# POLITECHNIKA WROCŁAWSKA

## WYDZIAŁ INŻYNIERII ŚRODOWISKA

### KATEDRA KLIMATYZACJI, OGRZEWNICTWA, GAZOWNICTWA I OCHRONY POWIETRZA

ROZPRAWA DOKTORSKA

## MODELOWANIE PROCESÓW WYMIANY CIEPŁA I MASY W WYMIENNIKU Z M–OBIEGIEM PRACUJĄCYM W URZĄDZENIACH KLIMATYZACYJNYCH

## MATHEMATICAL MODELING OF THE M-CYCLE HEAT AND MASS EXCHANGER USED IN AIR CONDITIONING SYSTEMS

mgr inż. Demis Pandelidis

Promotor: prof. dr hab. inż. Sergey Anisimov

Słowa kluczowe: wymiana ciepła, wymiana masy, obieg Maisotsenki, modelowanie matematyczne, pośrednie chłodzenie wyparne, analiza numeryczna, optymalizacja.

Key words: heat transfer, mass transfer, Maisotsenko cycle, mathematical modeling, indirect evaporative cooling, numerical simulation, optimization.

## Nomenclature

| Main symbols used in the text | | |
|---|---|---|
| $c_p$ | [J/(kg K)] | Specific heat capacity of moist air |
| $c_g$ | [J/(kg K)] | Specific heat capacity of water vapor |
| $c_W$ | [J/(kg K)] | Specific heat capacity of water |
| $d_h$ | [m] | Hydraulic diameter |
| $F$ | [m$^2$] | Surface area |
| $h$ | [m] | Height |
| $i$ | [kJ/kg] | Specific enthalpy of moist air |
| $G$ | [kg/s] | Moist air mass flow rate |
| $L, l$ | [m] | Streamwise length |
| $M$ | [kg/s] | Water vapor mass transfer rate |
| $N$ | [W] | Electrical power required for fan to operate |
| $p$ | Pa | Partial pressure of water vapor |
| $P_b$ | Pa | Atmospheric pressure |
| $q$ | [W/m$^2$] | Heat flux |
| $q^o$ | [kJ/kg] | Specific heat of water evaporation |
| $Q$ | [W] | Rate of heat transfer |
| $Q_1$ | [W] | Cooling capacity |
| $\hat{Q}$ | [W/m$^3$] | Specific cooling capacity per cubic meter of the heat exchanger's structure |
| $\hat{Q}_G$ | [W/(kg/s)] | Specific cooling capacity respected to 1 kg/s of primary airflow |
| RH | [%] | Relative humidity |
| $s$ | [m] | Fin pitch |
| $t$ | [°C] | Temperature |
| $\bar{t}$ | [°C] | Average temperature |
| $v$ | [m/s] | Air stream velocity |
| $V$ | [m$^3$/s] | Volumetric airflow rate |
| $V_{HMX}$ | [m$^3$] | Volume of the HMX structure |
| $W$ | [W/K] | Heat capacity rate of the fluid |
| $WC$ | [kg/s] | Water consumption |
| $x$ | [kg/kg] | Humidity ratio |
| $\bar{x}$ | [kg/kg] | Average humidity ratio |
| $X$ | [m] | Coordinate along primary airflow direction |
| $Y$ | [m] | Coordinate perpendicular to $X$ coordinate |
| $Z$ | [m] | Coordinate along fins direction |
| Special characters: | | |
| $\alpha$ | [W/(m$^2$ K)] | Convective heat transfer coefficient |
| $\beta$ | [kg/(m$^2$ s)] | Mass transfer coefficient |
| $\delta$ | [m] | Thickness |
| $\Delta p$ | [Pa] | Pressure drop |
| $\lambda$ | [W/(m K)] | Thermal conductivity |
| $\varepsilon$ | [-] | Effectiveness |
| $\sigma$ | [-] | surface wettability factor, $\sigma \in (0.0...1.0)$ |
| Non dimensional coordinates: | | |
| COP | [-] | Coefficient of performance |
| $f$ | [-] | Fuid friction coefficient |
| Le | [-] | Lewis factor |
| NTU | [-] | Number of transfer units |
| Nu | [-] | Nusselt number |
| Pr | [-] | Prandtl number |
| Re | [-] | Reynolds number |
| St | [-] | Stanton number |

| | | |
|---|---|---|
| $\bar{X}$ | [-] | $\bar{X}=X/L_X$ – relative $X$ coordinate |
| $\bar{Y}$ | [-] | $\bar{Y}=Y/L_Y$ – relative $Y$ coordinate |
| $\bar{Z}$ | [-] | $\bar{Z}=Z/h_{fin}$ – relative $Z$ coordinate |

| Subscripts/superscripts: | |
|---|---|
| 1 | Primary (main) airflow |
| 2 | Working (secondary) airflow in the wet channels in product part of the exchanger |
| 3 | Working (secondary) airflow in the dry channels in initial part of the exchanger |
| 4 | Working (secondary) airflow in the wet channels in initial part of the exchanger |
| $b$ | Beginning zone/respected to beginning zone |
| $cond$ | Heat transfer by thermal conduction |
| I$cond$ | First active zone of heat and mass transfer |
| I zone | Referenced to the first-order boundary conditions |
| II$cond$ | Referenced to the second-order boundary conditions |
| II$zone$ | Second active zone of heat and mass transfer |
| $const$ | Constant |
| $fin$ | Fins/ respected to fins structure |
| $g$ | Water vapor |
| $h$ | Referred to the channel height |
| $heat$ | Heat transfer |
| $HMX$ | Heat and mass exchanger |
| $i$ | Inlet |
| $(i,j)$, $(n,m)$ | Calculation nodes |
| $initial/work$ | Initial (working) part of the exchanger |
| $l$ | Latent heat flux |
| $mass$ | Mass transfer |
| $met$ | Coating material (metal foil or polyethylene) |
| $o$ | Outlet |
| $p$ | Plate surface |
| $plt$ | Channel plate |
| $product$ | Referenced to the product section of heat exchanger |
| $s$ | Sensible heat flux |
| $sat$ | Saturation state |
| $var$ | variable |
| $w$ | Water film |
| $WB$ | Wet bulb temperature/respected to wet bulb temperature |
| $X$ | Air streamwise in the dry channel |
| $Y$ | Air streamwise in the wet channel |
| • | Referenced to the elementary plate surface |
| •• | Referenced to the elementary fin surface |
| ' | Conditions at the air/water interface temperature |
| '' | Referenced to the plate surface |
| ∗ | Parameters after mixing |

| Specific nomenclature used for comparison of the different air conditioning systems (Section 10) | | |
|---|---|---|
| $CC$ | [-] | Cooling coil/ respected to cooling coil |
| $DW$ | [-] | Desiccant wheel/ respected to desiccant wheel |
| $E$ | [-] | Exhaust air parameters/ respected to exhaust air parameters |
| $ML$ | [kg/(s $n$)] | Human moisture loads in summer |
| $n$ | [-] | Number of room occupants |
| $Q_{RS}$ | [W] | Radiation cooling loads: walls |
| $Q_{CS}$ | [W] | Sensible cooling loads: windows |

| | | |
|---|---|---|
| $Q_{rS}$ | [W] | Radiation cooling loads: walls |
| $Q_{Win}$ | [W] | Sum of cooling loads: windows |
| $Q_o$ | [W] | Sensible cooling loads: occupants |
| $Q_T$ | [W] | Sensible cooling loads: technology |
| $Q_{Tot}$, | [W] | Total sensible cooling loads |
| $Q_L^H$ | [W] | Latent cooling loads: windows |
| $RE$ | [-] | Rotary exchanger/ respected to rotary exchanger |
| $reg$ | [-] | Regeneration air for desiccant wheel/ respected to regeneration air |
| $S$ | [-] | Supply air parameters/ respected to supply air parameters |
| $t_a$ | [°C] | Ambient air temperature |
| $t_E$ | [°C] | Exhaust air temperature |
| $t_R$ | [°C] | Temporary room temperature |
| $t_R^{Sum}$ | [°C] | Temporary room temperature in summer |
| $t_{RMax}^{Sum}$ | [°C] | Maximum room temperature in summer |
| $t_R^{Wint}$ | [°C] | Room temperature in winter |
| $\Delta t_{CC}$ | [°C] | Required temperature drop on cooling coil |
| $\xi$ | [kJ/kg] | Room process vector coefficient |

# Contents

**Appendix A. Calculation algorithm of the model describing the cross-flow evaporative cooler**

**Appendix B. Validation of the mathematical models of cross-flow
and regenerative evaporative air cooler against existing experimental data**

**Appendix C. Calculation algorithm for the model of the realistic M-Cycle air cooler
(universal section method)**

**Appendix D. Flow sheets of programming for the computer programs describing
cross-flow M-Cycle air cooler.**

**Appendix E. Analysis of the accuracy of the experiment performed by author**

**Appendix F. Validation against existing experimental data**

**Appendix G. Mathematical model of the modified counter-flow evaporative air cooler
(basic M-Cycle)**

**Appendix H. Additional information for Section 9.1.**

**Appendix I. Sensitivity analysis on the influence factors on the basis of regression models**

**Appendix J. Mathematical model of the desiccant wheel**

**Appendix K. Root code of the program describing ideal cross-flow M-Cycle air cooler**

## Abstract

This thesis investigates the indirect evaporative air cooler based on Maisotsenko cycle used in air conditioning systems: the cross-flow M-Cycle air cooler. The heat and mass transfer process were analyzed with ε-NTU-models, 14 mathematical models of the M-Cycle heat and mass exchangers (HMXs) were developed in total. At first the initial studies were performed with the basic evaporative cooling cycles, which allowed preparing initial assumptions for the mathematical model of the M-Cycle air cooler and to establish the most characteristic features of the combined heat and mass transfer in indirect evaporative air coolers.

In order to study the considered air cooler, the modified Runge-Kutta method and original algorithms, allowing to take into account uneven fin temperature distribution under combined heat and mass transfer conditions and effect of airflows mixing in wet channels under different arrangements of the initial part of the exchanger were applied to numerically solve the sets of differential equations under variable initial conditions. The computation model results were validated against experimental data obtained both from tests performed by author and from experimental data available in the existing literature. The positive results of this validation indicated that the sufficient accuracy in simulation could be obtained. The performance of the HMX was investigated and parametrically evaluated by transitional simulation under various ambient and working and operational conditions under different geometrical arrangements. The first analysis include the detail study of the combined heat and mass transfer processes inside considered air cooler. This allowed establishing that heat and mass transfer in cross-flow M-Cycle air cooler is characterized by a complex and diverse temperature and moisture distributions, which are different from the dependences found in typical evaporative heat exchangers. The second study was a sensitivity analysis under variable operational conditions, which allowed establishing factors which have most impact on the performance of the considered air cooler. The third analysis was performed to compare different M-Cycle air coolers, which allowed establishing which flow arrangement has the highest application potential. The results of the fourth study indicated that there are possibilities of improvement of the original M-Cycle HMX by modifying its geometrical arrangement and by modifying its construction for application in different types of air conditioning systems. The analysis allowed establishing the best proportions between initial and product part of the exchanger, the most effective perforation arrangements and the boundary temperatures determining which version of the cross-flow M-Cycle air cooler operates better in different type of air conditioning system. After above-mentioned analysis, the cross-flow M-Cycle heat exchanger was statistically analyzed and its structure was optimized. The statistical analysis allowed establishing the regression equations for "black box" models of the characteristic efficiency factors, including outlet air temperature, specific cooling capacity respected to the volume of HMX structure, dew point effectiveness and coefficient of performance (COP). The optimization was based on five independent variables (inlet air temperature and relative humidity, primary air mass flow rate, working to primary air heat capacity ratio and relative length of the initial part) and their influence on efficiency factors. The optimization allowed establishing the optimal geometrical and operational parameters of the exchanger and the climate conditions for its rational

operation. The analysis of the values of Harrington function in climate parameters from selected cities worldwide showed that investigated HMX can be applied in most of them and it is suitable for the Polish climate conditions.

The optimized HMX was analyzed in terms of its application potential in two air conditioning systems: typical air handling unit with cooling coil supplied by R410a mechanical compression system and the solar desiccant air conditioning system (SDEC) with rotary dehumidifier regenerated with air with relatively low temperature which can be obtained by the solar panels in moderate climate conditions. Both analysis showed that cross-flow M-Cycle air cooler has high application potential.

In case of the typical air conditioning system, HMX allowed for significant reduction of operational costs: up to 23 times. In the displacement system the considered air cooler is able to operate as the only cooling source, while in the mixing system it requires additional cooling coil during peak hours. In case of the desiccant systems, considered unit allowed achieving higher effectiveness than typical system equipped with direct evaporative coolers and rotary exchanger and it allowed keeping the comfort conditions inside the conditioned spaces at lower regeneration air temperature. The analysis of the different arrangements of the SDEC systems equipped with the cross-flow M-Cycle air cooler allowed finding the most effective solution in terms of cooling performance.

## Streszczenie

W niniejszej pracy doktorskiej przeanalizowano wymiennik z obiegiem Maisotsenki pracujący w urządzeniach klimatyzacyjnych, o krzyżowym schemacie przepływu powietrza. Procesy wymiany ciepła i masy były analizowane za pomocą ε-NTU modeli. Na potrzeby rozprawy opracowano łącznie 14 modeli różnych wymienników z M-obiegiem. Na początku pracy przeprowadzono badania wstępne z wykorzystaniem podstawowych obiegów pośredniego chłodzenia wyparnego, które pozwoliły przygotować wstępne założenia dotyczące modelu pośredniego wymiennika wyparnego z M-obiegiem oraz określić najważniejsze zależności dotyczące jednoczesnej wymiany ciepła i masy w różnych obiegach pośredniego chłodzenia wyparnego.

Do rozwiązania układu cząstkowych równań różniczkowo algebraicznych ze zmiennymi warunkami początkowymi, które opisują procesy zachodzące w badanym wymienniku, wykorzystano oryginalne, autorskie algorytmy bazujące na zmodyfikowanej metodzie Rungego- Kutty czwartego rzędu, które pozwoliły na uwzględnienie nierównomiernego rozkładu temperatury na ożebrowaniu w warunkach jednoczesnej wymiany ciepła i masy oraz pozwoliły uwzględnić proces mieszania się strumieni powietrza w badanym wymienniku. Wyniki uzyskane z modeli były walidowane, zarówno do istniejących danych eksperymentalnych jak i do wyników badań przeprowadzonych przez autora. Pozytywne wyniki walidacji pozwoliły stwierdzić, że model cechuje się wystarczającą dokładnością do badań pośredniego wymiennika z M-obiegiem. Pierwsza analiza przeprowadzona w pracy dotyczyła dokładnemu zbadaniu procesów wymiany ciepła i masy zachodzących wewnątrz badanego wymiennika wyparnego. Ustalono, że zachodzące procesy odbiegają w znaczący

sposób od procesów spotykanych w typowych wymiennikach wyparnych. Druga analiza dotyczyła sprawdzenia wrażliwości badanej jednostki na wybrane czynniki, co pozwoliło ustalić, który z nich ma największy wpływ na krzyżowy wymiennik z M-obiegiem. Trzecia analiza dotyczyła porównania różnych wymienników z M-obiegiem, dzięki której określono, która z badanych jednostek ma największy potencjał wdrożeniowy. Na podstawie wyników uzyskanych z czwartej serii symulacji stwierdzono, że można ulepszyć istniejącą konstrukcję wymiennik poprzez modyfikację jego parametrów geometrycznych oraz poprzez zmianę jego budowy w zależności od lokalizacji w systemach klimatyzacyjnych. Na podstawie symulacji ustalono, że efektywność wymiennika można podnieść poprzez zmianę aranżacji perforacji ścianek wymiennika oraz przez zmianę proporcji pomiędzy jego częścią występną i główną. Określono także parametry graniczne, dla których różne aranżacje wymiennika w systemach klimatyzacyjnych osiągają wyższą efektywność. W kolejnej serii badawczej przeanalizowano wymiennik statystycznie i zoptymalizowano jego strukturę. Analiza statystyczna pozwoliła na uzyskanie modeli „czarnej skrzynki" opierających się na równaniach regresji dla charakterystycznych wskaźników efektywności wymiennika: wyjściowej temperatury powietrza głównego, właściwej mocy chłodniczej odniesionej do jednostki wypełnienia wymiennika, sprawności odniesionej do temperatury punktu rosy powietrza na wejściu do jednostki oraz współczynnika efektywności COP. Optymalizację przeprowadzono dla pięciu zmiennych niezależnych (wejściowej temperatury i wilgotności powietrza, przepływu masowego powietrza głównego, stosunku pojemności cieplnej powietrza pomocniczego do głównego oraz względnej długości części wstępnej wymiennika). Dzięki procesowi optymalizacji ustalono optymalne wartości parametrów geometrycznych i roboczych wymiennika oraz określono strefy jego racjonalnego wykorzystania. Analiza zmienności funkcji Harringtona dla parametrów klimatycznych wybranych miast ze świata pokazała, że wymiennik z M-obiegiem nadaje się do wdrożenia w polskich systemach klimatyzacyjnych. Zoptymalizowany wymiennik został wykorzystany do testów jego potencjału wdrożeniowego w wybranych systemach klimatyzacyjnych: standardowego systemu klimatyzacyjnego z chłodnicą freonową oraz solarnego systemu klimatyzacyjnego opartego na osuszaczu sorpcyjnym, który regenerowany jest powietrzem o relatywnie niskiej temperaturze, która jest możliwa do uzyskania na panelach solarnych w umiarkowanych klimatach (tzw. system SDEC). Obydwie analizy potwierdziły bardzo wysoki potencjał wdrożeniowy jednostki. W przypadku typowego systemu klimatyzacyjnego wymiennik z M-obiegiem pozwolił na znaczne ograniczenie kosztów eksploatacyjnych ( do 23 razy w stosunku do typowego systemu). W przypadku systemów wentylacji wyporowej wymiennik może pracować jako jedyne źródło chłodu, w przypadku systemów wentylacji mieszającej jednostka potrzebuje dodatkowej chłodnicy pracującej jako szczytowe źródło chłodu. W przypadku systemów sorpcyjnych proponowana jednostka pozwoliła znacząco poprawić efektywność w stosunku do klasycznego systemu opartego na komorach zraszania i wymienniku obrotowym oraz pozwoliła na utrzymanie komfortowych warunków w klimatyzowanych pomieszczeniach w sytuacji, gdy rotor regenerowany był powietrzem o niskiej temperaturze. Po analizie różnych aranżacji systemów SDEC z krzyżowym wymiennikiem z M-obiegiem ustalono rozwiązanie najbardziej efektywne pod względem skuteczności ochładzania powietrza.

# 1. Introduction

## 1.1. Background of the study

The rapid growth of world energy consumption has raised serious concerns over the depletion of energy resources. The increasing world energy consumption is caused by the facts like continuous growth of world population, economic growth in emerging regions the development of communication networks and the promotion of life style of developed nations [1], [2].
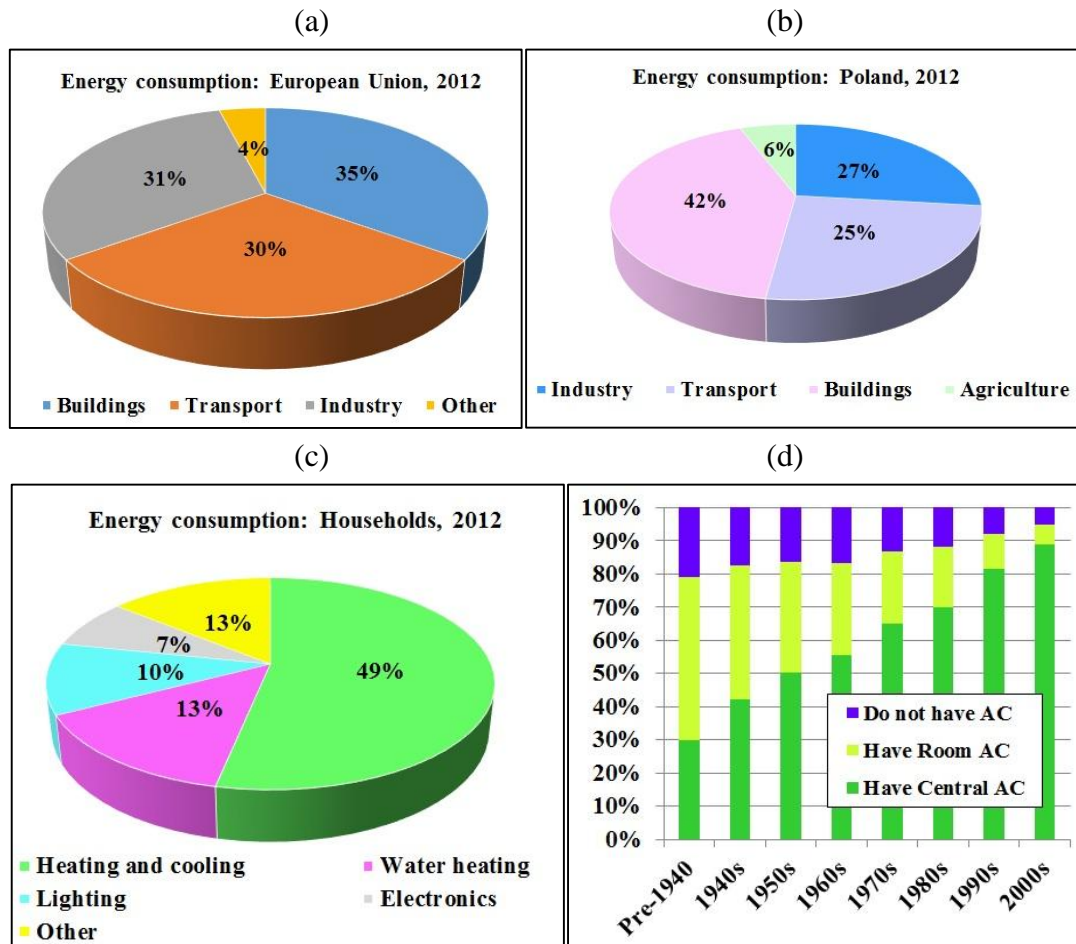
(a)                                                    (b)

(c)                                                    (d)

Fig. 1.1. Energy consumption in XXIst century. (a) Energy consumption in EU, 2012 [3]. (b) Energy consumption in Poland, 2012 [4]. (c) Energy consumption in households worldwide, 2012 [5]. (d) Increase in air conditioning in American Households [6].

Over the last two decades, the world primary energy consumption (fossil fuels) has increased by 49% [7]. The building sector accounts for a major part of the world's total end energy consumption. In 2012, energy consumption of buildings in EU countries accounted for 35% of total energy use (Fig. 1.1. (a)), higher than those for industry (31%) and transport (30%). In Poland, the proportion of energy consumption in buildings was 42% (30% of which are households), which is higher than average European consumption (Fig. 1.1. (b)). The building sector has the largest single potential for improving the efficiency of energy utilization. It can be seen that energy used for cooling is an important part of the total energy consumption (Fig. 1.1. (c)), which is continuously increasing due to the growing demand for better indoor comfort

conditions in buildings. In this regard, air conditioning systems have become more popular to supply comfortable environment (Fig. 1.1. (d)).

The refrigeration and air-conditioning systems use almost 15% of the total electricity produced today [8]. Currently, the mechanical-compression systems are covering almost 95% of the air-conditioning market [9], [10]. The energy policies of many countries worldwide focus on reducing the electrical energy consumption and implementing new technologies, which are considered as environmental friendly [8]. Due to the increasing need for air conditioning and the growing interest in energy savings, seeking ways to reduce fossil fuel consumption and to increase usage of the renewable energy during air-conditioning process in building sector is a matter of great importance.

In last two decades many novel devices based on the renewable energy were implemented for the heating purposes: novel heat recovery units, heat pumps, solar systems and many other. However, no devices based on the renewable energy which were widely applied in the cooling sector so far. This creates an important scientific challenge for researchers around the world. One of the novel solutions which is able to face the above-mentioned challenges is the direct and indirect evaporative air cooling. Evaporative air coolers utilize the latent heat of water evaporation to provide cooling and are less dependent on fossil fuels [2], [11], [12], they are also characterized by much higher COP factors in compare to the mechanical compression systems [2], [11], [12]. The higher COP shows that considered devices are able to reduce the significant part of energy consumption used for air conditioning. One of the best methods in achieving very low temperatures with indirect evaporative air cooling is the new thermodynamic cycle known as the Maisotsenko cycle (M-Cycle).

### 1.2. Historical overview

The first known appearance of practical use of evaporative air cooling occurred at around 2500 B.C., during which the ancient Egyptians made use of water containing porous clay jars for purpose of air cooling [13]. This mechanism was also applied into ancient Egypt buildings and further spread across the Middle East regions where the climate is usually hot and dry. There were also many examples of other forms of using evaporative air cooling in that time, such as porous water pots, water ponds, pools, and thin water chutes were put into the building constructions in order to create the cooling effect [13]. One of the earliest and most interesting methods of practical applications evaporative cooling into the ventilation system was the windcatcher (Fig. 1.2.), which was widely used in ancient Egypt and Persia thousands of years ago. The form of the system was the wind shafts on the roof, which caught the wind, passed it over subterranean water in a qanat and discharged the cooled air into the building [13], [14]. Nowadays Iranians are still using direct evaporative cooling but they have changed the windcatcher into a mechanical evaporative air cooler.
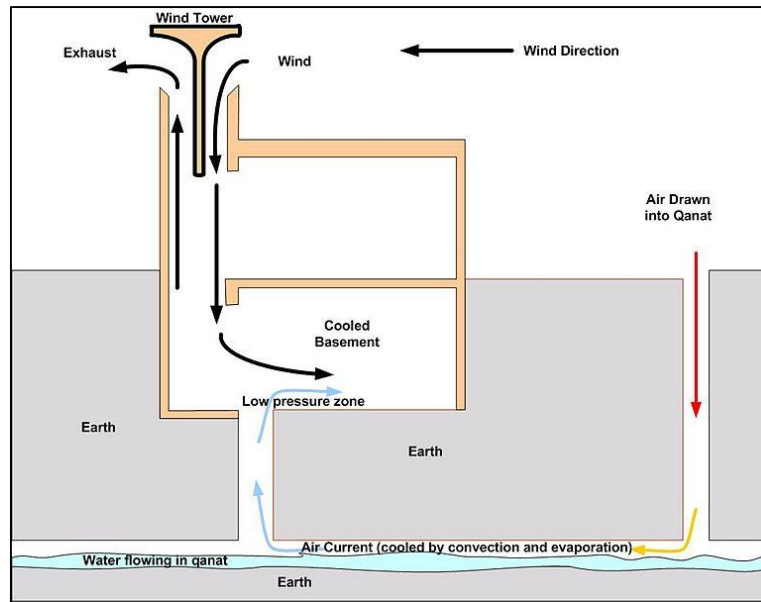
Fig. 1.2. The scheme of an ancient windcatcher [13].

The modern evaporative cooling devices became popular in the USA at the beginning of XX century [13]. In early 1900s, air washers were invented at New England and Southern Coastline and used for cleaning and cooling air in textile mills and factories. During that period, several air cooling devices including the direct and indirect coolers were also found in Arizona and California, because the dry climate of those states allowed achieving very low temperatures with evaporative cooling. In late 1930s, many houses and business spaces at Southwest were equipped with individually made water dripping air coolers which, when entering into early 1950s, were developed into the massively producing products and obtained wide range of market places including USA, Canada, and Australia [13].

Evaporative air cooling devices were based on simple and cheap solutions which made them very attractive for middle and lower-class costumers. A perfect example of such solutions is the misting fan (Fig. 1.3.(a)): it is a standard auxiliary fan equipped with a nozzle to spray the water mist in the air. This solution became very popular in touristic regions in south European countries such as Greece and Spain. The more advanced and effective version of the misting fan is the direct evaporative cooler (DEC), visible in Figure 1.3.(b). This device is equipped with a centrifugal fan and a porous material (usually cellulose or wood fibre) which is wetted with water. Such devices are very popular in the Middle East and the hot regions of China and India.
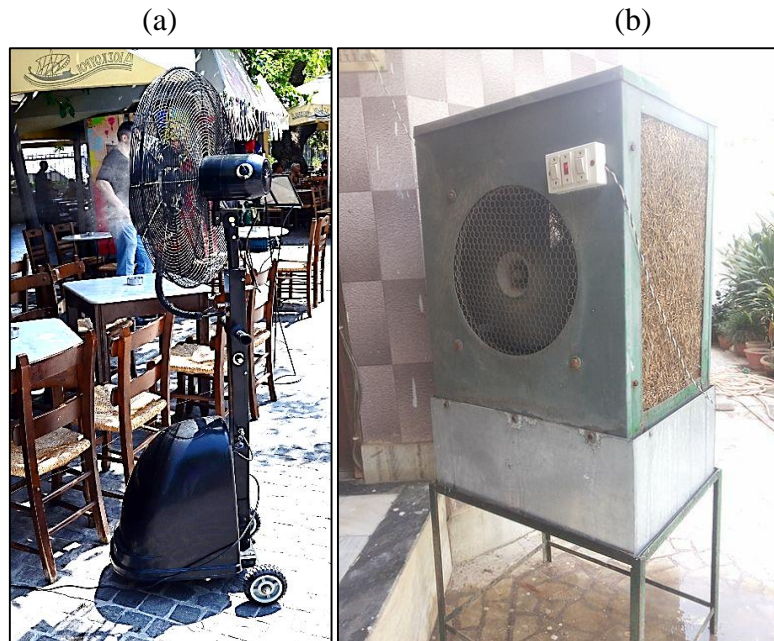
(a)                              (b)



Fig. 1.3. Evaporative cooling today. (a) A misting fan in Athens, Greece (author's photograph). (b) A traditional air cooler in Mirzapur, Uttar Pradesh, India [13].

Owing to the distinguished advantage of the Indirect Evaporative Coolers (IEC) over the direct one, i.e., no moisture added into the air thus enabling hygiene air quality, this type of air treatment has gained growing attention and fast development over the past few decades. Research, production and practical application related to the devices realizing indirect evaporative cooling process, called the heat and mass exchangers (HMXs) were all rapidly flourishing [2], [15], [16]. Many corporations around the world discovered the potential of evaporative cooling and they started applying such exchangers in their air handling units (AHUs). The most important world corporation which applied the evaporative air cooling include Air Group Australia, Carrier (USA), Coolerado (USA), Euroclima (Austria), Kampmann (Germany), Munters (Sweden), and about 25 other corporations around the world. This shows the increasing interest in novel solutions of evaporative air coolers, which would allow obtaining highest possible effectiveness and replacing part of the ineffective mechanical compression systems.

## 1.3. Evaporative air cooling cycles

### 1.3.1. Direct evaporative air cooling (DEC)

Direct evaporative air cooling is the oldest and the simplest method of cooling air with water in which the process air contacts directly with water. This type of systems has been widely used for the reasons of simple structure, cheap initial and operating costs [7]. Direct evaporative cooling system has approximately 0.70–0.95 effectiveness in terms of temperature depression [17]. Typical evaporative air cooler uses a water tank, a porous material which is wetted with water and a fan which moves the air through the wet porous material (Fig. 1.4.(a)). The most commonly used direct evaporative coolers are essentially metal cubes or plastic boxes with

large flat vertical air filters, called their walls (Fig. 1.4.(b)). The pads are kept moist by the water dripped continuously onto their upper edges and distributed further by gravity and capillarity. The process air is drawn by a fan. After being cooled and humidified in the channels between the pads, the air leaves the cooler. The falling water is usually kept in a tank below the pads, where it is recirculated into the system. Many coolers use two-speed or three-speed fans, so the users can modulate the leaving air states as needed [17].
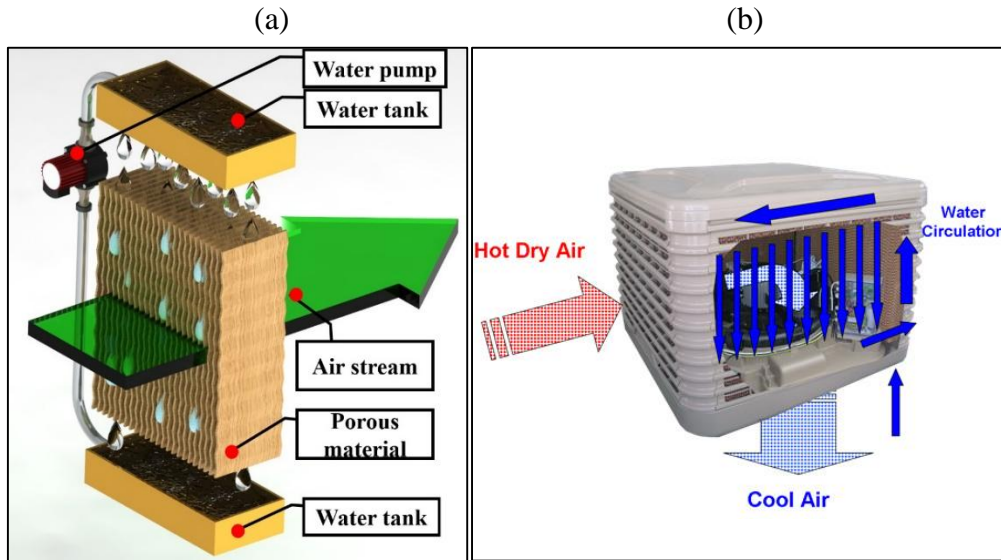


Fig. 1.4. Direct evaporative air coolers. (a) Operation scheme. (b) Scheme of a typical DEC unit [18].

Sometimes in the case of residential applications there are concerns on hygienic issues, if maintenance of water is poor. Direct evaporative cooling system adds moisture to the cool air (Fig. 1.5.), which also makes conditions more uncomfortable for humans. The process can be expressed as from to point $1_i$ in the psychrometric chart as shown in Fig. 1.5. The air handling process approximately follows the constant enthalpy line. Point $1_i$ represents the state of process air entering a cooler, point $1_o$ represents the state of the process air leaving the cooler. Theoretically, the process may end at wet bulb temperature of the incoming air. However, reaching the saturation state with direct evaporative air cooling is almost impossible [17].
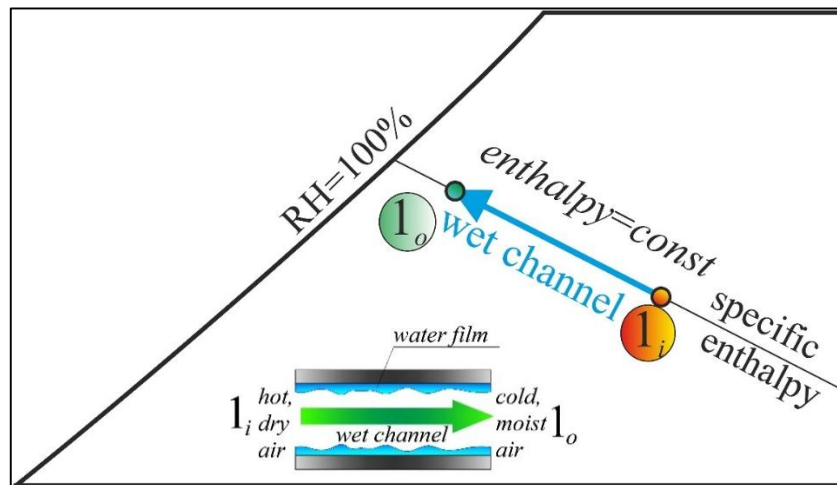


Fig. 1.5. Heat and mass transfer in DEC process

### 1.3.2. Indirect evaporative air cooling (IEC)

Indirect evaporative cooling system provides only sensible cooling to the process air without any moisture addition (Fig.1.6. (a)). An indirect evaporative air cooler passes primary (main) air over the dry side of the plate of the heat exchanger, and working (secondary) air over its opposite wet side [15], [16], [19]. The wet side absorbs heat from the dry and therefore it cools the dry side without adding moisture to the air (process $1_i–1_o$ in Fig.1.6. (a)), while the latent heat of vaporizing water is given to the wet side air (process $2_i–2_o$ in Fig.1.6. (a)).

Due to no moisture addition to the supply air, the IEC system is more attractive than direct evaporative devices for domestic applications. That is why there are often used in air handling units, like in case of Euroclima's ETA PAC air handling unit (Fig. 1.6.(b)). IEC units take the form of typical heat recovery recuperators: parallel-flow (Fig. 1.6.(c)), counter-flow (Fig. 1.6.(d)) and counter-flow (Fig. 1.6.(e)).
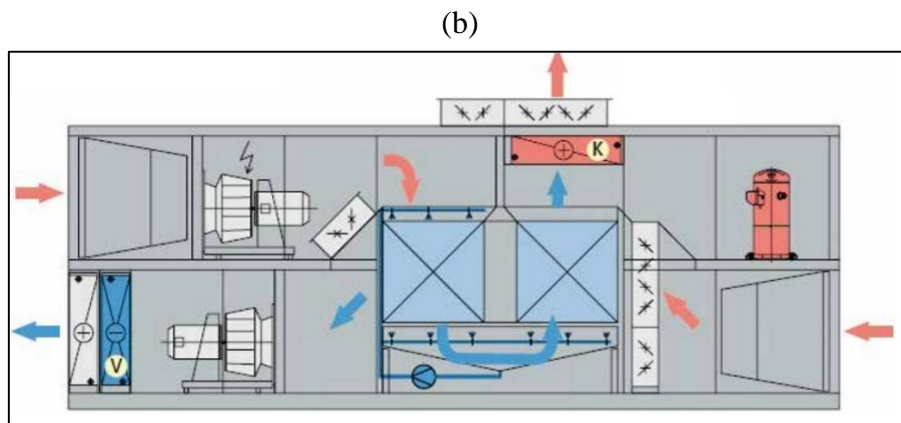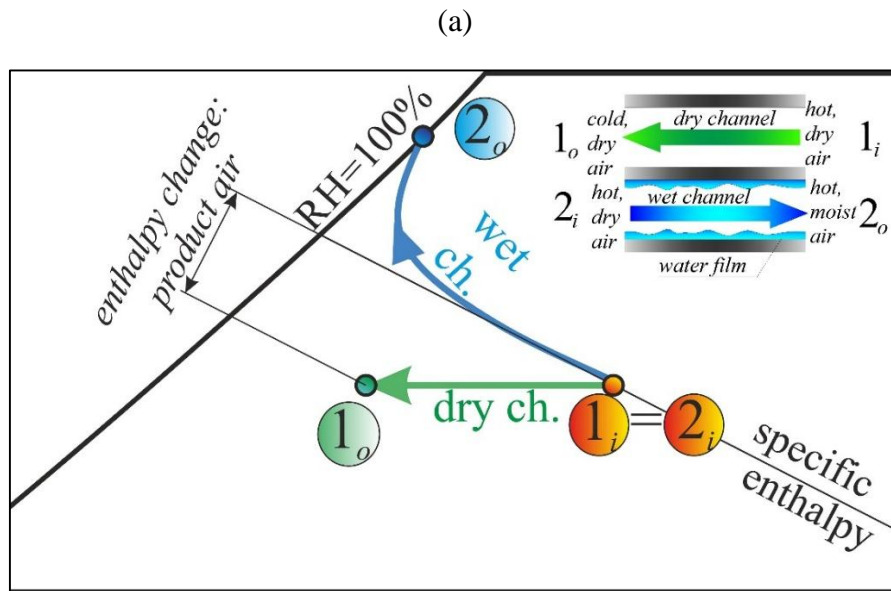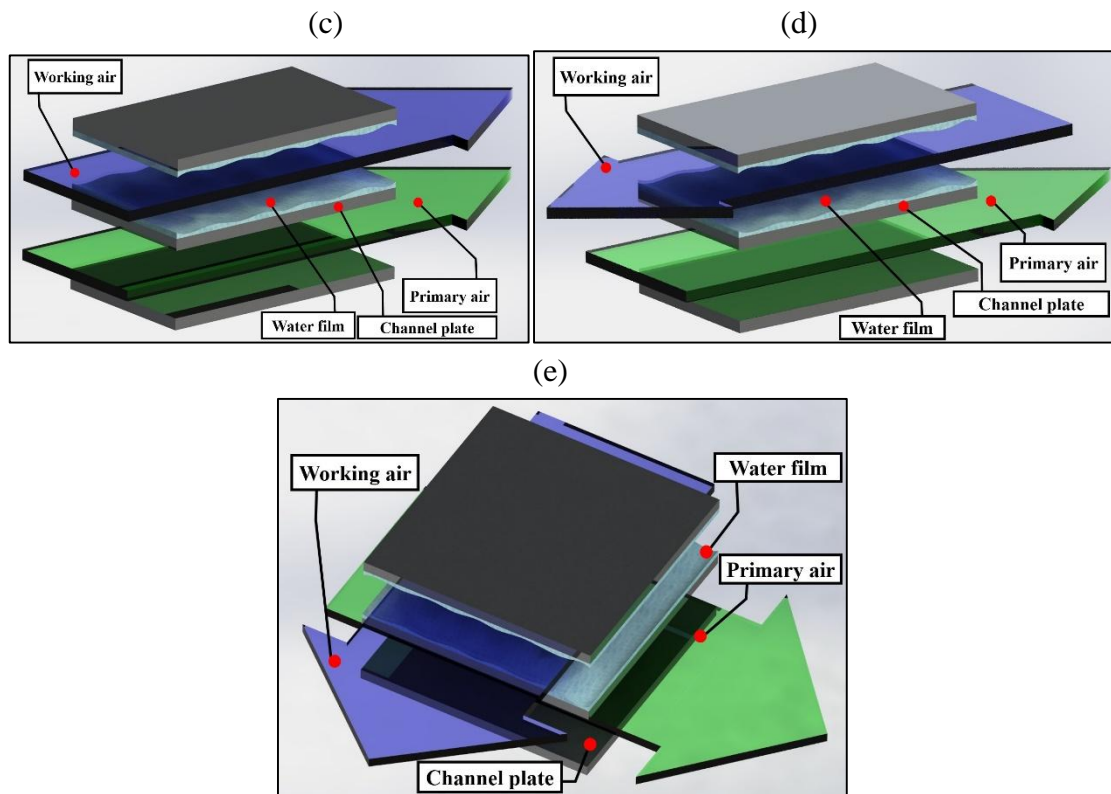
(a)



(b)

Fig. 1.6. Indirect evaporative cooling. (a) Heat and mass transfer on psychrometric chart. (b) ETA PAC air handling unit by corporation Euroclima equipped with double cross-flow indirect evaporative cooler [20]. (c) Parallel-flow IEC. (d) Counter-flow IEC. (e) Cross-flow IEC.

Some counter-flow IEC units are able to achieve high temperature efficiency, they are even able to achieve temperatures lower than the wet bulb temperature of the incoming air [21] However, the counter-flow units are hard to manufacture and most IECs are based on the cross-flow scheme. That is why the cooling effectiveness of most indirect coolers is generally low, typical units are able to cool the ambient air to the level of 0.40–0.60 of its inlet wet bulb temperature [2], [11], [22] which is the major drawback in wider application of indirect evaporative cooling systems.

## 1.4. Materials used for evaporative air coolers structure

The most important parts of any evaporative air cooler are the materials which are used for their structure. Types of materials differ in case of indirect and direct units (indirect evaporative air coolers must have one dry and one wet channel) and on the type of application. A wide range of material types can be used as a medium to evaporate water, i.e. metal, fibre, plastic, ceramics, zeolite and carbon [7], [23].

The wet sides of heat and mass exchanger are usually formed by the wicking and porous materials to enable water evaporation. The most important properties of the evaporative material are: wicking ability (capillary forces), thermal conductivity, hygroscopic and tensile strength [23]. A high wicking ability enables a fast, thin and uniform wetting on the wet surface of the plate, a high thermal conductivity allows a large amount of heat to be conducted from

the dry side of the plate to the wet side, a tensile strength should be well enough to process or shape into various geometries, a coating compatibility with a hydrophobic material should allow for the low thermal contact resistance between them [24]. The wicking material should also be relatively cheap and easy for cleaning and replacement [7], [24].

The dry sides of IECs are usually formed using hydrophobic materials which prevent water penetrating the from wet side. According to Duan [7] the wicking and evaporation capacities of the materials will be improved after the hydrophobic material coated on the evaporative medium surface.

In the case of an indirect evaporative chillers the structure is made of a materials similar to the ones used in cooling towers, i.e. PVC package or aluminum foil package (Fig. 1.7.(a) and (b)). According to the study performed by Jiang and Xie [25], the mass transfer coefficient of aluminum foil is two times greater than that of PVC padding, thus it has higher heat and mass transfer rate. The main disadvantage of the aluminum foil padding is its shorter life time and its relatively high cost. Different type of metals may be also used for the structure of IECs. The typical metal structure, however, has low porosity and it is not able to maintain the water for a longer period of time. For this reasons porous metal structures may be implemented on the wet side (i.e. wicked metal, metal foams or wools- Fig. 1.7.(c)). Metals as copper, aluminum and their coils are used for such structures [23].

In case of M-Cycle heat exchangers used in Coolerado Coolers [15], cellulose-blended fibre and polyethylene were used as the wicking and the hydrophobic coating materials (Fig. 1.7.(d)). Cellulose fibres are also often used as the material for direct evaporative air coolers. The special cellulous materials enable uniform and thin wetting on the working air side of heat exchanger without extra water, which allows focusing on the cooling of the product air. This is caused by the fact that the wicking of cellulose material disrupts the surface tension of water [24]. The cellulous fibres or kraft paperswork well when they are coated with hydrophobic synthetic resin, plastic or wax or a thin layer of aluminium to form the heat exchanger plates [26].

Another interesting type of evaporative media are the porous ceramic materials (Fig.1.7.(e)). This materials were investigated by Zhao et al. [23]. Porous ceramic tubes or pipes are the most favorite configurations for this type of material. Ceramic materials have several advantages, i.e. good construction facility, accessibility. Also, the ceramic exchangers have good filtering property, due to the fact that water evaporates in the pores without carrying of water droplets, which acts as a filter to avoid the propagation of bacteria [27].
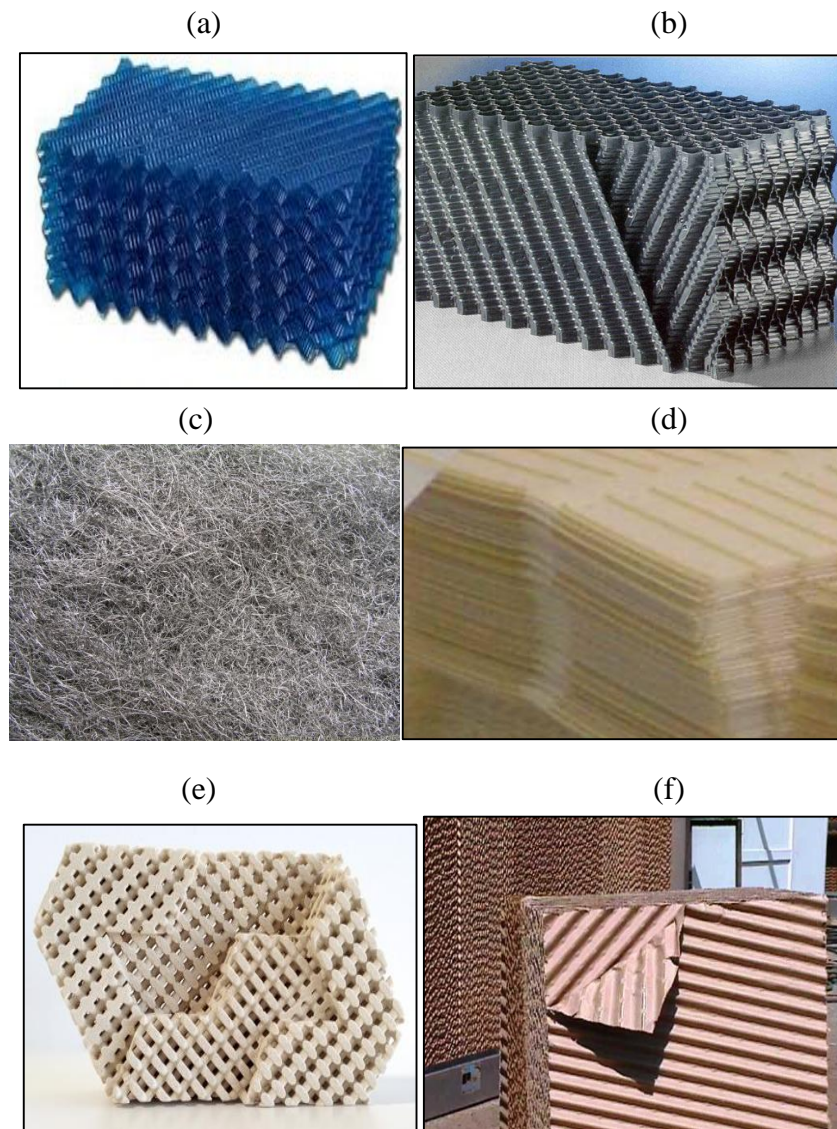
(a)                                      (b)

(c)                                      (d)

(e)                                      (f)

Fig. 1.7. Materials used for evaporative air coolers. (a) PVC package. (b) Aluminum package. (c) Metal wool porous structure. (d) Cellulose-blended fibre sheets. (e) Ceramic porous structure. (f) Rigid porous paper structure used for DEC packages.

Another type of materials are rigid evaporative media (Fig. 1.7.(f)). They were originally manufactured by Munters Corp. [7] and they shortly become widely used in direct evaporative coolers. Such materials have many advantages over other materials, including low pressure drop resulting in low operating costs, good wetting properties, low scaling, self-cleaning and long life time. In the process of fabrication, the corrugated cellulose media, treated chemically with antiriot and rigidifying resins, have been stacked together in different flute (Fig. 1.7.(f)).

Another materials considered to be used in evaporative air coolers are zeolite and carbon structures. According to Zhao [23],thermal properties of carbon materials are good enough to transfer both sensible and latent heat in evaporative air coolers. For such applications a carbon material with low porosity would show higher effectiveness, because it has less water-retaining capacity that would enable enhanced sensible heat transfer. Some carbon fibres can be made

into low porosity level (1% or below), and therefore, may be suitable for use in IECs. As for the zeolite structures, the synthetic zeolites are attractive for drying and separation, due to their affinity for water and other small diameter molecules. and also their ability to reject large diameter molecules [2], [23].This water retaining potential is satisfying to participate in the mass transfer duty in indirect evaporative air coolers [23]. The properties of several evaporative medium types were summarized by Zhao et al. [23] (Table 1.1).

Table 1.1. Prosperities of selected materials used of evaporative air coolers

| Type of material | Thermal conductivity, W/(m·K) | Porosity, % | Hardness/ shaping ability | Compatibility with coating | Contamination risk | Cost per sheet 10cm×10cm×0.5 mm (£) |
|---|---|---|---|---|---|---|
| Metal | High | 20-90 | High | Compatible with solid metal | Low (sintered metal) | 30-100 |
| Fibre | Low | 1-60 | Low | Compatible with polyethylene | High | <5 |
| Ceramic | Variable | 1-80 | High | Compatible with solid metal | High | 150-250 |
| Zeolite | Low | 40-80 | Medium | Compatible with polyethylene or wax | High | 150-250 |
| Carbon | Variable | Variable | Medium | Compatible with polyethylene or wax | High | 30-80 |

## 1.5. Methods of improving evaporative air coolers

The major concern in wider application of indirect evaporative air cooling units is their low thermal effectiveness [11]. Typical IECs are based on the cross-flow scheme, which results in low temperature drop. The counter flow units are difficult to apply, due to the complicated airflow scheme. Many researchers took their effort to increase the efficiency of evaporative air coolers in order to allow for their wider application in different climate conditions. Some of the methods concentrated on complex systems made of few types of exchangers, while some focused on more simple solutions. The following chapter presents most important methods of increasing the efficiency of IECs which were investigated or proposed in the previous studies.

### 1.5.1. Combination of systems

The simples way of increasing the evaporative air cooling process is the combination of systems, by using two or more indirect exchangers (such solution is used in ETA PAC air handling unit presented in Fig. 1.6.(b)) or a combination of indirect and direct evaporative air coolers (Fig. 1.8.). In such case, the first stage of the process is indirect evaporative cooling, which lowers both the dry-bulb and wet bulb temperature of the incoming air. Then the leaving air is delivered to the direct evaporative cooler where it is cooled and humidified. The working air for IEC may be the exhaust air from the conditioned space (but in this case it is not recommended due to the higher humidity) or the outdoor air. This system allows the air to be cooled below its wet bulb temperature [28], but it has two main disadvantages: first, the total system is larger and more expensive, second, it adds moisture to the airflow which make the

indoor conditions less comfortable. Due to the last reason it is recommended for hot and dry climate conditions.
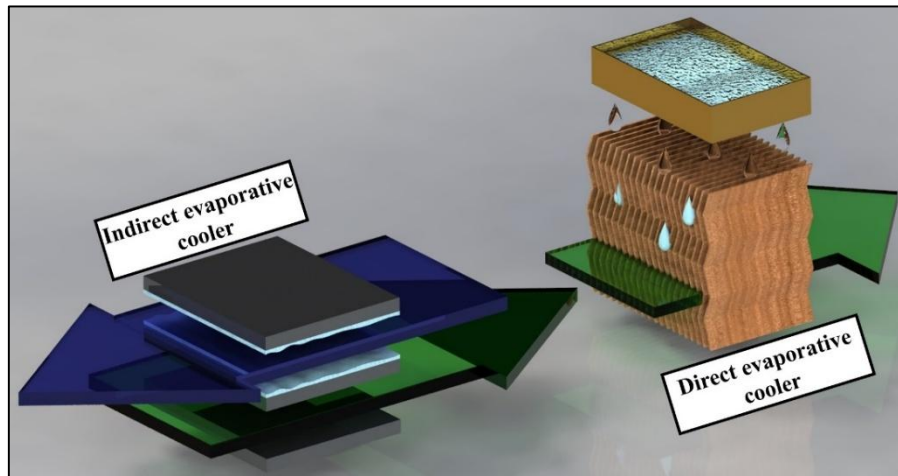


Fig. 1.8. A combined system of indirect and direct evaporative air coolers.

### 1.5.2. IEC with cooling coil (supplied by the typical refrigerant system)

A very simple method to achieve higher effectiveness of the IEC is a combination of evaporative air cooling and a typical mechanical compression system (Fig. 1.9.). Such idea was investigated by author in many papers [2], [29], [30], [31], [32]. The main advantage of such system is it's low sensitivity on the outdoor conditions.

In such system an IEC unit operates in conjunction with a cooling coil (or a direct-expansion (DX) refrigerant coil) to enable energy efficient air conditioning for buildings. The IEC works as a main cooling source and cooling coil works as a peak cooling source. In situation when evaporative air cooler is not able to provide satisfying indoor conditions, the mechanical compression system is switched on and additionally cools the airflow.

The best solution is the application of the IEC which could operate as the heat recovery exchanger (colder exhaust room air is delivered to the wet channels), which allows it to be less sensitive on the humidity of the outdoor air. Research presented by author shown that during most of the day time in Polish climate conditions, an IEC is able to provide comfortable conditions, the cooling coil needs to operate only for 4-5 hours [32]. After passing the wet channels, the working airflow may be used to cool the condenser of the mechanical compression refrigeration based system, thus further improving its performance due to the reduced cooling air temperature within the air condenser.

### 1.5.1. A combined system of IEC, DEC and cooling coil (supplied by the typical refrigerant system)

When extra low temperature air is needed at a special occasion such as freezing rooms [2], a combination of the three units, including indirect evaporative air cooler, direct evaporative air cooler and a cooling coil may be considered. The system operates similar to one described in the Section 1.5.2.
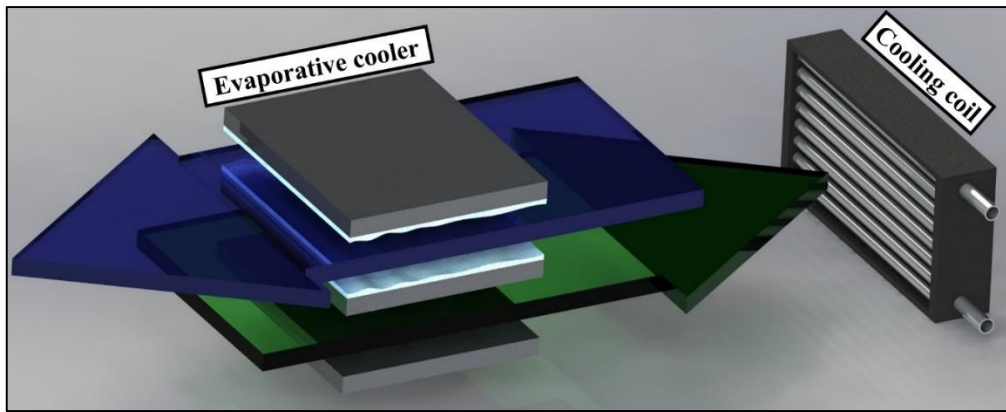
Fig. 1.9. A combined system of indirect evaporative air cooler and typical cooling coil.

## 1.5.2. SDEC system

Due to the novel discoveries air dehumidification process, systems with separate control of the temperature and humidity of the airflow become popular in recent years [2]. The concept of such systems is based on the idea to use a desiccant cycle to remove the moisture from the airflow and reduce its temperature with evaporative cooling process. The most popular solution of such system are Solar Desiccant Evaporative Cooling systems (SDEC), which use the solar energy to regenerate the desiccant material [33]. Owing to this advantage, SDEC system are characterized with a very low energy consumption.
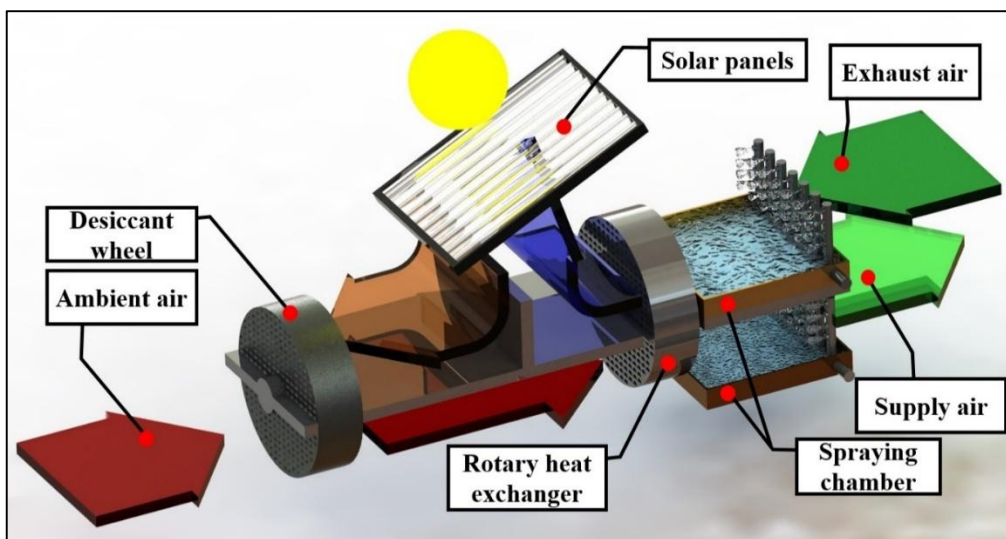


Fig. 1.10. Scheme of the typical SDEC system.

The typical system consists of a rotary desiccant wheel for dehumidification of the airflow, the rotary heat exchanger for first-step reduction of temperature and a spraying chamber for further cooling of the air stream (Fig. 1.10.). The exhaust air stream is also delivered to the spraying chamber, to reduce its temperature to the lowest possible level before it enters the rotary heat exchanger for the initial cooling of the process airflow. After passing the rotary wheel, the exhaust airflow is delivered to the solar panels, where its heated sensibly (Fig. 1.10.). If the solar panels are not able to provide enough heat the system may be additionally equipped with water or electrical heater. The hot air is delivered to the desiccant wheel, where it regenerates

the sorbent. After this process the exhaust air is discharged to the atmosphere. There are many arrangements of the SDEC systems (with IEC units, with a combination if DEC/IEC units and other combination of heat recovery exchangers and direct and indirect evaporative air coolers [33]). Solid desiccants used for the rotary dehumidifier include: silica gel, activated aluminum, lithium chloride, zeolites, molecule sieves, titanium silicide, polymer etc. All desiccants have a porous structure, which enables binding of moistures in the voids [2].

Author has investigated the subject of the SDEC systems as well [34], [35], [36]. The solution of the SDEC with air ground heat exchanger for pre cooling and partly dehumidifying the air before it enters the system was proposed (Fig. 1.11). The system was using an indirect evaporative air cooler instead of the spraying chambers and the rotary heat exchanger. The initial pre-cooling of the airflow in ground heat exchanger resulted in low humidity and relatively low temperature after passing the desiccant wheel, which allowed obtaining very low supply air temperatures (even 13°C at ambient air temperature equal 30°C [35], [36]).

The SDEC systems are claimed to have the potential to widely eliminate use of the mechanical compression systems and therefore, to become the new energy effective method for air conditioning [2], [33]. The main advantage of the system is that, the heat source could be either solar energy or a low grade waste heat which could further reduce the costs and fossil fuel consumption. The main disadvantages are the high investment costs, complex structure, complicated control system and a large size of the unit (the indoor system is larger than a typical AHU and it also requires a solar panels on the roof).
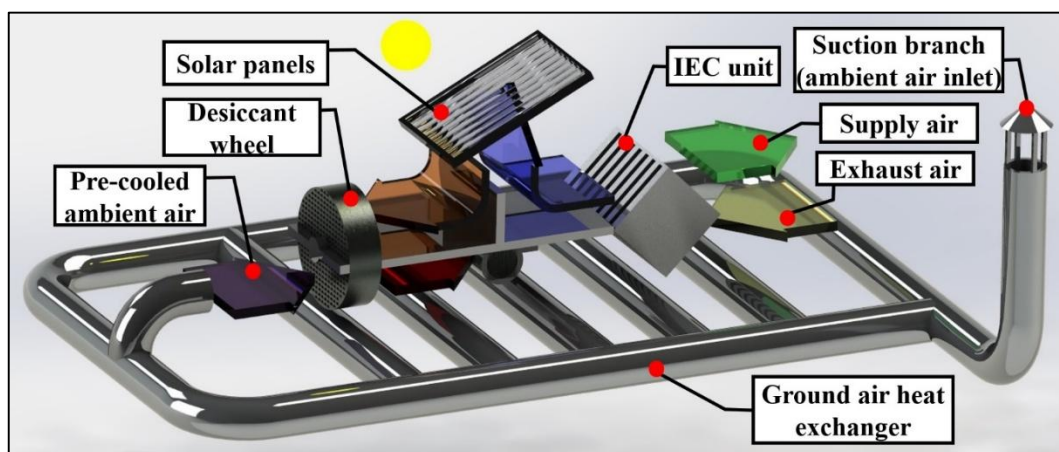


Fig. 1.11. SDEC system with IEC and air ground heat exchanger [34].

### 1.5.3. System with nocturnal cooling

Another interesting idea at first presented by Heidarinejad et al. [37], [38] is the nocturnal cooling system. In such solution the water is kept in a storage tank and it is cooled at night in the radiator heat exchangers located outside the building (Fig. 1.12.). During the next day, the cold water in the storage tank is delivered to the cooling coil as chilled water to decrease temperature of the outdoor air before it enters the evaporative air cooler. Then, the pre-cooled air passes through a evaporative air cooling system. Systems consisting only IEC cooling units or a two-stage combination of indirect-direct coolers are considered. Owing to the pre-cooling

effect the system allows achieving much lower outlet air temperatures. The main disadvantages of the system are similar to disadvantages of the SDEC system: costs, complexity, complicated control system, sensitivity to the damages and large size.

### 1.5.4. System with water ground heat exchanger

A system with water ground heat exchanger (Fig. 1.12.) works similarly to the nocturnal cooling solution, but in this case, instead of the nocturnal radiators, the system is equipped with a ground heat exchanger which cools the water before it enters a cooling coil to pre-cool the airflow for the evaporative air coolers [39]. This system also may use a single indirect evaporative air cooling unit or a combination of IEC and DEC exchangers.
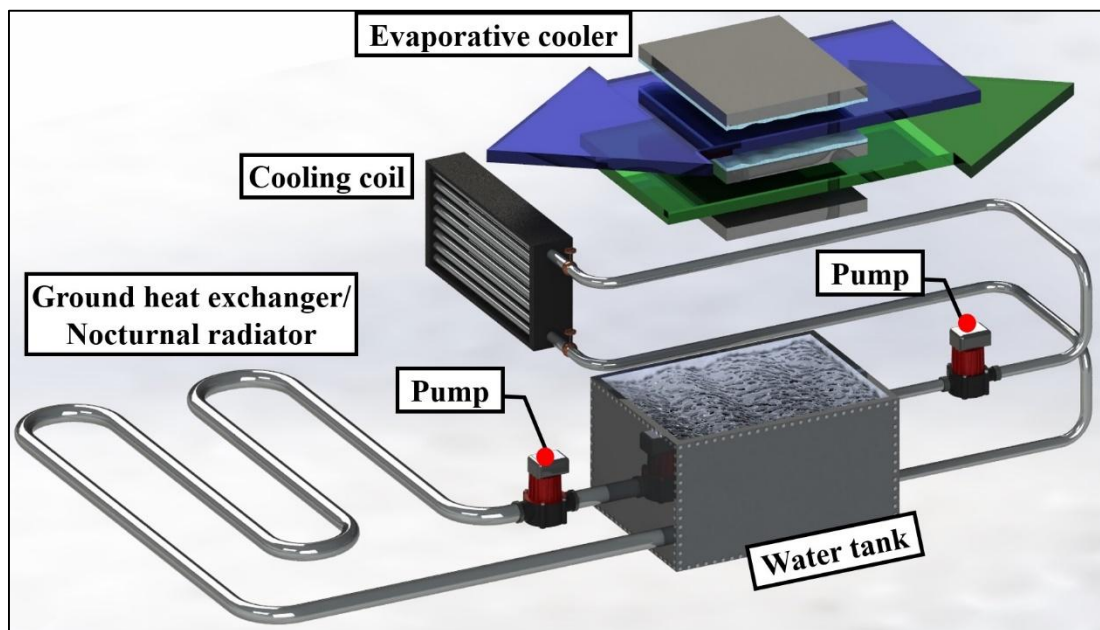


Fig. 1.12. System with nocturnal cooling or a water ground heat exchanger.

### 1.5.5. Maisotsenko cycle (M-Cycle)

The main problem with the typical indirect evaporative air cooling units is their low thermal efficiency. It is the main reason why the scientist around the world develop novel complex systems in order to obtain the low temperatures with IEC units. However, there is another way to obtain high efficiency of the indirect evaporative air cooling without using complicated systems and mechanical compression. This technique is based on the novel thermodynamic cycle, known as the Maisotsenko cycle or the M-Cycle, which is viewed as a technological breakthrough in renewable energy cooling cycles [15], [40], [41]. This cycle was named after its inventor, Prof. Valeriy Maisotsenko [15], [42].

The M-Cycle uses the same wet side and dry side of a plate as the conventional indirect evaporative cooler but with a much different airflow configuration which creates the new thermodynamic cycle [12], [15]. The Maisotsenko cycle combines with the thermodynamic processes of heat exchange in an indirect evaporative air cooler, based on the idea that the

working airflow is indirectly pre-cooled before it enters the wet channels (Fig. 1.13.). This results in much lower primary air temperatures which approach nearly the dew point temperature of the air incoming air (this cycle is sometimes called dew point evaporative cooling [2], [11], [43]). The simplest exchanger with the Maisotsenko cycle is the regenerative counter-flow unit (Fig. 1.13.). In this exchanger the primary and the working air streams are passing through the same dry channel (mixed primary and working air in the dry channels will be referred as the main flow) and are cooled without humidification (process $1_i-1_o=2_i$ in Fig. 1.13.). At the end of the dry channel part of the main flow (working air) is delivered to the wet channel, where it realizes the indirect evaporative cooling process (process $2_i-2_o$ in Fig. 1.13.). It is noteworthy that water is not evaporated into the product air stream. When exhausted, the working air stream is saturated and has a temperature less than the incoming air, but greater than the wet bulb temperature (Fig. 1.13.).

The best way to explain the general conception of the Maisotsenko cycle is to follow the steps of its inventor (Fig. 1.14). In the typical evaporative air cooler (Fig. 1.14.(a)) the primary and the working airflow are delivered to the exchanger separately. Prof. Maisotsenko tried to analyze what would happen if the primary airflow would be returned to the wet channel after passing the dry passage (Fig. 1.14.(b)). In such case, the incoming air ($1_i$) is passed over the dry side of the plates and then turned to the wet side ($1_o=2_i$). After it passes the wet channels it is exhausted out as air $2_o$. As the air passes over the dry side of the plate, it is cooled sensibly. The airstream in the dry channels is cooled by the same airstream in the wet channels. At the point where the air turns from the dry channel to the wet channel ($1_o=2_i$, Fig. 1.14.(b)) it reaches its dew point temperature of the incoming air ($1_i$).
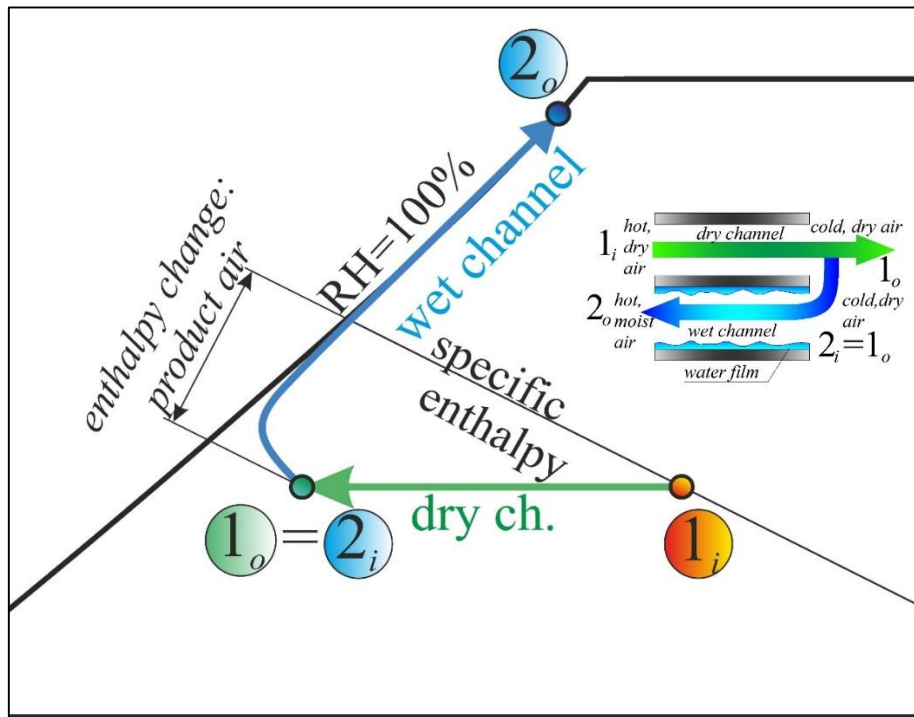


Fig. 1.13. The psychrometric interpretation of the Maisotsenko cycle in a regenerative HMX.

These theoretical results have been achieved on a regular basis in several prototype models, confirming that the temperature of the airstream, after passing along the dry side of the plate, approaches the dew point temperature [15]. In this process, however, the cooling capacity is equal to zero because the whole air stream is returned to the wet channel (no air is delivered to the occupants). At the end of the wet channel, the working air stream reaches the same enthalpy as the incoming air ($i_{2o} = i_{1i}$), the total process is then adiabatic (this exchanger would be later referred as the adiabatic counter-flow exchanger).

The key idea of the M-Cycle was to take advantage of the low temperature of the air at the end of dry channels in the adiabatic counter-flow exchanger. This was accomplished by dividing the main air stream at the end of the exchanger into the primary airflow (1), which was delivered to the occupants and the working airflow (2) which was returned to the wet channels (Fig. 1.14.(c)). This resulted in the simplest form of the M-Cycle: the regenerative heat and mass exchanger. This unit allowed obtaining low air temperatures, but it was characterized by the low cooling capacity, due to the fact that the air stream delivered to the exchanger was divided into the two air streams [19], [44], [45].

The final, "ideal" form of the M-Cycle is presented in Figure 1.14. (d). This form would later be referred as the modified counter-flow heat and mass exchanger. This exchanger was the ideological background behind the M-Cycle units which were later applied in the air conditioning systems. This exchanger uses three channels: one dry channel for the primary airflow (1) and one dry and one wet channel for the working airflow (2 and 3). Later in the text, the working air in the wet channels would always be referred by number 2, while the working air pre-cooled in the dry channels, which is not mixed with the primary airflow (like in the HMX visible in Fig. 11.5. (d)) would always be referred by number 3. This unit uses a separate channels for pre-cooling of the working airflow 3, which allows obtaining very low temperatures. It also allows avoiding the negative aspect of the lower cooling capacity in the regenerative unit, because the air is separated before it enters the exchanger. The modified counter-flow exchanger also uses perforation to distribute the working airflow evenly. The main disadvantage of this unit is that it uses three channels, which is an odd number, therefore it is not possible to create the repeatable channel structure with such arrangement.
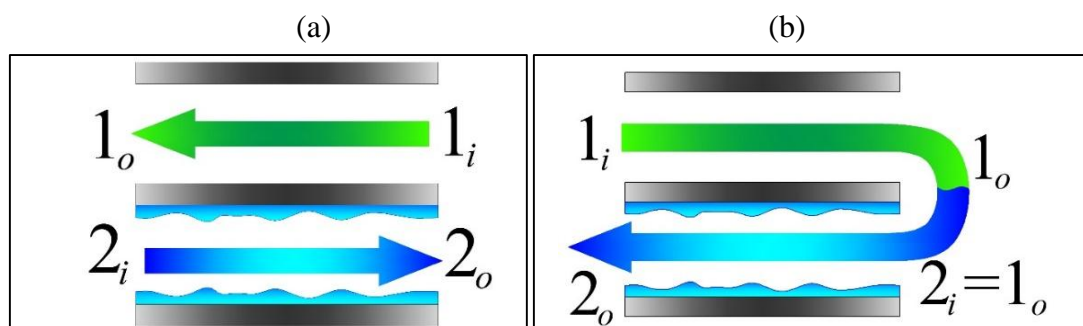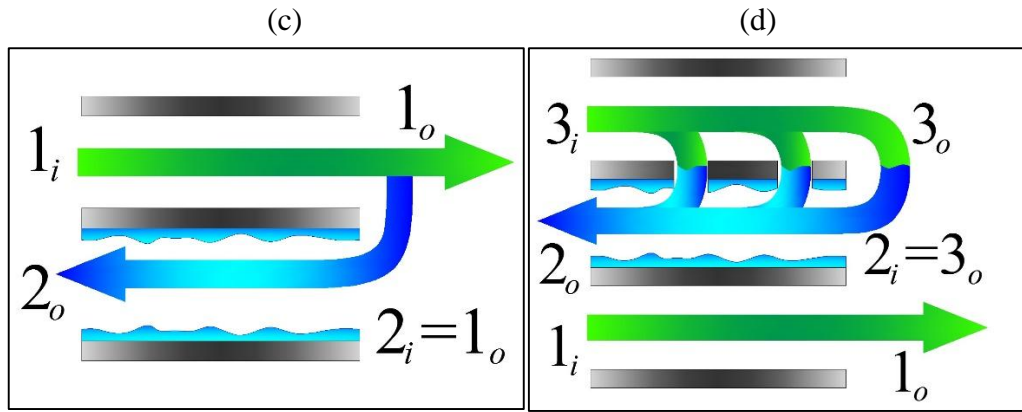
(a)                                          (b)

Fig. 1.14. Maisotsenko cycle development process. (a) Standard indirect evaporative air cooler. (b) Adiabatic counter-flow evaporative air cooler. (c) Regenerative M-Cycle evaporative air cooler. (d) Modified counter-flow evaporative air cooler with the M-Cycle.

Although the advantages of counter-flow arrangement are well known, pure counter flow in the plate heat exchanger is very difficult to realize due to the geometry of the channels (plates) with air entering and leaving on the same sides. In this regard, the M-Cycle has now been embodied in a cross-flow perforated heat exchanger (Fig. 1.15.). This unit is based on multiple branching of the working air 3 from the dry passages to the wet passage through the perforations in the plates over the length of the channel from their dry sides to the wet sides [15], [46]. This configuration has been further developed in the USA by Idalex Inc. and Coolerado Corporation, wherein the wet and dry ducts are divided into two separate sections which allows for pre-cooling of the dry air streams prior to their entry into the wet duct thereby resulting in an enhanced cooling efficiency (the structure of the applied cross-flow M-Cycle unit is visible in Fig. 1.15.(b)). The experimental results [2], [15], [40] confirmed that this air cooler allows obtaining significantly higher effectiveness than the typical indirect evaporative air coolers. The main challenge for this unit is to optimize its arrangement to achieve the highest efficiency using the less effective airflow arrangement (cross-flow instead of the counter-flow).
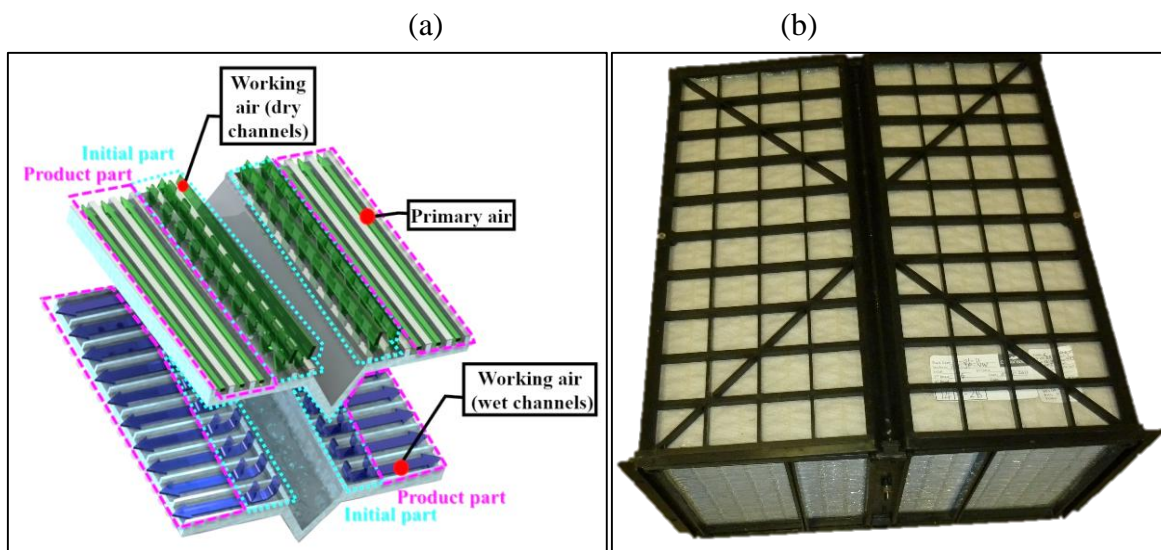


Fig. 1.15. Cross-flow Maisotsenko cycle HMX. (a) Scheme of the unit. (b) Actual air cooler manufactured by Coolerado Corp. (author's photograph).

## 1.6. Factors characterizing the performance of evaporative air coolers

The main factors which are usually used for the description of evaporative air coolers performance are described below:

- Temperature level of outlet primary airflow $\overline{t_{1o}}$: the basic factor describing to what level evaporative air coolers is able to cool the outdoor airflow.

- The wet bulb thermal effectiveness, defined as the ratio of the difference between intake and outlet primary air temperature to the difference between inlet primary air temperature and its wet bulb temperature [47]:

$$\varepsilon_{WB} = \frac{t_{1i} - \overline{t_{1o}}}{t_{1i} - t_{1i}^{WB}}$$

(1.1)

- The dew point thermal effectiveness, defined as the ratio of the difference between intake and outlet primary air temperature to the difference between inlet primary air temperature and its dew point temperature [47]:

$$\varepsilon_{DP} = \frac{t_{1i} - \overline{t_{1o}}}{t_{1i} - t_{1i}^{DP}}$$

(1.2)

- the obtained cooling capacity $Q_1$ referenced to the primary airflow temperature drop:

$$Q_1 = G_1 \cdot c_{p1} \cdot \left( t_{1i} - \overline{t_{1o}} \right)$$

(1.3)

Sometimes the cooling capacity is not a good factor for comparison of the evaporative air coolers, for example when they have different sizes. For more effective comparison it is better to use the cooling capacity respected to the volume of HMX structure, which allows telling how much cooling power can be provided with a unitary structure of the exchanger (this allows for comparison of the unit with different sizes [48]).

- the specific cooling capacity respected to the cubic meter of the unit's structure

$$\hat{Q} = Q_1 / V_{\text{HMX}}$$

(1.4)

where:

  o  $Q_1 = G_1 \cdot c_{p1} \cdot \left( t_{1i} - \overline{t_{1o}} \right)$ is the cooling capacity,

  o  $V_{\text{HMX}}$ is the volume of the exchanger structure ($V_{\text{HMX}} = 2(h + \delta_{plt}) l_X \, l_Y$).

The other effective method to calculate the relative cooling capacity is to respect it to the cooled air stream [12].

- the specific cooling capacity respected to the air mass flow rate

$$\hat{Q}_G = Q_1 / G_1 \tag{1.5}$$

Another factor which can be used for the effective comparison of the evaporative air coolers is the coefficient of performance (COP)

- the energy efficiency factor COP is calculated as the ratio of obtained cooling capacity to the electrical energy required for a fan to operate. There are two possibilities of calculating the theoretical energy efficiency [49]: respected to the primary airflow (COP$_1$) and respected to the primary and the working airflow (COP$_{1+2}$). The COP factors are calculated from the equations:

$$COP_1 = Q_1 / N_1 \tag{1.6}$$
$$COP_{1+2} = Q_1 / N_{1+2} \tag{1.7}$$

where:
- $N_1$ is the required fan power respected to the primary airflow: $N = \Delta p_{product} V_{product}$
- $N_{1+2}$ is the required fan power respected to the primary and the working airflow: $N = \Delta p_{work} V_{work} + \Delta p_{product} V_{product}$

Two different methods of calculating the COP are used because of the different aspects of operation of the evaporative exchangers in the context of whole air-conditioning system. The air from the working part is usually discharged to the atmosphere after passing the wet channels, whereas the product air passes the whole ventilation system (ducts, dampers, diffusers etc.). Therefore, the pressure drop along the primary air part is more important in the context of the total efficiency of the air conditioning system. The pressure drops are calculated on the basis of airflow friction loses along the channels [43], [50], [51]. The fluid friction coefficient for laminar flow in rectangular channels is obtained from the equation (1.8).

$$f = 96 / Re \tag{1.8}$$

Sometimes the evaporative air cooling units are also analyzed by their water consumption. However, the IEC units are characterized by a rather small water usage [43], [50], [51]. This fact connected with the negligible water price compared to the costs of electricity results in the fact that this factor is used very rarely [7], [43], [50], [51]..

- The water consumption is calculated by taking the moisture rise from inlet to outlet of working air and multiplying it by the secondary air mass flow rate.

$$WC = G_2 \cdot \left( \overline{x}_{2o} - x_{2i} \right) \tag{1.9}$$

### 1.7. Review of the main scientific achievements in increasing the efficiency of evaporative air coolers

Indirect evaporative air cooling is becoming very popular, especially in recent years. Between 2012 and 2015 there were almost 6000 papers connected with evaporative air cooling published in JCR indexed journals according to Scopus™. Below there is a short review over the main, selected achievements in improving the efficiency of evaporative air coolers.

One of the first concepts of achieving higher efficiency with indirect evaporative air cooling was presented in 1935, when Ray [52] published his patent of the air conditioning system where the ambient air was cooled below its inlet wet bulb temperature without mechanical refrigeration. This was achieved by combination of direct and indirect evaporative cooling (Fig. 1.16).

In 1976, in the former USSR, Prof. Valeriy Maisotsenko developed his first ideas of the M-Cycle utilized in the regenerative and counter-flow exchangers (Fig. 1.17). He patented his first devices (patents SU No 571669 and 979796 [42]), but during the Cold War it was very hard to get the attention of the scientist around the world. The final development of the M-Cycle unit had to wait to the XXIst century.
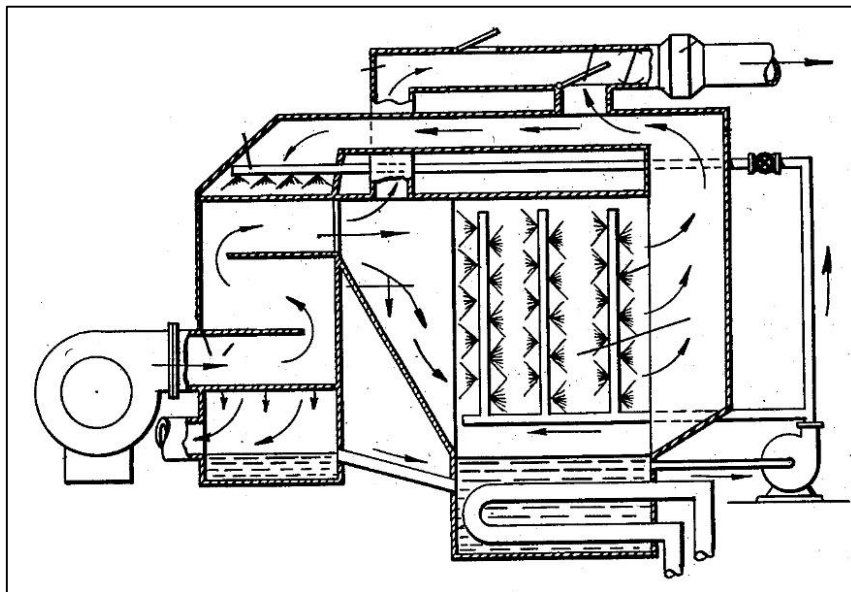


Fig. 1.16. The combined evaporative air cooler patented by Ray [52] in 1935.

The next noticeable idea comes from 1979, when Pescod [53] indicated by splitting a portion of the air produced by an indirect evaporative cooler and using it in the wet passage, the target wet bulb temperature of the cooling process will be lowered.

In 1981 Maclaine-Cross and Banks [54] referred to that idea in concept of the regenerative cross-flow evaporative air cooling. Assuming a linear slope for the saturation temperature-enthalpy relation of air, they suggested a simplified model, which was one of the first numerical

models describing the evaporative air cooling, which could be used to predict the cooler performance by analogy to dry surface heat exchangers. Their results showed that the target wet bulb temperature of the cooling process can be lowered in regenerative evaporative air cooler. The results predicted by the model were 20% higher than the experimental data.

In 1987 Crum et al. [28] indicated that wet bulb temperature of the ambient air can be achieved with multistage indirect evaporative air cooling process and with the combination of cooling towers and HMXs. Their study showed that the cooling tower-heat exchanger combination has the highest thermal potential for air-conditioning purposes.

In 1989 Hsu et al. [55] presented one of the first detail numerical models of basic indirect evaporative air cooling cycles. They investigated theoretically and experimentally three types of indirect evaporative coolers with different airflow arrangement: counter-flow, cross-flow and regenerative configuration. The proposed mathematical model was developed under the assumption that the water film is locally replenished and its local temperature may be calculated from the algebraic equation of overall energy balance. They concluded that the examined methods of evaporative cooling are capable to reach sub-wet bulb effectiveness about 1.30 at NTU ranging from 10 to 15.
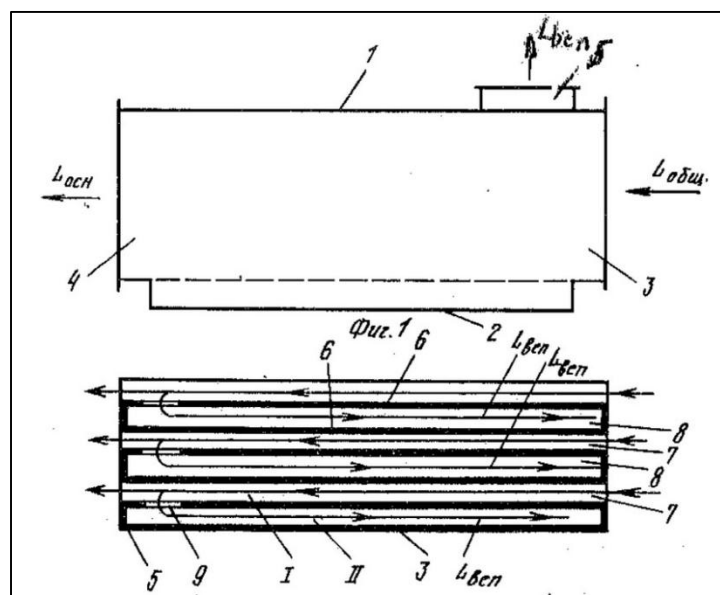


Fig. 1.17. The regenerative M-Cycle air cooler patented by Maisotsenko [42] in 1976.

In 1993 Erens and Dreyer [56] presented a comparison of three analytical methods available in literature. They established a method appropriate for use in accurate prediction which gave the assumption that the secondary air is supersaturated with water vapor. They also developed a more simplified method suitable for smaller sized systems and development of initial design scheme; this method had larger discrepancy with the experimental results.

In 1994 Navon and Arkin [57] studied the economic value and thermal comfort level of a system with combined direct and indirect evaporative cooling compared with a conventional air

conditioner. A life cycle cost calculation method was exploited to compare the annual equivalent cost in two cities of Israel with extreme summer conditions. The results show that the economic potential of the system based on evaporative air cooling is very promising considering the significant reduction of electricity cost in compare to the mechanical compression systems.

In 1997 El-Dessouky et al. [58] presented a theoretical investigation of the steady-state counter flow wet cooling tower. They developed a new expression relating the tower effectiveness to the modified number of transfer units and the capacity rate. The model considered the resistance to heat transfer in the water film, the nonunity of the Lewis number, and the curvature of the saturated air enthalpy curve. The substantial errors varied from $-2.5\ldots +4.3\%$ in calculating the cooled water outlet temperature, and errors from $-16.7\ldots\ +42.9\%$ in estimating the tower thermal characteristics. In the same year Tulsidasani et al. [59] analyzed the performance of a non-air-conditioned building, which was equipped with an IEC system. The analysis was performed for three different India's climatic conditions (dry/hot, humid/hot, humid/warm). They also studied impact of various parameters on thermal comfort of the building space. The results showed that the presented system was able to improve the thermal comfort inside the buildings in dry and hot climate conditions.

Year 1998 brought significant progress in mathematical modeling of indirect evaporative air cooling processes. Stoitchkov and Dimitrov [60] improved the cross-flow heat exchanger model developed by Maclaine-Cross and Banks. The improved model predicted exchanger performance with better approximation. This was accomplished by including the flowing water film, determination of mean water surface temperature and derivation of an equation for calculating the ratio of total to sensible heat taking into account the barometric pressure. Presented model was validated against existing experimental data. The discrepancies between the test results and model were at most 3.84%. Alonso et al. [61] developed a simplified mathematical model for calculating the outlet primary air temperature in the cross-flow heat and mass exchanger based on a model developed by Pescod [53]. In this study, an equivalent water temperature was introduced for the energy transfer, which assumed the whole process to an adiabatic saturation process. The model was verified and validated with other experimental data and Pescod and Erens 's models [53], [56]. The model was characterized by a good agreement with the experimental data. Guo and Zhao [62] investigated the impact of various parameters on the performance of a cross-flow HMX. The parameters included primary and working air velocities, channel width, inlet relative humidity and wettability of plate. A numerical method was used to solve differential equations. In this paper the numerical model was not validated against the experimental data or other models. The results indicated that a smaller channel width, a lower inlet relative humidity of the secondary air, a higher wettability of plate, and a higher ratio of secondary to primary air can result in increased thermal effectiveness.

In year 2000, Joudi and Mehdi [63] analyzed an indirect/ direct evaporative cooling system in a typical Iraq household. A two story house located in Baghdad was the object of the study.

Four different operational modes were analyzed and put into alternative use under changing cooling load conditions. The concept of variable air volume (VAV) was employed as a control strategy over the day by changing the supply airflow rate through a variable speed fan according to the variation in the cooling load. The results showed that indirect evaporative cooling would result in a comfortable indoor condition for most periods of system operation. A dedicated analyses and comparison among these operations suggested that the system would obtain a higher effectiveness when operating with the relatively cold indoor return air, instead of the warm outdoor fresh air.

In 2002 Prof. Valeriy Maisotsenko received his American Patents [64] of the M-Cycle heat and mass exchangers (Fig. 1.18): U.S. Patent No. 6,497,107 *Method and Apparatus of Indirect-Evaporation Cooling*; U.S. Patent No. 6,581,402 *Method and Plate Apparatus for Dew Point Evaporative Cooler*; U.S. Patent No. 6,705,096 *Method and Plate Apparatus for Dew Point Evaporative Cooler Using a Trough Wetting System*. This was the beginning of the commercial development of the Maisotsenko cycle in the United States and later in other parts of the world.

In 2003 Song and Lee [65] presented a theoretical analysis of the finned evaporative heat exchanger with a two-dimensional heat and mass transfer model. The model assumed that the Lewis number is unity and the water vapor saturation curve is linear. Based on the model, the characteristics of the heat and mass transfer were investigated in a plate-fin heat exchanger with the interstitial surface fully covered by thin water film. The cooling effect with application of evaporative cooling was found to be improved considerably compared with the sensible cooler, due to the thermal conductance between the fin and the air and due to the latent heat transfer caused by the water evaporation from the fin surface. It was also found that the cooling efficiency depends greatly on the fin thickness. If the fin was not sufficiently thick, the cooling enhancement by the evaporative cooling decreased.
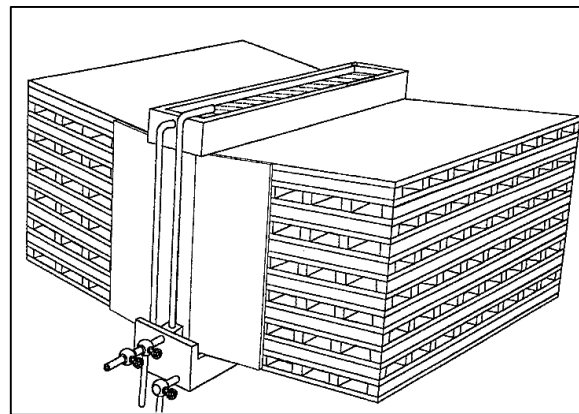


Fig. 1.18. One of the first versions of the cross-flow M-Cycle air cooler patented by Maisotsenko in 2002.

The year 2004 brought important results on more complicated evaporative air systems. El-Dessouky et al. [66] presented a combined IEC/DEC unit installed on a building in Kuwait, Iraq. The ambient air dry bulb temperature in summer reaches over 45°C. The test results indicated that the cooling effectiveness of the IEC/DEC system was in the range 0.9–1.05, but

the indirect evaporative air cooler contributed only 20–40% of the cooling effect. The thickness of the wet packing and water flow rate across the direct evaporative air cooler were found to have most significant impact on the system performance. These results showed good agreement with the literature data. Lebrun et al. [67] presented a simplified method describing the combined heat and mass transfer processes in direct and indirect contact cooling towers and evaporative condensers. The theoretical basis of the model was Merkel's theory. The results showed that a unified theoretical treatment may be applied to all evaporative exchangers analyzed. The key difference in the theory for each unit relates to the unique characteristics, the global heat transfer coefficients, or the corresponding thermal resistances of the fluids. An example for each case was shown, along with the validation of the models against catalogue data. Martinez et al. [68] analyzed two different types of evaporative systems. A returning air recovery system was used. The first system (with indirect evaporative cooler) worked like a flat interchanger made of aluminum, resulting in only sensible heat transfer from the primary airflow. The second system (with semi-indirect evaporative cooler) was made of solid porous ceramic pipes which separated the two airstreams, thus allowing for sensible and latent heat exchange with the primary airflow. The authors took care to make the system free of legionella, due to the pipes construction, which performed as a filter material, making it impossible for the bacterium to enter premises.

In 2005 Kloppers and Kröger [69] studied the effect of the Lewis factor, or Lewis relation, on the performance prediction of natural draft and mechanical draft wet-cooling towers. The history and development of the Lewis factor and its application in wet-cooling tower were discussed, a relation of the Lewis factor to the Lewis number was also investigated along with the influence of the Lewis factor on the prediction of the cooling tower performance. It was established that the amount of water that evaporates is a function of the actual value of the Lewis factor. If the inlet air temperature is relatively high, the influence of the Lewis factor on tower performance decreases.



Fig. 1.19. Different versions of the cross-flow M-Cycle HMXs which were tested over the years (author's photograph).

In 2006 Elberling [40] performed the first detail experimental testing of the cross-flow M-Cycle HMX, using an early-2005 model Coolerado Cooler. The goal was to assess the performance of the Coolerado Cooler for consideration in Pacific Gas and Electric Company's rebate program for evaporative coolers. A test plan was developed based on ASHRAE test standards for evaporative coolers. It was confirmed that the advantage of an indirect evaporative cooler is that it accomplishes low-cost evaporative cooling without adding any moisture to the air supplied to the conditioned space. However, the M-Cycle air cooler was characterized by a higher flow relative to typical direct evaporative coolers. The test confirmed that the unit would keep a space within the ASHRAE comfort zone over a wider range of outdoor conditions than other direct and indirect evaporative air coolers. A testing report indicated that the early version of the M-Cycle exchanger could obtain a wet bulb effectiveness of 81% to 91% with an average of 86% . In the same year M.N. Golubovic et al. [70] presented the new method of calculating the Lewis relation. This method was used to evaluate Lewis relation in the case of the flow of free air stream over a flat planar test specimen. The flat planar materials used to demonstrate the method in this work was made out of two different materials, bleached paper and bleached paper/Na-silicate. Also in 2006 Chengqin and Hongxing [71] developed an analytical model describing the heat and mass transfer in indirect evaporative cooling with parallel/counter-flow configurations. The model was based on conversion of the one-dimensional differential equations with assumption of humidity ratio of air in equilibrium with water surface to be a linear function of the surface temperature to the analytical solution. The results of the analytical solutions were found to be in good agreement with results of numerical integrations.

In 2007 Hettiarachchi et al. [72] studied the effect of the longitudinal heat conduction in the exchanger wall of a compact-plate cross flow indirect evaporative cooler. A ε-NTU method was used to analyze the heat and mass transfer processes. The equations were integrated with a block iterative numerical method. The model was validated against existing experimental data. The results indicate that the thermal performance deterioration of the evaporative coolers may become significant for some typical operating conditions and could be as high as 10%, while it lies less than 5% for most conservative conditions. In the same year Qiu [73] presented his PhD thesis over the small scale indirect evaporative air cooler prototype. The testing results showed that the real performance of the IEC unit was much lower than the values given by the catalogues. The key reason for reduced performance was the poor water distribution of the unit. He proposed a modification of the exchanger by installing a top water spraying device a integrated with a solar-powered PV panel which provided electrical energy for fans and pump. The modified unit was tested and the results showed that the cooling capacity and COP of the new unit were 3 times higher than that of the old device.

The year 2008 brought important progress in analysis of the Maisotsenko cycle. Gillan [15] presented the study of applied M-Cycle unit for Coolerado Corporation for a commercial purposes. He presented the theoretical basis of the M-Cycle, along with the cross-flow unit's development history. He also showed the values of outlet product air temperatures achieved by the device for different inlet air conditions. Zhao et al. [50] analyzed a regenerative M-Cycle heat and mass exchanger with numerical methods. According to their results, the optimal

average air velocities in the dry and wet channels should be in the range of 0.3 to 0.5 m/s, the recommended channel height is 6 mm or below and the working-to-intake air ratio should be around 0.4. Zhao et al. [23] also analyzed several types of evaporative media potentially used in forming the heat/mass evaporative exchangers. The materials included metals, fibres, ceramics, zeolite and carbon, in terms of their physical and thermal properties. By analyzing the heat and mass transfer principles, the study showed that the thermal conductivity and porosity of materials is less important in process of electing materials. The most important factors according to the paper are shape formation/holding ability, durability, compatibility with water-proof coating, contamination risk and cost of materials. It was found that the wick metals such as cooper and aluminum are the most suitable materials for the heat exchanger. In the same year Alizadeh [74]  analyzed the solar liquid desiccant air conditioner in the tropical climate of Queensland, Australia. The system used a polymer plate heat exchanger for dehumidification and indirect evaporative cooling, and a cooling pad as the direct evaporative cooler for the dry air leaving the plate heat exchanger. Lithium chloride desiccant was used as a desiccant in the experiments. The data obtained from performance monitoring of the solar system operating on a commercial site was compared with a previously developed model for the polymer exchanger. The comparison showed the good agreement between the experiments and model predictions- the inaccuracies were within the measuring errors. The tests indicated a satisfactory performance of the unit by independently controlling the air temperature and humidity inside the conditioned space. The study suggested that liquid desiccant system can be used in the HVAC industry, either as a packaged roof-top air conditioner, or as an air handler unit for commercial applications. The system could also be used for space heating in winter due to the property of desiccants to provide heat when wetted.

In 2009 Zhao et al. [75] investigated the feasibility of a novel evaporative cooling system for air conditioning in China. The paper included analyses of China weather conditions, investigation of availability of water for evaporative cooling, and assessment of cooling capacity of the system within various regions of China. It was concluded that the novel system is suitable for most regions of China, especially northern and west regions where the climate is hot and dry during the summer season, but it is less suitable for Guangzhou and Shanghai where climates are more humid. To overcome the humid climate they suggested a pre-treatment dehumidification process with silica-gel. The cooling output of the system was from 1.1 to 4.3 W per $m^3$/h air flow rate, depending on the region where the system was applied. In the same year Heidarinejad et al. [37] studied the cooling performance of two-stage indirect/direct evaporative cooling system with experimental methods. The study was performed on a two-stage evaporative cooling experimental setup consisting of an indirect evaporative cooling stage followed by a direct evaporative cooling stage. Two air simulators were provided to simulate outdoor design condition of different cities of Iran. Results showed that under various outdoor conditions, the effectiveness of IEC stage varied over a range of 0.55–0.61 and the effectiveness of IEC/DEC unit varied over a range of 1.08–1.11. Aspects of achieving comfort conditions and power saving were also investigated. The presented system was able to provide comfort conditions in the regions in Iran where direct evaporative cooling alone were not able to provide

them during summer time. The year 2009 brought also another important analysis of the Maisotsenko cycle: Kozubal and Slayzak [76] tested a Coolerado hybrid system (unit H80- Fig. 1.20), which combined an indirect evaporative cooler with the classical mechanical compression cooling coil. The performance of the hybrid system were investigated experimentally in a laboratory. The system operates as follows: The outdoor air mixes with the return air before entering into the indirect evaporative section. About 50% of the entering mixed air is cooled by the evaporative section and then passes through an evaporator coil to be delivered to the occupants by a fan. Other part of the entering air- the working air, is cooled and humidified in the indirect evaporative module and then passes through the condenser coil. The working air gains some heat from the fluid in condenser and exhausts to outside. The results of test showed that the total cooling capacity of the unit was 16.8 kW with a total COP of 15.2 at the outdoor air condition of 32.2°C dry-bulb and 17.7°C wet bulb temperature.
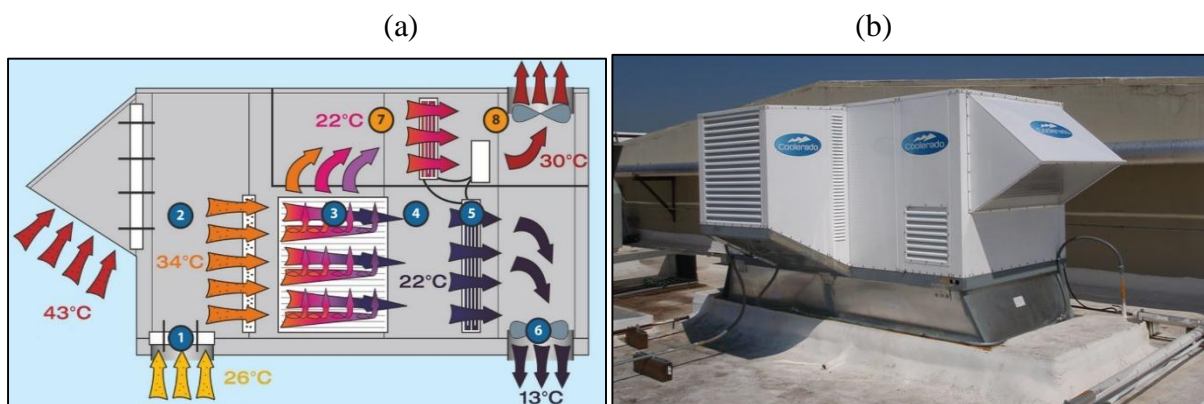
(a) (b)



Fig. 1.20. The Coolerado's hybrid H80 unit based on the M-Cycle HMX and a mechanical compression system [76]. (a) Operation scheme. (b) The actual unit.

The second decade of the XXIst century brought many important achievements in developing and analyzing the most effective indirect evaporative air cooling systems.

In 2010 Heidarinejad et al. [38] presented a hybrid system of nocturnal radiative cooling, cooling coil, and direct evaporative cooling in Tehran. The results obtained demonstrate that overall effectiveness of hybrid system is more than 100%. They suggested that presented system can be considered as an alternative to the mechanical vapor compression systems Farmahini-Farahani and Heidarinejad [77] also presented a novel system which was a combination of nocturnal radiative cooling and two-stage evaporative cooling. The effectiveness of the system was investigated for four different cities having different climatic conditions. The results obtained indicated that the proposed system can become a new alternative for typical cooling systems in some hot regions. In the same year Riangvilaikul and Kumar [9], [10] presented a numerical and experimental study of the M-Cycle regenerative dew point indirect evaporative cooler (Fig. 1.21). The study developed a numerical model to simulate the heat and mass transfer process. The governing equations were solved by employing finite differential approach and Newton iterative method. The modelling results were validated against their experimental data under various inlet air conditions (typically covering dry, moderate and humid climates) and for different intake air velocities (1.5–6 m/s). Reasonable

agreement was achieved between the numerical and experimental results, giving 5–10% of deviation in terms of the outlet air temperature and effectiveness, respectively. The study showed that the predicted dew point effectiveness varied significantly from 0.65 to 0.86 when the inlet air humidity changed from 6.9 g/kg to 26.4 g/kg at the constant inlet temperature of 35°C. They suggested that the intake air velocity should be set below 2.5 m/s, the channel spacing gap should be less than 5 mm, the channel length should be larger than 1 m and the ratio of the working to intake air should be set between 0.35 and 0.6.
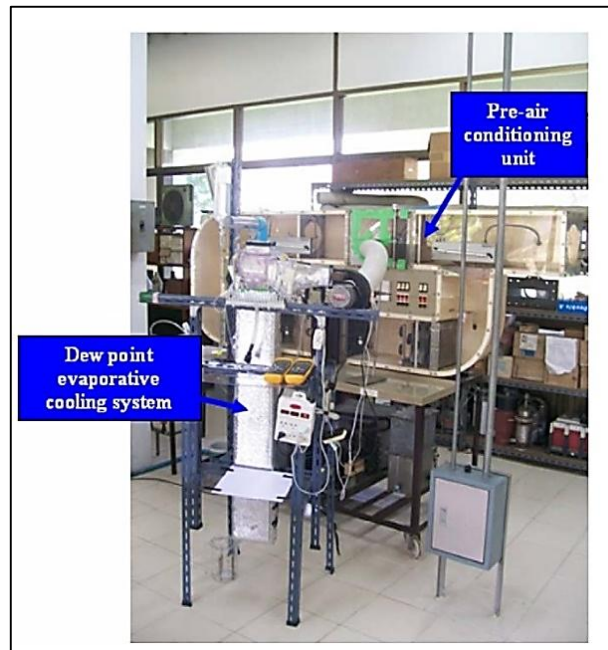


Fig. 1.21. Testing bench used by Riangvilaikul and Kumar [9].

On the base of one-dimensional model Hasan [11] numerically analyzed four types of indirect evaporative cooler configurations to achieve sub-wet bulb temperature: three two-stage coolers (counter-flow, parallel flow and combined parallel-regenerative flow) and single-stage counter flow regenerative cooler. The main idea of these exchangers is manipulating the airflow arrangement by branching the working air from the part of process airflow, which is indirectly pre-cooled before it enters the wet passages. He concluded that the highest wet bulb effectiveness of up to 1.31 may be achieved in the case of the combined parallel-regenerative type, proposed by Anisimov et al. [78]. Also in 2010, Jiang and Xie [25] developed a novel indirect evaporative chiller which was able produce The chiller comprised of two parts: the air-to-water counter-flow heat exchanger and the air-to-water counter-flow padding tower. The first prototype chiller was constructed and installed in Xingjiang Province of China, in which a relatively lower ambient wet bulb and dew point temperature is in presence. The long-term testing indicated that the unit can produce the water with temperature varying in range from 14 to 21°C with the COP around 9.
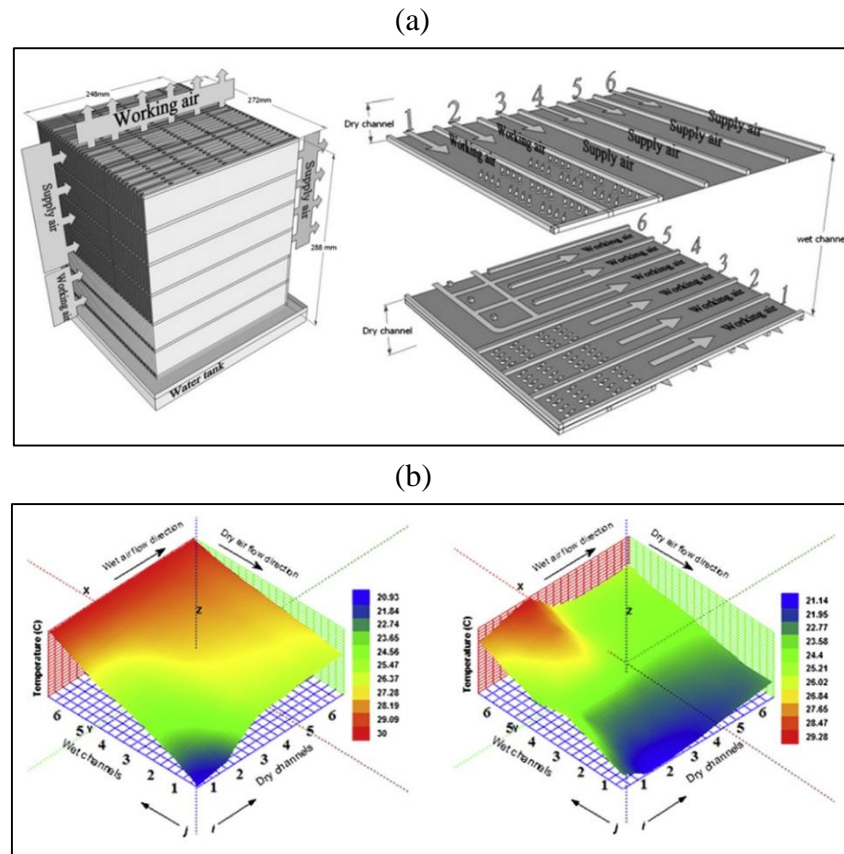
(a)



(b)



Fig. 1.22. ISAW TAC-150 cross-flow M-Cycle HMX investigated by Zhao et al. [43]. (a) Unit's scheme. (b) Temperature distribution: primary and the working air strams.

The year 2011 brought another important studies connected with M-Cycle. Zhan et al. [43] presented the first numerical study of the cross-flow Maisotsenko cycle heat and mass exchanger used in a small scale Chinese air conditioner ISAW TAC-150.The numerical model was established and solved using the finite-element method. The model was developed using the Engineering Equation Solver environment and validated by existing experimental data. Correlation between the cooling effectiveness, COP and selected parameters was presented. It was established that lower channel air velocity, lower inlet air relative humidity, and higher working-to-product air ratio yielded higher cooling effectiveness. They recommended average air velocities in dry and wet channels to be lower than 1.77 m/s and 0.7 m/s, respectively. The optimal working to primary air ratio according to the paper is 0.5, while the recommend channel height is 4 mm. The M-Cycle air cooler was compared with the typical cross-flow air cooler and achieved a 16.7% higher cooling effectiveness. The interesting trend was visible in the temperature distribution achieved with the model in the wet channels (Fig. 1.22) there were no trend in increasing temperature of the working air, which was reported to be typical for the M-Cycle air coolers. For example, such trend was observed in experimental study presented at the same year by Zube and Gillan [46].

In an attempt to better understand the fundamental physics occurring inside the cross-flow Maisotsenko cycle HMX, Zube and Gillan [46] studied the exchanger with experimental methods. Their experiment included measuring the parameters inside the exchanger using

thermocouple. This was done by dividing each set of channels into a two-dimensional grid and collecting measurements at each node location. Each of parameters was averaged based on the grid resolution and presented according to their location within the heat mass exchanger.

Using the models established in their previous studies [50] and [43], Zhan et al. [51] presented a comparative study of the performance of cross-flow and regenerative M-Cycle heat exchangers for dew point cooling. The results showed the regenerative exchanger offered greater (around 20% higher) cooling capacity, as well as greater (15% to 23% higher) dew point and wet bulb effectiveness when equal in physical size and under the same operating conditions. The cross-flow system, however, had a 10% higher Energy Efficiency (COP). Also in 2011 Duan [7] presented her PhD thesis describing the novel regenerative M-Cycle HMX. Duan's research analyzed the feasibility of using a new dew point cooling system in China and European countries, taking into account of local weather conditions, availability of water source and water consumption. It was concluded that the M-Cycle based dew point system is suitable for most regions within EU countries and China, but unsuitable for some regions where the air is too humid to be dealt, e.g., Venice, Rome, Shanghai, Guangzhou etc. The cooling output of the system ranges from 1.6 to 5.2 $W/m^3/h$ airflow rate, depending upon the region where the system is applied. Compared to a conventional mechanical vapor compression refrigeration based system, the dew point system has significant higher potential in saving energy costs. The estimated payback period of the dew point system is around 1.05−1.8 years. In the same year Miyazaki [79] analyzed M-Cycle for integrated air cooling system, driven by the solar energy using the ε–NTU method. The model was validated against experimental data with reasonable agreement from both simulation and experimental results (within 5 and 10%). Also in 2011 Jaber and Ajib [80] designed an indirect evaporative air-conditioning for the typical Mediterranean residential buildings and studied the economic benefit relating to utilization of such a system. The results indicated that most of the cooling load of the buildings could be matched by using an IEC unit with the airflow rate of 1100 l/s. The payback time of the implementation would be less than two years. In his article, Chen [81] analyzed a wet porous cooling plate which was used for a building wall. Cooling effect was achieved due to the evaporation in the porous plate. Chen also developed mathematical model on the heat and mass transfer in the unsaturated porous media to analyze the influences of ambient conditions and the porous plate thickness on the cooling performance of the porous evaporative plate. It was established that the ambient wind speed and the thickness of porous plate have significant influence on the average temperature of the porous plate. Kulkarni and Rajput [82] published a paper about a two stage indirect/direct evaporative cooler with wet surface plate heat exchanger type indirect stage and different shapes and cooling media in direct stage. The cooling pads made up of wood wool, rigid cellulose and aspen fiber were used as media in direct stage. The results show that saturation efficiency of direct evaporative cooler varies in the range of 0.983 to 0.719. Overall efficiency of the unit varies in the range of 1.195 to 0.743 and outlet temperature of air between 27.3 °C and 32.4 °C. Bruno [83] analyzed the operational characteristics of a novel dew point indirect evaporative cooling unit equipped with a counter-

flow heat exchanger using the experimental methods. The new unit was used as a pre-cooling device of a typical air conditioner in the commercial application. The obtained wet bulb effectiveness was in range 1.18–1.29, while the average outlet air temperature was 17.3°C. Also in year 2011 Tavakoli and Hosseini [84] presented the analysis of a steady state laminar 3D cross flow, between two sinusoidal corrugated parallel plates, with perpendicular directions of the corrugation for evaporative coolers. They suggested that in different residential, agricultural or industrial applications, the proper size of the domain or Reynolds number can be estimated through the resulted diagrams.

The year 2012 resulted in another important discoveries in the subject of indirect evaporative air cooling. Hasan [22] presented the analysis of the novel indirect evaporative air cooler based on the modified of the ε–NTU method, the wet bulb effectiveness achieved in this study was up to 1.2. The main idea for achieving a sub-wet bulb temperature by the presented unit is based on indirect pre-cooling of the working air before it enters the wet passage. It is shown that a modified analytical model for indirect evaporative coolers could be based on the ε–NTU method with proper adjustments. The model results showed good agreement with results from existing experimental measurements and a numerical model. During the same year Farmahini-Farahani and Heidarinejad [85] expanded their idea of the system based on a combination of nocturnal radiative cooling and two-stage evaporative cooling. The effectiveness of the system was investigated for four different cities having different climatic conditions. The results obtained indicated that the proposed system can become a new alternative for typical cooling systems in some hot regions. The energy saving of the novel system is between 75 and 79% higher than of the mechanical vapor compression systems. Caliskan et al. [86] presented energy and exergy analysis along with environmental impact and sustainability parameters of the Maisotsenko cycle. Three various novel air coolers based on M-Cycle were evaluated using energy and exergy analyses. The results indicated that maximum exergy efficiency is found to be 0.191 for a reference temperature of 23.88 °C where the optimum operation takes place. In their other paper [87], the thermodynamic analyses of the thermal storage system of buildings was presented. The results showed that necessary power demand of the building can be received by the thermochemical or sensible supported systems. Khalajzadeh et al. [39] analyzed a novel integrated system of ground heat exchanger and indirect evaporative air cooler in the summer conditions of Tehran. A ground-coupled circuit pre-cools the entering air of an indirect evaporative cooler. The simulation reveals that the combination of the ground-coupled circuit and the indirect evaporative cooler can easily provide comfort conditions. The obtained results showed that novel hybrid system significantly decreases the air temperature below the ambient wet bulb temperature. Worek et al. [88] showed the possibility of using the cross-flow M-Cycle heat and mass exchanger in desiccant-indirect evaporative air-cooling system for various operational conditions (Fig. 1.23). The air exiting the desiccant wheel can vary in temperature from 32.2°C if a heat recovery wheel is used to 82.2°C if no heat exchanger is used, it must be cooled before it can be used in any conditioned space. It was established that the unique heat and mass exchanger utilizing the M-Cycle allows the desiccant system to provide cooling and to dehumidify the air with far less energy input. Also, the M-Cycle HMX was able to cool the

air to low temperatures without an additional heat exchanger, which would increase the overall cost of the system. Another study connected with solar desiccant system was performed by Finocchiaro et al. [89]. In this system, air-to-air packaged wet heat exchangers are used to maximize the exploitation of the evaporative cooling potential associated with the exhaust air stream. The thermodynamic cycle is first theoretically described, and then an example of a real application at the Solar Laboratory of the University of Palermo was shown. Different energy performance figures, such as thermal and electrical COP, were presented and discussed.
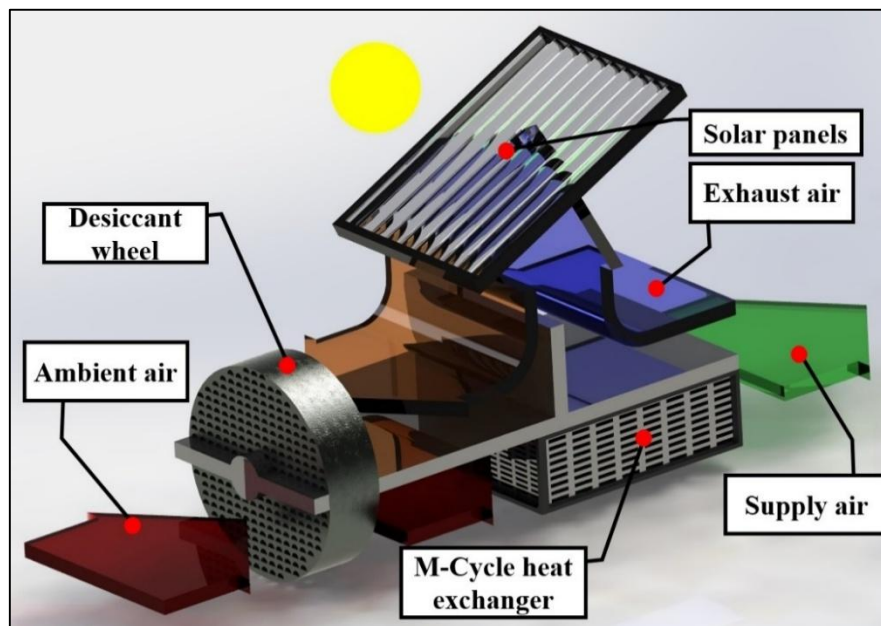


Fig. 1.23. The SDEC system with the M-Cycle HMX.

Interesting studies were published in 2013 as well. Boukhanouf et al. [90] presented a computer model and experimental results of an indirect evaporative cooling system for air conditioning in hot and dry climate regions. The system uses porous/fired clay materials as wet media for water evaporation. The primary air and working airflows were in counter-flow direction. Modelling results were conducted for ambient air dry bulb temperature ranging from 30°C to 45°C and relative humidity lower than 65%. The results indicated that supply air would be cooled below the wet bulb temperature. Kanzari et al. [91] analyzed the sub-wet bulb temperature air cooling unit with a numerical methods. The exchanger used the ceramic porous material for the plate construction. The wet bulb effectiveness obtained by this unit was 1.17. During the same year, Bellemo et al. [8] analyzed desiccant cooling system with regenerative indirect evaporative air cooler. The system included a desiccant wheel, dew point evaporative air coolers, a heat recovery unit and a heat source. An empirical model was built based on polynomial fits to manufacturer data. The model was validated with manufacturer data. The models enable calculations of the steady state operation of the system. Another analysis of desiccant - indirect evaporative air cooler was performed by Woods and Kozubal [92]. They analyzed a liquid desiccant air conditioner with regenerative evaporative cooler. Each stage was a stack of channel pairs, where a channel pair is a process air channel separated from an exhaust air channel with a thin plastic plate. In the first stage, a liquid desiccant film, which lines the

process air channels, removed the moisture from the air through a porous hydrophobic membrane. An evaporating water film weted the surface of the exhaust channels and transfers the enthalpy of vaporization from the liquid desiccant into an exhaust airstream, cooling the desiccant and enabling lower outlet humidity. Several experiments were performed on the prototypes over a range of inlet temperatures and humidifies, process and exhaust air flow rates, and desiccant concentrations and flow rates. The model developed by authors predicted the experiments within ±10%. Uckan et al. [93] also analyzed the novel configuration of desiccant-evaporative air-conditioning system. They used experimental methods. Experiments were carried out to investigate the total performance of the system and performance of the components used during summer season in a hot and humid climate. Effectiveness values for both heat exchangers and evaporative coolers were calculated through their work. In addition to the cooling capacity, coefficient of performance (COP) and energy consumption of the system were also evaluated. Results show that the effectiveness for the heat exchangers and evaporative coolers are very high under different outdoor conditions. Another study performed in 2013 was done by Lee et al. [94]. They investigated method to improve the compactness of the regenerative evaporative cooler: three different configurations, i.e., the flat plate type, the corrugated plate type, and the finned channel type are investigated and compared to find the most compact configuration. The key point in the derivation of the proposed simple model for the heat exchange on the fin surface is introduction of the linear air saturation line and the linear function between enthalpy of the humid air and its wet bulb temperature. These simplifications allowed solving the heat conduction equations for the fin analytically.

The year 2014 brought further exploring of potential in highly-efficient evaporative air cooling processes. Cui et al. [95] developed a simplified analytical model for indirect evaporative heat exchangers via a modified log mean temperature difference (LMTD) method designed for sensible heat exchangers. The authors suggested their method is a good solution for fast calculation for engineering purposes. The model has been demonstrated to be a practical method to provide an accurate result with a short computational time. Jradi and Riffat [96] parametrically studied the modified cross-flow dew point indirect evaporative air cooler based on the M-Cycle. In this study a numerical analysis is carried out for a modified dew point cooling system based on a proposed psychrometric energy core (PEC) with a cross-flow heat and mass exchanger for buildings air-conditioning applications. A detailed numerical model was developed for the energy core with the cross-flow exchanger using Matlab environment. On the base of optimization investigation the 1.12 wet bulb effectiveness of the proposed dew point cooling system was attained. Rogdakis et al. [41] presented experimental and numerical study of the M-Cycle HMX in Greek climate conditions. The obtained results indicated that the M-Cycle HMXs can operate with high efficiency in the hot and dry Mediterranean climate, thus they can satisfy the necessary cooling power required for air conditioning. El-Agouz and Kabeel [97] analyzed performance of desiccant air conditioning system with geothermal energy. The thermal analysis of air conditioning system with its different components desiccant wheel, solar collector, heat exchanger, ground heat exchanger and water spray evaporative cooler is presented. Three different air conditioning cycles are simulated in the current study

for different zones like: hot-dry zone, warm-dry zone, hot-humid zone and the warm-humid zone. The highest obtained COP of the desiccant air conditioning system was 1.03 while the lowest COP was 0.15. Sosa and Gómez-Azpeitia [98] presented a field study of indirect evaporative air coolers and shading devices; indirect evaporative cooling, a combination of shading devices and thermal mass and a combination of indirect evaporative cooling, solar protection, thermal mass and nocturnal radiative cooling. The article shown high potential of application of such systems in dry and warm climate conditions. Gao et al. [99] experimentally analyzed an integrated liquid-desiccant indirect evaporative air-cooling system with the M–cycle. The results showed that the dehumidification process in the first stage of the cycle has direct impact on the cooling capacity in the second stage, when the inlet parameters of the airflow or desiccant are changed. The energy balances obtained were in the range of ±20% for all experimental conditions.

Evaporative air cooling is still intensively studied in 2015. The results already established proved the high potential of such cycles in air conditioning systems. The future perspectives of dew point IEC systems seems very promising, however there are still many important things that need to be discovered. The studies presented in 2015 include many new ways of increasing the effectiveness of evaporative air cooling cycles and new methods of analyzing them. Montazeri et al. [100] simulated the impact of selected parameters on evaporative cooling efficiency with computational fluid dynamics methods. The selected parameters were: air temperature, air humidity ratio, airflow velocity, water temperature and droplet size distribution. The results showed that the sensible cooling capacity of the system can be improve by more than 40% if, for the given inlet water temperature (35.2 °C), the temperature difference between the inlet air and the inlet water droplets increases from 0 °C to 8 °C. Zenga et al. [101] studied a solar hybrid one-rotor two-stage desiccant cooling and heating system with numerical methods. The system was made up of a one-rotor two-stage desiccant cooling unit, with design cooling capacity for 5 kW, and a solar collector array of 15 m$^2$. Performance model of the system was created in TRNSYS environment. Numerical results agreed with the experimental data. The simulation results showed that about 60% of the humidity load can be totally handled by the one-rotor two-stage desiccant cooling unit, and about 40% of the heating load can be handled by the solar energy. Cruz and Krüger [102] analyzed passive indirect evaporative cooling in Brazilian climate conditions. Different arrangements of passive air coolers were tested in the experiment. The obtained results showed that the presented solution can provide comfortable conditions in the most of the cities where the experiment took place. Authors suggested that the passive system could have a great applicability in Brazil with a strong potential for improving indoor comfort conditions and to promote a reduction of the energy demand on HVAC. Heidarinejad and Moshari [103] presented a new mathematical model of an indirect evaporative cooling system, which included the longitudinal heat conduction in the channel plate and the effect of spray water temperature change as well. The mathematical model was used for simulation of combined system of indirect/direct evaporative cooling. The results indicated that presented solution is able to achieve 50% higher wet bulb effectiveness than typical indirect evaporative air cooler. Cui et al. [104] presented the performance analysis of

indirect evaporative heat exchanger pre-cooling the air for typical mechanical compression cooling coil in hot and humid climate. The study was performed with numerical methods. The obtained results suggested that that the proposed exchanger is able to cover about 47% of the cooling load from the ambient air, therefore it is able to provide important energy savings. Balyani et al. [105] presented the analysis of best cooling strategy based on thermal comfort and 3e analyses for small scale residential buildings at diverse climatic conditions. The proposed systems were analyzed based on 3E (energy, economic, and environmental) as well as thermal comfort analyses. It was established that in temperate and humid, very hot and semi-humid, and temperate and wet cities, desiccant-enhanced evaporative cooling was the best solution.

It should be mentioned that there were also three review articles about the evaporative air cooling published in years 2004-2013. The review performed by Duan et al. [2] described the general achievements in direct and indirect evaporative air cooling around the world, the review performed by Xuan et al. [17] focused on research and application of evaporative air cooling in China, while the review presented by Wani et al. [106] analyzed only the potential and applications of the Maisotsenko cycle. Indirect and direct evaporative air cooling was also widely discussed in the review about technical development of rotary desiccant dehumidification and air conditioning published by La et al. [107], in the review about strategies of achieving better energy-efficient air conditioning by Chua et al. [108] and in the review about the polymer compact heat exchangers by Zaheed et al. [109]. Table 1.2 presents the summary of parametric data of main analyzed indirect evaporative air coolers.

Table 1.2. Parametric data chosen for analysis of the selected IEC units.

| Parameters | Unit | Alonso | Stoitchkov | Guo | Zhan, Qiu | Elberling | Riangvilaikul |
|---|---|---|---|---|---|---|---|
| Flow pattern | | Cross-flow | Cross-flow | Cross-flow | M-Cycle cross-flow | M-Cycle cross-flow | M-Cycle Counter-flow |
| $t_{1i}$ | °C | 35..45 | 24..36 | 25..45 | 25..40 | 26.7..43.8 | 25..45 |
| $t_{1i}^{WB}$ | °C | 19.5..23.3 | 17.7..28.3 | N/A | 17.9..30.3 | 18.1..23.9 | 10.7..32.5 |
| $t_{2i}$ | °C | 23.5..27.2 | 22..28 | 25.0 | N/A | N/A | N/A |
| $t_{2i}^{WB}$ | °C | 16.8..18.6 | 16..21 | 11.4..23.8 | N/A | N/A | N/A |
| $w_1$ or $V_1$ | m/s or m³/h | 80 m³/h | 3.3 m/s | 0.5..4.5 m/s | 130 m³/h | 1910..5000 m³/h | 2.4 m/s |
| $W_2/W_1$ | - | 0.5 | 0.5 | 0.5..2 | 0.5 | 0.5 | 0.33 |
| $L_X$ | m | 0.3 | 0.4..0.7 | 0.2 | 0.25 | N/A | 1.2 |
| $h$ | mm | 3.0 | 3.5 | 2..10 | 4 | N/A | 5 |
| $t_{1o}$ | °C | 20.8..24.8 | 17.2..23.6 | 21.3..26.3 | 18..30 | 19.9..25.6 | 15.6..32.1 |
| $\varepsilon_{WB}$ | - | 0.77..0.93 | 0.79..0.88 | 0.78..0.95 | 0.5..0.65 | 0.81..0.91 | 0.92..1.14 |

It can be easily observed that many existing studies are focusing on new methods of increasing the effectiveness of evaporative air coolers. These methods can be divided into the four main groups:

1. Using multistage cooling within one unit or using the combination of IECs or IEC/DEC units.
2. Searching for new materials for the structure of evaporative air coolers. This include applying specially designed porous materials for channel construction. Such plates allow for very even water film distribution, keeping the water consumption at minimal value at the same time.
3. Using combined airflow schemes to achieve higher effectiveness of indirect evaporative air coolers.
4. Searching for the optimal operating modes of the evaporative air coolers on the base of multi-objective optimization and determining the climatic regions where IECs are suitable to provide thermal comfort conditions.

It should be mentioned that using complicated systems, such us multistage combination of direct and indirect air coolers or adding additional elements to the system such as cooling coil connected with the nocturnal cooled water may significantly increase its costs and make it difficult to control with the automatic controllers. The complicated systems are also more sensitive for potential damages (the more parts the system contains, the more of them may be damaged). The most important problem, however, is the size of the cooling equipment. The construction of the buildings nowadays lives very few space for the technological support, due to the fact that space is very expensive. The real estate prices have significantly increased in the XXIst century (price for the square meter of room space in Poland has doubled between years 2000 and 2011 [110]), therefore architects design buildings in the way where most of it space can be sold to potential customers. This leaves a very small room for the technical equipment , therefore the application of complicated evaporative systems in new buildings is limited.

This shows that the M-Cycle heat and mass exchanger has the highest potential of application in the modern air conditioning systems, due to its high efficiency and size which is similar to the typical exchangers used in air handling units [15]. Therefore it becomes important to scientifically analyse the Maisotsenko cycle HMX for air conditioning applications in order to increase its efficiency, optimize the unit and find suitable climatic conditions for its effective operation.

It can be clearly seen from the literature review that the cross-flow M-Cycle HMX, which is the only form of the cycle currently applied in the air conditioning systems, have been investigated by a very few studies. The experimental studies have confirmed the high performance of the HMX [40], [76], but they were not able to optimize the unit or make the significant modifications to its structure due to the high costs. Most of the current numerical work concentrated on the regenerative counter-flow M-Cycle which is harder to be applied in practice due to the unfavourable airflow scheme [15]. There was only one numerical model for the cross-flow M-Cycle HMX, but it described only a small-scale Chinese exchanger (the length of the channel was only 25 cm) and it was based on the simplified assumptions (it did not

include the fins in the exchanger structure and it have not got an algorithm which would allow for the detail analysis of air streams mixing process in the initial part of the HMX). This model was also validated using the very small unit, under a limited conditions and with a very small airflow rate (Primary airflow rate was only 130 $m^3$/h, working airflow rate was 65 $m^3$/h) [2], [43]. The small scale and limited operating conditions of the ISAW TAC-150 exchanger allowed only for initial analysis and were probably the reasons of different temperature trends between numerical results and experimental data presented by Zube and Gillan [46]. There was also a simplified algebraic "black box" model presented by Rogdakis in he's PhD thesis [111], but this model was not based on the differential equations and it cannot be used for analysis of heat transfer phenomenon inside the HMX, it allows, however, for satisfying calculation of the outlet air temperatures.

As described above, there are no studies concentrated on the detail numerical analysis of the Maisotsenko cycle cross-flow indirect evaporative air cooler, which include studding the heat transfer processes on the finned surface taking into account the different character of the associated heat and mass transfer at the entrance and exit part of the wet channels and with describing the phenomenon of air streams mixing in the wet working channel of the exchanger. This leaves an important scientific gap which limits the possibilities of increasing the effectiveness of the M-Cycle air coolers. In this regard it becomes highly important to deliver the detail theoretical model of the cross-flow M-Cycle heat and mass exchanger for the dew point evaporative cooling in order to study the heat and mass transfer process inside the unit, increase the efficiency of the original exchanger and optimize the structure of the unit to make it suitable for a wide range of climate conditions.

For the above mentioned reasons this study focuses on the numerical analysis of the cross-flow Maisotsenko cycle heat exchanger. The study will be based on the mathematical model which differs from the previously conducted ones as follows: it is based on the detail differential equations, it includes the complete conduction equations for the finned surface and the correction coefficients considering different temperatures of water evaporated from the channel plate and the fin surface and for the different heat of vaporization from the fin and plate surface. The model is also supplemented with detail algorithm describing the process of air streams mixing in the wet channels of the perforated initial part of the air cooler.

### 1.8. Subject of the study

The subject of the study is the cross-flow M-Cycle heat and mass exchanger used in air conditioning systems. The scheme of the exchanger is visible in Figure 1.24: it is a perforated heat exchanger, with operation based on multiple branching of the air from the dry passages to the wet passage through the perforations over their length of the plates the plates from their dry sides to the wet sides [15], [64]. This configuration has been further developed in the USA by Idalex Inc. and Coolerado Corp., wherein the wet and dry ducts are divided into two separate sections which allows for pre-cooling of the dry air streams prior to their entry into the wet duct. The working mechanism of the M-Cycle HMX is described as follows. Part of the surface on the dry side is designed for the primary air (Fig. 1.24) to pass through and the rest is allocated

to working air (working air in dry channels in Fig. 1.24). Both the product and working air are guided to flow over the dry side along parallel flow channels. The working air initially enters the dry channels where it is precooled sensibly before it is fractioned into multiple streams which are directed into the wet channels. There are numerous holes distributed regularly on the area where the working air is retained and each of these allows a certain percentage of air to pass through and enter the wet side of the sheet. The air is gradually delivered to the wet side (working air in wet channels in Fig. 1.24) as it flows along the dry side, forming an even distribution of airstreams over the wet surface. The pre-cooled air, delivered to the wet side, flows over the wet surface along channels arranged at right angles to the dry side channels, absorbing heat from the working and product air. Owing to its pre-cooling effect, the working air in the wet side (working air wet channel) has a much lower temperature and therefore, is able to absorb more heat from its two adjacent sides. As a result, the cooling effectiveness of the new structure is higher than that of the traditional cross-flow exchanger [40], [43], [111].
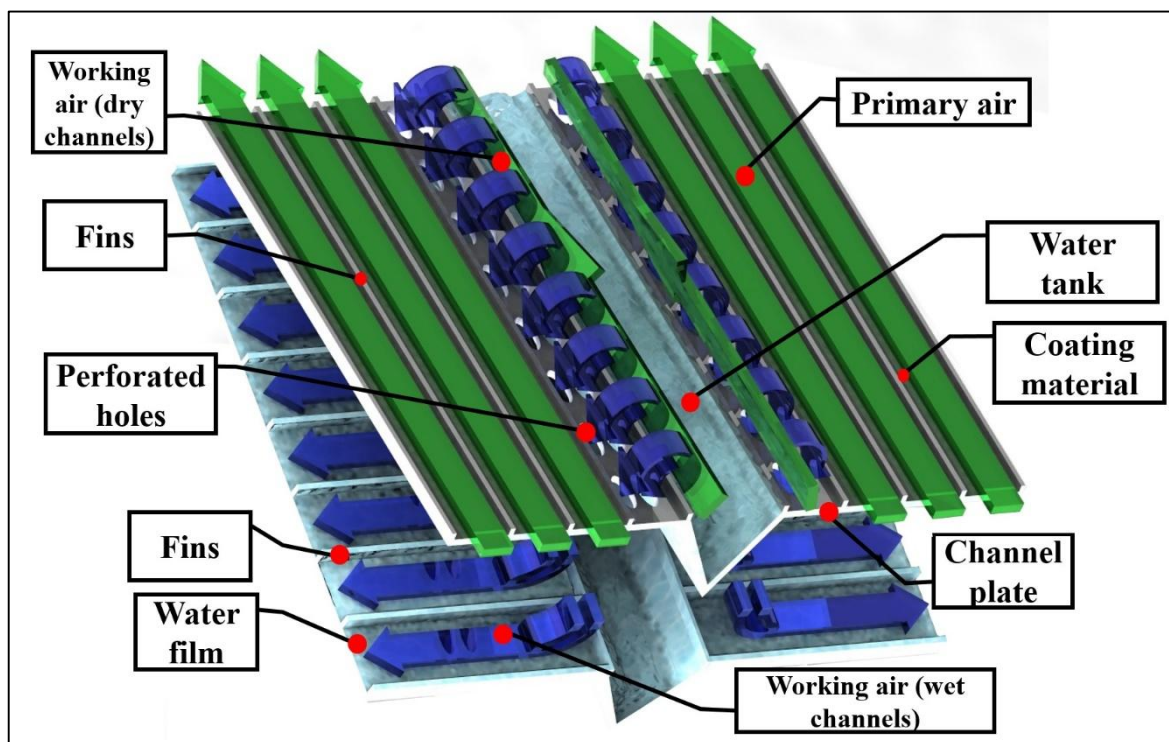


Fig. 1.24. Scheme of the M-Cycle HMX analyzed in this study.

The structure of the exchanger is presented in Figure 1.25. The heat exchanger is made into the typical recuperators box-shaped structure (Fig. 1.25.(a)), where dry and wet channels are placed alternately one after another (Fig. 1.25.(b)). It should be noticed that the current structure of heat exchanger is made of two identical units placed on the two sides of the water tank (Fig. 1.24 and Fig. 1.25.(c)). For the numerical analysis the location of identical structures is not important, therefore the mathematical model will describe only one side of the heat exchanger (Fig. 1.25.(d) and (e)). The construction of the plate heat exchanger uses a special medium with the characteristics of high water retention and wickability as the wet channel: unit consists of numerous sheets made of porous material (cellulose fibre), which are creating the

wet channel. The sheets are stacked together. One side of each sheet is also coated with impervious material (polyethylene) to avoid penetration of water (Fig. 1.25.(d) and (e)). Sheets covered with impervious material are creating dry channel. Considered heat exchanger operates in a cross flow pattern. Exchanger's channels are also fined (Fig. 1.25.(b), (d) and (e)). Fins purpose, besides improving heat transfer, is to provide structure as well as guide air movement within the heat exchanger. Fins run along the length of each sheet, and the width of the next sheet to form a cross flow of air streams within the exchanger. There are also numerous regularly distributed holes made in the wall separating dry and wet channel in the working part of the exchanger (Fig. 1.25.(d) and (e)). This configuration gradually diverts air from the dry working channel to the wet channels. Unit's primary and working channels are flat rectangular-shaped (Fig. 1.25.). For the case of currently produced M-Cycle exchanger a cellulose-blended fibre and polyethylene were used as the wicking and the hydrophobic coating [15], [112]. A patented technology for M-Cycle exchanger construction reports that special cellulose material enables uniform and thin wetting on the wet side of the heat exchanger without extra water and therefore focusing on the cooling of the process air [15], [112]. In the studied case, the plate of the exchanger is 0.4 mm thick; height of each channel is equal 3.2 mm; width of each channel is equal 25 mm; fins width is equal 2.0 mm. Due to limitations in current manufacturing methods, the real HMX sheet dimensions are not exact and have tolerances associated with them (Fig. 1.25.(a) and (b)). The channel dividers are made from beads of polyethylene plastic and are attached to the sheet using a mechanical system similar to a hot glue gun [15], [112]. The flow rate of the warm polyethylene and the speed of the machine affect the bead thickness and height. And adjusting this device to produce a specified bead dimension is a trial and error process. Therefore the working air sheets and product air sheets can be different heights, but on any one sheet, the heights are consistent (Fig. 1.25.). In presented analysis, as a simplification, it is assumed that all channels have the same height and width.
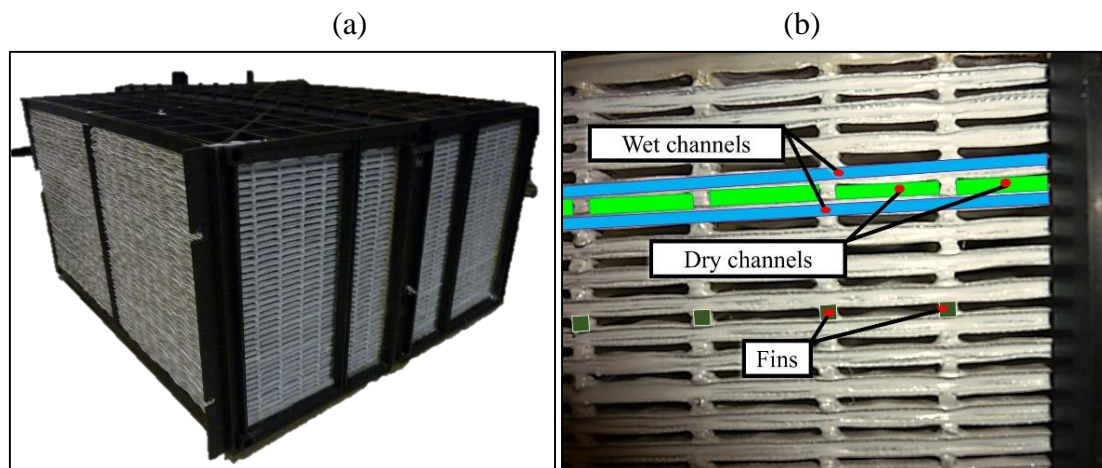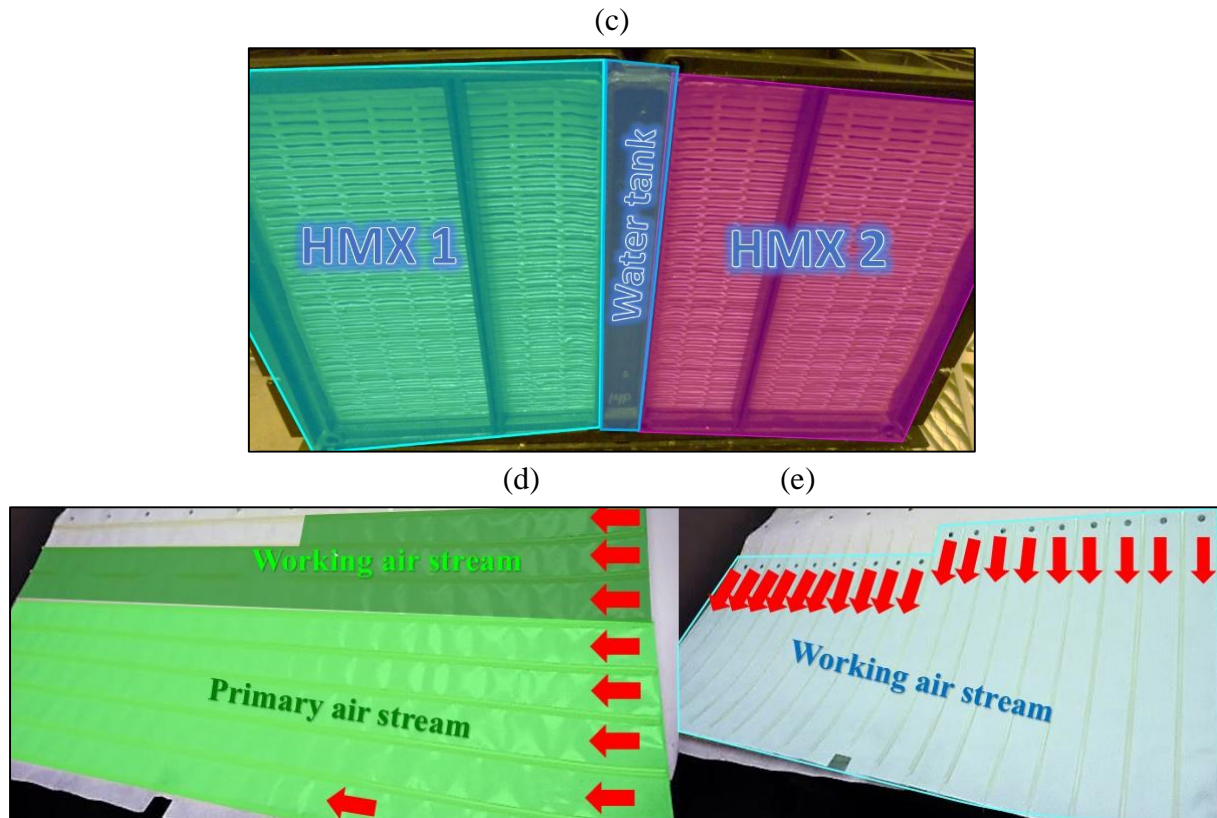
(a) (b)

(c)



(d)                                    (e)

Fig. 1.25. Structure of the M-Cycle HMX analyzed in this study (author's photographs). (a) The general look of the structure. (b) Dry and wet channels. (c) Connection of two HMXs in one unit with the water tank. (d) Dry channels structure (single HMX). (e) Wet channels structure (single HMX).

The most important part of considered exchanger is its initial part, where the working airflow is pre-cooled before entering the primary part. This element of the structure differs the M-Cycle HMX from the typical cross-flow evaporative cooler (Fig. 1.26). Therefore it can be undoubtedly concluded that its arrangement has highest impact on the performance of the M-Cycle HMX and it should be detail studied. Figure 1.26. shows the general nomenclature which will be used for the description of the exchanger analyzed in this study. To make the description of the exchanger easier it will be described divided into the two parts: initial and product. As it was mentioned before, the primary air stream will be marked as 1,the working air stream in wet channels which contacts with the primary air will be marked as 2. The working air in the dry channels which contacts only with working air in the wet channels will be marked as 3, while the working air in the wet channels which contacts only with the secondary air stream in the dry channels will be marked as 4 (Fig. 1.26). The air streams 2,3 and 4 are all part of one working air stream ($G_2 = G_{3i} = G_{4o}$). It can be seen that in general conception, the initial part of the cooler have dry and wet channels, just like the product side, however, in its initial part the airflow in the dry channels is constantly decreasing, due to the fact that parts of the working air in the dry channels are transferred to the wet channel. Therefore the mass flow rate along the dry working air channels is variable (Fig. 1.26(a)) and at the final part of the exchanger the working air stream is equal to 0 (the whole airflow is transferred to the wet side). It is also visible that similar situation occur inside the wet channels (Fig. 1.26(b)). Along the channel length the working airflow 4 is constantly increasing. At the end of the initial part it reaches its

final value ($G_{4o}= G_{2i}$). At the product part of the exchanger the working airflow is constant through the entire channel length ($G_{2i}= G_{2o}$).
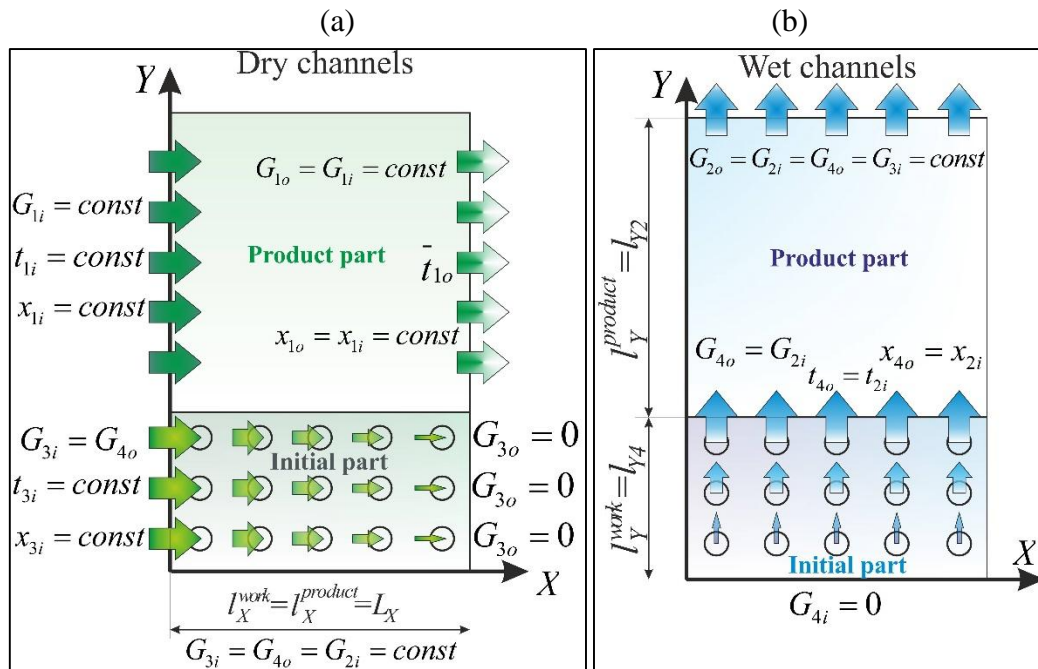


Fig. 1.26. Dry and wet channels of the M-Cycle HMX analyzed in this study. (a) Dry channels. (b) Wet channels.

The theoretical ideal arrangement of the initial part is presented in Figure 1.27.(a). It consist of the even dense perforation in every dry and wet channels in order to distribute the airflow evenly. However, due to the limitations in production methods this arrangement cannot be used in practice: the perforated holes have to be larger. The arrangement of the initial part in currently produced unit is visible in Figure 1.27.(b). The original HMX has shorter first dry working air channel than the other two working air channels. There are also no holes in the third dry channel, because the airflow is transferred to the second dry channel through the gaps in fins (Fig. 1.27.(b)). This version of the exchanger was obtained on the basis of experimental tests, with have natural limitations, connected with costs and the time of the project. The Coolerado Corporation is still testing the different perforation arrangements in order obtain maximal effectiveness of the M-Cycle exchanger (Fig. 1.27.(c) and (d)). Such analysis can be easily performed with the mathematical model, which allows for fast and cheap comparison between different perforation configurations. Due to the great importance of the initial part of the unit, the significant part of the presented study will focus on the analysis and optimization of the working air precooling in the initial part using the mathematical model.
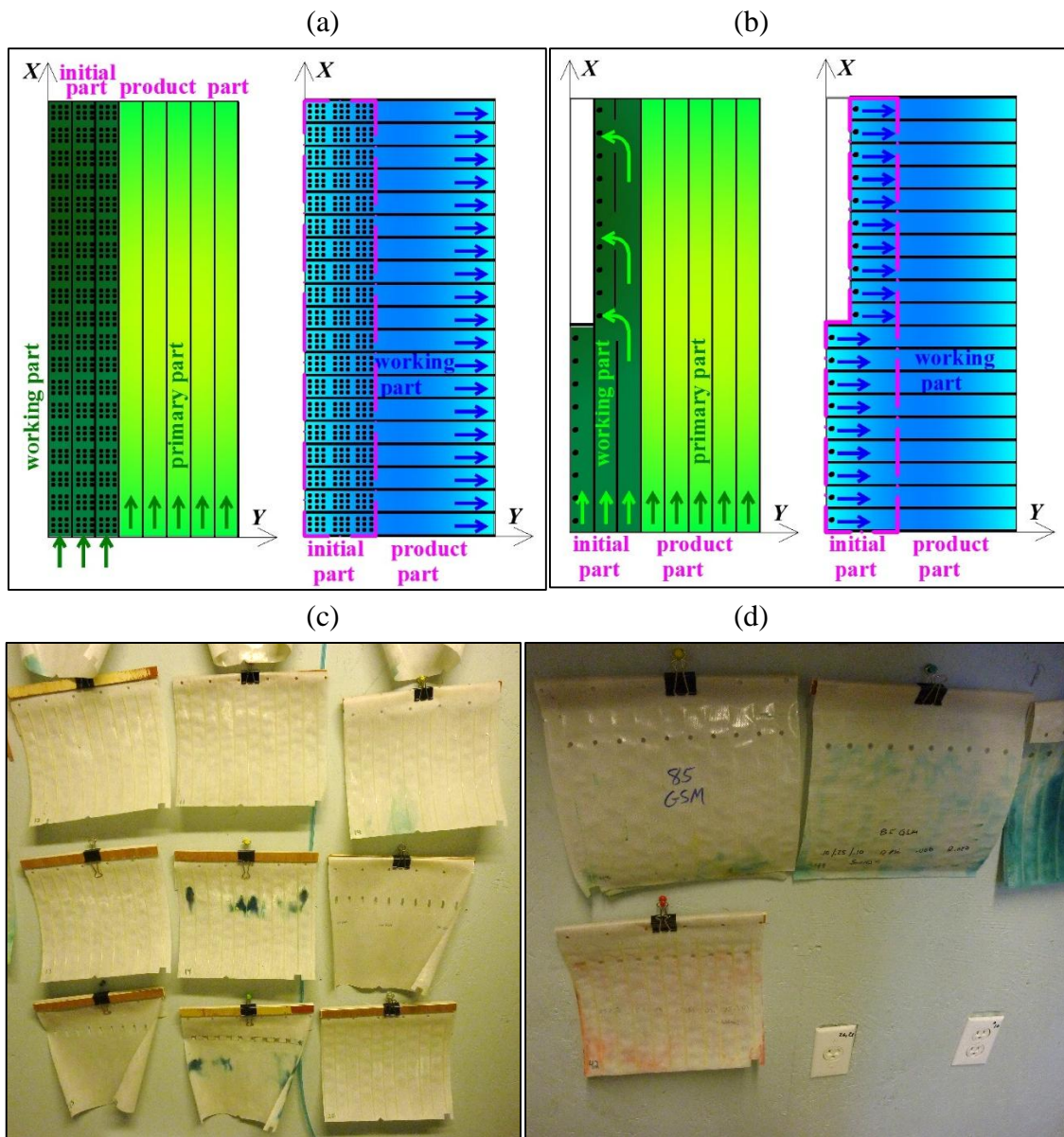
Fig. 1.27. Different arrangements of the initial part in the cross-flow M-Cycle air cooler. (a) Ideal arrangement (dense perforation). (b) Currently produced arrangement obtained with the numerical results. (c) Different arrangements tested at the Coolerado Corp. part 1. (d) Different arrangements tested at the Coolerado Corp. part 2.

### 1.9.Thesis, subject and scope of the presented Ph.D. dissertation

The analysis of the existing literature allowed for creating the thesis of the presented Ph.D.:

*"It is possible to establish the M-Cycle heat and mass exchanger which can be practically used in Polish climate conditions"*

The following thesis lead to the subject of the work, which is detail numerical analysis of the cross-flow M-Cycle HMX, analysis of its application in Polish climate conditions and optimization of its structure. The subject requires a certain scope of work, which is:

- − Creating mathematical models for the basic evaporative air cooling cycles for the initial studies.
- − Creating the assumptions for the mathematical model of the M-Cycle HMX on the basis of the initial studies results.
- − Creating the mathematical model of the M-Cycle HMX for the ideal cycle conditions (very dense and even perforation).
- − Creating the mathematical model of the M-Cycle HMX for practical conditions which include different arrangements of the initial part.
- − Validation of the mathematical models against the experimental data collected by author and against existing experimental data.
- − Analysis of heat and mass transfer processes inside the M-Cycle HMX.
- − Analysis of impact of operational and geometrical factors on the unit's performance.
- − Propositions of improving the performance of the HMX on the basis of numerical analysis.
- − Analysis of application in the Polish climate conditions.
- − Comparison analysis between different M-Cycle heat exchangers.
- − Proposition of the different versions of the exchanger to obtain higher performance.
- − Comparison analysis between the proposed exchangers and the original unit
- − Optimization of the structure of the original HMX for different climate conditions.

## 2. Initial studies

*The results of this section were published in "S. Anisimov, D. Pandelidis, Theoretical study of the basic cycles for indirect evaporative air cooling, International Journal of Heat and Mass Transfer, 84 (2015) 974–989"* [113].

The description of heat and mass transfer process in the cross-flow M-Cycle indirect evaporative air cooler is complex and it requires solving many important mathematical problems (e.g. algorithmic solution of the coupled heat and mass transfer on the finned surface). For this reason the this part of presented thesis is focused on the analysis of basic evaporative air cooling cycles, which are much simpler to be mathematically described. A key objective of this section is to analyze the simple cycles for indirect evaporative air cooling (parallel-flow-P, counter-flow- C, cross-flow- CR and regenerative - R: Fig. 2.1), in order to understand their performance, advantages and disadvantages of each cycle, identify difficulties and barriers remaining in their application, find out routes toward enhancing their performance and establish basic knowledge necessary for further development of the mathematical model describing more complex evaporative air coolers, such as cross-flow M-Cycle heat and mass exchanger. It is important to mention that the regenerative heat and mass exchanger is the most simple form of the Maisotsenko cycle (Fig. 2.1.(d)). Therefore, analysis of heat and mass transfer process occurring in this exchanger may bring many important observations regarding the physical phenomena utilized in this thermodynamic process. Another important information is that M-Cycle unit studied in this thesis is based on the cross-flow arrangement. Analysis of the processes occurring in the typical cross-flow unit (Fig. 2.1.(c)) may also bring many important observations necessary for future development of the mathematical model of the cross-flow M-

Cycle HMX. It is especially important to develop an effective algorithm which allows to calculate the partial differential equations of heat and mass transfer, which are reacquired to describe the cross-flow arrangement (see Section 2.1.). The study will be conducted with original mathematical models presented in the next section of this chapter.
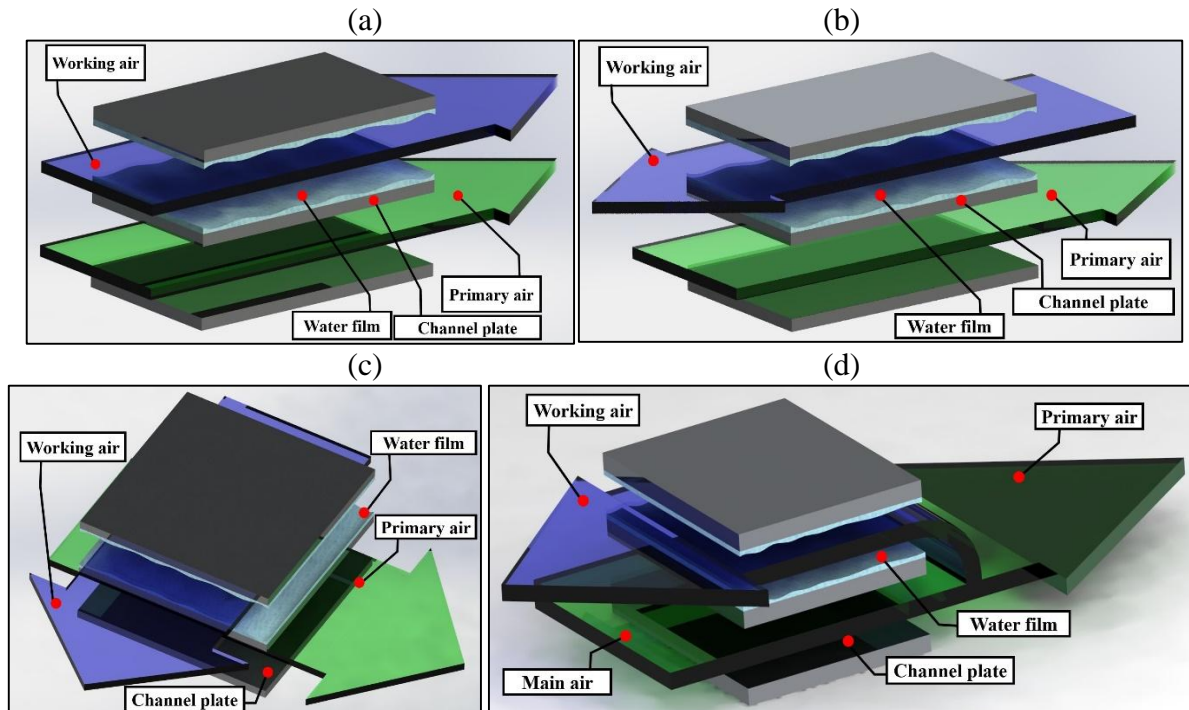


Fig. 2.1. Basic cycles for indirect evaporative air cooling analyzed in the section. (a) parallel-flow (P). (b) counter-flow (C). (c) cross-flow (CR). (d) regenerative flow (R).

## 2.1. Mathematical models of the basic indirect evaporative cooling cycles

The general concept of heat and mass transfer mechanism in indirect evaporative air coolers is different than of the typical sensible recuperators. In traditional dry recuperators, during summer operation, one air stream is cooled sensibly at the cost of sensible heating of the second air stream [2], [16]. The humidity ratio of both streams remain unchanged. In case of indirect evaporative coolers this process runs differently: the primary air stream is cooled by the *sensible heat transfer* at the cost of heating the working airflow with the *total heat* (a sum of latent heat of water evaporation and sensible heat). The direction of the sensible heat in the wet channel however may vary (the working airflow might be sensibly cooled or heated), but the general direction of the *total heat is always heating* the working airstream. This process may be described in terms of the specific enthalpy change: the specific enthalpy of the primary air stream is always decreasing, whereas the enthalpy of the working air stream is always increasing. There are three main methods used for mathematical modelling of heat and mass transfer processes in evaporative cooling units [12]:

- Models based on the Reynolds equations,

- Models based on the boundary layer equations,

- Models based on the ε–NTU method.

---

Mathematical models based on the Reynolds and boundary layer equations allow obtaining detail information about thermal parameters in every portion of studied object. However, this models are often very hard to solve in modern indirect evaporative units, because they are often characterized by complicated airflow and water distribution [114], [115]. The complicated structure of the models often requires many simplifications about exchangers' geometry and airflow characteristics, which may lead to inaccurate results [114], [115]. That is why in the presented thesis preference is given to the mathematical model based on the modified ε–NTU method [114], [115], [116], [117]. Models based on such method assume that airflow is treated as a gaseous fluid with constant temperature, velocity and mass transfer potential which are equal to bulk average values in sections normal to the exchangers plate [114], [115]. The ε–NTU method was used to describe indirect evaporative air coolers with satisfactory agreement with the experimental results by Hasan [22] and Miyazaki [79].The assumptions for the presented numerical models are listed below.

- Heat losses to the surroundings are negligible.
- Steady state operation.
- Driving force of mass transfer is a gradient of humidity ratio (water vapor's partial pressure).
- Airflow is an ideal, incompressible gas mixture of dry air and water vapor.
- Airflow is in the longitudinal direction and is not mixed vertically.
- Longitudinal molecular diffusion of water vapor in air and longitudinal heat conduction along the wall as well as inside the fluids in the direction of airflow are negligible.
- Water film is stagnant.
- Kinetic properties of airflow and water film are constant and equal to bulk average values.
- The passage walls are impervious to mass transfer.
- Consumed water rate corresponds to sufficient evaporation and keeping up the material of plates in hygroscopic saturated condition. This causes that airflow heat capacity to be much larger than that of the water film (i.e., $W_2 \gg W_w$).
- The temperature of the water film, the sensible heat transfer coefficient $\alpha$ and the Lewis factor depend on the operating conditions [113], [118].

It is important to mention that in novel evaporative coolers, such as the cross-flow M-Cycle the channel plates are made of the porous material which is constantly wetted with water, therefore the water film inside the unit is stagnant [64]. Due to this fact, the models of the basic evaporative cooling cycles are based on the same assumption. However, it was earlier established by Holmberg that in case of the exchangers like evaporative coolers, the slowly moving water film can also be treated as stagnant [119]. This was also confirmed by similar results obtained from numerical the studies of the same evaporative heat exchangers with the assumption of moving water film and with assumption of stagnant water layer [16], [78].

The example schematics of heat and mass transfer in calculation control volumes in the dry and wet channels, which shows the operating mechanism of mathematical model is presented for the parallel,counter and cross-flow IECs in Fig. 2.2. The processes occurring regenerative HMX are identical to processes occurring in the counter-flow IEC, therefore they are omitted.
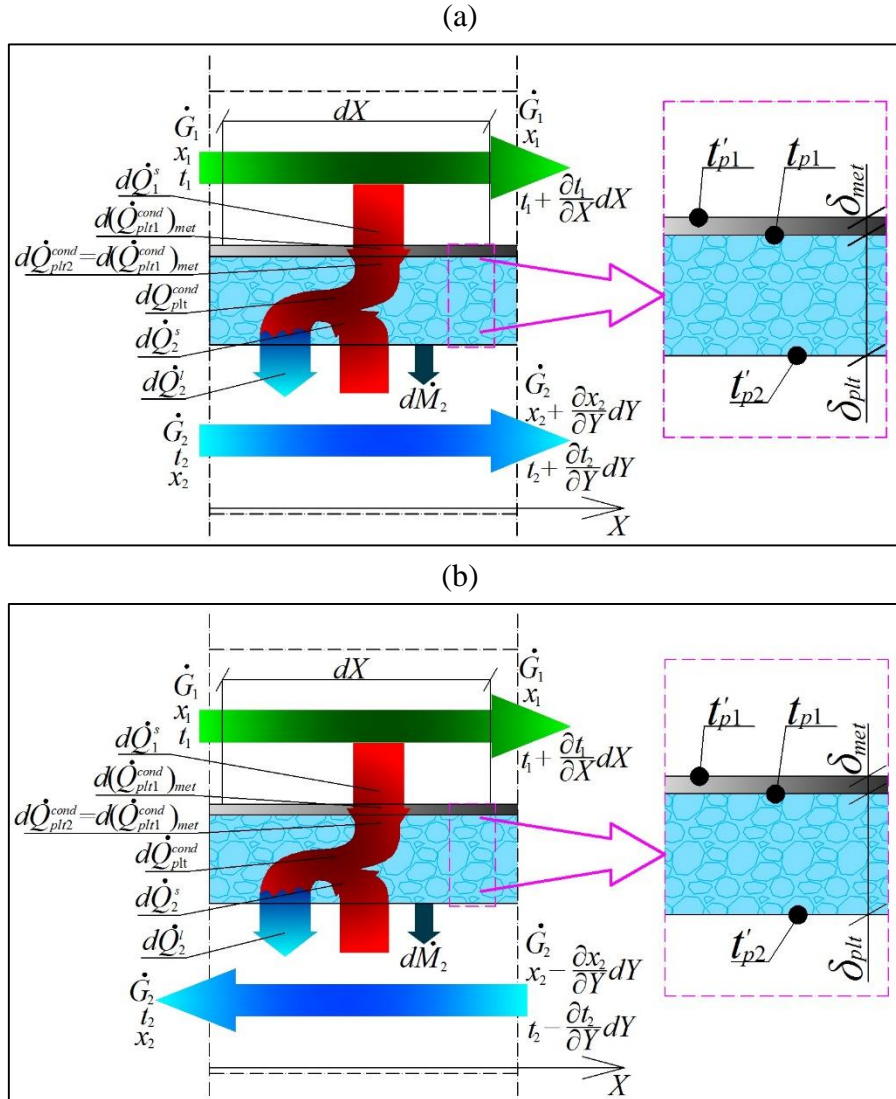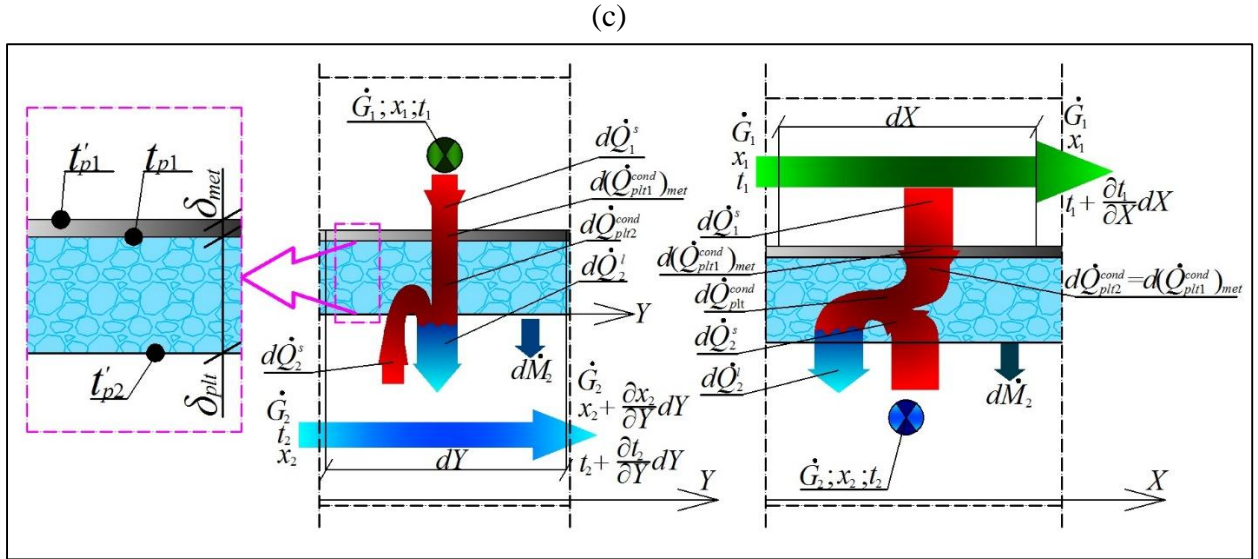
(a)



(b)

(c)



Fig. 2.2. Schematic of heat and mass transfer in differential control volumes in the product part of the investigated HMXs. (a) parallel-flow exchanger. (b) counter-flow and regenerative exchangers. (c) cross-flow exchanger.

The mathematical model is based on the heat and mass balance equations for the separated airflows, which are presented below [113], [114], [115].

- For the primary airflow 1:

➢ The balance equations includes only sensible heat transfer (see Fig. 2.2).

    o For the parallel-flow, counter-flow and regenerative IEC:

$$\dot{G}_1 c_{p1} \frac{dt_1}{dX} dX = -d\dot{Q}_1^s \tag{2.1}$$

where $\dot{G}_1 = (dY/L_Y)G_1$.

Rearranging Eq. (1) gives the following relationship

$$\frac{dt_1}{d\bar{X}} = \mathrm{NTU}_1 (t_{p1} - t_1) \tag{2.2}$$

where: $\mathrm{NTU}_1 = \alpha_1 F_1 / (G_1 c_p)$

Differential equations of energy conservation balance for the cross-flow IEC are just the same as in the case of P,C and R IEC, but they should be converted to the partial differential equations taking into account airflows direction. The sensible heat transfer equation for the cross-flow evaporative air cooler is given as:

$$\frac{\partial t_1}{\partial \bar{X}} = \mathrm{NTU}_1 (t_{p1} - t_1) \tag{2.3}$$

- For the working air stream 2.

➢ The energy conservation balance (Fig. 2.2).

  ○ For the parallel-flow IEC:

$$\dot{G}_2 c_{p2} \frac{dt_2}{dX} dX = -d\dot{Q}_2^s + c_{g2}\left(t'_{p2} - t_2\right)d\dot{M}_{p2} = -d\dot{Q}_{p2}^s + c_{g2}\left(t'_{p2} - t_2\right)d\dot{M}_{p2} \tag{2.4}$$

where $\dot{G}_2 = \left(dY/L_Y\right)G_2$.

The equations of energy conservation balance are identical for the counter-flow and regenerative exchanger, the only difference between mathematical description of those devices lies in the initial conditions (Fig. 2.3). Differential equations of energy conservation balance for the counter-flow and regenerative IEC are identical to the equations describing parallel-flow IEC, but they are characterized by the different sign, due to the different airflow direction.

  ○ For the counter-flow and regenerative IEC:

$$\dot{G}_2 c_{p2} \frac{dt_2}{dY} dY = -c_{g2}\left(t'_{p2} - t_2\right)d\dot{M}_{p2} + d\dot{Q}_2^s = -c_{g2}\left(t'_{p2} - t_2\right)d\dot{M}_{p2} + d\dot{Q}_{p2}^s \tag{2.5}$$

where $\dot{G}_2 = \left(dY/L_Y\right)G_2$.

Differential equations of energy conservation balance for the cross-flow IEC are just the same as in the case of parallel-flow IEC, but they should be converted to the partial differential equations taking into account airflows direction.

  ○ For the cross-flow IEC:

$$\dot{G}_2 c_{p2} \frac{\partial t_2}{\partial Y} dY = -d\dot{Q}_2^s + c_{g2}\left(t'_{p2} - t_2\right)d\dot{M}_{p2} = -d\dot{Q}_{p2}^s + c_{g2}\left(t'_{p2} - t_2\right)d\dot{M}_{p2} \tag{2.6}$$

where $\dot{G}_2 = \left(dX/Lx\right)G_2$.

Rearranging of the Eqs. (2.3-2.6) gives the following relationships:

  ○ For the parallel-flow IEC:

$$\frac{dt_2}{d\overline{X}} = \mathrm{NTU}''_2\left[\left(t'_{p2} - t_2\right) + \left(\frac{\sigma_p}{\mathrm{Le}}\right)_2\left(\frac{c_g}{c_p}\right)_2\left(t'_{p2} - t_2\right)\left(x'_{p2} - x_2\right)\right] \tag{2.7}$$

  ○ For the counter-flow and regenerative IEC:

$$\frac{dt_2}{d\overline{X}} = -\mathrm{NTU}''_2\left[\left(t'_{p2} - t_2\right) + \left(\frac{\sigma_p}{\mathrm{Le}}\right)_2\left(\frac{c_g}{c_p}\right)_2\left(t'_{p2} - t_2\right)\left(x'_{p2} - x_2\right)\right] \tag{2.8}$$

      ○ For the cross-flow IEC:

$$\frac{\partial t_2}{\partial \bar{Y}} = \text{NTU}_2^{''}\left[\left(t_{p2}' - t_2\right) + \left(\frac{\sigma_p}{\text{Le}}\right)_2\left(\frac{c_g}{c_p}\right)_2\left(t_{p2}' - t_2\right)\left(x_{p2}' - x_2\right)\right] \tag{2.9}$$

Where:

- $\text{NTU}_2^{''} = \alpha_2 F_2/\left(G_2 c_p\right)$,

- $\bar{X} = X/L_X$,

- $\bar{Y} = Y/L_Y$.

    ➢ The mass balance equation for the water vapor (Fig. 2.2):

      ○ For the parallel-flow IEC:

$$\dot{G}_2\frac{dx_2}{dX}dX = d\dot{M}_2 = d\dot{M}_{p2} \tag{2.10}$$

As in the case of the energy balance, the differential equations of mass conservation balance for the exchanger R and C are identical to the equations describing IEC P, but they are characterized by the different sign, due to the different airflow direction.

      ○ For the counter-flow and regenerative IEC:

$$\dot{G}_2\frac{dx_2}{dX}dX = -d\dot{M}_2 = -d\dot{M}_{p2} \tag{2.11}$$

In the case of the cross-flow HMX, equations of mass conservation balance are just the same as for parallel-flow IEC, but, as in case of energy balance equations, they should be converted to the partial differential equations taking into account airflows direction.

      ○ For the cross-flow IEC:

$$\dot{G}_2\frac{\partial x_2}{\partial Y}dY = d\dot{M}_2 = d\dot{M}_{p2} \tag{2.12}$$

Rearranging of the Eqs. (2.3-2.6) gives the following relationships:

      ○ For the parallel-flow IEC:

$$\frac{dx_2}{d\bar{X}} = \text{NTU}_2^{''}\left(\frac{1}{\text{Le}_2}\right)\sigma_{p2}\left(x_{p2}' - x_2\right) \tag{2.13}$$

      ○ For the counter-flow and regenerative IEC:

$$\frac{dx_2}{d\bar{X}} = -\text{NTU}_2^{''}\left(\frac{1}{\text{Le}_2}\right)\sigma_{p2}\left(x_{p2}' - x_2\right) \tag{2.14}$$

      ○ For the cross-flow IEC:

$$\frac{\partial x_2}{\partial \bar{Y}} = \text{NTU}_2^{''}\left(\frac{1}{\text{Le}_2}\right)\sigma_{p2}\left(x_{p2}' - x_2\right) \tag{2.15}$$

Additionally all mathematical models are supplemented by energy balance equations developed:

> For the airflow/plate surface interface in the dry primary airflow passage 1 (see Fig. 2.2)

$$d\left(\dot{Q}_{plt}^{cond}\right)_{met} = d\dot{Q}_1^s \qquad (2.16)$$

which can be converted using the following set of energy balance equation

$$\begin{cases} d\dot{Q}_{plt}^{cond} = d\left(\dot{Q}_{plt}^{cond}\right)_{met} \\ t'_{p1} \approx \left(t'_{p1}\right)_{met} \approx t_{p1} \end{cases} \qquad (2.17)$$

to the following form

$$\left(\frac{\lambda_{plt}}{\delta_{plt}}\right)\left(t_{p1} - t'_{p2}\right) \approx \alpha_1\left(t_1 - t_{p1}\right) \qquad (2.18)$$

> Overall energy balance for the filling surface (see Fig. 2.2)
  o For the parallel-flow and cross-flow IEC:

$$d\dot{Q}_1^s + d\dot{Q}_2^s = d\dot{Q}_2^l \qquad (2.19)$$

Conversion of Eq. (2.19) gives the following relationship

$$\left(\frac{W_1}{W_2}\right)NTU_1\left(t_{p1} - t_1\right) + NTU_2\left(t'_{p2} - t_2\right) + NTU_2\left(\frac{\sigma_p q^o}{c_p Le}\right)_2\left(x'_{p2} - x_2\right) = 0 \qquad (2.20)$$

The developed sets of differential equations are supplemented by the initial conditions, establishing the initial air stream parameters (Fig. 2.3).

- For the airflow parameters at the entrance to the dry channels (all exchangers: Fig. 2.3):

$$t_1\Big|\begin{matrix} = t_{1i} \\ \overline{X} = 0.0 \\ \overline{Y} = (0.0\ldots1.0) \end{matrix} \quad ; \quad x_1\Big|\begin{matrix} = x_{1i} \\ \overline{X} = (0.0\ldots1.0) \\ \overline{Y} = (0.0\ldots1.0) \end{matrix} \qquad (2.19)$$

- For the airflow parameters at the entrance to the wet channels.
  o For parallel-flow IEC (Fig. 2.3(a)):

$$t_2\Big|\begin{matrix} = t_{2i} = t_{1i} \\ \overline{X} = 0.0 \\ \overline{Y} = (0.0\ldots1.0) \end{matrix} \quad ; \quad x_2\Big|\begin{matrix} = x_{2i} = x_{1i} \\ \overline{X} = 0.0 \\ \overline{Y} = (0.0\ldots1.0) \end{matrix} \qquad (2.20)$$

    ○   For counter-flow IEC (Fig. 2.3(b)):

$$t_2 \begin{vmatrix} = t_{2i} = t_{1i} \\ \bar{X} = 1.0 \\ \bar{Y} = (0.0 \dots 1.0) \end{vmatrix} \quad ; \quad x_2 \begin{vmatrix} = x_{2i} = x_{1i} \\ \bar{X} = 1.0 \\ \bar{Y} = (0.0 \dots 1.0) \end{vmatrix} \quad (2.21)$$

    ○   For regenerative IEC (Fig. 2.3(c)):

$$t_2 \begin{vmatrix} = t_{2i} = t_{1o} \\ \bar{X} = 1.0 \\ \bar{Y} = (0.0 \dots 1.0) \end{vmatrix} \quad ; \quad x_2 \begin{vmatrix} = x_{2i} = x_{1o} = x_{1i} \\ \bar{X} = 1.0 \\ \bar{Y} = (0.0 \dots 1.0) \end{vmatrix} \quad (2.22)$$

    ○   For cross-flow IEC (Fig. 2.3(d)):

$$t_2 \begin{vmatrix} = t_{2i} = t_{1i} \\ \bar{X} = (0.0 \dots 1.0) \\ \bar{Y} = 0.0 \end{vmatrix} ; \quad x_2 \begin{vmatrix} = x_{2i} = x_{1i} \\ \bar{X} = (0.0 \dots 1.0) \\ \bar{Y} = 0.0 \end{vmatrix} \quad (2.23)$$

(a)                         (b)

(c)                         (d)
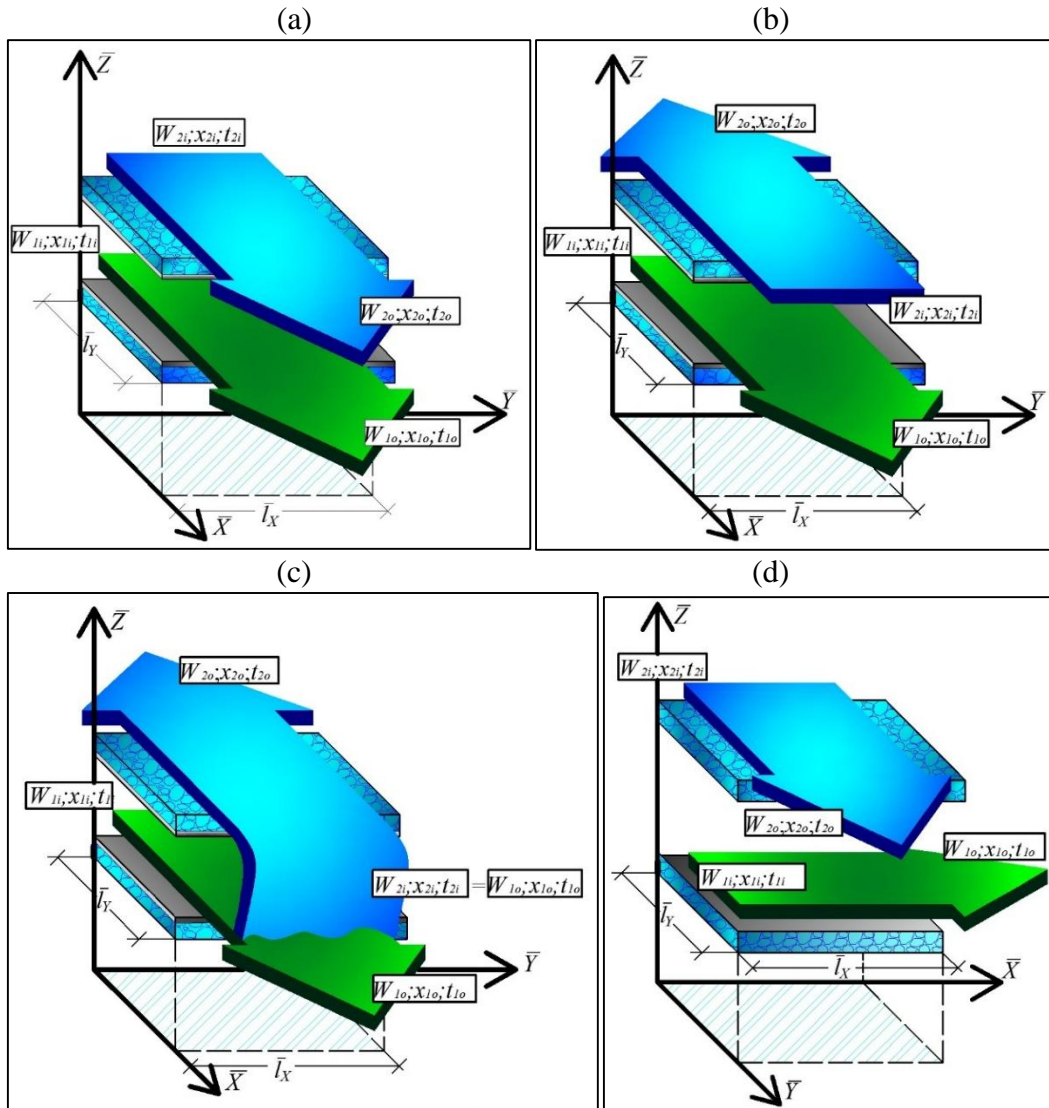


Fig. 2.3. Initial conditions at the entrance to appropriate air channels. (a) Parallel-flow HMX. (b) Counter-flow HMX. (c) Regenerative HMX. (d) Cross-flow HMX.

The presented numerical models are also supplemented by empirical equation describing the relation between water vapor's temperature and it's saturation pressure [113]

$$p^{sat} = 6.107\, exp\left(0.0726t - 2.912\cdot 10^{-4}t^2 + 8.33\cdot 10^{-7}t^3\right) \tag{2.24}$$

The humidity ratio of the water on plate surface is calculated from the Eq. (2.25)

$$x^{sat} = 0.622\frac{p^{sat}}{P_b - p^{sat}}, \text{ kg water/kg dry air} \tag{2.25}$$

The convection heat transfer coefficients are calculated using the Nusselt number. The air streams are assumed as a laminar flow due to the relatively low channel height and relatively low velocity [116], [120]. The Nusselt number is calculated differently in the two thermodynamic regions: the undeveloped region at entrance to the channel ($l \leq l_b$) and the fully-developed flow ($l > l_b$). The length of the first region can be calculated from:

$$l_b/d_h = 0.05\,\mathrm{Re}\,\mathrm{Pr} \tag{2.26}$$

In the first region the Nusselt number is calculated from Eqs. (2.27) or (2.28), which depend on the boundary conditions (height is considered as specific dimension of the channel) [116], [120]:

$$\mathrm{Nu}_{heat}^{Icond} = 1.533\left(\mathrm{Re}_h\mathrm{Pr}\left(h/l\right)\right)^{1/3} \tag{2.27}$$

$$\mathrm{Nu}_{heat}^{IIcond} = 1.755\left(\mathrm{Re}_h\mathrm{Pr}\left(h/l\right)\right)^{1/3} \tag{2.28}$$

For the fully-developed airflow, the Nusselt number is constant [116], [120]. The Nusselt numbers for a rectangular channel are listed below.

$$\mathrm{Nu}_h^{Icond} = 3.77 \tag{2.29}$$
$$\mathrm{Nu}_h^{IIcond} = 4.12 \tag{2.30}$$

Mass transfer coefficient is designated from well-known Lewis relationship [70].
$$\beta = \alpha/\left(c_p\,\mathrm{Le}\right) \tag{2.31}$$

The Lewis factor is obtained on the basis of ratio of the Stanton number for heat transfer to the Stanton number for mass transfer (Sherwood number [70]). The Nusselt numbers may be used instead of the Stanton numbers with a certain approximation [118], [121], [122]:

$$\mathrm{Le} = \mathrm{St}_{heat}/\mathrm{St}_{mass} \approx \mathrm{Nu}_{heat}/\mathrm{Nu}_{mass} \tag{2.32}$$

Increasing the number of channels in modern indirect evaporative air coolers, using combined airflow arrangement, partial wetting of the channel plates cause increasing the longitudinal gradient of the plate temperature, and the pattern of the plate nonisothermality may vary even within the same channel. A longitudinal plate nonisothermality can be described by suitable

function of temperature difference between airflow and plate surface: linear, exponential or combined [12]. All kinds of nonisothermality caused by a deformation of the temperature distribution in the thermal boundary layer make essential impact on heat transfer process in the channels of HMXs. While developing $\varepsilon$-NTU model the above-mentioned effect should be taken into account by introduction of appropriate functional relationship of heat transfer coefficient adequate to changing boundary conditions on the plate surface of the channel. In this regard it is necessary to elaborate on the issue of the Lewis relation unity [121], [122] in the wet channels of indirect evaporative air coolers. It should be noted that it is necessary to have a preliminary information about a character of the longitudinal profile of the temperature and humidity ratio differences between the water film surface and working airflow to determine the values of NTU and Lewis factor, required for the solution of the developed set of differential equations. If one uses a purely pragmatic approach, preference should be given to the iterative process of numerical simulation. In this this case, the shapes of a longitudinal gradients of the temperature and humidity ratio in the dry and wet channels are preliminary assumed. At discrepancy between the assumed and obtained (as result of simulation) character of temperature and humidity ratio profiles, the shapes of a longitudinal gradients should be corrected. Such sequence of iterative computations is being kept until the adequacy of longitudinal heat and mass transfer potentials profiles at the beginning and at the end of iteration has been reached. The developed algorithm was realised in the digital computer program. The computer program evaluation tests were performed with the help of calculations of different variants, describing problems with familiar analytical solutions. The numerical algorithm used to solve the differential equations and flow sheet of programing for the cross-flow evaporative air cooler is presented in **Appendix A**, the validation of the mathematical model describing cross-flow and regenerative air cooler against existing experimental data is presented in **Appendix B**.

## 2.2. Results and discussion

### 2.2.1. Analysis of the Lewis relation

High priority of analyzing the Lewis relation unity is not in doubt, as practically all known numerical studies investigating indirect evaporative coolers in the recent years were based on the assumption that the value of the Lewis relation is equal to 1.0 [2], [22], [50]. On the other hand, "classical" studies performed by Berman [123], [124], Bogoslowski [125], Guhman [126], Kokorin [127] and Maisotsenko [128] revealed a violation of this relationship in a number of cases. An explanation of this phenomenon should be sought in the analysis of the conformity of heat and mass transfer processes realized in the wet channels of IEC to the assumptions made for derivation of the Lewis relation.

A derivation of the Lewis relation is based on the Kirpichov-Guhman theorem, which defines the following similarity conditions [126]: *two phenomena are similar if they are described by the same set of differential equations and have the similar conditions of unambiguity*.

Satisfaction of the first condition for IECs is not in doubt, as heat and mass transfer processes are described by identical differential equations. It should be noted that impact of accompanying exchange phenomena (such as the Stefan flux, thermal diffusion, diffusion thermal conductivity) is negligible for air-vapor mixture under conventional operational conditions of the evaporative units [114], [127], [128].

The similarity conditions for heat and mass transfer processes realized in the wet channels of indirect evaporative heat and mass exchangers includes meeting the following requirements:

- geometrical similarity of the channels and the boundary conditions where the heat and mass transfer process occurs,
- similarity of the temperature and humidity ratio (partial pressure of water vapor) fields,
- similarity of the physical characteristics of the air streams,
- similarity of the velocity and static pressure changes fields.

Evaluation of the implementation of these conditions, conducted by Kokorin [127], confirmed the existence of similarity for the majority of the analysed HMXs. For the purpose of a detailed study of the coupled heat and mass transfer in the channels of IECs under different airflow arrangements we highlighted the first two conditions, the implementation of which is not always evident.

The parallel-flow indirect evaporative coolers are characterized by constant or relatively small changes of water film temperature and changes of the air temperature (Fig. 2.4) and humidity ratio in the working wet channels (Fig. 2.4(f)) are similar to the changes of the airflow thermodynamic parameters observed under adiabatic humidification conditions. In this case, the boundary conditions for the heat and mass transfer are the same along the whole wet channel and the profiles of temperature and the humidity ratio differences are similar up to a sign (Fig. 2.4(b) and (f)). As a consequence of meeting all the similarity conditions, the Lewis relation is equal to unity and the ratio of heat transfer to mass transfer coefficient is constant and equal to the theoretical value ($\alpha/\beta = c_p$).

Counter-flow, cross-flow and regenerative IECs are distinguished by essential changes of the thermodynamic parameters of the water film and coupled heat and mass transfer are characterized by a number of features (Fig. 2.4(a),(c)-(e),(g)-(i)). It should be noted that mass transfer in these exchangers is characterized by constant direction of mass flux in the wet channels and unchanged character of the longitudinal profile of the humidity ratio differences between the water film surface and working airflow (Fig. 2.4(a),(g)-(i)), while sensible heat transfer is characterized by the two active heat transfer zones, in which the heat flux direction changes to the opposite and the characters of the longitudinal profiles of the temperature differences between the air stream and plate surface are different ($2_i-\Omega$ and $\Omega-2_o$ in Fig 2.4(a),(c)-(e)). The working airflow 2 temperature decreases at the initial portion of the wet channel ($2_i-\Omega$ in Fig. 2.4(a),(c)-(e)), reaching a minimum value and then it starts increasing at the final part of the wet portion (segment $\Omega-2_o$ in Fig. 2.4(a),(c)-(e)). At the inlet portion of the wet channels (*first zone* in Fig. 2.4(a),(c)-(e),(g)-(i)) the heat and mass transfer fluxes are

directly opposite and the characters of the longitudinal profile of the temperature and humidity ratio differences between the water film surface and working airflow are different. At the exit part of the wet channels (*second zone* in Fig. 2.4(a),(c)-(e),(g)-(i)) the sensible and latent heat are transferred from the water film surface to the working airflow and the regularities of the changes of the temperature and humidity ratio differences between the water film surface and working airflow are identical. This can be explained as follows: the high values of temperature and humidity ratio differences at the entrance of secondary flow channels ($2_i-\Omega$) cause intensive water evaporation and secondary airflow cooling as a result (Fig. 2.4). At the same time, the plate temperature $t'_{p2}$ gradually increases because virtually constant sensible heat flow from adjacent primary air stream begins to exceed the evaporative cooling effect. Therefore, the temperatures of the secondary air stream $t_2$ and the plate surface at a certain distance from the flow inlet become equal (point $\Omega$ in the Fig. 2.4(a),(c)-(e)). As a result of water film temperature rising on the terminal parts of the plate, the temperature of the plate surface $t'_{p2}$ becomes higher than secondary airflow temperature $t_2$. Thus, the coupled heat and mass transfer process at the exit part of the secondary flow channels is characterized by the change of sensible heat flux direction at unchanged mass flux direction (see Fig. 2.4(a),(c)-(e)).
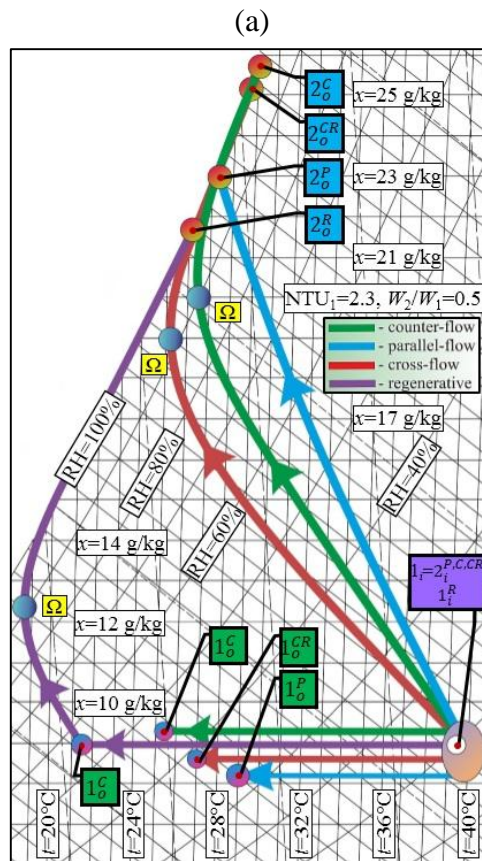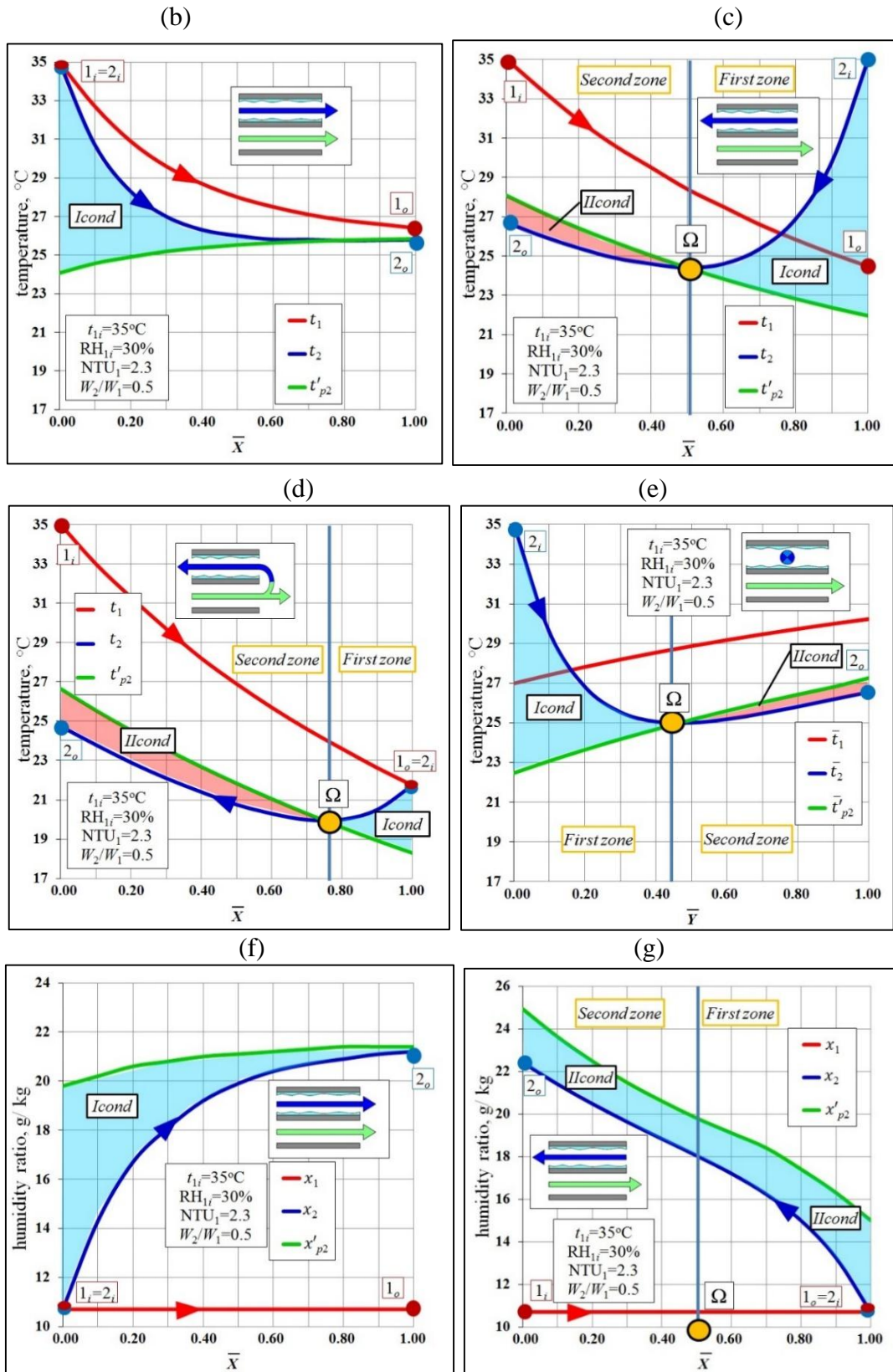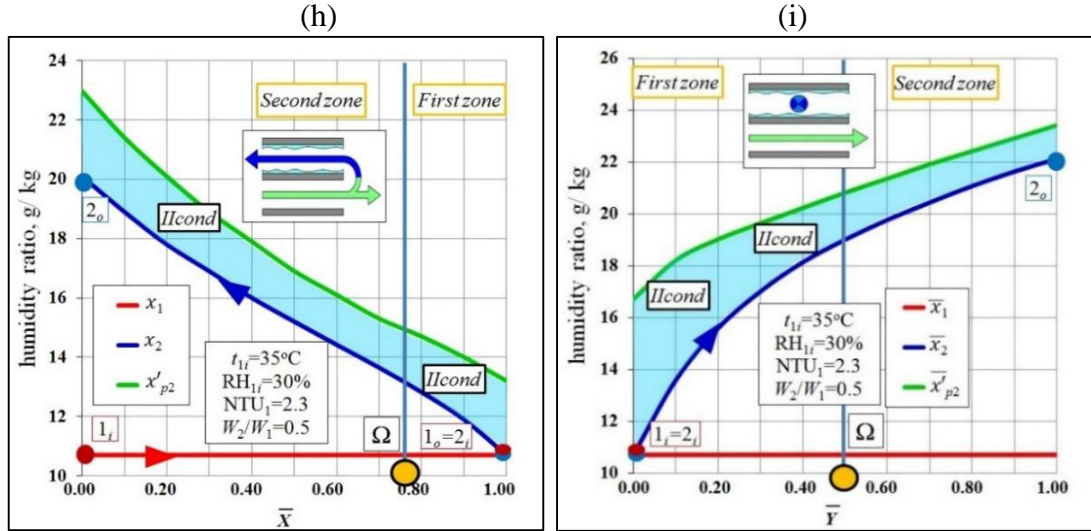
(a)

(b)

(c)

(d)

(e)

(f)

(g)

Fig. 2.4. Combined heat and mass transfer analysis for the basic evaporative cycles. (a) Psychrometric chart. (b) Temperature distribution in parallel-flow IEC. (c) Temperature distribution in counter-flow IEC. (d) Temperature distribution in regenerative IEC. (e) Temperature distribution in cross-flow IEC. (f) Humidity ratio distribution in parallel-flow IEC. (g) Humidity ratio distribution in counter-flow IEC. (h) Humidity ratio distribution in regenerative IEC. (i) Humidity ratio distribution in cross-flow IEC.

Analysis of the longitudinal profile of the humidity ratio differences between the water film surface and working airflow in the wet channels shows that the mass transfer processes are characterized by a linear function of the humidity ratio differences $\Delta x_2 = (x'_{p2} - x_2)$ with respect to the working airflow direction, which corresponds (in accordance with the approach of Žukauskas [120]) to the boundary conditions of the second type ($M \approx$ const).

$$\text{Nu}_{mass} = \text{Nu}_{mass}^{\text{I} zone} = \text{Nu}_{mass}^{\text{II} zone} = \text{Nu}_{mass}^{\text{II} cond} = 4.12$$

(2.33)

Having conducted a similar analysis for the heat transfer processes at the exit part of the wet channels (Fig. 2.4(c)-(e)), it can be concluded that heat transfer in this part of the HMX also occurs under boundary conditions of the second type ($q \approx$ const), thus the value of the Nusselt number for the *second zone* is equal to [116], [120]:

$$\text{Nu}_{heat}^{\text{II} zone} = \text{Nu}_{heat}^{\text{II} cond} = 4.12$$

(2.34)

Unlike the exit portion of the wet channels, heat transfer in the *first zone* is implemented under exponential change of the temperature differences $\Delta t_2 = (t'_{p2} - t_2)$, which corresponds to the boundary conditions of the first type [120]. In this case the Nusselt number is equal to [116], [120]:

$$\text{Nu}_{heat}^{\text{I} zone} = \text{Nu}_{heat}^{\text{I} cond} = 3.77$$

(2.35)
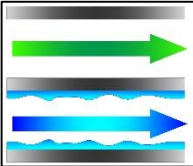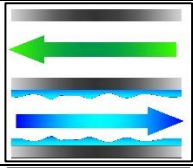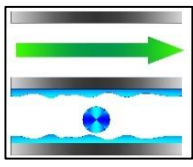
Obtained values of the Nusselt numbers allow for evaluation the Lewis factor values for each heat transfer zone separately:

$$\text{Le}^{\text{I}\,zone} = \text{Nu}_{heat}^{\text{I}\,zone} \Big/ \text{Nu}_{mass}^{\text{I}\,zone} = 3.77/4.12 = 0.91 \neq 1.0 \tag{2.36}$$

$$\text{Le}^{\text{II}\,zone} = \text{Nu}_{heat}^{\text{II}\,zone} \Big/ \text{Nu}_{mass}^{\text{II}\,zone} = 4.12/4.12 = 1.0 \tag{2.37}$$

The obtained results indicate a violation of the unity for the Lewis relation associated with the violation of the similarity of the temperature and humidity ratio differences between the water film surface and working airflow at the intake part of the wet channels. Agreeing with a number of researchers [123], [124], [127] that using the mean logarithmic temperature difference for the heat transfer coefficient evaluation under conditions of changing heat flux direction leads to *pseudo*-violation of the unity for the Lewis relation, which can be avoided by dividing the whole heat and mass exchange surface into parts, it should be noted that in this case, even within separate zones, a *real* violation of unity for the Lewis relation occurs [12], [113]. When comparing the results of numerical simulations obtained in this study and values obtained in experimental studies [118], it was found that Lewis factor varies in a fairly narrow range of values from 0.9 to 1.1 (Table 2.1). It was observed that working to primary air ratio, air inlet parameters and the NTU value have significant impact on the Lewis factor value (Table 2.1). Therefore it is necessary to include appropriate corrections in the mathematical models describing presented indirect evaporative air coolers, to check the Lewis relation unity in every calculation process.

Table 2.1. Lewis factor values for selected $W_2/W_1$ ratios at $t_{1i}$=35°C, RH$_{1i}$=30%, NTU$_1$=2.3

| Exchanger | | $W_2/W_1$= 0.3 | | $W_2/W_1$= 1.0 | | $W_2/W_1$= 2.0 | |
|---|---|---|---|---|---|---|---|
| | | First zone | Second zone | First zone | Second zone | First zone | Second zone |
|  | $\text{Nu}_{heat}$ | 3.77 | - | 3.77 | - | 3.77 | - |
| | $\text{Nu}_{mass}$ | 3.77 | - | 3.77 | - | 3.77 | - |
| | $\text{Le} = \dfrac{\text{Nu}_{heat}}{\text{Nu}_{mass}}$ | 1.0 | - | 1.0 | - | 1.0 | - |
|  | $\text{Nu}_{heat}$ | 3.77 | 4.12 | 3.77 | 4.12 | 4.12 | 4.12 |
| | $\text{Nu}_{mass}$ | 3.77 | 4.12 | 4.12 | 4.12 | 3.77 | 4.12 |
| | $\text{Le} = \dfrac{\text{Nu}_{heat}}{\text{Nu}_{mass}}$ | 1.0 | 1.0 | 0.91 | 1.0 | 1.09 | 1.0 |
|  | $\text{Nu}_{heat}$ | 3.77 | 4.12 | 3.77 | 4.12 | - | - |
| | $\text{Nu}_{mass}$ | 3.77 | 4.12 | 4.12 | 4.12 | - | - |
| | $\text{Le} = \dfrac{\text{Nu}_{heat}}{\text{Nu}_{mass}}$ | 1.0 | 1.0 | 0.91 | 1.0 | - | - |
|  | $\text{Nu}_{heat}$ | 3.77 | 4.12 | 3.77 | 4.12 | 4.12 | 4.12 |
| | $\text{Nu}_{mass}$ | 3.77 | 4.12 | 4.12 | 4.12 | 3.77 | 4.12 |
| | $\text{Le} = \dfrac{\text{Nu}_{heat}}{\text{Nu}_{mass}}$ | 1.0 | 1.0 | 0.91 | 1.0 | 1.09 | 1.0 |

## 2.4.2. Comparative analysis of presented exchangers

In this section the basic evaporative cycles are compared in terms of their cooling effectiveness. Is should be mentioned that basic evaporative air cooling cycle were analyzed by author in many articles, the most important are: [129]- comparative analysis of different regenerative air coolers, [21]- analysis of the counter-flow evaporative air cooler, [130]- analysis of the cross-flow air cooler at different climate conditions, [44], [19]- comparison of the basic evaporative exchangers at different operational conditions, [16]- analysis of two different arrangements of the cross-flow indirect evaporative air cooler. Two efficiency factors were selected as representative to analyze the presented heat exchangers [113]:

- the dew point thermal effectiveness (see. Eq. (1.2) in section 1.6)
- the specific cooling capacity respected to the cubic meter of the unit's structure (where volume of the exchanger structure is given as: $V_{HMX}=2(h+\delta_{plt})l_X\,l_Y$, m$^3$; see. Eq. (1.4) in section 1.6).

Figure 2.5 presents the water film temperature distribution in the primary airflow direction. It can be seen that the plate temperature distribution is characterized by significant changes which cannot be omitted in analysis of considered exchangers. The changes in water film temperature are varying between 1÷4°C for the parallel-flow exchanger (Fig. 2.5(a)), from 6−11°C for the regenerative and the counter-flow exchanger (Fig. 2.5(b) and (c)) and from 2 to 4.5°C for the cross-flow exchanger (Fig. 2.5(d)). In the case of the counter-flow, cross-flow and the regenerative HMX the water film temperature is decreasing in the primary airflow direction, which allows receiving lower outlet temperatures than parallel-flow unit (Fig. 2.5). In this regard a particular attention was paid to the procedure of plate temperature calculation. The values of the local plate temperature $t_p$ satisfied to Eq. (2.20) were determined on each step of integration by means of the Wegstein's iteration method used for solving general nonlinear equations in the form $t_p = f(t_p)$.
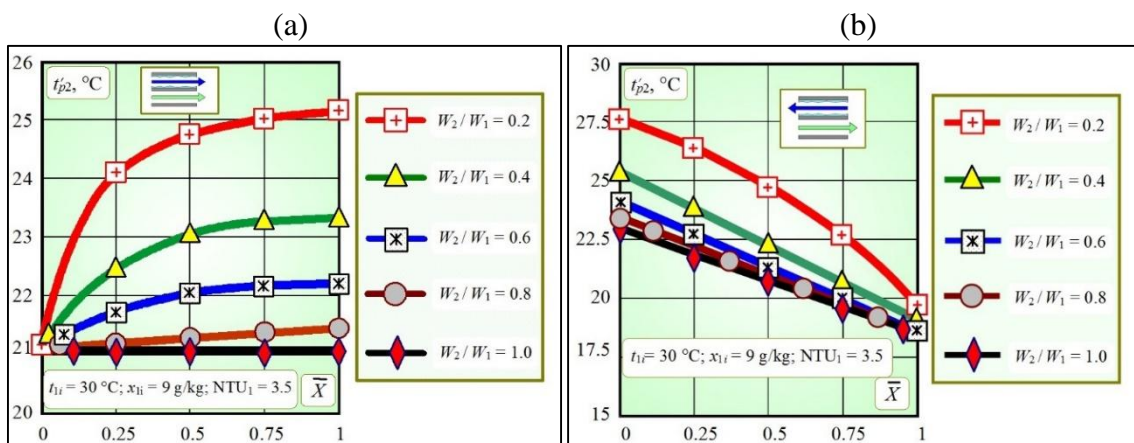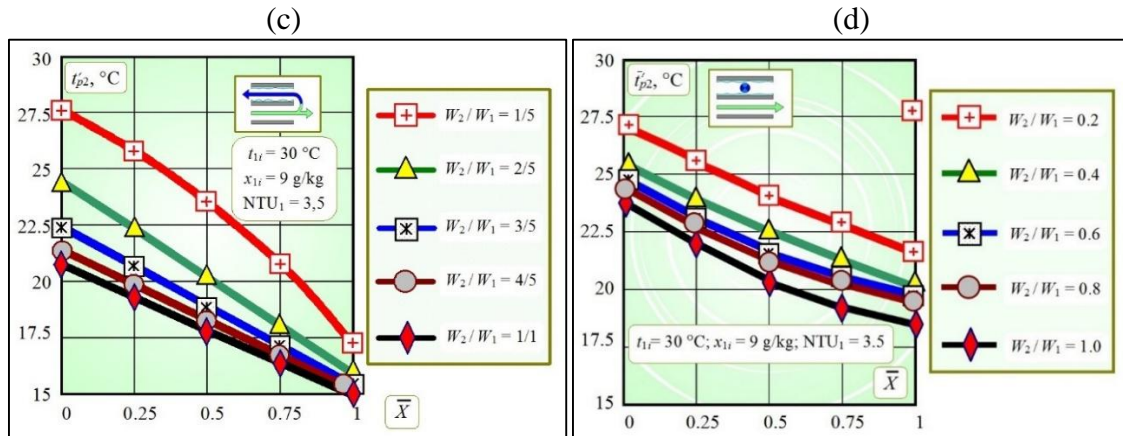
Fig. 2.5. Water film temperature distribution. (a) Parallel-flow IEC. (b) Counter-flow IEC. (c) Regenerative IEC. (d) Cross-flow IEC.

The received dew point temperature effectiveness and specific cooling capacity rate as functions of dimensionless operating parameters ($NTU_1$ number and $W_2/W_1$ ratio) are presented in Figure 2.6. It can be seen that the regenerative exchanger achieves highest dew point effectiveness (Fig. 2.6(a) and (b)). However, the regenerative IEC is characterized by a low values of specific cooling capacity (Fig. 2.6(c) and (d)). This paradoxical effect is caused by the lower final value of the primary airflow rate in the regenerative IEC, because part of the main stream is returned to the working air channel [19], [30], [113]. This follows from the fact that construction of the regenerative air cooler assumes that both the secondary and the primary air streams are flowing through the same dry channel and at the end of the HMX they are separated (the secondary airflow enters the wet channel, while the product airflow is delivered to the conditioned apartments: see Figs. 2.1(d) and 2.3(c)). In the other types of HMXs (i.e. parallel-flow, counter-flow and cross-flow) primary and working air streams are separated before entering the corresponding channels. For example, at constant secondary to primary air ratio equal to 0.5, assuming that inlet primary airflow rate in the dry channel is equal to 1000 m³/h, outlet product airflow for the parallel-flow, counter-flow and cross-flow HMXs will be equal 1000 m³/h, while for the regenerative HMXs only 500 m³/h, because half of the primary airflow has to be returned to the wet channel as working air stream. In case of regenerative unit the product airflow delivered to the conditioned apartments is always smaller than the main airflow at the inlet to the dry channels. The analysis of specific cooling capacity $\hat{Q}$ shows that the structure of regenerative HMXs is used ineffectively: the lower outlet temperature cannot overcome the negative effect of the product airflow reduction, therefore the $\hat{Q}$ indexes for such exchangers are lower than of the typical evaporative air coolers. According to the above specified characteristics of the heat and mass transfer processes in the analyzed heat exchangers it can be assumed that the novel constructions of such devices can be developed to utilize the most advantageous aspects of the basic airflow schemes.
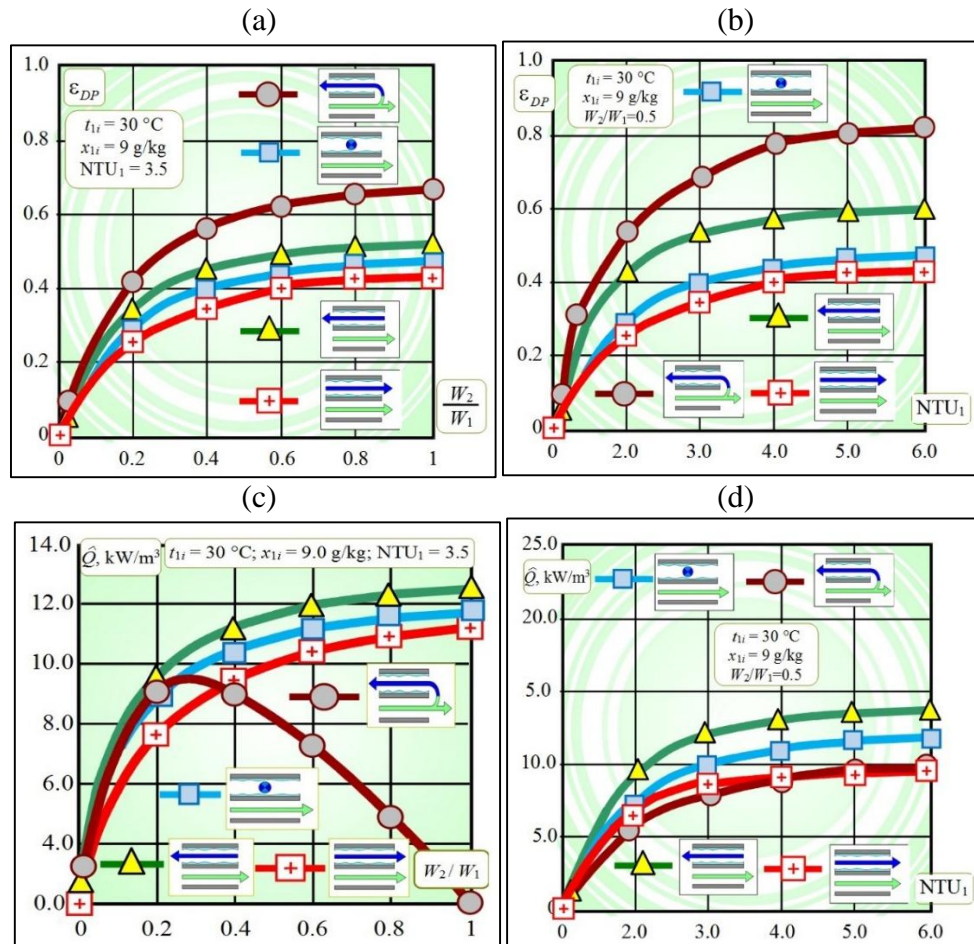
(a)

(b)



(c)

(d)



Fig. 2.6. Characteristic effectiveness indexes as a function of dimensionless operating parameters. (a) Dew point effectiveness as a function of $W_2/W_1$ ratio. (b) Dew point effectiveness as a function of $NTU_1$ number. (c) Specific cooling capacity as a function of $W_2/W_1$ ratio. (d) Specific cooling capacity as a function of $NTU_1$ number.

## 2.5. Conclusions from the section 2

A numerical study describing four different indirect evaporative air coolers (parallel-flow, counter-flow, regenerative and cross-flow) were presented in this section. Simulations were performed on the basis of original mathematical models developed for each exchanger. The obtained results include detail description of the heat transfer processes occurring inside the dry and wet channels and performance analysis of the basic evaporative air coolers.

The main conclusions are listed as follows:

- The coupled heat and mass transfer in parallel-flow exchangers is characterized by the similar temperature and humidity ratio distribution profiles, therefore for these exchangers the Lewis factor is equal to 1.

- Heat and mass transfer processes in the wet channel of cross-flow, counter-flow and regenerative IEC are characterized by creation of two particular heat and mass transfer zones, where the sensible heat flux in the dry channel changes its direction form cooling to heating of the working airflow. Detail analysis of the

temperature and humidity ratio distributions and boundary conditions, characterizing the coupled heat and mass transfer process in each of these determined zones, revels the violation of the Lewis relation unity under a certain inlet and operation conditions.

- o On the basis of above-mentioned conclusions it can be assumed that the mathematical model of the cross-flow M-Cycle air cooler must include the correction coefficient for the Lewis factor in case of the violation of the Lewis relation. The model must also include the assumption of two active heat and mass transfer zones in the working air channels.

- The regenerative M-Cycle heat exchanger allows achieving the highest dew point effectiveness, but it is characterized by lower values of specific cooling capacity due to the fact that primary and working airflow are separated at the end of the dry channel.

- o It can be clearly seen that the Maisotsenko cycle allows for highest thermal effectiveness, however in the regenerative flow arrangement its cooling capacity is very low in compare to the other units. The main challenge in practical application of the M-Cycle air coolers is to find a way to avoid the negative effect of delivering both working and primary air (main airflow) to the same dry channel and spate them at the exit part. From this standpoint the cross-flow M-Cycle air cooler, which is the subject of this thesis is one of the best opportunities, due to the fact that in its case the primary and working airflow are separated at the entrance part of the exchanger (see. Fig. 3.1 in section 3).

## 3. Mathematical model of the cross-flow Maisotsenko cycle heat and mass exchanger

*The results of this section were published in "S. Anisimov, D. Pandelidis, Numerical study of the Maisotsenko cycle heat and mass exchanger, International Journal of Heat and Mass Transfer, 75 (2014) 75–96"* [12]

### 3.1. Initial assumptions

Analysis of the basic evaporative cooling cycles allowed preparing the initial assumptions for the mathematical model of the cross-flow Maisotsenko cycle heat and mass exchanger. The numerical model of the studied unit is presented in this section. Fig. 3.1 shows the general configuration of the Maisotsenko cycle HMX. The working mechanism of the cross-flow M-Cycle exchanger was previously described in section 1.9.

It should be reminded that due to limitations in current manufacturing methods, the real HMX sheet dimensions are not exact and have tolerances associated with them. The working air sheets and product air sheets can be different heights, but on any one sheet, the heights are consistent [46], [112], [131]. In the model, as a simplification, it is assumed that all channels have the same height and width. The schematic structure of the exchanger, along with the nomenclature used for its description is presented in Figure 3.2.(a), whereas the photographs of

the real exchanger, including the general look of the unit, the look of the channels and the plate creating the dry and wet portion of the exchanger are presented in Figs. 3.2.(b)-(e). General assumption of the heat and mass transfer mechanism are identical to the assumptions previously developed for the basic indirect evaporative air cooling cycles (presented in section 2.1).
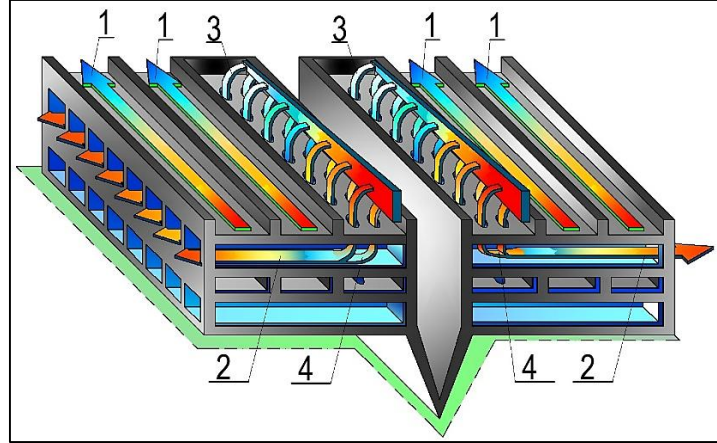


Fig. 3.1. M-Cycle heat and mass exchanger structure. 1: primary airflow. 2: working airflow (wet channels in product part). 3: working airflow (dry channels in initial part). 4: working airflow (wet channels in initial part).

(a)



(b)                                                    (c)

(d) (e)
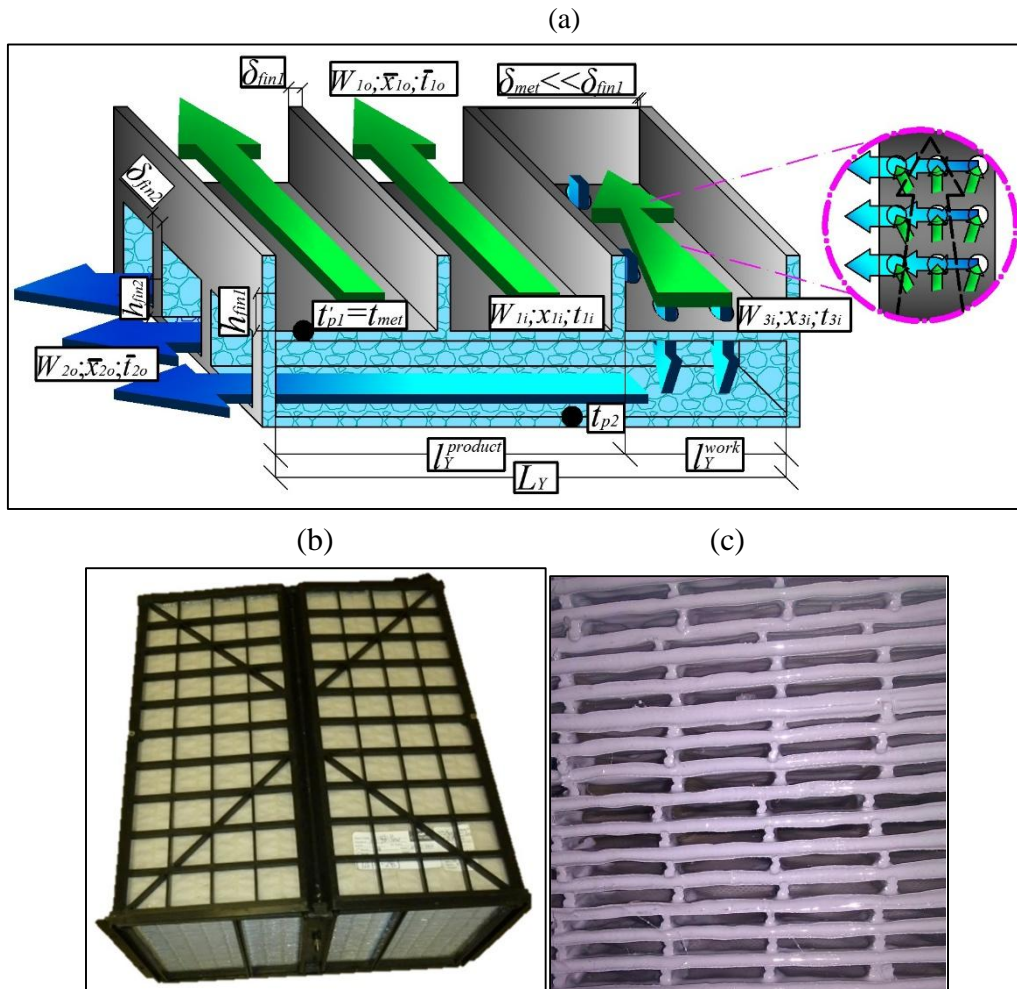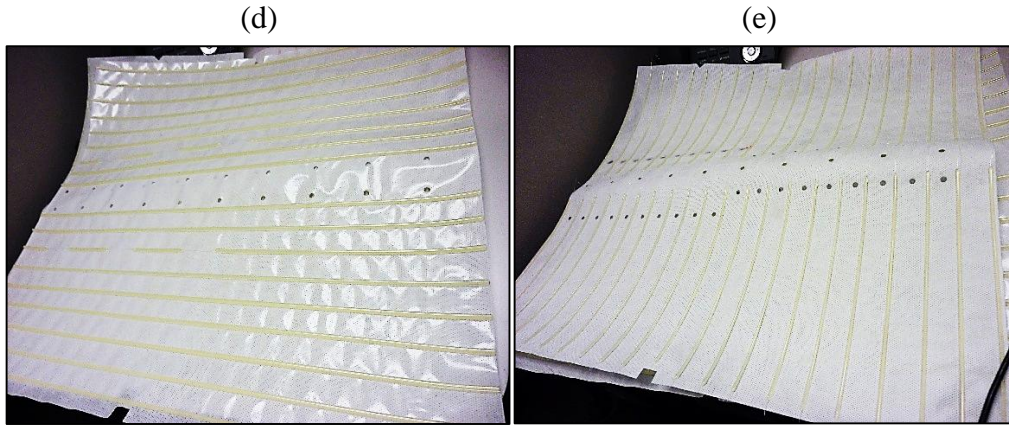


Fig. 3.2. Maisotsenko cycle HMX structure characteristics (all photographs are made by author). (a) Structure of wet and dry channels with nomenclature. (b) General view of the device. (c) Channels structure. (d) Dry channel with coating material. (d) ) Wet channel with wicking material.

### 3.2. Model development

Developing the mathematical model describing M-Cycle HMX requires solving the main problem, connected with algorithmic description of air streams mixing in the initial part of the unit, caused by atypical scheme of airflow management in the channels of considered device. In this connection basic differential equations of heat and mass balance should be supplemented by algebraic equations, describing air streams mixing.
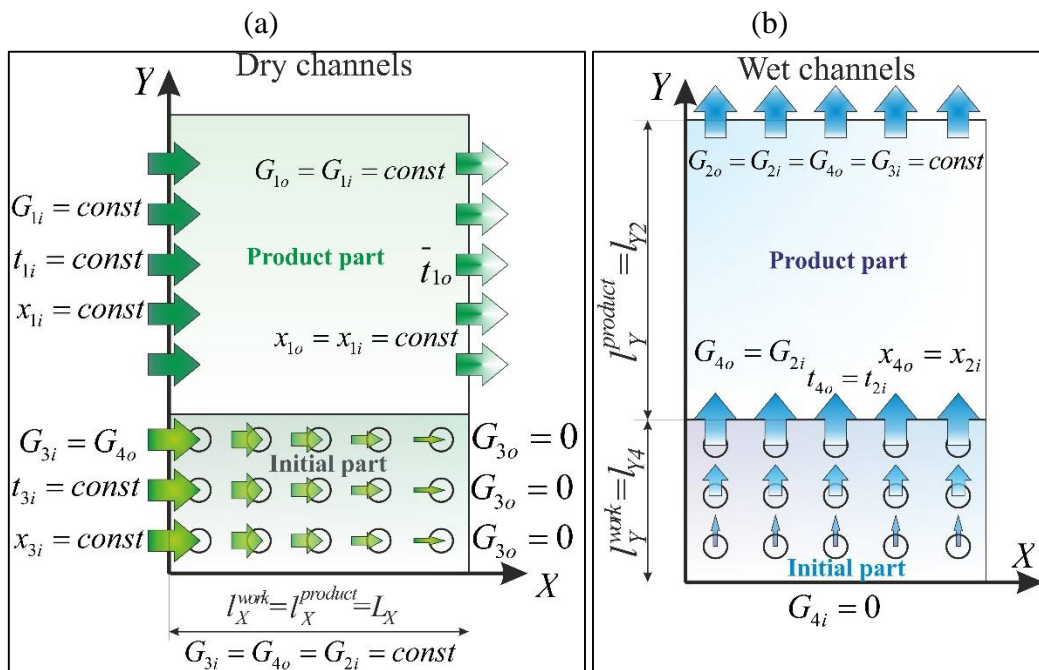
(a) (b)



Fig. 3.3. Maisotsenko Cycle mathematical model assumptions for the air streams. (a) Dry channels. (b) Wet channels.

From the standpoint of the heat and mass transfer processes occurring in the channels M-Cycle HMX can be divided into two main sections: the first one is a typical cross-flow indirect evaporative cooler (product part, which is responsible for cooling the primary airflow:

---

Fig. 3.3(a)), and the second one responsible of pre-cooling of the working airflow and formation of effective temperature distribution at the inlet to the wet channels in the product part of the heat exchanger (Fig. 3.3(b)). In this regard, depending on the section analysed, the working air stream will be considered and marked as three different flows 2, 3, 4 (Fig. 3.3). In the product portion the pre-cooled working airflow 2 is exchanging heat with the primary airflow 1, like in typical cross-flow indirect evaporative cooler (but with non-uniform initial distribution of the working airflow's temperature and humidity ratio at the inlet part of the channel 2). The air stream 3 (dry channels in initial part- Fig. 3.3(a)) and 4 (wet channels in initial part- Fig. 3.3(b)) are responsible for pre-cooling of the working air. The above-mentioned parts of working air will be marked by quantitatively equal air streams 2, 3 and 4, where 2 is the stream in the product air 1, 3 is working air in the dry initial channels and 4 is working air in the wet initial channels. The balance equations for the airflow 3 consider only sensible heat transfer, while set of equations for airflows 2 and 4 describes combined heat and mass transfer. Streams 3 and 4 are mixed in the wet channels in the initial part (Fig. 3.3). Air mass flow rate in the wet passage 4 is increasing parallel to $Y$ axis, because single parts of the stream 3, are delivered separately into the channels, and they are enlarging air stream 4 stream after each hole.

## 3.1. Mathematical model equations

The mathematical model of the cross flow type M-Cycle evaporative cooler was developed on the heat and mass balance considerations in the form of partial differential equations made up for separated air streams and realized in orthogonal coordinate system (Fig. 3.4). The model was made including the result established with the preliminary developed models of the basic evaporative cooling cycles (Section 2). It assumes the different heat transfer characteristics at the beginning and exit part of the wet channels (Fig. 3.4(a)-(d)). The main addition to the model of the cross-flow M-Cycle air cooler are the heat and mass transfer through the structure with fins in the dry and wet channel (Fig. 3.4). The heat transfer through conducting on fins in the dry channel (Fig. 3.4.(e)) and in the wet channel (Fig. 3.4.(c) and (d)) requires solving additional set of differential equations and application of different calculation algorithm for the energy balance.

In this section the mathematical model equations will be presented only for the product part of the exchanger (primary air stream 1 and working air stream 2). This follows from the fact that the general balance equations for the heat and mass transfer in the initial and product part are identical, the only difference lies in the variable NTU number for the air stream 3 and 4, which is caused by the changing airflow rate when parts of air stream 3 are transferred to the wet channel and they are mixing with the air stream 4 (the algorithm of calculation for the initial part is explained in Section 3.2)
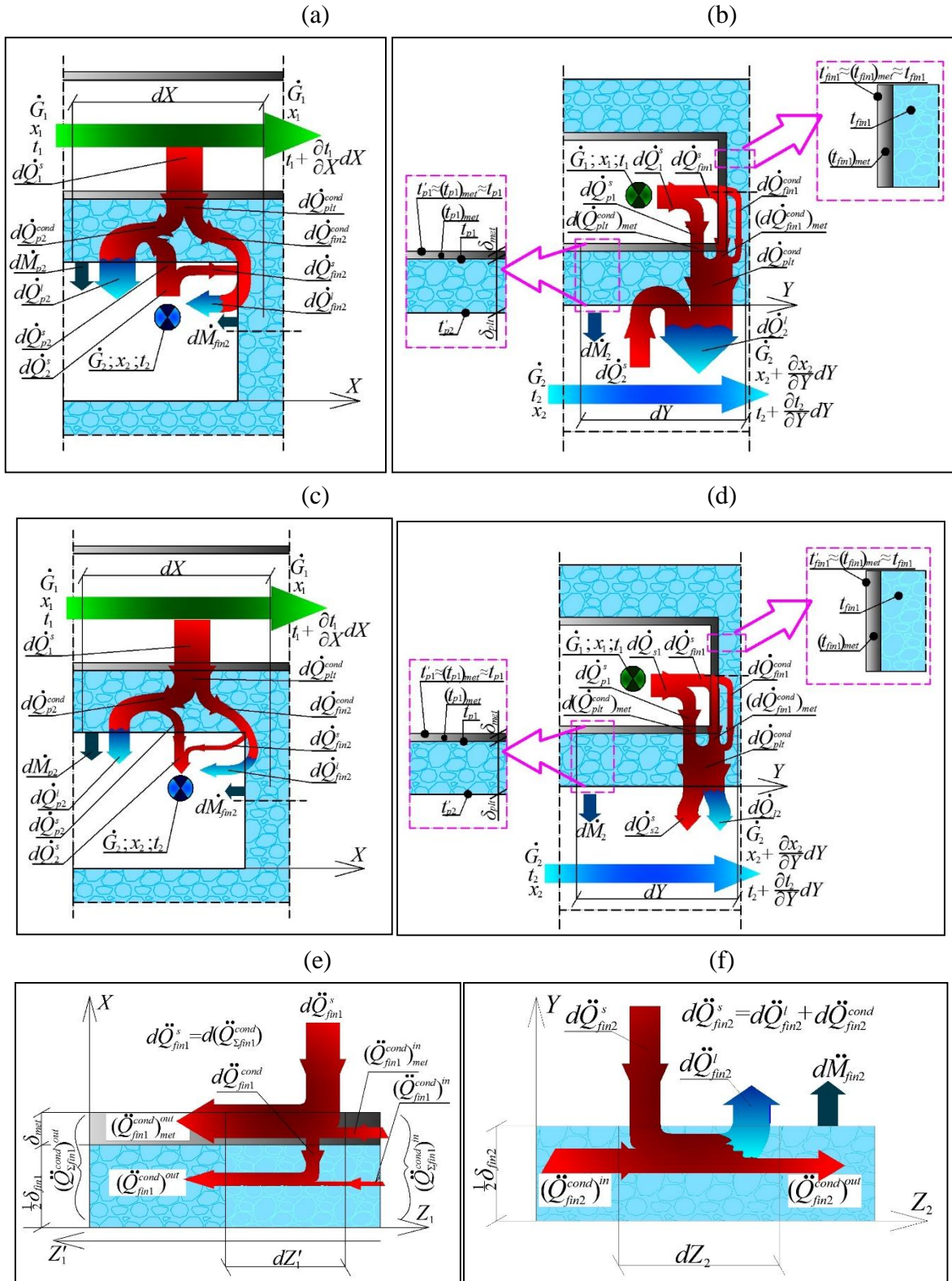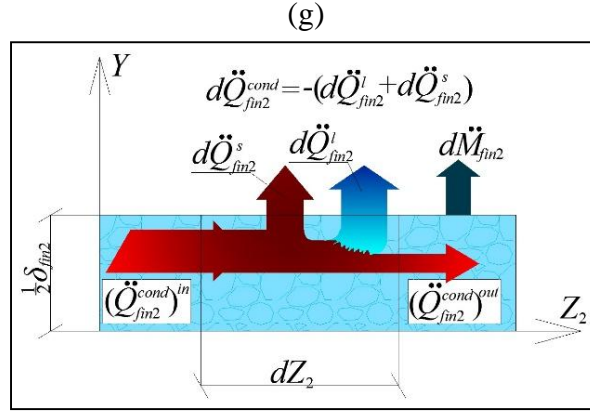
(a)

(b)

(c)

(d)

(e)

(f)

Fig. 3.4. Schematic of heat and mass transfer in differential control volumes in the product part of the investigated HMX. (a) At the entrance part of the wet channel (detail view on the wet channel). (b) At the entrance part of the wet channel (detail view on the dry channel). (c) At the exit part of the wet channel (detail view on the wet channel). (d) At the exit part of the wet channel (detail view on the dry channel). (e) For the dry channel fin. (f) For the wet channel fin at the entrance part of the wet channel. (g) For the wet channel fin at the exit part of the wet channel.

The following balance equations can be written for the air streams passing through control volume in the product part of the HMX (Fig. 3.4 (a)–(g))

- For the air stream in the dry channel:
  - The energy balance considering the sensible heat transfer through the surface of the fin and channel plate (see Fig. 3.4(a)–(d)):

$$\dot{G}_1 c_{p1} \frac{\partial t_1}{\partial X} dX = -d\dot{Q}_1^s = -\left( d\dot{Q}_{p1}^s + d\dot{Q}_{fin1}^s \right) \tag{3.1}$$

where $\dot{G}_1 = (dY/L_Y) G_1$.

Rearranging Eq. (3.1) gives the following relationship

$$\frac{\partial t_1}{\partial \bar{X}} = \mathrm{NTU}_1'' \left( t_{p1} - t_1 \right) \left[ \left( 1 - \frac{\delta_{fin1}}{s_{fin1}} \right) + \frac{2 h_{fin1}}{s_{fin1}} \left( \bar{t}_{fin1} - t_1 \right) \right] \tag{3.2}$$

where $\displaystyle \bar{t}_{fin1} = \int_{\bar{Z}_1 = 0}^{\bar{Z}_1 = 1} \left( t'_{fin1} - t_1 \right) d\bar{Z}_1$

- For the air stream in the wet channel considering the coupled sensible and latent heat transfer through the surface of the fin and channel plate:

  - The energy balance:
    - At the entrance part of the wet passage (Fig. 3.4(a)–(b))

$$\dot{G}_2 c_{p2} \frac{\partial t_2}{\partial Y} dY = -d\dot{Q}_2^s + \left[ c_{g2} \left( t'_{p2} - t_2 \right) d\dot{M}_{p2} + c_{g2} \left( \bar{t}_{fin2} - t_2 \right) d\dot{M}_{fin2} \right] =$$
$$= -\left[ d\dot{Q}_{p2}^s + d\dot{Q}_{fin2}^s \right] + \left[ c_{g2} \left( t'_{p2} - t_2 \right) d\dot{M}_{p2} + c_{g2} \left( \bar{t}_{fin2} - t_2 \right) d\dot{M}_{fin2} \right] \tag{3.3}$$

- At the exit part of the wet passage (see Fig . 3.4(c)–(d))

$$\dot{G}_2 c_{p2} \frac{\partial t_2}{\partial Y} dY = +d\dot{Q}_2^s + \left[ c_{g2} \left( t'_{p2} - t_2 \right) d\dot{M}_{p2} + c_{g2} \left( \overline{t}'_{fin2} - t_2 \right) d\dot{M}_{fin2} \right] =$$
$$= +\left[ d\dot{Q}_{p2}^s + d\dot{Q}_{fin2}^s \right] + \left[ c_{g2} \left( t'_{p2} - t_2 \right) d\dot{M}_{p2} + c_{g2} \left( \overline{t}'_{fin2} - t_2 \right) d\dot{M}_{fin2} \right]$$

(3.4)

where $\dot{G}_2 = (dX/L_X)G_2$, $\overline{t}'_{fin2} = \int\limits_{\overline{Z}_2=0}^{\overline{Z}_2=1} \left( t'_{fin2} - t_2 \right) d\overline{Z}_2$ .

Rearranging Eqs. (3.3) and (3.4) gives the following relationship regardless of the analyzed part of the wet passage

$$\frac{\partial t_2}{\partial \overline{\overline{Y}}} = \mathrm{NTU}_2'' \left( \frac{1}{\overline{l}_{Y2}} \right) \left\{ \left[ \left( 1 - \frac{\delta_{fin2}}{s_{fin2}} \right) \left( t'_{p2} - t_2 \right) + \frac{2h_{fin2}}{s_{fin2}} \left( \overline{t}'_{fin2} - t_2 \right) \right] + \right.$$
$$\left. + \left[ \left( 1 - \frac{\delta_{fin2}}{s_{fin2}} \right) \left( \frac{\sigma_p}{\mathrm{Le}} \right)_2 \left( \frac{c_g}{c_p} \right)_2 \left( t'_{p2} - t_2 \right) \left( x'_{p2} - x_2 \right) + \frac{2h_{fin2}}{s_{fin2}} \left( \frac{1}{\mathrm{Le}_2} \right) \left( \frac{c_g}{c_p} \right)_2 \sigma_{fin2} \left( \overline{t}'_{fin2} - t_2 \right) \left( \overline{x}'_{fin2} - x_2 \right) \right] \right\}$$

(3.5)

➢ The mass balance for the water vapor inside the wet channel considering the evaporation from the plate and fin surface in the wet channel

$$\dot{G}_2 \frac{\partial x_2}{\partial Y} dY = d\dot{M}_2 = \left( d\dot{M}_{p2} + d\dot{M}_{fin2} \right)$$

(3.6)

Rearranging Eqs. (3.6) gives the following differential equation

$$\frac{\partial x_2}{\partial \overline{\overline{Y}}} = \mathrm{NTU}_2'' \left( \frac{1}{\overline{l}_{Y2}} \right) \left( \frac{1}{\mathrm{Le}_2} \right) \left[ \left( 1 - \frac{\delta_{fin2}}{s_{fin2}} \right) \sigma_{p2} \left( x'_{p2} - x_2 \right) + \frac{2h_{fin2}}{s_{fin2}} \sigma_{fin2} \left( \overline{x}'_{fin2} - x_2 \right) \right]$$

(3.7)

where, $\overline{x}'_{fin2} = \int\limits_{\overline{Z}_2=0}^{\overline{Z}_2=1} \left( x'_{fin2} - x_2 \right) d\overline{Z}_2$ .

The energy balance for a differential control volume of the fin in the dry channel can be presented as the heat conduction equation considering only sensible heat transfer on the surface of the fin (see Fig. 3.4 (e))

$$\begin{cases} \left( \ddot{Q}_{\Sigma fin1}^{cond} \right)^{in} + d\ddot{Q}_{fin1}^s = \left( \ddot{Q}_{\Sigma fin1}^{cond} \right)^{out} \\ \left( \ddot{Q}_{\Sigma fin1}^{cond} \right)^{in} = \left( \ddot{Q}_{fin1}^{cond} \right)^{in} + \left( \ddot{Q}_{fin1}^{cond} \right)^{in}_{met} \\ \left( \ddot{Q}_{\Sigma fin1}^{cond} \right)^{out} = \left( \ddot{Q}_{fin1}^{cond} \right)^{out} + \left( \ddot{Q}_{fin1}^{cond} \right)^{out}_{met} \end{cases}$$

(3.8)

Rearranging the set (3.8) and assuming that $t'_{fin1} = \left( t_{fin1} \right)_{met} = t_{fin1}$, the heat conduction equation for the composite fin can be written as

$$\frac{\partial^2 t_{fin1}}{\partial \overline{Z}_1^2} = -m_{fin1}^2 h_{fin1}^2 \left( t_1 - t_{fin1} \right)$$

(3.9)

Where fin temperature coefficient is equal:

$$m_{fin1}^2 = \frac{2\alpha_1}{\lambda_{fin1}\delta_{fin1} + 2(\lambda_{fin1})_{met}(\delta_{fin1})_{met}}$$

(3.10)

Under the following boundary conditions (see Fig. 3.5)

$$t_{fin1}\Big|_{\bar{Z}_1=0} = t'_{p1} = t_{p1} \quad ; \quad \partial t_{fin1}/d\bar{Z}_1\Big|_{\bar{Z}_1=1.0} = 0$$

(3.11)

the differential equation (3.9) can be solved analytically:

$$\left(\frac{\partial t_{fin1}}{d\bar{Z}_1}\right)_{\bar{Z}_1=0} = m_{fin1}h_{fin1}(t_1 - t_{p1})\,\text{th}(m_{fin1}h_{fin1})$$

(3.12)

$$(t_{fin1} - t_1) = (t_{fin1} - t_1)_{\bar{Z}_1=0}\frac{\text{ch}\left[m_{fin1}h_{fin1}(1-\bar{Z}_1)\right]}{\text{ch}(m_{fin1}h_{fin1})} = (t_{p1} - t_1)\frac{\text{ch}\left[m_{fin1}h_{fin1}(1-\bar{Z}_1)\right]}{\text{ch}(m_{fin1}h_{fin1})}$$

(3.13)

Using Eqs. (3.13) the energy balance equation (3.2) can be converted to the final form

$$\frac{\partial t_1}{\partial \bar{X}} = \text{NTU}_1''(t_{p1} - t_1)\left[\left(1 - \frac{\delta_{fin1}}{s_{fin1}}\right) + \frac{2}{m_{fin1}s_{fin1}}\text{th}(m_{fin1}h_{fin1})\right]$$

(3.14)

The energy balance for a differential control volume of the fin in the wet channel should be described taking into account combined sensible and latent heat exchange on the surface of the fin. It should be mentioned that the combined heat and mass transfer equations on the fin surface cannot be solved analytically [12], [78].

> The energy balance at the entrance part of the wet channel (see Fig. 3.4(f))

$$\left(\ddot{Q}_{fin2}^{cond}\right)^{in} + d\ddot{Q}_{fin2}^s = d\ddot{Q}_{fin2}^l + \left(\ddot{Q}_{fin2}^{cond}\right)^{out}$$

(3.15)

> The energy balance at the exit part of the wet channel (see Fig. 3.4(g))

$$\left(\ddot{Q}_{fin2}^{cond}\right)^{in} = d\ddot{Q}_{fin2}^s + d\ddot{Q}_{fin2}^l + \left(\ddot{Q}_{fin2}^{cond}\right)^{out}$$

(3.16)

Rearranging Eqs. (3.15) and (3.16) and assuming that $t'_{fin2} = t_{fin2}$, the following relationship can be obtained (regardless of the analyzed part of the wet channel):

$$\frac{\partial^2 t_{fin2}}{\partial \bar{Z}_2^2} = -m_{fin2}^2 h_{fin2}^2\left[(t_2 - t'_{fin2}) - \left(\frac{\sigma_{fin}}{c_p\text{Le}}\right)_2(x'_{fin2} - x_2)q_{fin2}^o\right]$$

(3.17)

Where the fin temperature coefficient is given as:

$$m_{fin2}^2 = \frac{2\alpha_2}{\lambda_{fin2}\delta_{fin2}}$$

(3.18)

Additionally the M-Cycle mathematical model was supplemented by energy balance equations developed:

➢ For the plate surface in the dry passage considering transfer through coating and wicking material (see Fig. 3.4(b) and (d))

$$d\left(\dot{Q}_{plt}^{cond}\right)_{met} = d\dot{Q}_{p1}^s$$

(3.19)

which can be converted taking into account the following set of energy balance equations

$$\begin{cases} d\dot{Q}_{plt}^{cond} = d\left(\dot{Q}_{plt}^{cond}\right)_{met} + d\dot{Q}_{\Sigma fin1}^{cond} \\ d\dot{Q}_{\Sigma fin1}^{cond} = d\dot{Q}_{fin1}^s \end{cases} \quad ;$$

(3.20)

to the following form:

$$\dot{Q}_{plt}^{cond} = d\dot{Q}_{p1}^s + d\dot{Q}_{fin1}^s$$

(3.21)

Rearranging the Eq. (3.21) and taking into account analytical relationship (3.12), the energy balance (3.19) can be written as:

$$\left(\frac{\lambda_{plt}}{\delta_{plt}}\right)\left(t_{p1} - t'_{p2}\right) = \alpha_1\left(t_1 - t_{p1}\right)\left[\left(1 - \frac{\delta_{fin1}}{s_{fin1}}\right) + \left(\frac{2}{m_{fin1}s_{fin1}}\right)\text{th}\left(m_{fin1}h_{fin1}\right)\right]$$

(3.22)

➢ For the surface of the exchanger structure (the complete energy balance for dry and wet channels)

• At the entrance part of the wet passage (see Fig. 3.4(a)–(b))

$$d\dot{Q}_1^s + d\dot{Q}_2^s = d\dot{Q}_2^l$$

(3.23)

which can be converted to the form

$$\left(d\dot{Q}_{p1}^s + d\dot{Q}_{fin1}^s\right) + d\dot{Q}_{p2}^s = d\dot{Q}_{p2}^l + d\dot{Q}_{fin2}^{cond}$$

(3.24)

• At the exit part of the wet passage (see Fig. 3.4(c)–(d))

$$d\dot{Q}_1^s = d\dot{Q}_2^s + d\dot{Q}_2^l$$

(3.25)

after rearrangement the Eq. (3.25) can be written as:

$$\left(d\dot{Q}_{p1}^s + d\dot{Q}_{fin1}^s\right) = d\dot{Q}_{p2}^s + d\dot{Q}_{p2}^l + d\dot{Q}_{fin2}^{cond}$$

(3.26)

Conversion Eqs. (3.24) and (3.26) gives the following relationship regardless of the

analyzed part of the wet passage

$$\left(\frac{W_1}{W_2}\right)NTU_1''\left(t_1-t_{p1}\right)\left[\left(1-\frac{\delta_{fin1}}{s_{fin1}}\right)+\frac{2}{m_{fin1}s_{fin1}}th\left(m_{fin1}h_{fin1}\right)\right]+NTU_2''\left(t_2-t_{p2}'\right)\left(1-\frac{\delta_{fin2}}{s_{fin2}}\right)=$$

$$=NTU_2''\left(1-\frac{\delta_{fin2}}{s_{fin2}}\right)\left(\frac{\sigma_p q_p^o}{c_p Le}\right)_2\left(x_{p2}'-x_2\right)-NTU_2''\frac{2}{m_{fin2}^2 s_{fin2}h_{fin2}}\left(\frac{\partial t_{fin2}}{\partial \bar{Z}_2}\right)_{\bar{Z}_2=0} \tag{3.27}$$

After simple transformation Eq. (3.27) can be adapted to describe the initial condition for the Eq. (3.17)

$$\left(\frac{\partial t_{fin2}}{\partial \bar{Z}_2}\right)_{\bar{Z}_2=0}=\frac{m_{fin2}^2 s_{fin2}h_{fin2}}{2NTU_2''}\left\{\left(\frac{W_1}{W_2}\right)NTU_1''\left(t_{p1}-t_1\right)\left[\left(1-\frac{\delta_{fin1}}{s_{fin1}}\right)+\frac{2}{m_{fin1}s_{fin1}}th\left(m_{fin1}h_{fin1}\right)\right]+$$

$$+NTU_2''\left(1-\frac{\delta_{fin2}}{s_{fin2}}\right)\left[\left(t_{p2}'-t_2\right)+\left(\frac{\sigma_p q_p^o}{c_p Le}\right)_2\left(x_{p2}'-x_2\right)\right]\right\} \tag{3.28}$$

which significantly simplifies iterative procedure of the local plate temperature computation at each node of integration step.

To complete, the set of simultaneous partial differential equations (3.5), (3.7), (3.9), (3.14), (3.17), (3.22), (3.28) the boundary conditions, establishing initial thermodynamic parameters values of exchanged air streams at the entrance to the appropriate channels of the product part of the heat exchangers (see Fig. 3.3) are needed.

- For the primary airflow at inlet to the dry channel

$$t_1\bigg|_{\substack{\bar{X}=0 \\ \bar{Y}=\bar{l}_{Y4}\div1.0}}=t_{1i} \qquad ; \qquad x_1\bigg|_{\substack{\bar{X}=0\div1 \\ \bar{Y}=\bar{l}_{Y4}\div1.0}}=x_{1i}=const \tag{3.29}$$

- For the working airflow at inlet to the wet channel

$$t_{2i}\bigg|_{\substack{\bar{X}=0\div1.0 \\ \bar{Y}=\bar{l}_{Y4}}}=t_{4o}\bigg|_{\substack{\bar{X}=0\div1.0 \\ \bar{Y}=\bar{l}_{Y4}}}; \qquad x_{2i}\bigg|_{\substack{\bar{X}=0\div1.0 \\ \bar{Y}=\bar{l}_{Y4}}}=x_{4o}\bigg|_{\substack{\bar{X}=0\div1.0 \\ \bar{Y}=\bar{l}_{Y4}}} \tag{3.30}$$

the boundary conditions for the fin in the wet channel (Fig. 3.5):

$$t_{fin2}\bigg|_{\bar{Z}_2=0}=t_{p2}'=t_{p2} \quad ; \qquad \partial t_{fin2}/\partial\bar{Z}_2\bigg|_{\bar{Z}_2=1.0}=0 \tag{3.31}$$

and the boundary conditions for the fin in the dry channel which were previously presented in the Eq. (3.11).
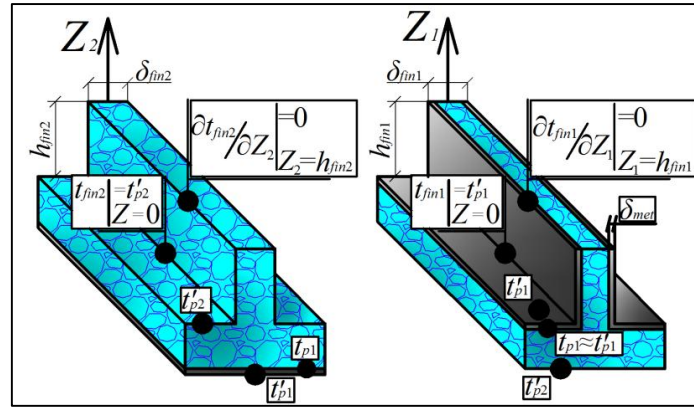
Fig. 3.5. A schematic of the fin geometry and details of thermal boundary conditions for the fins in dry and wet channels.

The developed ε–NTU–model of the heat and mass transfer in the working part of the investigated evaporative cooler are based on the same balance differential equations as for the process part. For this reason the model for the working part of heat exchanger is omitted in the presented work. The difference lies only in the other boundary conditions for the air streams, which are listed below.

- For working air at inlet to the dry channel

$$t_3\bigg|_{\substack{\overline{X}=0 \\ \overline{Y}=0\div\overline{l}_{Y4}}} = t_{3i} = t_{1i} \quad ; \quad x_3\bigg|_{\substack{\overline{X}=0\div1 \\ \overline{Y}=0\div\overline{l}_{Y4}}} = x_{3i} = x_{1i} = const \tag{3.32}$$

- For working air at inlet to the wet channel

$$t_4\bigg|_{\substack{\overline{X}=0\div1.0 \\ \overline{Y}=0}} = t_3\bigg|_{\substack{\overline{X}=0\div1.0 \\ \overline{Y}=0}} ; \quad x_4\bigg|_{\substack{\overline{X}=0\div1.0 \\ \overline{Y}=0}} = x_3\bigg|_{\substack{\overline{X}=0\div1.0 \\ \overline{Y}=0}} = x_{3i} = x_{1i} = const \tag{3.33}$$

Furthermore, during integration of the governing differential equations the variable air mass flow rates in the dry and wet channels caused by permanent mixing of the air from dry channel with the air in the wet channel are included in each node of the elementary control volume. It's worth noting that balance equations for airflow in the dry and wet channels in product and initial part are identical. The only difference is that the NTU of working streams 3 and 4 is variable during the heat and mass transfer processes, because their flow value isn't constant (air stream 3 is decreasing and 4 is increasing).

### 3.3. Mathematical model calculation algorithm

In order to formulate the complete numerical model of the Maisotsenko Cycle heat and mass exchangers, the important final needs to be solved: it is necessary to develop an algorithmic description of the air streams mixing process. This is connected with the unique airflow distribution in the dry and wet channels required to utilize the Maisotsenko Cycle in the cross-

flow exchangers. This section discusses the algorithm which allows calculating the equations in the initial and product part of the exchanger. There are two methods which can be applied to model the processes in the initial part: the assumption of "ideal" perforation (very dense and even, discussed in Section 3.3.1) and the "realistic" perforation with larger holes which don't have to be distributed regularly on the channel plate (this method is presented and discussed in **Appendix C**). Flow sheets of programing for both methods are presented in **Appendix D**, while the root code for the computer program is presented in **Appendix L.**

### 3.3.1. Ideal M-Cycle air cooler (dense perforation)
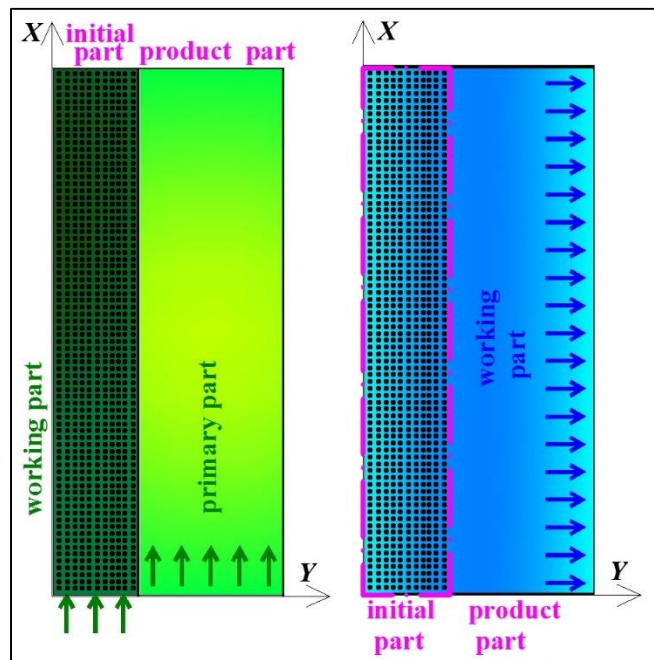


Fig. 3.6. A schematic of the "ideal" perforation in the initial part of the cross-flow Maisotsenko cycle air cooler.

The "ideal" cross-flow Maisotsenko cycle heat and mass exchanger is presented in Figure 3.6. The perforation in the initial part in its case is dense and evenly distributed. The initial and the product part are rectangular both in dry and wet part of the exchanger. The algorithmic description of the initial part of the unit assumes that mixing process is included in the process of integration of differential equations as changing initial conditions in every calculation node.

The algorithm of numerical calculation in the product part of the exchanger is shown in the Fig. 3.7(a). The product part of the heat exchanger is calculated as a typical cross-flow air cooler (with similar algorithm to the previously presented in the section 2.2). Processes in the working part of the heat exchanger (Fig. 3.7(b) and (c)) are more complicated, due to the fact that air streams 3 and 4 are mixing in the wet channel. For this reason the calculation process is shown for the single cells in the dry and wet channel: working air processes description is analyzed for air stream 3 and 4 separately. The air stream 4 in the wet channel is considered at first (Fig. 3.7(b)).

(a)
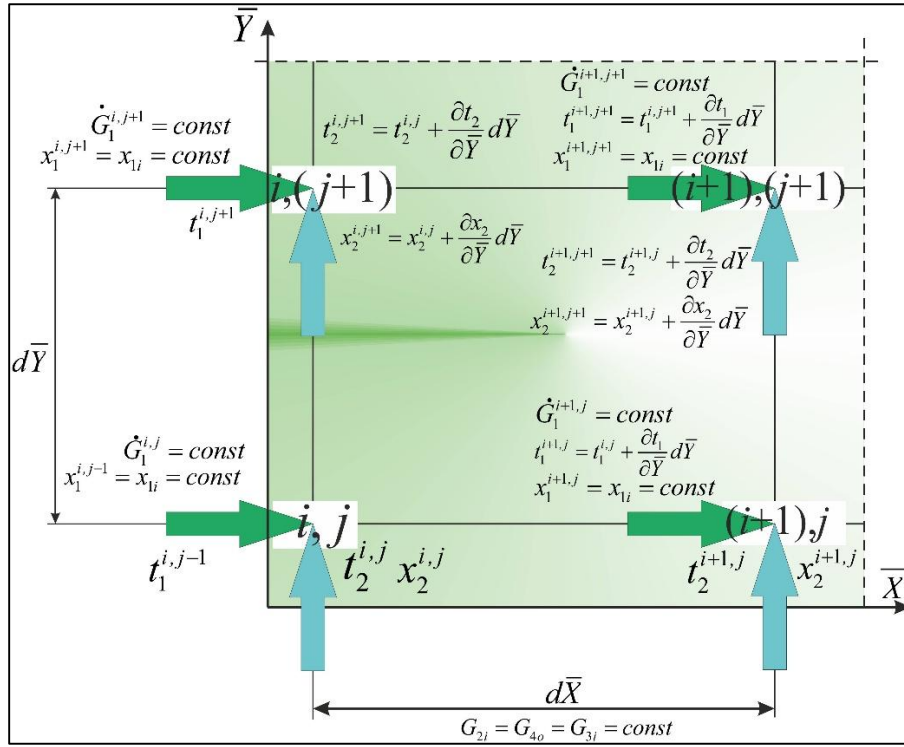


(b)
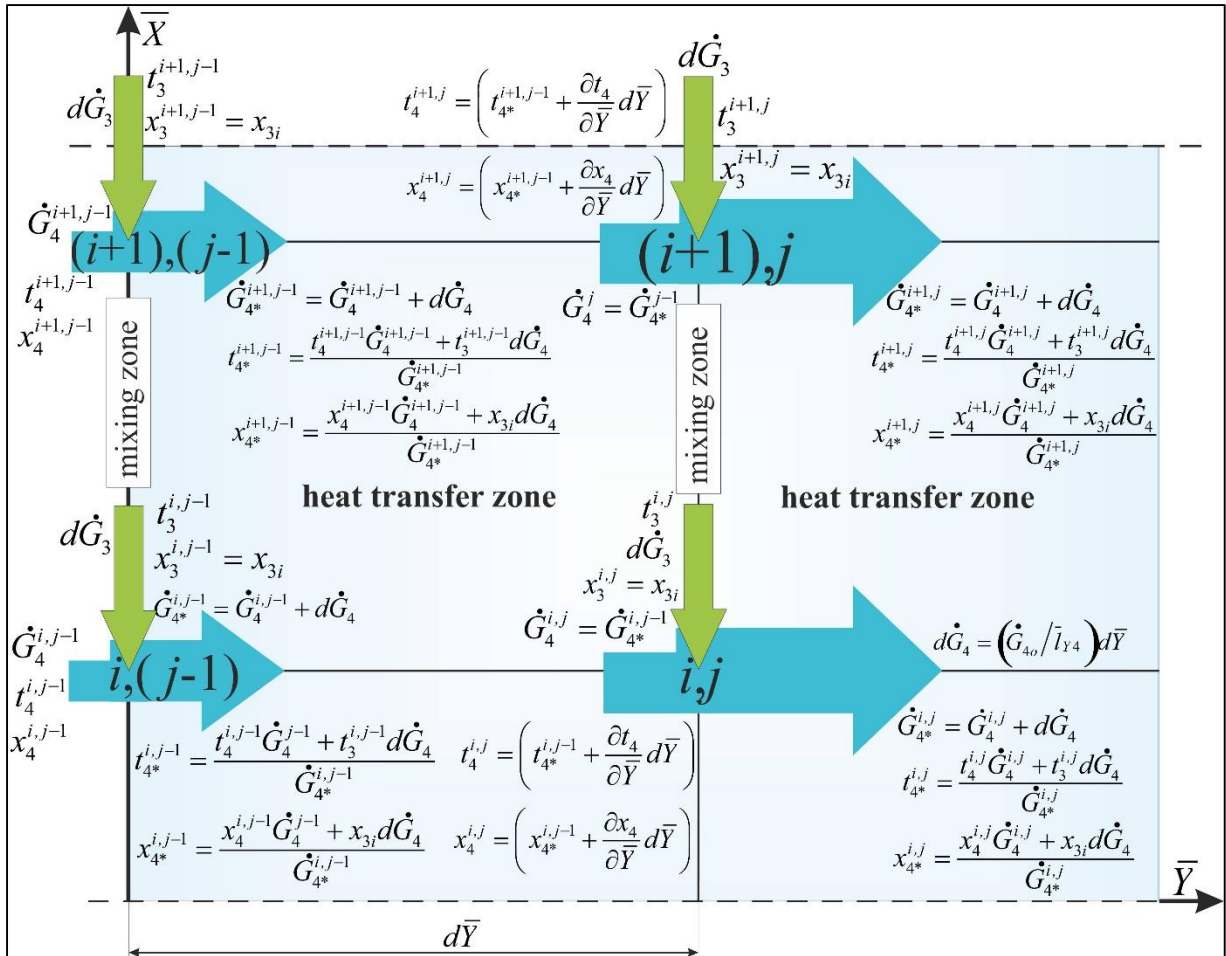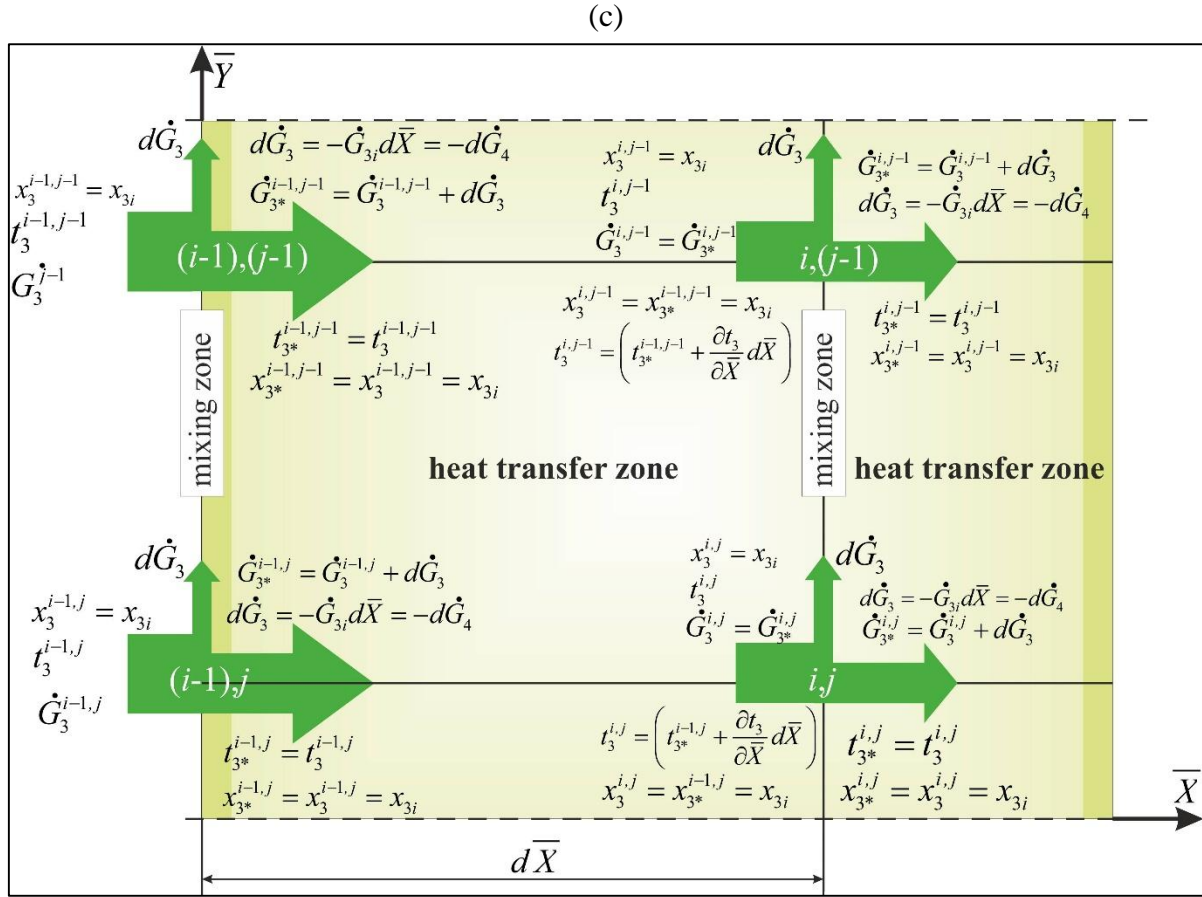
(c)



Fig. 3.7. Maisotsenko Cycle mathematical model calculation algorithm illustrations. (a) Processes in the product part. (b) Processes in the wet channels of the initial part (working air stream 4). (c) Processes in the dry channels of the initial part (working air stream 3).

The initial calculation nodes are $(i,j-1)$ and $(i+1,j-1)$. The nodes are entered by two elementary parts of the air stream 4 with parameters: $t_4^{i,j-1}$; $t_4^{i+1,j-1}$ and $x_4^{i,j-1}$; $x_4^{i+1,j-1}$.

In the first node: $(i,j-1)$, <u>there are two unitary air streams at its entrance: part of the air stream 4</u>, with parameters $t_4^{i,j-1}$ and $x_4^{i,j-1}$ <u>and unitary part of the air stream 3</u> $(d\dot{G}_3)$, with parameters $t_3^{j-1,i}$ and $x_3^{j-1,i} = x_{3i}$. Precisely in node $(i,j-1)$ those <u>unitary streams are mixed</u> (mixing zone in the Fig. 3.7(b)) and the <u>airflow 4 is increased</u> by the value of $d\dot{G}_3$ and it is equal: $\dot{G}_{4*}^{i,j-1} = \left(\dot{G}_4^{i,j-1} + d\dot{G}_4\right)$, where index "*" indicates the conditions after mixing. The final <u>parameters of the air stream 4*</u> can be defined from the heat and mass balance when mixing humid air with the algebraic equation:

$$t_{4*}^{i,j-1} = \frac{t_4^{i,j-1}\dot{G}_4^{i,j-1} + t_3^{j-1,i}d\dot{G}_4}{\dot{G}_{4*}^{i,j-1}} \tag{3.34}$$

where $d\dot{G}_4 = -d\dot{G}_3$ − is the part of the air stream 3 delivered from the dry channel.

The humidity ratio of air stream 4 has changed as follows:

$$x_{4*}^{i,j-1} = \frac{x_4^{i,j-1}\dot{G}_4^{i,j-1} + x_3^{j-1,i}d\dot{G}_4}{\dot{G}_{4*}^{i,j-1}} \tag{3.35}$$

Analogously, parameters of elementary air stream 4 in node $(i+1,j-1)$ after mixing are given as:

$$t_{4*}^{i+1,j-1} = \frac{t_4^{i+1,j-1}\dot{G}_4^{i+1,j-1}+t_3^{j-1,i+1}d\dot{G}_4}{\dot{G}_{4*}^{i+1,j-1}}; \; x_{4*}^{i+1,j-1} = \frac{x_4^{i+1,j-1}\dot{G}_4^{i+1,j-1}+x_3^{j-1,i+1}d\dot{G}_4}{\dot{G}_{4*}^{i+1,j-1}} \tag{3.36}$$

Before the next calculation node, the air stream 4 exchanges heat with air stream 3 in the dry channel, therefore <u>its humidity ratio changes</u> by the value $\frac{\partial x_4}{\partial \bar{Y}} d\bar{Y}$ and its temperature changes by the value $\frac{\partial t_4}{\partial \bar{Y}} d\bar{Y}$ (heat transfer zone in the Fig. 3.7(b)). The <u>final parameters</u> of the air stream 4 after this processes, which become the <u>beginning parameters in the next calculation nodes</u> $(i,j)$ and $(i+1,j)$, can be calculated from the equations:

$$t_4^{i,j} = \left(t_{4*}^{i,j-1} + \frac{\partial t_4}{\partial \bar{Y}} d\bar{Y}\right); \qquad x_4^{i,j} = \left(x_{4*}^{i,j-1} + \frac{\partial x_4}{\partial \bar{Y}} d\bar{Y}\right) \tag{3.38}$$

$$t_4^{i+1,j} = \left(t_{4*}^{i+1,j-1} + \frac{\partial t_4}{\partial \bar{Y}} d\bar{Y}\right) \qquad x_4^{i+1,j} = \left(x_{4*}^{i+1,j-1} + \frac{\partial x_4}{\partial \bar{Y}} d\bar{Y}\right) \tag{3.39}$$

In the next calculation node $(i,j)$, considered elementary air stream is mixed again with the part of the air stream 3 $(d\dot{G}_3)$ with parameters $t_3^{j,i}$ and $x_3^{j,i} = x_{3i}$ (mixing zone in the Fig. 3.7(b)). Airflow 4 increases and it is equal $\dot{G}_{4*}^{i,j} = \dot{G}_4^{i,j} + d\dot{G}_4$. The values of temperature and humidity ratio are calculated using the same method as in case of node $(i,j-1)$. After mixing, before the next calculation node, air stream 4 exchanges heat and mass which results in temperature changing by the value $\frac{\partial t_2}{\partial \bar{Y}} d\bar{Y}$ and humidity ratio by $\frac{\partial x_2}{\partial \bar{Y}} d\bar{Y}$ and so on. Parameters in other calculation steps are designated analogously.

<u>The final value of the air mass flow rate $\dot{G}_{4o}$ is equal to the air mass flow rate $\dot{G}_{2i}$ at inlet to the working air channel in the product part of the heat exchanger:</u> $\dot{G}_{4o} = \dot{G}_{2i} = \dot{G}_{3i} = \dot{G}_{2o} = const$ (see Fig. 3.3). Moreover, <u>the inlet parameters of the air stream 2 are equal to</u> the outlet parameters of the <u>air stream 4 in the inital part of the heat exchanger</u> (Fig. 3.3): $t_{2i} \dot{=} t_{4o}$, $x_{2i} \dot{=} x_{4o}$.

Processes in the dry channels of the initial part (for air stream 3) are less complicated, <u>because airflow mixing is realized only in the wet channel 4 of the initial part of the heat exchanger</u> (see Figs. 3.1, 3.2(a), 3.3 and 3.7(c)). Heat transfer in the dry channel of the initial part is analyzed using on an example cell with 4 nodes (Fig. 3.7(c)), starting points for calculation process are $(j-1,i-1)$ and $(j,i-1)$. Let us consider single node $(j,i-1)$. At the entrance the air stream 3 has following parameters: $t_3^{i-1,j}$ and $x_3^{i-1,j}$. In the point $(j,i-1)$ <u>elementary part of the airflow 3 equal $d\dot{G}_3$ with temperature $t_3^{i-1,j}$ and humidity ratio $x_3^{j,i-1}$ is separated from the air stream 3 and it is delivered to the wet channel</u>, where it is mixed with the air stream 4 (mixing zone Fig. 3.7(b), (c)). The airflow 3 is decreased by the value of $d\dot{G}_3 = -d\dot{G}_4$. It is assumed that the <u>airflow 3 does not change its temperature during the mixing process</u> ($t_3^{j,i-1} = t_{3*}^{j,i-1}$), <u>humidity ratio also remains unchanged</u> ($x_3^{j,i-1} = x_{3*}^{j,i-1}$). <u>Before the next calculation</u>

node the air streams 3 and 4 are exchanging heat: temperature of the flow 3 is changed by the value $\frac{\partial t_3}{\partial \bar{X}} d\bar{X}$ (heat transfer zone- Fig. 3.7(c)). Humidity ratio of the airflow 3 is always constant, because this air stream is in the dry channel ($x_{3i} = x_3^{i,j} = x_{3*}^{i-1,j} = const$) where no mass transfer occurs. The final temperature of the air stream 3 before the next calculation step (initial condition for the next step) is equal: $t_3^{j,i} = t_3^{j,i-1} + \frac{\partial t_3}{\partial \bar{X}} d\bar{X}$. In the next calculation node ($j,i$) part of the air stream $d\dot{G}_3$ with the parameters $t_3^{j,i}$ and $x_3^{j,i}$ is separated and delivered to the wet channel and so on. Parameters in other calculation steps are designated analogously: the final conditions after previous calculation node are always the initial conditions for the next calculation step.

Final air mass flow rate $\dot{G}_3$ at the end of the dry part is equal to zero, due to the fact that airflow 3 is entirely delivered to the wet channel 4 (see Fig. 3.3).

## 4. Validation of the mathematical model

*The results of this section were published in "S. Anisimov, D. Pandelidis, A. Jedlikowski, V. Polushkin, Performance Investigation of a M-Cycle cross-flow heat exchanger used for indirect evaporative cooling, Energy, 76 (2014) 593–606 " [132] and "S. Anisimov, D. Pandelidis, Numerical study of the Maisotsenko cycle heat and mass exchanger, International Journal of Heat and Mass Transfer, 75 (2014) 75–96" [12].*


Mathematical model of the M-Cycle air cooler was validated both against data obtained from author's own experimental research (Section 4.1) and by existing experimental data (**Appendix F**). In both cases the model achieved satisfying accuracy which allowed it to be used for analysis of the real M-Cycle air cooler.

### 4.1. Validation against author's experimental data

### 4.1.1. Description of the measurement station

Author performed experimental study on the measurement station provided by the Coolerado Corporation in Denver, CO, USA. The testing bench was created according to the ASHRAE Standard 133-2001 for testing the evaporative air coolers [133].

Operating conditions were simulated by placing the HMX inside a test chamber ( Fig. 4.1). The desired inlet airflow parameters are provided by an air preconditioning unit which is consist of: supply fan F2, an electrical heater H and a vapor air humidifier VH (Fig. 4.1(a),(d) and (f)). The pretreated airflow is delivered to the HMX by the main fan (F1 in Fig. 4.1(a), (b) and (c)). Airflow is filtered before it enters the HMX (AF in Fig. 4.1(a), (b) and (c)). The ratio of working to primary air mass flow rate is controlled by auxiliary fans (SF, EF in Fig. 4.1(a) and (c)) and a set of previous calibrated orifice plates on both the product and exhaust side of the HMX (SI and EI in Fig. 4.1(a) and (c)). The airflow rate is measured upon the pressure drop on each orifice plate by manometer (Ma in Fig. 4.1(a) and (g)). The accuracy of the airflow characteristics of the orifice plates was tested and pre-calibrated by comparing the results with

the results obtained from measuring the same airflows with ANSI ASHRAE Standard 143-2007 Test Chamber with accuracy of 1.0%. In order to additionally raise HMX inlet air humidity, exhaust air could also be turned back to the testing chamber, by switching the damper (D in Fig. 4.1(a)). Water is delivered to the exchanger directly from the pipeline (WS in Fig. 4.1(c)).

Three sets of experiments were conducted in the following form:

1. Variable inlet air conditions ($t_{1i}$ and $x_{1i}$), other parameters remain unchanged.
2. Variable air mass flow rates ($G_1$ and $G_2$), other parameters remain unchanged.
3. Investigation of local temperature and humidity ratio distribution of the airflows inside the dry and wet channels of the exchanger.

To evaluate the performance of the investigated evaporative air cooler the following relevant parameters were measured:

- Dry and wet bulb temperature (DB and WB in Fig. 4.1(a) (c) and (e)) of the airflow entering and leaving the exchanger (dry and wet channels).
- Pressure drop at the orifice plates to calculate the airflow rate.
- Temperature of the airflow inside the dry (DB) and wet channel (DB and WB) at several measurement points (for experiment number 3: Fig. 4.1(h)).

Measurement equipment was installed in the key points of the experimental setup (Fig. 4.1). The studies were performed under steady-state conditions when all the measured values exhibited negligible change over a long period. Each experiment was repeated to ensure consistency (and repeatability) of the measured data.

Inlet and outlet dry and wet bulb temperatures are measured with the VWR Traceable thermometer (accuracy 0.5°C, WB and DB in Fig. 4.1(a) and (b)). In the channels of heat exchanger dry and wet bulb temperatures are measured with Omega K-type thermocouple, ungrounded (accuracy 0.5°C), OMEGACLAD XL sheath, 1.55 mm probe diameter with ceramic mini connector (part number: SCAXL-062U-22SHX). The thermocouple is connected to a Fieldpiece ATH4 accessory head and then to a Fieldpiece HS26 stick meter with a digital readout. In order to measure the wet bulb temperature in the working air channels of the exchanger the probe of the manometer was covered with porous primer paint and wetted with water. This allowed keeping the probe wetted with water inside the channels. Thermocouple covered with primer paint was pre-calibrated for measuring the wet bulb temperature by comparing the readings from this thermocouple and analogous thermocouple covered with wetted material as typical wet bulb measuring thermometer (Fig. 4.1(h)). The readings were identical, therefore the probe covered with porous paint is considered as accurate to measure the wet bulb temperature inside the channels of the exchanger. The same method was also used by Zube and Gillan to study the cross-flow M-Cycle heat and mass exchanger with experimental methods [46]. Coolerado Corporation takes care about the appropriate calibration and accuracy of the measurement devices in order to keep the experimental data most valid for their production and to satisfy the ASHRAE standards [46]. Thermometers and thermocouples were pre-calibrated and verified before the tests in an isothermal bath using a precise sensors with the accuracy of 0.2°C and achieved very good agreement, therefore their accuracy will be considered as 0.2°C.

The dimensions of the exchanger used in the experiment are listed in Table 4.1. It should be reminded that even though the sizes of the channels in the tested exchanger are not identical, due to the manufacturing methods used by Coolerado Corporation, they are assumed to be the same for all of the channels.

Table 4.1. Assumed exchanger construction parameters

| Channel type | Flat, rectangular |
|---|---|
| Channel height | 3.2 mm |
| Coating material | Polyethylene ($\lambda$= 0.6 W/(m K)) |
| Coating material thickness | 0.02 mm |
| Wicking material | Cellulose fibre ($\lambda$=0.04 W/(m K)) |
| Plate thickness | 0.4 mm |
| Exchanger length | 0.50 m |
| Exchanger width | 0.22 m |
| Channel width | 25 mm |
| Fins width | 1.9 mm |
| Number of dry and wet channels | 42 |

(a)

(b)



(c)

(d)



(e)                                                                              (f)



(g)                                                                              (h)



Fig. 4.1. Testing bench at Coolerado Corporation facilities in Denver, CO, USA (all photographs are made by author). (a) General scheme of the measurement station. (b) Photo of the bench inside the test chamber. (c) Three-dimensional visualization of the testing bench inside test chamber with all equipment. (d) Three-dimensional visualization of the pre-condition unit. (e) Thermometers used in the experiment. (f) Photo of the testing chamber. (g) Manometer used in the experiment. (h) Calibration of the Omega K-type thermocouple used for measuring the wet bulb temperature inside the channels of the exchanger (comparison of probe with the primer paint and probe cover with wetted material).

Note the naming convention relative to the "right" and "left" side of the HMX with respect to the symmetry plane (see Fig. 1.26). Since the physical performance is the same on either side of the symmetry plane, temperature measurements of the airflow inside the exchanger were taken only on the right half of the HMX.

To simplify the data collection and analysis, only one set of complementary dry (product) and wet (exhaust) plates is chosen on the right half of the HMX (Fig. 4.2) to represent the performance of the air inside the channels. This assumes the performance of each layer, or set of half-plates, within the HMX does not change across the vertical height of the stack, or across the plane of symmetry. It also assumes the quantity of heat transferred way from the product channel is split evenly between the two exhaust channels that run both above and below it. These assumptions are verified using an infrared camera to visually inspect the product exit temperature profile of the entire HMX (see Fig. 4.2(c) and (d)). The measurement locations for each product and exhaust plate are taken according to a carefully chosen two-dimensional grid, set in the horizontal plane (see Fig. 4.2(e)-(h)).Measurements are taken at each alphanumeric node location, where the individual grids are overlaid on top of each of their respective product and exhaust half-plates.

The analysis of the accuracy of the performed experiment, along with checking the energy balance between primary and working airflow during measurements is presented in **Appendix E**. Equation (4.1) was used to calculate the discrepancies (this method was used in other studies connected with indirect evaporative air cooling, e.g. [60]).

$$((\bar{t}_{1o})^{\text{experiment}} - (\bar{t}_{1o})^{\text{model}} / (\bar{t}_{1o})^{\text{experiment}}) \cdot 100\% \qquad (4.1)$$
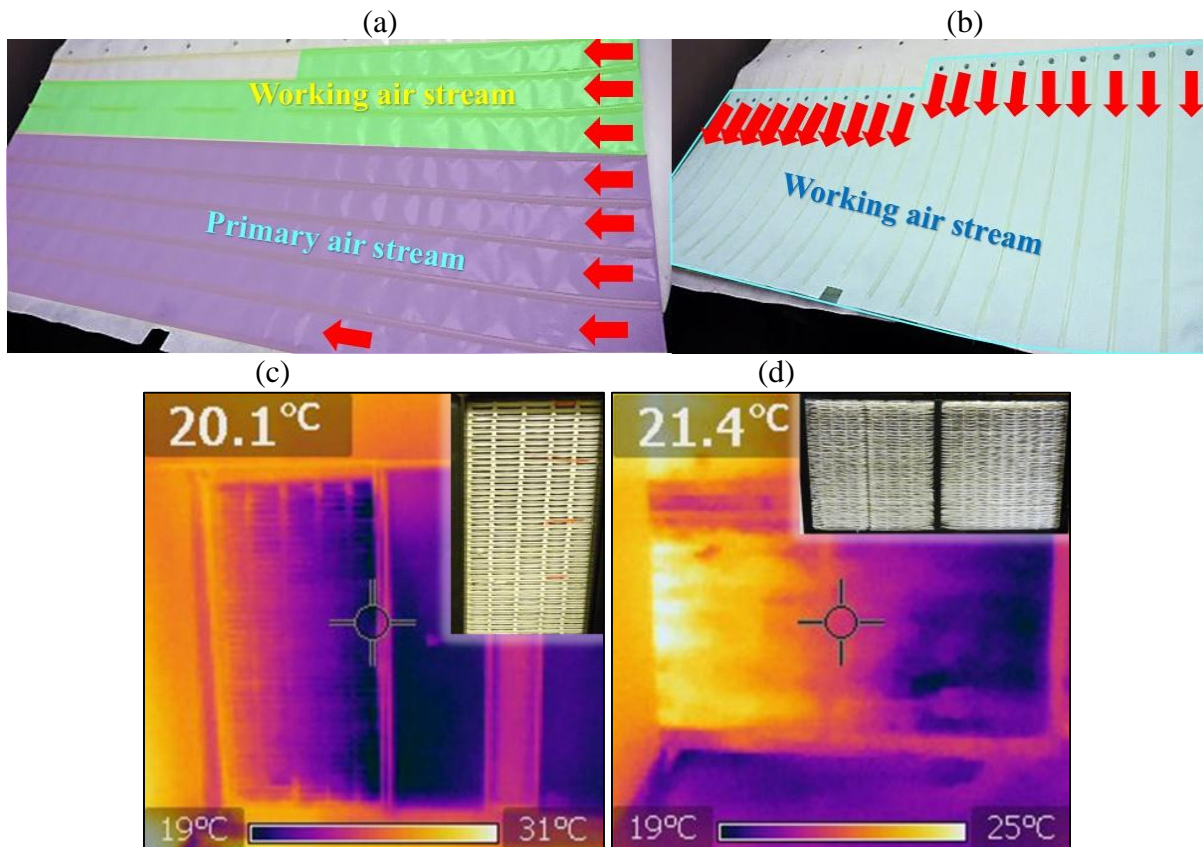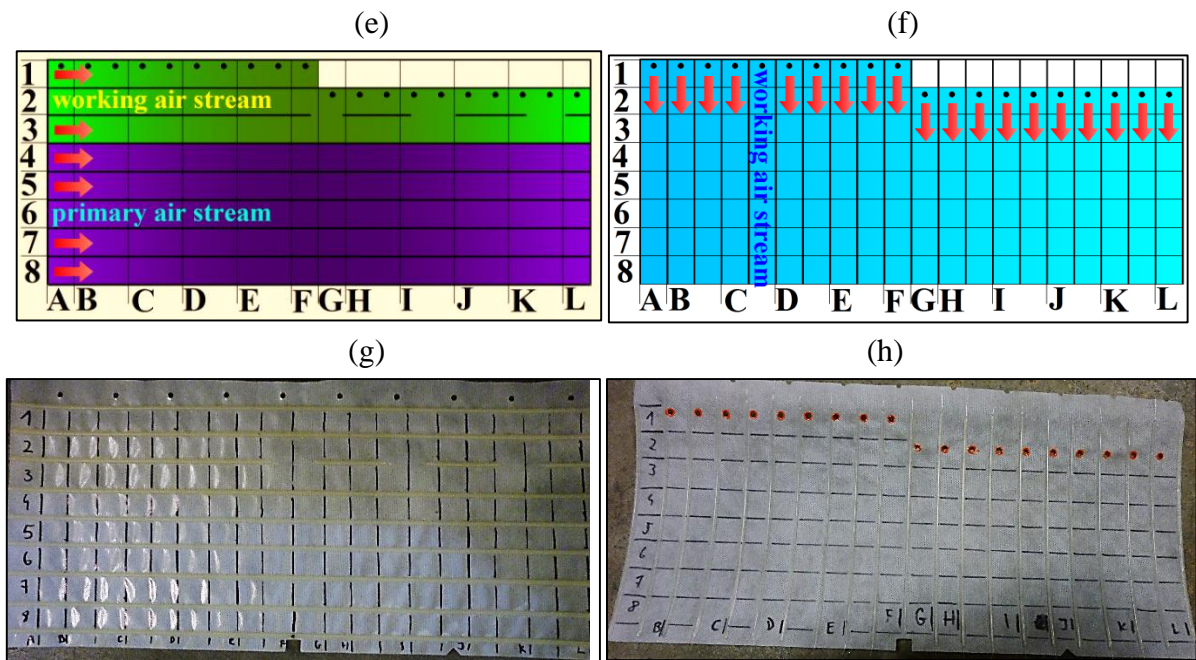
(a) (b)



(c) (d)

Fig. 4.2. (a) Photo of the dry plate (all photographs are made by author). (b) Photograph of the wet plate. (c) Infra-red photograph of the product part of the exchanger. (d) Infra-red photograph of the exhaust part of the exchanger. (e) Measuring points inside the dry part of the exchanger: scheme. (f) Measuring points inside the wet part of the exchanger: scheme. (g) Measuring points inside the dry part of the exchanger: channel plate with the signed points. (h) Measuring points inside the wet part of the exchanger: channel plate with the signed points.

### 4.1.4. Comparison under different inlet air parameters

This section presents the comparison between the numerical and experimental results at variable inlet temperature and humidity ratio, while other parameters remained unchanged. The model was set to the same operating conditions as for the experimental cases, including the exchanger geometry and inlet airflow conditions. In order to make adequate comparative analysis between the model and experimental results only tests concerning similar levels of operating parameters were conducted. Comparison was presented for three hypothetical conditions. These are: moderate ($x_{1i}$ =11.2 g/kg), humid ($x_{1i}$ =16.5 g/kg) and very humid ($x_{1i}$ =25.0 g/kg). The results are visible in Figure 4.3., including outlet temperatures, specific cooling capacity, wet bulb effectiveness and dew point effectiveness. The continuous line in Fig. 4.3(a)–(d) represents the model, while the points represent the experimental results. Deviation of the primary air stream outlet temperature is up to 4% (the highest differences in outlet temperatures are up to 0.5°C). The highest differences in specific cooling capacities obtained by the model and experiment are equal 0.8 kW/(kg/s), the deviation is at most 10%. The maximal differences between the wet bulb and dew point obtained by model and the experiment are 10%.
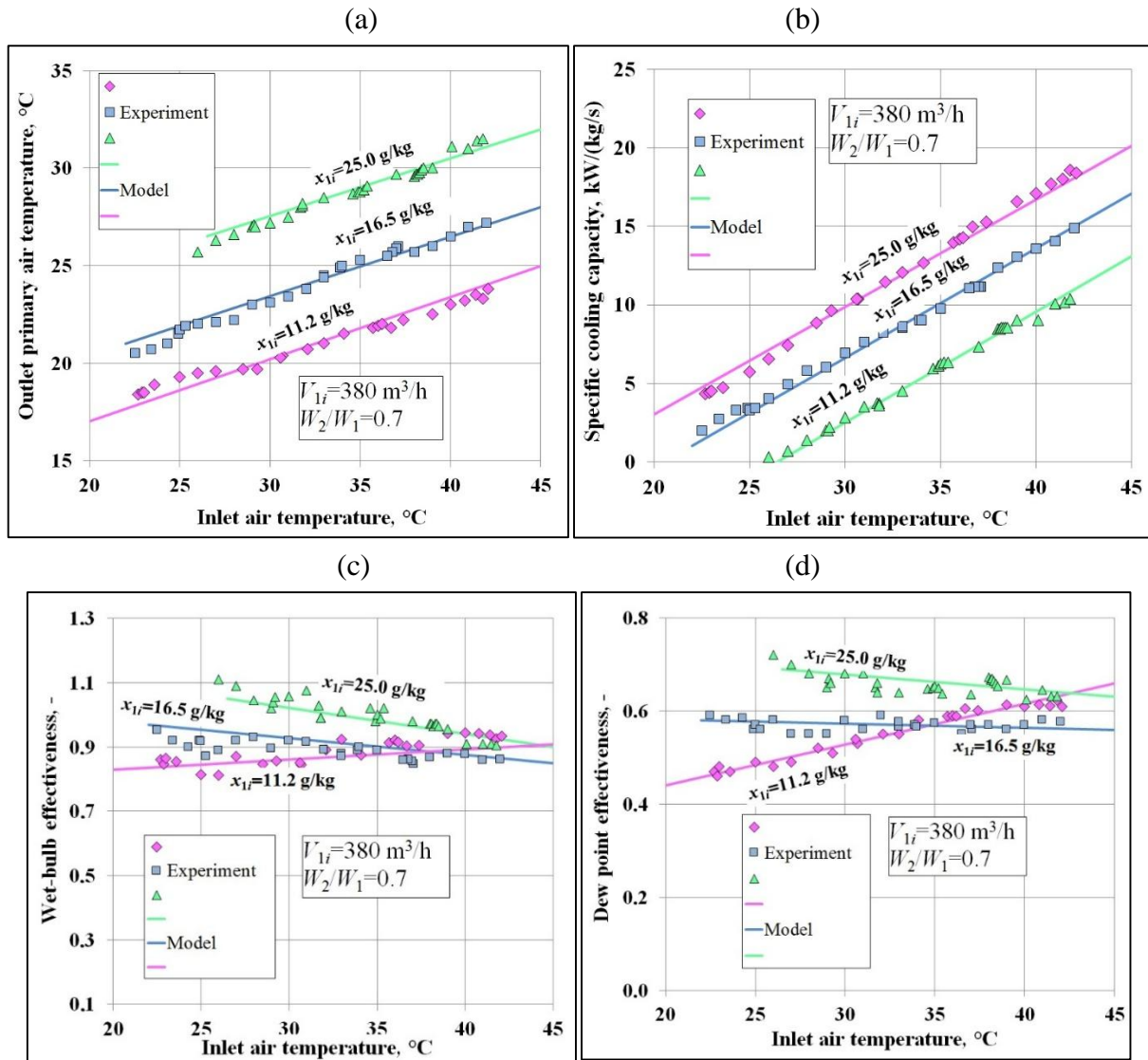
(a)

(b)



(c)

(d)



Fig. 4.3. Comparison between model and experiment under variable inlet air temperature at different levels of humidity ratio. (a) Average outlet product airflow temperature $\bar{t}_{lo}$. (b) Specific cooling capacity $\hat{Q}_G$ (respected to 1 kg/s of product airflow). (c) Wet bulb effectiveness $\varepsilon_{WB}$. (d) Dew point effectiveness $\varepsilon_{DP}$.

## 4.1.5. Comparison under variable airflow rate

This section presents the comparison between the model and the experiment under variable airflow rate at fixed inlet parameters and working to primary air ratio. The results of the comparison are presented in Figure 4.4. It can be seen that the maximal deviation between outlet temperature of the primary air stream is equal 0.1°C, the discrepancies are at most 1%. In case of the specific cooling capacity the differences are at most 0.93 kW/(kg/s), while the discrepancies are at most 1%. The maximal differences between the wet bulb and dew point obtained by model and the experiment are 1%.
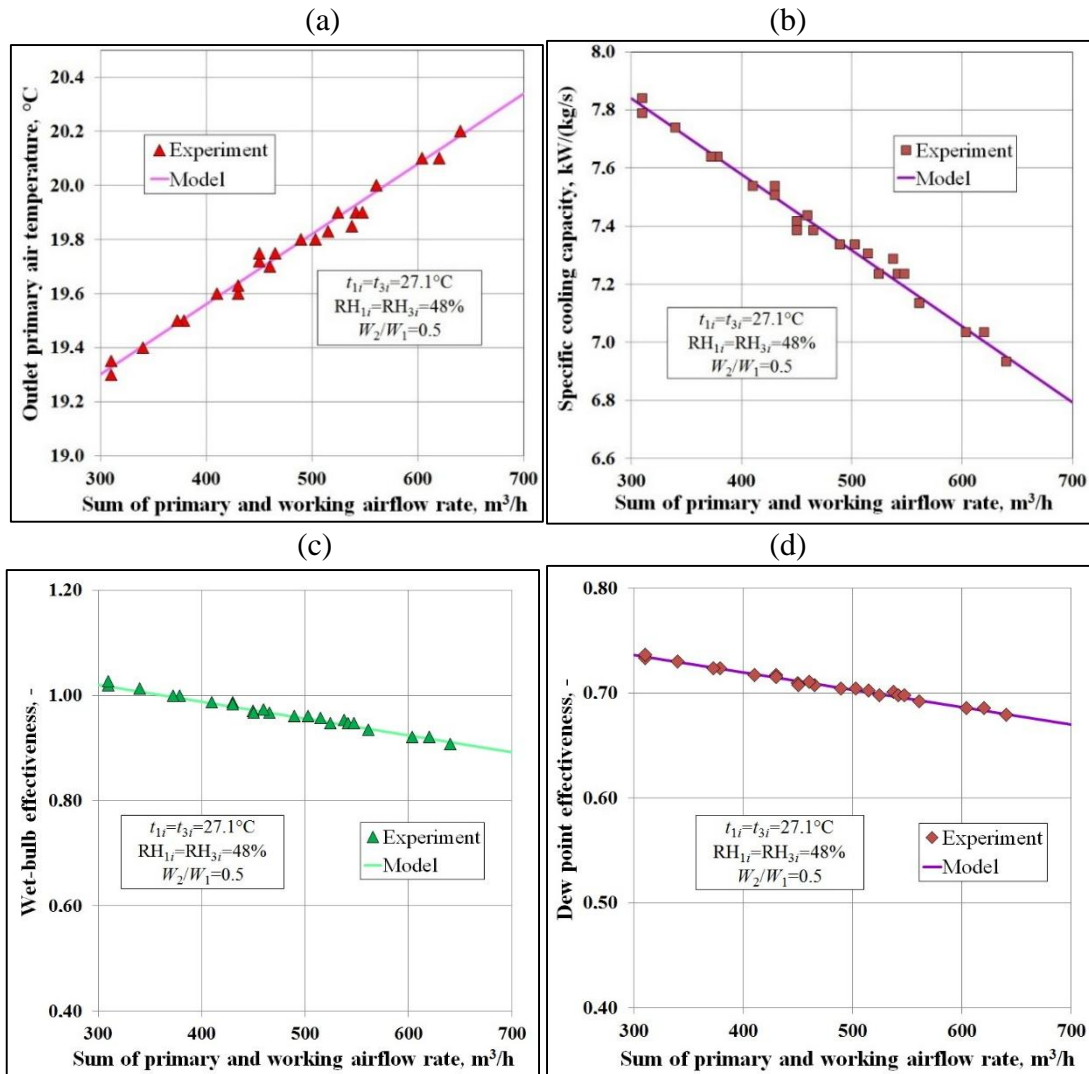
Fig. 4.4. Comparison between model and experiment under variable airflow rate. (a) Average outlet product airflow temperature $\bar{t}_{l_o}$ .(b) Specific cooling capacity $\hat{Q}_G$ . (c) Wet bulb effectiveness $\varepsilon_{WB}$ . (d) Dew point effectiveness $\varepsilon_{DP}$ .

## 4.1.6. Correlations between the model and the experiment in average outlet parameters

This section discusses the general comparison between the average outlet air parameters (i.e. outlet primary and working air temperature and working air humidity ratio) obtained by model and the experiment. The comparison is based on the correlation charts presented in Figure 4.5. The correlation between the experimental and the simulation data is equal 0.996 for predicting outlet product air temperature (Fig. 4.5(a)). For the working airflow, the correlation for outlet temperature is equal 0.998 (Fig. 4.5(b)). For outlet humidity ratio of the working air stream, the correlation is equal to 0.997(Fig. 4.5(b)). Additionally the correlation for the wet bulb effectiveness was also calculated and established as equal to 0.979 (Fig. 4.5(d)). It can be seen that the model achieved high agreement in terms of predicting the outlet parameters and the correlations obtained are very close to 1.
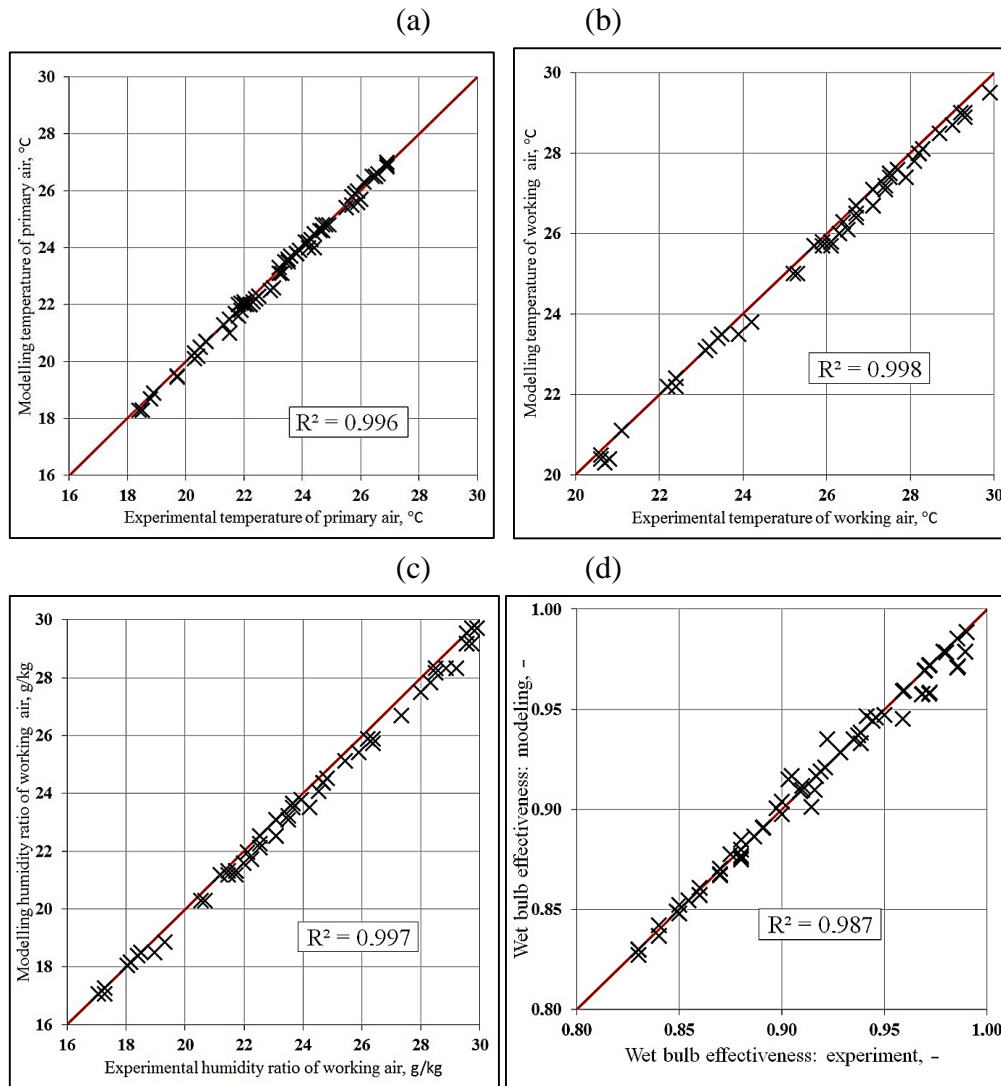
Fig. 4.5. Correlation between the model and the experiment. (a) Average outlet temperature of the primary flow $\bar{t}_{1o}$. (b) Average outlet temperature of the working flow $\bar{t}_{2o}$. (c) Average outlet humidity ratio of the working flow $\bar{x}_{2o}$. (d) Wet bulb effectiveness.

### 4.1.7. Comparison of the distribution of air parameters inside the channels

Modeling results compared with experimental data, including the primary and working air stream temperature profiles are shown in Fig. 4.6. It should be mentioned that the readings of the parameters inside the exchanger are very sensitive to the position of the thermocouple, distribution of the airflow and other factors. Therefore, the purpose of this comparison is to find out, if trends of temperature profiles between model and experiment are similar, not to achieve an ideal agreement. The similar trends in the parameters inside the exchanger can be assumed as additional confirmation that the model predicts the processes occurring in the cooler properly. The results are visible in Figure 4.6, the comparison is presented for two hypothetical conditions: moderate (Fig. 4.6(a) and (b)) and hot and humid (Fig. 4.6(c) and (d)).

Deviation in the primary air stream temperature profiles is at most 0.8°C for moderate conditions (Fig. 4.6(a)) and 0.95°C for hot and humid conditions (Fig. 4.6(c)). In case of the working airflow temperatures the differences are at most 0.9°C for moderate conditions (Fig.

4.6(b)) and 1.05°C for hot and humid conditions (Fig. 4.6(d)). The obtained values are considered to be satisfying. It should be mentioned that final temperatures of the primary and working air stream (at point are very close to experimental results (differences are at most 0.4°C). Average temperature differences for moderate conditions for the primary air stream are equal 0.56°C and 0.67°C for working air stream. In case of the hot and humid conditions the average temperature differences are equal 0.66°C and 0.72°C for primary and working air stream respectively.
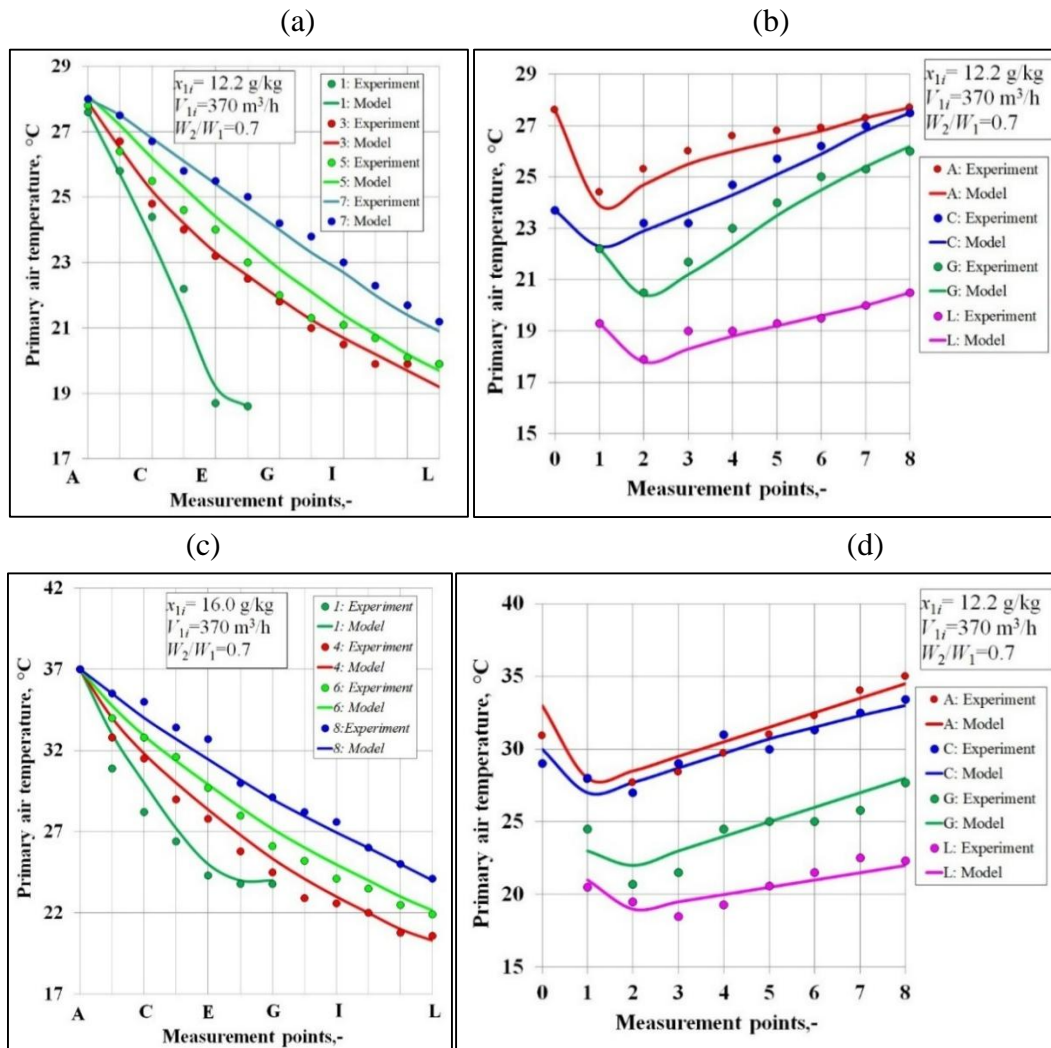
(a) (b)

(c) (d)



Fig. 4.6. Comparison of temperature distribution across the channels of the exchanger. (a) Profiles of primary and working air temperature in the dry channel. (b) Profiles of working air temperature in the wet channel. (c) Profiles of primary and working air temperature in the dry channel. (d) Profiles of working air temperature in the wet channel.

The comparison the trends in temperature distribution along the dry and wet channels of the exchanger additional method was used. Once all the temperature measurements were recorded for sets of product and working channels, the values were displayed on a three-dimensional surface plot across the exchange plate. The results are visible in Figure 4.7. It can be seen that the trends are generally similar, however the experimental results sometimes show atypical oscillations, which can be explained by the measurement inaccuracies. It can be seen that both

model and the experiment show that the air stream in the dry channels is not cooled evenly: there is almost 3°C (experiment) or 2°C (model) difference between local outlet temperatures between sections 3 and 5 (Fig. 4.7(a) and (b), location of measurement points is presented in Fig. 4.2(e)-(h)).

The differences between temperature trends in the wet channel are higher than in case of the dry channel (Fig. 4.7(c) and (d)), however the trend remains similar. It can be seen that for the presented conditions there is a trend that temperature of the working air is decreasing at the beginning of the wet channel (points 1-2) and starts increasing in its terminal part (points 4-8). The higher temperatures are closer to the inlet of the exchanger (points A-C) and lower at the terminal part of the dry channel of the exchanger (points J-L).
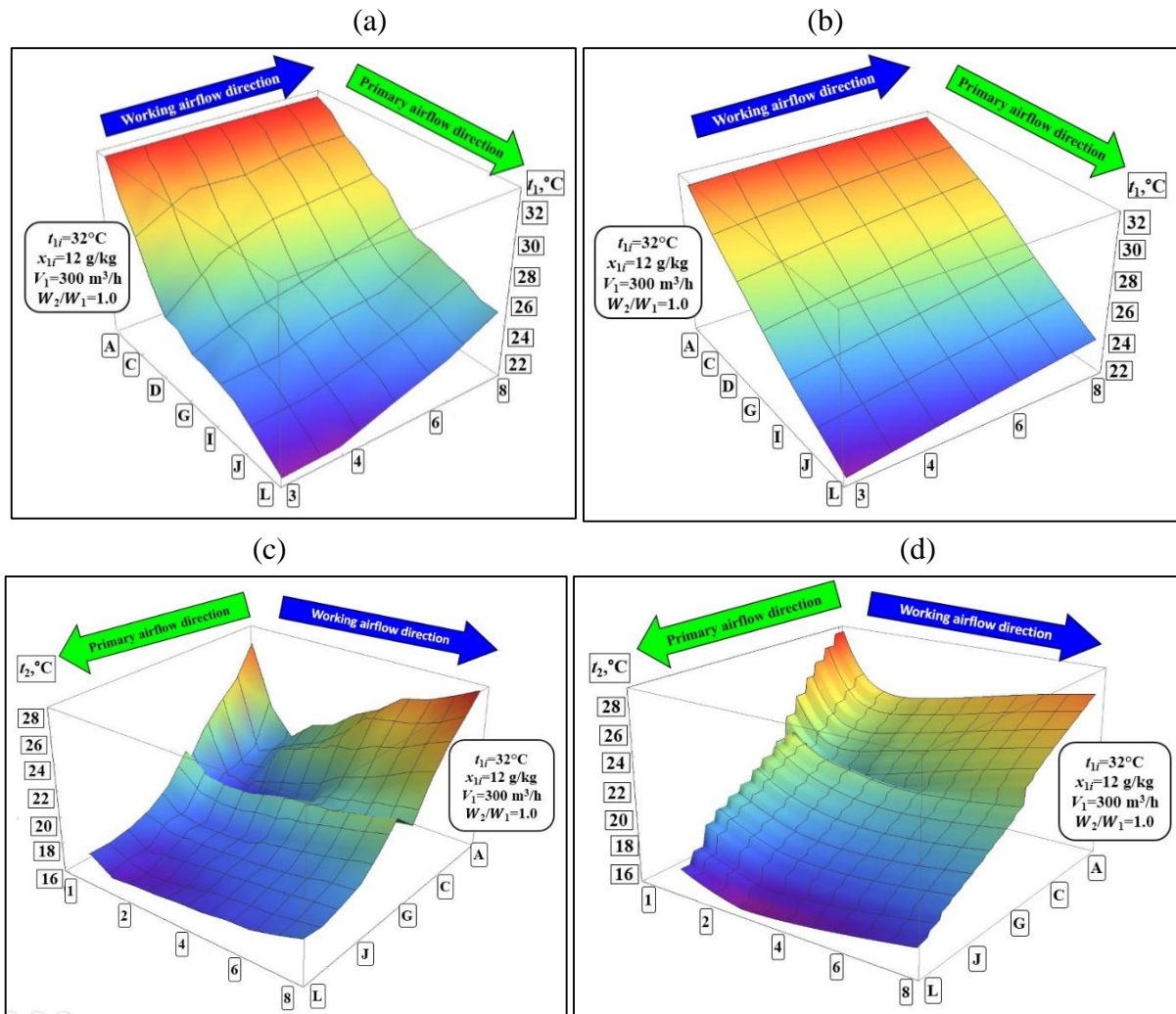
(a) (b)



(c) (d)

Fig. 4.7. Comparison of temperature distribution across the channels of the exchanger. (a) Profiles of primary air temperature in the dry channel: experiment. (b) Profiles of primary air temperature in the dry channel: model. (c) Profiles of working air temperature in the wet channel: experiment. (d) Profiles of working air temperature in the wet channel: model.

Another comparison was presented using the psychrometric chart in order to fully compare process in the wet channel obtained from the model and the experiment. The results are visible in Figure 4.8. In case of the experiment the measurement points were connected with

the straight lines in order to make the trends inside the wet channel more visible (Fig. 4.8(a) and (c)). It can be seen that also in this case the trend in results obtained by model and the experiment is similar. It can be seen that in both cases that the highest evaporation rates occur at the beginning of the wet channel: about 50% of growth in humidity ratio takes place in sections 1 and 2 for the wet channel connected with dry channel 1 (Fig. 4.8(a) and (b)) and in sections 2 and 3 in case of the wet channel connected to the dry channel 2 and 3 (Fig. 4.8(a) and (b), for the sections numeration see Fig. 4.2(e)-(h)). In both cases the working air temperature decreases at the beginning of the wet channel and rises at its terminal part.
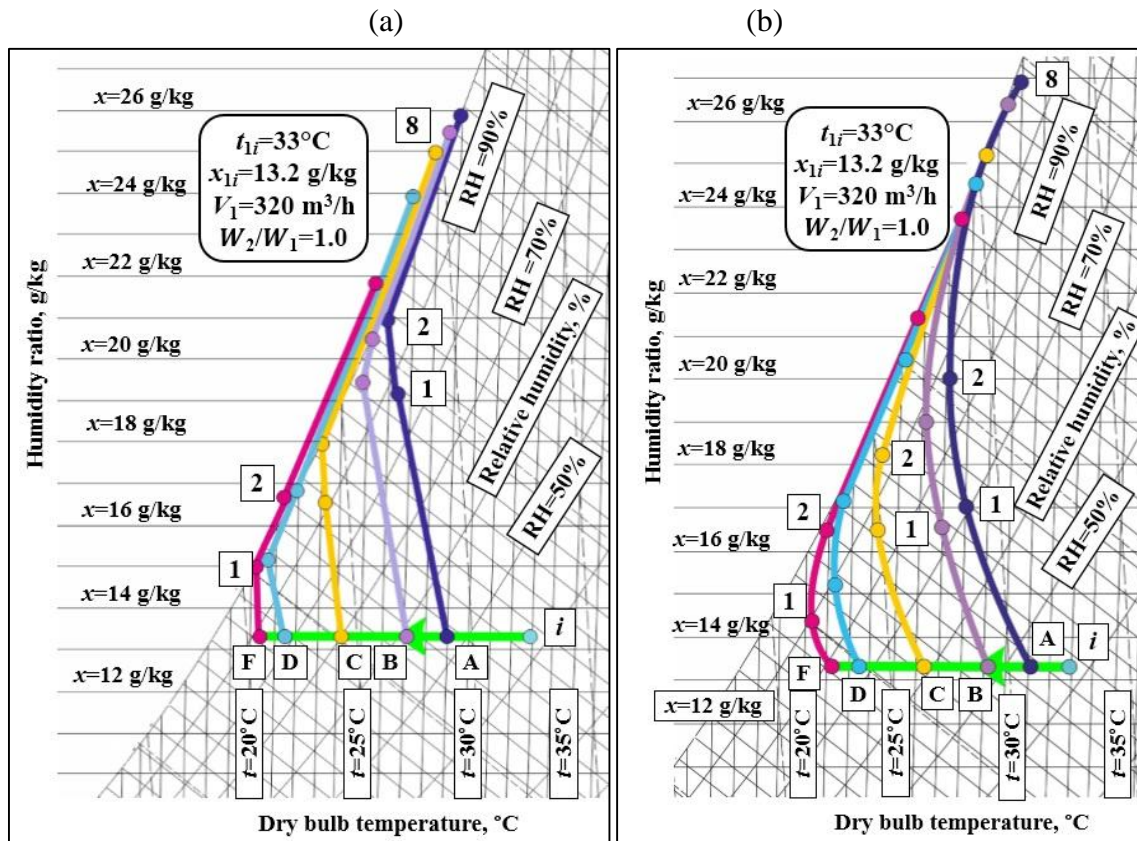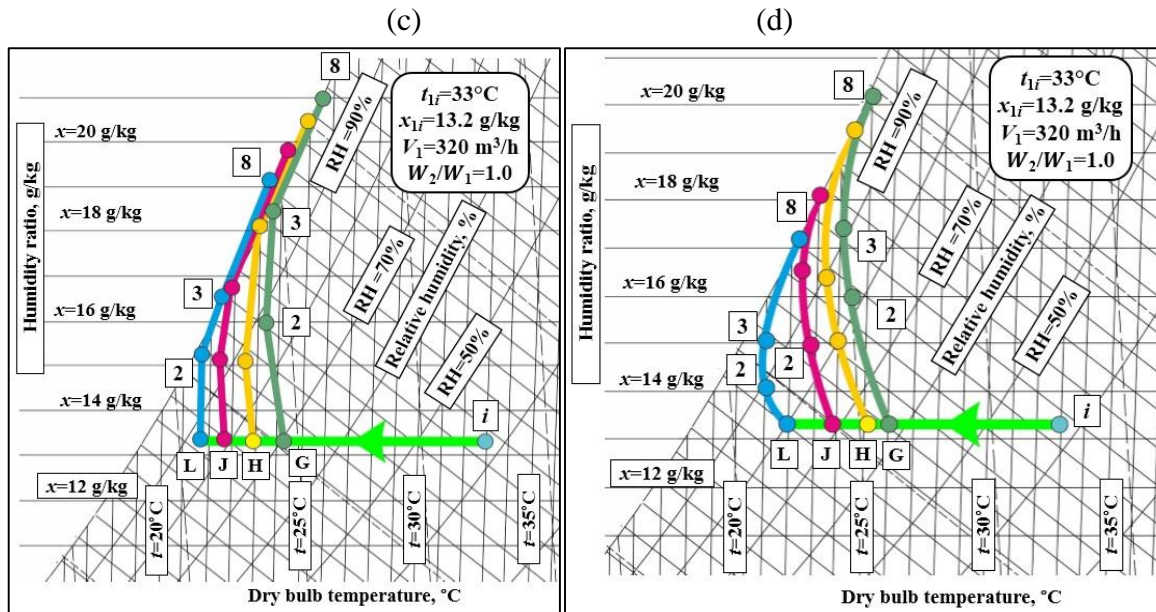
(a)    (b)

Fig. 4.8. Psychrometric paths of the working air stream inside the heat exchanger. (a) For the dry channel 1 and wet channels $A-F$: experiment. (b) For the dry channel 1 and wet channels $A-F$: model. (c) For the dry channel 1 and 2 and wet channels $G-L$: experiment. (d) For the dry channel 1 and 2 and wet channels $G-L$: model.

### 4.2. Conclusions from the section

The section investigated the validation of the mathematical model describing M-Cycle cross-flow heat exchanger used for indirect evaporative air cooling. The presented experimental results confirmed that inlet air can be cooled down below the wet bulb temperature: the wet bulb effectiveness ranged between 0.85 and 1.15, whereas the dew point effectiveness varied between 0.15 and 0.78 for different inlet conditions. The dry and wet bulb effectiveness does not vary much during continuous operation under real range of ambient air condition changes. The cooling capacity varied between 1 to 19 kW for every kg/s of airflow. Temperature difference for inlet and outlet airflow for dry air conditions varied between 5.2 and 20.1°C (for inlet air temperatures range 20–45°C).

The simulation results obtained from the numerical model was validated using experimental data obtained by author at Coolerado Corporation testing bench, which included measuring average outlet parameters of the primary and working air streams and by measuring the airflow parameters inside dry and wet channels of the exchanger and with data obtained by other authors in the existing studies (**Appendix F**). In all cases the model showed good agreement and trend. In case of the average outlet parameters the modeling results were very close to the experimental data, whereas in case of the parameters inside the exchanger they showed satisfactory agreement and very similar trend. The maximal differences between the average outlet primary air temperature obtained by model and the experiment were 0.5°C, however the average differences were about 0.15-0.25°C, which is a very good agreement in terms of the engineering standpoint (usually the typical accuracy of the control systems for air conditioning is 0.5°C). The validation against existing experimental data showed similar

agreement, which confirms that the model is accurate to predict the performance of the real cross-flow M-Cycle air cooler and it can be used to analyze its performance.

# 5. Analysis of heat and mass transfer processes inside the exchanger

*The results of this section were published in "S. Anisimov, D. Pandelidis, Numerical study of the Maisotsenko cycle heat and mass exchanger, International Journal of Heat and Mass Transfer, 75 (2014) 75–96"* [12] *and "D. Pandelidis, S. Anisimov, Numerical analysis of the heat and mass transfer processes in selected M-Cycle heat exchangers for the dew point evaporative cooling, Energy Conversion and Management 90 (2015), 62–83"* [134].

### 5.1. Ideal cross-flow M-Cycle heat and mass exchanger

### 5.1.1. Initial part

Processes occurring in the initial part of the exchanger are shown in Figure 5.1. It can be seen that temperature of air stream 3 decreases evenly in the *X* axis direction (Fig. 5.1(a) and (b)). Wet bulb effectiveness in the dry channel varies from 0.2 at the inlet part ($\bar{X}$=0.1) to 1.72 in the final part ($\bar{X}$=1.0). Average wet bulb effectiveness in the dry channels of the initial part is equal to 1.07. Working air stream 3 is then effectively pre-cooled before entering the wet channel.

In the wet channel the active zones of heat and mass transfer are significantly deformed in compare to the typical evaporative air cooling units (see Section 2). This can be easily seen on the psychrometric chart (Fig. 5.1(a)), on the temperature and humidity ratio profiles (Fig. 5.1(c) and (d)) and on the surface plots (Fig. 5.1(e) and (f)). After reaching the wet channel through the first hole ($\bar{Y} = 0.01$ in the Fig. 5.1(c)), humidity ratio intensively increases (Fig. 5.1(c) and (d)). Enhancement of humidity ratio is coupled with a decreasing temperature of the airflow (Fig. 5.1(c) and (f)). In the cross-section $\bar{Y} = 0.06$ (air stream 4- after mixing), the humidity ratio rapidly decreases and the temperature increases by about 5°C (Fig. 5.1(c) and (e)). Dehumidification of air intensifies the evaporation of water, resulting in a renewed enhancement of the humidity ratio (Fig. 5.1(c) and (f)) and reduction of temperature (Fig. 5.1(c) and (e)). This is due to the warm and dry portions of the air stream 3 from the dry channel, which are delivered to the wet portion of the device by perforated holes. In each section of $\bar{X}$ and $\bar{Y}$ axis, the working air stream 3 is always hotter and dryer than the working air stream 4 in the wet channel. Therefore mixing of those two airflows in the wet portion always results in increasing the working airflow temperature and decreasing its humidity. This causes the rapid increase in humidity ratio, combined with reduction of the working airflow temperature after each hole. Temperature and humidity ratio oscillation range is reduced along the $\bar{Y}$−axis, since the mass flow 4 enlarges, while the same amount of dry air stream 3 is delivered from the dry channel through each hole. At the end of the wet part, elementary component of airflow 3 has small heat capacity *W* comparing to the air stream 4, and therefore causes fewer disturbances to the temperature and the humidity ratio profiles (Fig. 5.1(c), (e) and (f)). Oscillations are smaller when perforation is denser. Figure 5.1(c) presents temperature and humidity ratio profiles for exchanger with 10 perforated holes along $\bar{Y}$ axis and Fig. 5.1(d) shows exchanger

with 20 holes along $\bar{Y}$ axis. It can be seen that at first oscillations of temperature and humidity ratio are identical in both cases. This is due to the same proportion in air mass flow rates in the which enter through the first hole and through the second hole (respectively 1/10 of the total airflow for the HMX with 10 holes and 1/20 for the exchanger with 20 holes). It can be seen that in the HMX with 20 holes oscillations are quickly becoming unnoticeable, while in the first case they are quite distinct: at the end of the channel 4 temperature oscillations values are equal 1°C (10 holes) and 0.4°C (20 holes), humidity ratio oscillations are equal 2 g/kg and 1 g/kg respectively (Fig. 5.1(c) and (d)).

Another interesting phenomenon can be seen in the surface plots (Fig. 5.1(e) and (f)). Temperature and humidity ratio plots differ: temperature oscillations are less visible in part of the wet channel 4 under the terminal part of the dry channel 3 (from $\bar{X}$=0.6 to $\bar{X}$=1.0 temperature variations are minimal). However, in the same region humidity ratio oscillations are much more visible. This is due to the fact that humidity ratio of air stream 3 is constant along the whole dry channel, while its temperature is variable. In the final part of the dry channel  air stream 3 is cold, thus after it is delivered to the wet channel its temperature does not change by substantial values. Mixing of cold airflow 4 in the wet channel with cold airflow 3 from the dry channel cannot cause significant temperature oscillations, therefore temperature plot becomes smoother along the $\bar{X}$ axis (Fig. 5.1(e)). However, humidity ratio of air stream 3 is constant in the whole dry initial part, therefore it causes higher oscillations in humidity ratio profiles in the wet channel (Fig. 5.1(f)). Although variations in humidity ratio are more visible than temperature variations, humidity ratio surface plot becomes smoother along the $\bar{X}$ axis as well. This can be explained as follows: when air stream is cooled with constant humidity ratio, its relative humidity is close to the saturation state in the final part of the dry channel (Fig. 5.1(a)) and therefore its ability to assimilate water vapor becomes low. Humidification of the air stream 4 delivered from the final part of the dry channel runs ineffectively, therefore its humidity ratio is similar to its inlet value. Therefore, when air streams 3 and 4 are mixing, the oscillations in humidity ratio profiles are less visible along the $\bar{X}$ axis.

(a)
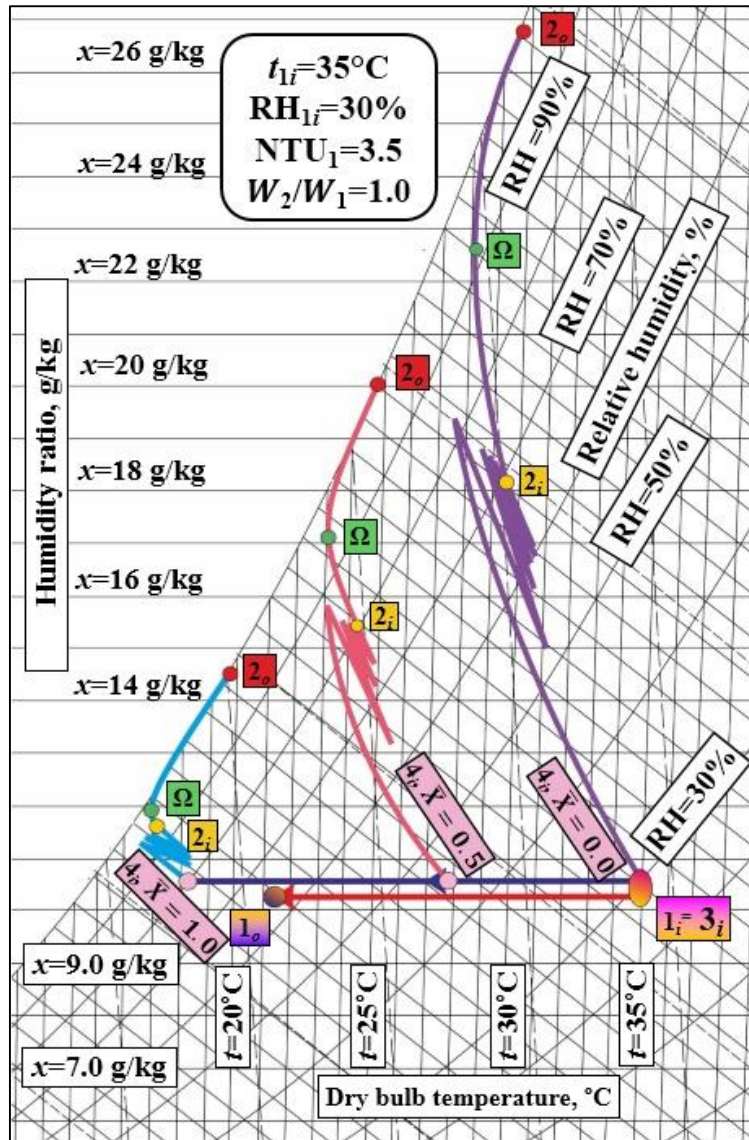


(b)
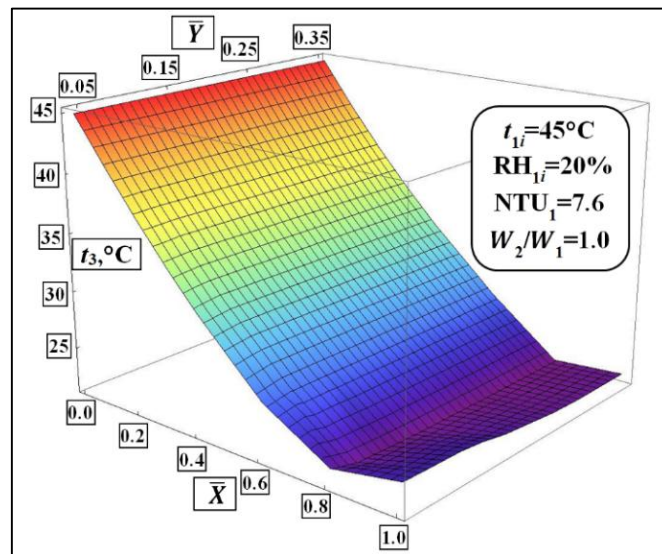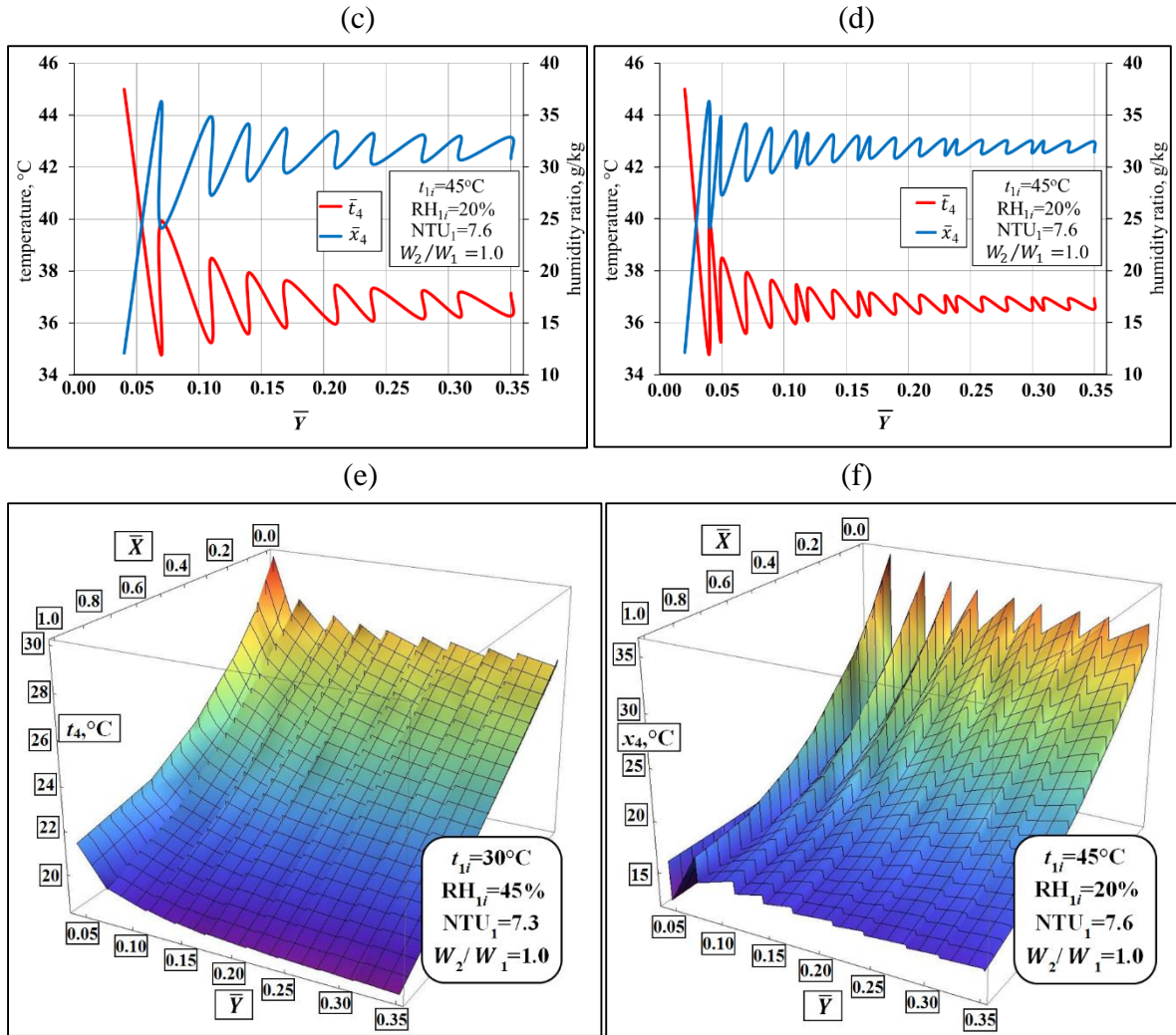
Fig. 5.1. Simulation results for the initial part of the HMX. (a) Heat and mass transfer processes on the psychrometric chart. (b) Air stream 3 temperature distribution (dry channel). (c) Temperature and humidity ratio profiles (average values) in the wet channel along $\bar{Y}$ axis (exchanger with 10 holes). (d) Temperature and humidity ratio profiles (average values) in the wet channel along $\bar{Y}$ axis (exchanger with 20 holes). (e) Air stream 4 temperature distribution: surface plot. (f) Air stream 4 humidity ratio distribution: surface plot.

The average outlet relative humidity for air stream 4 is 75–80%, depending on the initial part length ($l_Y^{work}$). It means that air stream is very close to the saturation state when it enters the product part of the considered HMX. When initial part is relatively long (e.g. $l_Y^{work}=0.35l_Y$), outlet relative humidity of the air stream 4 can be very high - up to 95-97%. However, the length of the initial part along the $\bar{Y}$ axis does not affect the outlet temperature of the air stream 3 (maximal change in airflow 3 outlet temperature, for $l_Y^{work}$ varying from 0.1 to $0.35L_Y$, is equal 0.5°C). This allows assuming that initial part should not be too long along the $\bar{Y}$ axis, because water evaporation is used only for cooling of the working airflow instead of cooling the primary airflow. This problem is discussed in Section 8.

It should be mentioned that due to the high deformation of the heat and mass transfer plots in the wet channels of the initial part, for the exchanger with dense perforation the active

zones of heat and mass transfer (see Section 2) are very hard to observe. They occurrence will be discussed during analysis of the processes in the realistic M-Cycle air coolers in Section 5.2.

### 5.1.2. Product part

Heat and mass transfer processes occurring in the product part of the exchanger are more simple than in the initial part, due to the fact that no mixing process occurs. However, due to the different temperature distribution, they are more difficult in compare to the typical cross-flow air cooler. Results are visible in Figure 5.2. The analysis of temperature distribution in the working cross-flow passages in the product part of the heat exchanger reveals the existence of two particular heat and mass transfer zones ($2_i-\Omega$ and $\Omega-2_o$ in Fig. 5.2(a) and (b)), as in case of the basic evaporative air cooling cycles. It can be seen that the coupled heat and mass transfer process at the exit part of the working airflow channels is characterized by the change of sensible heat flux direction at unchanged mass flux direction (Fig. 5.2(b)-(d))). Rising of the working air stream 2 temperature causes that sensible heat flux in the wet channel changes its sign (it is visible in heat transfer plots: Fig. 5.2(b) and (c)). The sign of the heat transfer represents the direction of the heat flux, the change of sign from negative to positive means that the working air stream was cooled at first and it is heated later. It is important to mention that working airflow starts to become heated relatively quickly (after 1/3 of the wet channel in the product part of the exchanger– Fig. 5.2(c) and (e)), which means that working airflow is cooled at a shorter distance in the wet channel than it is heated.

The phenomenon of occurrence of two active heat and mass transfer zones is widely discussed in the Section 2, therefore it is not analyzed in this Section. From the analysis of this phenomenon, it is concluded that existence of such particular heat and mass transfer areas with different boundary conditions of heat transfer and mass transfer on the plate surface of wet channels in the product part of the HMX leads to the violation of Lewis relation unity, as it is in case of the counter-flow, cross-flow and regenerative indirect evaporative air cooler: $\mathrm{Le} = \mathrm{St}_{heat}/\mathrm{St}_{mass} \approx \mathrm{Nu}_{heat}/\mathrm{Nu}_{mass} \approx 0.9$ (see Section 2 and [12]).

(a)
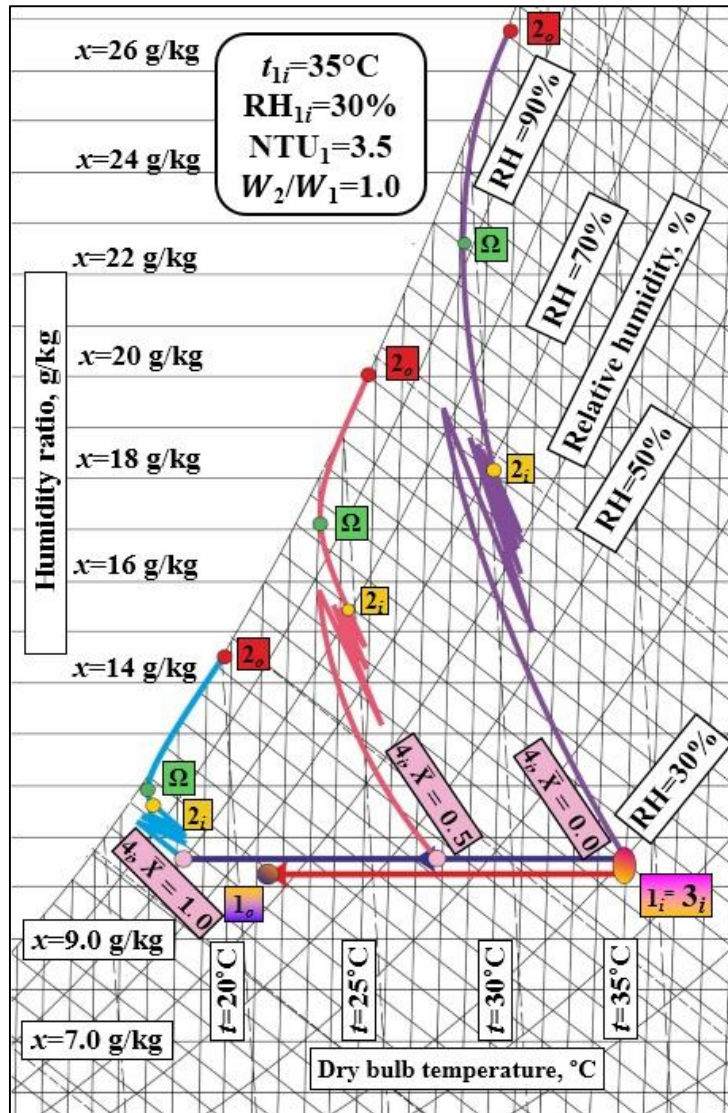


(b)
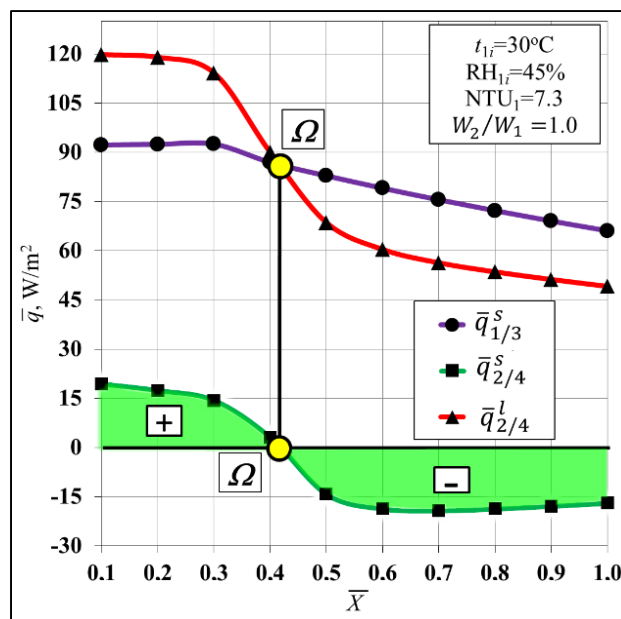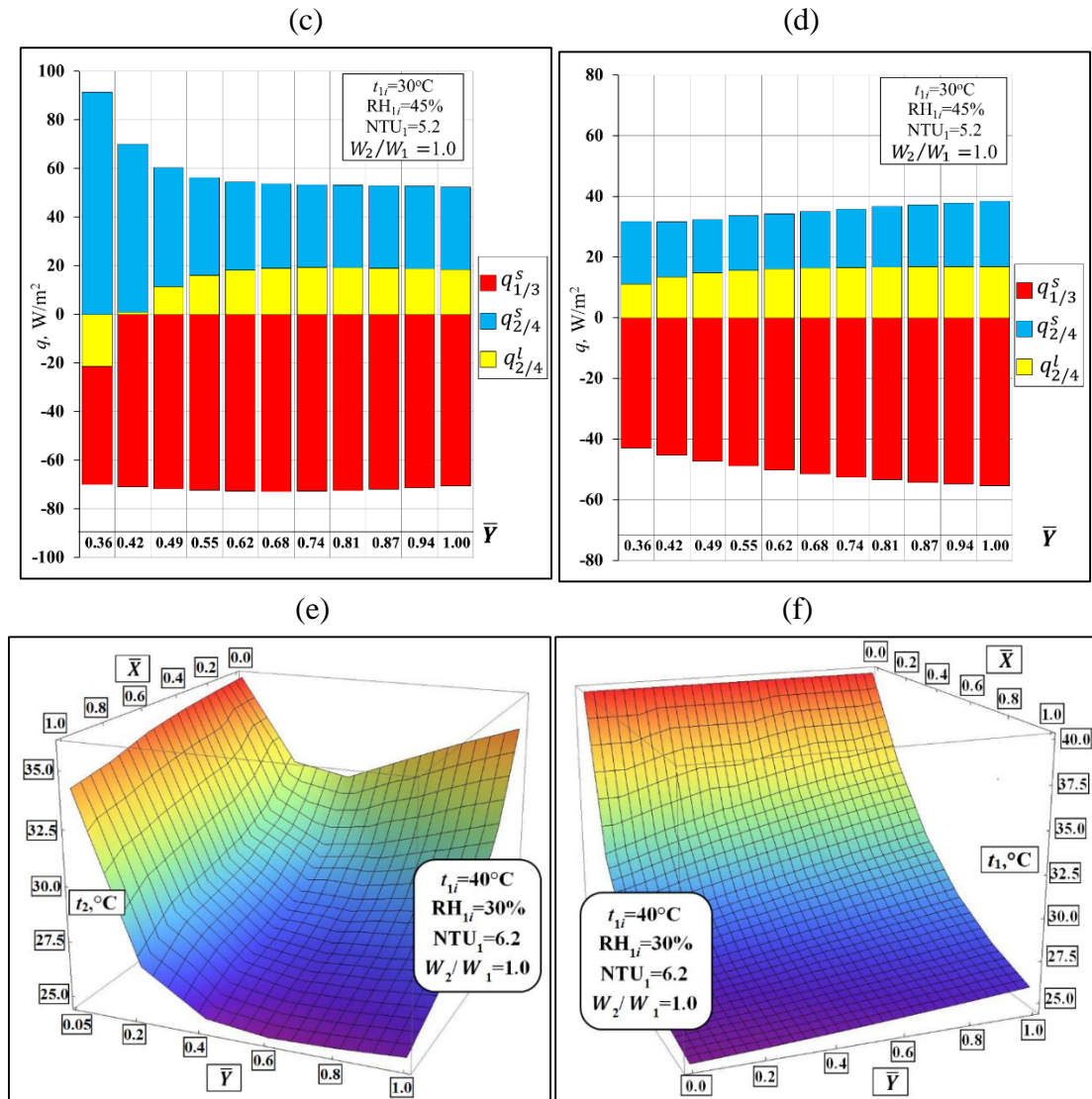
Fig. 5.2. Simulation results for the product part. (a) Heat and mass transfer processes on the psychrometric chart. (b) Average heat flux distribution along the $\bar{Y}$ axis. (c) Local sensible and latent heat flux distribution along the $\bar{Y}$ axis (section $\bar{X}$=0.5) - bar chart. (d) Local sensible and latent heat flux distribution along the $\bar{Y}$ axis (section $\bar{X}$=1.0)- bar chart. (e) Air stream 2 temperature distribution: surface plot. (f) Air stream 1 temperature distribution: surface plot.

The occurrence of two active heat and mass transfer zones is present in all cases analyzed in this thesis, which allows presuming that it is occurring regularly in the Maisotsenko cycle heat and mass exchangers. This is the desired effect, because it allows increasing the specific enthalpy difference between the working air stream at inlet and outlet of the exchanger, resulting in lower product air temperature which is later delivered to the conditioned spaces. The phenomenon has a negative effect as well, because it reduces the heat transfer potential in the place where it occurs (lower temperature difference between the working and primary airflow), therefore the primary airflow is cooled unevenly (Fig. 5.2(f)). It can be seen that airflow near the terminal part of the wet channel ($\bar{Y} \approx 0.9 - 1.0$) is characterized by higher temperature than airflow neat the initial part of the working air channel ($\bar{Y} \approx 0.0 - 0.1$).

Wet bulb effectiveness obtained from the simulations for this exchanger is varying between 0.65 to 1.67, depending on the inlet conditions, airflow velocity in channels and geometrical parameters of the device. Average wet bulb effectiveness obtained is varying between 1.10 and 1.3%. Producer claims that wet bulb effectiveness of this unit is in range 0.94… 1.20 [135]. Maximal dew point effectiveness obtained from the simulations is equal 0.88.

## 5.2. Different arrangements of the realistic M-Cycle air cooler

This section discusses the analysis of heat transfer processes in 7 different arrangements of the cross-flow M-Cycle air cooler, selected after consultation with Coolerado Corporation and Prof. Valeriy Maisotsenko (Fig. 5.3 and 5.4). The purpose of this analysis is to analyze the heat and mass transfer phenomena for details which are very hard to observe in the ideal cooler due to a very dense perforation. The performance of the units will be compared in the Section 8. The analysis of the realistic arrangements of the heat exchangers requires different calculation algorithm than ideal M-Cycle air cooler (the method is presented in **Appendix C**). The dry and wet channels of the considered HMXs are presented respectively in Figure 5.3 and 5.4. Primary and working channels are flat and rectangular-shaped as in the original air cooler. The dimensions assumed in this study are:

- The wet and dry channel height is equal 3.0 mm.
- The wet and dry channel width is equal 24 mm.
- The total number of wet channels is 19, the total number of dry channels is 8, as in the original M-Cycle air cooler.
- It is assumed that the airflow is distributed evenly through the channels (e.g. for exchanger with 5 primary air channels and 3 dry working air channels, in each channel 1/5 of the primary airflow is delivered, while for each working channel 1/3 of the working airflow is delivered). Inside the dry working air channels, air is spread evenly through the holes (e.g. for exchanger with 3 dry working air channels with 10 holes each, air stream delivered through one hole is 1/10 of 1/3 of the total working air stream). The problem of airflow distribution inside the M-Cycle air cooler is discussed in Section 8.

The units selected for the analysis along with their characteristics are listed bellow. Original HMX, marked as Variant 0 (V0) is presented in Fig. 5.3(a)). It has a shorter first dry initial channel than the other two initial channels (1st Fig. 5.3(a)). There are no holes in the third dry channel (3rd: Fig. 5.3(a)), the airflow is transferred to the second dry channel through the gaps in fins (2nd : Fig. 5.3(a)). Variant 1 HMX (V1: Fig. 5.3(b)) has the same number of the dry working air channels, but with even hole distribution in every channel (19 holes in each initial channel). Variant 2 (V2: Fig. 5.3(c)) is characterized by the 3 dry working air channels, where in the first channel holes are distributed regularly, while in the other two working air channels holes are distributed one the chess-board scheme. Variant 3 exchanger (V3 Fig. 5.3(d)) has the three dry working air channels with regularly distributed holes, but one of the working air

channels is placed closer to the end of the wet part. Variant 4 HMX (V4 Fig. 5.3(e)) is the modified version of V1 HMX with two dry working air channels and 6 primary air channels. Variant 5 HMX (V5 Fig. 5.3(f)) is the modified version of the original exchanger with two dry working air channels and 6 primary air channels. Variant 6 HMX (V6 Fig. 5.3(g)) is the modified version of the V3 unit with two dry working air channels and 6 primary air channels. Variant 7 HMX (V7 Fig. 5.3(h)) is the modified version of V4 HMX with one dry working air channel and 7 primary air channels. All of considered devices have the same size and the same number of the wet channels (Fig. 5.4). Wet channels for all of analysed exchangers have the same length, except units V0 and V5, where channels from $10^{th}$ to $19^{th}$ are shorter, due to the construction of the dry initial part (Fig. 5.4(a) and (f)). For all other devices, the wet part is identical, it differs only by the way the dry working air stream is delivered.

Due to the different construction of the real M-Cycle air coolers, which in some cases (i.e. V3 and V6 units) make very difficult to determine which part of the wet channel belongs to the initial and which to the product part of the exchanger, for the purpose of this analysis working air stream in the wet channels is always marked as 2. Primary air stream is, as always, marked 1 and working air stream in the dry channels is marked as 3.
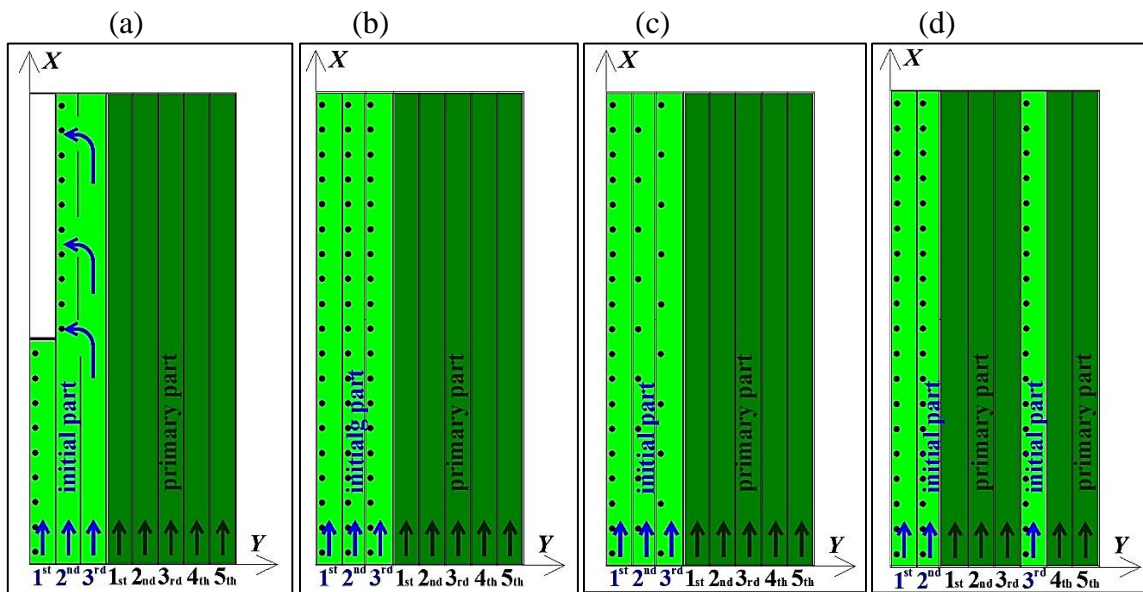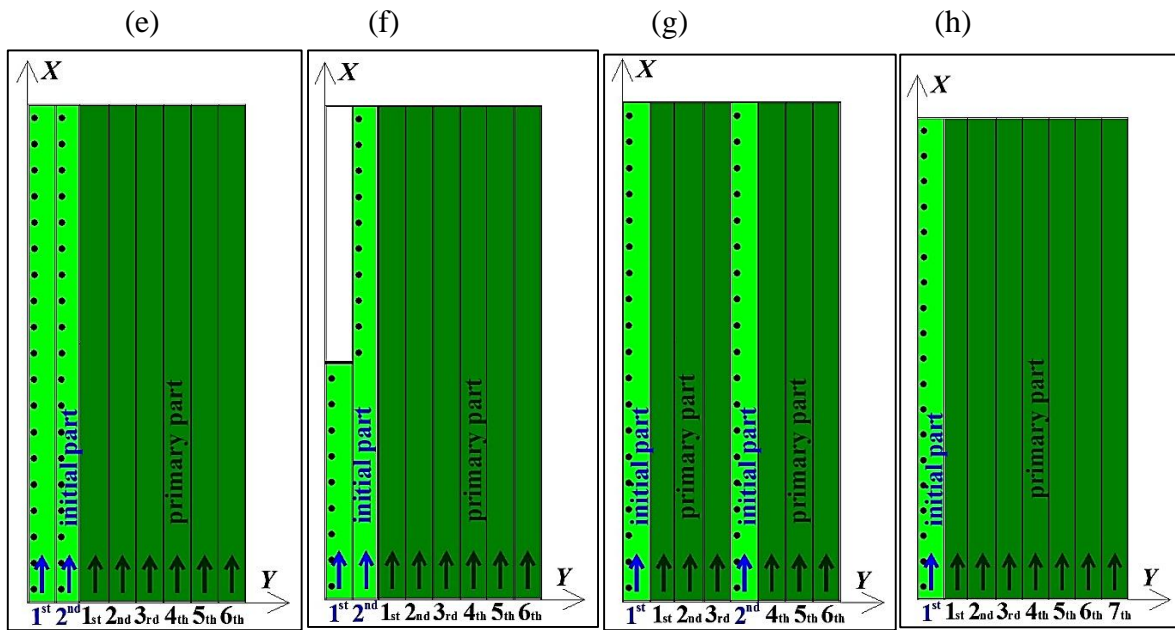
Fig. 5.3. Dry channels characteristics (nomenclature $1^{st}, 2^{nd}$…: number of dry initial part channels; $1_{st}$; $2_{nd}$…: number of product part channels). (a) Original HMX (V0). (b) Variant 1 (V1). (c) Variant 2 (V2). (d) Variant 3 (V3). (e) Variant 4 (V4). (f) Variant 5 (V5). (g) Variant 6 (V6). (h) Variant 7 (V7).
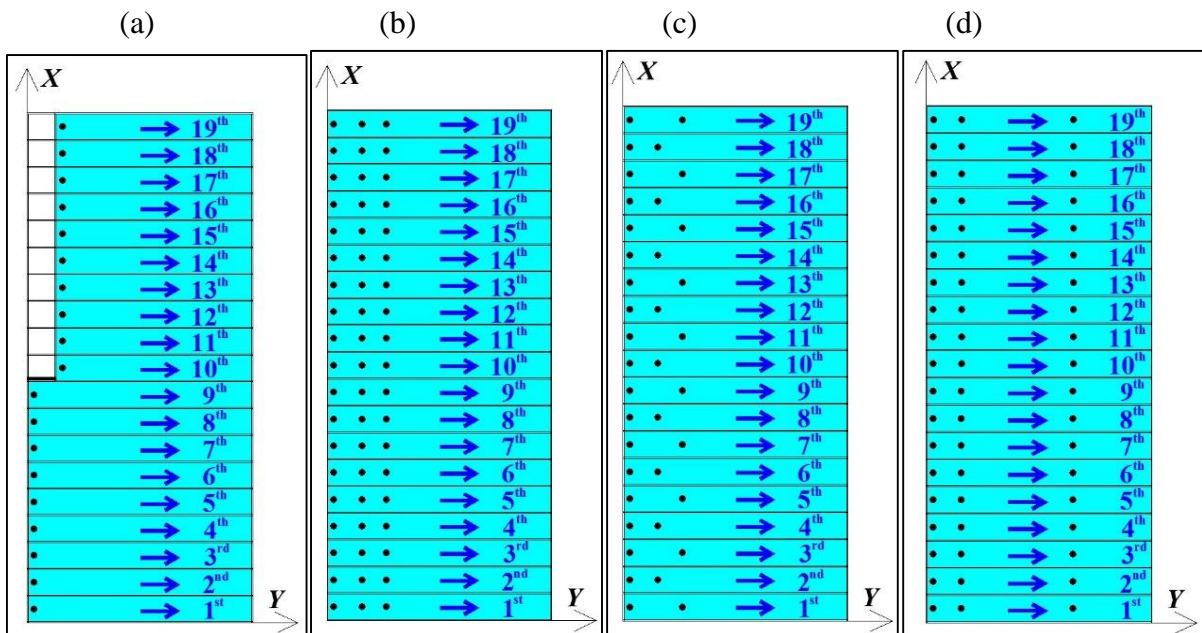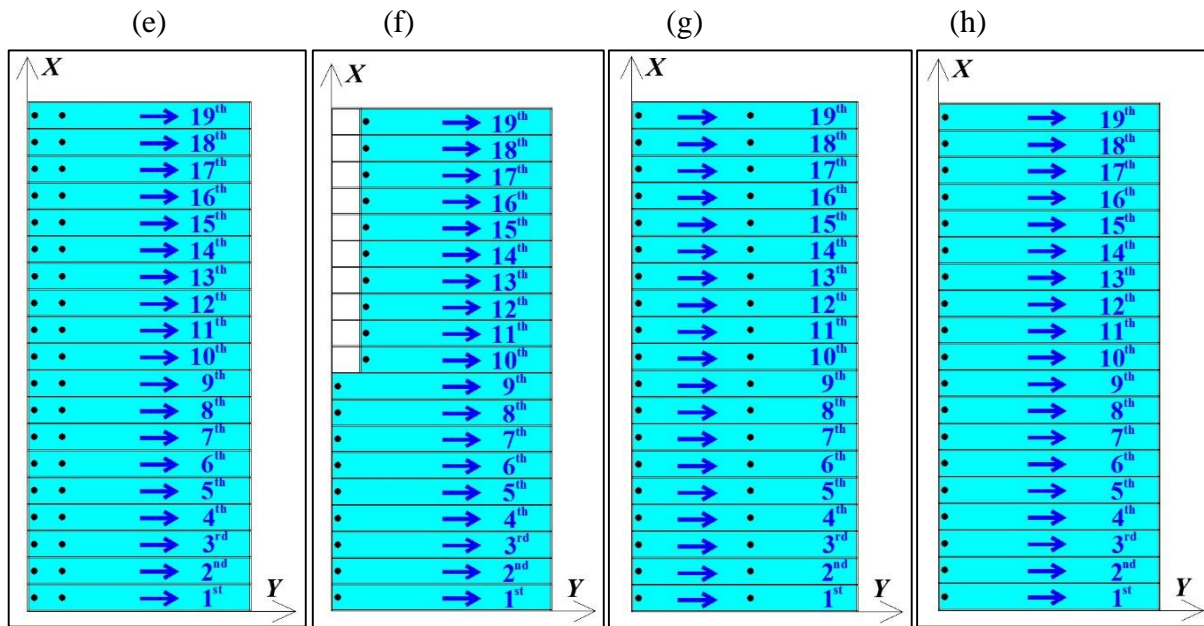
Fig. 5.4. Wet channels characteristics (nomenclature $1^{st}, 2^{nd}\ldots$: number of wet working air channels). (a) Original HMX (V0). (b) Variant 1 (V1). (c) Variant 2 (V2). (d) Variant 3 (V3). (e) Variant 4 (V4). (f) Variant 5 (V5). (g) Variant 6 (V6). (h) Variant 7 (V7).

The first series of simulations were dedicated to the heat and mass transfer processes occurring inside each of the investigated exchangers when primary and working airflow rates and inlet parameters were maintained as constant values. The simulation results are arranged into the four groups: air temperature distribution inside the dry channels (Fig. 5.5) and the wet channels (Fig. 5.6), humidity ratio distribution inside the wet channels (Fig. 5.7) and air parameters distribution on the psychrometric chart (Fig. 5.8).

Air temperature distribution inside the dry channels of the considered exchangers is presented on the surface plots (Fig. 5.5). It can be seen that the temperature distribution inside each exchanger significantly differs. There are visible disturbances (step changes) in the temperature profiles. The disturbances are caused by the different NTU values in the working and the primary air channels, due to the different heat exchange surface and different air stream velocity. The different NTU values results in different efficiency of the cooling process inside the primary and the working air channel. It can be seen that the working airflow achieves lower temperatures than the primary airflow, except for the unit V7, in which the NTU value in the dry working air part is very low (Fig. 5.5(h)).

Referring to Fig. 5.5(a), there are few main differences between the temperature distribution inside the original device (V0) and the rest of the analyzed variants. There are disturbances in temperature profiles in the two working air channels: $2^{nd}$ and $3^{rd}$ according to nomenclature presented in Fig. 5.3(a), which are located between points $\bar{Y}=0.15–0.45$; $\bar{X}=0–1.0$ in Fig. 5.5(a). The disturbances occur in points: $\bar{X}=0.5$, $0.7$ and $0.9$ and they are caused by the transfer of the air stream from the $3^{rd}$ channel to the $2^{nd}$ channel through the gaps in the fins (see. Fig. 5.3(a)). The construction of other exchangers does not allow to transfer the air

stream between the dry channels, therefore there are no disturbances in their dry working air channels.

(a)

(b)



(c)

(d)

(e)
(f)



(g)
(h)
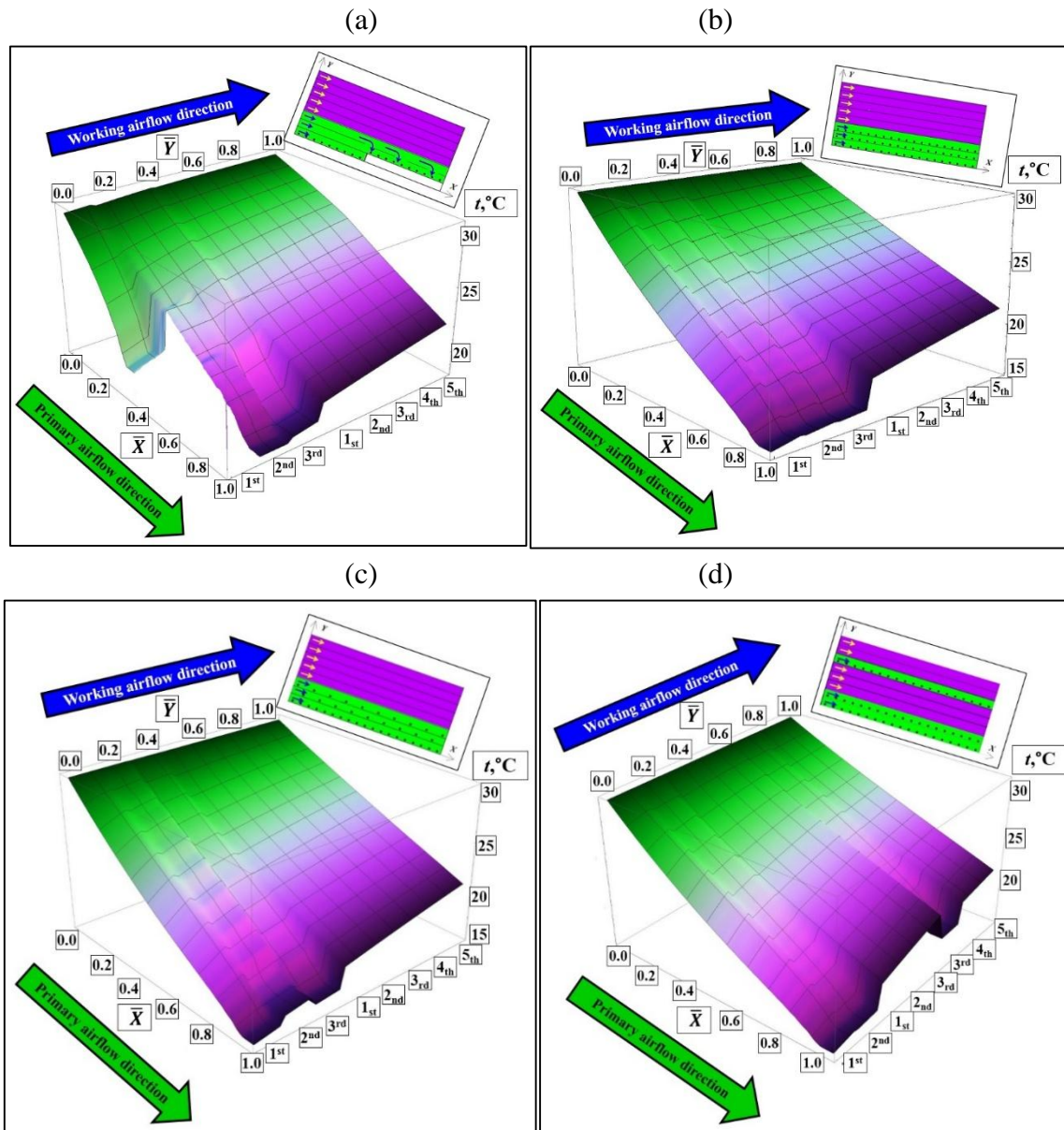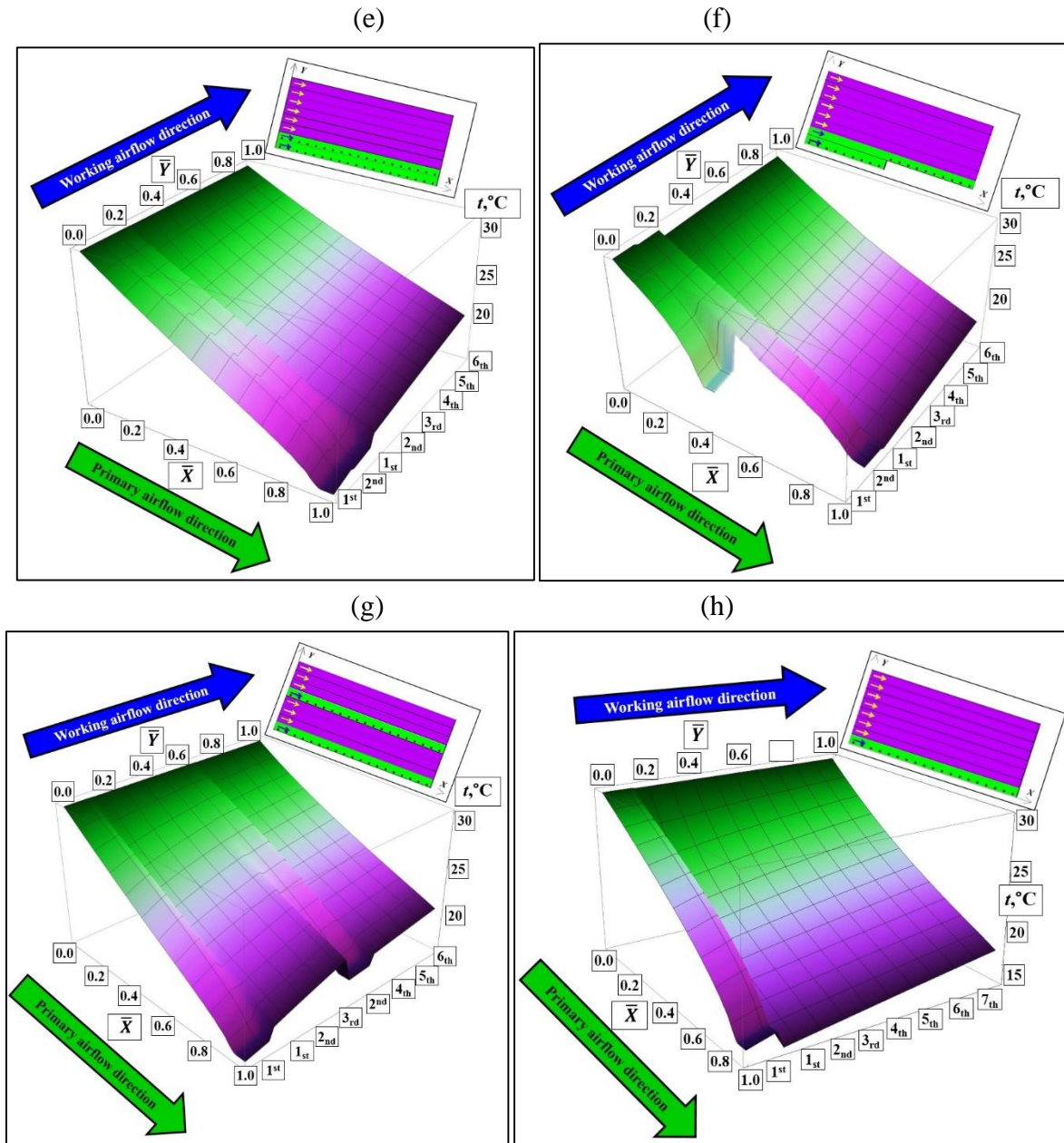


Fig. 5.5. Air temperature distribution inside the dry channels: surface plots. Inlet conditions: $t_{1i}$=30°C, RH$_i$=40%, $V_1$=300 m$^3$/h, $W_2/W_1$=1.0. (a) V0. (b) V1. (c) V2. (d) V3. (e) V4. (f) V5. (g) V6. (h) V7.

Air temperature distribution inside the wet channels is presented on the surface plots (Fig. 5.6(a)−(h)). Processes occurring in the wet part of the exchangers differ significantly from the processes in the dry side. Also, the temperature distribution inside each exchanger significantly differs. It can be seen that the plots describing variants with air streams mixing in the wet channel (see Fig. 5.6(b)−(e) and (g)) deviates from the variants V0, V5 and V7, in which mixing process does not occur (Fig. 5.6(a), (f) and (h)). V7 unit shows even temperature change along the whole wet part, there are no profile disturbances and deformations on the plot (Fig. 5.6(h)). In the V0 and V5 devices there is no air stream mixing in the wet channels, however the plot is deformed, because of the uneven length of the wet channels (the length of the wet channels can be seen in Fig. 5.4(a) and (f)).

In the devices where the mixing process occurs (V2–V4 and V6) the air temperature profiles are deformed as it was visible in case of the ideal M-Cycle air cooler analyzed in previous section: at the beginning of the wet channel, the temperature of the air stream intensively decreases, but at a certain point it is increases abruptly. After a sharp increment, the temperature starts decreasing again. The number of oscillation peaks and their location depends on the holes arrangement (see Fig. 5.4) and it is caused by the mixing of the hotter air stream from the dry channel with the colder airflow inside the wet channel. When exchanger has got no holes located in the way of the working air stream along the channels, the oscillation phenomenon is absent (variants V0, V5 and V7: Fig. 5.6(a), (f) and (h)).

(a)                                              (b)



(c)                                              (d)

(e)

(f)

(g)

(h)
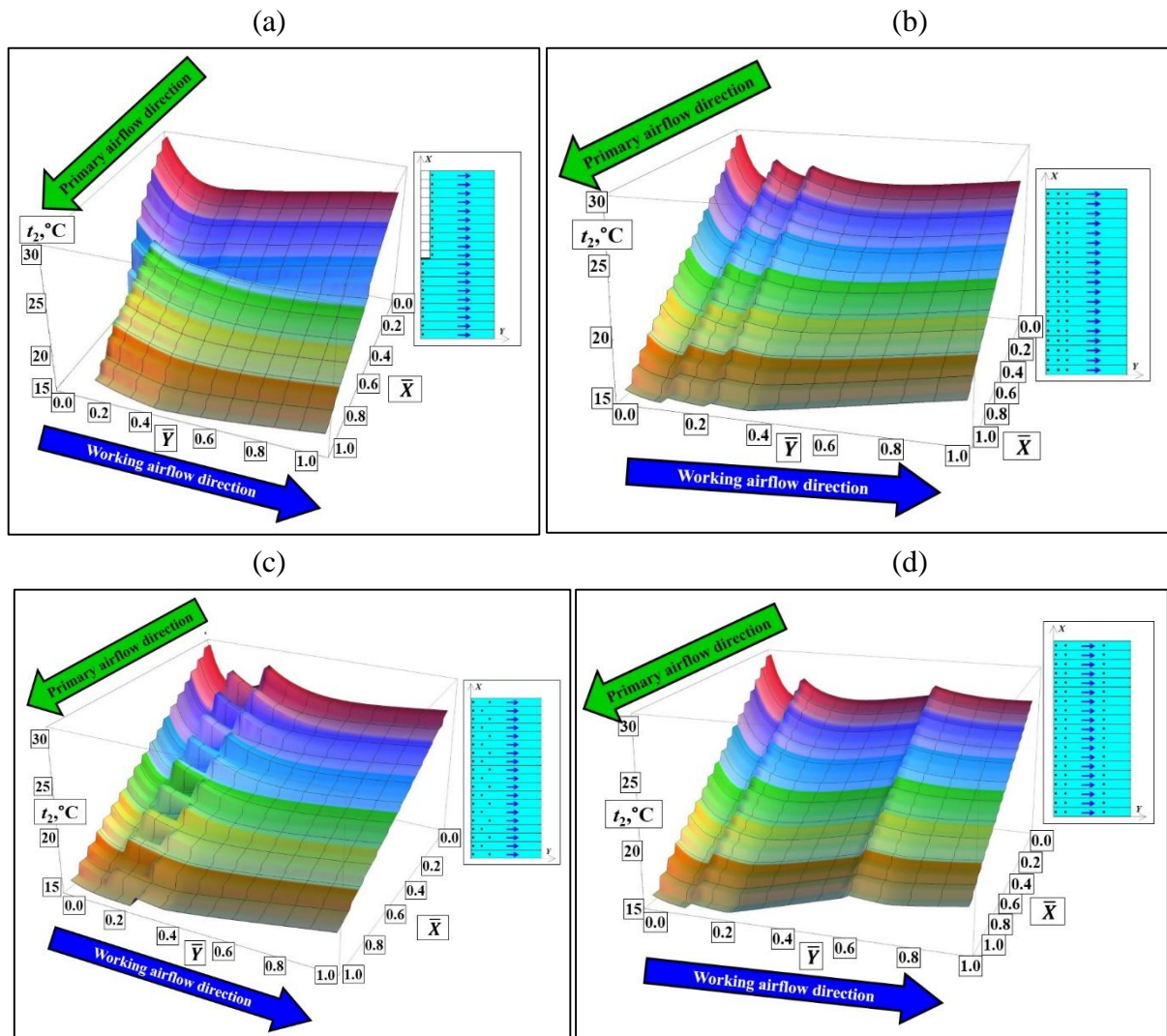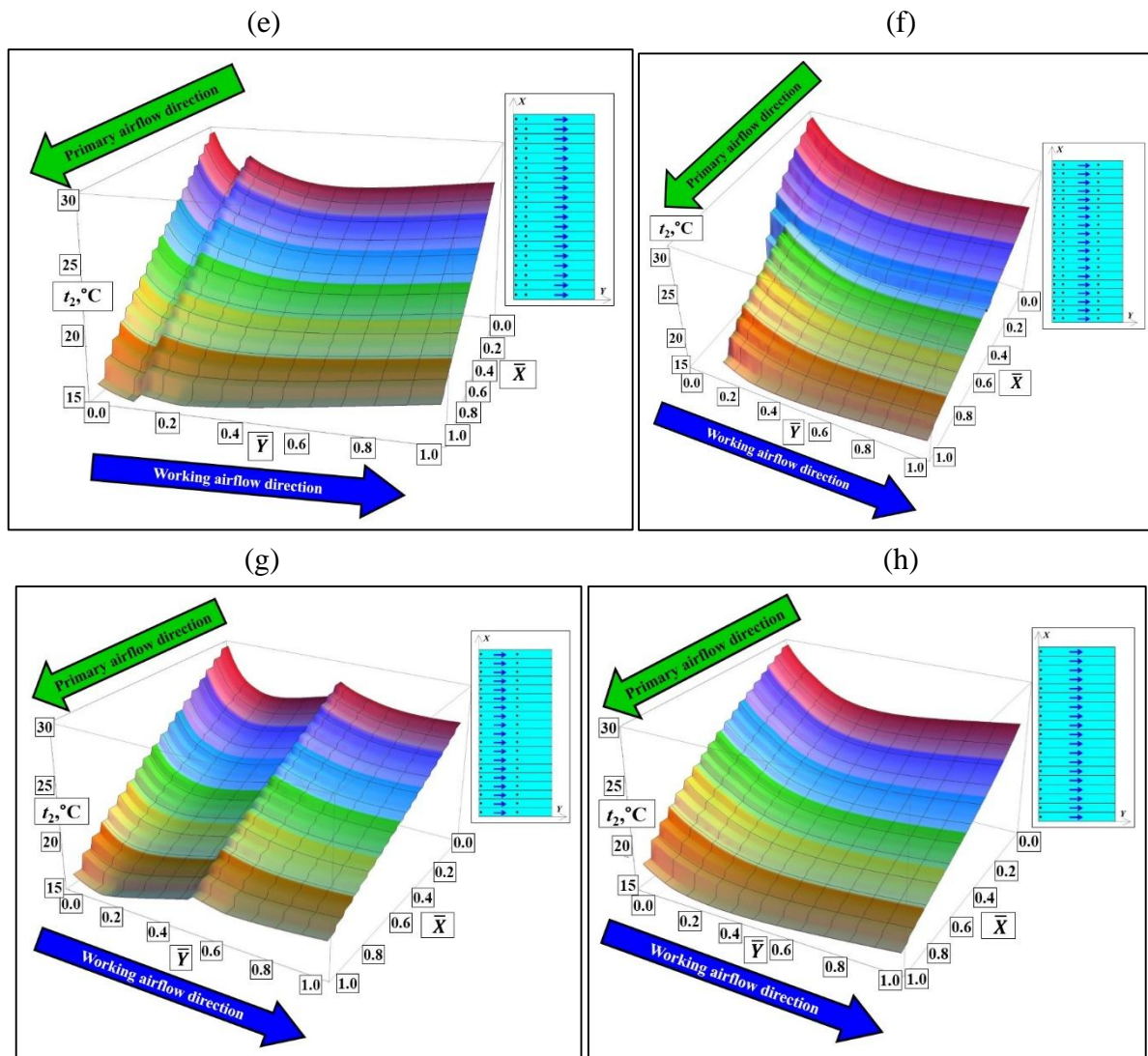
Fig. 5.6. Air temperature distribution inside the wet channels: surface plots. Inlet conditions: $t_{1i}$=30°C, RH$_i$=40%, $V_1$=300 m$^3$/h, $W_2/W_1$=1.0. (a) V0. (b) V1. (c) V2. (d) V3. (e) V4. (f) V5. (g) V6. (h) V7.

Figure 5.7 shows distribution of the humidity ratio in the wet channels of the analyzed exchangers. It is clearly visible that the mixing process in the units V1−V4 and V6 also affects the humidity ratio profiles (Fig. 5.7(b)−(e) and (g)). It can be seen that the oscillations in the humidity ratio profiles are more visible than oscillations on the temperature plots.

It can be also seen in all the plots that the humidity ratio profiles in the part closer to the end of the dry channel ($\bar{X} = 0.95 − 1.0$ in Fig. 5.7) differs a little from the rest of the plot. This is caused by the almost adiabatic humidification process, which is occurring when the working air stream 3 enters the wet channel through the last hole − no airflow remains in the dry working channel, therefore the airflow is cooled in the direct evaporative cooling process.

(a)

(b)

(c)

(d)

(e)

(f)
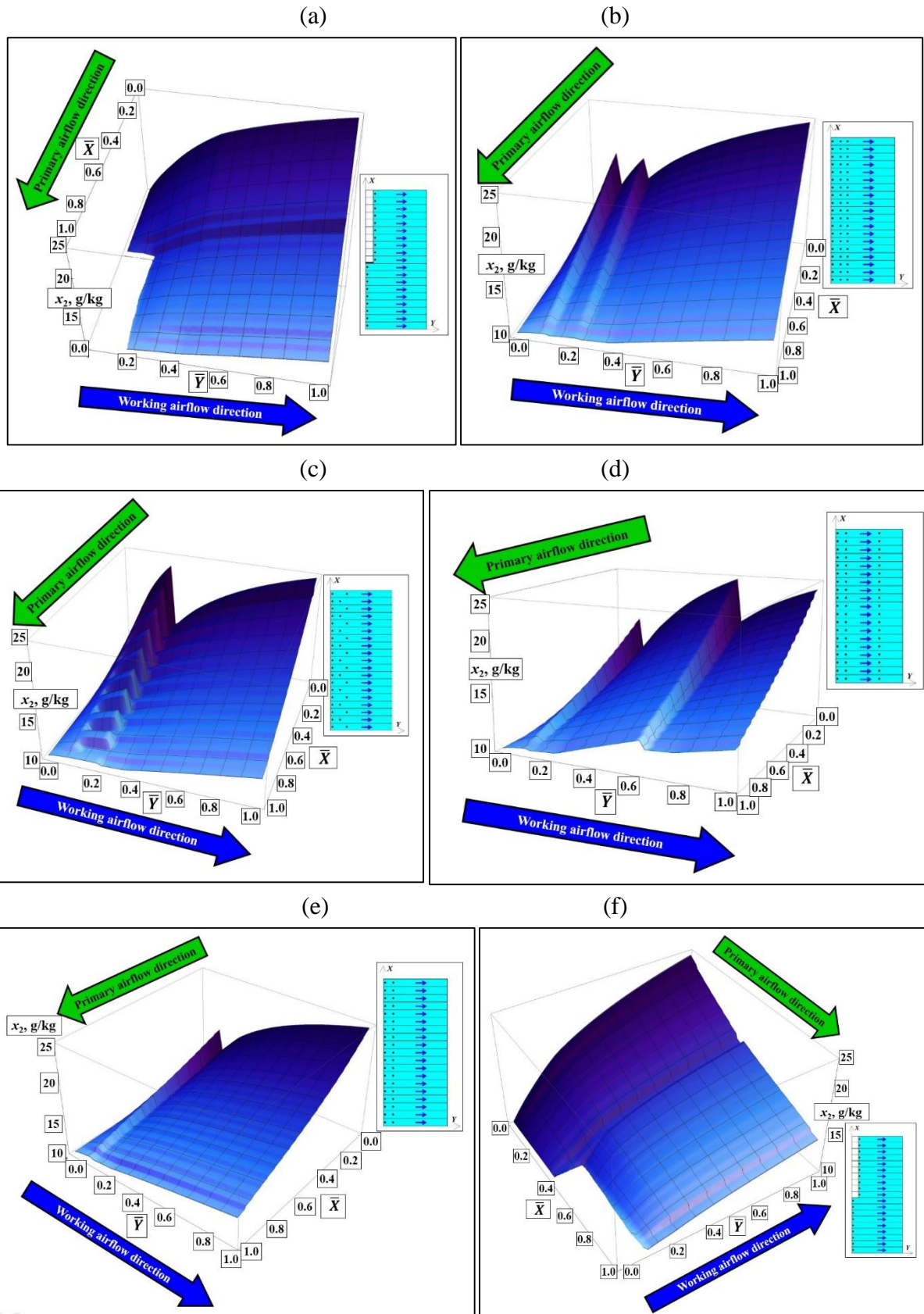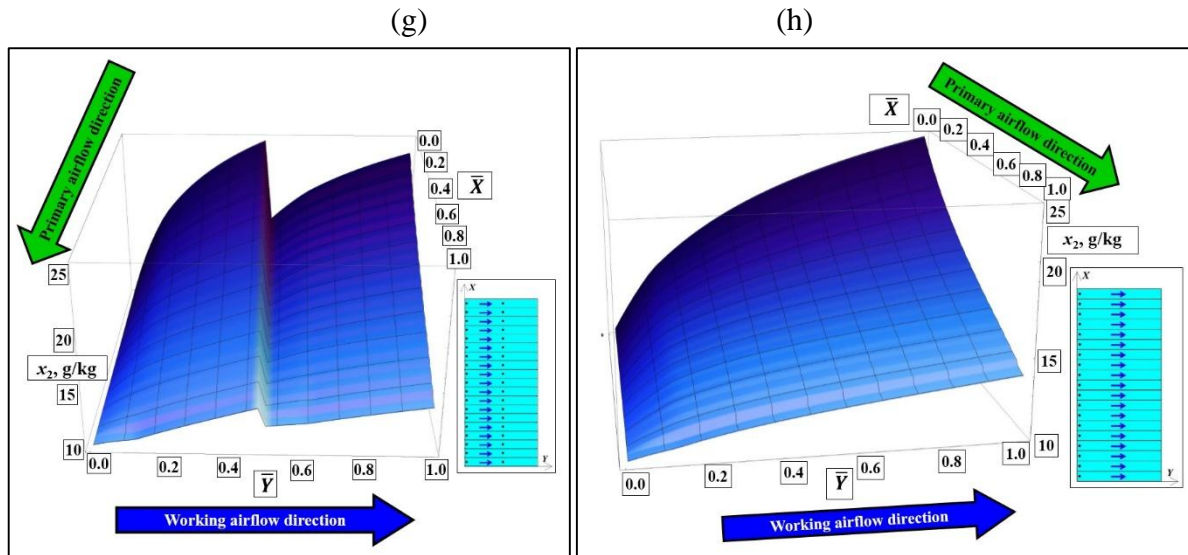
Fig. 5.7. Humidity ratio distribution inside the wet channels: surface plots. Inlet conditions: $t_{1i}$=30°C, RH$_i$=40%, $V_1$=300 m$^3$/h, $W_2/W_1$=1.0. (a) V0. (b) V1. (c) V2. (d) V3. (e) V4. (f) V5. (g) V6. (h) V7.

The simultaneous changes of the airflow temperature and humidity ratio for the can be seen in psychrometric charts (Fig. 5.8). It can be seen that the phenomenon of active heat and mass transfer zones occurs in the realistic M-Cycle air coolers as well. This phenomenon is particularly pronounced in the variants V0,V5 and V7, because the temperature and humidity ratio profiles are not deformed by the process of the air streams mixing. In the case of the perforated heat and mass exchangers, the effect of the sensible heat flux direction changing in the wet channel occurs repeatedly (working air stream temperature decreases and increases alternately) due to the mixing of the air streams (Fig. 5.8(b) and (j)). This phenomenon is much easier to observe in case of the realistic exchangers, due to the fact that in case of the untis with very dense perforation the repeating mixing of the air streams makes the results (plots) very hard to analyze and interpret (see section 5.1). The analysis of heat transfer processes in the realistic units allows assuming that similar process (multiple existence of active heat and mass transfer zones) occurs in the ideal M-Cycle HMX with dense perforation as well.

It can be seen that the temperature change of the working air stream after mixing with the air from the dry channel is relatively small, since the process is almost isothermal (minimal temperature change with significant changes in humidity ratio, Fig. 5.8). From that it can be concluded that the latent heat flux in the working air channel is significantly higher than the sensible heat flux.

(a)



(b)



(c)



(d)
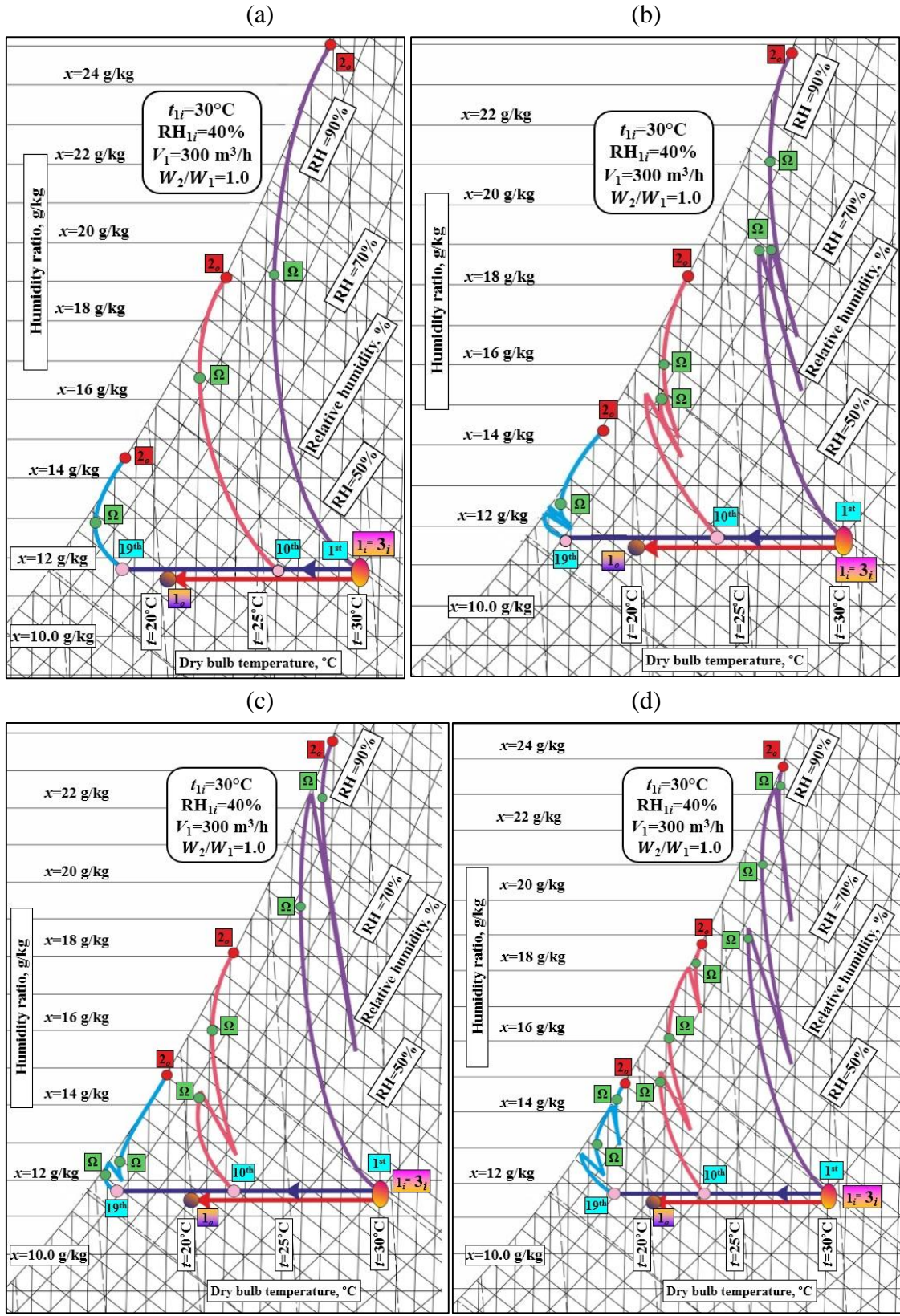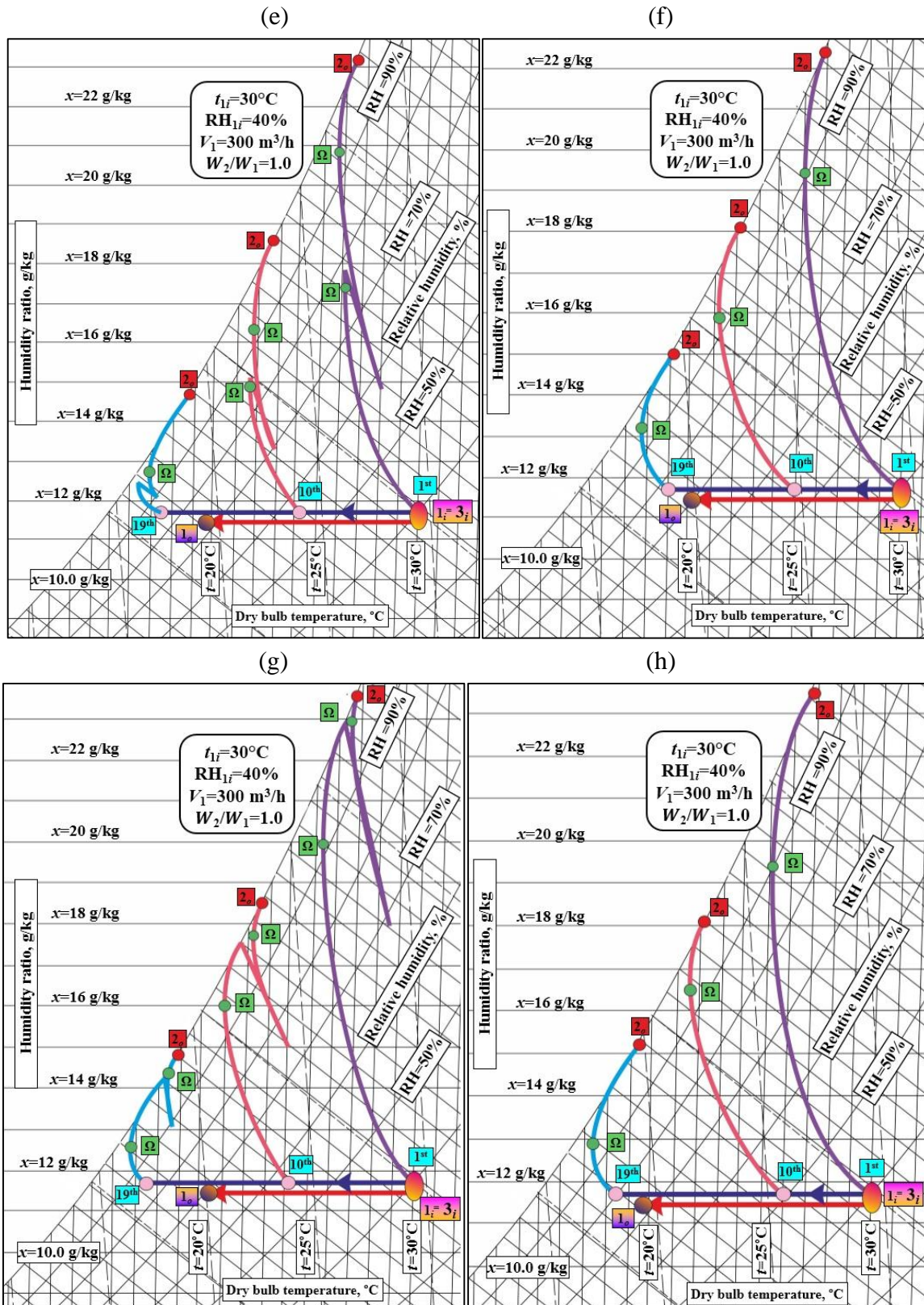
Fig. 5.8. Simulation results on the psychrometric charts. Inlet conditions: $t_{1i}$=30°C, RH$_i$=40%, $V_1$=300 m$^3$/h, $W_2/W_1$=1.0. (a) V0. (b) V1. (c) V2. (d) V3. (e) V4. (f) V5. (g) V6. (h) V7.

### 5.3. Analysis of the heat and mass transfer surface

Another analysis was carried out, to establish how the structure of the M-Cycle HMX affects heat and mass transfer processes. Simulations were performed for three different types of heat transfer structure: flat channels (rectangular-shaped), square channels and triangle channels. Assumptions are presented in Table 5.1

Table 5.1. Assumptions for numerical simulation channels type.

| Type of channel | Dimension a, mm | Dimension b, mm | Height, mm |
|---|---|---|---|
| Flat rectangular («F») | 18 | 3 | 3 |
| Square («S») | 6 | 6 | 6 |
| Triangle («T») | 6 | 6 | 5 |

Results are presented in Figure 5.9. It has been seen that shape of the channels has significant impact on the heat flux distribution. When the channel is flat, heat and mass transfer is mainly realized through the plate surface and less through fins. This configuration is used in currently produced cross-flow M-Cycle HMXs. In this case, from total sensible heat flux from the dry channel, 88% is delivered through the plate surface and only 12% through the fin surface. In the wet channel 13% of sensible heat transfer and 13% of latent heat transfer takes place on the fin surface, while 87% takes place through the plate surface. Substantially different situation occurs when channels have different shape (i.e. square or triangle), when fins are much denser than in the flat channel. In these cases, most of the heat flux (both sensible and latent) is delivered through fins. For square channel, 55% of sensible heat in the dry channel, 62% of sensible heat in the wet channel and 59% of latent heat is transferred through the fins surface. In case of the triangular channel heat transferred the thorough fins in the dry channel is equal to 81% of total sensible heat flux. In the wet channels, 45% of sensible and 82% of the latent heat flux is transferred through fins.

Figure 5.9(b) presents heat flux distribution along $\bar{X}$ axis for the HMX with rectangular channel «F». It can be seen that proportion of heat flux distribution through fins and plate surface is almost constant over the whole channel. In section $\bar{X}$=0.1, 12% of the sensible heat in the dry channel is exchanged through fins, while in the section $\bar{X}$=1.0 it is 12.2%. In the wet part, 13% of latent and sensible heat is transferred through the fins in the section $\bar{X}$=0.1. In section $\bar{X}$=1.0 it is 12.9% and 12.93% respectively. Analogous situation occurs in case of the heat flux distribution along the $\bar{Y}$ axis (Fig. 5.9(c)). In the section $\bar{Y}$=0.1 12% of the sensible heat flux in the dry channel is transferred through fins and in the section $\bar{Y}$=1.0 this value remains unchanged (still 12%). In the wet channel, between sections $\bar{Y}$=0.1 and $\bar{Y}$=1.0, heat transfer through the fins changes from 13% to 12.5% for the sensible heat and from 13% to 12,8% for the latent heat. For the HMX with square and triangle channels, proportion of heat flux distribution is less uniform. In section $\bar{Y}$=0.1 29% of the sensible heat in the dry channel is transferred through fins for HMX with square channels and 40% for the HMX with triangle channels. In section $\bar{Y}$=1.0 it is 60.2% for square channel and 95.1% for triangular channel. In the wet channel, in section $\bar{Y}$=0.1, 59.4% of latent heat is transferred through fins in case of «S»

and 82.3% in the case of «T», while for sensible heat transfer it is 41% for «S» and 31% for «T». In the section $\bar{Y}=1.0$, 63.2% of latent heat is transferred through the fins in case of «S» and 82.3% in case of «T», while for sensible heat transfer it is 61.4% for «S» and 35% for «T». Heat transfer distribution proportions along the $\bar{X}$ axis for square and triangular channel are analogous to those along the $\bar{Y}$ axis.

It is important to note that changes of plate and fin material heat conductivity have a very little impact on the effectiveness of the heat and mass transfer. Simulations were carried out, varying fins and plate heat conductivity from 0.1 to 100 W/(m·K), while keeping the other parameters unchanged. In all analyzed cases, the changes of heat flow values were negligible (Fig. 5.9(g)). For flat channel heat flux transferred through fins has changed by 0.4%, while for square and triangle channels it has changed by 0.5%. This is due to the small channels dimensions: temperature gradient along the fin is close to zero. In the «R» case, temperature along the fin from $\bar{Z}=0.0$ to $\bar{Z}=1.0$ changes by the value of 0.01°C, in «S» case it changes by 0.03°C and in «T» case by 0.04°C when thermal conductivity is changed from 0.1 to 100 W/(m·K). For such small height of channels, change of its thermal resistance cannot affect the heat transfer processes significantly. Plate and fins thermal conductivity has also very little impact on the general performance of the HMX (e.g. outlet temperature of the primary air stream $t_{1o}$ and specific cooling capacity $\hat{Q}_G$). Outlet temperatures for the HMX with flat channels were equal: $t_{1o}^{\lambda=0.1}=19.7°C$ and $t_{1o}^{\lambda=100}=19.4°C$. For the unit with square channels: $t_{1o}^{\lambda=0.1}=19.7°C$ and $t_{1o}^{\lambda=100}=19.4°C$, and for the exchanger with the triangle channels: $t_{1o}^{\lambda=0.1}=19.7°C$ and $t_{1o}^{\lambda=100}=19.4°C$. This fact allows presuming that heat conductivity of material used for the structure of the HMXs is less important in compare to other factors (e.g. ability of even water distribution, durability, shaping ability etc.). It is important to underline that thermal conductivity of the plate and fins in the wet channel is the resultant of porous material and water heat conductivity, so it will always be relatively low [12].

The next study was performed in order to establish the influence of the uniformity of water distribution on heat and mass transfer processes. Varying the surface wettability factor σ from 0.5 to 1.0, while all other parameters remain unchanged. The results are presented in Fig. 5.9(h). Obtained results show that uniform wetting of filling has more substantial influence on cooling efficiency than heat conductivity of the strcture. Outlet temperature for exchanger with flat channel was 3°C higher when only half of the surface was wetted (σ=0.5) in compare to the fully wetted exchanger (Fig. 5.9(h)). Specific cooling capacity $\hat{Q}_G$ related to the 1 kg/s mass airflow was 3 kW lower for half-wetted HMX. The trend is the same for different inlet conditions (Fig. 5.9(h)). For the HMX with the square channels difference in outlet temperatures was 3.2°C, while for the exchanger with triangle channels it was 3.1°C.

(a)

(b)

(c)

(d)

(e)

(f)

(g)  (h)



Fig. 5.9. Simulation results for heat transfer surface. (a) Average latent and sensible heat flux on the plate and fins surface- exchanger with the flat channels (bar chart along the $\bar{X}$ axis). (b) Average latent and sensible heat flux on the plate and fins surface- exchanger with flat channels (bar chart along the $\bar{Y}$ axis). (c) Local latent and sensible heat flux on the plate and fins surface- exchanger with the square channels (bar chart along the $\bar{X}$ axis: section $\bar{Y}$-0.5). (d) Local latent and sensible heat flux on the plate and fins surface- exchanger with the square channels (bar chart along the $\bar{X}$ axis: section $\bar{Y}$-1.0). (e) Local latent and sensible heat flux on the plate and fins surface- exchanger with the triangle channels (bar chart along the $\bar{X}$ axis: section $\bar{Y}$-0.5). (f) Local latent and sensible heat flux on the plate and fins surface- exchanger with the triangle channels (bar chart along the $\bar{X}$ axis: section $\bar{Y}$-1.0). (g) Outlet temperature and specific cooling capacity $\hat{Q}_G$ for the different $\lambda$ coefficient values (■- HMX with square channels; ▲- HMX with triangle channels; ▬- HMX with flat channels). (h) Outlet temperature and specific cooling capacity $\hat{Q}_G$ for different $\sigma$ coefficient values (HMX with flat channels).

## 5.4. Conclusions from the section

The performance of the Maisotsenko HMX was investigated and parametrically evaluated by transitional simulation under various ambient and working/operating conditions to analyze the heat and mass transfer processes occurring in dry and wet channels.

It was found that the processes of heat and mass transfer are characterized by a complex and diverse temperature and moisture distributions, which are significantly different from the dependence found in typical evaporative heat exchangers. The analysis of these distributions in the initial part of HMX shows that heat and mass transfer process in the wet channel are strongly deformed and characterized by temperature and humidity oscillation due to continuous mixing the wet airflow 4 with dry airflow 3. Numerical simulation brings out the existence of two particular heat and mass transfer areas in the wet channels, when sensible heat flux changes its sign at unchanged mass flow direction (working airflow is reversely heated and cooled and constantly humidified). This behaviour is similar to the basic indirect evaporative air coolers (see Section 2), however in case of the cross-flow M-Cycle HMX the active heat and mass zones may occur reversely many times in one device due to the mixing of the air streams (this is easier to observe in case of the realistic units with few perforations, because in the ideal M-

Cycle HMX with dense perforation the continuous mixing of the air streams 3 and 4 makes the plots very hard to read and interpret).

From the analysis of this phenomenon, it is concluded that existence of different heat transfer areas changes the boundary conditions of coupled heat and mass transfer on the plate surface and makes correct calculation of heat transfer performance on the base of logarithmic temperature difference method impossible and leads to violation of Lewis relation unity as in case of the typical cross-flow and counter flow indirect evaporative air coolers (see Section 2). It should be noted that such change of local sensible heat flux direction in the wet channel of the product part causes a generally positive effect, because it allows for more effective cooling of the primary airflow (higher specific enthalpy difference between the inlet and outlet working airflow).

It can be also concluded that the different shape of the channels significantly affect the heat and mass transfer distribution inside the exchanger. The analysis showed that in case of the flat channels most of the heat is transferred through plate, while in case of the units with square and triangle channels most of the heat is transferred through the fins.

It was also established that thermal conductivity of the plate and fins surface has a little impact on the heat transfer distribution and the performance of the exchanger, while the surface wettability factor is characterized by a high impact on the cooling performance of the cross-flow M-Cycle air cooler.

## 6. Analysis of impact of selected factors on the cooling performance

*The results of this section were published in "S. Anisimov, D. Pandelidis, Numerical study of the Maisotsenko cycle heat and mass exchanger, International Journal of Heat and Mass Transfer, 75 (2014) 75–96"* [12] *and "D. Pandelidis, S. Anisimov, Numerical analysis of the heat and mass transfer processes in selected M-Cycle heat exchangers for the dew point evaporative cooling, Energy Conversion and Management 90 (2015), 62–83"* [134].

This section presents the analysis of impact of the main operational and geometrical factors on the cooling performance of the cross-flow M-Cycle indirect evaporative air cooler. Four main parameters (indices) have been selected to study the operational performance of the investigated HMX:

- Temperature level of outlet primary airflow $t_{1o}$ ,
- Dew point thermal effectiveness $\varepsilon_{DP,}$
- The specific cooling capacity respected to the 1 kg/s of the primary airflow $\hat{Q}_G$.

Operational and geometrical parameters varied in this section are:

- Inlet air temperature $t_{1i} = t_{3i}$ ,
- Inlet air relative humidity $RH_{1i} = RH_{3i,}$
- Inlet air humidity ratio $x_{1i} = x_{3i,}$
- Channel height $h,$

- Channel shape,
- Dry channel length $L_X$,
- Wet channel length $L_Y$,
- Primary airflow velocity $v_1$,
- Working to primary heat capacity ratio $W_2/W_1$.

### 6.1. Impact of inlet airflow parameters

### 6.1.1. Inlet air temperature

Varying the inlet air temperature between 25°C and 45°C while all other parameters remain unchanged, the simulation was carried out using the established computer model. The results are presented in Figure 6.1(a) and (b). A trend in increasing supply air temperature, cooling capacity and dew point effectiveness of the HMX coincides with increasing inlet air temperature. This is due to the fact that working airflow mass transfer potential is almost constant when it has constant inlet relative humidity, however, higher temperature facilitates the evaporation of the water (large temperature difference between the water film and the air), therefore warmer airflow is cooled more effectively. It is noteworthy that relatively small temperature difference occurs between inlet and outlet temperatures obtained. Although the temperature of inlet air changes by 20 degrees (from 25°C to 45°C), the maximal difference in outlet temperatures is equal 13°C ($t_{1o}^{25°C}$=12,7°C and $t_{1o}^{45°C}$=25,7°C for RH$_{1i}$= 30%− Fig. 6.1(a)). The dew point effectiveness also increases with the inlet air temperature, e.g. by 23% for RH$_{1i}$ = 30% (from 0.66 to 0.89− Fig. 6.1(a)) and by 17% for RH$_{1i}$ = 45% and RH$_{1i}$ = 60%. Specific cooling capacity $\hat{Q}_G$ varies between 2−15 kW/(kg/s) for RH$_{1i}$ = 30% and 8−25.5 kW/(kg/s) for RH$_{1i}$= 60% (Fig. 6.1(b)). This shows that this indirect evaporative HMX is more efficient at higher inlet air temperatures, suggesting it is more suited to a high- temperature environment.

### 6.1.2. Inlet air relative humidity

Figure 6.1(c) and (d) shows the simulation results for the inlet air with constant temperature and variable relative humidity. When the relative humidity of inlet air increases from 20 to 60% (for $t_{1i}$=45°C), accordingly the dew point effectiveness increases from 0.836 to 0.954. However, at the same time outlet temperature increases and the specific cooling capacity decreases, respectively from 21.3 to 35.8°C and from 27.4 to 20.2 kW/(kg/s). Based on the lowest predicted outlet temperature value, the air cooler is most efficient in dry and hot climates (Fig. 6.1(a)–(d)), however, dew point temperature effectiveness (and wet bulb effectiveness shows the opposite trend: it increases with increasing inlet relative humidity. Such paradoxical conclusion proves that efficiency related to wet bulb or dew point temperature is not an adequate indicator for evaporative coolers performance, when it's considered as the only efficiency factor. A possible explanation of such behavior lies in the nonlinearity of the saturation line. As one can see from psychrometric chart the nonlinear character of saturation

line is that a certain change of humidity ratio at lower level of dry bulb temperature provides greater changers of dew point temperature values. Such character of dependence $t_{1i}^{DP} = f\left(x_{1i}\right)$ at different levels of dry bulb temperature (presented in psychrometric chart in Figure 6.1(e)) explains the change of wet bulb effectiveness trends visible in Fig. 6.1(c) and (d). This can be be also explained with an example using the definition of dew point effectiveness. From Eq.(4.1) dew point effectiveness is given as:

$$\varepsilon_{DP} = \frac{t_{1i} - \overline{t_{1o}}}{t_{1i} - t_{1i}^{DP}}$$

When HMX operates with saturated inlet air the unit cannot cool the air at all, however $t_{1i} = t_{1o} = t_{DP}$, so dew point effectiveness reaches its maximum. At $RH_{1i}$ =90% the temperature drop across the HMX was only 1.9°C, which shows that general performance of the evaporative cooler is low at a humid climate. As the dew point effectiveness shows similar trends in both increasing inlet air temperature and increasing inlet relative humidity, but with different outcome to the considered HMX performance, it can be concluded that the dew point effectiveness cannot be considered to independently characterize the performance of the device.

### 6.1.3. Inlet air temperature and relative humidity combined (constant humidity ratio)

The impact of combined air inlet thermodynamic parameters on cooling efficiency was analyzed through assuming constant inlet air humidity ratio and varying inlet air temperature (which resulted in variable inlet air relative humidity), while other parameters remain unchanged. The results are presented in Figure 6.1(f) and (g). It was established that combined inlet air temperature and relative humidity have significant impact on the cooling efficiency. When humidity ratio remained constant, relative humidity was decreasing with increasing temperature. Therefore, positive impact on cooling effectiveness caused by high temperature is increased by positive influence of lower relative humidity. Primary air stream outlet temperature changes only by 3 degrees, while air entrance temperature changes by 20 degrees. Relationship is quite linear-type. With higher humidity ratio, the positive influence of lower RH (at constant air temperature) is less effective, due to fact that relative humidity increases proportionally with humidity ratio. For example: air stream with inlet humidity ratio equal 8 g/kg and inlet temperature equal 30°C obtains outlet temperature which is 3°C lower than of the air stream with analogous inlet temperature and inlet humidity ratio equal 12 g/kg (Fig. 6.1(f) and (g)).

(a)



(b)



(c)



(d)



(e)

(f)                              (g)



Fig. 6.1. Impact of air inlet parameters on cooling effectiveness. (a) Dew point effectiveness and outlet product air temperature as a function of inlet air temperature (constant inlet relative humidity). (b) Specific cooling capacity and outlet product air temperature as a function of inlet air temperature (constant inlet relative humidity). (c) Dew point effectiveness and outlet product air temperature as a function of inlet air relative humidity (constant inlet temperature). (d) Specific cooling capacity and outlet product air temperature as a function of inlet air relative humidity (constant inlet temperature). (e) Impact of the inlet relative humidity on the dew point effectiveness. (f) Dew point effectiveness and outlet product air temperature as a function of inlet air temperature (constant inlet humidity ratio). (g) Specific cooling capacity and outlet product air temperature as a function of inlet air temperature (with constant inlet humidity ratio).

Analysis also shows that the inlet temperature of the air stream is relatively less important than inlet relative humidity (Fig. 6.1). For example, the same recuperator can cool the airflow with inlet temperature equal 30°C and $RH_{1i}$ =30% to 15.8°C and air with $t_{1i}$ =40°C and $RH_{1i}$ = 18% to 17.2°C. Comparing these two hypothetical scenarios presents a 10 degree difference in inlet temperature and only a 1.4°C difference in outlet temperature. The analysis of combined inlet air temperature and relative humidity impact on the cooling efficiency allows presuming that considered evaporative cooler works with maximal effectiveness in hot, dry climates. The effectiveness will be lowest at moist and cold regions and quite satisfying in colder, but dry climate conditions.

## 6.2. Impact of geometric parameters of the exchanger

This section investigates impact of geometric parameters of the exchanger (height of the channels and length along *X* and *Y* axis) on the dew point effectiveness, outlet air temperature and specific cooling capacity.

### 6.2.1. Channel height

To investigate the impact of channel height on cooling performance of the exchanger simulations were carried out varying the channel height from 2.5 to 20 mm while keeping other parameters unchanged. The results are presented in Figure 6.2(a) and (b). It can be seen that

both the dew point effectiveness and cooling capacity decrease with increasing channel height, while outlet air temperature increases. For the 2.5 mm channel, the obtained outlet primary air temperature was equal 19.2°C, while for the 20 mm channel, it was equal 28.0°C (for $t_{1i} = 30$°C and $RH_{1i} = 45\%$). The difference in obtained outlet air temperatures for exchanger with lowest and highest channel height was at most 15°C. Therefore, channel height has a significant impact on cooling efficiency and it needs to be taken under consideration in analysis of M-Cycle air coolers. From the efficient heat transfer standpoint, the channels should be relatively low-pitched. However, a small channel height results in increased flow resistance and decreased energy efficiency, if airflow rate remains unchanged. Therefore, it is reasonable to keep constant airflow velocity in the channels, i.e. use higher number of smaller channels instead of few bigger channels.

### 6.2.2. Channel shape

Analysis of the impact of channel shape on the cooling effectiveness was performed for three type of channels established in Table 5.1 (flat, square and triangle– shaped). The dimensions of the channels was selected on the basis of consultation with Prof. Maisotsenko and Coolerado Corporation to satisfy their manufacturing methods and to satisfy the relations for the characteristic Nusselt numbers for the heat transfer presented in [116]. Results are presented in Figure 6.2(b) and (c). All simulations were performed varying the heat transfer surface (different type of channels are characterized by a different surface) and boundary conditions for heat and mass transfer (for different type of channels shape [116]) assuming constant air velocity in each channel and all other parameters unchanged. Results show that for considered conditions flat channels allow achieving highest cooling efficiency. Outlet temperature obtained by HMX with flat channels is up to 1.3°C lower than triangle channels and up to 3.43°C lower than square channels. Obtained dew point effectiveness for unit with flat channels is respectively up to 10.1% and 23.0% higher from units with triangle and square channels (Fig. 6.2(c)). Similar trend is visible in case of the specific cooling capacity. This is caused by the most advantageous combination of thermal characteristics and height for the flat rectangular channel. Nusselt numbers for flat rectangular channel are equal $\mathrm{Nu}_h^{Icond} = 5.597$ and $\mathrm{Nu}_h^{IIcond} = 6.49$, for square channel $\mathrm{Nu}_h^{Icond} = 2.976$ and $\mathrm{Nu}_h^{IIcond} = 3.608$ and for triangle channel $\mathrm{Nu}_h^{Icond} = 2.47$ and $\mathrm{Nu}_h^{IIcond} = 3.11$. This shows that heat transfer coefficient α is highest for the flat channel (assuming the same value of characteristic length). However, flat channel has much smaller heat transfer surface (the dimensions are presented in Tab. 5.1) than square and triangle channels. Flat channels are more effective than triangle and square channel with considered dimensions, due to the lower channel height, which is essential for effective heat transfer (see Section 6.2.1) and due to the higher convective heat transfer coefficient α and mass transfer coefficient $\beta$. Effectiveness of exchanger with triangle channels is higher than of the unit with square channels, because triangle channel compensates higher Nusselt number of square channel with larger heat transfer surface.

Results presented in Section 6.2.1 show that cooling performance of the cross-flow M-Cycle HMXs increases with lower channel height (Fig. 6.2(a) and (b)), therefore if triangle/square channel would have the same height as flat channel, they would be more effective, due to the higher heat transfer surface. However, the direct comparison of the effectiveness for different shaped channels is hard to perform. It is important to mention that for very low channel height it is easier to construct the flat channel. This shows that economical and constructing issues must be taken under consideration. In this Section analysis was based on the assumption that the flat channel should has lower height than square and triangle channel, otherwise it would not be "flat". This assumption was also made, due to the manufacturing methods used by the Coolerado Corporation . The currently produced cross-flow M-Cycle exchanger is based on the flat channels [112]. It is impossible to create channels with analogues height with square or triangle shape using the same technique, because the hot polyethylene would plaster the channels. Therefore, flat channels are easier to be structurally implemented in evaporative air coolers, because it is harder to create evenly shaped triangle or square channels with a micro-porous polymeric material. It is also harder to distribute the water evenly on triangle or square-shaped fins. Therefore in many cases it is reasonable to use flat channels with low height instead of square and triangle channels with larger heat transfer surface.
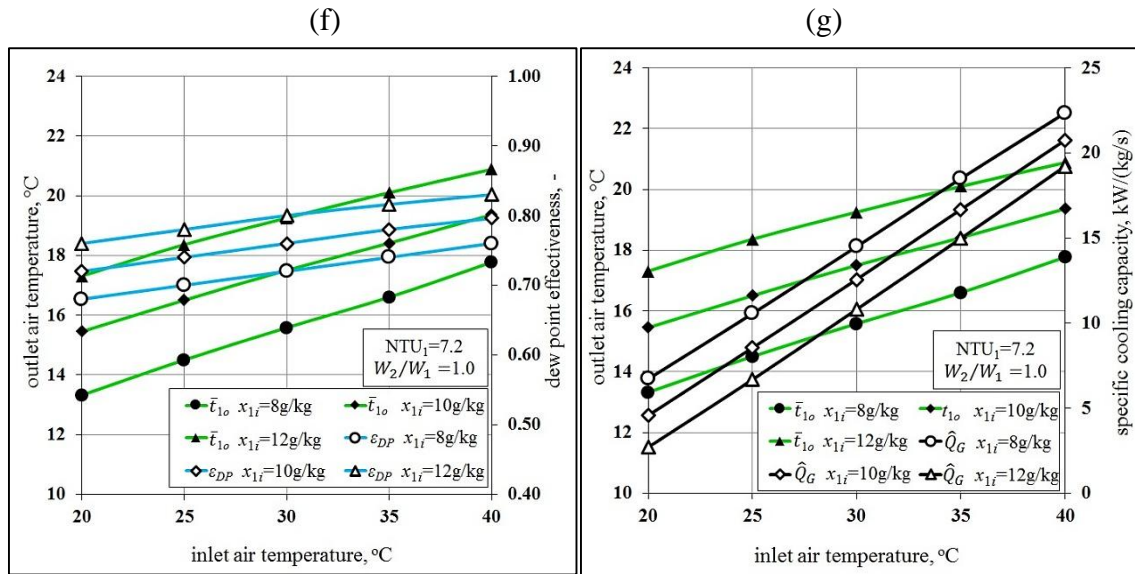
(a) (b)

Fig. 6.2. Impact of exchanger geometry on cooling efficiency. (a) Dew point effectiveness and outlet product air temperature as a function of channel height (HMX with flat channels). (b) Specific cooling capacity and outlet product air temperature as a function of channel height (HMX with flat channels). (c) Dew point effectiveness and outlet product air temperature as a function of $L_X$ ( ■- HMX with square channels; ▲- HMX with triangle channels; ▬- exchanger with flat channels). (d) Specific cooling capacity and outlet product air temperature as a function of $L_X$. (e) Dew point effectiveness and outlet product air temperature as a function of $L_Y$ (HMX with flat channels). (f) Specific cooling capacity and outlet product air temperature: function of $L_Y$ (HMX with flat channels).

## 6.2.3. Exchanger length

Varying the length of the exchanger along the $X$ axis (dry channel length) from 0.25 m to 1.0 m, while keeping all other parameters unchanged, simulations were carried out to investigate the impact of channel length on the cooling performance. As shown in Fig. 6.2(c) and (d), dew point effectiveness and specific cooling capacity increase with increasing dry channel length $L_X$, whereas the outlet air temperature present the adverse trend under this variation. This shows that M-Cycle HMX should have relatively long dry channel $L_X$. The

increasing of the length can lead to the enhancement of the heat and mass transfer process by increasing the contact time and area. It should be additionally noted that longer dry channel allows for more effective cooling of secondary air stream 3 as well. Colder working air can cool the primary airflow to the lower temperature level. However, longer channel causes higher pressure loss and it results in inefficient use of the structure of the exchanger: the positive effect of lower outlet air temperature is compensated with the disproportionate increase in the heat exchange surface required to obtain the lower temperature. Therefore the length of the exchanger should be determined with compromise method.

Another set of simulations was performed to analyze the impact of length along the *Y* axis on the cooling efficiency. Simulations were carried out varying the length of the exchanger along the *Y* axis (wet channel length) from 0.25 m to 1.25 m, while keeping all other parameters unchanged. The results shown in Fig. 6.2(e) and (f) are presented for the HMX with flat channels for fixed inlet relative humidity (results for exchangers with different shaped channels were analogous). It can be seen that outlet air temperature decreases with increasing wet channel length, whereas dew point effectiveness and specific cooling capacity rate are increasing. The trend, however, is not as distinctive as in the case of dry channel length. Differences in outlet temperatures for the shortest and longest channel are similar, but when compared the differences after each step, it can be seen that temperature drops are becoming linear for $L_Y$ and parabolic for $L_X$. This can be explained as follows: the working air stream becomes saturated relatively fast, therefore, when the wet channel is long, the heat and mass transfer in its final part becomes less effective and primary airflow is not cooled evenly. Therefore, the average outlet temperature does not achieve very low values. The effectiveness of HMX, when only $L_Y$ is variable (under constant velocity conditions), should be treated as asymptotic. To verify that hypothesis, simulations were performed, assuming $L_Y$=10 m. Outlet temperature was only 1.0°C lower, than for the HMX with $L_Y$=1.25 m.

### 6.3. Impact of other operational parameters

### 6.3.1. Airflow velocity

The results of simulations performed to study the impact of the airflow velocity on the performance of considered air cooler are presented in Figure 6.3(a) and (b). When declared primary airflow velocity increases (at fixed working to primary heat capacity ratio), the primary air mass flow rate increases in proportion, so does the working mass flow rate in wet channels. Simulations were carried out, varying the primary airflow velocity from 1.8 to 6.8 m/s while keeping other parameters unchanged As shown in Figure 6.3(a) the specific cooling capacity rate related to the 1 kg/s mass airflow rate increases with increasing primary airflow velocity (i.e with increasing air mass flow rate). However, at the same time, outlet air temperature increases, while dew point effectiveness decreases: respectively from 15.6 to 20.6°C and from 90 to 64% (see Fig. 6.3(b)). The increasing trend of the outlet product air temperature index with the variation of the airflow velocity can be explained on the base of energy balance equations developed for the primary air stream (on the basis of Eq. 4.13): the higher outlet air

temperature $\bar{t}_{1o}$ is caused by the lower NTU value, due to the high air mass flow rate. Higher air mass flow rate also results in increased specific cooling capacity, because the changes in outlet air temperature are relatively small in compare to the growth of the airflow rate, therefore the cooling capacity is higher in proportion with increasing velocity. It should be noted that when $G_1 \rightarrow \infty$ the $\hat{Q}_G \rightarrow \infty$, however $\bar{t}_{1o} \rightarrow t_{1i}$. That is why the construction of considered exchanger should guarantee a relatively low value of the airflow velocity in the channels. However, air stream velocity should not be too low, because the differences in outlet temperature do not change that much for low airflow velocities, for example $t_{1o}$ for $v$=1.8 m/s is equal 19.3°C and for $v$=3.0 m/s it is equal 20.2°C (Fig. 6.3(a)). Additionally, the unit with very low airflow velocity in channels would have too large dimensions

### 6.3.2. Working to primary air heat capacity ratio

For the fixed values of primary airflow velocity (simulations were performed for three different values, equal 2, 3 and 4 m/s), the influence of working to primary air heat capacity ratio on outlet air temperature, dew point effectiveness and cooling capacity was investigated. Studies were performed through changing $W_2/W_1$ ratio from 0.25 to 3.0 by interval of 0.25. The results are shown in Figure 6.3(c) and (d). It is visible that outlet air temperature decreases $W_2/W_1$ ratio changing from 0.25 to 1.0 and it remains practically constant (temperature change is equal 0.02°C, which is negligible) for $1.0<W_2/W_1\leq3.0$. The same trend is clearly visible for dew point effectiveness and cooling capacity (Fig. 6.3(c) and (d)). The nature of these trends can be explained as follows: when working air mass flow rate is smaller than the primary air mass flow rate, its heat capacity and ability to assimilate water vapor is relatively small. Sensible heat flux from the product channel is equal $G_1 c_p (t_{1o} - t_{1i})$ and it is completely delivered to the wet channel. Total heat flux in the wet channel is equal $G_2(i_{2o} - \bar{\iota}_{2i})$. Because $G_2$ is smaller than $G_1$, specific enthalpy drop (and therefore temperature drop) in the dry channel must be smaller, to fulfill the balance equation. That is why primary air stream is cooled less effectively, when it is larger than working air stream. When air streams are equal (i.e. their heat capacities are equal), the efficiency of cooling becomes high. When working airflow is larger than primary airflow, its heat capacity allows for good assimilation of water vapor and sensible heat, but (when geometric parameters of the exchanger are constant) higher mass flow rate reduces the NTU of working air (lower heat transfer potential), which compensates the positive effect of higher heat capacity. This results in almost constant performance indexes for working to primary air heat capacity ratio higher than 1.
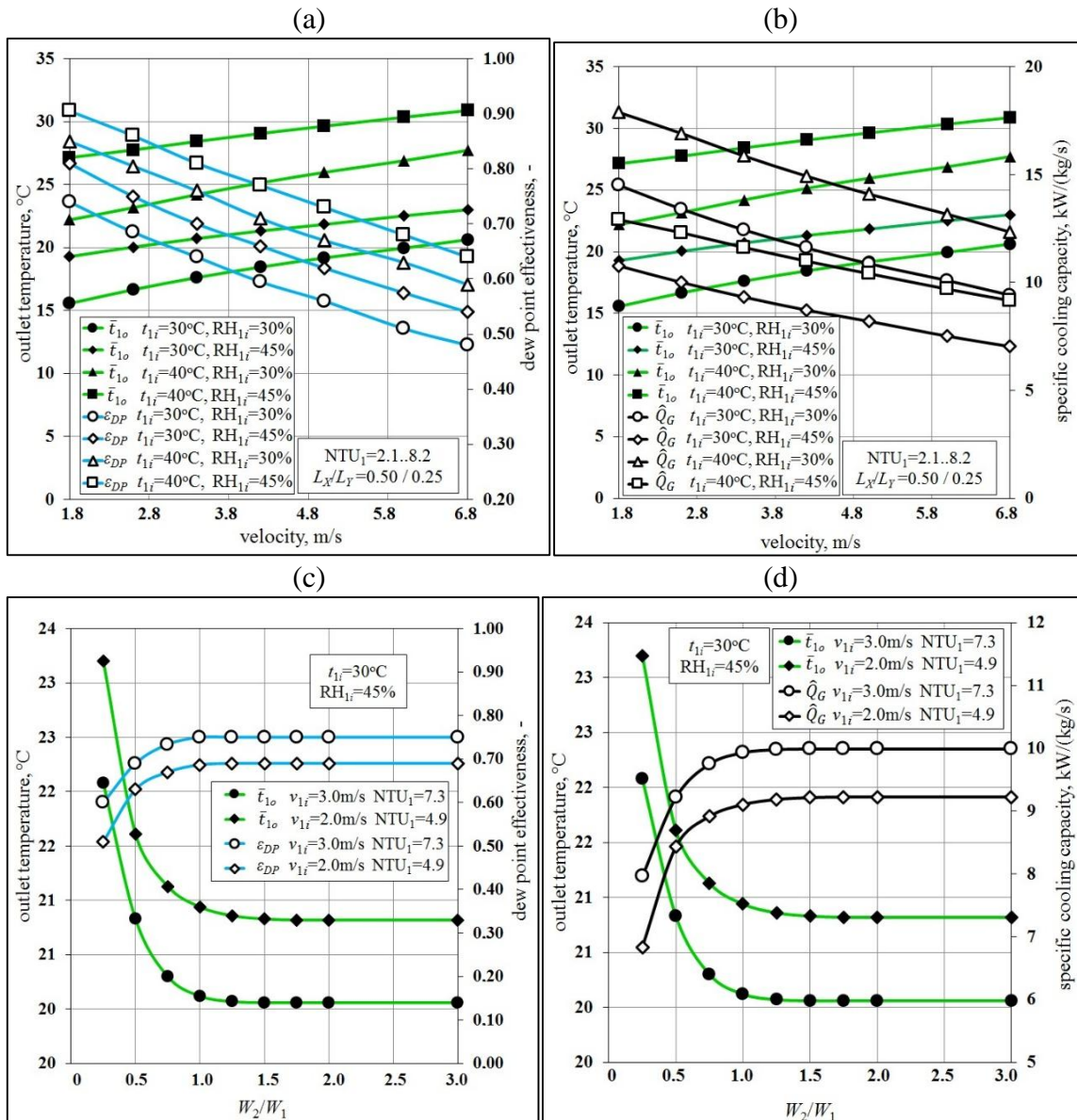
Fig. 6.3. Impact of operational parameters on cooling effectiveness. (a) Dew point effectiveness and outlet air temperature as a function of airflow velocity. (b) Specific cooling capacity and outlet air temperature as a function of airflow velocity. (c) Dew point effectiveness and outlet air temperature as a function of $W_2/W_1$ ratio. (d) Specific cooling capacity and outlet air temperature as a function of $W_2/W_1$ ratio.

### 6.4. Conclusions from the section

The performance of the Maisotsenko HMX was investigated and parametrically evaluated by transitional simulation under various ambient and working/operating conditions in terms of cooling efficiency. Sensitivity analysis was performed to determine which design parameters have the most impact on the HMX performance under various ambient and operating conditions in terms of outlet air temperature, dew point effectiveness and specific cooling capacity.
It was established that:

- M-Cycle is most effective in hot and dry climates and it is less effective in cold and humid climate conditions,

- the energy efficiency of the considered HMX is affected by its geometrical and operational parameters: length, height and shape of the channels, uniformity of water distribution, as well as it is affected by the intake air velocity and the working-to-intake air ratio, but it depends less on the conductive conductance through fins,

- considered heat exchanger can be relatively long in the primary airflow direction, but it should not be too long along the working airflow direction,

- the efficiency of the exchanger increases for working to primary air heat capacity ratio increasing from 0 to 1 and it remains relatively constant when it is higher than 1.0,

- dew point effectiveness (and wet bulb effectiveness) is not an adequate indicator to analyze the M-Cycle air cooler performance, when it is considered as only efficiency factor. In some cases (i.e. high inlet air relative humidity) dew point effectiveness can increase while the other performance factors are decreasing. An optimized design of the M-Cycle heat exchanger is a compromise between dew point effectiveness and cooling capacity.

## 7. Comparison of different M-Cycle air coolers

*The results of this section were published in "S. Anisimov, D. Pandelidis, J. Danielewicz, Numerical analysis of selected evaporative exchangers with the Maisotsenko cycle, Energy Conversion and Management 88 (2014) 426–441"* [45].

It was earlier mentioned in the instruction (Section 1) and in the initial analysis (Section 2) that there is a number of heat and mass exchangers utilizing different forms of the M-Cycle. The main exchangers are presented in Fig. 7.1. The first HMX (Fig 7.1(a)) is the ideological basis of the M-Cycle and it was the first kind of the heat exchanger which allowed to present the principals of this physical process [15]. This kind of HMX is created on the base of counter-flow exchanger, but its structure is modified to realize the M-Cycle. The second HMX is the unit with the simplest construction and airflow arrangement: the regenerative HMX (Fig. 7.1(b)). The heat and mass transfer process in this exchanger was discussed in Section 2. The regenerative HMX can also be equipped with perforation (Fig. 7.1(c)). It should be mentioned that devices presented in Figure 7.1(a)–(c) are harder to manufacture than the unit with the cross-flow arrangement [15]. That is why the most popular HMX with the M-Cycle (produced by the Coolerado Corporation) is based on the cross-flow arrangement (see Fig. 7.1(d)). Due to this fact another type of the cross-flow M-Cycle exchanger was proposed by author (Fig. 7.1(e)). The proposed device differs from the original HMX by the direction of the working air stream in the dry channels: it flows in the opposite direction than the primary air stream, while in the original unit it flows in the same direction (Fig. 7.1(d) and (e)).

It should be noted that the cross-flow is currently produced commercially. Also some companies around the world applied the regenerative exchangers in their air handling units [2]. The original M-Cycle exchanger, however, is not commercially produced, due to the complex structure. Despite the exchanger presented in Fig. 7.1(a) is not produced, its operating principle

is the base of the M-Cycle and its efficiency is assumed to be the highest [15]. In this regards, it is important to compare the effectiveness of existing M-Cycle devices with their ideological roots. That is why study presented in this Section focuses on comparing different types of the M-Cycle HMXs with numerical methods. Five different exchangers with the M-Cycle are put to the comparative analysis (Fig. 7.1(a)–(e)):

-Modified counter-flow HMX (variant 1,V1, Fig. 7.1(a)).

-Regenerative HMX (variant 2,V2, Fig. 7.1(b)).

-Perforated regenerative HMX with 5 holes (variant 3, V3, Fig. 7.1(c)).

-Original cross-flow HMX (variant 4, V4, Fig. 7.1(d)).

-Modified cross-flow HMX proposed by author, where primary and working air stream flow in the opposite direction in the dry channels (variant 5, V5, Fig. 7.1(e)).
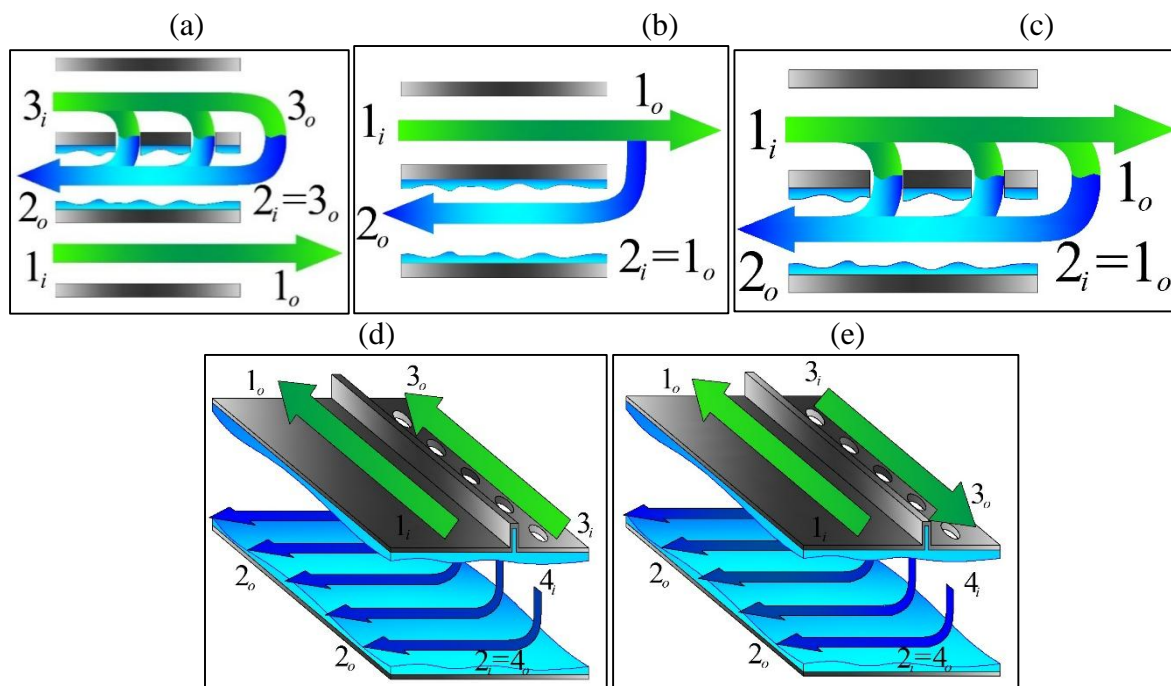


Fig. 7.1. Different versions of the airflow arrangement in the M-Cycle heat and mass exchangers. (a) Modified counter- flow HMX. (b) Regenerative HMX. (c) Regenerative HMX with perforation. (d) Cross-flow HMX. (e) Modified cross-flow HMX.

## 7.1. Assumptions for V1, V3, V5 heat exchangers

There are three new heat and mass exchangers presented in this Section (units V1, V3, V5) and each of them requires a new model (Fig. 7.2). However, the models describing HMXs V3 and V5 are similar to the ones already presented in this thesis. Differential equations describing exchanger V3 are identical to the ones describing the regenerative exchanger (presented in Section 2), the only difference lies in the fact that this unit has to include the mixing algorithm (Fig. 7.2(b)) similar to the cross-flow M-Cycle exchanger (presented in Section 3). Mixing algorithm for the perforated regenerative HMX was presented by author in [136], therefore it will not be discussed in this section. In case of the V5 HMX, the model is exactly identical to the model of the original cross-flow M-Cycle unit (presented in Section 3), the only difference

lies in the initial conditions, because in case of this unit the working airflow enters the HMX from the opposite side (Fig. 7.2(c)). For the above-mentioned reasons it was decided that presentation of the differential equations describing heat and mass transfer in the V3 and V5 exchanger will be omitted. The only model presented in this thesis (in **Appendix G**) is the model of the original unit (V1), because its structure is different from the cross-flow and regenerative HMXs and it requires additional discussion. The general assumption for unit V1 are presented in Figure 7.2(a). The analysis of any evaporative air cooler with numerical methods requires a repeatable structure of the channels. The V1 HMX (Fig. 7.1(a)) is equipped with three channels, which is an odd number and it is not repeatable. That is why this unit had to be transformed into a modified structure in order to perform numerical analysis (see Fig. 7.2(a)). In case of this unit the working air is delivered to the middle channel and it is separated to two wet channels which contact with the primary air from the opposite side. This structure can be made as repeatable and such exchanger can be constructed.

(a)

(b)



(c)
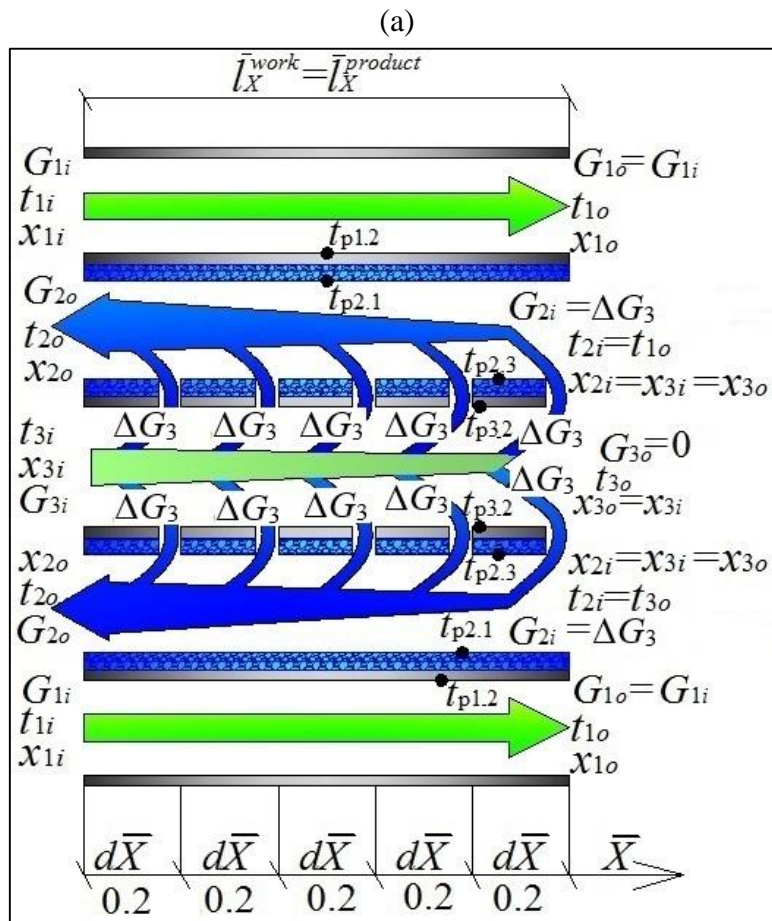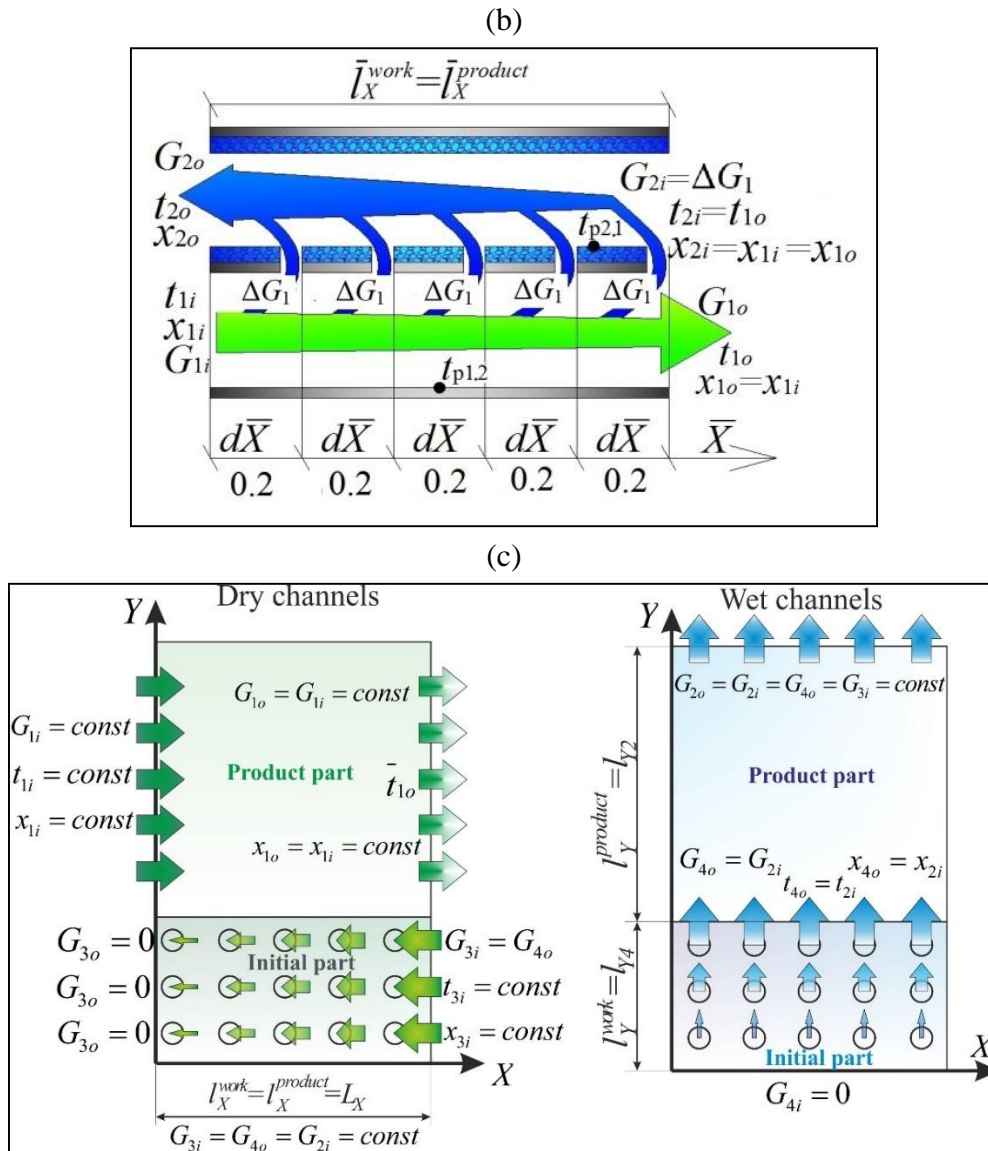


Fig. 7.2. Airflow distribution in the dry and wet channels. (a) Modified counter-flow HMX (V1). (b) Regenerative HMX with perforation (V3). (c) Modified cross-flow HMX (V5).

For the purpose of mathematical modeling, the primary air stream is marked as 1, the working airflow in the wet channels which contacts with the primary air is marked as 2. In the V2 and V3 HMXs the working and primary air stream are both flowing through the same dry channel, therefore the number 1 refers to the main air stream which is the sum of primary and working airflow (see Fig. 2.1 (d) and 7.2(b)). In case of the V1, V4 and V5 HMXs, the working air is delivered to the separated dry channels. In this case the number 1 refers only to the primary airflow. The working airflow in the dry channels for V1,V4 and V5 units is marked as 3 (see Fig. 3.3 and Fig. 7.2(a) and (c)). It can also be seen that only in HMXs V4 and V5 occurs the situation when working air in the wet channels contacts at first with the working air in the dry channels and later with the primary air. The working airflow in the wet channels in the initial part of the HMXs V4 and V5 is marked as 4 (as it was discussed in the Section 3), while the same airflow in the wet channel in the product part of the HMXs is marked as 2.

### 7.2. Results and discussion

### 7.2.1. General assumptions

Three main parameters (indices) have been selected to study the operational performance of the investigated HMXs:

- Outlet primary airflow temperature $\overline{t_{1o}}$.
- The wet bulb thermal effectiveness $\varepsilon_{WB}$.
- The specific cooling capacity respected to the cubic meter of the unit's structure $\hat{Q}$.

Assumptions for the simulations are listed below.

- All exchangers have the same dimensions (0.5 m×0.5 m×0.5 m), the same channel height (4 mm) and the same plate thickness (0.3 mm of wet porous material and 0.02 mm coating impervious material).
- All simulations were performed for primary airflow velocity equal 3 m/s, at constant ratio $W_2/W_1$ and $W_3/W_1$ (except the simulations performed under variable airflow velocity and working to primary heat capacity ratio).
- Due to the different structure of analyzed exchangers they have different assumed working to primary heat capacity ratio: it was established in Section 6 that cross-flow HMXs operate with the highest effectiveness for the $W_2/W_1=1$. However, the construction of V2 and V3 HMXs does not allow to keep $W_2/W_1$ ratio equal 1, because all the primary air stream from the dry channel would have to be delivered to the wet channel, thus the cooling capacity of these units would be equal to zero. The main target of this Section is to compare the M-Cycle exchangers in operating conditions close to optimal, therefore the working to primary heat capacity ratio for V2 and V3 units is assumed on the basis of existing literature studies. Articles [9], [10], [50], [137], [48] show that $W_2/W_1$ ratio for regenerative HMX should be keep at the level close to 0.3, therefore this level is assumed for the purpose of this analysis. For other HMXs (V1, V4 and V5) working to primary heat capacity ratio is assumed as equal to 1.0 (except the analysis under variable the working to primary heat capacity ratio).

### 7.2.2. Results

The results of numerical simulations, including the outlet air temperatures $\bar{t}_{1o}$ and specific cooling capacity per cubic meter of the HMX structure $\hat{Q}$, are presented in Figures 7.3(a)–(e). The studies were performed for different types of conditions:

a) Constant inlet air relative humidity $RH_{1i}$ and variable inlet air temperature $t_{1i}$ (Fig. 7.3(a)).
b) Constant inlet air temperature $t_{1i}$ and variable inlet relative humidity $RH_{1i}$ (Fig. 7.3(b)).

c) Variable primary airflow velocity $v_1$ (Fig. 7.3(c)).
d) Variable value of number of transfer units referred to the primary airflow channel $NTU_1$ at constant primary airflow velocity $v_1$ and working to primary heat capacity ratio (i.e. variable heat transfer surface- Fig. 7.3(d)).
e) Variable working to primary heat capacity ratio at constant primary airflow velocity $v_1$ (Fig. 7.3(e)).

The results of computer simulations for variable inlet air temperature and constant inlet relative humidity are presented in Figure 7.3(a). It can be seen that all of the exchangers show the same trend in increasing supply air temperature $\bar{t}_{1o}$ and specific cooling capacity rate $\hat{Q}$ with increasing inlet air temperatures $t_{1i}$ as the cross-flow M-Cycle air cooler in the previous section. It can be also seen that although outlet temperature $\bar{t}_{1o}$ is lower for the conditions with lower inlet air temperature, the temperature difference between inlet and outlet air $(t_{1i}-\bar{t}_{1o})$ is greater for airflow with the higher temperature $t_{1i}$. The example of differences can be seen in Table 7.1.

Table 7.1. Differences between inlet and outlet air temperatures $(t_{1i}-\bar{t}_{1o})$ for two inlet conditions.

| HMX | $(t_{1i}-\bar{t}_{1o})$ difference (for $t_{1i}=25°C$) | $(t_{1i}-\bar{t}_{1o})$ difference (for $t_{1i}=45°C$) |
|---|---|---|
| V1 | 8.9 | 14.8 |
| V2 | 7.7 | 13.9 |
| V3 | 7.3 | 13.4 |
| V4 | 7.7 | 13.5 |
| V5 | 7.2 | 12.7 |

It can be observed that V1 HMX obtains the lowest value of the outlet air temperature for all the conditions presented in Figure 7.3(a) and in Table 7.1, but at the same time it is characterized by the lowest value of specific cooling capacity index $\hat{Q}$. The regenerative HMX (V2) obtains higher outlet air temperatures than the V1 HMX, but it obtains lower outlet air temperatures than V3,V4 and V5 HMXs (selected values of outlet air temperatures are presented in Tab. 7.2). The original cross-flow HMX (V4) is characterized by the highest specific cooling capacity in comparison with all other considered HMXs (Fig. 7.3(a) and Tab. 7.2), but outlet product air temperatures $\bar{t}_{1o}$ obtained by the V4 unit are higher than the temperatures obtained by the  units V1 and V2. The V5 HMX is characterized by the highest outlet product air temperature among the considered variants, but its specific cooling capacity index is higher than of the units V1-V3. Discrepancies in the outlet product air temperatures and specific cooling capacities for all considered HMXs do not exceed 1.9°C and 11.3 kW/m$^3$ respectively (Tab. 7.2).
Another set of simulations was performed varying inlet primary air relative humidity, while keeping all other parameters unchanged. The results are presented in Figure 7.3(b). It can be seen that also in this case all the exchangers show similar trend: when the relative humidity of inlet air is increased from 30% to 70% (for $t_{1i}=30°C$), accordingly the outlet product air temperature raises and the specific cooling capacity drop for all analyzed units.

Table 7.2. Outlet air temperature $\bar{t}_{1o}$ and specific cooling capacity $\hat{Q}$ for inlet air temperature equal 30°C.

| HMX | $\bar{t}_{1o}$, °C | $\hat{Q}$, kW/m³ |
|-----|------|------|
| V1 | 19.6 | 14.5 |
| V2 | 20.6 | 18.2 |
| V3 | 21.3 | 17.0 |
| V4 | 20.8 | 25.8 |
| V5 | 21.5 | 23.9 |

The example values of obtained $\bar{t}_{1o}$ and $\hat{Q}$ can be seen in Table 7.3. Figure 7.3(b) and Table 7.3 bring another interesting observation: the outlet product air temperatures obtained by devices V1 and V5 deviate significantly from the rest of the HMXs (outlet air temperature of unit V0 is significantly lower than of other units and outlet temperature of unit V5 is significantly higher), while the outlet air temperatures obtained by units V2-V4 are relatively similar. This trend is more visible for the inlet air with lower relative humidity and less visible for inlet air with higher RH (Fig. 7.3(b)). However the specific cooling capacity dependence shows different trend (Tab.7.3 and Fig. 7.3(b)): V4 and V5 units obtain higher specific cooling capacity, which gradually deviates from other HMXs. Specific cooling capacity obtained by units V2 and V3 is similar, while for the unit V1 it is always the lowest from all the obtained results.

Table 7.3. Outlet air temperature $\bar{t}_{1o}$ and specific cooling capacity $\hat{Q}$ for inlet RH equal 45%.

| HMX | $\bar{t}_{1o}$, °C | $\hat{Q}$, kW/m³ |
|-----|------|------|
| V1 | 22.2 | 10.9 |
| V2 | 23.0 | 13.8 |
| V3 | 23.2 | 13.0 |
| V4 | 23.1 | 19.5 |
| V5 | 23.5 | 18.1 |

The next set of simulations was presented at variable airflow velocity. The results of simulations are presented in Fig. 7.3(c). It can be seen that all the exchangers show similar trend: their specific cooling capacity increases with airflow velocity, while the outlet increases. The results of this set of simulations are summarized in Table 7.4.

Table 7.4. Outlet air temperature $\bar{t}_{1o}$ and specific cooling capacity $\hat{Q}$ for different air stream velocities.

| HMX | $\bar{t}_{1o}$, °C $v_1$=2 m/s | $\hat{Q}$, kW/m³ $v_1$=2 m/s | $\bar{t}_{1o}$, °C $v_1$=6 m/s | $\hat{Q}$, kW/m³ $v_1$=6 m/s |
|-----|------|------|------|------|
| V1 | 21.0 | 9.0 | 25.0 | 14.4 |
| V2 | 21.6 | 11.0 | 25.3 | 18.7 |
| V3 | 22.3 | 10.1 | 25.3 | 18.5 |
| V4 | 21.9 | 16.0 | 25.2 | 27.2 |
| V5 | 22.8 | 14.6 | 25.4 | 26.1 |

As can be seen in the Figure 7.3(c) and Table 7.4, the trends in outlet product air temperatures differ from the trends presented in Figures 7.3(a) and (b). With increasing air stream velocity the outlet air temperatures obtained by considered devices become similar: maximum

differences in obtained outlet air temperatures are equal 0.4°C (for $v_1$=6 m/s: Tab. 7.4), however, V1 HMX still achieves lowest outlet air temperatures.

Table 7.5. Outlet air temperature $\bar{t}_{1o}$ and specific cooling capacity $\hat{Q}$ for two levels of NTU.

| HMX | $\bar{t}_{1o}$, °C; $NTU_1$=1.85 | $\hat{Q}$, kW/m³; $NTU_1$=1.85 | $\bar{t}_{1o}$, °C; $NTU_1$=3.5 | $\hat{Q}$, kW/m³; $NTU_1$=3.5 |
|---|---|---|---|---|
| V1 | 21.5 | 10.7 | 18.5 | 17.3 |
| V2 | 22.3 | 14.8 | 19.7 | 20.0 |
| V3 | 22.8 | 14.5 | 20.8 | 18.0 |
| V4 | 22.3 | 23.7 | 20.0 | 26.5 |
| V5 | 22.9 | 20.2 | 21.5 | 23.6 |

The results of numerical simulation of the considered HMXs for variable NTU number, when all other parameters are fixed as constant, are presented in Figures 7.3(d) and (e). It can be seen that the outlet product air decrease, while specific cooling capacity increases with increasing NTU number for all analyzed exchangers. The examples are presented in Table 7.5.

It can be seen that increasing NTU number (i.e. increasing heat transfer surface) can significantly improve the efficiency of considered exchangers (Tab. 7.5, Fig. 7.3(d) and (e)). However, at a certain point the effectiveness of the HMXs grows asymptotically, due to the natural limitations of heat and mass transfer process [114], [116]. That is why the enhancement of heat transfer surface should take place when the calculated value of NTU for considered HMX is relatively low (e.g. 0.5÷2).

It can be seen that with decreasing NTU number wet bulb effectiveness of the considered HMXs becomes similar, which is predictable due to the nature of heat and mass transfer processes realized in the evaporative air coolers [113], [138]: when NTU→0 the $\varepsilon_{WB}$→0 for all of analyzed HMXs. With increasing NTU number, the effectiveness becomes significantly different (see Fig. 7.3(e)). It can be observed that for higher NTU numbers (NTU=3÷3.5 in Fig. 7.3(d)), the trend in outlet product air temperatures obtained by considered devices becomes similar to the trends obtained for variable inlet air temperature and relative humidity (Fig. 7.3(a) and (b)).
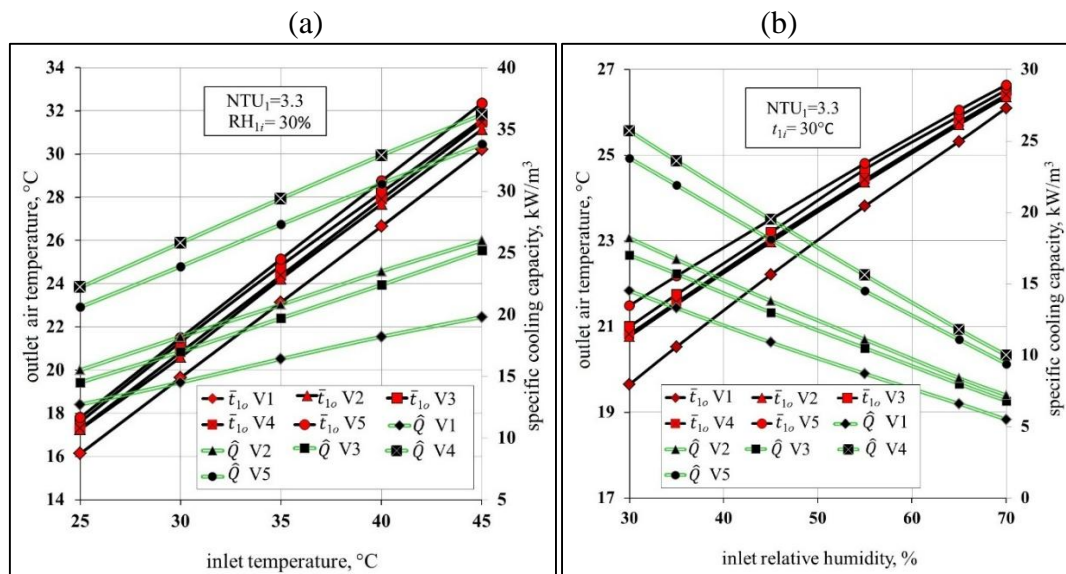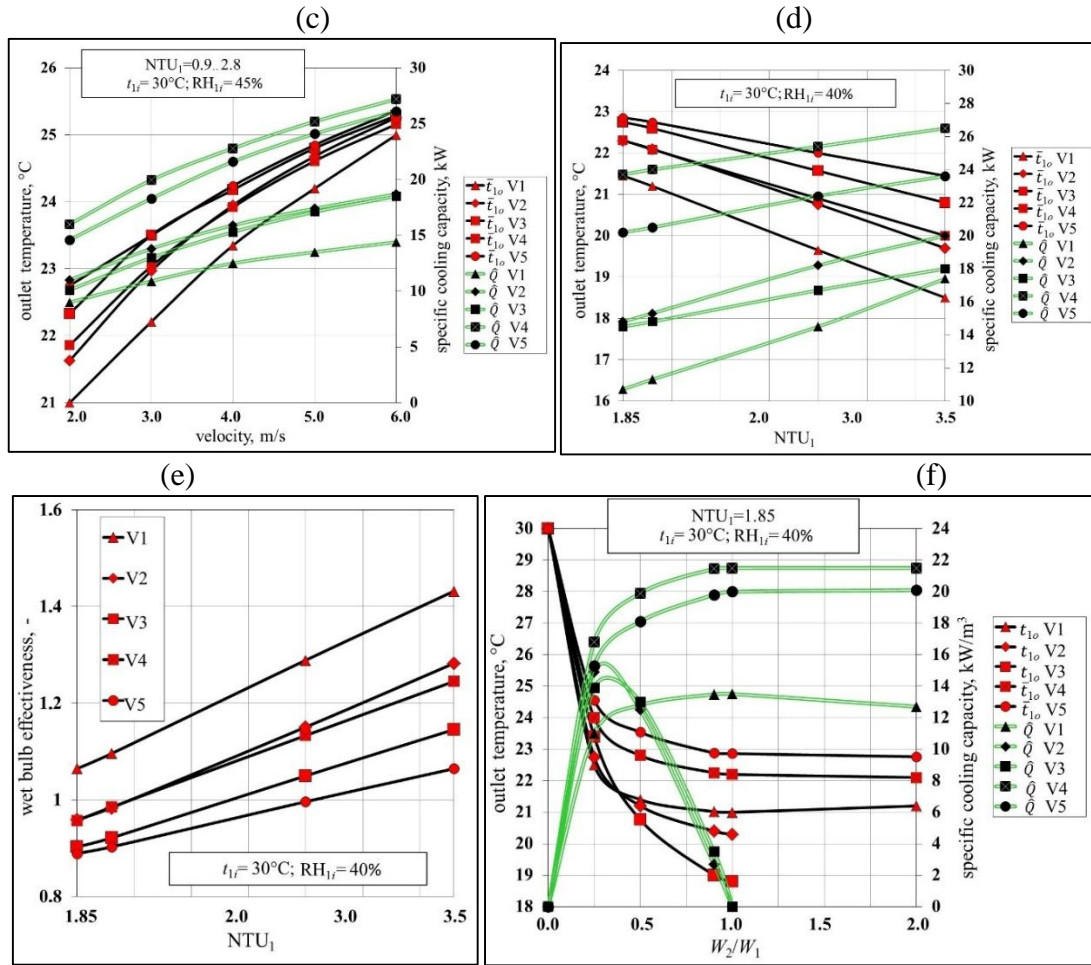


(a)                    (b)

Fig. 7.3. Numerical simulation results. (a) Average outlet product air temperature $\bar{t}_{1o}$ and specific cooling capacity $\hat{Q}$ vs. inlet air temperature (at constant inlet air relative humidity). (b) $\bar{t}_{1o}$ and $\hat{Q}$ vs. inlet air relative humidity (at constant inlet air temperature). (c) $\bar{t}_{1o}$ and $\hat{Q}$ vs primary airflow velocity (at constant inlet air parameters). (d) $\bar{t}_{1o}$ and $\hat{Q}$ vs NTU (at constant inlet air parameters). (e) Wet bulb effectiveness vs NTU (at constant inlet air parameters). (f) $\bar{t}_{1o}$ and $\hat{Q}$ vs. S/P ratio (at constant inlet air parameters).

Figure 7.3(f) shows the results of numerical simulation for constant inlet air parameters and variable $W_2/W_1$ ratio. It can be observed that both wet bulb effectiveness $\varepsilon_{WB}$ and $\hat{Q}$ for all analyzed devices show different trends than in other cases studied in this section. The outlet air temperature becomes significantly higher for all of HMXs when working to primary heat capacity ratio becomes low. The examples of changes in outlet air temperatures are presented in Table 7.6.

Table 7.6. Outlet air temperature $\bar{t}_{1o}$ and specific cooling capacity $\hat{Q}$ for different levels of $W_2/W_1$.

| HMX | $\bar{t}_{1o}$, °C; $W_2/W_1$ =0.25 | $\hat{Q}$, kW/m³; $W_2/W_1$ =0.25 | $\bar{t}_{1o}$, °C; $W_2/W_1$ =0.3 | $\hat{Q}$, kW/m³; $W_2/W_1$ =0.3 | $\bar{t}_{1o}$, °C; $W_2/W_1$ =0.5 | $\hat{Q}$, kW/m³; $W_2/W_1$ =0.5 |
|---|---|---|---|---|---|---|
| V1 | 22.5 | 11.0 | 22.0 | 11.3 | 21.4 | 12.1 |
| V2 | 22.8 | 14.9 | 22.3 | 15.2 | 21.2 | 13.5 |
| V3 | 23.4 | 13.9 | 22.4 | 14.3 | 20.8 | 13.6 |
| V4 | 24.0 | 16.8 | 23.3 | 18.2 | 22.8 | 19.9 |
| V5 | 24.6 | 15.3 | 24.1 | 16.6 | 23.5 | 18.1 |

For working to primary heat capacity ratio equal 1.0, the specific cooling capacity of units V2 and V3 is equal to zero (the main air stream is completely transferred to the wet channel, therefore no primary air stream is delivered to the conditioned spaces). It can be seen that for $W_2/W_1 > 0.4$ units V2 and V3 always achieve lower outlet air temperatures than V1 HMX, while for $W_2/W_1 > 0.6$ the specific cooling capacity of exchangers V2 and V3 becomes lower than of the V1 unit. When V4 and V5 HMXs have the same $W_2/W_1$ ratio as units V1−V3, they always achieve higher outlet air temperatures, but at the same time their specific cooling capacity is always higher than of the units V1−V3. It can also be observed that for HMXs V1,V4 and V5 the $W_2/W_1$ ratio equal to 1.0 allows obtaining relatively low outlet temperatures, while for $W_2/W_1$ ratio higher than 1.0 the obtained temperatures become almost constant (Fig. 7.3(f)). Analysis of data, presented in Figure 7.3(f) and Table 7.6 shows that $W_2/W_1$ ratio for V1,V4 and V5 unit should be close to 1.0, while for devices V2 and V3 it should be kept in the range of (0.3−0.45) in order to obtain satisfactory temperature efficiency and relatively high cooling capacity.

The comparison of optimal $W_2/W_1$ ratio for regenerative HMX obtained in this study and in other studies available from the literature can be seen in Table 7.7. The influence of selected operational parameters on the efficiency factors for considered HMXs is presented in Table 7.8.

Table 7.7. Optimal $W_2/W_1$ ratios for V2 HMX available in literature.

| Obtained data | Riangvilaikul and Kumar [9], [10] | Zhao et al. [50] | Anisimov* [78] |
|---|---|---|---|
| $(W_2/W_1)^{opt} = (0.3–0.45)$ | $(W_2/W_1)^{opt} = 0.33$ [9] <br> $(W_2/W_1)^{opt} = (0.35–0.6)$ [10] | $(W_2/W_1)^{opt} = (0.3–0.5)$ | $(W_2/W_1)^{opt} = (0.14–0.27)$ |

* − presented values referred to the heat exchanger under combined airflow arrangement

Table 7.8. Influence of selected operational parameters on efficiency of V1-V5 HMXs.

| Efficiency indexes | $t_{1i} \uparrow$ | $RH_{1i} \uparrow$ | $v_1 \uparrow$ | $NTU_1 \uparrow$ | S/P $\uparrow$ (in the range of S/P = (0–1.0)) | | |
|---|---|---|---|---|---|---|---|
| $\bar{t}_{1o}$ | $\uparrow$ | $\uparrow$ | $\uparrow$ | $\downarrow$ | $\downarrow$ | | |
| $(t_{1i}-\bar{t}_{1o})$ | $\uparrow$ | $\downarrow$ | $\downarrow$ | $\uparrow$ | $\uparrow$ | | |
| $\hat{Q}$ | $\uparrow$ | $\downarrow$ | $\uparrow$ | $\uparrow$ | $\uparrow$ (for V1,V4 and V5 units) <br> $\uparrow$ (V2, V3 units $W_2/W_1$= (0..0.37)) <br> $\downarrow$ (V2, V3 units $W_2/W_1$ = (0.37..1.0)) | | |
| $\varepsilon_{WB}$ | $\uparrow$ | $\uparrow$ | $\downarrow$ | $\uparrow$ | $\uparrow$ | | |

## 7.2.3. Discussion

A multivariant set of simulations showed that the outlet air temperatures obtained by the considered HMXs are relatively similar. In this regard other factors must be taken under consideration (e.g. specific cooling capacity). In most cases presented in this study (the results are presented in Figures 7.3(a)−(e)), the lowest level of outlet air temperature was achieved by the modified counter-flow HMX (V1), while the highest specific cooling capacity was achieved by the cross-flow exchanger (V4). At the same time V1 unit was characterized by the lowest cooling capacity. The highest outlet air temperatures were achieved by V5 HMX.

The lowest specific cooling capacity obtained by the V1 HMX follows from the fact that this unit requires three working airflow channels (one dry working air channel and two wet ones) for one primary airflow channel. It can be seen that 75% of exchanger's volume is used for working airflow (25% for pre-cooling in the dry channels and 50% for evaporative cooling in the wet channels). Such airflow arrangement allows for very effective cooling of the primary airflow, but the benefits cannot overcome the drawbacks connected with using too much of heat exchanger volume for the working air stream. Since the specific cooling capacity $\hat{Q}$ is respected to the volume of the HMX its value is lowest for the unit which requires larger structure to cool the airflow. In case of the V1 unit its structure is used ineffectively, therefore its specific cooling capacity is lowest from the analyzed devices. The obtained results show that V1 unit, despite showing high temperature effectiveness, is not suitable for the commercial purposes.

V2 and V3 units are characterized by higher level of $\hat{Q}$ than V1 HMX, but they are always achieving lower $\hat{Q}$ than exchangers V4 and V5. This follows from the fact that construction of the regenerative air coolers assumes that both working and primary air streams flow through the same dry channel and at the end of the HMX they are separated (the working airflow enters the wet channel, while the primary airflow is delivered to the conditioned apartments, see Section 2). In the cross-flow HMXs these air streams are separated before entering the corresponding channels. This shows that the structure of regenerative HMXs is also used ineffectively: the lower outlet temperature cannot overcome the negative effect of the reduction of the primary airflow, therefore the specific cooling capacity are low for these devices.

Another interesting observation is that for the $W_2/W_1$ ratio lower than 0.47 the perforated regenerative recuperator V3 is characterized by higher outlet product air temperature $\bar{t}_{1o}$ (lower cooling performance) than the V2 HMX (see Fig. 7.3(f), Tab. 7.6). However, when S/P ratio becomes higher than 0.47, V3 unit is characterized by lower outlet air temperatures than V2 device (see Fig. 7.3(f), Tab. 7.6). This effect can be explained by the following considerations. There are three main opposite trends of simultaneous heat and mass transfer processes in the perforated exchangers under mixing conditions of the primary airflow with the working airflow in the wet cannels: the positive trend is reducing the humidity ratio of the working air stream (after mixing with the dry air from the primary channel), another positive trend is that in perforated units air mass flow rate decreases along the dry channel, because part of the main flow are continuously delivered to the wet channel (reduction of the air stream increases NTU value) and the negative trend is increasing the working air temperature inside the wet channel. It can be seen that for the lower levels of working to intake air ratio, the negative effect overcomes the positive. For the ratio higher than 0.47, the positive effect of reducing the working air stream humidity ratio and decreasing of the airflow overcomes the negative influence of the warm primary air entering the wet channel. Therefore, under such kind of operating conditions, the perforated unit is characterized by the higher efficiency than the regenerative HMX. However, it can be also observed from Figure 7.3(f) that specific cooling capacity for both units significantly decreases for specific cooling capacity ratio higher than 0.34, therefore keeping the higher temperature effectiveness reduces specific cooling capacity.

It is important to underline that in most of the cases considered the cross-flow exchanger V4 shows higher temperature effectiveness than perforated regenerative HMX and very similar temperature effectiveness to the exchanger V2. Theoretically, when those three exchangers have the same $W_2/W_1$ ratio, the V4 unit is characterized by the lower, but still quite similar temperature effectiveness, while its specific cooling capacity index is much higher in every case, which shows that its structure is used more effectively. The efficiency of V4 and V1 unit is also relatively similar (the difference in outlet air temperatures between V4 and V1 is at most 2°C). It is an unusual situation when cross-flow exchanger achieves higher or similar performance to the counter flow devices. To understand this phenomenon it is necessary to study the temperature distribution inside the HMXs (Fig. 7.4(a)–(e)). It can be seen that units with high temperature effectiveness (V1 and V2) show almost constant local temperature difference between the plate surface and the primary air stream (see Fig. 7.4(a) and (b)). For the V3 unit the plate surface temperature distribution is partly disturbed in places where mixing of the air streams occurs (Fig. 7.4(c)). The disturbance of temperature profiles are also visible in case of the V1 unit (Fig. 7.4(a)). It can be seen that V4 unit shows just the same character of temperature distribution as in the case of units V1 and V2: temperature difference between the plate surface and the primary air stream is nearly constant (Fig. 7.4(d)). At the same time V5 unit shows different trend: the temperature difference $(\bar{t}_1-\bar{t}_{p1})$ is the highest at the inlet part of the HMX and it is lowest at the terminal part of the dry channel. This effect is caused by the different character of inlet temperature distributions of the working airflow in the wet channels of the product part of these exchangers, which corresponds to the outlet working airflow temperature distribution in the initial part of these units $(\bar{t}_{2i}=\bar{t}_{4o})$. In case if the V4 unit working airflow temperature is highest at the beginning and lowest at the final part of the primary air channel. Thus temperature distribution on the plate surface in the primary airflow channels is similar to the temperature distribution observed in the counter-flow heat exchangers (Fig. 7.4(a)–(e)): the temperature difference between the plate surface and the primary air stream is almost constant through the whole channel. That is why the effectiveness of the original M-Cycle cross-flow HMX (V4) is significantly higher than typical indirect evaporative air coolers. At the same time, initial section in modified cross-flow HMX (V5) creates a temperature distribution, which is similar to parallel-flow exchangers: heat transfer is the highest at the inlet part and the lowest at the outlet part of the HMX. This effect can also be observed on the chart showing heat flux distribution on the surface of the dry channels (Fig. 7.4(f)): counter-flow exchangers V1–V3 and V4 unit are characterized by relatively constant heat flux along the dry channel (in V3 unit the heat flux profile is disturbed by mixing of air streams, but its average value is still relatively constant). In V5 unit over a half of the total heat transfer rate occurs at the inlet part of the primary air channels $(\bar{X}=(0–0.3)$ in Fig. 7.4(f)). That is why V5 HMX is characterized by the lowest temperature efficiency. However, considered exchanger still obtains higher specific cooling capacity than units V1–V3 and it can be successfully adapted to supply-exhaust recuperation in air handling units, therefore its performance should be examined by additional detailed studies (this aspect is widely discussed in the next section).

Although V2 HMX showed higher temperature effectiveness than cross-flow units V4 and V5, implementation of pure counter flow arrangement in plate heat exchangers is very difficult due to the geometry of the channels (plates) with air entering and leaving on the same sides. In this regard, it can be assumed that the original cross-flow M-Cycle HMX (V4) is more reasonable for the commercial purposes. Its temperature effectiveness is close to the regenerative HMX, its cooling capacity is high, while its construction is easier to develop [2], [112], [138].
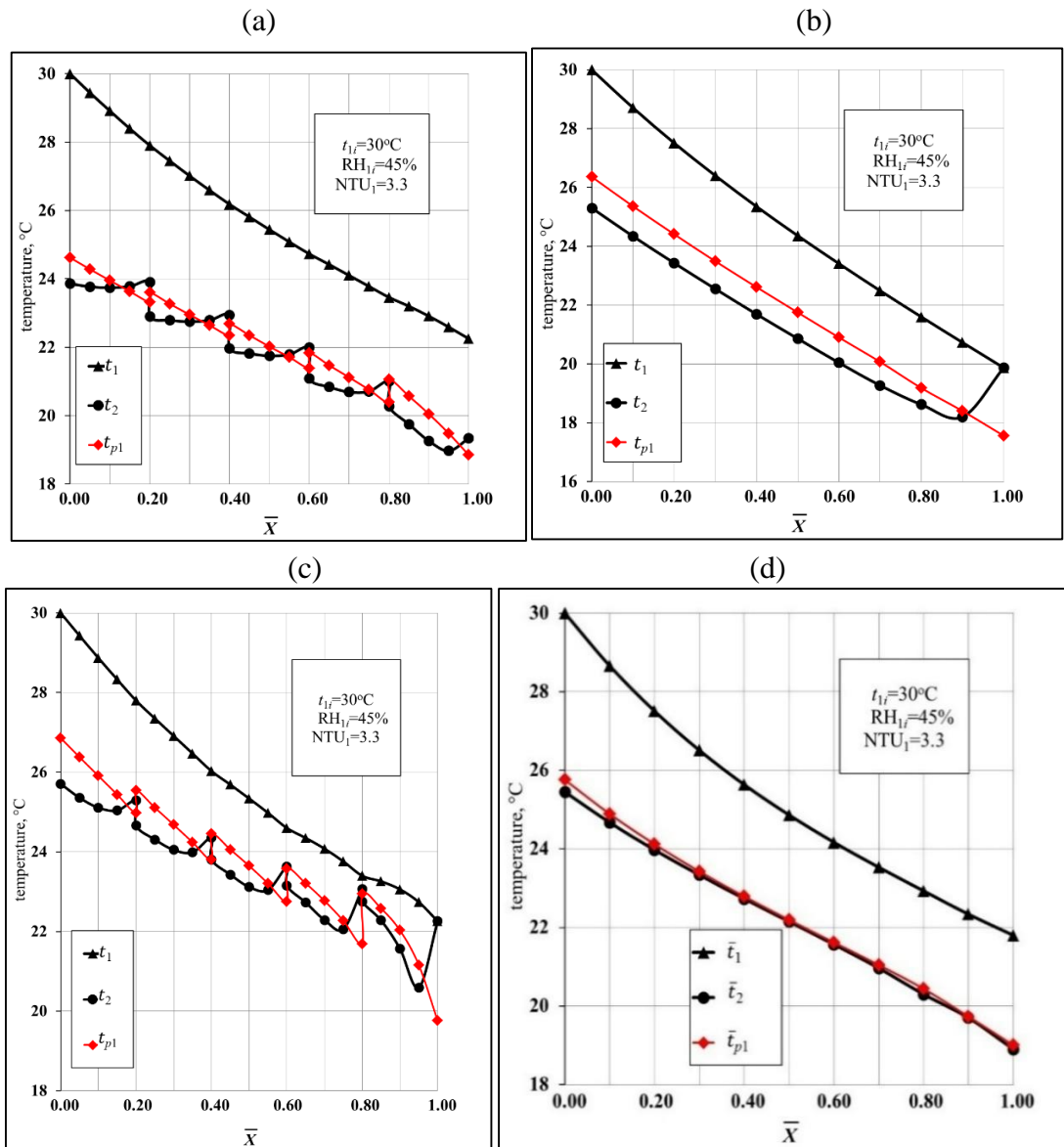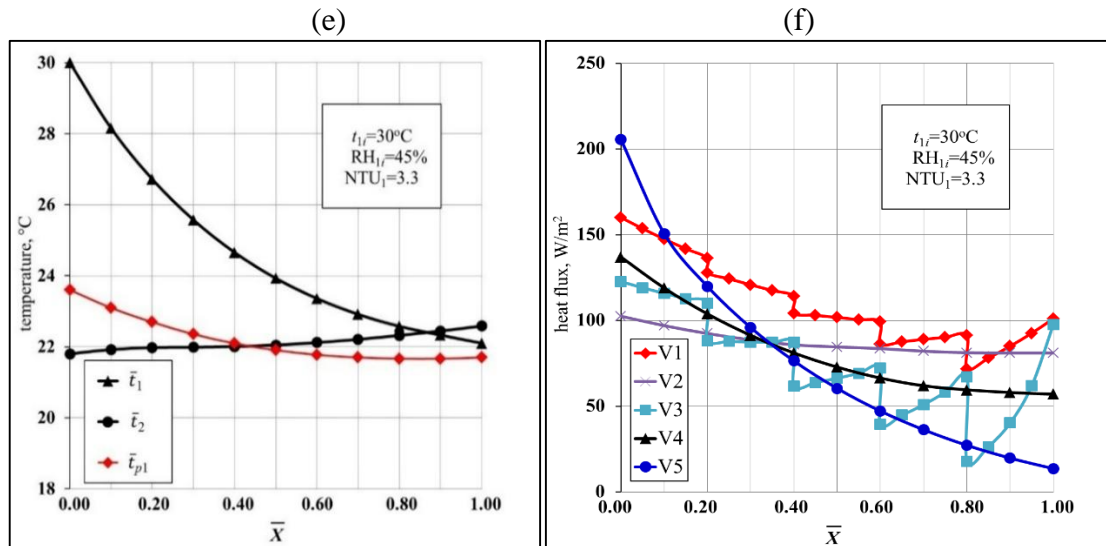
(a)                                                    (b)



(c)                                                    (d)

Figure 7.4. Temperature and heat flux distribution in the channels of the considered HMXs. (a) Temperature distribution for V1 HMX. (b) Temperature distribution for V2 HMX. (c) Temperature distribution for V3 HMX. (d) Temperature distribution for V4 HMX. (e) Temperature distribution for V5 HMX. (f) Heat flux distribution for units V1−V5.

## 7.3. Conclusions from the section

The performance of five M-Cycle HMXs was investigated and parametrically evaluated by transitional simulation under various ambient and working/operating conditions in terms of cooling efficiency. It was established that:

- The performance of the considered exchangers strongly depends on inlet air temperature and humidity, value of the NTU number, intake air velocity and working to primary air heat capacity ratio,

- The modified counter-flow HMX, which was the ideological base of the M-Cycle shows the highest temperature effectiveness, but its structure is used ineffectively, which results in the lowest specific cooling capacity from the considered units,

- Perforated regenerative exchangers show higher temperature efficiency than the typical regenerative units for the working to intake air ratio higher than 0.47, due to the more effective distribution of the airflow in the wet channels. For $W_2/W_1 < 0.47$ the typical regenerative units are more effective than their perforated equivalents,

- The temperature effectiveness of the cross-flow M-Cycle HMX is similar to the counter-flow M-Cycle HMXs, while its specific cooling capacity is higher and construction is easier to design, therefore cross-flow M-Cycle HMX seems to be the reasonable unit for commercial purposes,

- The high effectiveness of the original cross-flow M-Cycle HMX is caused by effective inlet working air temperature distribution in the wet channel, generated by its initial part,

- The modified cross-flow M-Cycle HMX is less effective than the original cross-flow unit when they operate at the same inlet conditions. The differences in the efficiency between the two exchangers seems surprising, since their construction is almost similar,

the only difference is the different airflow direction inside the dry channel in the initial portion of the exchanger. However, this small construction difference results in a completely different temperature distribution inside the dry product air channel of the two units, which has a significant impact on their cooling performance. Original cross-flow HMX has more effective temperature distribution inside the product part, which allows it to obtain higher cooling effectiveness.

## 8. Propositions of improvement of the cross-flow M-Cycle HMX

*The results of this section were published in "D. Pandelidis, S. Anisimov, W.M. Worek, Performance study of the Maisotsenko Cycle heat exchangers in different air-conditioning applications, International Journal of Heat and Mass Transfer 81 (2015), 207–221 [29], D. Pandelidis, S. Anisimov, Numerical analysis of the heat and mass transfer processes in selected M-Cycle heat exchangers for the dew point evaporative cooling, Energy Conversion and Management 90 (2015), 62–83 [134] and D. Pandelidis, S. Anisimov, Numerical analysis of the selected operational and geometrical aspects of the M-Cycle heat and mass exchanger, Energy and Buildings, 87 (2015) 413-424 [49].*

### 8.1. Modified cross-flow M-Cycle air cooler

The results presented Section 7 showed that for the same inlet conditions the original cross-flow M-Cycle air cooler (Fig. 8.1(a)) always obtains a lower outlet temperatures than the modified cross-flow HMX proposed by author (Fig. 8.1(b)), due to the more effective temperature distribution inside its channels. However, the modified exchanger was not intended to operate on the same inlet conditions to the primary channel and dry working air channel. Its construction allows to operate in supply-exhaust system as typical heat recovery unit, whereas the original unit needs to operate with the same inlet conditions for both channels.

(a)                                             (b)
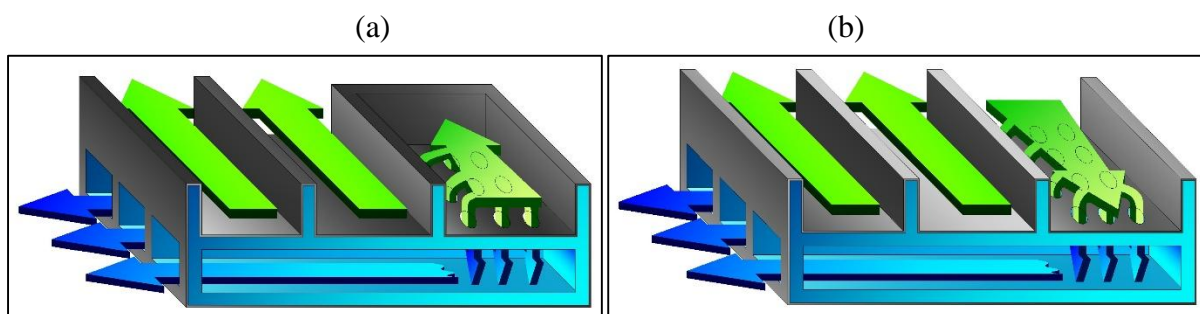


Fig. 8.1. Analyzed HMXs. (a) Original cross-flow HMX (HMX1). (b) Modified cross-flow HMX (HMX2).

Both units can be used as an individual cooling coils, which are the only source of cooling power in the system. However, in many air conditioning systems, especially in the public buildings and offices, the separate rooms typically use fan coil units to provide individual comfort for the occupants (Fig. 8.2). The exhaust air in case of the systems with the original HMX is removed to the outside (Fig. 8.2(a)). The modified HMX allows to be implemented in the supply-exhaust airflow system in the typical air-handling units (Fig. 8.2(b)). Therefore its

working channel can operate on the exhaust air, which is colder, and due to the fan coil unit, often dryer than the ambient air. The system presented in Figure 8.2(b) can be replaced with a system equipped with a heat pump, presented in Figure 8.2(c). The operation base in this case is the same as in supply-exhaust system with the fan coil units and the exhaust air from the evaporative cooler is additionally used to cool the condenser of a heat pump. Operation in supply-exhaust systems makes the exchanger less sensitive to the outdoor conditions. To make the original HMX less dependent on ambient air parameters in more humid climates, there is a possibility to use it in a system with a desiccant wheel (Fig. 8.2(d)), which dries the airflow and simultaneously increases its temperature [88]. The arrangements visible in Fig. 8.2 require different operational conditions for the presented HMXs, with different temperatures and relative humidities of the primary and the working airflow entering primary and working air channels of each exchanger. It is essential to establish the conditions for which it is more reasonable to use one HMX instead of another. In this section such an evaluation will be conducted using the numerical models. For the comparison purpose the original cross-flow unit is marked as HMX1 (Fig. 8.1(a)), while the modified unit is marked as HMX2 (Fig. 8.1(b)).

It should be mentioned that this section compares only the performance of the HMXs in different systems, not the systems itself. This is caused by the fact that comparison of the whole systems requires a very long economic analysis (investment and operational costs of different arrangements in different conditions) which in many cases is not relevant to the air conditioning systems user. For example, the typical air conditioning system may be significantly improve by replacing it for the SDEC system with the desiccant wheel, however, such transformation is expensive, complicated and requires a lot of time. It is much simpler to apply a simple, additional evaporative air cooler to the existing system and achieve the financial benefits immediately. This becomes even more important in current times, when prices of different kinds of energy and fuels are very unstable. In most cases the potential user needs to know only which of the potential exchangers would be more effective in his air conditioning system, which is the key reason behind this comparison: analyze application potential of the two considered air coolers and establish the ranges of their reasonable operation. More discussion about application of the cross-flow M-Cycle air cooler in air conditioning systems is presented in Section 10.
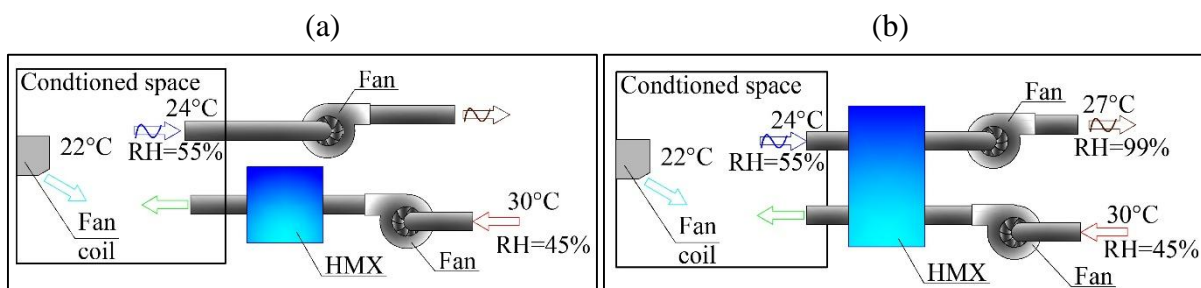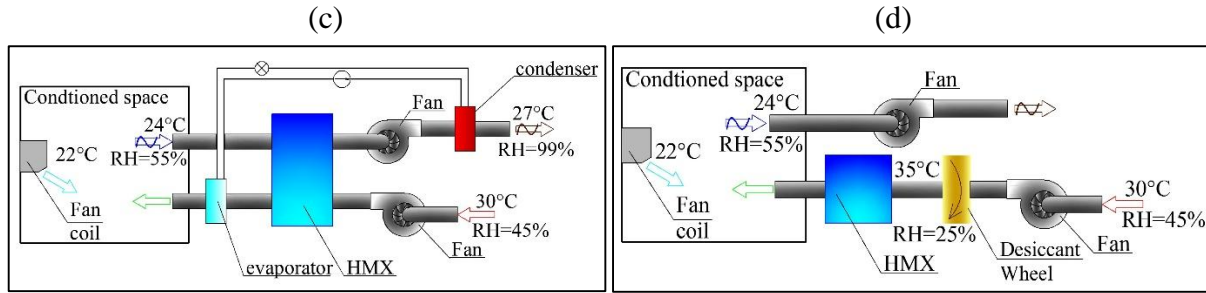


(a)                                              (b)

Fig. 8.2. Analyzed heat exchangers in different applications for air conditioning systems. (a) HMX1 in air conditioning system with fan coils. (b) HMX2 in air conditioning system with fan coils. (c) HMX2 in air conditioning system with heat pump. (d) HMX1 in air conditioning system with desiccant wheel.

The reference operating conditions for the analyzed exchangers are presented in Table 8.1. The considered exchangers are compared for the two hypothetical inlet conditions, representing different operational possibilities for the air conditioning system:

1. For HMX1 inlet temperature and humidity of the working and the primary air streams are the same, while HMX2 has different values of the primary and the working air inlet temperature and humidity (comparison between the HMX1 working in the supply air system presented in Fig. 8.2(a) and HMX2 working in the supply-exhaust air system shown in Fig. 8.2(b) and (c)). In this case, the inlet temperature of the working airflow is lower than the inlet temperature of the primary airflow for HMX2,

2. HMX1 has hot and dry inlet air conditions (the same for the primary and the working airflow), while HMX2 has different values for the primary and the working air inlet temperature and humidity (comparison between HMX1 working in the desiccant system presented in Fig. 8.2(d) and HMX2 working in the supply-exhaust air system visible in Fig. 8.2(b) and (c)).

Table 8.1. The reference operating conditions for the analyzed exchangers

| Length, m | Width, m | Channel height, mm | Working to primary air ratio, - | Primary air stream velocity, m/s | Number of primary and working air channels |
|---|---|---|---|---|---|
| 0.5 | 0.5 | 3.0 | 1.0 | 3.0 | 42 |

Three main parameters (indices) have been selected to study the operational performance of the investigated HMXs:

- Outlet primary airflow temperature $\overline{t_{1o}}$.
- The wet bulb thermal effectiveness $\varepsilon_{WB}$.
- The specific cooling capacity respected to the cubic meter of the unit's structure $\hat{Q}$.

### 8.1.1. Results and discussion

A set of simulations was performed in order to compare the effectiveness of the considered exchangers in the different operational conditions in the air conditioning systems. Figure 8.3(a) presents comparison of systems visible in Figure 8.2(a) and (b). Here HMX1 is

---

using only on ambient air, while in HMX2 the ambient air enters only the primary air channels and the working air channels are operating on the exhaust air from the conditioned space. Depending on the type of conditioned space, the exhaust air may have a different temperature and relative humidity; however the temperature inside the conditioned space is colder than the ambient temperature, while its relative humidity is usually higher. Simulations were conducted for an ambient air temperature equal 30°C, and the relative humidity of the ambient air was varied from 25 to 50%. The exhaust air temperature was changed from 21 to 26°C, with 1°C increments, while its relative humidity was changed from 40 to 60%. The charts (Fig. 8.3(a),(c) and (e)) are presented for constant levels of inlet temperatures of the primary airflow ($t_{1i}$), which are listed in frames in the upper part of the charts. For HMX1 the inlet temperatures represent different operation in air conditioning system (operation only on ambient air or in a system with a desiccant wheel). HMX2 operates on the ambient airflow in the primary air channels and exhaust air from the conditioned spaces in the working air channels. The $X$ axis in Figs. 8.3(a),(c) and (d) represents the temperature of the exhaust air, which enters the channels of the HMX2. It is important to mention that the parameters of the exhaust air do not affect the outlet air temperatures obtained by HMX1 (for this unit $t_{1i} = t_{3i}$), therefore values of $t_{1o}$ for this unit are presented as a constant lines. Blue lines represent the outlet air temperatures obtained by the HMX1 for constant inlet air temperature ($t_{1i} = t_{3i}$) and different inlet relative humidities of the working airflow (listed in the frame on the right side of each chart). The black lines represent the outlet temperatures obtained by the HMX2 for constant level of inlet primary air temperature ($t_{1i}$), variable inlet working air temperature (presented on the $X$ axis) and variable inlet working air relative humidity (listed in frame on the right side of each chart).

It can be seen that the inlet parameters have significant impact on the efficiency of considered systems. For moderate climate conditions (RH=45 to 50%) outlet temperatures obtained by HMX1 were equal 21.8°C and 20.8°C. At the same time, for the typical indoor conditions ($t$=24 to 26°C; RH=50 to 60%) HMX2 achieved outlet temperatures varying from 19.0°C ($t_{3i}$=24°C and RH$_{3i}$=50%) to 21.75°C ($t_{3i}$=26°C and RH$_{3i}$=60%). This shows that HMX2 operating on the exhaust air stream at the entrance to the working channels has more effective performance than the HMX1, which operates only on the ambient air. This phenomenon can be explained by analyzing the heat flux profiles (Fig. 8.3(b)). Although the heat flux profile for the HMX2 operating on the exhaust air is still similar to the profiles characteristic for the parallel-flow exchangers, the heat transfer rate is higher than the heat transfer rate of the same unit using ambient air. The higher value of the heat transfer rate, caused by the lower temperature of the working air, results in more efficient cooling of the primary air. As a result, HMX2 can achieve higher effectiveness than the HMX1 operating on outside air in moderate climates (Fig. 8.3(a)). However, in more dry climatic conditions (RH=35 to 40%) HMX1 achieves higher efficiency than HMX2 using exhaust air (for most of the typical indoor conditions). It can be seen that the detail analysis of the ambient and indoor air parameters is essential to achieve the highest efficiency of the designed air-conditioning system.

The next set of simulations was performed in order to compare the HMX1 operating in system with the desiccant wheel (see Fig. 8.2(d)) with HMX2 operating on the exhaust air (see Fig. 8.2(b) and (c)). The desiccant wheel dehumidifies the ambient air and it additionally

increases its temperature. Depending on the material used for the wheel structure and the range of the dehumidification process, the air temperature may increase or decrease depending on the conditions. For HMX2, the inlet temperature of the primary stream was assumed to be 30°C, while for HMX1 two types of the inlet conditions were selected for this study: dehumidification with a small increase in inlet temperature ($t_{1i}=t_{3i}=32.5$°C; $RH_i$=varied) and dehumidification with a higher increase in inlet temperature ($t_{1i}=t_{3i}=35.0$°C; $RH_i$=varied). The results of the comparison are shown in Figure 8.3(c) and (d), respectively. It can be observed that for the inlet temperature equal to 32.5°C and $RH_i \leq 25\%$, HMX1 achieves lower outlet temperatures than HMX2 operating on the exhaust air with the typical indoor conditions (Fig. 8.3(c)).
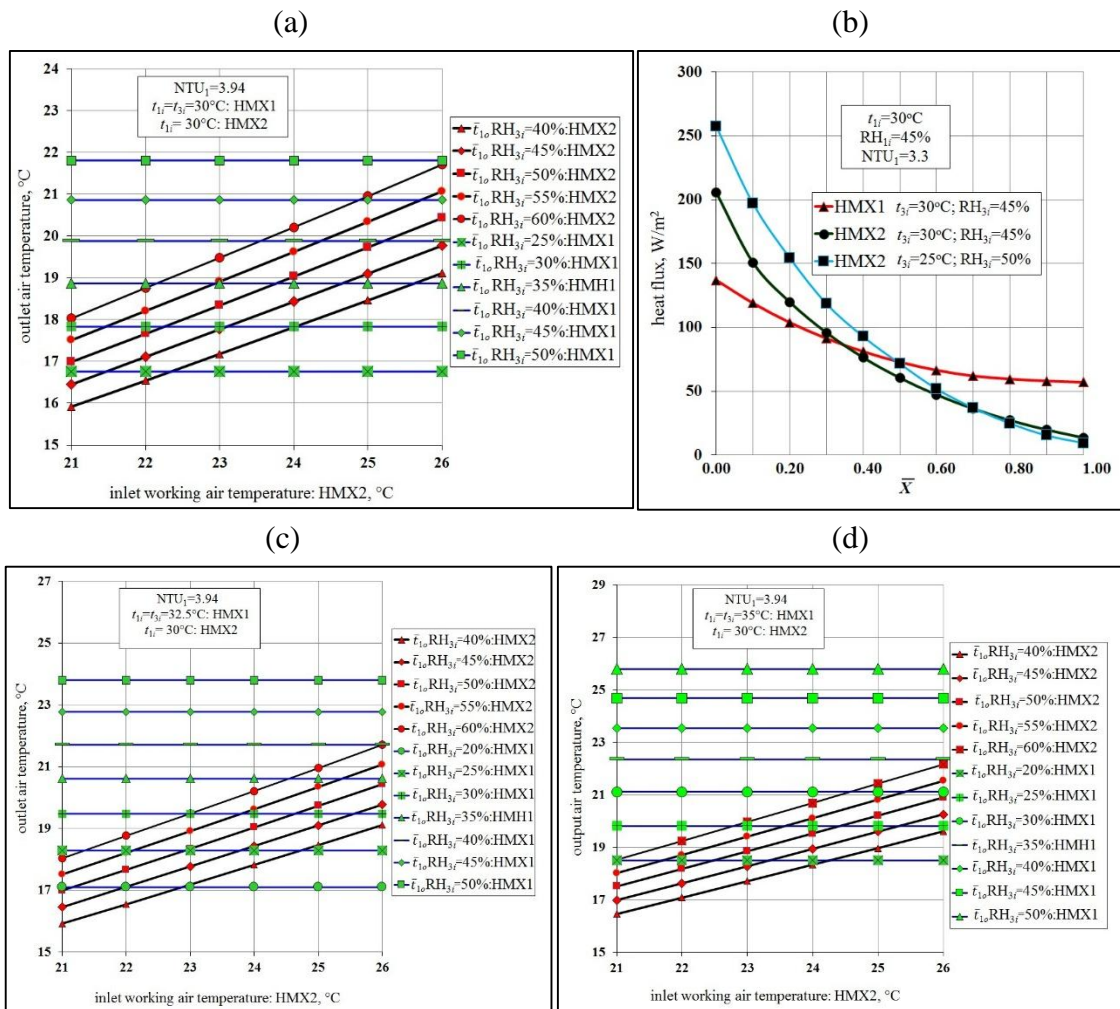
(a)  (b)



(c)  (d)



Fig. 8.3. Simulation results for HMXs operating in different air conditioning systems. (a) Outlet temperatures HMX1: t1i=30°C; RH1i=25 to 50%; HMX2: t1i=30°C; t3i=21 to 26°C; RH3i=40 to 60%. (b) Heat flux distribution inside the primary air channels. (c) Outlet temperatures: HMX1: t1i=32.5°C; RH1i=20 to 50%; HMX2: t1i=30°C; t3i=21 to 26°C; RH3i=40 to 60%. (d) Outlet temperatures: HMX1: t1i=35°C; RH1i=20 to 50%; HMX2: t1i=30°C; t3i=21 to 26°C; RH3i=40 to 60%.

When the temperature of the inlet air is raised to the higher level after dehumidification, the HMX1 obtains higher outlet temperatures (Fig. 8.3(d)). In this case, for the inlet temperature equal to 35.0°C and $RH_{1i}= RH_{3i}=25\%$, HMX1 achieves higher outlet temperatures than HMX2

operating using exhaust air with typical indoor conditions. However, for relative humidities equal to 20%, HMX1 shows better performance than HMX2 for the most of the typical indoor conditions (Fig. 8.3(d)). This shows that the inlet air stream for HMX1 has to be dehumidified to very low values of the relative humidity to overcome the performance of HMX2 operating on the exhaust air.

Table 8.2 presents the outlet temperature, specific cooling capacity and the wet bulb effectiveness obtained by HMX1 and HMX2 for the selected inlet parameters. The analysis of Table 8.2 illustrates another interesting observation: HMX1 for the inlet conditions of $t_{1i}=t_{2i}=32.5°C$; $RH_{1i}=RH_{3i}=20\%$ obtained lower outlet temperature than HMX2 (for $t_{1i}=30°C$; $t_{3i}=24°C$ and $RH_{3i}=40\%$), however its wet bulb effectiveness is 0.33 points lower. HMX2 (for $t_{1i}=30°C$; $t_{3i}=24°C$ and $RH_{3i}=40\%$) obtained a lower outlet temperature than HMX1 (for $t_{1i}=35.0°C$ and $RH_i=20\%$), however its specific cooling capacity is 4.4 kW/m$^3$ lower. This shows that the wet bulb effectiveness and the specific cooling capacity are not adequate to describe the performance of the HMXs operating in different arrangements in the air-conditioning systems. The higher specific cooling capacity for the air with higher inlet temperature is caused by the higher difference between inlet and outlet primary air temperatures $\left(t_{1i}-\bar{t}_{1o}\right)$. Greater temperature difference $\left(t_{1i}-\bar{t}_{1o}\right)$, for the higher temperature of the inlet airflow causes a very intensive evaporation process in the wet channels, which improves the efficiency of cooling process and results in greater cooling capacity $\hat{Q}$. However, the additional cooling capacity is used only for the reduction of the primary airflow temperature to the level before the air stream was heated in dehumidification process and thus it does not give any energy benefit.

Table 8.2. Outlet temperature, specific cooling capacity and wet bulb effectiveness of HMX1 and HMX2

| | HMX1: $t_{1i}=32.5°C$ $RH_{1i}=20\%$ | HMX1: $t_{1i}=35.0°C$ $RH_{1i}=20\%$ | HMX2: $t_{1i}=30°C$ $t_{3i}=24°C$ $RH_{3i}=40\%$ | HMX2: $t_{1i}=30°C$ $t_{3i}=24°C$ $RH_i=50\%$ |
|---|---|---|---|---|
| $\bar{t}_{1o}$,°C | 17.1 | 18.5 | 18.17 | 19.35 |
| $\hat{Q}$, kW/m$^3$ | 33.4 | 35.5 | 31.1 | 28.0 |
| $\varepsilon_{WB}$, - | 1.14 | 1.15 | 1.47 | 1.33 |

An explanation of the trends in the wet bulb effectiveness presented in Table 8.2 is that the wet bulb effectiveness refers to the wet bulb temperature of the primary air. In case of HMX2, the air stream entering the wet channel has a different temperature, relative humidity and therefore different wet bulb temperature. In this case, the efficiency factor based on the primary air's wet bulb temperature is not informative and can lead to an incorrect conclusions. Therefore it should not be used for the description of indirect evaporative exchangers with different primary and working air inlet parameters.

The boundary values of the exhaust air parameters at the entrance to the working air channel of HMX2, which allow obtaining higher efficiency than HMX1 are presented in Table 8.3. It can be seen on the basis of Table 8.3 and Figure 8.3 that in many cases the HMX2 can show a better performance than HMX1, especially for the colder indoor parameters. This leads

to a conclusion that "free" energy available in cold exhaust air should not be wasted by extracting this air to the atmosphere. It also seems reasonable in some cases to use heat recovery exchangers (or a partially recirculated exhaust air stream) in systems with HMX1 instead of using a desiccant wheel.  To analyze this aspect, another set of simulations were performed.

In this analysis the two types of the heat recovery methods were assumed to be placed before HMX1. First a recirculation with efficiency equal 50% (recovery of the sensible and latent heat: Fig. 8.4(a)) and a cross-flow recuperator with the temperature effectiveness equal to 0.50 (recovery of the sensible heat only: Fig. 8.4(b)). The ambient air parameters assumed are an inlet temperature of 30°C and an inlet relative humidity equal to 45%. The exhaust air temperature varies from 21 to 26°C, while its relative humidity varies from 45 to 55%. The outlet temperatures obtained by HMX1 with the heat recovery units was compared with outlet temperatures obtained by the same unit in the system with the desiccant wheel (inlet parameters of $t_{1i}$=35.0°C; $RH_i$=20 to 30%). The results of the comparison are shown in Fig. 8.4(c).

Table 8.3. Selected boundary temperature and relative humidity values for the exhaust air entering the working air channels in HMX2 allowing overcoming the performance of HMX1

| HMX1; $t_{1i}$=30°C | HMX2; $t_{1i}$=30°C |
|---|---|
| $RH_{1i}$=30% | $RH_{3i}$=40%: $t_{3i}$<23°C<br>$RH_{3i}$=50%: $t_{3i}$<22.2°C |
| $RH_{1i}$=40% | $RH_{3i}$=50%: $t_{3i}$<25.3°C<br>$RH_{3i}$=60%: $t_{3i}$<23.5°C |
| $RH_{1i}$=45% | $RH_{3i}$=50%: $t_{3i}$<25.8°C<br>$RH_{3i}$=60%: $t_{3i}$<25.0°C |
| HMX1; $t_{1i}$=32.5°C | HMX2; $t_{1i}$=30°C |
| $RH_{1i}$=20% | $RH_{3i}$=40%: $t_{3i}$<22.9°C<br>$RH_{3i}$=45%: $t_{3i}$<22.0°C |
| $RH_{1i}$=25% | $RH_{3i}$=40%: $t_{3i}$<24.8°C<br>$RH_{3i}$=50%: $t_{3i}$<23.0°C |
| $RH_{1i}$=30% | $RH_{3i}$=45%: $t_{3i}$<25.6°C<br>$RH_{3i}$=50%: $t_{3i}$<24.8°C |
| HMX1; $t_{1i}$=35.0°C | HMX2; $t_{1i}$=30°C |
| $RH_{1i}$=20% | $RH_{3i}$=40%: $t_{3i}$<24°C<br>$RH_{3i}$=50%: $t_{3i}$<23.2°C |
| $RH_{1i}$=25% | $RH_{3i}$=40%: $t_{3i}$<26.3°C<br>$RH_{3i}$=50%: $t_{3i}$<24.4°C |
| $RH_{1i}$=30% | $RH_{3i}$=50%: $t_{3i}$<26.4°C<br>$RH_{3i}$=60%: $t_{3i}$<24.5°C |

Blue lines in Figure 8.4(c) represent the outlet temperatures obtained by the HMX1 in the system with the desiccant wheel for constant level of inlet airflow temperature ($t_{1i}$= $t_{3i}$) and different inlet working airflow relative humidities (listed in the frame on the right side of each chart). The parameters of the exhaust air do not affect the operation of the HMX in the system with the desiccant wheel, therefore the results for this system are presented as a constant values.

The *X* axis in Fig. 8.4(c) represents the temperature of the exhaust air, which enters either heat recovery exchanger or a recirculation chamber (where it exchanges sensible heat or it is mixed with the ambient air with parameters listed above). The black lines represent the outlet airflow temperatures obtained by the HMX1 operating with heat recovery units or recirculation system for constant inlet primary air temperature ($t_{1i}$), variable exhaust air

temperature (presented on the *X* axis) and exhaust air relative humidity (listed in frame on the right side of each chart). The relative humidity of the exhaust air does not affect the heat transfer process in heat recovery recuperator, since it is only used to exchange sensible heat.
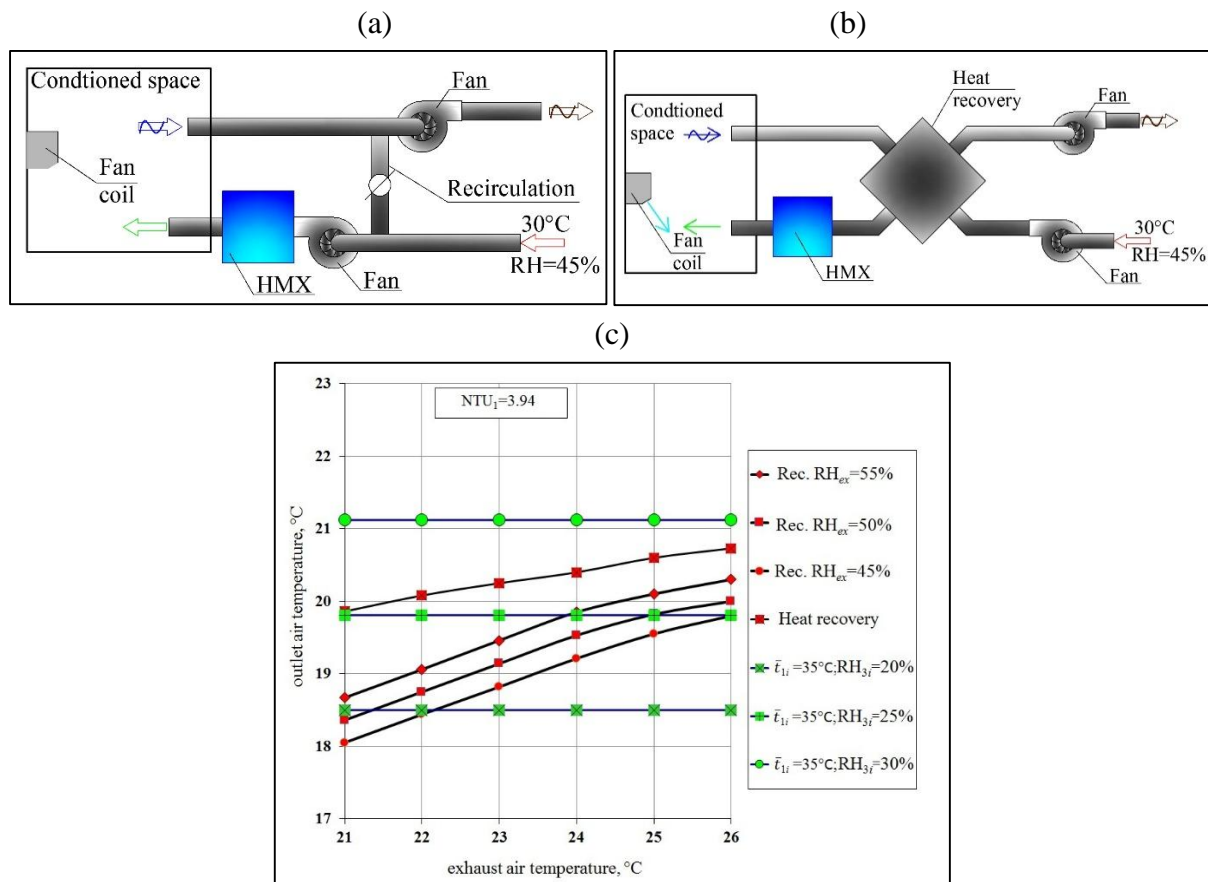
(a)                                    (b)



(c)



Fig. 8.4. Heat recovery units before the HMX1. (a) System with cross-flow recuperator; (b) System with recirculation. (c) Simulation results for the HMX1 operating with heat recovery unit, recirculation and desiccant wheel.

It can be seen that performance of the HMX1 operating on partly recirculated air is very close to the performance of the same unit in the system with the desiccant wheel. At the same time HMX1 working with the cross-flow recuperator obtained a relatively high outlet temperature (higher by $0.5$ to $2.1°C$ than the same exchanger with the recirculation), showing that the recovery of latent heat is essential for achieving the highest effectiveness of the indirect evaporative exchangers with the M-Cycle. The main disadvantage of the recirculation is the reduction in the supply air quality, which in some cases makes this solution impossible to apply in air-conditioning systems with higher hygienic requirements.

### 8.1.2. Conclusions from the Subsection 8.1

The operational parameters of the HMXs were varied in order to compare their cooling performance in the different types of air-conditioning systems. The basic operating parameters were given in Table 7.1. The results obtained in this study show the effectiveness of the indirect

evaporative air-conditioning system strongly depends on many factors, therefore, several possibilities of operational options for the indirect evaporative HMXs should be carefully examined in order to achieve the highest energy efficiency. In systems where the air stream is additionally cooled by a mechanical compression system, a recirculation or a supply-exhaust system with the HMX2 may be considered. In very humid climates, it may be reasonable to use system with the desiccant wheel. In more dry climates, for typical indoor conditions, a system with HMX1 working as the main source for cooling can be applied.

The discrepancies in effectiveness characterizing the considered HMXs were explained on the basis of the unique features of heat and mass transfer phenomenon occurring in each of the units. It was established that:

- HMX2 operating on the exhaust air with the typical indoor parameters in the working air channels shows higher effectiveness than HMX1 operating on ambient air in moderate climate conditions.
- HMX1 operating in the system with the desiccant wheel shows higher efficiency tha HMX2 operating on indoor air, when air stream is highly dehumidified ($RH_i$ =25% and lower).
- The material used for the desiccant wheel construction should allow for intense dehumidification of the air stream and a relatively small temperature increase in order to obtain the lowest outlet temperatures.
- In systems, where the air stream is additionally cooled by a mechanical compression system, it is reasonable to partly recirculate the exhaust air stream in systems with HMX1.
- The wet bulb effectiveness and the specific cooling capacity are not informative when comparing the indirect evaporative exchangers operating on the different primary and working air inlet parameters.

### 8.2. Airflow distribution and modifications of the initial part

This section investigates the possibilities of improving the original cross-flow M-Cycle HMX by varying its relative geometric and operational parameters, which were previously discussed with Prof. Valeriy Maisotsenko and Coolerado Corporation. From the literature it can be found that in the commercially produced M-Cycle HMX sometimes faces the problem of uneven airflow distribution inside the wet channels [46], [49]. It is important to study, how much the uneven airflow distribution affects the efficiency of the considered HMX. The additional problems are connected with the geometry of the exchanger: is it reasonable to increase the size of the exchanger by adding additional dry channels to the initial part or perhaps it is reasonable to increase the size of the initial part at cost of the primary part for better pre-cooling of the working airflow. All the comparisons will be presented at a simplest version of realistic M-Cycle air cooler with the same dimensions as the original exchanger (8 dry and 19 wet channels, with see Section 3), but with simple channel arrangement which would make all the problems easier to observe (Fig. 8.5).

Four main parameters (indices) have been selected to study the operational performance of the investigated HMXs:

- Outlet primary airflow temperature $\overline{t_{1o}}$.
- The obtained cooling capacity $Q_1$ (obtained from Eq. (1.3)).
- Two coefficients of performance:
    - respected to the primary airflow ($COP_1$ obtained from Eq. (1.6))
    - respected to the primary and the working airflow ($COP_{1+2}$ obtained from Eq. (1.7)).

Two different methods of calculating the COP were assumed due to the different aspects of operation of the considered exchanger in the context of whole air-conditioning system. The air from the working part is discharged to the atmosphere after passing the wet channels, while the primary air passes the whole ventilation system (ducts, dampers, diffusers etc.). Therefore, the pressure drop along the primary air part is more important in the context of the total efficiency of the air conditioning system. The pressure drops are calculated on the basis of airflow friction loses along the channels (see Section 1 and [2], [43], [49], [50]).

The water consumed by the M-Cycle air cooler was omitted, due to its low costs comparing to the costs of consumed electricity [2], [43], [49], [50]. The COP factors are assumed as ideal values. They are based on theoretical energy consumption. In practice the energy used for a fan to operate can be higher [2], [43], [49], [50]. However this factors are only used to make the comparison of different exchangers easier. This method of calculation was assumed by other studies connected with indirect evaporative air cooling [2], [7], [43], [50]
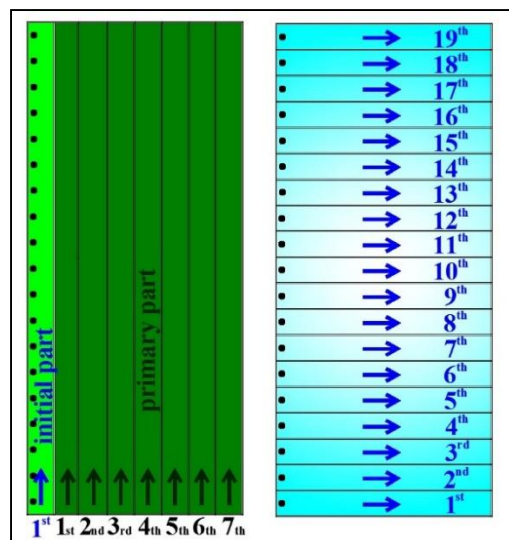


Fig. 8.5. Basic unit for the analysis (dry and wet channels with numeration respectively).

### 8.2.1. Impact of uneven flow distribution in the wet channels on cooling performance

Four different airflow distributions (selected on the basis of consultation with the producer of the exchanger- Coolerado Corporation and Prof. Valeriy Maisotsenko ) are compared (Fig. 8.6): the unit with even distribution of the working airflow inside the wet channels (1- Fig. 8.6 (a)), the unit with uneven airflow distribution, where 40% of the working airflow  is transferred to the first five channels (2- Fig. 8.6 (b)), the unit with uneven airflow distribution, where 45% of the working airflow  is transferred to the first five channels (3- Fig. 8.6(c)), the unit with uneven airflow distribution, where 60% of the working airflow  is transferred to the first five channels (4- Fig. 8.6(d)). The primary airflow in the currently produced HMXs is distributed rather evenly through the dry channels [46], therefore in this study the uniform distribution of the primary airflow is assumed. The results are presented in Figure 8.7.
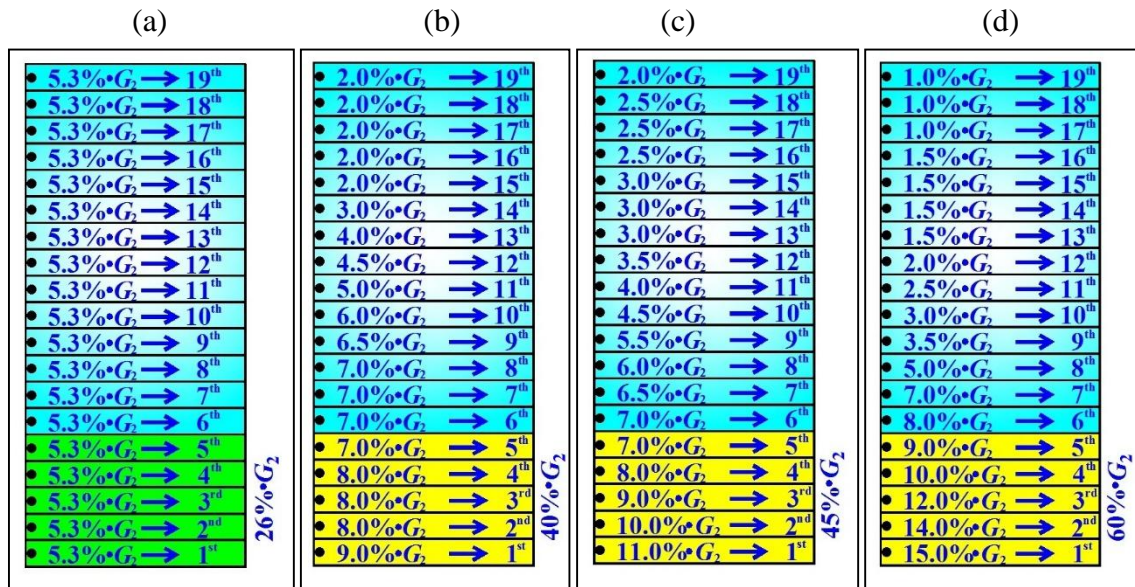


Fig. 8.6. Assumed airflow distributions inside the wet channels. (a) Even airflow distribution. (b) Uneven airflow distribution: 40% of the working air stream is transferred through the first five channels. (c) Uneven airflow distribution: 45% of the working air stream is transferred through the first five channels. (d) Uneven airflow distribution: 60% of the working air stream is transferred through the first five channels.

Figure 8.7 shows increase in outlet air temperatures and decline in cooling capacity, $COP_1$ and $COP_{1+2}$ with increasing disproportion of the airflow distribution. Non-uniform distribution of the airflow inside the wet channels results in different air stream velocity, which affects the heat and mass transfer process between the primary and working airflow. The higher pressure drop, caused by increased velocity in the initial channels has a negative impact on the $COP_{1+2}$, which drops from 142 to 56 between unit 1 and 4 (Fig. 8.7(g)). The differences in outlet temperatures are in range 0.8...2.5°C (Fig. 8.7(a) and (b)), while for the cooling capacity the differences are in range 100-300 W (Fig. 8.7(c) and (d)).
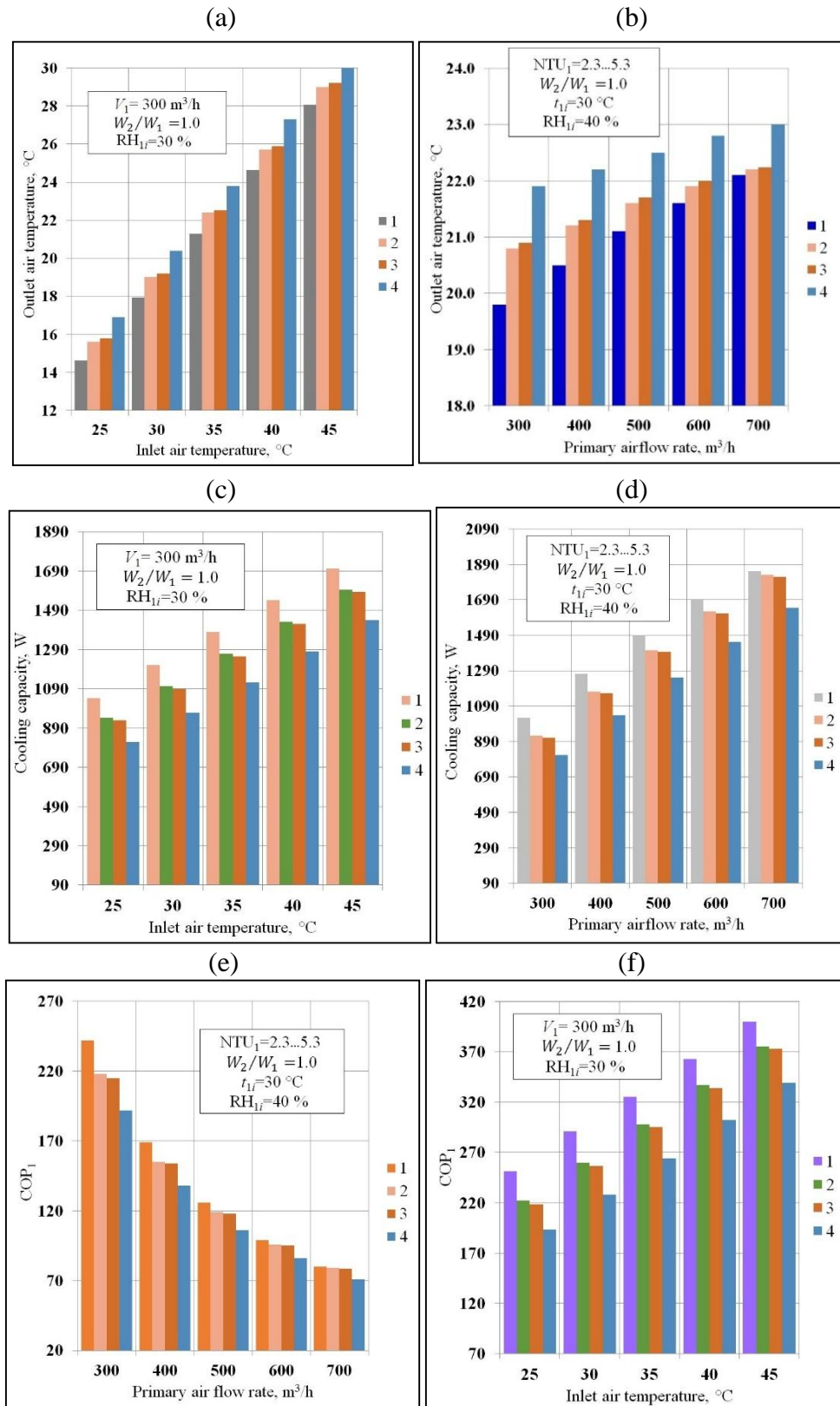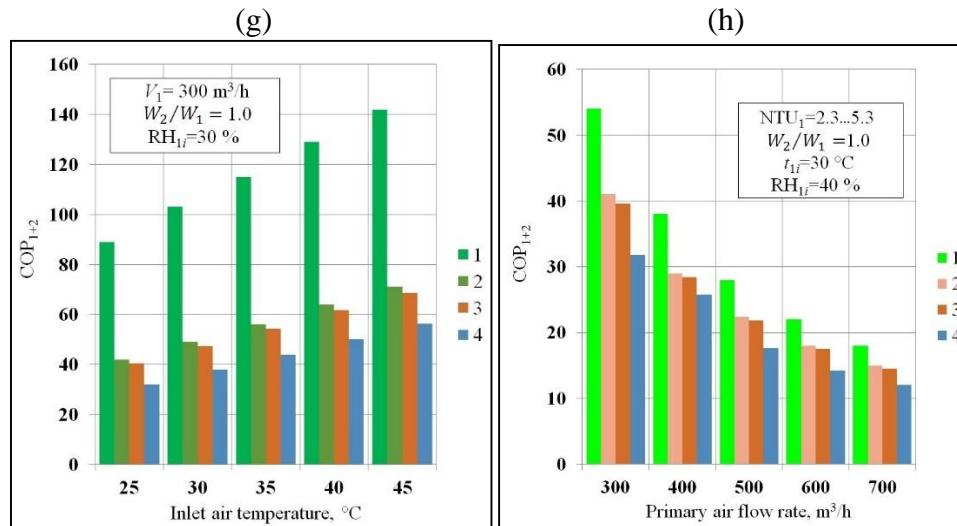
(a)



(b)



(c)



(d)



(e)



(f)

(g)                    (h)



Fig. 8.7. Impact of uneven airflow distribution on the cooling performance. (a) Outlet air temperature-function of inlet air temperature. (b) Outlet air temperature- function of the primary airflow rate. (c) Cooling capacity- function of inlet air temperature. (d) Cooling capacity- function of the primary airflow rate. (e) $COP_1$- function of inlet air temperature. (f) $COP_1$- function of the primary airflow rate. (g) $COP_{1+2}$- function of inlet air temperature. (h) $COP_{1+2}$- function of the primary airflow rate.

Table 8.4. Lowest temperature of the pre-cooled working airflow in the dry channels

| Exchanger | $t_{1i}$=25°C | $t_{1i}$=30°C | $t_{1i}$=35°C | $t_{1i}$=40°C | $t_{1i}$=45°C |
|---|---|---|---|---|---|
| Lowest temperature of the working airflow in the dry channels- unit 1 | 13.3 | 17.5 | 21.1 | 24.6 | 28.3 |
| Lowest temperature of the working airflow in the dry channels- unit 2 | 14.1 | 17.5 | 21.1 | 24.5 | 28.2 |
| Lowest temperature of the working airflow in the dry channels- unit 3 | 14.0 | 17.4 | 21.0 | 24.4 | 28.1 |
| Lowest temperature of the working airflow in the dry channels- unit 3 | 13.3 | 16.7 | 20.1 | 23.6 | 27.1 |

The temperatures of the working airflow at the end of the dry channel are presented in Table 8.4. It can be seen that the disproportions in airflow distribution have rather positive impact on the pre-cooling of the secondary airflow: the temperature of the working airflow decreases with increased non-uniformity of the airflow spreading. This can be explained by the quick reduction of the airflow rate along the dry working air channel. Lower airflow rate increases the NTU number which results in more effective pre-cooling of the working airflow. However, at the same time all of performance factors drop for units 1-4 (Fig. 8.7). This shows that the ability to achieve low temperatures of the working airflow is not the only factor which has significant impact on cooling performance. The principal point of achieving the high effectiveness with the M-Cycle HMX is keeping an unique temperature distribution along the primary air channels, which is similar to the temperature distribution found in the counter-flow exchangers (see Section 7). The effective temperature distribution results in almost constant heat flux transfer through the entire length of the primary air channel (this was established and widely discussed in the previous Section). The disproportional spreading of the working airflow has negative impact on the temperature distribution and heat flux transfer due to the different heat capacities of the secondary airflow inside each wet channel. As a result, the effectiveness of

devices with non-uniform airflow distribution is lower than of the units with evenly spread working air stream (Fig. 8.7). It can be seen that this operational aspect has a significant impact on the efficiency of the M-Cycle exchangers. Therefore, the M-Cycle HMXs should be produced with a structure which allows for even spreading of the working airflow through the channels (Fig. 8.8). Quasi-uniform airflow distribution is technically achievable without great costs. All of the methods are based on equalizing the pressure drop along the wet working air channels. The first way is based on increasing the resistance of the channels at entry region of the exchanger (Fig. 8.8(a)). This can be obtained by using different size of the channels, or by adding additional  elements to increase hydraulic resistance of the channels in the entry region (smaller holes or partial blockades at the end of the channel). Another method is to place a damper at the end of the working air channels in the entry region. This methods are sometimes used in different types of heat exchangers and they can be easily implemented in evaporative air coolers. However, increasing the channel resistance causes additional costs to the production process (this costs are not high, but sometimes even small difference in price does matter). There is another possibility to achieve quasi-uniform airflow distribution inside the channels with much lower production costs (Fig. 8.8(b)). The simplest way to achieve quasi-uniform airflow distribution inside the channels is the appropriate placement of the working air exhaust diffusers in air handling units. The location of the exhaust diffusers should be chosen in the way to create the Tichelmann airflow scheme (the same pressure drop from intake to exhaust diffuser through every working air channel). In the typical AHUs equipped with the M-Cycle HMX [135], the diffuser is placed right in front of the wet channel (first scheme in Fig. 8.8(b)). However, in all of those devices there is enough space to locate the diffuser to create the Tichelmann flow scheme (Fig. 8.8(c)). That method does not cause great costs to the production process and can effectively provide the uniform airflow distribution.

Since it was established that the uniform airflow distribution allows obtaining highest effectiveness of the cross-flow M-Cycle air coolers, in all other studies in the presented thesis the uniform distribution inside the primary and working air channels is assumed.

(a)
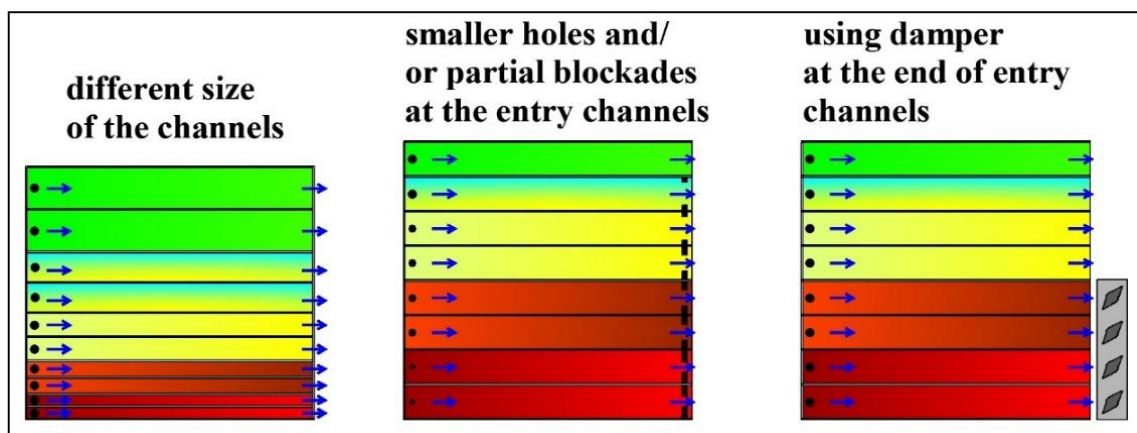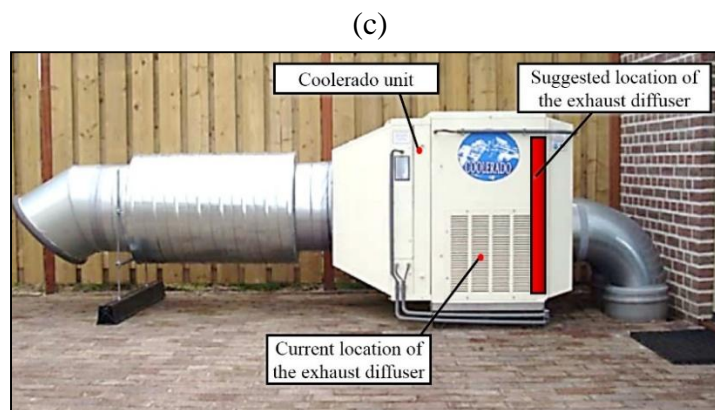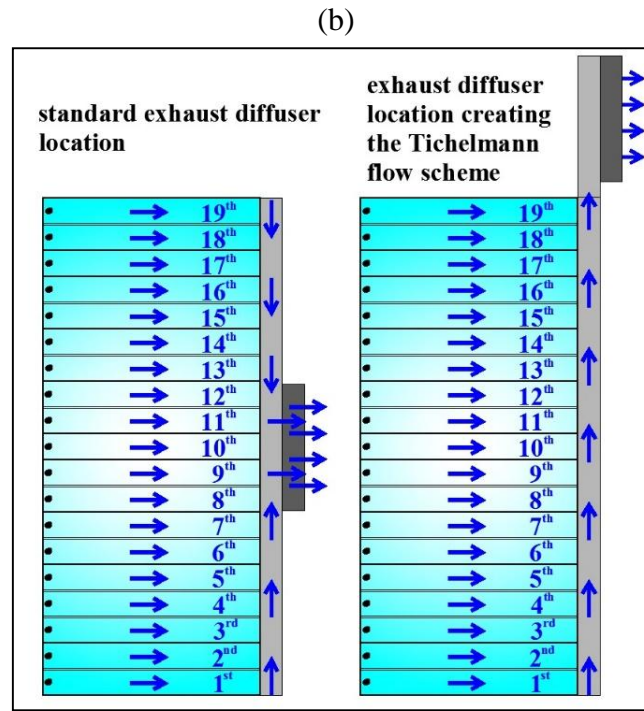
(b)



(c)



Fig. 8.8. Different methods of achieving even airflow distribution. (a) Increasing hydraulic resistance of the channels at the entry region. (b) Using a Tichelmann airflow scheme. (c) Suggested location of the exhaust diffuser in Coolerado units to create the Tichelmann airflow scheme.

### 8.2.2. Influence of the size of the initial part on the cooling performance

In this section the influence of the size of the dry working air portion on the cooling performance of the M-Cycle heat exchanger is presented. Three types of the HMXs are analyzed in this section (Fig. 8.9): the basic unit with seven primary and one dry working air channel (marked as 1- Fig. 8.9(a)), the unit with seven primary and two working air channels (marked as 2- Fig. 8.9(b)) and the unit with seven primary and three working air channels (marked as 3- Fig. 8.9(c)). The results, including outlet air temperatures, cooling capacity, $COP_1$ and $COP_{1+2}$ are visible in Figure 8.10. In this section, as in all Sections in the presented thesis except section 8.2.1, it is assumed that the airflow is distributed evenly through the channels.
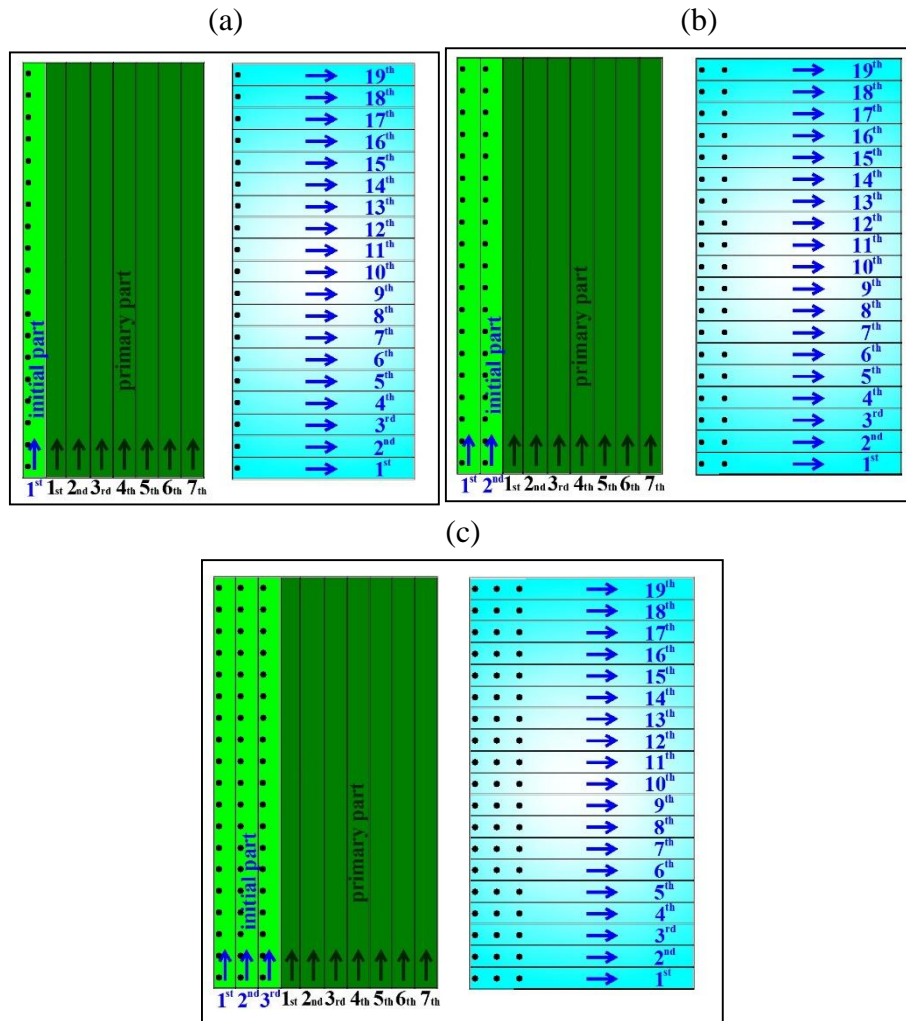
(a)                                    (b)



(c)



Fig. 8.9. Assumed heat exchangers. (a) Basic unit- 1. (b) Basic unit with additional dry working air channel- 2. (c) Basic unit with two additional dry working air channels- 3.

A trend in decreasing outlet air temperature (Fig. 8.10(a) and (b)), increasing cooling capacity (Fig. 8.10(c) and (d)), $COP_1$ (Fig. 8.10(e) and (f)) and $COP_{1+2}$ (Fig. 8.10(g) and (h)) of the evaporative coolers coincides with increasing dry working air part. This is due to a more effective pre-cooling of the working airflow. The larger heat transfer surface in the initial part and the lower air stream velocity increase the NTU value and, as a result, the effectiveness of heat transfer process. The lowest temperatures of the pre-cooled working airflow at the end of the dry channel are presented in Table 8.5. It can be seen that there are significant differences between temperatures obtained by the presented exchangers. For example, for conditions $t_{1i}$=45°C the working airflow in the basic unit was cooled in the dry channels to 28.3°C, while in the exchanger 3 it was cooled to 24.5°C (almost 4°C difference). Such discrepancies allows for more effective cooling of the primary air stream, resulting in higher efficiency of the units with larger secondary air part.

Table 8.5. Lowest temperature of the pre-cooled working airflow in the dry channels

| Exchanger | $t_{1i}$=25°C | $t_{1i}$=30°C | $t_{1i}$=35°C | $t_{1i}$=40°C | $t_{1i}$=45°C |
|---|---|---|---|---|---|
| Lowest temperature of the working airflow in the dry channels- unit 1 | 13.3 | 17.5 | 21.1 | 24.6 | 28.3 |
| Lowest temperature of the working airflow in the dry channels- unit 2 | 11.2 | 14.6 | 18.1 | 21.7 | 25.5 |
| Lowest temperature of the working airflow in the dry channels- unit 3 | 9.8 | 13.3 | 16.7 | 20.6 | 24.5 |

The differences in outlet primary air temperature, cooling capacity, $COP_1$ and $COP_{1+2}$, between considered configurations increase with increasing airflow rate (Fig. 8.10(b),(d),(f) and (h)). The discrepancies in outlet temperatures are in range 0.8-1.5°C. It can be concluded that increasing the dry initial portion results in higher effectiveness of the HMX. However, larger working air portion enlarges the size of the exchanger, which can be problematic in application of the HMX in air-conditioning systems. Space in new buildings is extremely expensive and technical equipment needs to be relatively small. The air handling units (AHUs) are expected to use minimal space in conditioned buildings. The larger HMX requires AHU, which may often by characterized by too large size for typical buildings, especially in systems operating with high airflow rates. The overall size of the exchanger should then be determined on the basis of a multi-criteria optimization, which takes into account economic factors. However, such analysis is very hard to perform, since it is difficult to value the required space in respect to the obtained cooling performance. The logical assumption is to keep the size of the exchanger as small as possible to obtain satisfactory efficiency. Due to the fact that producer (Coolerado Corporation) wants to keep the size of the exchanger unchanged, in other Sections of presented thesis the external dimensions of the exchanger will remain identical to the original unit (see Table 4.1).
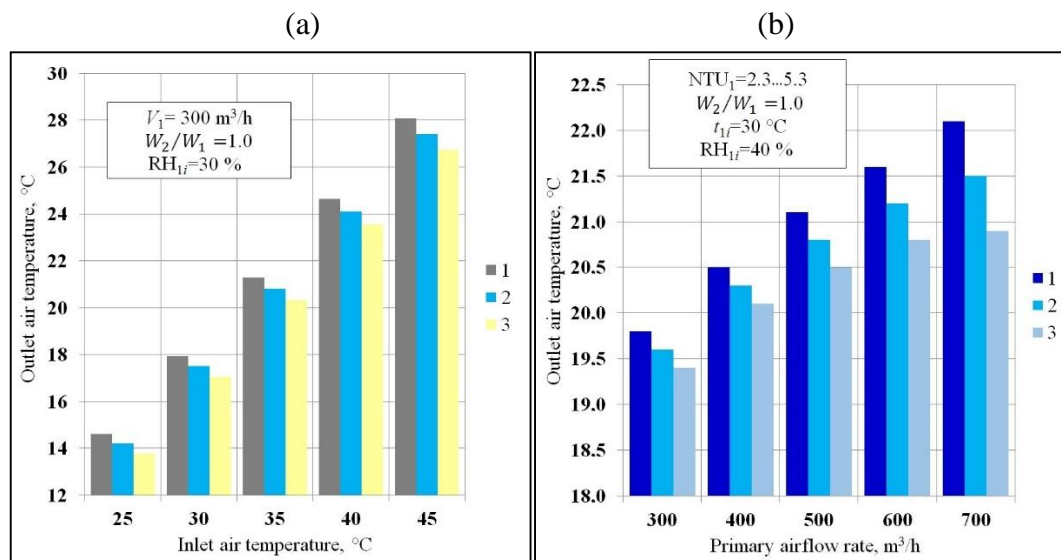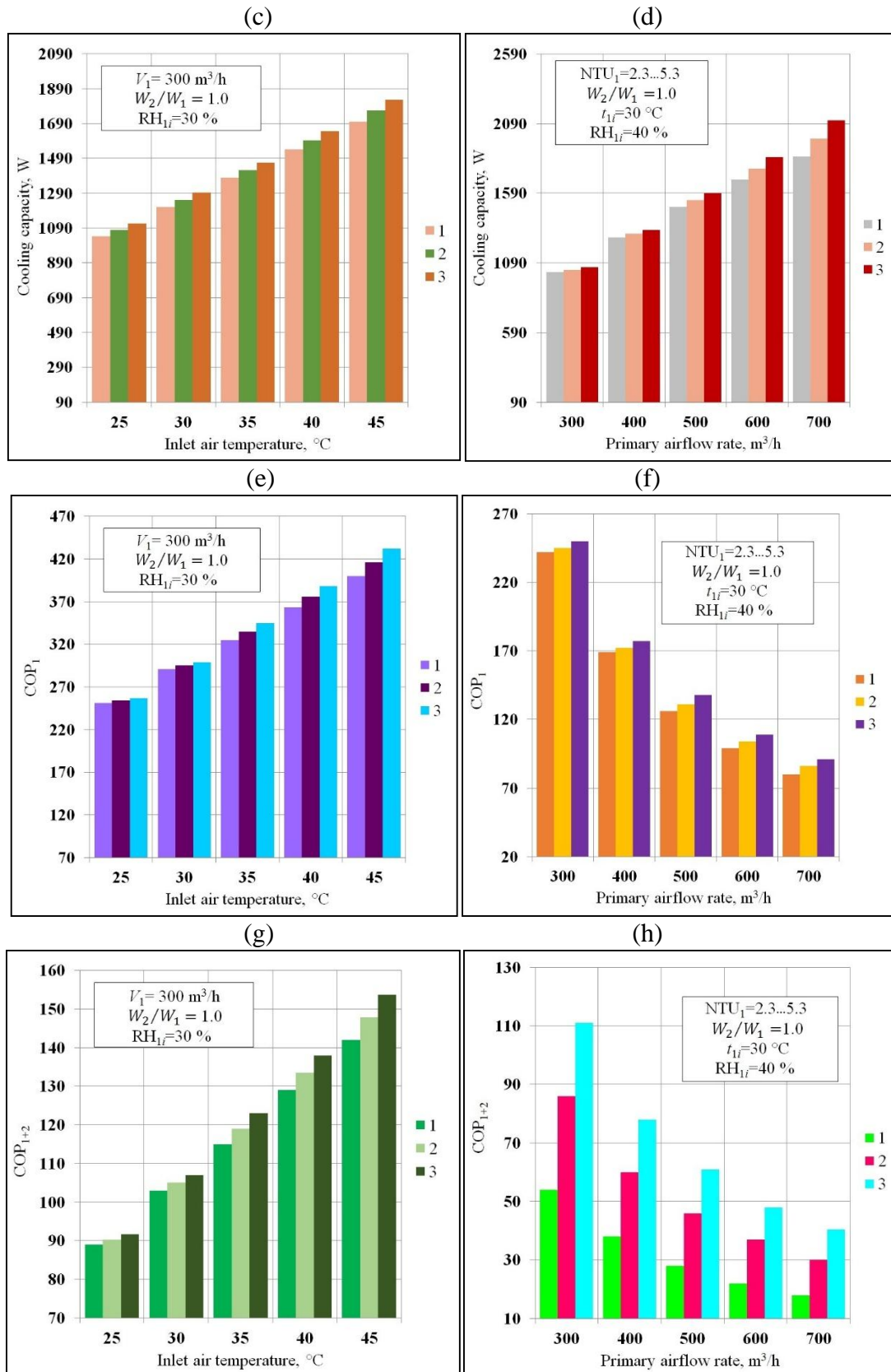
(a) (b)

Fig. 8.10. Influence of the size of the initial part on the cooling performance. (a) Outlet air temperature- function of inlet air temperature. (b) Outlet air temperature- function of primary airflow rate. (c) Cooling capacity- function of inlet air temperature. (d) Cooling capacity- function of primary airflow rate. (e) $COP_1$- function of inlet air temperature. (f) $COP_1$- function of primary airflow rate. (g) $COP_{1+2}$- function of inlet air temperature. (h) $COP_{1+2}$- function of primary airflow rate.

### 8.2.3. Impact of increasing the initial part at cost of product part on cooling performance

In the previous subsection it was established that larger dry working air portion of the exchanger improves its performance. However, the increased dry working air side caused important problem: it increased the overall size of the exchanger. As it was previously mentioned in other Sections in this thesis the external dimensions are assumed as constant and equal to the dimensions of original exchanger. However, this still leaves many important issues to investigate. This section focuses on one important aspects of exchanger arrangement: is it justified to increase the size of initial part at the cost of the product part. In this case, the total size of the exchanger remains constant. Three HMXs are be compared (Fig. 8.11): the basic unit with seven primary and one dry working air channel (marked as 1- Fig. 8.11(a)), the unit with six primary and two working air channels (marked as 2- Fig. 8.11(b)) and the unit with five primary and three working air channels (marked as 3- Fig. 8.11(c)). The results are presented in Figure 8.12.
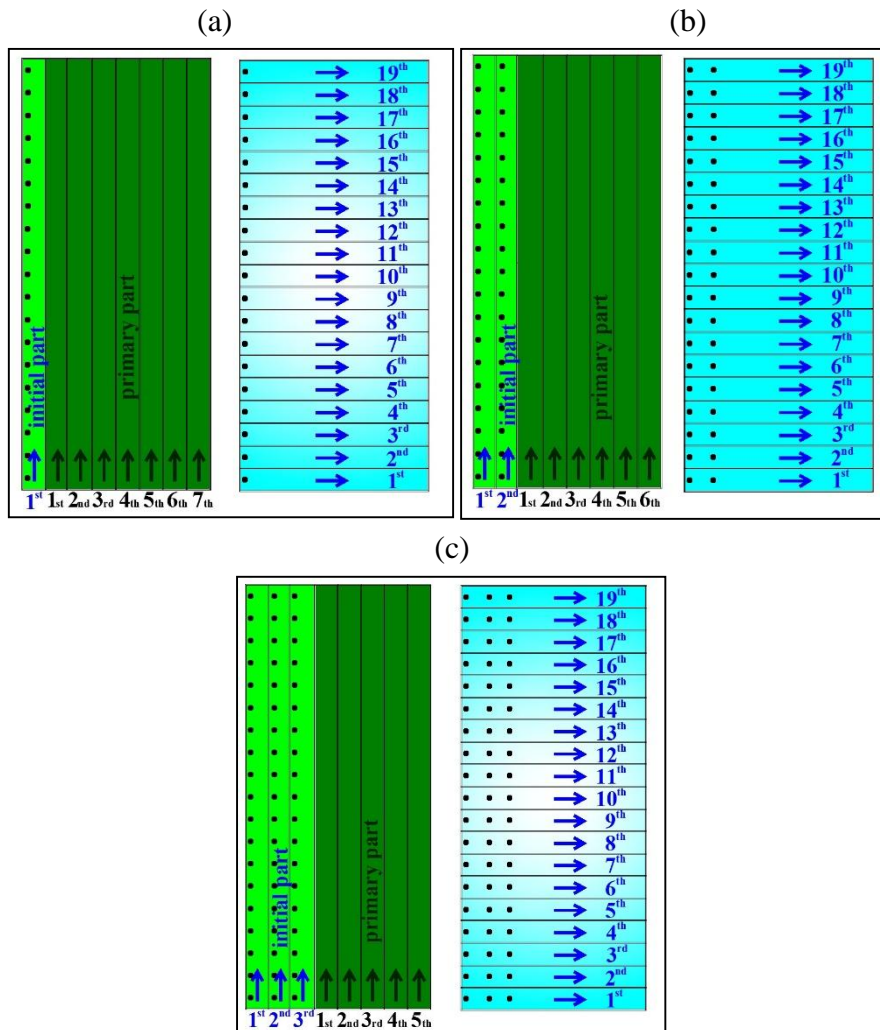


Fig. 8.11. Assumed heat exchangers. (a) Basic unit- 1. (b) Unit with six primary air channels and two dry working air channels- 2. (c) Unit with five primary air channels and three dry working air channels- 3.

It can be seen that for the lower airflow rates units 1 and 2 are characterized by the same outlet product air temperatures and the same cooling capacity. HMX 3 achieves higher outlet temperatures and lower cooling capacity, but it is characterized by the highest $COP_{1+2}$. For higher airflow rates (Fig. 8.12(b),(d),(f) and (g)) unit with one working air channel (Exchanger 1) achieves lower outlet temperatures and higher cooling capacity than Units 2 and 3. It can be concluded that size of the primary part in respect to the size of the initial part is an important construction issue. The trends in outlet temperatures and cooling capacities obtained by units 1 and 2 can be explained as follows. In unit 1, larger heat transfer surface in the product part increases the $NTU_1$ value. At the same time, lower heat transfer surface in the initial part has negative impact on the pre-cooling of the secondary air stream (lower NTU value). For smaller airflow rates, when efficiency of the investigated devices is high (due to the very low velocity in channels, which maximizes the NTU number), the effective pre-cooling of the working airflow in the Exchanger 2 allows for overcoming the higher heat transfer surface in the product part of the Exchanger 1. However, when the airflow rate becomes high, it minimizes the NTU in both parts. In this case, the ability to of Unit 1 to achieve the higher $NTU_1$ overcomes the negative effect of ineffective pre-cooling of the working airflow. That is why the Unit 1 becomes more efficient than Unit 2 with increased airflow rate.

It can be seen that Unit 1 is characterized by higher $COP_1$ and lower $COP_{1+2}$ than units 2 and 3. However, in case of the M-Cycle air conditioning systems the COP factors in many cases may lead to the wrong conclusions about the overall efficiency of the system. Systems based on indirect evaporative air coolers are characterized by very low energy consumption ($COP_1$ in range 170-420, $COP_{1+2}$ in range 20-160 in compare to 2-4 COP for traditional air-conditioners [2], [43], [51]). The small differences in a power required by a fan to operate (at most 22 W in the presented study) can lead to a significant savings by obtaining higher cooling capacity (up to 185 W in the presented case). Moreover, the indirect evaporative air coolers are characterized by relatively low pressure drops along the channels. In many cases, the fan operating in such systems would consume a larger dose of electrical energy than it is necessary for the system to work, due to the too low pressure drop combined with relatively high airflow rate, which is often unsuitable for fans performance characteristic [2], [43], [51]. From this standpoint, it is justified to increase the initial part at cost of the product part only if it does not have negative impact on the cooling performance. Concluding, the unit 2 (proportion of initial part to product part equal 2:6) in is a more favorable choice in the systems with lower airflow rates, while the Unit 1 (proportion of initial part to product part equal 1:7) is more suitable for systems characterized by higher airflow rates.

The problem of size of the initial part and its arrangements is additionally discussed in the subsection 8.3, where HMXs with different arrangements of the initial part are compared with the original M-Cycle air cooler. The final conclusions are presented for both section 8.2 and 8.3, after the whole data is established and discussed.
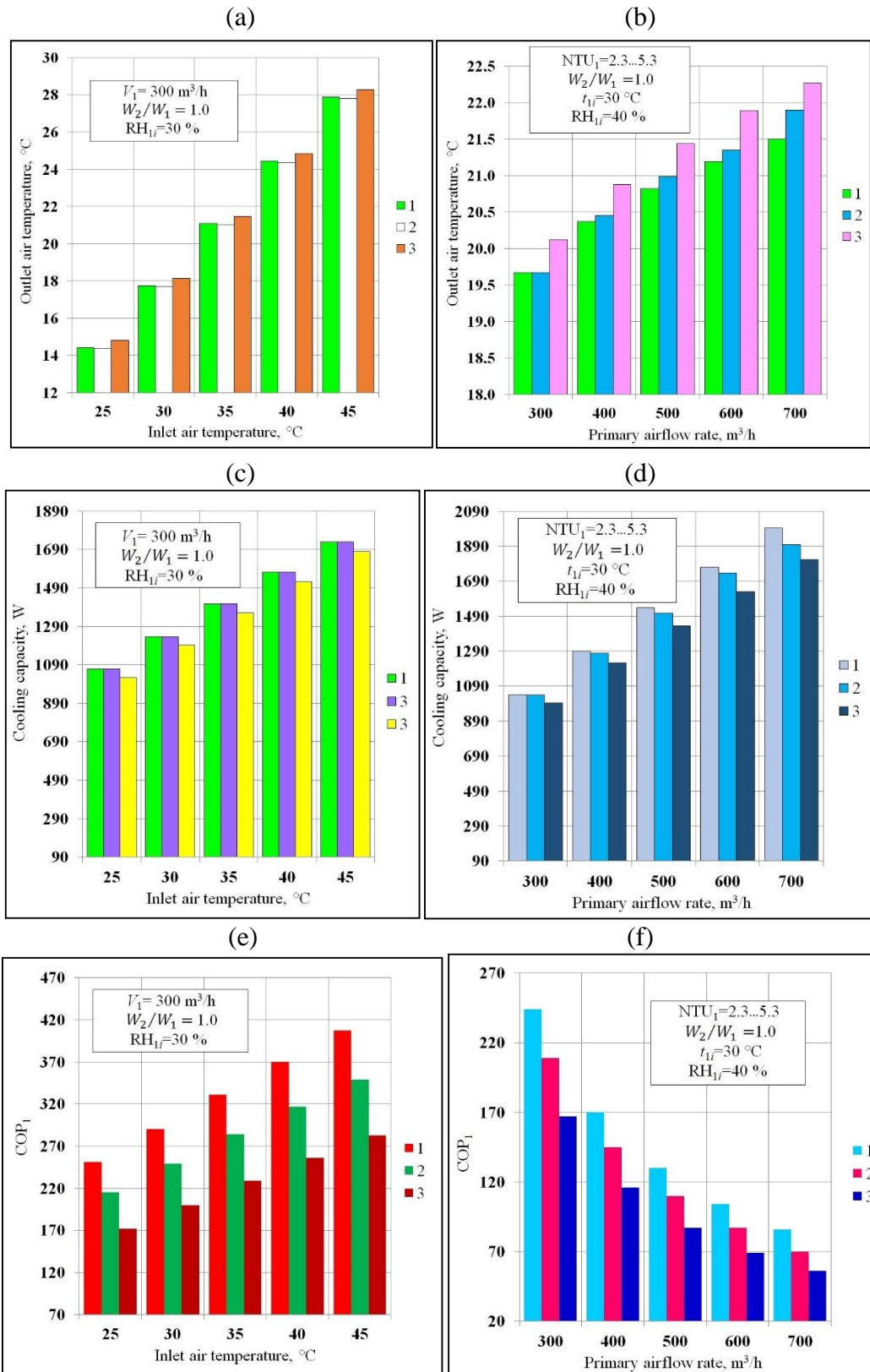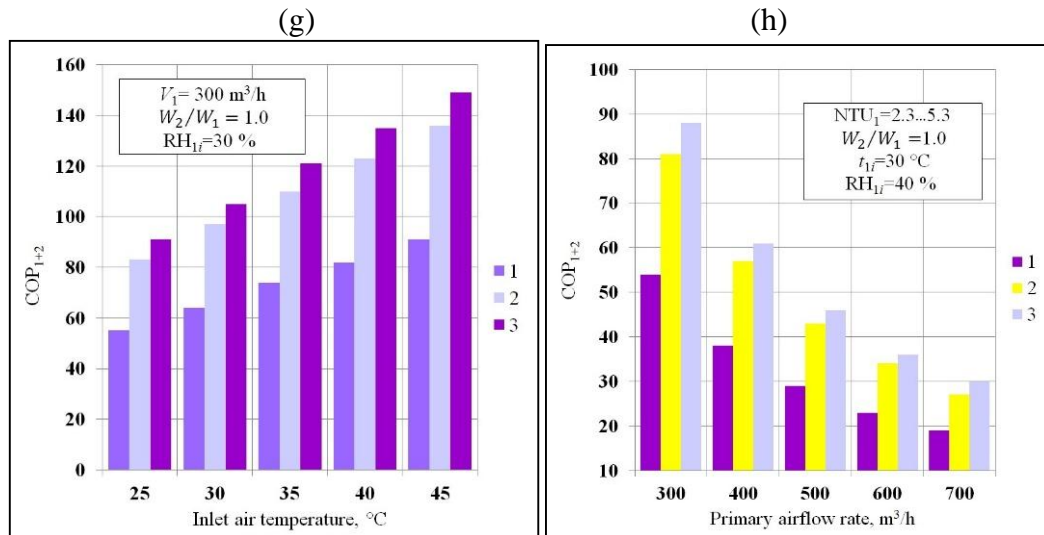
(a)



(b)



(c)



(d)



(e)



(f)

Fig. 8.12. Impact of increasing the initial part at cost of product part on cooling performance. (a) Outlet air temperature- function of inlet air temperature. (b) Outlet air temperature- function of the primary airflow rate. (c) Cooling capacity- function of inlet air temperature. (d) Cooling capacity- function of the primary airflow rate. (e) $COP_1$- function of inlet air temperature. (f) $COP_1$- function of the primary airflow rate. (g) $COP_{1+2}$- function of inlet air temperature. (h) $COP_{1+2}$- function of the primary airflow rate.

## 8.3 Different arrangements of the initial part

In this section the analysis is performed in order to establish impact of the different arrangements of the initial and product part of the exchanger on its cooling performance. Seven different variant of the exchangers, selected on the basis of consultation with Coolerado Corporation and Prof. Valeriy Maisotsenko, are compared (Fig. 8.13). The detail description of the devices is presented in Section 5.2. First unit (Variant 0, V0: Fig. 812(a)) is the original M-Cycle HMX. Variant 5 (V5, Fig. 8.13(f)) is also based on the original exchanger, but it has one less initial channel. Variants 1,4 and 7 (V1, V4 and V7, Fig. 8.13 (b),(e) and (h)) are the exchangers analyzed in Section 8.2.3 (Impact of increasing the initial part at cost of product part on cooling performance). They are analyzed again in this section as reference units for the comparison. Exchangers V3 and V6 have one of the initial channels placed near the terminal part of the wet channel (Fig. 8.13(d) and (g)), while unit V2 is a modified version of exchanger V1, with the perforations in the initial part located on the chessboard scheme (Fig. 8.13(c)).

As it can be seen the units differ with the perforations arrangement, location and in some cases length of the dry initial channels.

Three main parameters (indices) have been selected to study the operational performance of the investigated HMXs:

- Outlet primary airflow temperature $\overline{t_{1o}}$ .
- The wet bulb thermal effectiveness $\varepsilon_{WB}$ .
- The specific cooling capacity obtained by the exchangers $Q_1$.
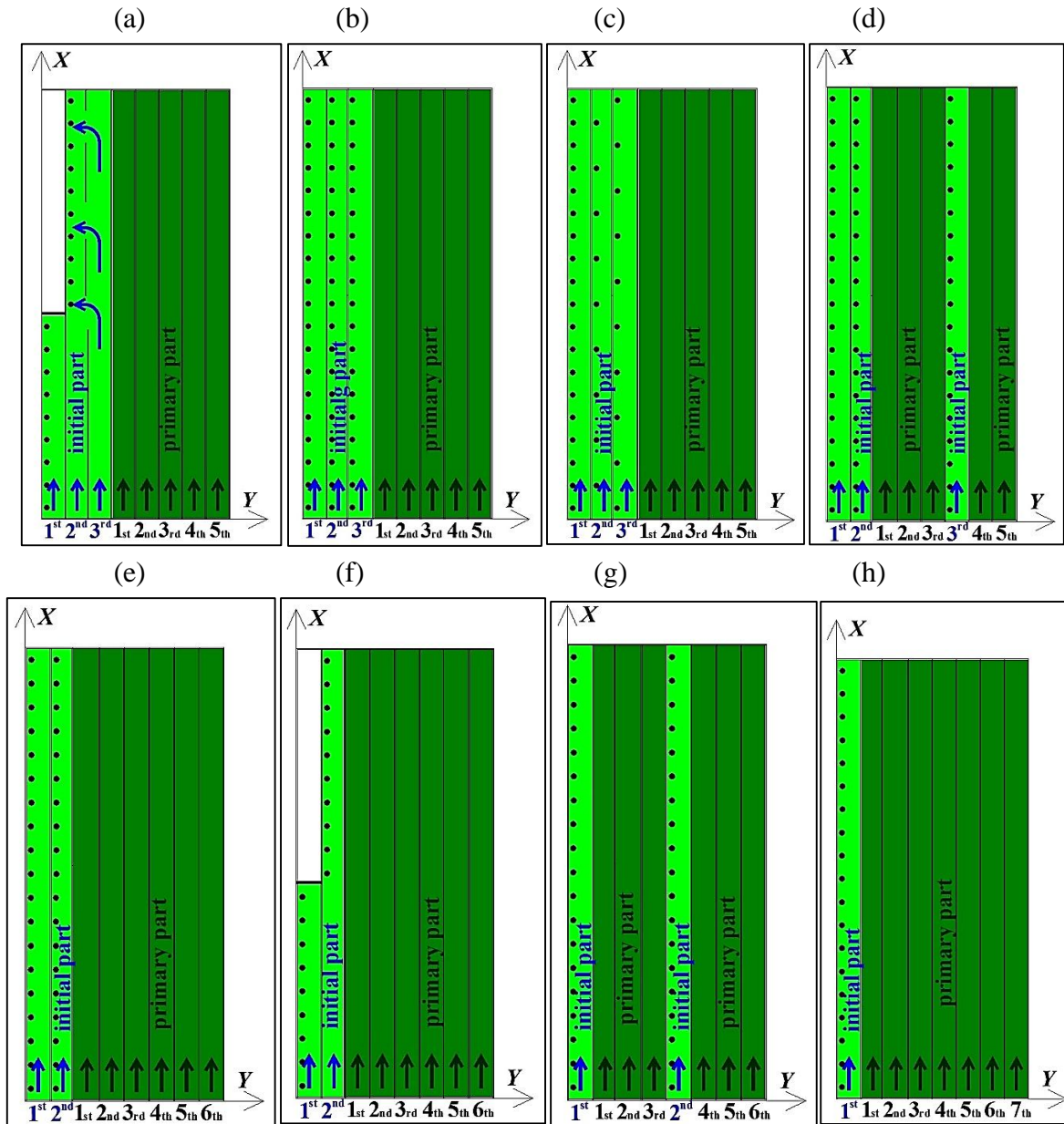
Fig. 8.13. Dry channels characteristics (nomenclature $1^{st}, 2^{nd}$…: number of dry initial part channels; $1_{st}$; $2_{nd}$…: number of product part channels). (a) Original HMX (V0). (b) Variant 1 (V1). (c) Variant 2 (V2). (d) Variant 3 (V3). (e) Variant 4 (V4). (f) Variant 5 (V5). (g) Variant 6 (V6). (h) Variant 7 (V7).

Due to the fact that all of the exchangers have the same external dimensions and proportion between size of the initial and product part of the units is analogous to the proportion in units V1,V4 and V7 the COP factor was omitted for this comparison. The obtained results for all of analyzed exchangers are similar to the results presented in Section 8.2.3 (the results for unit V0,V2 and V5 are slightly different, but the differences are negligible), therefore presenting additional analysis with the theoretical COP factor would mean repeating the unnecessary information. Additionally, as it was previously mentioned, the energy connected with the operation of the fan is small in compare to the cooling power obtained by the M-Cycle air coolers [49], therefore it is more reasonable in this Section to compare the cooling power obtained by the devices instead of the COP factors.

### 8.3.1. Comparison under variable climate conditions

Figure 8.14 (a) shows the dependency of the outlet air temperature $t_{1o}$ under variation of the inlet air temperature $t_{1i}$ at a constant relative humidity level $RH_{1i}$, Figure 8.14(b) illustrates the wet bulb effectiveness as a function of the inlet air temperature under the same operating conditions. It can be observed that units V7 and V4 are characterized by the lowest outlet air temperature, while the original HMX V0 is characterized by the highest outlet air temperature. Units V3 and V6 achieved second and third worst effectiveness respectively. Exchangers V1,V2 and V5 achieved similar effectiveness, lower than units V4 and V7, but higher than other HMXs. The obtained results show that all devices achieve the lowest temperature for inlet temperature equal 25°C (the lowest value obtained for this conditions was 14.9°C (V4 and V7), the highest was 15.4°C (V0)).
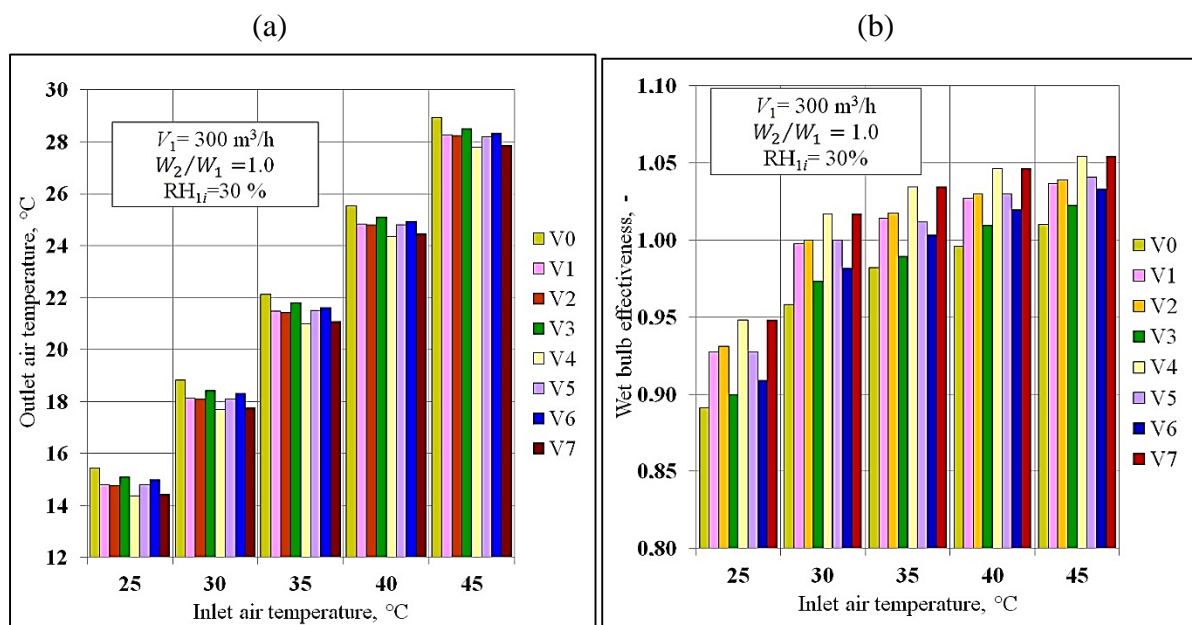
(a)  (b)



Fig. 8.14. Simulation results for constant inlet relative humidity and variable temperature. (a) Outlet temperatures. (b) Wet bulb effectiveness.

Figures 8.15(a) and (b) show the simulation results for the inlet air with constant temperature and variable relative humidity. It can be seen that also in this case the lowest temperatures are achieved by exchangers V4 and V7. Simulation results for the constant inlet humidity ratio and variable temperature are shown in Figure 8.15(c)–(e). The trends in effectiveness obtained by the considered exchangers are similar to the trends presented in Figures 8.14 (a): the lowest outlet temperature is achieved by the V4 and V7 units, while the highest outlet temperature is obtained by the V0 unit.

Data presented in Figures 8.14 and 8.15 allows for the general comparison between the analyzed variants. It can be seen that the original HMX V0 is characterized by the worst temperature efficiency, while the devices V4 and V7 are the most efficient. The difference in outlet air temperatures between the most efficient units and the less efficient ones are up to 2.0°C. Such difference can lead to important energy savings, especially in large ventilation

systems with significant airflows (e.g. for the supply airflow rate equal 20 000 m$^3$/h that difference results in 13.4 kW energy savings). Therefore the differences between the HMXs can be treated as significant and they show that there is still an opportunity to improve the original device.

### 8.3.2. Comparison under variable airflow rates

Figure 8.16 (a) shows the dependency of the outlet air temperature $t_{1o}$ under variable primary airflow rate at constant inlet air temperature and relative humidity and at constant working to primary air heat capacity ratio equal to 1.0. Analysis of the results brings out another interesting observation: the trends in exchangers efficiency are different from the ones obtained for the climatic analysis (see Figs. 8.14 and 8.15). With increasing airflow rate outlet air temperature obtained by the unit V4 is higher than of the V7 unit (Fig. 8.16 (a) and (b)). The same trend can be generally observed between all of exchangers with smaller initial part and larger product part (i.e. units V5 and V6): all of them achieve higher efficiency than their equivalents with larger initial part (i.e. units V0 and V3).



(a)  (b)

(c)  (d)

(e)
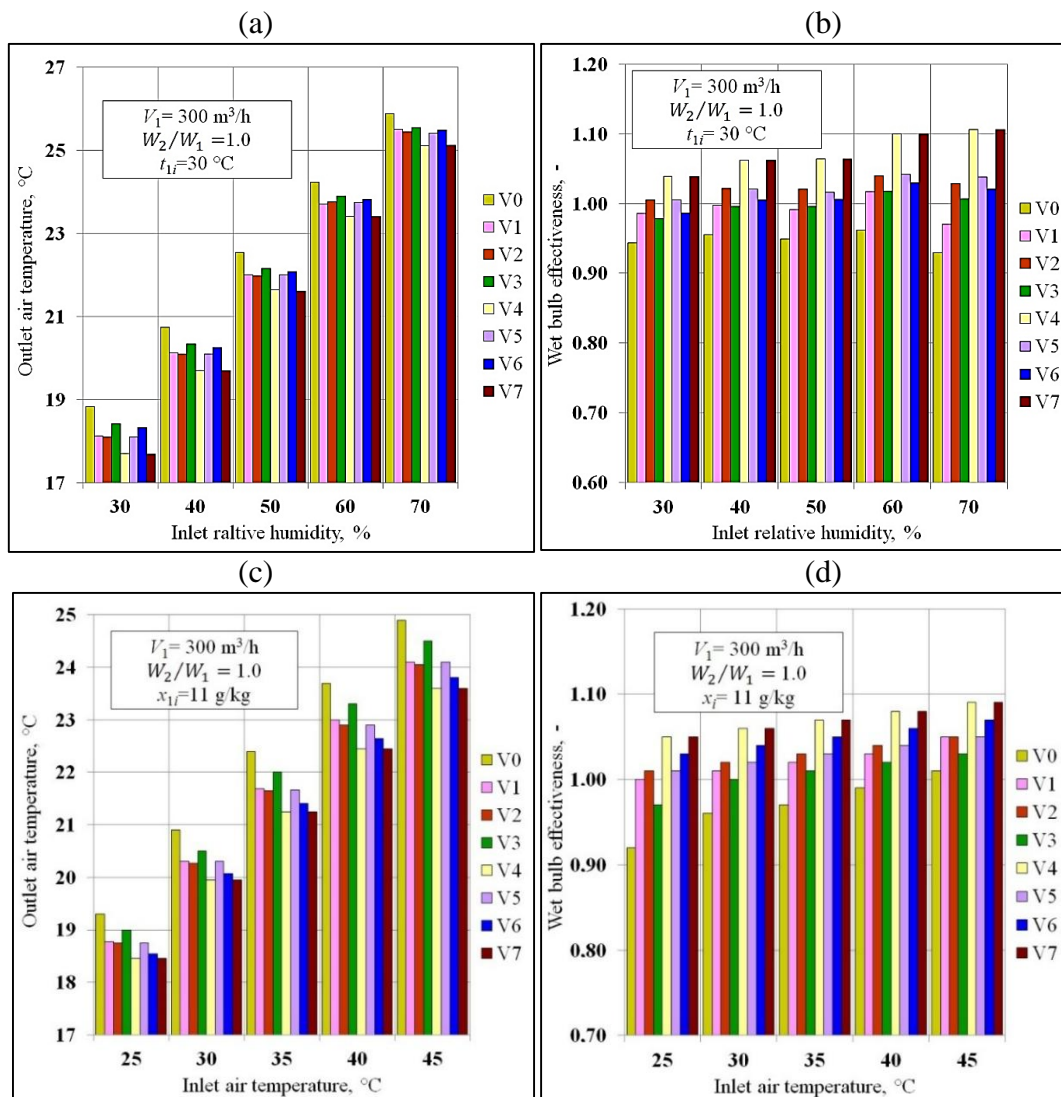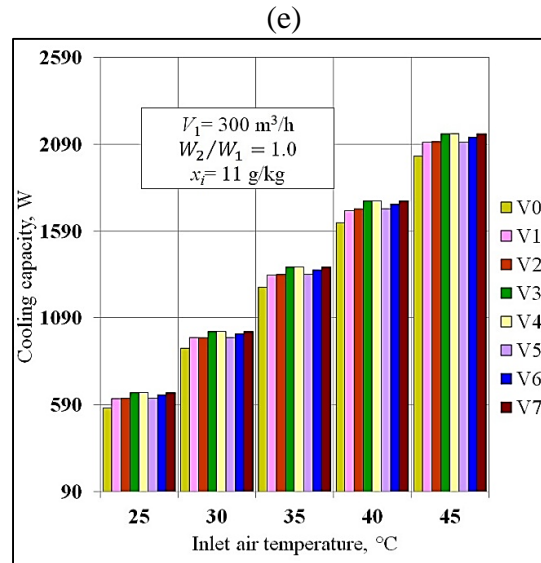


Fig. 8.15. Impact of inlet air humidity on cooling effectiveness. (a) Outlet air temperatures (constant inlet air temperature, variable inlet relative humidity). (b) Wet bulb effectiveness (constant inlet air temperature, variable inlet relative humidity). (c) Outlet air temperatures (constant inlet humidity ratio). (d) Wet bulb effectiveness (constant inlet humidity ratio). (e) Cooling capacity (constant inlet humidity ratio).

The different trends in cooling effectiveness of units with different proportions between initial and product part can also be seen in Fig. 8.16(c): when the primary and the working air volumetric flow rates are equal 300 m³/h, analogous variants of exchangers which differ only by the size of initial part achieve the similar outlet air temperatures. When the primary airflow rate is constant and the working airflow is increasing, in many cases units with larger product part are characterized by the higher efficiency (i.e. units V4 achieves higher effectiveness than unit V7, exchangers V1 and V2 obtain lower outlet temperatures than exchanger V5), however the discrepancies in the outlet temperatures are generally low. When the working airflow is constant and the primary airflow increases, units with smaller initial part are characterized by the lower outlet air temperature and the discrepancies are higher (Fig. 8.16(c)). It can be seen that the effectiveness of the exchangers with different size of initial and product part become similar with increasing working airflow rate (Figure 8.16(d)). However, after the airflows become equal the drop in the outlet air temperature becomes low and the function is almost asymptotical (it was established in Section 6.3.2 that the effectiveness of cross-flow M-Cycle HMXs is the highest for working to primary air heat capacity ratio close to 1.0).

This results from this section generally confirm the results obtained in Section 8.2.3: in all cases the size of initial in respect to the size of the product part is the major construction issue. All of the analyzed exchangers have the same dimensions, but some of them differ in number of primary and the working air channels in the dry part: V0, V1, V2 and V3 HMX are characterized by 3:5 proportions between the dry working air channels and the primary channels, the proportion for units V4, V5 and V6 is 2:6, while for V7 unit it is 1:7. It can be seen that the V5 unit, which has the same construction as the original device V0, but larger primary part (one less working channel to one additional primary channel) always achieves higher efficiency than V0 HMX. The same trend is visible in case of units V3 and V6:

exchanger V6 always achieves higher effectiveness than V3 unit, however, in this case the differences are less significant.

However, the initial part arrangement is also important: is clearly visible that the efficiency of units with the same size of initial and product portion differs. The lower cooling effectiveness of the V0 HMX can be explained by a relatively small heat capacity rate of the airflow in the wet channels in the first half of the exchanger under the assumption of even airflow distribution (see the description in Section 5.2): the 1/27 of total working airflow gets to the wet channel through each hole in the 1$^{st}$ dry working air channel. For example in the V1 and V4 unit its 1/19 of the total airflow. The smaller heat capacity rate results in worse ability to assimilate water vapor and sensible heat. Additionally, before getting to the main part, air stream in the wet channel assimilates the heat from the working airflow in the other two dry channels. As a result, it gets relatively hot and saturated before it enters the main part(it can be seen in Figure 5.8(a) that the working airflow at the beginning of the V0 unit is more hot and humid in compare to the other exchangers). In the other half of V7 exchanger, the heat capacity of airflow in the wet channel is higher, but it can't totally fix the negative effect from the first half of HMX. The analysis shows that it is better to distribute the secondary airflow evenly through the entire exchanger. It can be seen that the V5 unit, which construction allows for higher heat capacity in working air channels at the beginning of the HMX achieves much higher effectiveness, than its original equivalent. However, it still does not achieve the same effectiveness as devices V4 and V7 with very even airflow distribution through each hole.

The analysis also shows that placing one of the dry working air channels closer to the end of the wet channel (units V3 and V6), does not improve the cooling efficiency. Although V3 unit shows a little better performance than the original HMX, it is still pretty ineffective comparing to the rest of the analyzed devices. The unit V6 is the most ineffective unit from devices with two dry working air channels.
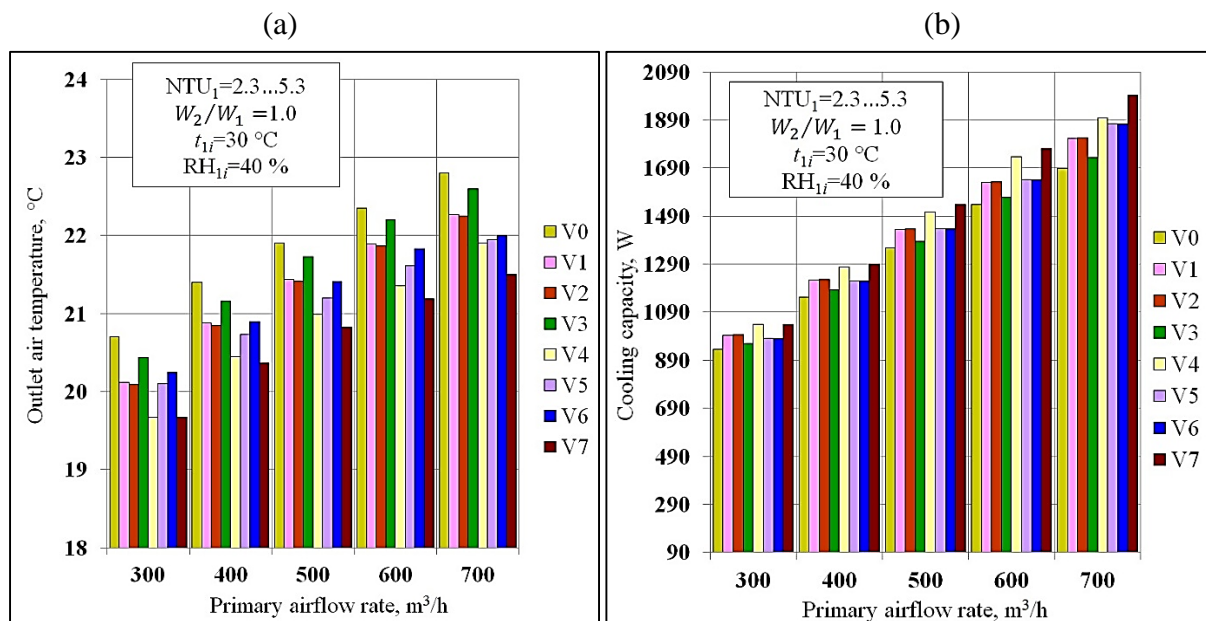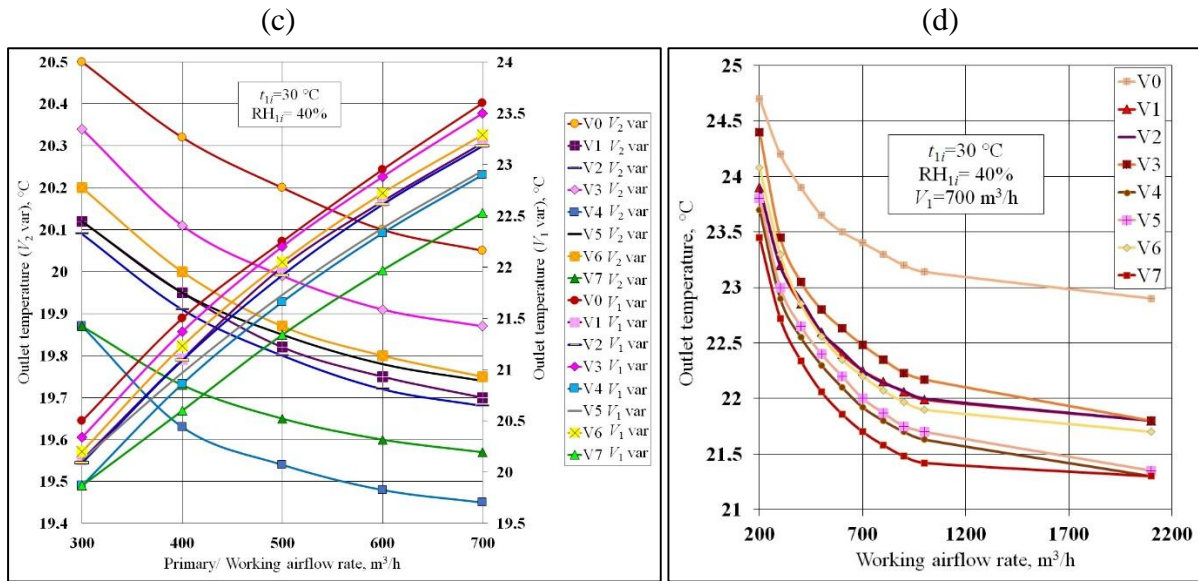
(a)  (b)

(c)                                                                    (d)



Fig. 8.16. Simulation results for different airflow rates. (a) Outlet air temperatures for variable primary and working airflow (working to primary airflow ratio equal 1). (b) Cooling capacity for variable primary and working airflow (working to primary airflow ratio equal 1). (c) Impact of variable working and primary airflow on outlet air temperatures for V0,V4 and V7 units. (d) Impact of different working to primary airflow ratios on cooling performance of  selected units.

## 8.4. Conclusions from Sections 8.2 and 8.3

This sections present the comparative study of the different arrangements of the cross-flow M-Cycle air cooler. The units were compared under different conditions, which include uneven airflow distribution, increasing initial part while keeping the product part unchanged, increasing the initial part at cost of the product part and under different arrangements of the initial part.  The results showed that it is possible to improve the original construction of the heat exchanger even under the same external dimensions.  It was established that:

- It is important to keep even airflow distribution inside the wet channels. Uneven distribution leads to significant decreasing in cooling performance. It is important to find effective ways of maintaining the even airflow in the working air channels, such as using different size of the holes in the plate or more efficient hydraulic schemes of the system (Tichelmann airflow scheme),

- Increasing the dry working air portion of the exchanger results in improving exchanger performance. However, the larger size of the wet portion enlarges the total size of the exchanger. This creates an important practical barrier in wider deployment of the M-Cycle HMXs.  The geometrical size is important aspect in air-conditioning units that is why the indirect evaporative air coolers should be characterized by the similar size in compare with the conventional vapor compression refrigeration systems,

- Increasing the dry working air portion of the exchanger at a cost of primary air portion is justified when it allows obtaining higher cooling performance. On the basis of presented analysis, for lower airflow rates the proportion of the working to primary air portion should be kept at level 2:6, in order to improve the system COP, while for the higher airflow rates this proportion should be equal 1:7,

- The hole arrangement and size of the working and primary part in the dry channels have significant impact on cooling efficiency,
- The most effective arrangement of the cross-flow M-Cycle HMX with the same dimensions as the original unit should guarantee the even airflow distribution, even perforation inside the initial part, which is located on one side of the exchanger and proportion between product and initial part equal 6:2 or 7:1.

# 9. Statistical analysis and optimization of the cross-flow M-Cycle HMX

*The results of this section were published in "D. Pandelidis, S. Anisimov, Application of a statistical design for analyzing basic performance characteristics of the cross-flow Maisotsenko cycle heat exchanger, International Journal of Heat and Mass Transfer 95 (2016), 45–61* [139]*.*

In this section the cross-flow M-Cycle heat and mass exchanger is analyzed with statistical methods and it structure is optimized. The analysis of the M-Cycle exchanger is based on the assumptions that external dimensions of the exchanger are fixed and identical to the original unit (the exchanger examined is created of two identical parts presented in Fig. 1.26, with 0.22 m width ($L_Y$) each and with total length ($L_X$) equal 0.5 m, all other parameters are presented in Table 4.1). The statistical analysis and optimization is performed for three performance factors:

- the specific cooling capacity per cubic meter of the heat exchanger's structure $\hat{Q}$
- the dew point thermal effectiveness $\varepsilon_{DP}$
- the coefficient of performance $COP_{1+2}$. To simplify the notation, in this Section $COP_{1+2}$ is marked as COP.

Additionally the regression equation is also established for the outlet temperature of the primary airflow $\overline{t_{1o}}$ in order to create a simple black-box model which allows for simple calculation for the engineers. Important terminology used in this section:

- $k$- The number of influence factors ($k=5$)
- $n^*$- The number of experimental runs in the factorial portion of the design ($n^*=2^k=32$)
- $n_r$- The number of repetitions of experiments at the center point of the design ($n_r=8$)
- $n_\alpha$ - The number of axial points in the design ($n_\alpha=2k=10$)
- $n$- The number of experimental runs ($n=n^*+n_r+n_\alpha=50$)
- $X_i, X_j$- Coded independent variables.

## 9.1. Statistical analysis

### 9.1. Regression equations for the performance factors

A five-level ($-\alpha$, $-1.0$, $0.0$, $+1.0$, $+\alpha$) full factorial circumscribed central composite design (CCD) was applied for identifying the relationship between the response functions and independent variables and fitting a second-order response surface. Five independent variables (Fig. 9.1 and Table 9.1) were selected as the most influential on the performance of the investigated HMX and their levels were chosen on the basis of the preliminary studies

performed in this thesis. The independent variables studied were: inlet air temperature $t_i$, inlet air relative humidity $RH_i$, supply air mass flow rate $G_{1i}$, working to primary airflow heat capacity ratio $W_2/W_1$ and a relative width of the initial part of the exchanger $\bar{l}_Y^{work}$ (representing the size of the initial part of the exchanger, in compare to the size of the product part designed for cooling process of the supply airflow). The coded and actual levels of the chosen independent variables are presented in Table 9.1.
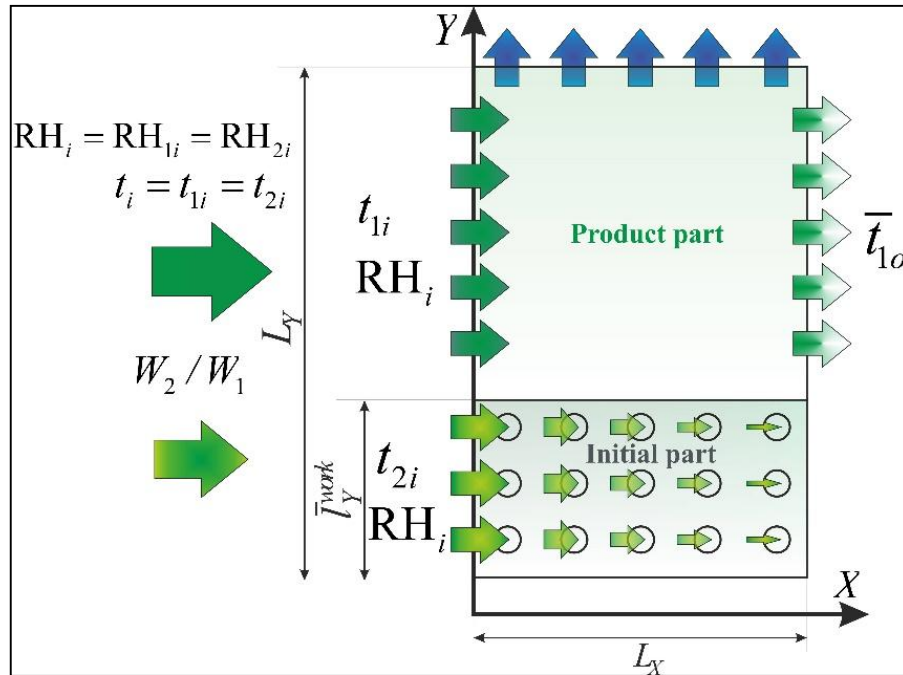


Fig. 9.1. Independent variables chosen for the modeling purpose

Table 9.1. Independent variables and their coded and actual levels for CCD

| Independent variable | Units | Symbol | Coded levels | | | | |
|---|---|---|---|---|---|---|---|
| | | | Axial $(-\alpha)$ | $-1$ | $0$ | $+1$ | Axial $(+\alpha)$ |
| $t_i$ | °C | $X_1$ | 25 | 28.75 | 32.5 | 36.25 | 40 |
| $RH_i$ | % | $X_2$ | 30 | 40 | 50 | 60 | 70 |
| $G_1$ | kg/s | $X_3$ | 0.1 | 0.14 | 0.18 | 0.22 | 0.26 |
| $W_2/W_1$ | – | $X_4$ | 0.6 | 0.8 | 1.0 | 1.2 | 1.4 |
| $\bar{l}_Y^{work}$ | – | $X_5$ | 0.125 | 0.25 | 0.375 | 0.5 | 0.625 |

There are many different methods to select a useful value of $\alpha$ (axial points). Commonly values of $\alpha$ for full factorial orthogonal design are determined on the base of the following equation [140]:

$$\alpha^4 + 2^k \alpha^2 - 2^{k-1}\left(k + 0,5 n_R\right) = 0 \tag{9.1}$$

In the case of the number of factors involved ($k$=5) and the replicate number of central points ($n_R$=8) the value of $\alpha$ is equal 2.0. The points in the center of the plan were chosen on the basis

of the performed experiment (see Section 4), the other parts of the plan were filled with the results obtained from the numerical model. The CCD for the outlet primary airflow temperature for the 50 experimental runs (including 32 experimental points in the factorial portion of the CCD, 10 axial points and 8 replicates at the centre points) is presented in Table 9.2. The CCDs for the specific cooling capacity, dew point effectiveness and the theoretical COP are presented in **Appendix H**.

The response surface regression procedure using the second-order polynomial model was implemented for estimation of the response in the investigated range of independent variables [140], [141], [142].

$$\hat{Y} = b_\mathrm{o} + \sum_{j=1}^{j=k} b_j X_j + \sum_{j=1}^{j=k-1} \sum_{u=j+1}^{j=k} b_{ju} X_j X_u + \sum_{j=1}^{j=k} b_{jj} X_j^2$$

(9.2)

where $\hat{Y}$ is the predicted response (outlet primary airflow temperature/ dew point effectiveness/ specific cooling capacity/ COP$_1$), $b_\mathrm{o}$, $b_j$, $b_{ju}$, $b_{jj}$ are regression coefficients for the intercept, linier, intersection and quadratic terms, respectively, and $X_j$, $X_u$ are the coded independent variables affecting the response $\hat{Y}$.

The overall predictive capability of the model was tested using regression analysis of the coefficient of determination ($R^2$) and absolute average deviation (AAD) values by comparing predicted responses with the experimental data. The $R^2$ and ADD were determined in accordance with Eq. (9.3) and Eq. (9.4) respectively [141], [142].

$$R^2 = 1 - \sum_{i=1}^{n} \left( \left( \hat{Y}_i - Y_i \right)^2 \Big/ \left( Y_{avg} - Y_i \right)^2 \right)$$

(9.3)

$$\mathrm{AAD} = \left\{ \left[ \sum_{i=1}^{n} \left( \left| Y_i - \hat{Y}_i \right| \Big/ Y_i \right) \right] \Big/ n \right\} \times 100\%$$

(9.4)

where $Y_{avg}$ is the average experimental value, which is expressed as

$$Y_{avg} = \sum_{i=1}^{n} Y_i \Big/ n$$

(9.5)

The satisfactory values of the coefficients of determination $R^2$ calculated as 0.999, 0.998, 0.996, 0.989 (Fig. 9.2) and AAD values calculated as 0.25%, 0.9%, 0.65% and 6.0% (see **Appendix H**) show that the models obtained define the true behavior of the system and it can be used for the analysis of the cross-flow M-Cycle exchanger.

The significance of the regression coefficients was analyzed through Student′s $t$-test, and non-significant coefficients were excluded to obtain a reduced model. The Student coefficients were

calculated separately for the intercept, linear, quadratic and interaction coefficients by the following equation [140]:

$$t_j = b_j / s_{bj}$$

(9.6)

where $b_j$ is regression coefficient and $s_{bj}$ is standard deviation of each regression coefficient.

Standard deviations (SD) of the regression coefficients were estimated on the base of the value of repeatability standard deviation $s_R$ calculated for the set of the center points of the CCD by Eqs. (9.7)–(9.12):

- For the intercept term $b_o$:

$$s_{bo} = s_R / \sqrt{n} = s_R / \sqrt{50}$$

(9.7)

- For the $j^{th}$ linear coefficient $b_j$:

$$s_{bj} = s_R / \sqrt{2^{k-1} + 2\alpha^2} = s_R / \sqrt{2^{5-1} + 2 \cdot 2.0^2} = s_R / \sqrt{24}$$

(9.8)

- For the $ju^{th}$ interaction coefficient $b_{ju}$:

$$s_{bju} = s_R / \sqrt{2^{k-1}} = s_R / \sqrt{2^{5-1}} = s_R / 4$$

(9.9)

- For the quadratic coefficient $b_{jj}$:

$$s_{bjj} = s_R / \sqrt{2^{k-1}\left(1 - \overline{X_j^2}\right)^2 + 2\left(\alpha^2 - \overline{X_j^2}\right)^2 + \left(n_R + 2k - 2\right)\left(\overline{X_j^2}\right)^2} =$$

$$= s_R / \sqrt{2^{5-1}\left(1 - 0.8\right)^2 + 2\left(2^2 - 0.8\right)^2 + \left(8 + 2 \cdot 5 - 2\right)0.8^2} = s_R / 5.6$$

(9.10)

where

$$\overline{X_j^2} = \sum_{i=1}^{i=n} X_{ji}^2 / n = 40/50 = 0.8$$

(9.11)

The repeatability variance $s_R^2$ for the set of the center points of the CCD ($i=43\ldots50$) were calculated by the following equation:

$$s_R^2 = \sum_{i=43}^{i=50} s_i^2 / f_R = \sum_{i=43}^{i=50} s_i^2 / 7$$

(9.12)

where $f_R = (n_R - 1) = 7$ − the number of degrees of freedom of the repeatability variance $s_R^2$
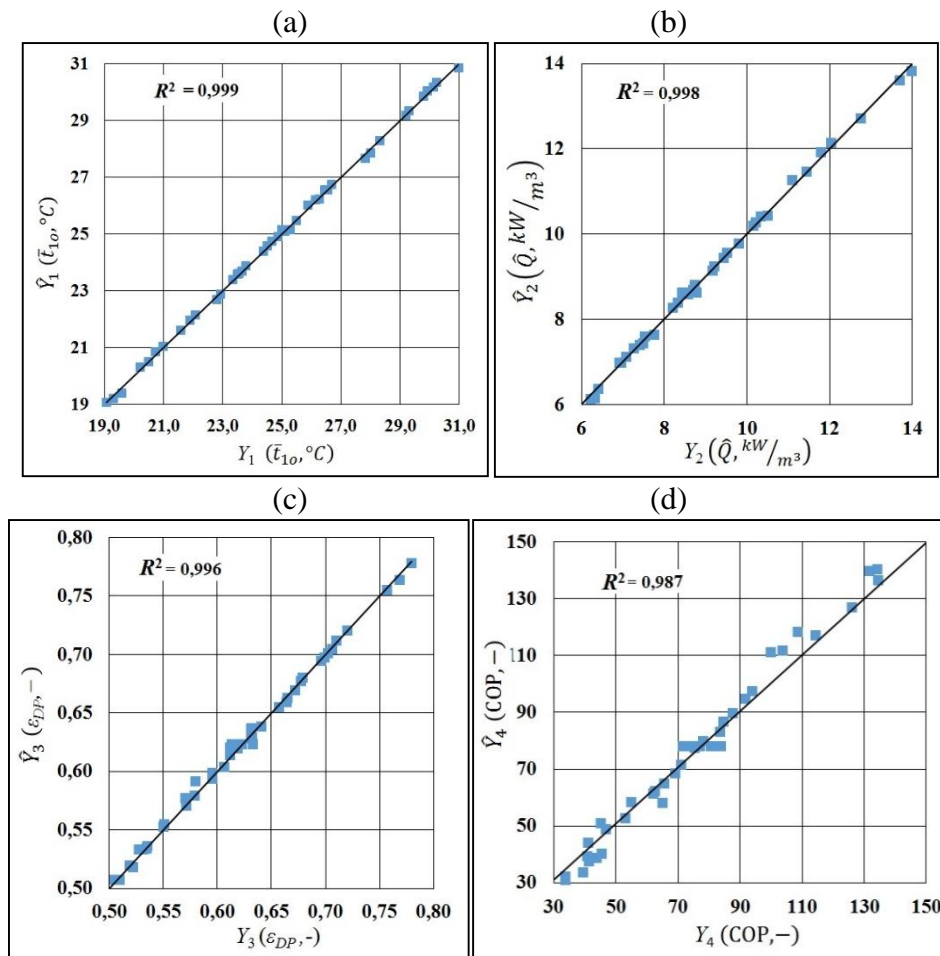
Fig. 9.2. The coefficients of determination $R^2$ for regression equations of the analyzed factors. (a) Outlet product airflow temperature. (b) Specific cooling capacity. (c) Dew point effectiveness. (d) COP.

Table 9.2. CCD setting in the original and coded form* of the independent parameters ($X_1 \ldots X_k$) and experimental results for the response variable $\hat{Y}_{1i}$ (outlet product airflow temperature $\overline{t}_{1o}$ )

| Types of | Run | $X_1$, | $X_2$, | $X_3$, | $X_4$, | $X_5$, | Observed | Predicted | Deviations |
|---|---|---|---|---|---|---|---|---|---|
| | 1 | 36.25(+1) | 60(+1) | 0.22(+1) | 1.2(+1) | 0.5(+1) | 31.0 | 30.9 | 0.1 |
| | 2 | 36.25(+1) | 60(+1) | 0.22(+1) | 1.2(+1) | 0.25(−1) | 30.1 | 30.2 | -0.1 |
| | 3 | 36.25(+1) | 60(+1) | 0.22(+1) | 0.8(−1) | 0.5(+1) | 31.1 | 31.1 | 0.0 |
| | 4 | 36.25(+1) | 60(+1) | 0.22(+1) | 0.8(−1) | 0.25(−1) | 30.3 | 30.4 | -0.1 |
| | 5 | 36.25(+1) | 60(+1) | 0.14(−1) | 1.2(+1) | 0.5(+1) | 29.8 | 29.8 | 0.0 |
| | 6 | 36.25(+1) | 60(+1) | 0.14(−1) | 1.2(+1) | 0.25(−1) | 29.2 | 29.1 | 0.1 |
| | 7 | 36.25(+1) | 60(+1) | 0.14(−1) | 0.8(−1) | 0.5(+1) | 29.9 | 30.0 | -0.1 |
| | 8 | 36.25(+1) | 60(+1) | 0.14(−1) | 0.8(−1) | 0.25(−1) | 29.3 | 29.3 | 0.0 |
| | 9 | 36.25(+1) | 40(−1) | 0.22(+1) | 1.2(+1) | 0.5(+1) | 27.8 | 27.7 | 0.1 |
| The full factorial portion of the CCD ($n*=2^k=32$) | 10 | 36.25(+1) | 40(−1) | 0.22(+1) | 1.2(+1) | 0.25(−1) | 26.5 | 26.6 | -0.1 |
| | 11 | 36.25(+1) | 40(−1) | 0.22(+1) | 0.8(−1) | 0.5(+1) | 28.0 | 27.9 | 0.1 |
| | 12 | 36.25(+1) | 40(−1) | 0.22(+1) | 0.8(−1) | 0.25(−1) | 26.7 | 26.8 | -0.1 |
| | 13 | 36.25(+1) | 40(−1) | 0.14(−1) | 1.2(+1) | 0.5(+1) | 25.9 | 26.0 | -0.1 |
| | 14 | 36.25(+1) | 40(−1) | 0.14(−1) | 1.2(+1) | 0.25(−1) | 24.9 | 24.9 | 0.0 |
| | 15 | 36.25(+1) | 40(−1) | 0.14(−1) | 0.8(−1) | 0.5(+1) | 26.1 | 26.2 | 0.0 |
| | 16 | 36.25(+1) | 40(−1) | 0.14(−1) | 0.8(−1) | 0.25(−1) | 25.1 | 25.1 | 0.0 |
| | 17 | 28.75(−1) | 60(+1) | 0.22(+1) | 1.2(+1) | 0.5(+1) | 24.4 | 24.4 | 0.0 |
| | 18 | 28.75(−1) | 60(+1) | 0.22(+1) | 1.2(+1) | 0.25(−1) | 23.7 | 23.7 | 0.0 |
| | 19 | 28.75(−1) | 60(+1) | 0.22(+1) | 0.8(−1) | 0.5(+1) | 24.5 | 24.5 | 0.0 |
| | 20 | 28.75(−1) | 60(+1) | 0.22(+1) | 0.8(−1) | 0.25(−1) | 23.8 | 23.8 | 0.0 |
| | 21 | 28.75(−1) | 60(+1) | 0.14(−1) | 1.2(+1) | 0.5(+1) | 23.4 | 23.4 | -0.1 |
| | 22 | 28.75(−1) | 60(+1) | 0.14(−1) | 1.2(+1) | 0.25(−1) | 22.8 | 22.7 | 0.1 |
| | 23 | 28.75(−1) | 60(+1) | 0.14(−1) | 0.8(−1) | 0.5(+1) | 23.5 | 23.6 | -0.1 |
| | 24 | 28.75(−1) | 60(+1) | 0.14(−1) | 0.8(−1) | 0.25(−1) | 23.0 | 22.9 | 0.0 |
| | 25 | 28.75(−1) | 40(−1) | 0.22(+1) | 1.2(+1) | 0.5(+1) | 21.9 | 21.9 | 0.0 |
| | 26 | 28.75(−1) | 40(−1) | 0.22(+1) | 1.2(+1) | 0.25(−1) | 20.8 | 20.8 | -0.1 |
| | 27 | 28.75(−1) | 40(−1) | 0.22(+1) | 0.8(−1) | 0.5(+1) | 22.1 | 22.1 | 0.0 |
| | 28 | 28.75(−1) | 40(−1) | 0.22(+1) | 0.8(−1) | 0.25(−1) | 21.0 | 21.0 | 0.0 |
| | 29 | 28.75(−1) | 40(−1) | 0.14(−1) | 1.2(+1) | 0.5(+1) | 20.2 | 20.3 | -0.1 |
| | 30 | 28.75(−1) | 40(−1) | 0.14(−1) | 1.2(+1) | 0.25(−1) | 19.3 | 19.2 | 0.1 |
| | 31 | 28.75(−1) | 40(−1) | 0.14(−1) | 0.8(−1) | 0.5(+1) | 20.5 | 20.5 | 0.0 |
| | 32 | 28.75(−1) | 40(−1) | 0.14(−1) | 0.8(−1) | 0.25(−1) | 19.6 | 19.4 | 0.2 |
| | 33 | 40.0(+α) | 50(0) | 0.18(0) | 1.0(0) | 0.375(0) | 31.3 | 31.2 | 0.0 |
| | 34 | 25.0(−α) | 50(0) | 0.18(0) | 1.0(0) | 0.375(0) | 19.1 | 19.1 | 0.0 |
| The axial (star) portion of the CCD ($n_a=2k=10$) | 35 | 32.5(0) | 70(+α) | 0.18(0) | 1.0(0) | 0.375(0) | 28.3 | 28.3 | 0.0 |
| | 36 | 32.5(0) | 30(−α) | 0.18(0) | 1.0(0) | 0.375(0) | 21.6 | 21.6 | 0.0 |
| | 37 | 32.5(0) | 50(0) | 0.26(+α) | 1.0(0) | 0.375(0) | 26.3 | 26.2 | 0.1 |
| | 38 | 32.5(0) | 50(0) | 0.1(−α) | 1.0(0) | 0.375(0) | 23.6 | 23.6 | 0.0 |
| | 39 | 32.5(0) | 50(0) | 0.18(0) | 1.4(+α) | 0.375(0) | 25.1 | 25.1 | 0.0 |
| | 40 | 32.5(0) | 50(0) | 0.18(0) | 0.6(−α) | 0.375(0) | 25.5 | 25.5 | 0.0 |
| | 41 | 32.5(0) | 50(0) | 0.18(0) | 1.0(0) | 0.625(+α) | 26.6 | 26.5 | 0.0 |
| | 42 | 32.5(0) | 50(0) | 0.18(0) | 1.0(0) | 0.125(−α) | 24.7 | 24.7 | -0.1 |
| | 43 | 32.5(0) | 50(0) | 0.18(0) | 1.0(0) | 0.375(0) | 25.2 | 25.1 | 0.0 |
| | 44 | 32.5(0) | 50(0) | 0.18(0) | 1.0(0) | 0.375(0) | 25.0 | 25.1 | -0.1 |
| Set of the center points of the CCD ($n_R=8$) | 45 | 32.5(0) | 50(0) | 0.18(0) | 1.0(0) | 0.375(0) | 25.3 | 25.1 | 0.2 |
| | 46 | 32.5(0) | 50(0) | 0.18(0) | 1.0(0) | 0.375(0) | 25.2 | 25.1 | 0.0 |
| | 47 | 32.5(0) | 50(0) | 0.18(0) | 1.0(0) | 0.375(0) | 25.0 | 25.1 | -0.1 |
| | 48 | 32.5(0) | 50(0) | 0.18(0) | 1.0(0) | 0.375(0) | 25.3 | 25.1 | 0.2 |
| | 49 | 32.5(0) | 50(0) | 0.18(0) | 1.2(0) | 0.5(0) | 25.2 | 25.1 | 0.0 |
| | 50 | 32.5(0) | 50(0) | 0.18(0) | 1.2(0) | 0.25(0) | 25.0 | 25.1 | -0.1 |

* Values in parenthesis are the coded forms of variables.

Estimated repeatability and regression coefficients deviations are given in Table 9.3.

Table 9.3. Repeatability and regression coefficients deviation

| Response model | Deviation | | | | |
|---|---|---|---|---|---|
| | $s_R$ | $s_{bo}$ | $s_{bj}$ | $s_{bju}$ | $s_{bjj}$ |
| $\hat{Y}_1$ ($\bar{t}_{1o}$) | 0.0159 | 0.0178 | 0.0257 | 0.0315 | 0.0225 |
| $\hat{Y}_2$ ($\hat{Q}$) | 0.0217 | 0.0208 | 0.0301 | 0.0368 | 0.0263 |
| $\hat{Y}_3$ ($\varepsilon_{DP}$) | $8.6 \cdot 10^{-4}$ | 0.0013 | 0.0019 | 0.0023 | 0.0016 |
| $\hat{Y}_4$ (COP) | 5.12 | 0.724 | 1.04 | 1.28 | 0.914 |

If the value of $t_j$ calculated by Eq. (9.6) is higher than critical value of $t$-distribution $t_{p,f} = t_{0.05,7} = 2.37$ (under assumed level of statistical significance $p=0.05$ and degree of freedom for the set of the center points of the CCD $f = n_R - 1 = 7$) then the analyzed coefficient is considered statistically significant [140]. Table 9.4 presents the results of significance test for regression coefficients for the outlet primary airflow temperature. Tests for other factors are listed in **Appendix H**.

Table 9.4. Test of significance for regression coefficients of predicted model equation for $\hat{Y}_1$ (outlet product airflow temperature $\bar{t}$1o)

| Term | Coefficient estimated | $t_j$ | $t_{p,f}$ | Statistically significant |
|---|---|---|---|---|
| $b_0$ | 25.1 | 1411 | | *Yes* |
| $b_1$ | 3.04 | 118 | | *Yes* |
| $b_2$ | 1.67 | 65 | | *Yes* |
| $b_3$ | 0.66 | 25.7 | | *Yes* |
| $b_4$ | -0.09 | 3.60 | | *Yes* |
| $b_5$ | 0.45 | 17.5 | | *Yes* |
| $b_{12}$ | 0.19 | 6.04 | | *Yes* |
| $b_{13}$ | 0.041 | 1.31 | | No |
| $b_{14}$ | 0.008 | 0.26 | | No |
| $b_{15}$ | 0.031 | 0.97 | | No |
| $b_{23}$ | -0.161 | 5.10 | 2.37 | *Yes* |
| $b_{24}$ | 0.0275 | 0.87 | | No |
| $b_{25}$ | -0.104 | 3.30 | | *Yes* |
| $b_{34}$ | 0.01 | 0.32 | | No |
| $b_{35}$ | 0.0575 | 1.82 | | No |
| $b_{45}$ | 0.0006 | 0.02 | | No |
| $b_{11}$ | 0.0076 | 0.33 | | No |
| $b_{22}$ | -0.048 | 8.30 | | *Yes* |
| $b_{33}$ | -0.058 | 9.89 | | *Yes* |
| $b_{44}$ | 0.0342 | 5.87 | | *Yes* |
| $b_{55}$ | 0.1233 | 21.18 | | *Yes* |

After excluding the insignificant model terms and decoding the independent input variables, the final forms of regression equations fitted by regression analysis were derived as follows:

$$\hat{Y}_1(\bar{t}_{1o}) = -10.8 + 0.558t_i + 0.154RH_i + 49.5G_1 - 2.17W_2/W_1 + 1.84\cdot\overline{l_Y^{work}} +$$
$$+5.10\cdot10^{-3}t_i\cdot RH_i - 0.40RH_i\cdot G_1 - 0.40RH_i\cdot\overline{l_Y^{work}} -$$
$$-4.80\cdot10^{-4}RH_i^2 - 36.0G_1^2 + 0.855(W_2/W_1)^2 + 7.89(\overline{l_Y^{work}})^2 \tag{9.13}$$

$$\hat{Y}_2(\hat{Q}) = -6.45 + 0.347t_i + 1.27\cdot10^{-2}RH_i + 70.3G_1 + 2.48W_2/W_1 + 4.18\cdot\overline{l_Y^{work}} -$$
$$-5.83\cdot10^{-3}t_i\cdot RH_i + 0.907t_i\cdot G_1 + 9.92\cdot10^{-2}RH_i\cdot\overline{l_Y^{work}} -$$
$$-0.615RH_i\cdot G_1 - 36.6G_1\cdot\overline{l_Y^{work}} + 5.80\cdot10^{-4}RH_i^2 - 74.4G_1^2 -$$
$$-0.975(W_2/W_1)^2 - 9.15\cdot(\overline{l_Y^{work}})^2 \tag{9.14}$$

$$\hat{Y}_3(\varepsilon_{DP}) = 0.129 + 1.86\cdot10^{-2}t_i + 5.98\cdot10^{-3}RH_i - 2.18G_1 + 0.158W_2/W_1$$
$$+ 0.361\overline{l_Y^{work}} - G_1\cdot\overline{l_Y^{work}} - 1.14\cdot10^{-4}t_i^2 - 3.07\cdot10^{-5}RH_i^2 + 3.24G_1^2 -$$
$$-1.14\cdot10^{-4}(W_2/W_1)^2 - 0.647\cdot(\overline{l_Y^{work}})^2 \tag{9.15}$$

$$\hat{Y}_4(\text{COP}) = 688 + 9.39t_i - 6.90RH_i - 757W_2/W_1 - 3.23\cdot10^3G_1 + 1.09\cdot10^3\cdot\overline{l_Y^{work}} -$$
$$-16.2t_i\cdot G_1 - 4.26t_i\cdot W_2/W_1 + 15.8RH_i\cdot G_1 + 3.48RH_i\cdot W_2/W_1 - 3.67RH_i\cdot\overline{l_Y^{work}} -$$
$$-1.45\cdot10^3G_1\cdot\overline{l_Y^{work}} + 1.19\cdot10^3G_1\cdot W_2/W_1 - 262W_2/W_1\cdot\overline{l_Y^{work}} +$$
$$+4.52\cdot10^3G_1^2 + 223(W_2/W_1)^2 - 309(\overline{l_Y^{work}})^2 \tag{9.16}$$

It should be noted that the currently produced Maisotsenko cycle HMXs are designed at fixed size of the initial part ($\overline{l_Y^{work}}$ =0.375) and fixed level of the working to primary air heat capacity ratio ($W_2/W_1$= 1.0). To make the calculation of the equations more convenient for engineers the simplified versions of the equations describing the currently produced HMXs were also established:

$$\hat{Y}_1(\bar{t}_{1o}) = -10.3 + 0.560t_i + 0.120RH_i + 49.5G_1 + 5.10\cdot10^{-3}t_i\cdot RH_i - 0.40RH_i\cdot G_1 -$$
$$-4.80\cdot10^{-4}RH_i^2 - 36.0G_1^2 \tag{9.17}$$

$$\hat{Y}_2(\hat{Q}) = -4.66 + 0.347t_i + 5.0\cdot10^{-2}RH_i + 56.6G_1 -$$
$$-5.83\cdot10^{-3}t_i\cdot RH_i + 0.907t_i\cdot G_1 - 0.615RH_i\cdot G_1 + 5.80\cdot10^{-4}RH_i^2 - 74.4G_1^2 \tag{9.18}$$

$$\hat{Y}_3\left(\varepsilon_{DP}\right) = 0.272 + 1.86 \cdot 10^{-2} t_i + 5.98 \cdot 10^{-3} \mathrm{RH}_i - 2.18 G_1 -$$
$$- 1.14 \cdot 10^{-4} t_i^2 - 3.07 \cdot 10^{-5} \mathrm{RH}_i^2 + 3.24 G_1^2 \tag{9.19}$$

$$\hat{Y}_4\left(\mathrm{COP}\right) = 423 + 5.13 t_i - 4.79 \mathrm{RH}_i - 2.59 \cdot 10^3 G_1 -$$
$$- 16.2 t_i \cdot G_1 + 15.8 \mathrm{RH}_i \cdot G_1 + 4.52 \cdot 10^3 G_1^2 \tag{9.20}$$

In some cases it might be easier for engineers to calculate the performance factors using air volumetric flow rate. The simplified equations were also established for air volume flow rate varying in the range of $(220\ldots540)$ m$^3$/h.

$$\hat{Y}_1\left(\overline{t}_{1o}\right) = -10.3 + 0.560 t_i + 0.120 \mathrm{RH}_i + 16.5 \cdot 10^{-3} V_1 +$$
$$+ 5.10 \cdot 10^{-3} t_i \cdot \mathrm{RH}_i - 1.30 \cdot 10^{-4} \mathrm{RH}_i \cdot V_1 - 4.80 \cdot 10^{-4} \mathrm{RH}_i^2 - 4.0 \cdot 10^{-6} V_1^2 \tag{9.21}$$

$$\hat{Y}_2\left(\hat{Q}\right) = -4.66 + 0.347 t_i + 5.0 \cdot 10^{-2} \mathrm{RH}_i + 1.89 \cdot 10^{-2} V_1 -$$
$$- 5.83 \cdot 10^{-3} t_i \cdot \mathrm{RH}_i + 3.02 \cdot 10^{-3} t_i \cdot V_1 - 2.05 \cdot 10^{-4} \mathrm{RH}_i \cdot V_1 +$$
$$+ 5.80 \cdot 10^{-4} \mathrm{RH}_i^2 - 8.26 \cdot 10^{-6} V_1^2 \tag{9.22}$$

$$\hat{Y}_3\left(\varepsilon_{DP}\right) = 0.272 + 1.86 \cdot 10^{-2} t_i + 5.98 \cdot 10^{-3} \mathrm{RH}_i - 8.5 \cdot 10^{-4} V_1 -$$
$$- 1.14 \cdot 10^{-4} t_i^2 - 3.07 \cdot 10^{-5} \mathrm{RH}_i^2 + 3.60 \cdot 10^{-7} V_1^2 \tag{9.23}$$

$$\hat{Y}_4\left(\mathrm{COP}\right) = 423 + 5.13 t_i - 4.79 \mathrm{RH}_i - 0.863 V_1 -$$
$$- 5.4 \cdot 10^{-3} t_i \cdot V_1 + 5.3 \cdot 10^{-3} \mathrm{RH}_i \cdot V_1 + 5.02 \cdot 10^{-3} V_1^2 \tag{9.24}$$

The overall statistical significance of the polynomial model equations (9.13)–(9.24) was examined on the base of the Fisher's test (lack-of-fit test) by calculating the $F$-ratio between the lack-of-fit variance $s_{lof}^2$ and the repeatability variance $s_R^2$ for the center points of the CCD

$$F = s_{lof}^2 \big/ s_R^2 \tag{9.25}$$

The lack-of-fit variance was calculated by the following equation

$$s_{lof}^2 = \sum_{i=1}^{i=n} s_i^2 \bigg/ f_{lof} \tag{9.26}$$

where $f_{lof} = (n - l)$ – the number of degrees of freedom of the lack-of-fit variance, $l$ – the number of significant model terms.

If the value of $F$ calculated by Eq. (9.25) is lower than critical value of $F$-distribution $F(p, f_{lof}, f_R)$ under assumed level of statistical significance $p=0.05$ and degree of freedom for the set of the center points $f_R=7$ then the fitted model is considered statistically significant [140]. Table

9.5 presents the results of the adequacy test which demonstrate a high significance of the developed regression models.

Table 9.5. Adequacy model estimation

| Response model | Degrees of freedom | | Variance | | $F$ | $F(p, f_{lof}, f_R)$ | Adequacy of the model |
|---|---|---|---|---|---|---|---|
| | $f_R$ | $f_{lof}$ | $s_R^2$ | $s_{lof}^2$ | | | |
| $\hat{Y}_1$ ($\bar{t}_{lo}$) | 7 | 37 | 0.016 | 0.010 | 0.67 | 2.270 | + |
| $\hat{Y}_2$ ($\hat{Q}$) | 7 | 35 | 0.217 | 0.013 | 0.63 | 2.285 | + |
| $\hat{Y}_3$ ($\varepsilon_{DP}$) | 7 | 38 | $8.6 \cdot 10^{-5}$ | $4.6 \cdot 10^{-5}$ | 0.53 | 2.262 | + |
| $\hat{Y}_4$ (COP) | 7 | 33 | 26.21 | 48.30 | 1.84 | 2.303 | + |

## 9.2. Optimization of the cross-flow M-Cycle HMX

This section presents the multi-criteria optimization of the cross-flow M-Cycle heat and mass exchanger. The optimization is performed on the basis of three previously established performance factors (specific cooling capacity, dew point effectiveness and theoretical COP). The optimization is performed for five influence factors (inlet air temperature and relative humidity, primary air mass flow rate, working to primary air heat capacity ratio and relative length of the initial part) varying in range established in the central composite design for the statistical analysis (see Table 9.1). To simplify the calculation process, optimization is based on the black-box model established from the regression equations (9.14)-(9.16). The analysis of sensitivity of the performance factors on influence factors is presented in **Appendix I**.

### 9.2.1. Single parameter optimization

The single parameter optimization was performed to obtain accurate information about impact of influence factors on heat and mass transfer processes occurring in considered heat exchanger. The analysis of performance was carried out for each individual quality criterion separately. The selected results are visible in Figure 9.3. The analysis of influence of the independent influence factors on the performance of the M-Cycle HMX leads to the important conclusion: variation of some factors leads to the increasing of one of the performance characteristics and decreasing of another. It can be seen that increasing the product air mass flow rate results in reduction of dew point effectiveness by approximately 0.2 (Fig. 9.3(a)) and the COP by up to 150 (Fig. 9.3(b)), however at the same time it increases the specific cooling capacity by up to 6 kW/m$^3$ (Fig. 9.3(c)). The change of relative length of the initial part from 0.125 to 0.625 leads to increasing COP factor (by up to 90: Fig. 9.3(f)) and to decreasing dew point effectiveness and specific cooling capacity by up to 0.14 and 2.2 kW/m$^3$ respectively (Fig. 9.3(d) − (e)). Higher values of working to primary air heat capacity ratio cause COP to decrease by up to 180 and on the other hand they increase the dew point effectiveness and the specific cooling capacity by up to 0.05 and 0.5 kW/m$^3$ respectively (Fig. 9.3(g) − (i)).
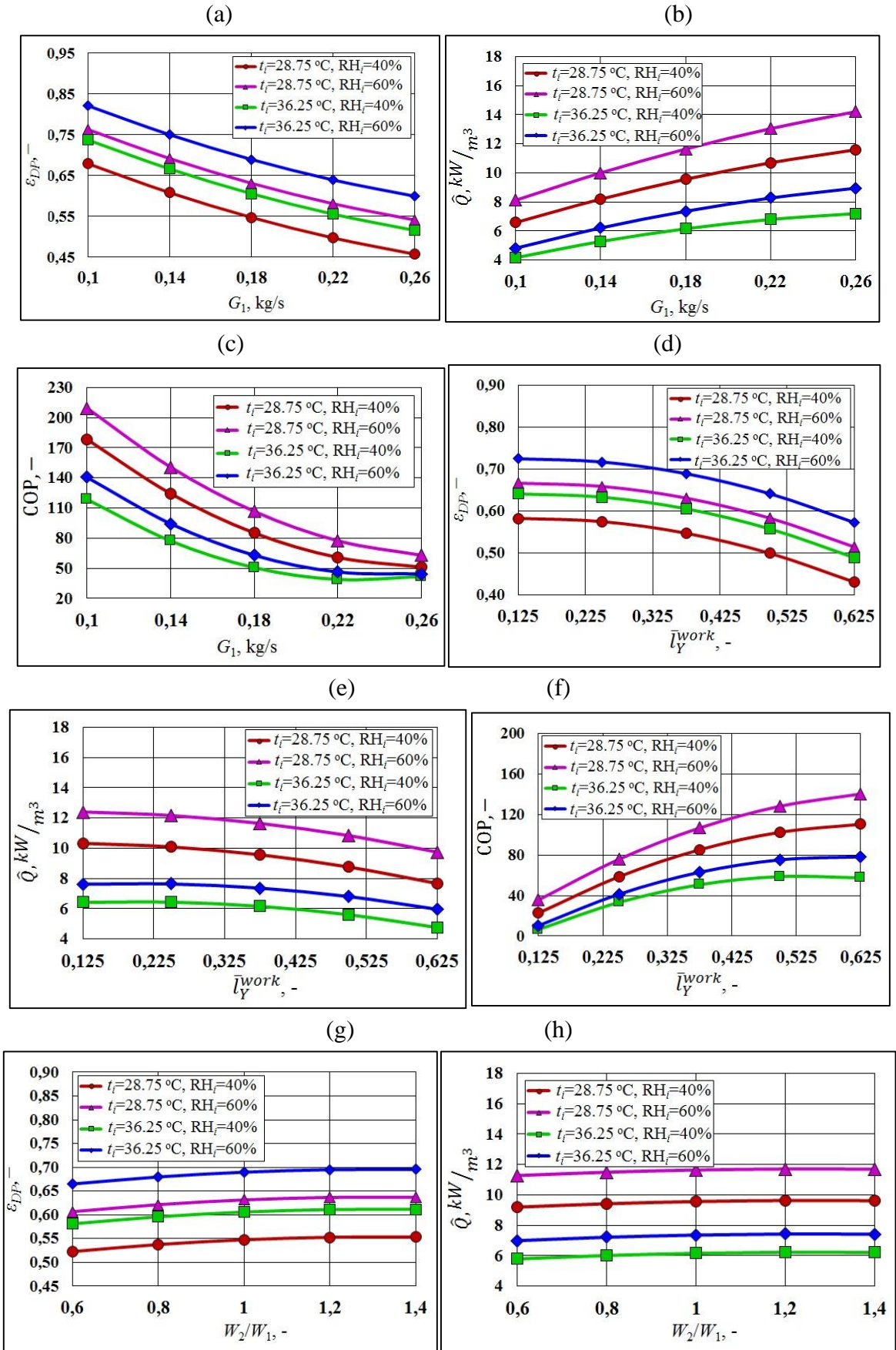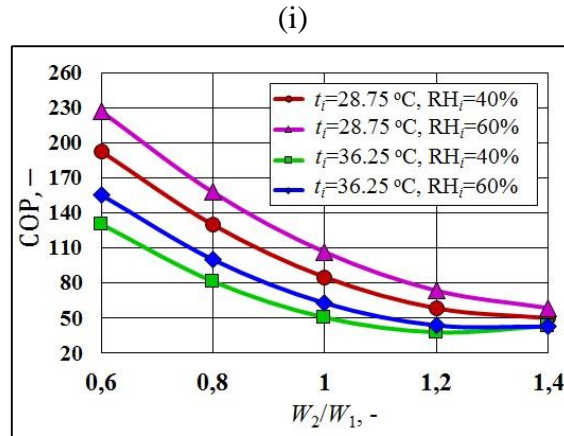
(a)



(b)



(c)



(d)



(e)



(f)



(g)



(h)

(i)



Fig. 9.3. Single-parameter optimization results. (a) Influence of $G_1$ on $\varepsilon_{DP}$. (b) Influence of $G_1$ on $\hat{Q}$. (c) Influence of $G_1$ on COP. (d) Influence of $\bar{l}_Y^{work}$ on $\varepsilon_{DP}$. (e) Influence of $\bar{l}_Y^{work}$ on $\hat{Q}$. (f) Influence of $\bar{l}_Y^{work}$ on COP. (g) Influence of $W_2/W_1$ on $\varepsilon_{DP}$. (h) Influence of $W_2/W_1$ on $\hat{Q}$. (i) Influence of $W_2/W_1$ on COP.

The obtained relationships indicate there is a possibility to obtain high effectiveness of analyzed heat and mass exchanger and opportunity to estimate the range of optimal operating conditions. However, a single-parameter optimization leads to the unsatisfactory results, connected with a discrepancy of extremums of selected characteristic quality indexes (Table 9.6). Optimization on the basis of specific cooling capacity leads to keeping the supply air mass flow rate on the highest level, which would result in very low dew point effectiveness and the COP. Optimization on the basis of dew point effectiveness results in low level of the COP and specific cooling capacity and so on. It is also visible that the COP is the most sensible performance factor: the variation of independent factors always lead to the significant changes of the COP. Such behavior of obtained response functions naturally necessitates to use multi-objective optimization methods on the base of developing a global quality index. However, generalization of the whole complex of contradictory individual optimization functions requires corrective procedure of individual quality criteria weights estimation [48]. Taking into account different character and sensitivity of impact of the independent parameters on the selected performance factors, this procedure would be crucial. The multi-criteria optimization which allows establishing the Pareto-optimal operating conditions and preferable climatic zones is presented in the next section.

Table 9.6. Single-parameter optimization results (for inlet conditions equal $t_{1i}$=32.5°C; RH$_{1i}$=50 %)

| Individual quality criteria | Optimal influence factors | | |
|---|---|---|---|
| | $(G_1)^{opt}$ | $(W_2/W_1)^{opt}$ | $(\bar{l}_Y^{work})^{opt}$ |
| Dew point thermal effectiveness $\varepsilon_{DP}$ | 0.1 | 0.6 | 0.6 |
| Specific cooling capacity per cubic meter of the HMX structure $\hat{Q}$ | 0.26 | 1.27 | 0.125 |
| Theoretical energy efficiency of the system *COP* | 0.1 | 1.32 | 0.2 |

### 9.2.2. Multi-parameter optimization

Many functions may be applied for mathematical analysis of relationships between individual quality criteria and univariate global quality index. In order to generalize the complex of contradictory individual optimization functions the individual desirability indexes were combined into one overall unitless values with Harrington's Desirability Function [143].

$$D = \prod_{i=1}^{n} d_i^{g_i},$$

(9.27)

- $d_i$ − desirability indexes of chosen quality criteria with the interval [0, 1].

-$g_i$ − weights of the individual quality criteria. The sum of weights is always equal to 1.0.

The individual quality indexes are transformed of the to the Harrington unitless desirability scale with one-sided specification using an appropriate form of the Gompertz-curve [78], [143], [144], [145], [146].

$$d_i = exp\left[-exp\left(-Y_i'\right)\right],$$

(9.28)

$Y_i'$ − the coded values of the quality indexes, obtained with a linear transformation

$$Y_i' = b_i + c_i Y_i,$$

(9.29)

*Transformation of the individual quality indexes to the non-dimensional scale*

The Gompertz-curves (Fig. 9) are determined using Eq. (9.29) with the Adler's method, where specification of two values of $Y_i$ and related values of $d_i$ [144], are determined on the highest and lowest values of the quality indexes: the lowest value is related to the boundary of "very bad conditions" ($d_i$=0.2 Fig. 9.4), whereas the highest value is related to the boundary of "very good conditions" ($d_i$=0.8 Fig. 9.4). Values chosen for this transformation were obtained in the center of the component design used for the description of the M-Cycle air cooler, due to the fact that they represent the typical moderate conditions, which are most representative for this kind of exchanger [12]. The values of the obtained indexes are presented in Tab. 9.7.

Table 9.7. Transformation of the individual quality indexes $Y_i$ in the Harrington's desirability scale

| Individual quality indexes | Dimension | Values of individual indexes related to $d_i$=0.2 | Values of individual indexes related to $d_i$=0.8 | Coefficients of linear transformation in Eq. (11) | |
|---|---|---|---|---|---|
| | | | | $b_i$ | $c_i$ |
| Dew point effectiveness $\varepsilon_{DP}$ | − | 0.53 | 0.78 | −4.62 | 7.84 |
| Specific cooling capacity $\hat{Q}$ | kW/m$^3$ | 4.73 | 11.75 | −1.81 | 0.28 |
| COP | − | 13 | 369 | −0.55 | 0.0055 |
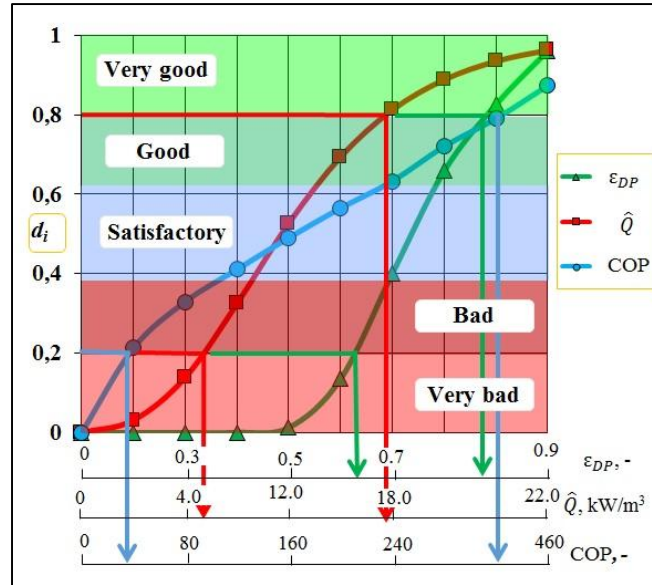
Fig. 9.4. The unitless scales of desirability for individual efficiency indexes.

*Choice of weights for selected individual quality criteria*

Optimization of the cross-flow Maisotsenko heat and mass exchanger requires estimation of weights for the individual quality criteria with appropriate corrective procedure. In many studies weights and individual quality indexes $Y_i$ are chosen using the experts opinions [145]. However, this method might be misleading in some cases, e.g. when a significant number of experts gives the contradictory opinions. For the above-mentioned reason, different method is applied in this study. The appropriate range of weight coefficients will be chosen with the method of minimizing their impact change of values of Harrington function. This is obtained with minimizing the following equation:

$$\sqrt{\left(\frac{\partial D^{opt}}{\partial g_1}\right)^2 + \left(\frac{\partial D^{opt}}{\partial g_2}\right)^2 + \left(\frac{\partial D^{opt}}{\partial g_3}\right)^2} \to \min \tag{9.30}$$

However, in order to minimize the above mentioned function, it is necessary to determine the relation of $D^{opt}$ as a function of weights:

$$D = f(g_1, g_2, g_3) \tag{9.31}$$

Demis Pandelidis

Table 9.8. The matrix of simplex-lattice design for the conditions t1i = 32.5°C and RH1i = 50%.

| No. | $g_1(\varepsilon)$ | $g_2(\hat{Q})$ | $g_3(COP)$ | $\varepsilon_{DP}$ | $\hat{Q}$ | COP | $d_1(\varepsilon_{DP})$ | $d_2(\dot{Q})$ | $d_3(COP)$ | $D^{opt}$ | $G_1^{opt}$ | $(W_2/W_1)^{opt}$ | $(\bar{l}_Y^{work})^{opt}$ |
|---|---|---|---|---|---|---|---|---|---|---|---|---|---|
| 1 | 0 | 0 | 1 | 0.65 | 4.7 | 369 | 0.53 | 0.2 | 0.8 | 0.8 | 0.1 | 0.6 | 0.6 |
| 2 | 0 | 1 | 0 | 0.59 | 11.75 | 38 | 0.39 | 0.8 | 0.25 | 0.8 | 0.26 | 1.27 | 0.125 |
| 3 | 1 | 0 | 0 | 0.78 | 5.9 | 62 | 0.8 | 0.32 | 0.29 | 0.8 | 0.1 | 1.32 | 0.2 |
| 4 | 0 | 0.2 | 0.8 | 0.66 | 5.5 | 328 | 0.57 | 0.27 | 0.76 | 0.61 | 0.11 | 0.6 | 0.52 |
| 5 | 0.2 | 0 | 0.8 | 0.68 | 5.1 | 348 | 0.62 | 0.24 | 0.78 | 0.74 | 0.1 | 0.6 | 0.52 |
| 6 | 0.2 | 0.8 | 0 | 0.6 | 11.7 | 42 | 0.39 | 0.8 | 0.25 | 0.69 | 0.26 | 1.3 | 0.125 |
| 7 | 0 | 0.8 | 0.2 | 0.55 | 10.9 | 85 | 0.26 | 0.75 | 0.34 | 0.64 | 0.26 | 0.6 | 0.23 |
| 8 | 0.8 | 0 | 0.2 | 0.75 | 5.5 | 262 | 0.75 | 0.28 | 0.67 | 0.73 | 0.1 | 0.6 | 0.28 |
| 9 | 0.8 | 0.2 | 0 | 0.76 | 6.4 | 64 | 0.77 | 0.37 | 0.3 | 0.67 | 0.11 | 1.3 | 0.23 |
| 10 | 0 | 0.4 | 0.6 | 0.61 | 7.4 | 220 | 0.42 | 0.47 | 0.6 | 0.54 | 0.16 | 0.6 | 0.44 |
| 11 | 0.4 | 0 | 0.6 | 0.72 | 5.4 | 320 | 0.69 | 0.26 | 0.75 | 0.72 | 0.1 | 0.6 | 0.43 |
| 12 | 0.4 | 0.6 | 0 | 0.64 | 9.9 | 14 | 0.52 | 0.69 | 0.2 | 0.62 | 0.2 | 1.3 | 0.125 |
| 13 | 0 | 0.6 | 0.4 | 0.52 | 10.4 | 105 | 0.19 | 0.72 | 0.38 | 0.56 | 0.26 | 0.6 | 0.33 |
| 14 | 0.6 | 0 | 0.4 | 0.74 | 5.5 | 291 | 0.73 | 0.28 | 0.71 | 0.72 | 0.1 | 0.6 | 0.35 |
| 15 | 0.6 | 0.4 | 0 | 0.7 | 8.1 | 27 | 0.66 | 0.53 | 0.22 | 0.61 | 0.15 | 1.3 | 0.17 |
| 16 | 0.2 | 0.2 | 0.6 | 0.72 | 5.4 | 320 | 0.69 | 0.26 | 0.75 | 0.6 | 0.1 | 0.6 | 0.43 |
| 17 | 0.2 | 0.6 | 0.2 | 0.61 | 9.4 | 113 | 0.42 | 0.65 | 0.4 | 0.54 | 0.2 | 0.6 | 0.22 |
| 18 | 0.6 | 0.2 | 0.2 | 0.75 | 5.6 | 246 | 0.75 | 0.29 | 0.64 | 0.6 | 0.1 | 0.67 | 0.31 |
| 19 | 0.2 | 0.4 | 0.4 | 0.65 | 7.4 | 206 | 0.54 | 0.47 | 0.58 | 0.53 | 0.15 | 0.6 | 0.34 |
| 20 | 0.4 | 0.2 | 0.4 | 0.73 | 5.5 | 295 | 0.72 | 0.28 | 0.71 | 0.59 | 0.1 | 0.6 | 0.36 |
| 21 | 0.4 | 0.4 | 0.2 | 0.68 | 7.2 | 184 | 0.62 | 0.45 | 0.54 | 0.53 | 0.14 | 0.62 | 0.26 |

This function cannot be obtained with the typical central composite design method, due to the fact that sum of the weights must always be equal to 1. Such function can be obtained, however, with three factor simplex-lattice design typically used for the design of mixture experiments (in case of mixtures the same situation occurs: sum of all components must be equal to one). Application of this method requires establishing simplex-lattice designs for every combination of the relative humidity and temperature form the central composite design describing the operation of the exchanger (Tab. 9.8). This generates a 25 matrixes with 19 weight combinations (475 test points). Every matrix allows generating four-dimensional ternary plots, which allow studding the variation of the optimal values of Harrington function, individual quality indexes and the influence factors as the functions of weight coefficients. Due to the high number of the test points and results only the obtained values will be present only for the temperature and relative humidity combination from the center of central composite design ($t_{1i}$=32.5°C, RH$_{1i}$=50%). The test matrix is presented in Table 9.8, the ternary plots are visible in Figure 9.5.

It can be seen that Harrington function of desirability shows high sensitivity on the weight values (Fig. 9.5(a)). However, in the central part of the plot, the region with lower sensitivity is clearly visible. This allows assuming that the weight coefficients which have lower impact on the $D$ value can be established. It is clearly visible that all influence factors ($G_1$, $W_2/W_1$ and $\bar{l}_Y^{work}$) are highly sensitive on the weight values and it is hard to determine the region where the

impact of the weights values is lower (Fig. 9.5(b)-(d)). However, this is supposed to be expected, due to the fact that all of the influence factors show opposite trend on the variation on operation conditions (see section 4.1. for single parameter optimization). The only small exception is the ternary plot of $W_2/W_1$ factor, which has a small stable region (Fig. 9.5(c)). This is caused by the fact that sensitivity of dew point effectiveness and specific cooling capacity on this factor is much smaller than on the primary air mass flow rate and relative length of the initial part. It can also be seen that optimal values of quality indexes and their transformed, dimensionless values show high sensitivity on the weight factors (Fig. 9.5(e)-(i)). However, in this case the plots are little less sharp than of the influence factors and quasi-stable regions might be established.

(a)

(b)

(c)

(d)

Fig. 9.5. Ternary plots obtained from the simplex-lattice design for inlet airflow conditions $t_{1i}$ = 32.5°C and RH$_{1i}$ = 50%. (a) Impact of weights values on the Harrington function. (b) Impact of weights values on the $G_1^{opt}$. (c) Impact of weights values on the $(W_2/W_1)^{opt}$. (d) Impact of weights values on the $(\overline{l_Y^{work}})^{opt}$. (e) Impact of weights values on the $(\varepsilon_{DP})^{opt}$. (f) Impact of weights values on $d_1(\varepsilon_{DP})^{opt}$. (g) Impact of weights values on the $(\hat{Q})^{opt}$. (h) Impact of weights values on the $d_2(\hat{Q})^{opt}$. (i) Impact of weights values on the $(COP)^{opt}$. (j) Impact of weights values on the $d_3(COP)^{opt}$.

Using above described method, the functions $D=f(g_1, g_2, g_3)$ for the all combinations of climate conditions were determined. For every combination the low-sensitivity eights were determined using Eq. 9.31. The obtained values were averaged in order to obtain universal values which might be suitable for all climate conditions. The final weights for selected individual quality criteria were determined as follows: $g_{\varepsilon_{DP}} = (0.22 \pm 0.01)$, $g_{\hat{Q}} = (0.41 \pm 0.02)$, $g_{COP} = (0.37 \pm 0.01)$
.

*Results of the optimization*

Computer simulations, carried out on the base of experiment methods design, allowed determining Pareto-optimal performance characteristics [144] of investigated HMX, which were scored on the Harrington scale of desirability (see Fig. 9.4), and generalize them in unitless form (Fig. 9.6(a)-(c)). Figure 9.6 shows the analysis of impact of the pairs of individual influence factors on the values of Harrington desirability function when the rest of influence factors are kept fixed in the center of the central composite design. Figures 9.6(a) and (b) show the impact of primary air mass flow rate and relative length of the initial part on the desirability function. It can be seen that the $D^{opt}$ reaches the values close to 0.5 for the $\overline{l_Y}^{work}$ varying between 0.3 and 0.45 and $G_1$ varying between 0.12 and 0.17 kg/s. Figures 9.6(c) and (d) show the impact of primary air mass flow rate and working to primary air ratio. The highest values of Harrington function are obtained for $G_1$ varying from 0.12 to 0.18 kg/s and $W_2/W_1$ changing between 0.6 and 0.7. Figures 9.6(c) and (d) show the impact of working to primary air heat capacity ratio and relative length of the initial part on the desirability function. It is clearly visible that the highest values of the function are obtained for the $\overline{l_Y}^{work}$ varying between 0.3 and 0.45 and $W_2/W_1$ changing between 0.6 and 0.7.

It should be mentioned that impact of the above-mentioned factors on the desirability function are different for the different climate conditions. Figure 9.7 shows the impact of the same pairs of factors on the desirability function for conditions from the axial points in the central composite design ($-\alpha$: $t_{1i} = 25°C$, $RH_{1i} = 30\%$; $+\alpha$: $t_{1i} = 40°C$, $RH_{1i} = 70\%$).
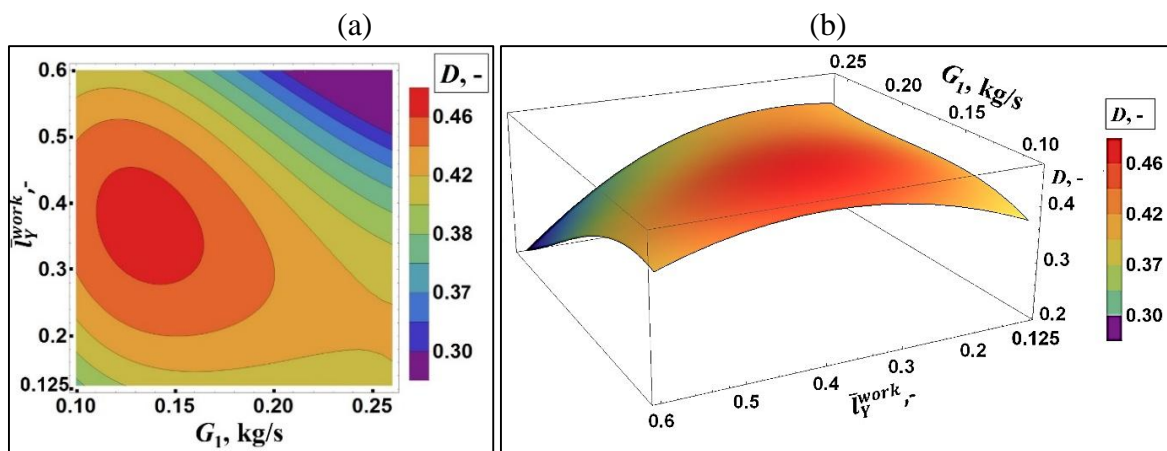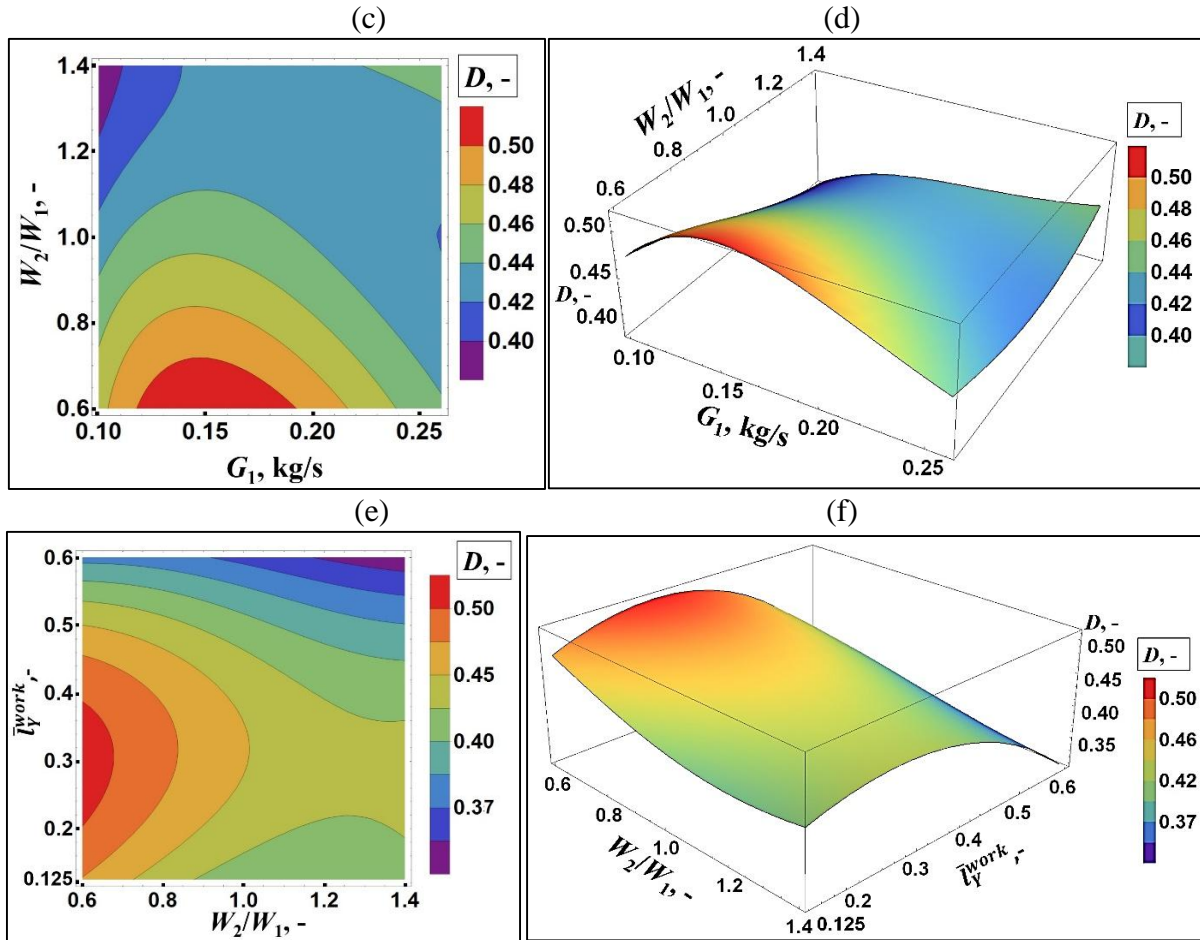
(a)          (b)

Fig. 9.6. Character of the Desirability Index $D$ under conditions $t_{1i} = 32.5°C$ and $RH_{1i} = 50\%$. (a) At the fixed level of the $W_2/W_1$: contour plot. (b) At the fixed level of the $W_2/W_1$: three-dimensional plot. (c) At the fixed level of the $\overline{l}_Y^{work}$: contour plot. (d) At the fixed level of the $\overline{l}_Y^{work}$: three-dimensional plot. (e) At the fixed level of the $G_1$: contour plot. (f) At the fixed level of the $G_1$: three-dimensional plot.

It can be seen that the Harrington function reaches highest values for the significantly different values of the influence factors: in case for the pair $G_1$ and $\overline{l}_Y^{work}$ the optimal values of the Harrington function are obtained for primary air mass flow rate varying from 0.245 and 0.26 kg/s and relative initial part length varying from 0.125 to 0.25. and when other influence factors are fixed at $-\alpha$ values (Fig. 9.7(a)). When values of the influence factors are fixed at $+\alpha$, the highest values of the desirability function are obtained for $G_1 = 0.1…0.145$ and $\overline{l}_Y^{work} = 0.125…0.45$. It can be seen that similar trend can be observed for other pairs of factors (i.e. $G_1$ and $W_2/W_1$; $W_2/W_1$ and $\overline{l}_Y^{work}$ : Fig. 9.7(c)-(f)). Also, it is clearly visible that different values of the geometrical and operational factors ($G_1$, $W_2/W_1$ and $\overline{l}_Y^{work}$ ) significantly affect the optimal climatic zones (Fig. 9.7(g) and (h)). It can be observed that it is impossible to optimize the structure of the exchanger at fixed climate conditions. The only reasonable way is to optimize the unit is to determine optimal values of $G_1$, $W_2/W_1$ and $\overline{l}_Y^{work}$ at all combinations of the temperature and relative humidity from the central composite design (Tab. 9.1) and establish the averaged ones, which allow to achieve satisfactory level of the Harrington function at most of the climate conditions. Using the optimal values of the geometrical and operational factors

established this way, the climate conditions allowing for rational operation of the heat and mass exchanger can be obtained.

(a)

(b)

(c)

(d)

(e)

(f)

(g)                                              (h)



Fig. 9.7. Character of the Desirability Index. (a) At the fixed level of the $W_2/W_1$, $t_{1i} = 25.0°C$ and $RH_{1i}$ = 30%. (b) At the fixed level of the $W_2/W_1$, $t_{1i} = 40.0°C$ and $RH_{1i} = 70\%$. (c) at the fixed level of the , $t_{1i} = 25.0°C$ and $RH_{1i} = 30\%$. (d) At the fixed level of the $\bar{l}_Y^{work}$, $t_{1i} = 40.0°C$ and $RH_{1i} = 70\%$. (e) at the fixed level of the $G_1$, $t_{1i} = 25.0°C$ and $RH_{1i} = 30\%$. (f) At the fixed level of the $G_1$, $t_{1i} = 40.0°C$ and $RH_{1i} = 70\%$.(g) At the fixed level of the $G_1$=0.1, $W_2/W_1$=0.6, $\bar{l}_Y^{work}$ =0.125. (h) At the fixed level of the $G_1$=0.26, $W_2/W_1$=1.4, $\bar{l}_Y^{work}$ =0.625.

The obtained averaged results of the multi-criteria optimization at different climate conditions allowed estimating optimum operating conditions (Fig. 9.8). The range of optimal geometrical and operating conditions, which were obtained from the Harrington scale of desirability and preference [78], [143], [144] is presented in Table 9.9. The established optimal operating characteristics were used to find suitable climatic zones for the cross-flow M-Cycle HMX (Fig. 9.9). It can be seen that obtained parameters allow for the satisfying operation of the analyzed heat and mass exchanger in most of the typical climate conditions. The not suitable climate conditions are those characterizing really moist regions (RH≥65%) and the colder climates (temperature level close to 25°C). The most unsuitable conditions are cold and moist climates. However, in such regions, the air conditioning demand is usually much lower than in hotter parts of globe. In hot and very moist climates M-Cycle cross-flow heat exchanger has to operate with additional dehumidifier (e.g. desiccant wheel or classic cooling coil). It should be mentioned that presented exchanger can operate effectively in the same temperature range under inlet relative humilities lower than 30%, however, it is a well-known fact that evaporative air cooler show best performance under very dry climates, therefore it was pointless to perform such analysis in this Section.

Table 9.9. Ranges of optimal operating conditions for the M-Cycle heat and mass exchanger

| Factor | Optimal range of values |
|---|---|
| $(G_1)^{opt}$ | 0.16...0.2 |
| $(W_2/W_1)^{opt}$ | 0.9...1.1 |
| $(\bar{l}_Y^{work})^{opt}$ | 0.2…0.3 |
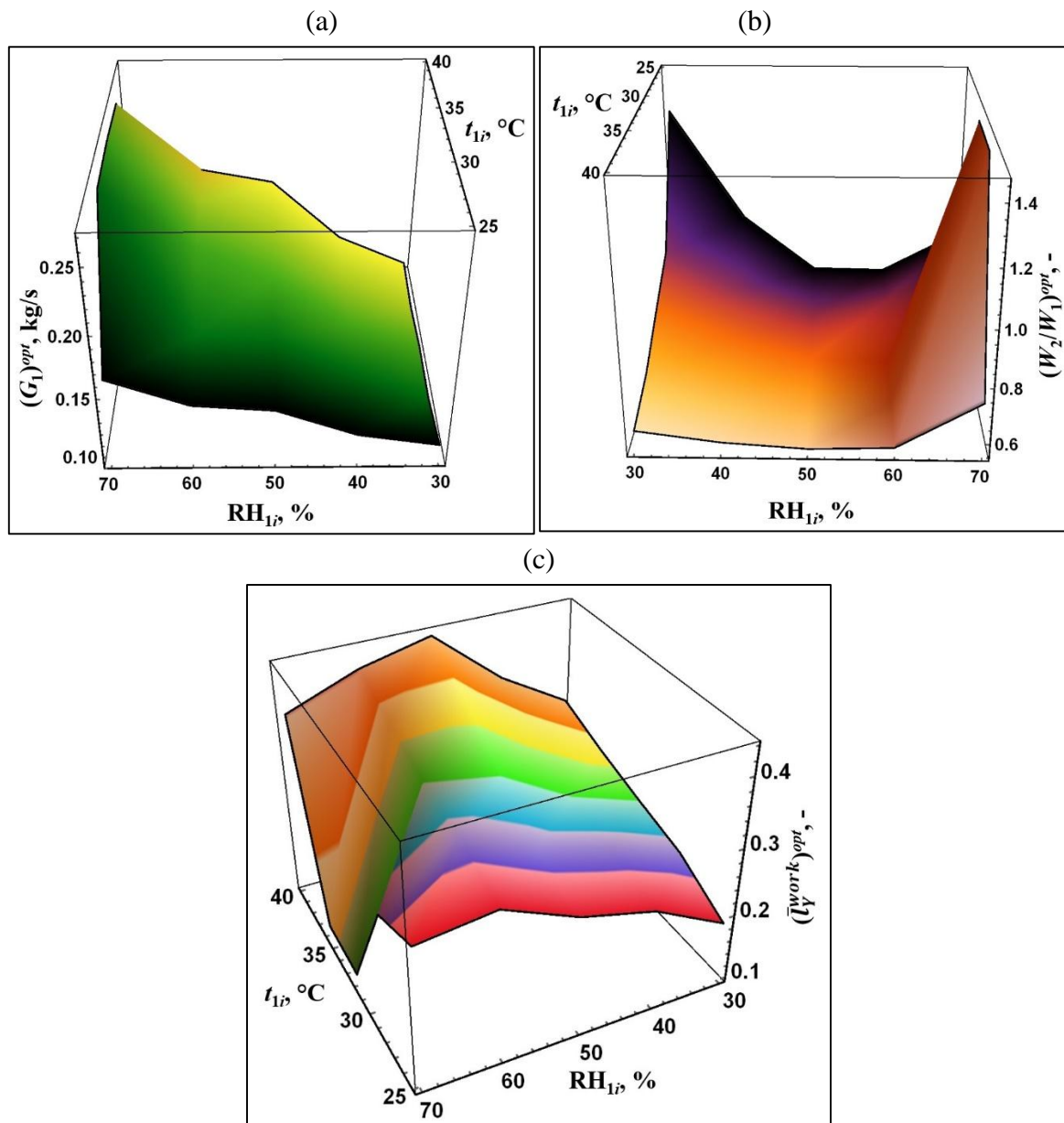
(a)  (b)

(c)



Fig. 9.8. Optimal individual values of influence factors at different climate conditions. (a) Primary air mass flow rate. (b) Working to primary air ratio. (c) Relative length of the initial part of exchanger.

The suitability of the M-Cycle heat and mass exchanger to the selected world cities was analyzed and established in Table 9.10. It can be seen that the presented exchanger allows obtaining satisfying effectiveness in many of the world regions, therefore it has a potential of wide application around the world. In many countries the presented exchanger cannot operate as the only cooling device for the building, however, it can still provide significant energy savings as an element of the typical air conditioning system (as a pre-cooler or post-cooler for the typical cooling coil) or as an element of the desiccant air conditioning system- this problem is widely discussed in the next section.
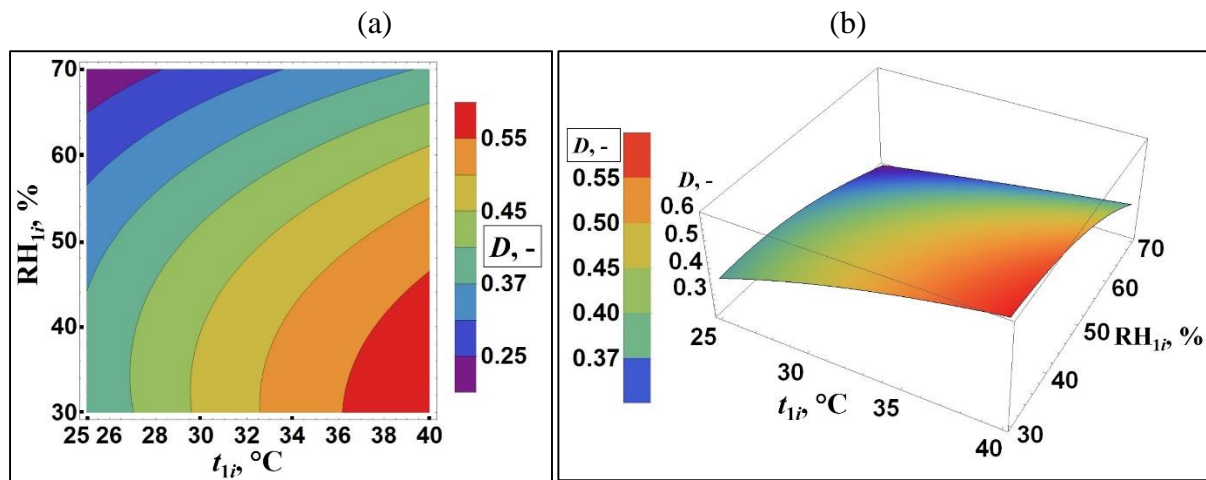
(a)                                          (b)



Fig. 9.9. Climatic zones of preferable application of the HMX. (a) Contour plot. (b) Three-dimensional plot.

Table 9.10. Suitability of the M-Cycle heat and mass exchanger to the selected world cities

| Country | City | Temperature, °C | Relative humidity, % | Suitable |
|---|---|---|---|---|
| China | Beijing | 37.4 | 45 | Yes |
| China | Shanghai | 38 | 47 | Yes |
| Czech Republic | Prague | 27.7 | 42 | Yes |
| **Denmark** | **Copenhagen** | **24** | **51** | **No** |
| Finland | Helsinki | 26.7 | 46 | Yes |
| Germany | Berlin | 29.2 | 44 | Yes |
| Greece | Athens | 33.8 | 31 | Yes |
| Hungary | Budapest | 30.6 | 36 | Yes |
| **Italy** | **Rome** | **30.9** | **62** | **No** |
| Japan | Tokio | 33.1 | 57 | Yes |
| Poland | Warsaw | 32 | 50 | Yes |
| Portugal | Lisbon | 32.1 | 31 | Yes |
| Russia | St. Petersburg | 27 | 53 | Yes |
| Spain | Madrid | 36.1 | 29 | Yes |
| Turkey | Izmir | 35.5 | 55 | Yes |
| United Kingdom | London | 28 | 48 | Yes |
| United States | New York | 35.5 | 45 | Yes |
| United States | Denver. CO | 33 | 25 | Yes |
| United States | Los Angeles | 29 | 50 | Yes |

## 9.3. Conclusions from the Section 9

This Section presents the statistical analysis and optimization of the cross-flow M-Cycle HMX. Four performance factors were selected as the representative responses (outlet primary airflow temperature, specific cooling capacity, dew point effectiveness and the theoretical COP) and five independent variables were chosen as the parameters which have the most impact on the exchanger's performance (inlet air temperature and relative humidity, supply air mass flow rate,

working to primary air heat capacity ratio and relative width of the dry initial part of the exchanger).

The accuracy and overall predictive capability of the model developed was examined using regression analysis of the coefficient of determination and absolute average deviation by comparing predicted responses with the experimental data. The satisfactory values of the $R^2$ and AAD as well as the positive results of the $F$-test indicated that the models obtained are statistically significant, may represent the true behavior of the system and can be used for the analysis of the cross-flow M-Cycle heat exchanger. The quadratic regression models were presented in different forms to make the calculation of the developed equations more convenient for engineers. The obtained equations were used to examine the impact of independent variables on the performance factors. It was also established that sensibility of this impact is different for different investigated factors. The most influential parameters are supply air mass flow rate, inlet air temperature and relative humidity.

The optimization was performed with two methods: single-parameter and multi-parameter compromise method. The single parameter optimization lead to the unsatisfactory results, due to the different trends shown by the quality criteria under identical variation of input parameters. However, this process allowed establishing the level of sensitivity of each quality index on the input parameters.

The multi-parameter optimization was based on analysis of the Harrington function of desirability. The weight coefficients for the optimization process were with the assumption to minimize their impact change of values of Harrington function. The analysis of the impact was based on the simplex-lattice design method, which allowed establishing weight coefficients appropriate for the analyzed climate conditions. The results of optimization allowed establishing Pareto-optimal operational and geometrical conditions (presented in Table 9.9) for the presented exchanger and establishing the optimal climate conditions for its effective operation (presented in Figure 9.9 and in Table 9.10).

## 10. Analysis of operation of the optimized HMX in selected air conditioning systems

### 10.1. Profitability analysis of application of the M-Cycle HMX in the typical air conditioning systems in Poland

This section investigates the possibility of application of the M-Cycle cross-flow indirect evaporative air cooler into the typical air conditioning systems in Polish climate conditions (Fig. 10.1). In all examples M-Cycle heat exchanger is placed in the typical air handling unit (Fig. 10.1(a)) with cooling coil supplied with R410 refrigerant. In this solution HMX operates as a main cooling source, whereas the cooling coil is used as a peak cooling source, which provides additional cooling. It should be noted that optimized M-Cycle HMX includes the constant primary airflow rate and working to primary air heat capacity ratio (540 m$^3$/h and 1.0 respectively). Due to this fact, in order to provide higher airflow rates the exchanger needs to

be blocked in groups, as it is in the typical Coolerado air coolers (Fig. 10.1(c)). The system is compared with a typical air handling unit with rotary heat exchanger (Fig. 10.1(b)). The analysis is performed for two example applications of such systems, which include:

- Three identical offices with windows exposed on south, east and west direction: mixing ventilation (Fig. 10.1(d)),
- Three identical offices with windows exposed on south, east and west direction: displacement ventilation (Fig. 10.1(e)),

The assumptions for the characteristics of the office spaces are listed as follows:

- Month of comparison: July,
- Location: Wroclaw, Poland,
- Area: 50 m$^2$,
- Occupation: 5 people,
- Typical construction window with double glass, with glass surface equal 10 m$^2$,
- One outdoor wall, not heat transfer through the inside walls, floor and ceiling,
- Hours of operation: 7 a.m.- 7 p.m.,
- Cooling loads from technology are constant and equal to 1 kW,
- Maximum room temperature in summer $t_{RMax}^{Sum}=t_R=25°C$,
- The efficiency of the rotary heat exchanger is constant and equal to 0.7,
- Room temperature is controlled using following equation [31], [32]:

$$t_R^{Sum} = \frac{t_R^{Wint}+t_a}{2}, °C \tag{10.1}$$

  o Where:
    o $t_R^{Sum}$- temporary room temperature in summer, °C,
    o $t_R^{Wint}$- room temperature in winter, $t_R^{Wint}=20°C$,
    o $t_a$- temporary ambient air temperature, °C.
- Assumed temperature difference between supply and exhaust air (to calculate the airflow rate): 6°C,
    o In case of the mixing ventilation the exhaust air temperature is assumed as equal to the human occupation zone temperature ($t_E= t_R$),
    o In case of the displacement ventilation the exhaust air temperature is assumed to be a 3°C higher than human occupation zone temperature ($t_E= t_R+3°C$) during the occurrence of the maximal cooling loads.

(a)
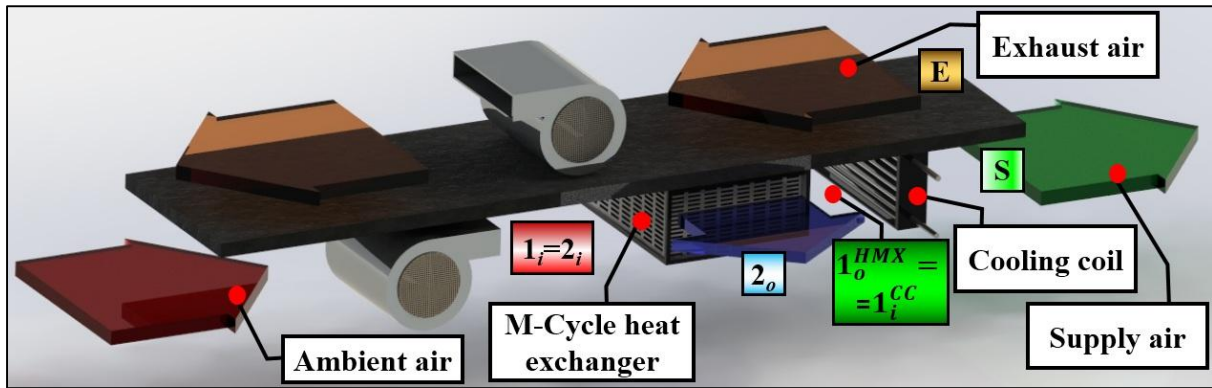


(b)
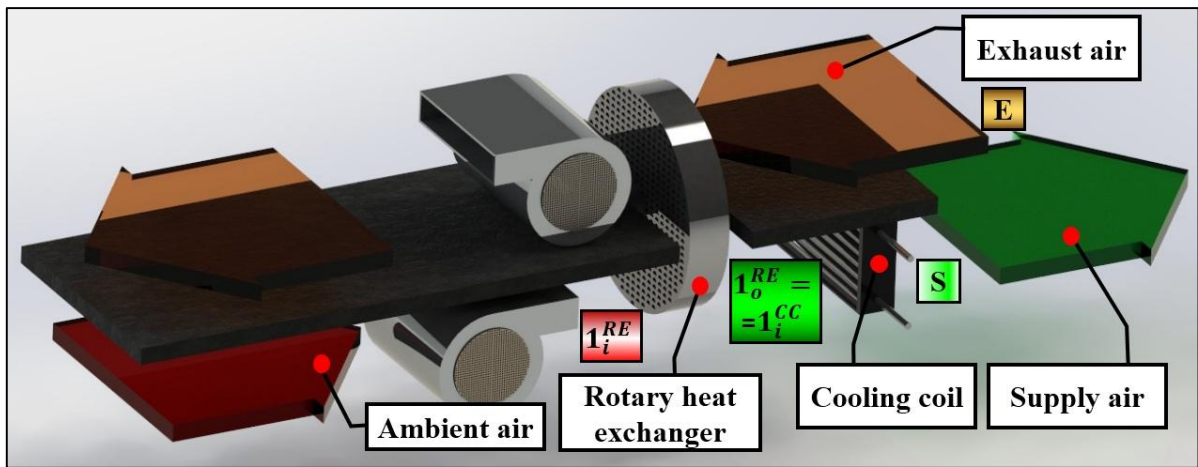


(c)                                              (d)
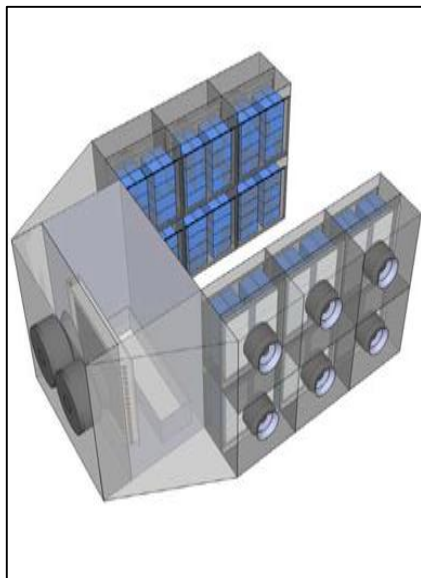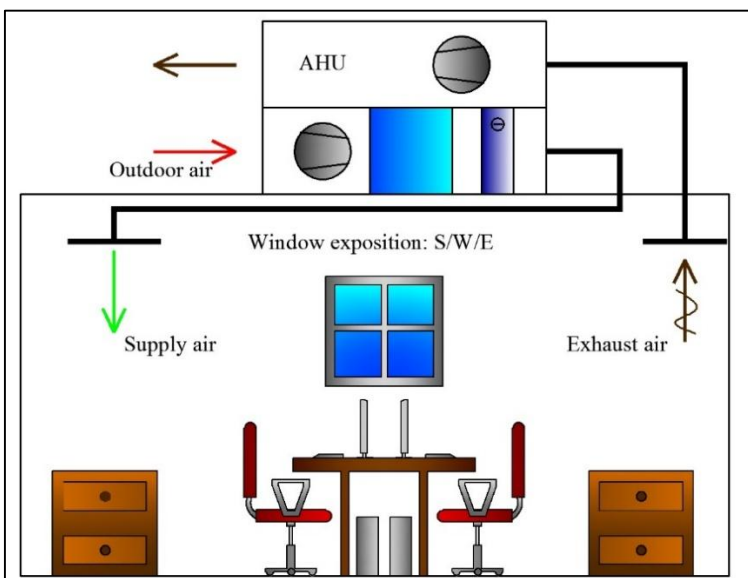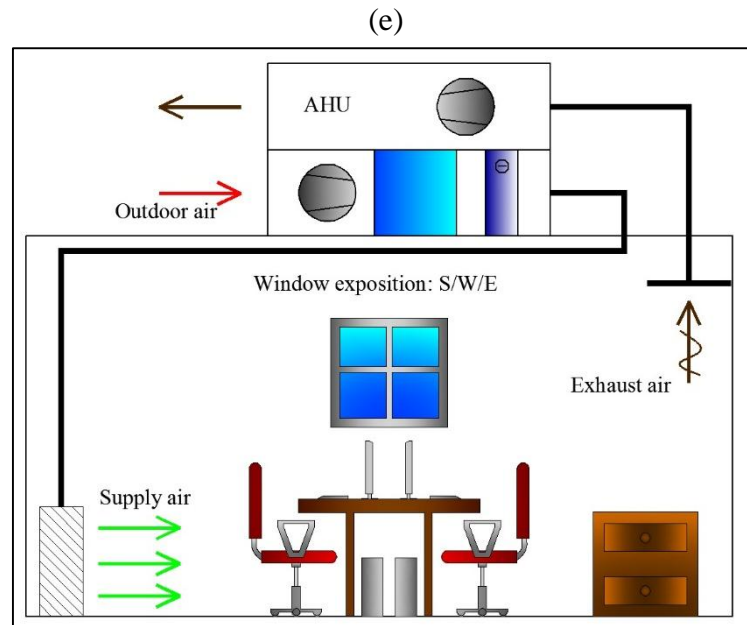
(e)



Fig. 10.1. Analyzed systems. (a) AHU with the M-Cycle unit. (b) AHU with the rotary heat exchanger. (c) Coolerado AHU with 240 M-Cycle HMXs blocked in one device (with cooling capacity equal 315 kW). (d) Scheme of the system with mixing ventilation. (e) Scheme of the system with displacement ventilation.

The example calculation of cooling loads was performed for the office with wall located on the southern side, the results are established in Table 10.1. Analogous calculations was performed for the offices with wall located on the western and eastern side of the building (the simplified results are presented in Tables 10.2 and 10.3). It can be seen that the maximal cooling loads for the "south room" occur at 12.00 a.m. and are equal 1.89 kW, in the "west room" they occur at 4 p.m. and are equal 3.72 kW, whereas in the "east room" they occur at 8.00 a.m. and are equal 2.17 kW. The required airflow rates calculated with the assumption of 6°C temperature difference between supply and exhaust airflow are equal:

- $V_S$=1610 m$^3$/h (3 HMXs),
- $V_S$=1850 m$^3$/h (4 HMXs),
- $V_S$=1080 m$^3$/h (2 HMXs).

Table 10.1. Calculation of the cooling loads for the room with wall on the south side

| | 7 a.m. | 8 a.m. | 9 a.m. | 10 a.m. | 11 a.m. | 12 a.m. | 1 p.m. | 2 p.m. | 3 p.m. | 4 p.m. | 5 p.m. | 6 p.m. | 7 p.m. | Hour |
|---|---|---|---|---|---|---|---|---|---|---|---|---|---|---|
| $t_a$,°C | 20.4 | 22.6 | 24.6 | 26.1 | 27.4 | 28.4 | 29.3 | 29.8 | 30.0 | 29.9 | 29.5 | 28.5 | 27.0 | Outdoor temperature |
| $t_R$,°C | 20.2 | 21.3 | 22.3 | 23.1 | 23.7 | 24.2 | 24.7 | 24.9 | 25.0 | 25.0 | 24.8 | 24.3 | 23.5 | Required room temperature |
| $Q_{RS}$,W | 35 | 25 | 16 | 10 | 6 | 4 | 4 | 6 | 10 | 16 | 22 | 29 | 37 | Radiation cooling loads: walls |
| $Q_{CS}$,W | 3 | 21 | 37 | 49 | 59 | 67 | 74 | 78 | 80 | 79 | 76 | 68 | 56 | Sensible cooling loads: windows |
| $Q_{rS}$,W | 140 | 506 | 874 | 1312 | 1657 | 1818 | 1749 | 1473 | 1081 | 713 | 215 | 178 | 131 | Radiation cooling loads: walls |
| $Q_{Win}$,W | 144 | 527 | 911 | 1360 | 1716 | 1885 | 1823 | 1551 | 1161 | 793 | 291 | 246 | 187 | Sum of cooling loads: windows |
| $Q_o$,W | 404 | 384 | 369 | 361 | 354 | 348 | 345 | 344 | 344 | 344 | 346 | 353 | 364 | Cooling loads: occupants |
| $Q_T$,W | 1000 | 1000 | 1000 | 1000 | 1000 | 1000 | 1000 | 1000 | 1000 | 1000 | 1000 | 1000 | 1000 | Cooling loads: technology |
| $Q_{Tot}$,W | **1582** | **1936** | **2296** | **2731** | **3076** | **3236** | **3171** | **2901** | **2515** | **2152** | **1659** | **1628** | **1587** | **Total cooling loads** |

Table 10.2. Cooling loads for the room with wall on the west side

| | 7 a.m. | 8 a.m. | 9 a.m. | 10 a.m. | 11 a.m. | 12 a.m. | 1 p.m. | 2 p.m. | 3 p.m. | 4 p.m. | 5 p.m. | 6 p.m. | 7 p.m. | Hour |
|---|---|---|---|---|---|---|---|---|---|---|---|---|---|---|
| $t_a$,°C | 20.4 | 22.6 | 24.6 | 26.1 | 27.4 | 28.4 | 29.3 | 29.8 | 30.0 | 29.9 | 29.5 | 28.5 | 27.0 | Outdoor temperature |
| $t_R$,°C | 20.2 | 21.3 | 22.3 | 23.1 | 23.7 | 24.2 | 24.7 | 24.9 | 25.0 | 25.0 | 24.8 | 24.3 | 23.5 | Required room temperature |
| $Q_{Tot}$,W | **1558** | **1565** | **1575** | **1583** | **1590** | **1598** | **2244** | **2893** | **3454** | **3720** | **3637** | **3175** | **1767** | **Total cooling loads** |

Table 10.3. Cooling loads for the room with wall on the east side

| | 7 a.m. | 8 a.m. | 9 a.m. | 10 a.m. | 11 a.m. | 12 a.m. | 1 p.m. | 2 p.m. | 3 p.m. | 4 p.m. | 5 p.m. | 6 p.m. | 7 p.m. | Hour |
|---|---|---|---|---|---|---|---|---|---|---|---|---|---|---|
| $t_a$,°C | 20.4 | 22.6 | 24.6 | 26.1 | 27.4 | 28.4 | 29.3 | 29.8 | 30.0 | 29.9 | 29.5 | 28.5 | 27.0 | Outdoor temperature |
| $t_R$,°C | 20.2 | 21.3 | 22.3 | 23.1 | 23.7 | 24.2 | 24.7 | 24.9 | 25.0 | 25.0 | 24.8 | 24.3 | 23.5 | Required room temperature |
| $Q_{Tot}$,W | **2115** | **2171** | **2118** | **1975** | **1776** | **1673** | **1659** | **1644** | **1628** | **1620** | **1592** | **1576** | **1552** | **Total cooling loads** |

### 10.1.1. Mixing ventilation

Using the previously established supply airflow rates and the required room temperatures during operation hours, the supply air temperatures were established for every room (Table 10.4). The outlet air temperatures obtained from the HMX were established using the mathematical model based on the regression equations and the climatic curve for the Wroclaw conditions [31], [32] (Fig. 10.2). It should be noted that the airflow rates inside HMXs in each system are similar (537 m³/h for S system, 463 m³/h for W system and 540 m³/h for E system), therefore the outlet air temperatures are assumed to be identical and equal to outlet temperatures obtained by the optimized exchanger (with primary airflow rate equal 540 m³/h).

Table 10.4. Required supply air temperatures, outlet temperatures: HMX, required temperature drop

| | 7 a.m. | 8 a.m. | 9 a.m. | 10 a.m. | 11 a.m. | 12 a.m. | 1 p.m. | 2 p.m. | 3 p.m. | 4 p.m. | 5 p.m. | 6 p.m. | 7 p.m. | Hour |
|---|---|---|---|---|---|---|---|---|---|---|---|---|---|---|
| $t_s^S$,°C | 17.3 | 17.7 | 18.0 | 18.0 | 18.0 | 18.2 | 18.8 | 19.5 | 20.3 | 21.0 | 21.7 | 21.2 | 20.6 | Required supply air temperature: S |
| $t_s^W$,°C | 17.7 | 18.8 | 19.8 | 20.5 | 21.1 | 21.6 | 21.0 | 20.2 | 19.4 | 18.9 | 18.9 | 19.1 | 20.6 | Required supply air temperature: W |
| $t_s^E$,°C | 14.4 | 15.3 | 16.4 | 17.6 | 18.8 | 19.6 | 20.1 | 20.4 | 20.5 | 20.5 | 20.3 | 19.9 | 19.2 | Required supply air temperature: E |
| $t_{1o}$,°C | 16.2 | 16.9 | 19.5 | 20.3 | 20.9 | 21.1 | 21.4 | 21.8 | 21.8 | 21.8 | 21.8 | 20.8 | 18.8 | HMX: outlet air temperature |
| $\Delta t_{CC}^S$,°C | - | - | 1.5 | 2.3 | 2.9 | 2.9 | 2.6 | 2.3 | 1.5 | 0.8 | 0.1 | - | - | |
| $\Delta t_{CC}^W$,°C | - | - | - | - | - | - | 0.4 | 1.6 | 2.4 | 2.9 | 2.9 | 1.7 | - | Cooling coil: required temperature drop |
| $\Delta t_{CC}^E$,°C | 1.8 | 1.6 | 3.1 | 2.7 | 2.1 | 1.5 | 1.3 | 1.4 | 1.3 | 1.3 | 1.5 | 0.9 | - | |
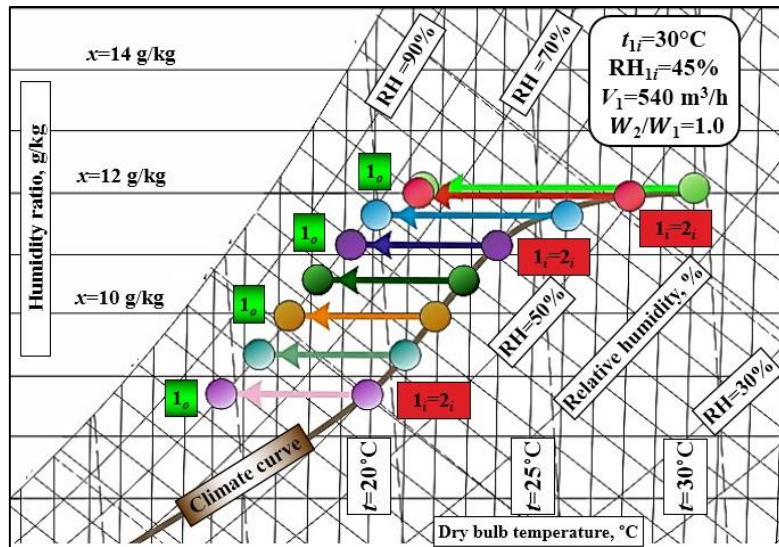


Fig. 10.2. Outlet air temperatures obtained by the HMX in Wroclaw climate.

With the known required temperature drop on the cooling coil and the airflow rates for each system the required cooling power for the mechanical compression systems during every hour can be calculated. The comparison between the systems equipped with the M-Cycle HMX and the traditional system with the rotary heat exchanger are presented in Figure 10.3. It can be seen that HMX generates significantly higher energy savings in compare to the rotary exchanger and, during some part of the day depending on the room exposition, it can operate as the only cooling source (Fig. 10.3(a),(c) and (e)). It can be seen that in case of the "south room" HMX provides cooling energy alone between 7 and 8 a.m. and between 5 and 7 p.m., during rest of the day it covers from 62 to 81% of the total required cooling power (Fig. 10.3(a)). In case of the room with western exposition HMX covers 80% of the daily cooling loads at in can operate as the main cooling source for 7 hours during the 13 hours operation time (Fig. 10.3(b)). In case of the "east room" HMX operates with the cooling coil during most of the day (except 7 p.m.) and it covers from 59 to 79% of the required cooling power. In the traditional system, rotary heat exchanger can cover up to 29% of the required cooling power for the "south room", up to 28% for the "west room" and up to 25% for the "east room".
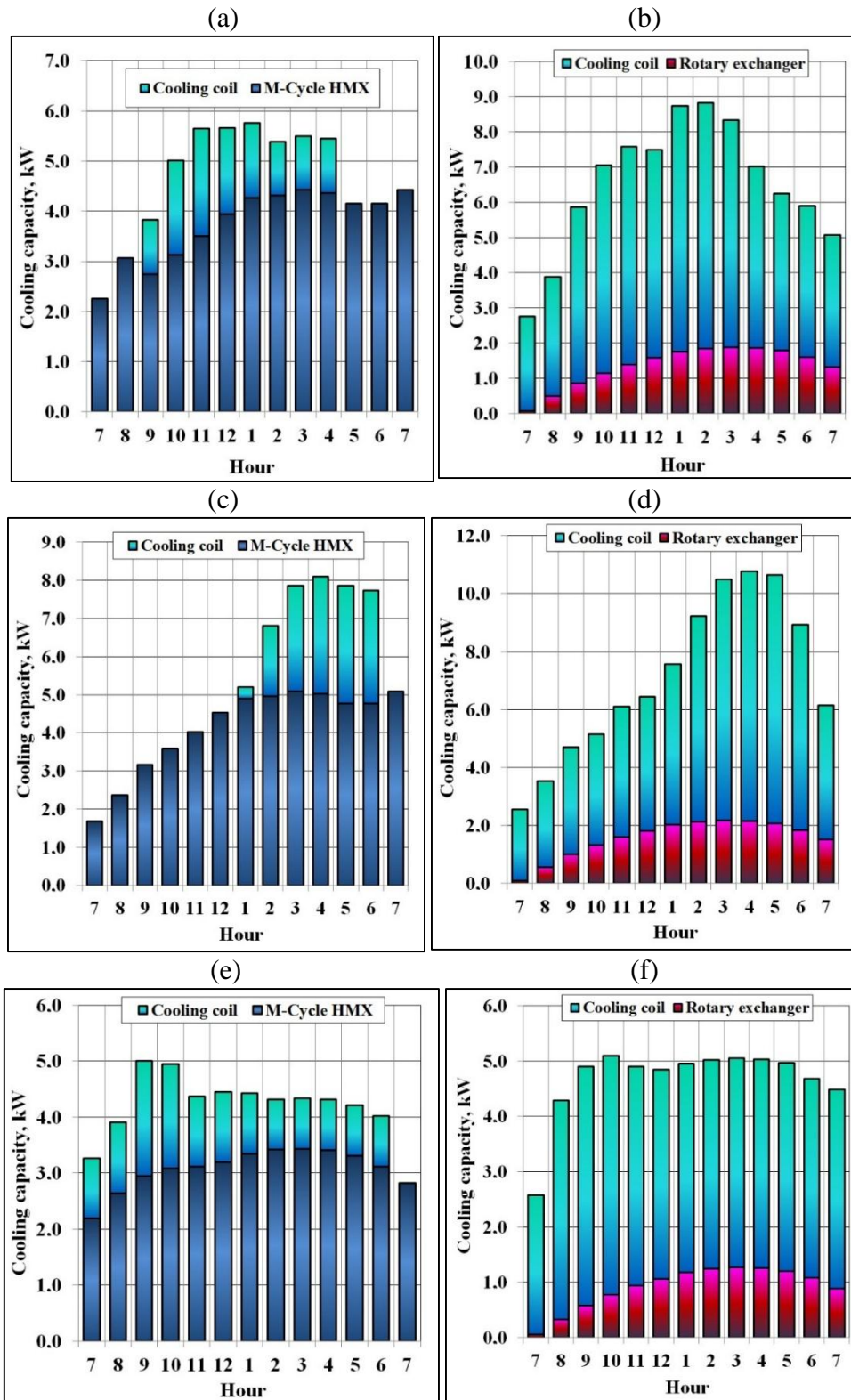
Fig. 10.3. Comparison between AC system with the M-Cycle HMX and traditional AC system. (a) Coverage of the required cooling capacities for "south room": M-Cycle system. (b) Coverage of the required cooling capacities for "south room": traditional system. (c) Coverage of the required cooling capacities for "west room": M-Cycle system. (d) Coverage of the required cooling capacities for "west room": traditional system. (e) Coverage of the required cooling capacities for "east room": M-Cycle system. (f) Coverage of the required cooling capacities for "east room": traditional system.

Analysis of Figure 10.3 brings another important observation: the summary cooling capacity of M-Cycle and traditional systems are different. The total cooling power obtained by the traditional system is always higher than of the system with the HMX. This is caused by the fact that, in order to provide appropriate air temperature, the cooling coil additionally dehumidifies the airflow (water vapor condenses on the cooler surface). Due to the fact that in the traditional system the cooling coil has to cool the airflow by a higher temperature difference, the condensation is proportionally higher in compare to the M-Cycle system: the required enthalpy difference for the cooling coil is up to six times higher (Fig. 10.4). It can be seen that application of the M-Cycle to the air conditioning systems allows not only for energy savings connected with sensible cooling of the airflow, but also by preventing from too high dehumidification of the airflow. In many cases the users of the air conditioning systems feel discomfort due to the too dry conditions in the apartments [15]. However, too low dehumidification of the airflow can lead to the discomfort as well. To analyze this aspect it is necessary to calculate the humidity loads in the conditioned spaces. The example calculation is performed for the southern room at the moment of highest humidity loads (i.e. highest indoor temperature equal 25°C). The occupation of the room include five people performing the sedentary office work with corresponding cooling loads equal $ML=30.5 \cdot 10^{-6}$ kg/s per person [147].

For five people the latent cooling loads can be calculated with the following equation:

$$Q_L^H = q^o \cdot n \cdot ML = 2500 \cdot 5 \cdot 30.5 \cdot 10^{-6} = 0.38 \text{ kW} \qquad (10.2)$$

The room process vector coefficient can be calculated from the equation (10.3)

$$\xi = (Q_L^H + Q_{Tot})/(n \cdot ML) = (2.52+0.38)/(5 \cdot 30.5 \cdot 10^{-6}) \approx 19,000 \text{ kJ/kg} \qquad (10.3)$$

Using the above-established data the psychrometric representation of the processes inside the room was prepared and presented in Figure 10.4. It can be seen that evaporative air cooler allows providing comfortable indoor environment ($t_R=25$°C, $RH_R=58\%$), however, under higher moisture loads there is a possibility that conditioned space might be too humid (Fig. 10.4(a)). Analogous analysis was performed for other rooms and in every case evaporative air cooler provided indoor parameters in range of thermal comfort zone, but in all analyzed cases the moisture loads are identical. Traditional air conditioning system allows keeping more dry conditions inside the room ($RH_R=53\%$), however, it is connected with much higher cooling capacity used to cool and dehumidify the airflow.

The above-mentioned problem can be solved with a simple control system algorithm. The most simple solution is to keep colder conditions in the conditioned spaces: for room temperature equal 25°C the highest acceptable indoor relative humidity is 60%, whereas for the room temperature equal 24°C it is about 70% [147], which can be easily provided by the evaporative systems even under relatively high moisture loads. Additionally, the control system can be equipped with the moisture sensor: if the humidity inside the conditioned spaces is too high, the cooling coil uses more power to cool and dehumidify the airflow. In all cases the M-Cycle system can provide comfortable conditions and generate high energy savings in compare to the

traditional system. It should be mentioned that nowadays in Europe the air handling units are often used to deliver only the necessary amount of fresh outdoor air to the occupants, whereas the indoor conditions are provided by the individual devices, such as fan coil units. In this case, the cooling system inside AHU is responsible only for cooling the outdoor air to the acceptable level, whereas the individual devices cover the cooling and moisture loads. Cross-flow M-Cycle HMX is an ideal solution for such systems, because it cools the airflow to the acceptable level at the minimal cost. In this type of AHUs evaporative air cooler can be used as the only cooling source to generate maximal energy savings.
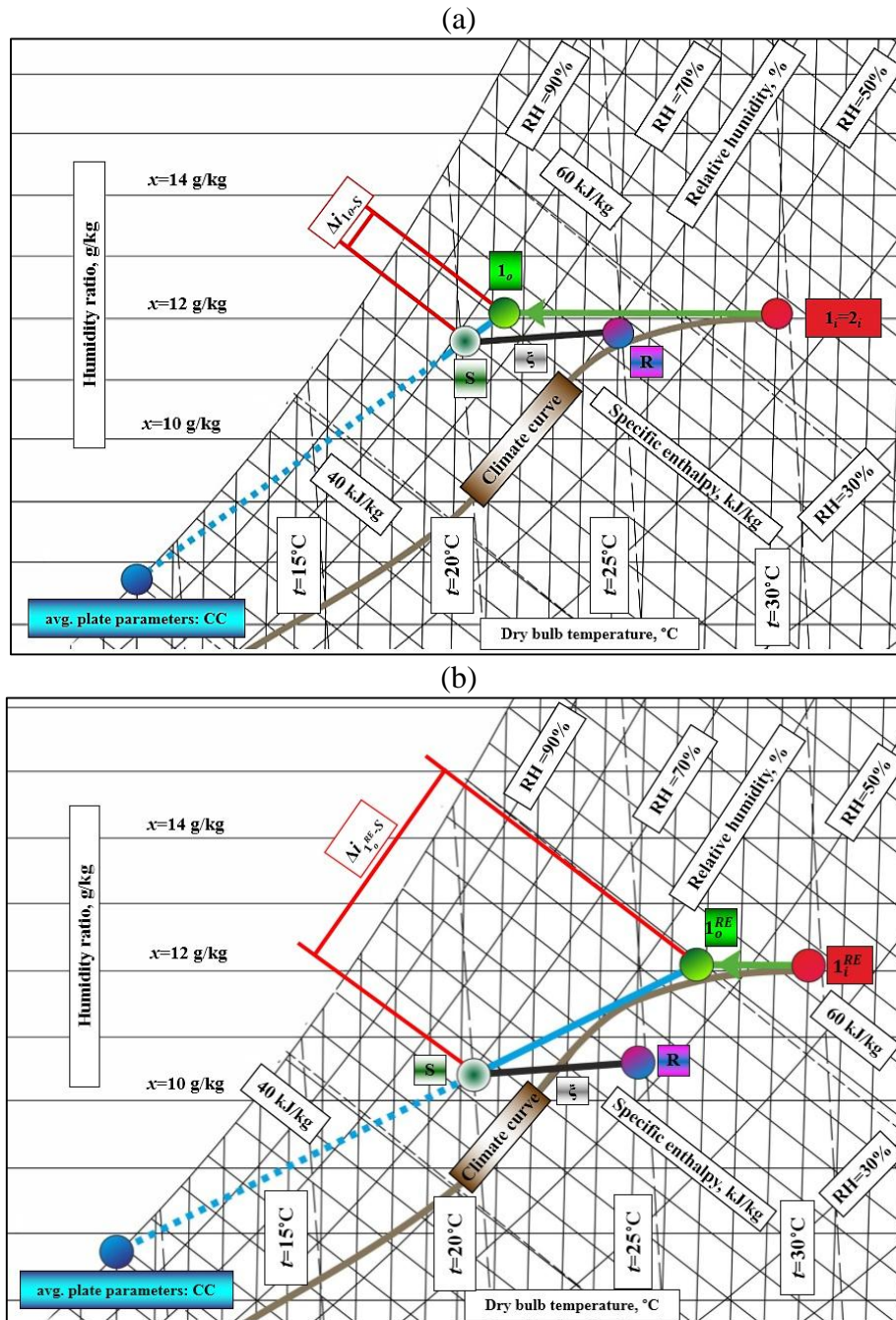


Fig. 10.4. Comparison between AC system with the M-Cycle HMX and traditional AC system on psychrometric chart. (a) "South room": M-Cycle system. (b) "South room": traditional system.

### 10.1.2. Displacement ventilation

One of the most popular solutions where air handling units are used to provide both fresh air and comfortable conditions are displacement systems, where air is delivered directly to the human occupation zone [147]. This type of ventilation is considered to be more healthy, due to the fact that in such systems air becomes thermally stratified, i.e., cool and fresh air is concentrated in the occupied zone, while warm, stale air is concentrated above, where it is exhausted [147]. In this Section the previously mentioned rooms with identical cooling loads and wall exposition are equipped with the displacement ventilation.

Table 10.5. Cooling loads for the room with wall on the west side

| | 7 a.m. | 8 a.m. | 9 a.m. | 10 a.m. | 11 a.m. | 12 a.m. | 1 p.m. | 2 p.m. | 3 p.m. | 4 p.m. | 5 p.m. | 6 p.m. | 7 p.m. | Hour |
|---|---|---|---|---|---|---|---|---|---|---|---|---|---|---|
| $t_a$,ºC | 20.4 | 22.6 | 24.6 | 26.1 | 27.4 | 28.4 | 29.3 | 29.8 | 30.0 | 29.9 | 29.5 | 28.5 | 27.0 | Outdoor temperature |
| $t_R$,ºC | 20.2 | 21.3 | 22.3 | 23.1 | 23.7 | 24.0 | 24.0 | 24.0 | 24.0 | 24.0 | 24.0 | 24.0 | 23.5 | Required room temperature |
| $t_s^S$,ºC | 18.7 | 19.5 | 20.2 | 20.5 | 20.8 | 21.0 | 21.0 | 21.3 | 21.6 | 22.0 | 22.4 | 22.5 | 22.0 | Required supply air temperature: S |
| $t_s^W$,ºC | 18.9 | 20.0 | 21.0 | 21.8 | 22.4 | 22.7 | 22.2 | 21.6 | 21.2 | 21.0 | 21.1 | 21.4 | 22.1 | Required supply air temperature: W |
| $t_s^E$,ºC | 17.3 | 18.3 | 19.4 | 20.3 | 21.2 | 21.9 | 22.4 | 22.6 | 22.7 | 22.7 | 22.5 | 22.1 | 21.4 | Required supply air temperature: E |
| $t_{1o}$,ºC | 16.2 | 16.9 | 19.5 | 20.3 | 20.9 | 21.1 | 21.4 | 21.8 | 21.8 | 21.8 | 21.8 | 20.8 | 18.8 | HMX: outlet air temperature |
| $\Delta t_{CC}^S$,ºC | - | - | - | - | 0.1 | 0.1 | 0.4 | 0.5 | 0.2 | - | - | - | - | Cooling coil: required temperature drop |
| $\Delta t_{CC}^W$,ºC | - | - | - | - | - | - | - | 0.2 | 0.6 | 0.8 | 0.7 | - | - | |
| $\Delta t_{CC}^E$,ºC | - | - | 0.1 | - | - | - | - | - | - | - | - | - | - | |

In this study, in order to avoid the problem of the tolerance on higher indoor relative humidity, the human occupation zone temperature is assumed as 24°C. Due to the fact that  airflow is delivered directly to the human occupation zone, its temperature cannot be too low. For the purpose of this analysis it is assumed that during the maximal cooling loads supply air temperature is 3°C. The assumed thermal gradient between the human occupation zone and the exhaust air during the maximal cooling loads is equal 3°C as well. Both temperature difference between supply air temperature and the human occupation zone and thermal gradient decrease in proportion to the temporary cooling loads to the maximal cooling loads. The airflows delivered to the rooms are identical to the airflows established in previous section due to the fact that temperature difference between supply and exhaust air during maximal cooling loads is still 6°C. The required supply air temperatures, along with the airflow temperatures provided by the M-Cycle HMX and the required temperature drop on cooling coil are presented in Table 10.5, the required cooling capacities of the AC systems are presented in Figure 10.5.

It can be seen that in case of the displacement system the M-Cycle air conditioner covers almost 100% of the daily cooling demand for all the rooms: temperature drops on the cooling coil are so low that they can be omitted. This is caused by the favorable requirements for the supply air temperature, which has to be higher in compare to the mixing ventilation to provide comfort in the human occupation zone. Traditional AC system has additional disadvantage in compare to

the M-Cycle system: it is sensible on the thermal gradient inside the conditioned spaces. When cooling loads in the rooms with displacement ventilation are high, the exhaust air temperature is much higher than temperature of the human occupation zone. This has a negative impact on the heat recovery process: in many cases the rotary heat exchanger has to be switched off. The negative impact on the thermal gradient is also visible in analyzed case: the heat recovery covered only 14, 10 and 15% of the daily cooling demand for south, west and east rooms respectively, whereas in the mixing ventilation system it was 21, 22 and 25%. It can be observed from the psychrometric chart (Fig. 10.6) that M-Cycle system is also able to provide comfortable conditions to the occupants under highest humidity loads.
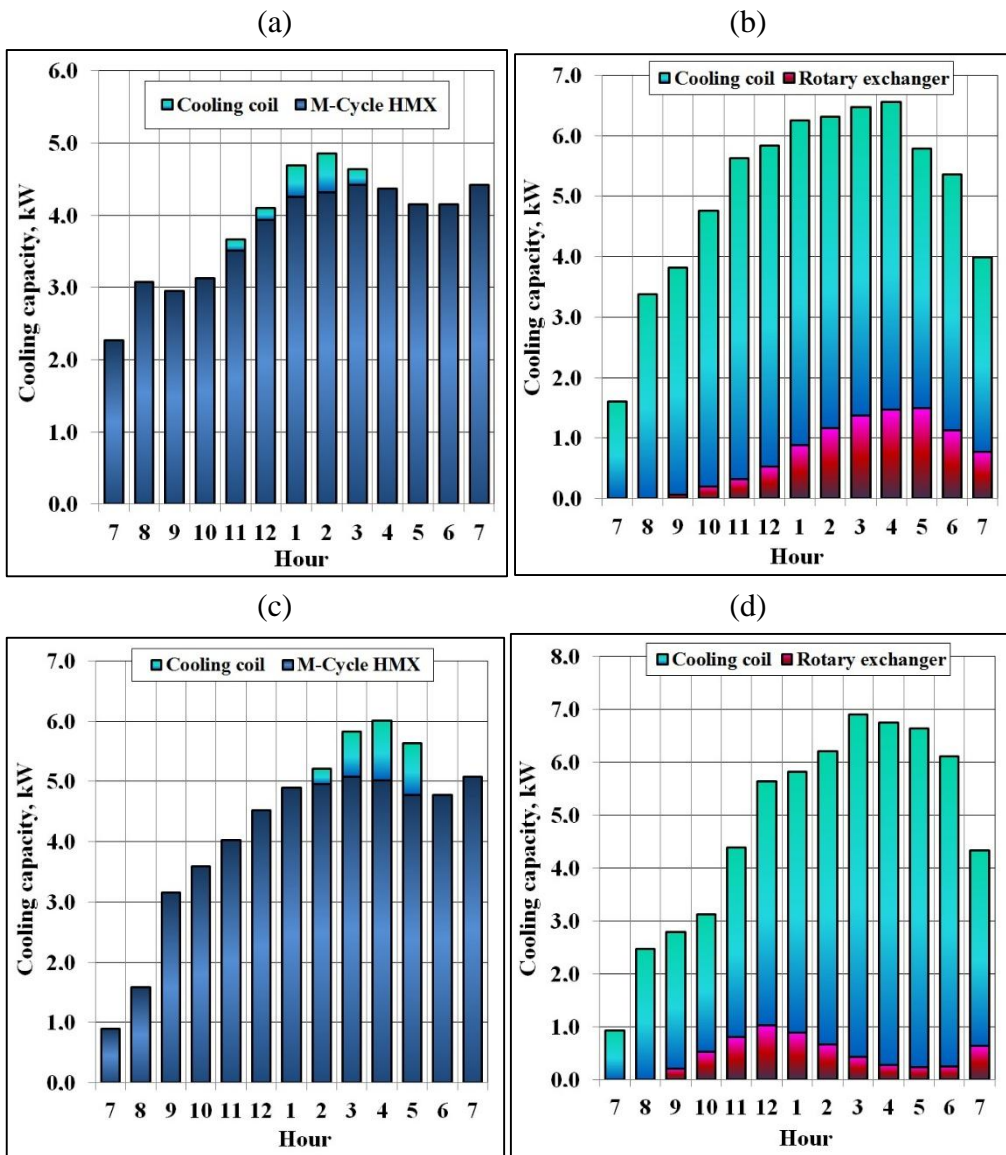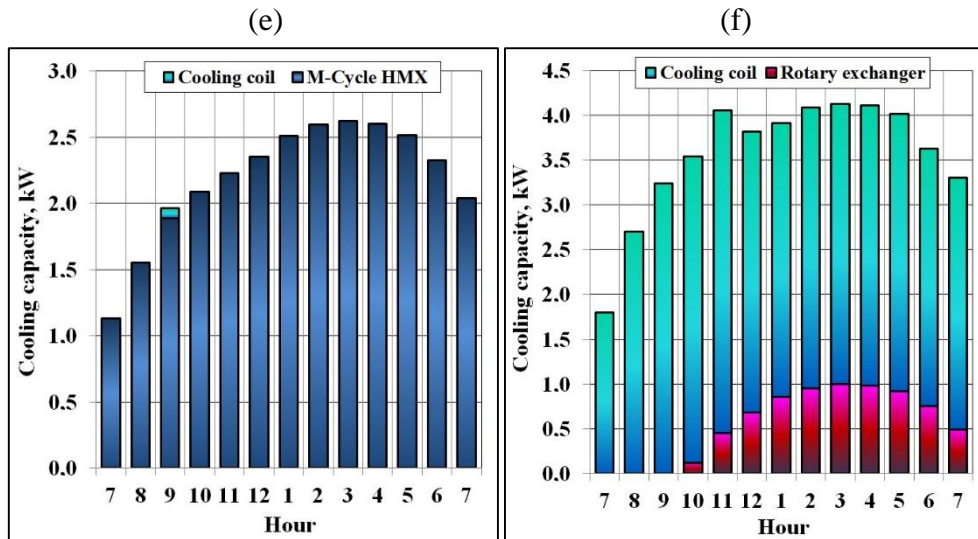
(a)           (b)

(c)           (d)

(e)              (f)



Fig. 10.5. Comparison between AC system with the M-Cycle HMX and traditional AC system. (a) Coverage of the required cooling capacities for "south room": M-Cycle system. (b) Coverage of the required cooling capacities for "south room": traditional system. (c) Coverage of the required cooling capacities for "west room": M-Cycle system. (d) Coverage of the required cooling capacities for "west room": traditional system. (e) Coverage of the required cooling capacities for "east room": M-Cycle system. (f) Coverage of the required cooling capacities for "east room": traditional system.

The results show that system equipped with the M-Cycle heat and mass exchanger is perfectly suitable for the displacement system and it is able to save high amount of energy in compare to the traditional air conditioning system. The cooling coil can be completely eliminated from the AHU equipped with the HMXs or it can be kept as a backup cooling source, which can be switched on when ambient air becomes to humid (e.g. during stormy day).
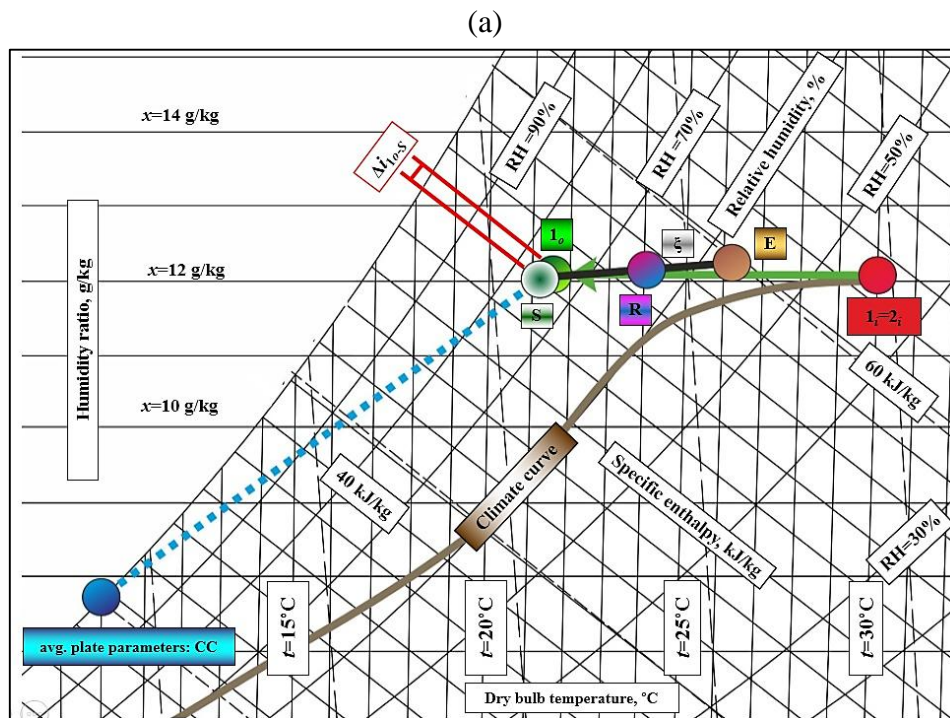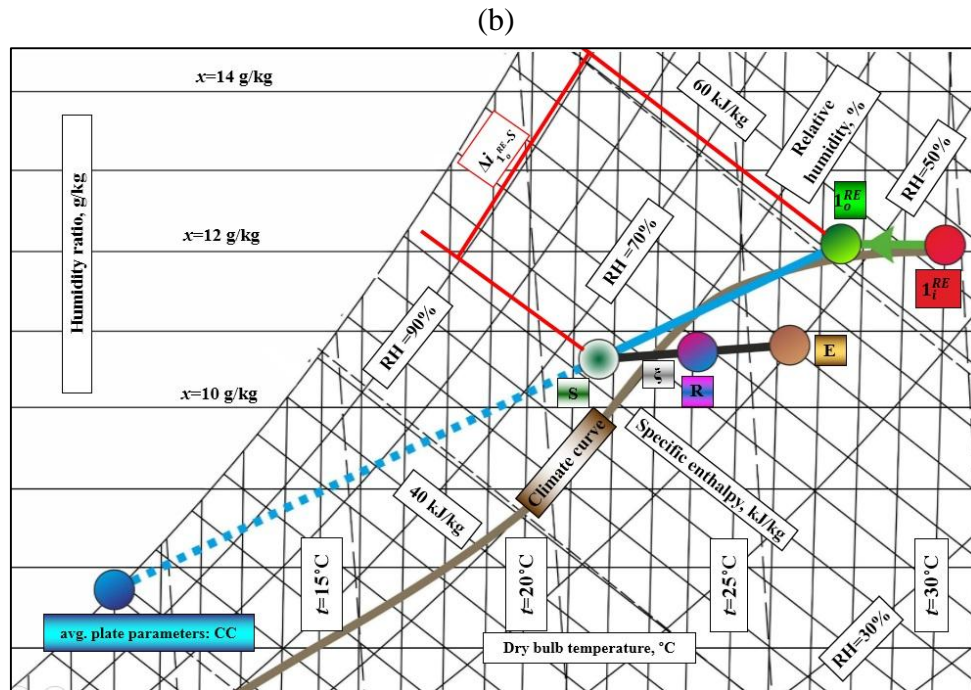
(a)

(b)



Fig. 10.6. Comparison between AC system with the M-Cycle HMX and traditional AC system on psychrometric chart. (a) "South room": M-Cycle system. (b) "South room": traditional system.

### 10.1.3. Financial benefits following from application of the M-Cycle HMX to the air conditioning systems

In this Section the daily operation costs of the M-Cycle and traditional AC systems are compared for the same previously-analyzed rooms with mixing and displacement ventilation. The purpose of this analysis is to show the level of financial benefits which can be achieved by application of the M-Cycle HMX to the air conditioning systems in Poland. Due to the fact that air handling units in Europe are not equipped with such cooler yet, the comparison of return of investment costs is impossible at the moment. However, on the basis of the information available from other regions of the world [112], [148], it can be assumed that investment costs for the M-Cycle air coolers are low (those air coolers are made of the composite materials which are cheap in compare to other materials used for the heat exchangers in AC units), therefore the difference in price between the typical and the M-Cycle systems should be minimal.

The operation costs in this comparison include:

- For the M-Cycle system:
  - Cost of using the additional R410a cooling coil during peak hours,
  - Cost of water consumption,
  - Cost of additional fan energy to pass the air through the M-Cycle air cooler (fan efficiency is assumed as equal to 0.7).
- For the traditional system:
  - Cost of using the R410a cooling coil.

Assumed costs of energy are listed below [31], [32], [149]:

- Cost of 1 hour of cooling with system based on R410a refrigerant is equal to 0.41 zł
- Cost of 1 $m^3$ of water is equal 3.2 zł

- Cost of 1 kWh of electrical energy is equal 0.60 zł

The results for the mixing ventilation are presented in Figure 10.7(a), the results for the displacement ventilation are presented in Figure 10.7(b). It can be seen that daily operation costs for the M-Cycle system are significantly lower in compare to the traditional solution: up to 4.6 times in mixing ventilation ("west" room) and up to 23 times lower in the displacement ventilation ("east" room). This is caused by the fact that operational costs of the evaporative air cooler are very low: the required fan energy for the optimized exchanger is about 35 W, the maximal daily water consumption was 140 dm$^3$ ("west" room), the minimal was equal 83 dm$^3$ ("east" room). The cost of this energy is incomparably lower than costs of operation of the mechanical compression refrigerant systems (most operation costs of the M-Cycle systems are caused by using cooling coil during peak hours). For the above-mentioned reasons, the M-Cycle systems are much cheaper in operation and application of such systems in Polish climate conditions is highly justified.
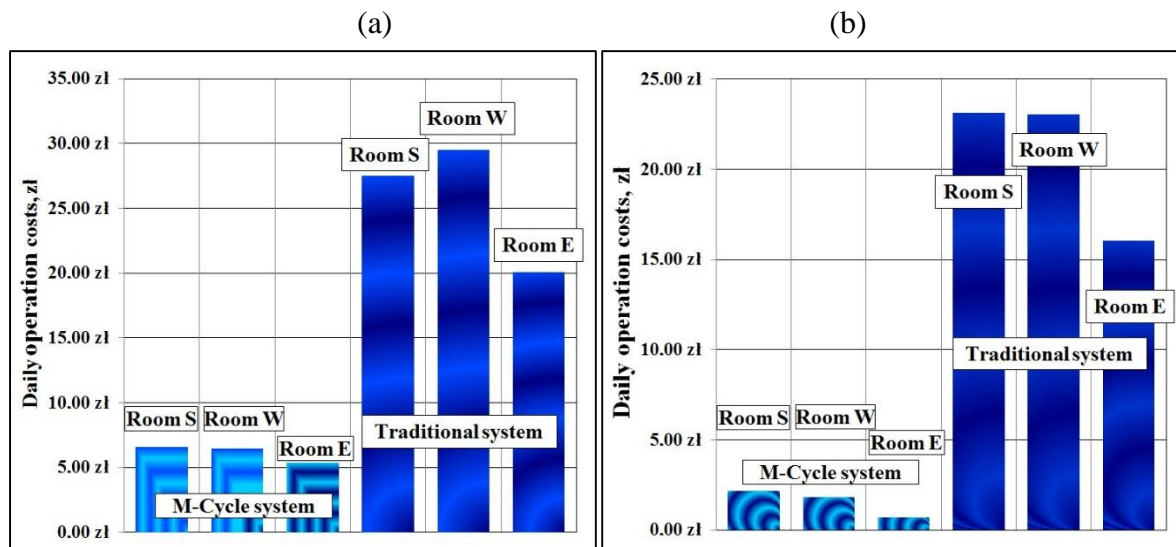
(a)                                          (b)



Fig. 10.7. Comparison between AC system with the M-Cycle HMX and traditional AC system: daily operation costs. (a) Mixing ventilation. (b) Displacement ventilation.

## 10.2.  Analysis of operation of the M-Cycle HMX in SDEC systems

Desiccant air conditioning systems are one of the promising ways which can improve the performance of traditional air conditioning systems [88], [150]. Such solutions are based on the combination of different heat exchangers. The typical idea (Fig. 10.8) includes a desiccant wheel for dehumidification of the airflow, a rotary heat exchanger for initial cooling of the dehumidified air stream and a spraying chamber, which cools and humidifies the airflow with evaporative cooling. The initial dehumidification allows for effective evaporative cooling which can provide comfort for typical indoor conditions. The exhaust air is also delivered to the spraying chamber, where it is cooled and humidified in order to increase the effectiveness of heat recovery process in the rotary exchanger. After passing the exchanger, the air is heated with solar panels or a typical air heater (or both) and it is used for the regeneration of the

desiccant wheel. The most effective desiccant systems use only solar energy to provide cooling-desiccant wheel is regenerated only with air heated in the solar panels (such systems are called Solar-Desiccant-Air Conditioning or SDEC: Fig. 10.8).
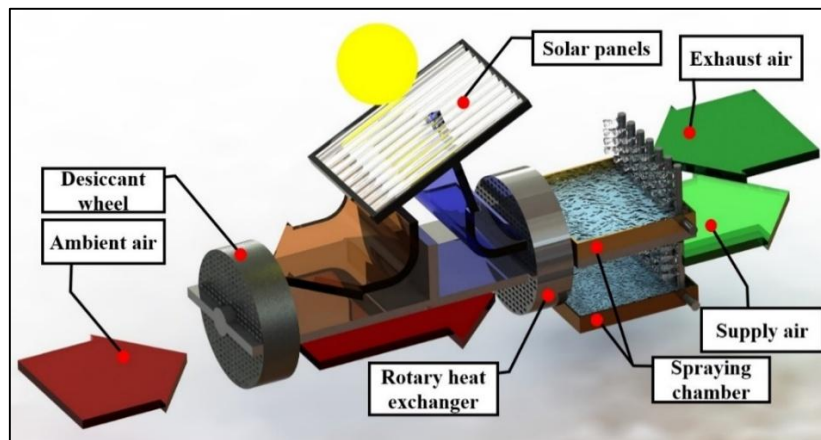


Fig.10.8. Scheme of the typical SDEC system.

The main disadvantages of SDEC systems are connected with direct evaporative air cooling: this system adds moisture to the air, which may result in an uncomfortable indoor conditions. Also the thermal effectiveness of the direct evaporative air cooler is limited by the wet bulb temperature of incoming air (in practice it is impossible to reach the wet bulb temperature with direct cooling). The additional disadvantage is the size of the system: the rotary heat exchanger and spraying chambers require a lot of volume in the system. For the above mentioned reasons, researchers are trying to apply new methods in desiccant air conditioning systems in order to increase their efficiency.

As it was previously mentioned, the best solution is to regenerate the dehumidifier using the heat from the solar panels, but they can only generate such high temperatures in very hot climates. Therefore, traditional desiccant systems are often limited to hot and humid climates (in hot and dry climates dehumidification of the airflow is redundant). In other climatic conditions, they can effectively operate when there is a source of the waste heat which can be used for heating of the airflow. In order to make such systems suitable for moderate climate conditions (such as central Europe and significant part of the United States), a new component needs to be added to the system which allows for effective operation under lower regeneration temperatures. One of such components is the cross-flow Maisotsenko cycle heat and mass exchanger (HMX) instead of the spray chambers and the rotary heat exchanger (Fig. 10.9(a)). This idea has not yet investigated numerically in the existing studies- the published data concentrated on the regenerative counter-flow unit in the desiccant systems [2]. A regenerative HMX allows obtaining low outlet temperatures, but due to the unfavorable airflow scheme it obtains lower cooling capacity than the cross-flow unit (see Section 7). This Section focuses on the numerical analysis of the desiccant system regenerated with air with lower temperature levels with the optimized cross-flow Maisotsenko cycle heat exchanger.

Two main elements of the desiccant system are numerically studied: the cross-flow M-cycle HMX (Fig. 10.9(a)) and the desiccant wheel (Fig. 10.9(b)). The primary airflow is delivered to

the occupants and later, as an exhaust airflow it is sensibly heated with the heat source (Fig. 10.9(a)). Other elements of the system are analyzed with simplified methods.
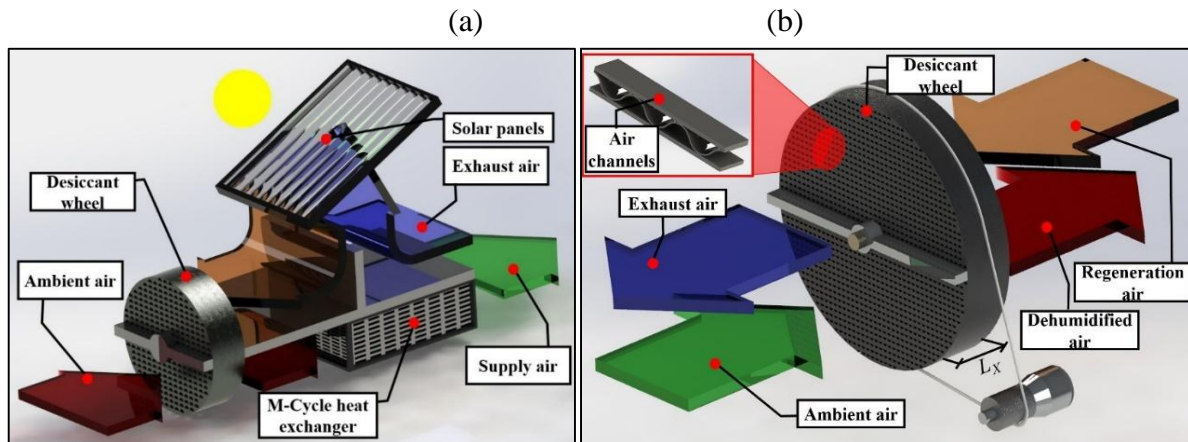
(a)                                      (b)



Fig. 10.9. Analyzed M-Cycle desiccant system. (a) The scheme of the system. (b) The scheme of the desiccant wheel.

The analysis in this Section is divided into two groups:

- General performance analysis of the cross-flow M-Cycle air cooler in SDEC systems (Section 10.2.1)
- Analysis of the different arrangements of the SDEC systems with the cross-flow M-Cycle air cooler in order to find the most effective solution from the heat transfer standpoint (Section 10.2.2)

The analyzed system is characterized by the parameters listed in Table 10.6. It is important to mention that the analysis of methods of heat production for the regeneration of the desiccant wheel is not analyzed in this section. However, the whole analysis will be presented for low values of regeneration air temperature (55-60°C), which can be produced by solar panels under typical summer conditions in moderate climate (such as central Europe), or any other low temperature heat source. The mathematical model of the desiccant wheel along with its validation is presented in **Appendix J**.

Table 10.6 Properties of analyzed cooling system components

| *Desiccant wheel* | |
|---|---|
| Specific heat capacity (silica gel), J/(kg K) | 750 |
| Channel type | Sinusoidal |
| Channel height, mm | 1.24 |
| Channel width, mm | 2.21 |
| Wall thickness, mm | 0.1 |
| Channel length, m | 0.1 |
| Rotor diameter, m | 0.45 |
| Percent of rotor surface used for regeneration airflow, % | 25 |
| Rotational speed, turns per hour | 8 |
| *Rotary heat exchanger* | |
| Constant temperature effectiveness, - | 0.75 |
| *Direct evaporative air coolers in traditional system* | |
| Constant wet bulb effectiveness, - | 0.80 |

## 10.2.1. Performance analysis of the cross-flow M-Cycle HMX in SDEC systems

The scheme of the system along with initial conditions is presented in Figure 10.10. The ambient air enters the desiccant wheel, where it is dehumidified. After that, the air is delivered to the HMX, where it is separated into the two air streams (the primary and working airflows). After passing the HMX, the primary airflow is delivered to the conditioned space, while the working airflow ($2_o$) is discharged to the atmosphere (Figure 10.10).
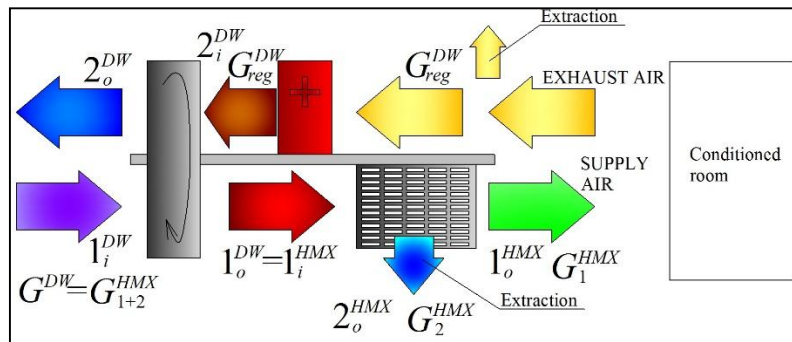


Fig. 10.10. General scheme of the system with initial conditions.

There are several additional assumptions for the system analyzed in this Section: the temperature and humidity ratio difference between the supply and exhaust air in conditioned room is 7°C and 1 g/kg respectively. The assumed temperature increase (caused by the compensation of the heat loads) between supply and indoor air is 6°C, also a 1°C temperature increase between indoor air and the exhaust air is assumed. Therefore, the "*safe*" supply air temperature, which allows keeping the indoor air temperature within thermal comfort conditions at about 25…25.5°C is 19…19.5°C.

*Comparison between traditional SDEC system and the solution with M-Cycle HMX*

The general comparison between the M-Cycle and traditional systems is presented on the psychrometric chart shown in Figure 10.11. It can be seen that there are significant differences in the air treatment in both analyzed systems. The supply air temperatures are similar (18.9°C for the system with M-Cycle and 19.1°C for the traditional system: Fig. 10.11(a) and (b)). The main advantage of the Maisotsenko cycle heat and mass exchanger is that it does not add moisture to the supply airflow, which gives two benefits: the air in the conditioned room (marked R in Fig. 10.11 (a) and (b)) lies in the thermal comfort zone, whereas in the case of the traditional system it is too humid (indoor air RH 50 to 65% in favor of the M-Cycle system). It should also be noted that the exhaust air, which is later used for regeneration of the desiccant matrix, is substantially dryer in the case of the novel system (humidity ratio 10.3 to 15 g/kg in favor of the novel system). This allows the use of regeneration air with lower temperature in comparison with the traditional system. In case of the M-Cycle system the regeneration air temperature, required to dehumidify the ambient air by approximately 2 g/kg, is 55°C, whereas for the traditional system it is 63°C. Moreover, when using the traditional system, it is not always possible to meet indoor air comfort conditions in terms of relative humidity. In order

to provide thermal comfort conditions it is necessary to increase regeneration air temperature (about 70°C), which significantly limits its application to only hot regions of the world. Such temperatures can be easily obtained when the conditioned object has a source of the waste heat with relatively high temperature, but in the case of only solar panels using it is very difficult to reach such temperature level of regeneration air for typical middle Europe climatic conditions [33].

Another important advantage of the M-Cycle unit is that it can provide a low supply air temperature using only one device, instead of three (one HMX instead of two direct evaporative air coolers and a rotary heat exchanger). Moreover, the heat and mass exchanger consumes a smaller amount of water, in many cases less than half that of the direct evaporative air cooler. The main disadvantage of the Maisotsenko cycle exchanger is that it requires a part of the dehumidified air to be delivered to the wet working channels and later extracted from the system. Therefore, in order to provide the same amount of air as the traditional system it would require a larger desiccant wheel, which might increase the cost of the system. However, the savings connected with the reduced number of the system components should overcome this cost disadvantage.

The system with the Maisotsenko cycle HMX can be also equipped with the rotary heat exchanger (Fig. 10.11 (c)). It can be seen that this configuration gives considerably lower supply and indoor air temperatures: 16.9°C and 22°C respectively (Fig. 10.11(c)). Unfortunately, this is connected with higher investment costs and the fact that an additional device brings a higher risk of potential malfunction. Moreover, such solution requires additional energy to operate the rotary exchanger. On the other hand, the ability to provide lower supply air temperature is an important advantage: in many cases the supply air temperature is critical in terms of choosing the air handling unit. Depending on the type of conditioned space and the investor requirements, this solution may be considered as an alternative to the system equipped only with the HMX. The simplified results from this system are also presented in this Section (under assumption of the constant temperature effectiveness of the rotary heat exchanger: Table 10.6) in order to show the theoretical capabilities of different systems with the cross-flow M-Cycle HMX.
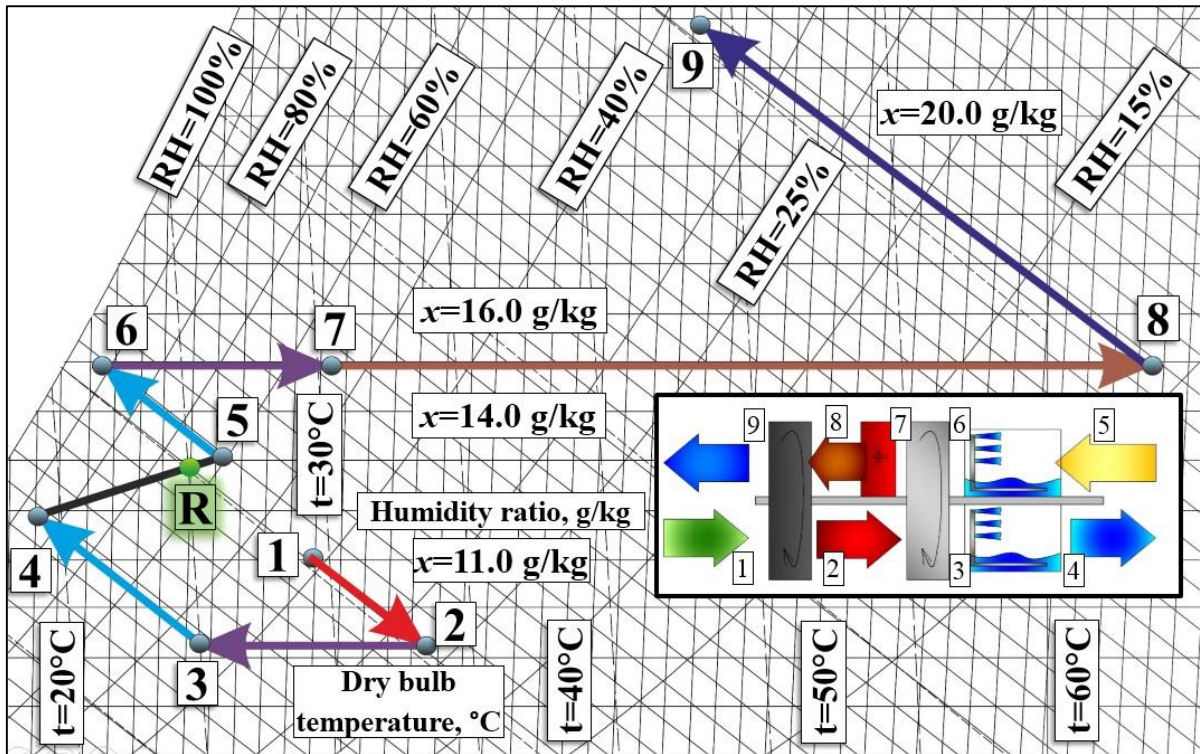
(a)



(b)
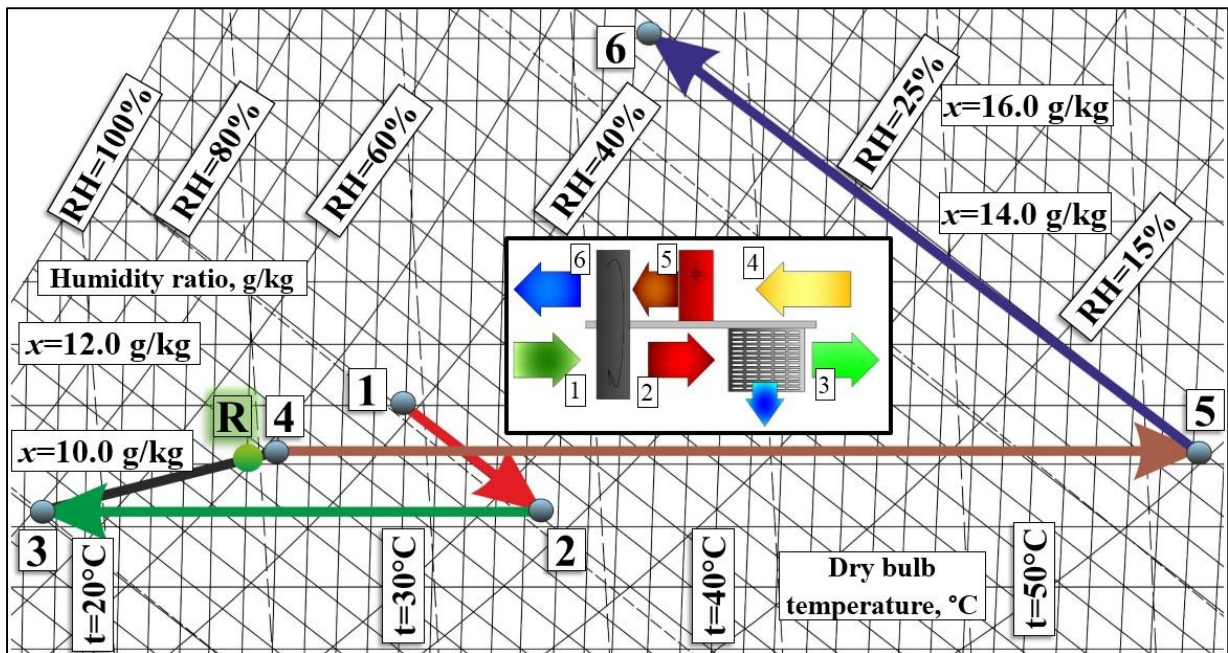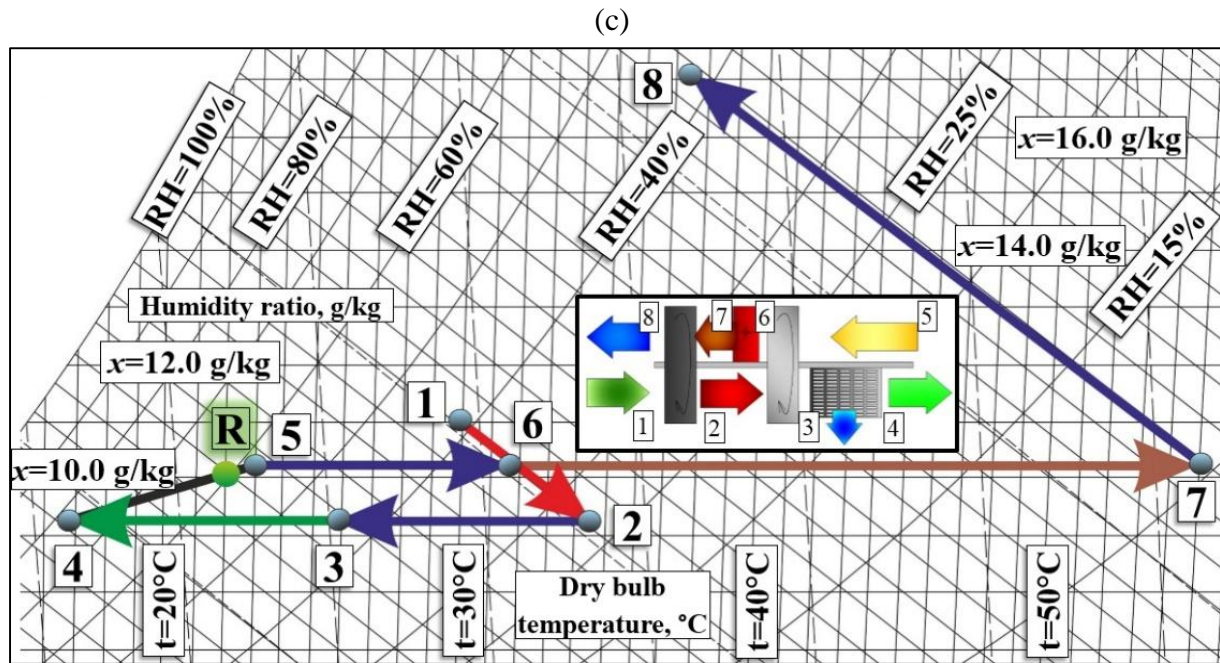
(c)



Fig. 10.11. Comparison between traditional and novel desiccant air conditioning systems. (a) Traditional system. (b) System with the M-Cycle HMX. (c) System with the M-Cycle HMX and rotary heat exchanger.

*Impact of inlet ambient air temperature on the system performance*

The impact of the inlet ambient air temperature on the performance of the two M-Cycle system is presented in Figure 10.12. The numerical simulations were performed with assumptions of constant exhaust air temperature equal to 26°C and the 1 g/kg humidity ratio increase between supply and exhaust airflow. The ambient airflow is equal 600 m$^3$/h, the regeneration airflow is equal 150 m$^3$/h.  It can be seen that increasing ambient air temperature results in higher supply air temperatures. This is caused by the fact that the dehumidification of ambient air at higher temperature is realized in desiccant matrix with lower efficiency. The moist air results in decreasing effectiveness of indirect evaporative cooling through the Maisotsenko cycle.  The system without rotary heat exchanger is more sensitive to the inlet air temperature changes: for the ambient air temperature varying from 25 to 40°C, the supply air temperature provided by this system increases by 3°C, whereas in the case of the system equipped with rotary exchanger, the change in supply air temperature is only 1.5°C. This is caused by the fact that the heat exchange in the rotary unit under summer conditions is less dependent on the humidity changes of the inlet airflow than the evaporative air cooling unit. The main disadvantage of the rotary exchanger is that it is limited by the exhaust air temperature and it cannot be used as the main cooling source. The system without a rotary exchanger requires additional heating of the regeneration airflow when the outdoor air temperatures are higher than 33°C in order to provide "safe" supply air temperature: for higher air temperatures, this system is not able to provide the supply air with a temperature equal 19.5°C or lower. The positive aspect is that when such temperatures occur, there is usually enough solar energy to provide higher regeneration air temperatures with solar panels.
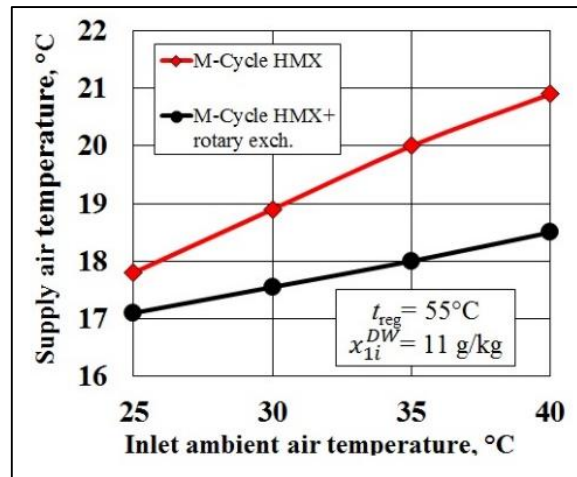
Fig. 10.12. Impact of inlet ambient air temperature on the system performance.

*Impact of inlet ambient air humidity ratio on the system performance*

The impact of the inlet ambient air humidity ratio on the performance of the analyzed system is presented in Figure 10.13. The simulations were performed under the assumption of constant exhaust air temperature equal 26°C and the 1 g/kg humidity ratio increase between supply and exhaust airflow. The ambient airflow is equal 600 m$^3$/h, the regeneration airflow is equal 150 m$^3$/h. It can be seen that the higher humidity ratio of the airflow has negative impact on the system performance, however, the impact of higher humidity ratio is not as negative as the higher inlet air temperature. This is due to the fact that air with higher humidity is dehumidified at higher efficiency in the desiccant wheel (however, the air with lower inlet humidity always achieves lower outlet humidity). Effective dehumidification partly reduces the negative impact of higher humidity ratio, so the evaporative cooling process provides lower outlet air temperatures. The system without rotary exchanger requires additional heating of the regeneration airflow to provide comfortable conditions when the incoming air has higher humidity ratio than 12 g/kg (Figure 10.13), whereas the system with the rotary exchanger doesn't require additional heating in the analyzed case.
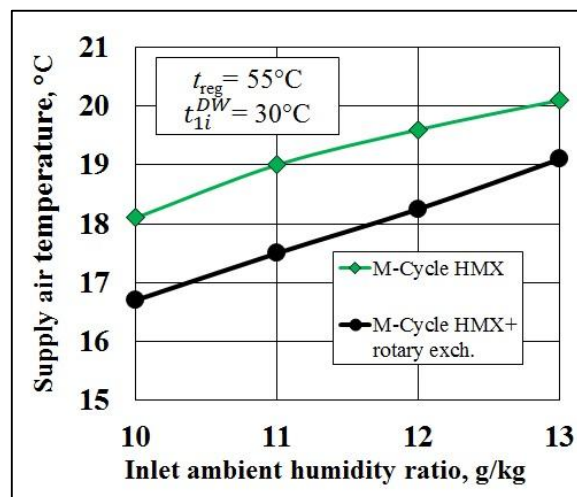


Fig. 10.13. Impact of inlet ambient air humidity ratio on the system performance.

*Impact of regeneration air temperature on the system performance*

The impact of the regeneration air temperature on the analyzed systems is presented in Figure 10.14. The simulations were performed under assumptions of constant exhaust air temperature equal 26°C and the 1 g/kg humidity ratio increase between supply and exhaust airflow. The ambient airflow is equal 600 m³/h, the regeneration airflow is equal 150 m³/h. Figure 10.14 clearly shows that higher regeneration air temperature has a positive impact on the effectiveness of M-Cycle system. Also, it can be seen that under presented conditions, even low regeneration air temperature (45°C) enables the supply air temperature to satisfy comfort conditions.

It can be also seen that the system with the rotary heat exchanger is more sensitive to the variation of regeneration air temperature. This is caused by the fact that the ambient airflow is more intensively heated, when the regeneration air temperature is higher. This results in a higher temperature difference between the outdoor and exhaust airflow, which results in more effective pre-cooling in the rotary exchanger before it enters the HMX.
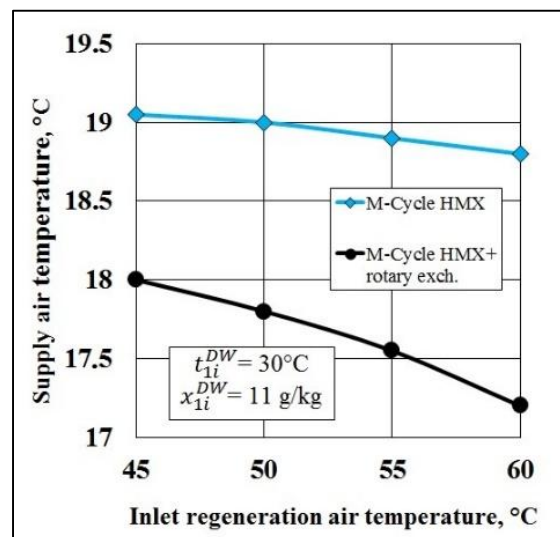


Fig. 10.14. Impact of regeneration air temperature on the system performance.

*Impact of ambient and regeneration airflow rate on the system performance*

The impact of ambient and regeneration airflow rate on the analyzed systems is shown in Figure 10.15. The simulations were performed under assumptions of constant exhaust air temperature equal to 26°C and the 1 g/kg humidity ratio increase between supply and exhaust airflow. It can be seen that the increased regeneration airflow improves the effectiveness of the system. The negative effect of the increased outdoor air stream follows from the fact that it decreases its number of heat transfer units (NTU) when the air is passing through the desiccant wheel and the HMX. However, both the systems are still able to provide satisfying supply air temperature in all of the analyzed cases. It is important to mention that increased ambient airflow results in higher cooling capacity (the drop in supply air temperature is compensated by increasing the mass airflow rate), therefore in some cases it may be reasonable to provide higher supply airflow rate at cost of its temperature.

The positive impact of increased regeneration airflow rate follows from its increased specific heat capacity, which allows removing the moisture from the desiccant wheel with higher effectiveness. However, the higher regeneration airflow requires more energy to be heated and it causes a higher pressure drop. Therefore, its value should be kept at the minimal level, which allows effective dehumidification of the ambient air. In some cases, it may be reasonable though to increase the regeneration airflow rate and heat it to the lower temperature level instead of keeping the smaller airflow, which has to be heated to the higher temperature.
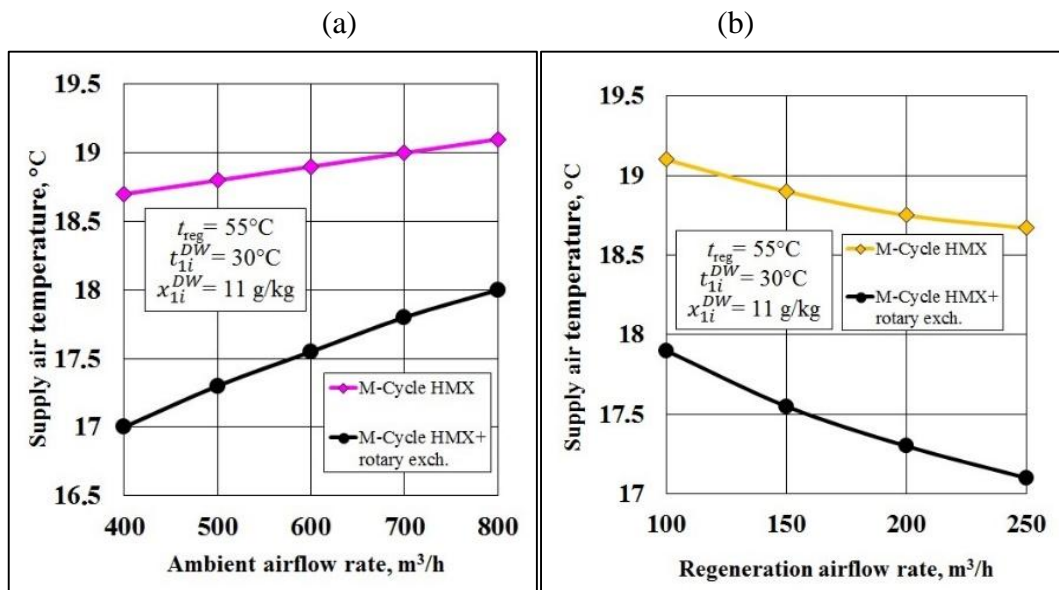


Fig. 10.15. Impact of airflow rates on the system performance. (a) Ambient airflow rate ($V_{reg}$=150 m³/h). (b) Regeneration airflow rate ($V_1$=600 m³/h).

*Impact of desiccant wheel rotational speed on the system performance*

The impact of desiccant wheel rotational speed on the performance of analyzed systems is presented in Figure 10.16. It can be observed that the increased rotational speed of the desiccant wheel may have both positive and negative impact on the efficiency of the system. When the dehumidifier turns very slowly (2-3 revolutions per hour) the effectiveness of the system is decreasing. The same effect occurs when the wheel turns very fast (15 revolutions per hour and higher). This follows from the fact that very fast rotational speed results in a high efficiency of heat transfer but the effectiveness of desiccant matrix regeneration significantly reduces. It can be seen that the optimal rotational speed for the analyzed case varies between 6 and 10 revolutions per hour.
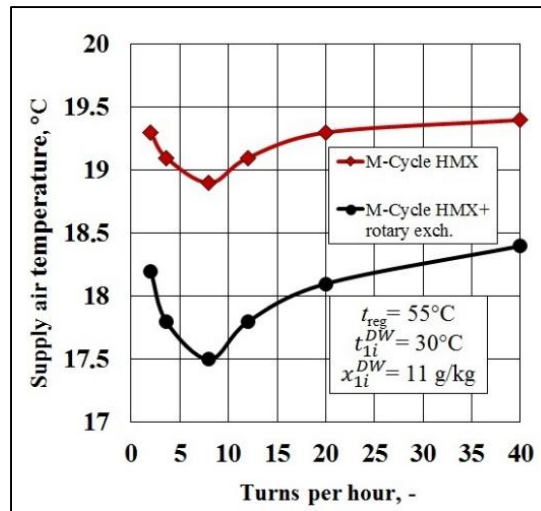
Fig. 10.16. Impact of airflow rates on the system performance.

*Impact of humidity ratio change between supply and exhaust airflow on the system performance*
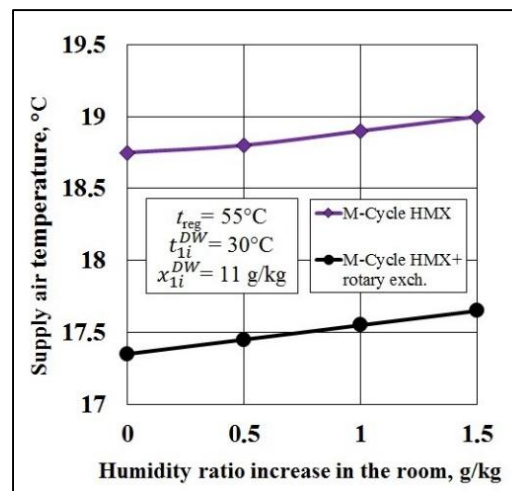


Fig. 10.17. Impact of humidity ratio change between supply and exhaust airflow on the system performance.

In the typical air conditioning applications, the larger part of the heating loads in the conditioned spaces are sensible heat loads (as it was presented in Section 10.1). However, in some cases the latent heat loads may also become significant (especially in crowded rooms). Therefore the humidity ratio of the exhaust airflow is usually different than of the supply airflow. It is important to study how much does it affect the performance of analyzed systems. The results of the numerical simulation are shown in Figure 10.17. It can be seen that increased humidity ratio of the regeneration airflow does not have a significant impact on the efficiency on the considered system. This follows from the fact that due to the use of the M-Cycle HMX, the airflow delivered to the conditioned space remains dry (the same humidity ratio as on the desiccant wheel outlet). Therefore, even after assimilation of latent heat loads in the room, the regeneration airflow is still relatively dry in compare to the air in the traditional desiccant system. This allows for satisfying regeneration of the desiccant material. For the above

mentioned reasons, the desiccant air conditioning system with the cross-flow M-Cycle HMX allows for operation on heat generated by the solar energy instead of relying on the external heat source in more world regions than the traditional solution.

### 10.2.2. Analysis of the different arrangements of the SDEC systems with the cross-flow M-Cycle air cooler

Cross-flow M-Cycle air cooler used in SDEC systems can operate in different arrangements (Fig. 10.18). It is important to analyze which solution is most effective. Three different arrangements of the M-Cycle systems are compared in this study (Fig. 10.18). First system (System 1) is the simplest solution (Fig. 10.18(a)): it contains the desiccant wheel, the M-Cycle HMX and the source of heat for the regeneration. It is the cheapest and less complicated solution, which also requires the smallest space. The second system (System 2) is equipped with additional rotary heat exchanger to pre-cool the primary air before it is delivered to the HMX and pre-heat the regeneration air before it is delivered to the source of heat (Fig. 10.18(b)). This system is more expensive and larger in scale, but it achieves lower temperatures with the pre-cooled air. The main problem with the above-mentioned systems is that half of the airflow delivered to the desiccant wheel is going to the wet channels of the exchanger. To overcome this disadvantage, the third system might be considered (System 3). This solution is most complicated from the analyzed three (Fig. 10.18(c)): it requires additional fan, which delivers the ambient airflow to the dry channels of the HMX without pre-treatment in the desiccant wheel. In moderate climate conditions the ambient air does not require dehumidification before it is delivered to the occupants, but without dehumidification the evaporative cooling process occurs less effectively. In System 3 only the working airflow, which is delivered to the initial part of the exchanger is dehumidified, while the primary airflow is delivered to the dry channels of the HMX directly from the outside with additional fan (in practice this would require a simple combination of the desiccant wheel and Coolerado ERV unit [151]). The third System is complicated and requires additional fan, which increases the costs, but it has important advantages: it requires smaller desiccant wheel to deliver the same amount of airflow to the occupants. The total price of the system, due to the smaller components may be similar to the System 2. The three above-mentioned systems will be put in the comparative analysis in order to determine their thermal efficiency under variable operational conditions. Due to the fact that air handling units adapted to operate in SDEC systems are not sold in Europe, the investment and operational costs are not analyzed in this section: the systems are only compared in terms of the obtained supply air temperature and cooling capacity.

(a)



(b)

(c)
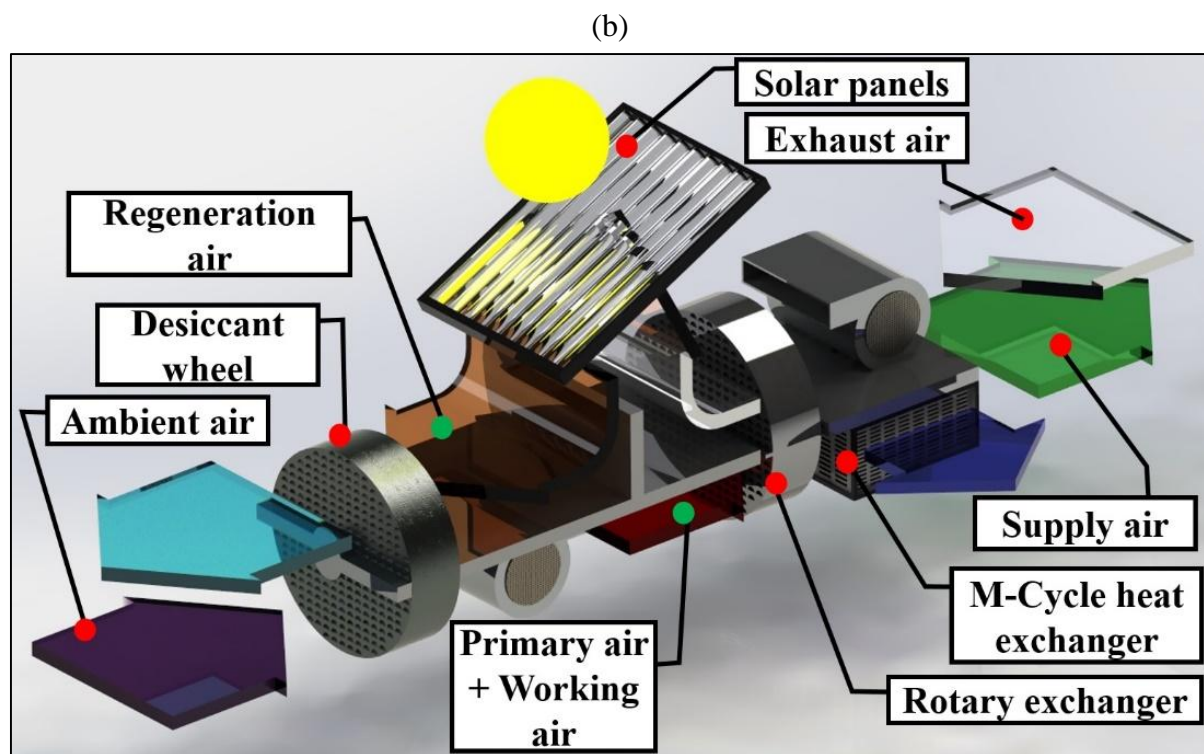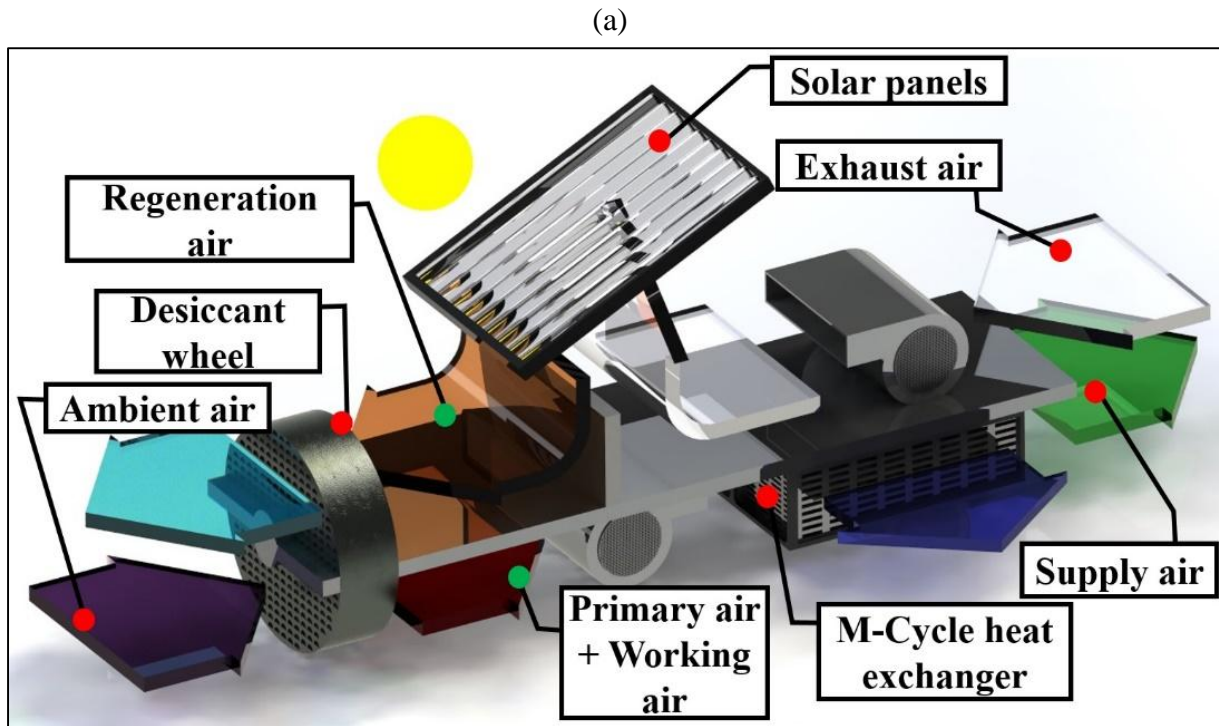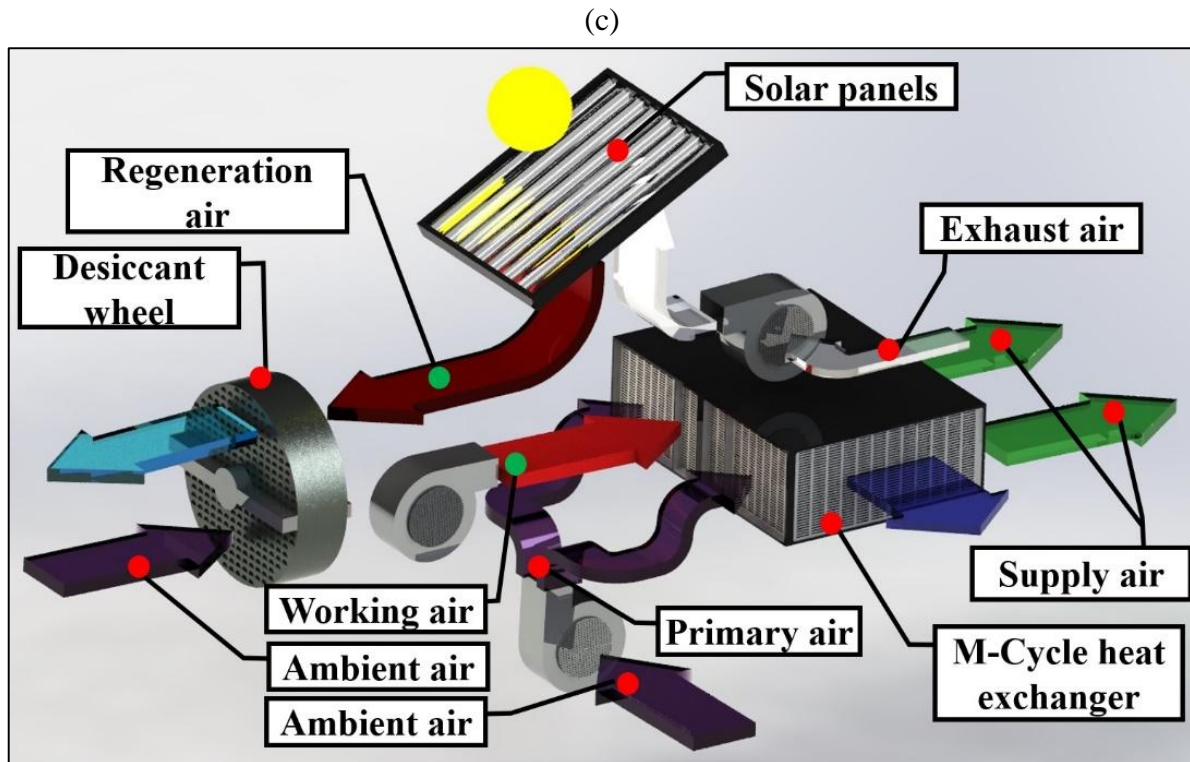


Fig. 10.18. Analyzed systems. (a) System 1. (b) System 2. (c) System 3.

The schematic of the systems along with the initial conditions is presented in Figure 10.19(a)-(c). Ambient air enters the desiccant wheel, where it is dehumidified. Depending on the system, after passing the dehumidifier, the airflow is to the product and initial part of the HMX (Fig. 10.19(a)- System 1), to the rotary exchanger and then to the dry and wet channels of the HMX (Fig. 10.19(b)- System 2), or it is delivered to the initial part of the HMX, while the ambient air is delivered to the product part (Fig. 10.19(c)- System 3). After passing the HMX, the primary airflow is delivered to the conditioned space, it assimilates the heating loads and it is exhausted, while the working airflow ($2_o$) is discharged to the atmosphere (Figure 10.19(a)-(c)). The cooling capacity of the systems is determined from the following equation:

$$Q_1 = G_1^{HMX} \cdot c_p \cdot (t_a - t_{1o}^{HMX}) \tag{10.4}$$

where:

$t_a$ – ambient air temperature, °C

The parameters of the desiccant wheel and rotary heat exchanger are presented in Table 10.6.
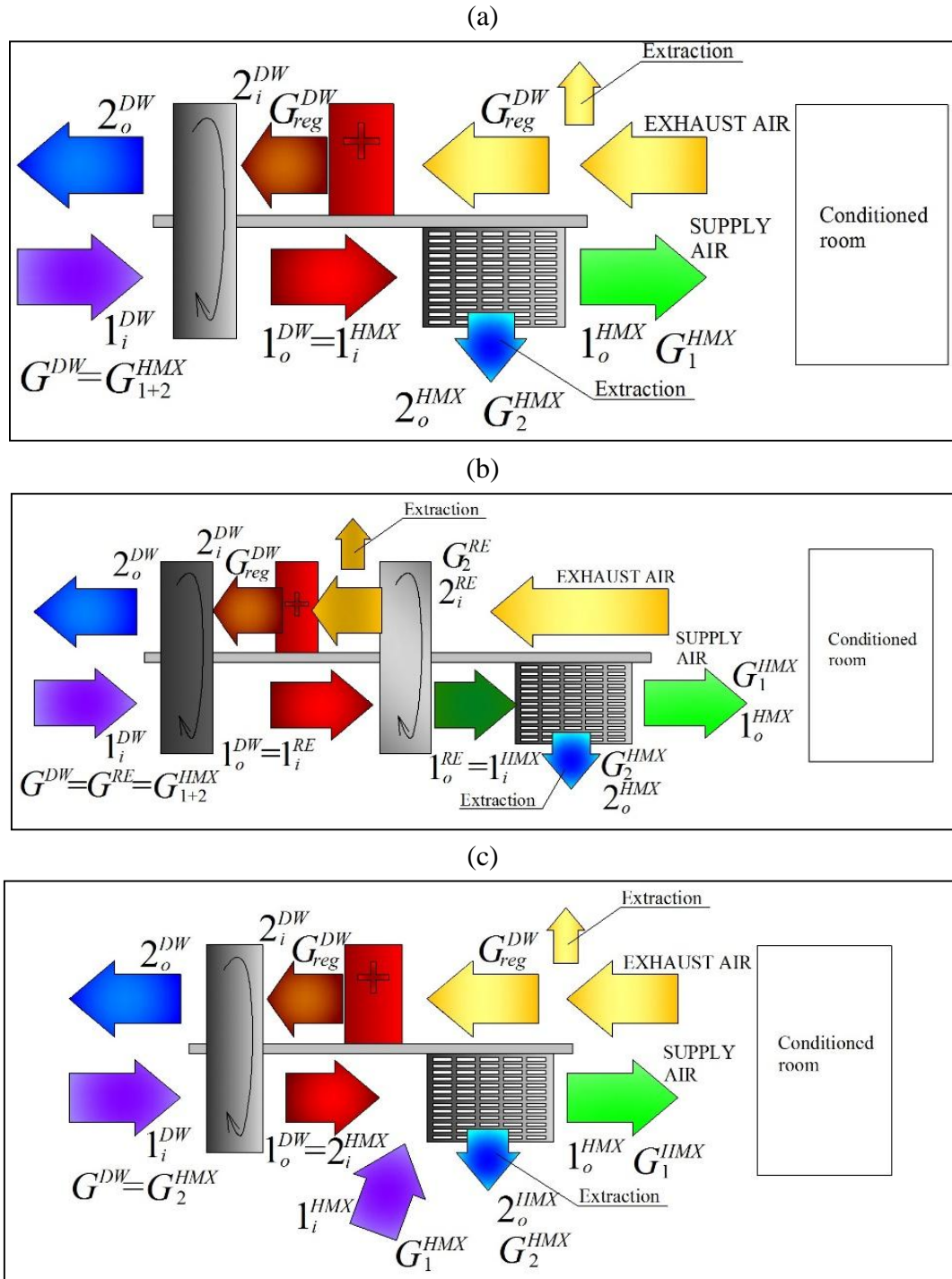
(a)



(b)



(c)



Fig. 10.19. Assumptions for mathematical model. (a) Inlet conditions: System 1. (b) Inlet conditions: System 2. (c) Inlet conditions: System 3.

*Comparison under the same supply airflow rate*

In this section the analysis is performed under assumption that all the systems are equipped with the same desiccant wheel, and all provide the same amount of air to the occupants (which means that the air at the entrance to the desiccant wheel for Systems 1 and 2 will be to times larger than in case of System 3). The regeneration airflow is the same for all analyzed systems. The assumed supply airflow is 300 m$^3$/h, which means that intake airflow for the desiccant

wheel is 600 m³/h for System 1 and 2 and 300 m³/h for System 3. The regeneration airflow for the desiccant wheel for all systems is equal 150 m³/h. The results are visible in Figure 10.20. The comparison under variable inlet temperature, including obtained supply air temperature and cooling capacity is presented in Figure 10.20(a) and (b) respectively. It can be seen that all systems are sensitive for inlet air temperature, however systems 1 and 3 are more sensitive than System 2. This is caused by the fact that the System 2 is equipped with rotary heat exchanger which pre-cools the incoming airflow before it is delivered to the exchanger. This shows the important advantage of the second system- it is less sensible on the ambient temperature. The benefits from the sensible pre-cooling of the dehumidified air also result in the highest effectiveness of the second system in the analyzed case: in obtains the lowest outlet temperature (the differences are up to 3°C: Figure 10.20(a)) and the highest cooling capacity (the differences are up to 0.25 kW: Figure 10.20(b)). It is important to mention that differences in obtained cooling capacity will increase along with the increased airflow rate. The main disadvantage of the System 2 is its sensitivity on the exhaust air parameters- with increasing exhaust air temperature, the effectiveness of the system is decreasing. In spaces with high cooling loads or in systems equipped with the displacement ventilation the exhaust air temperatures may reach high values and the effectiveness of the system may become similar to Sys. 1 and 3 (this was visible in case of the traditional air conditioning systems analyzed in Section 10.1). This may also happen in the places where exhaust air ducts are poorly isolated or are located in places like attics, where the space is significantly heated during summer time.

It can be seen that System 3 obtains higher effectiveness than System 1, but the differences are not as high as in case of System 2 and 1 (the differences are about 0.5-0.6°C: Figure 10.20(a) and (b)). The higher efficiency of System 3 follows from the fact that its primary airflow has lower inlet temperature. The dehumidification process in the desiccant wheel is connected with increasing airflow temperature, therefore the air stream delivered to the M-Cycle HMX is hot and dry. In case of the part of the airstream which is used as working air the high temperature does not make the significant difference because this airflow is indirectly pre-cooled in the initial part of the exchanger. However, in case of the primary air the higher air temperature makes a difference. It was previously established that higher inlet temperature results in higher temperature drop on the M-Cycle HMX, but obtained supply air temperature is always higher than in case of the primary air with lower inlet temperature (see Section 6). It can be seen that in desiccant systems there is no benefit from delivering the heated air to the primary channels, the benefits only follow from delivering the dehumidified air to the working channels. For the above mentioned reasons System 3 obtains lower supply air temperature (Figure 10.20(a) and (b)). It should be mentioned that air with higher temperature results in more intensive evaporation. Therefore, even though System 1 obtains higher outlet temperatures, it consumes more water than System 3. However, the advantage of the System 1 is that it can provide comfortable conditions even in the humid climate: in case of first system both airflows are dehumidified, therefore the air delivered to the conditioned spaces is dry. In case of the third system, the humidity ratio of the incoming air remains unchanged. This may lead to the uncomfortable conditions in the moist climates. However, in moderate climates the humidity ratio of the outdoor air usually does not have to be changed in order to provide comfort.

The comparison under variable inlet humidity ratio, including obtained supply air temperature and cooling capacity is presented in Figure 10.20(c) and (d) respectively. It can be seen that all systems are equally sensitive to inlet air humidity ratio. This follows from the fact that in this case the rotary heat exchanger cannot bring the same benefits for System 2, as it brings in case of higher inlet temperature. The rotary exchanger recovers only sensible heat, therefore it cannot additionally dehumidify the airflow. Therefore it can be seen that all analyzed systems are equally sensitive to the inlet ambient air humidity ratio. It also can be observed that there are similar trends in the differences between obtained outlet temperatures and cooling capacities. System 2 shows highest effectiveness, System 1 shows the lowest effectiveness: Figure 10.20(c) and (d)). It should be mentioned that the desiccant wheel in case of System 3 is regenerated with air with much higher humidity ratio than in case of System 1 and 2 (due to the fact that supply airflow has the same moisture content as the ambient air and it also assimilates the space latent heat loads). However, System 3 makes up for it by having the much lower airflow dehumidified in the desiccant wheel in compare to System 1 and 2. Also it benefits from delivering the air with lower temperature to the primary air channels of the M-Cycle HMX.
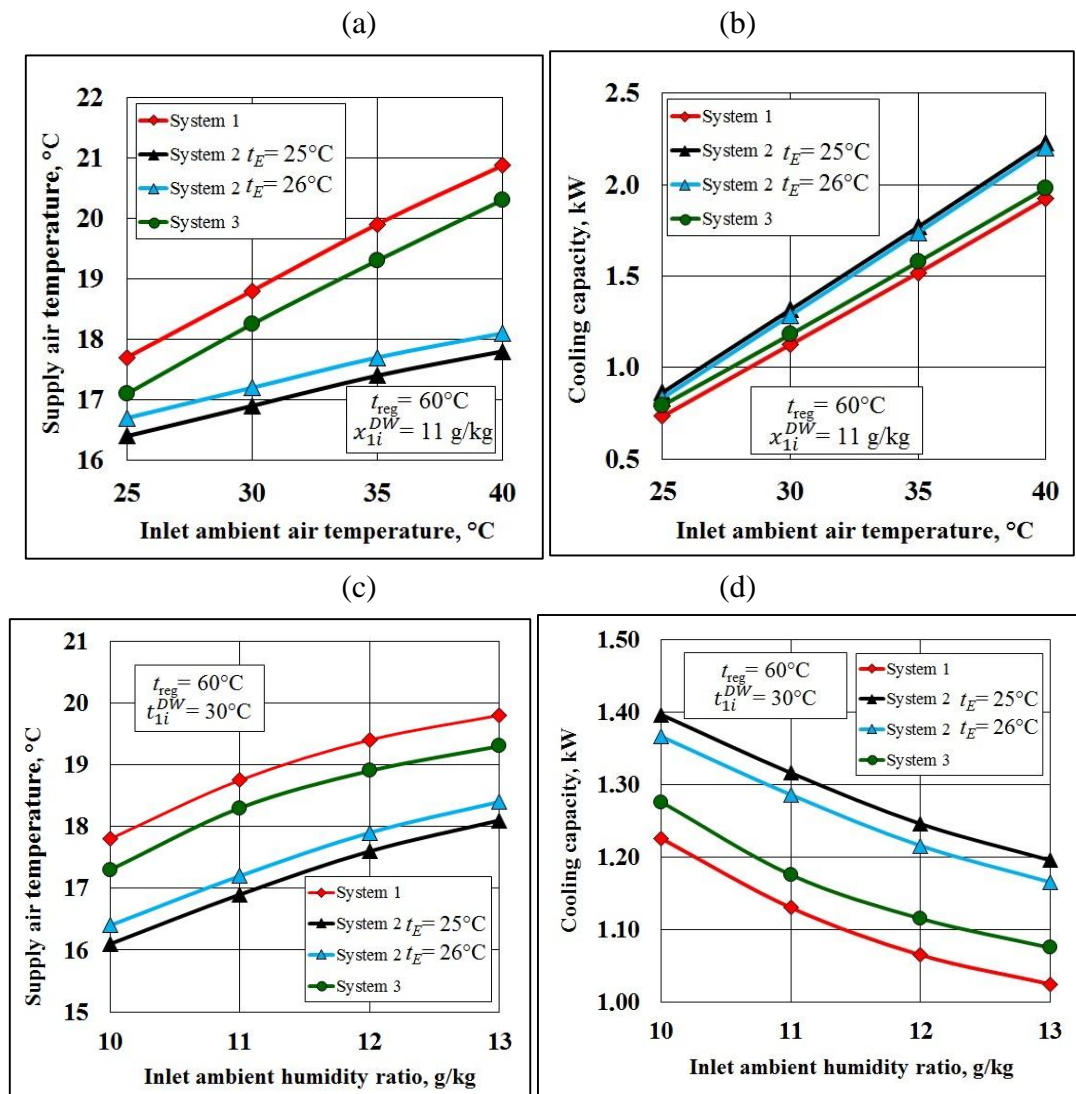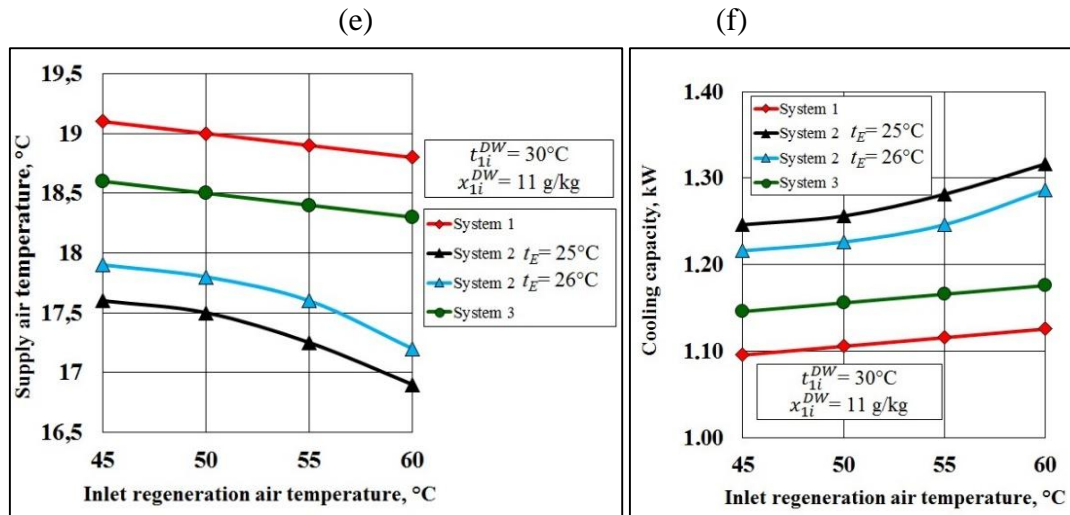
(a)  (b)

(c)  (d)

(e) (f)



Fig. 10.20. Comparison under the same supply airflow rate. (a) Comparison under variable inlet temperature: supply air temperatures. (b) Comparison under variable inlet temperature: cooling capacities. (c) Comparison under variable inlet humidity ratio: supply air temperatures. (d) Comparison under variable inlet humidity ratio: cooling capacities. (e) Comparison under variable regeneration air temperature: supply air temperatures. (f) Comparison under variable regeneration air temperature: cooling capacities.

The comparison under variable regeneration air temperature, including obtained supply air temperature and cooling capacity is presented in Figure 10.20(e) and (f) respectively. It can be seen that System 2 is more sensitive to regeneration air temperature than System 1 and 3. It can also be observed that generally all of the analyzed systems are not highly sensitive on the regeneration air temperature in moderate conditions (the drop in the supply air temperature for System 1 and 3 is only 0.4°C: Figure 10.20(e) and (f)). Generally regeneration of the desiccant wheel with lower temperature results in less effective dehumidification, the differences in the efficiency of the desiccant wheel are not that different. The significant differences would be visible when the dehumidifier would be regenerated with the very hot airflow (80°C and higher). However, the purpose of this study is to analyze the systems under conditions which can be obtained by solar panels in moderate climate. The low sensitivity on the low regeneration air temperature shows that presented solution allow for wide application around the world.

*Comparison under the same dehumidified airflow rate*

In this section the analysis is performed under assumption that all the systems are equipped with the same desiccant wheel, which dehumidifies the same airflow. This means that the supply airflow is different for systems 1 and 2 and System 3. The dehumidified airflow is 600 m³/h, which means that the supply airflow for System 1 and 2 is equal 300 m³/h and 600 m³/h for System 3. The regeneration airflow for the desiccant wheel for all systems is equal 150 m³/h. There is also an additional assumption: System 3 will be equipped with two parallel M-Cycle HMXs in order to maintain the same air stream velocity in the channels. All the simulations are performed under the same conditions as in previous section (variable inlet outdoor air

temperature, humidity ratio and regeneration air temperature). The results are visible in Figure 10.21.

It can be observed that in analyzed case System 3 obtains higher outlet temperatures than System 1 (Fig. 10.21(a),(c) and (e)), however the differences are not significant- up to 0.2°C (temperatures obtained by System 2 were removed in order to make the differences more visible). This follows from the fact that in case of the third system dehumidification process is less effective due to the higher humidity ratio of the regeneration air, but this negative effect is partly compensated by the lower inlet temperature of the primary airflow to the M-Cycle HMX. The main advantage of the System 3 is visible in Figure 10.21(b),(d) and (f): presented solution obtains significantly higher cooling capacity than System 1 and 2. This follows from the fact that arrangement of System 3 allows to provide higher airflow rate when it operates on the same amount of air delivered to the desiccant wheel as System 1 and 2. This results in two important benefits: first is that even though this solution obtains a little higher supply air temperatures than System 1, it makes up for it by keeping the higher airflow rate, second is that it needs less energy for the regeneration of the desiccant wheel. In many cases the cooling capacity is critical for the air conditioning system, because it shows how much cooling loads the considered system is able to cover. Therefore, in many cases System 3 may be characterized by more advantages than System 1 and 2: it can provide almost two time higher cooling capacity by using the same amount of energy for the regeneration of the desiccant wheel, it also consumes less water for the evaporation than System 1, due to the fact that it delivers colder air to the primary air channels. The main disadvantages of this solution are highest investment cost, largest size of the system and sensitivity on the outdoor air humidity in terms of providing comfort. All of the systems are sensible on the humidity ratio of the outdoor air, but in case of System 1 and 2, the incoming airflow may be dehumidified more effectively by using higher regeneration temperature. In case of System 3, only the working airflow is dehumidified, therefore under unfavorable outdoor conditions this solution may keep the conditioned spaces too humid.
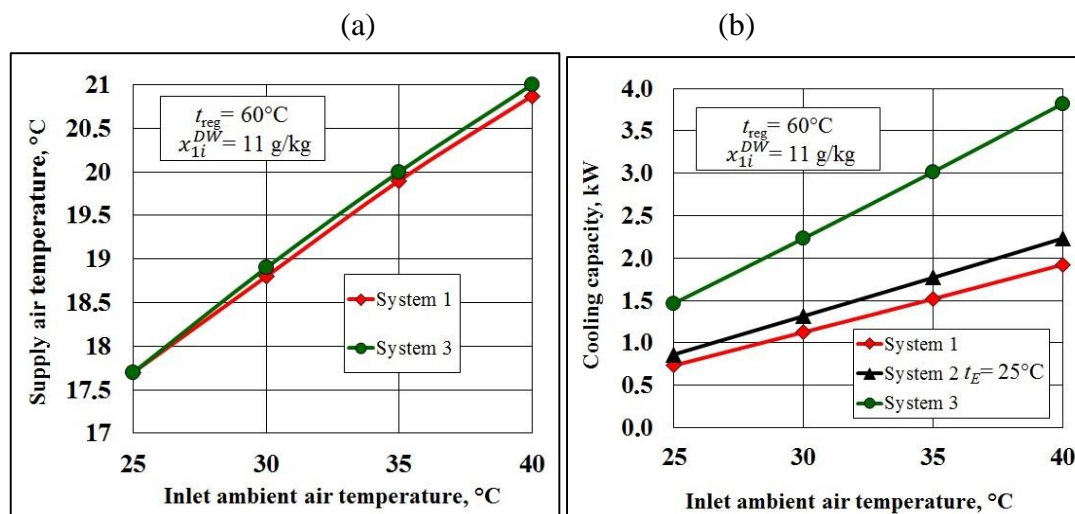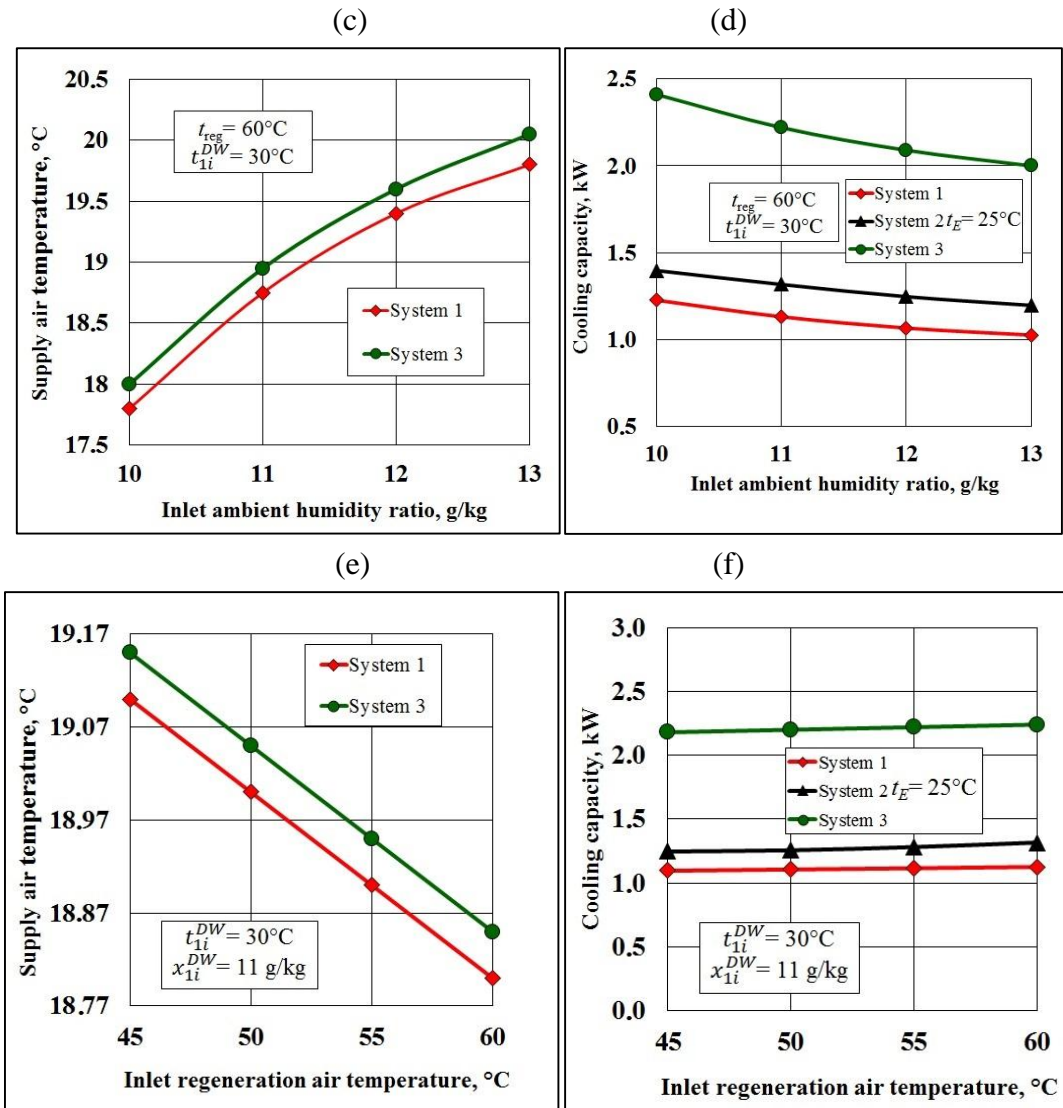
(a)                                    (b)

Fig. 10.21. Comparison under the same dehumidified airflow rate. (a) Comparison under variable inlet temperature: supply air temperatures. (b) Comparison under variable inlet temperature: cooling capacities. (c) Comparison under variable inlet humidity ratio: supply air temperatures. (d) Comparison under variable inlet humidity ratio: cooling capacities. (e) Comparison under variable regeneration air temperature: supply air temperatures. (f) Comparison under variable regeneration air temperature: cooling capacities.

*Propositions of most effective arrangements*

The presented analysis leads to several important conclusions and allows establishing the advantages and disadvantages of presented systems. The main advantage of System 1 and 2 over System 3 is low sensitivity on the ambient air conditions in terms of providing comfort to the conditioned spaces. The main advantage of System 3 over first and second system is possibility of achieving higher cooling capacity when it dehumidifies the same amount of air. The additional strong side of System 2 and 3 is that they deliver colder primary air to the exchanger, which results in lower supply air temperatures and lower water consumption (due to the fact that System 2 pre-cools both working and primary airflow with the rotary wheel, its temperature efficiency is higher and water consumption is lower). Using the above-mentioned

information the modifications of System 3 are proposed, in order to combine and utilize the advantages of all presented solutions. The modifications are visible in Figure 10.22.

The Modified System 3 is equipped with bypass of the desiccant wheel which allows it to operate like System 1 (when both primary and working airflow are delivered to the desiccant wheel) when outdoor conditions are too humid to provide comfort. It can operate as System 3 (half of the outdoor airflow is delivered to the bypass and then directly to the dry channels of the HMX as the primary air, while the other half goes to the desiccant wheel) when outdoor conditions allow to provide thermal comfort without dehumidification of the supply air (Fig. 10.22(a)). When the ambient conditions are dry enough to provide comfort without dehumidification, the whole air stream bypasses the desiccant wheel. This solution is also equipped with the mixing chambers before the primary air channels, which allows to change the proportion of how much primary airflow which is delivered to the desiccant wheel and how much directly to the exchanger. This solution allows for maximal energy savings and providing high thermal comfort at the same time.
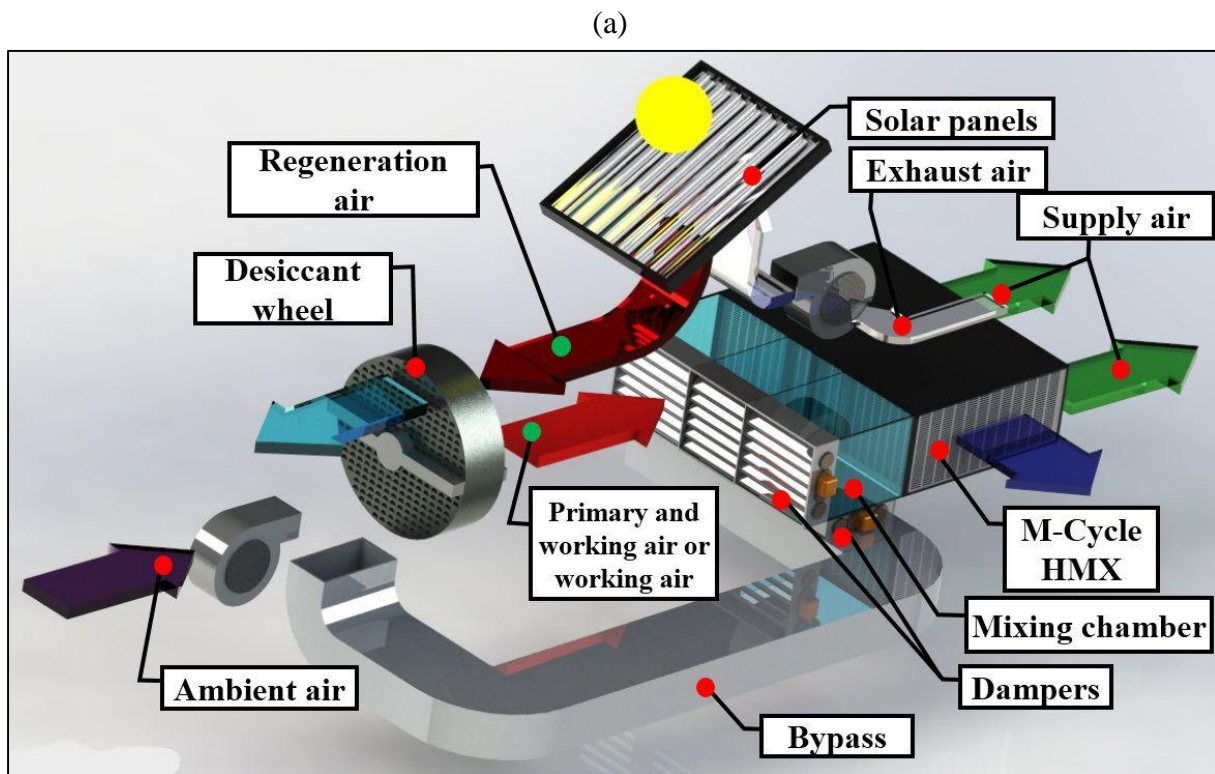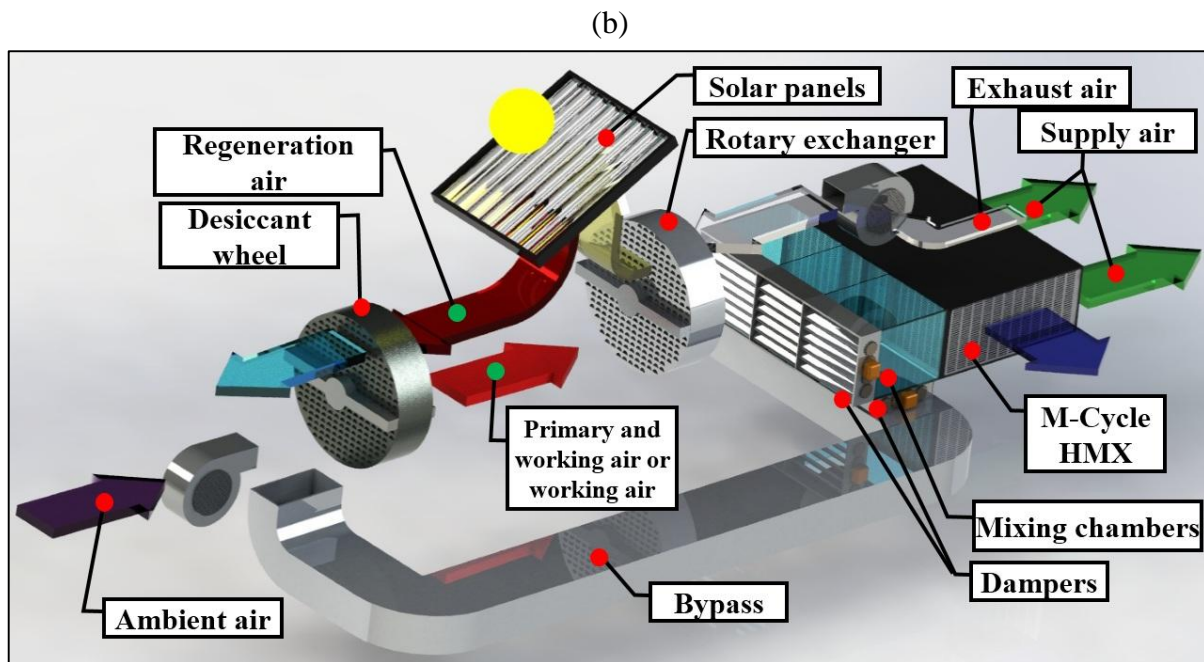
(a)

(b)



Fig. 10.22. Proposed modifications of System 3. (a) Modified System 3 with bypass. (b) Modified System 3 with bypass and rotary exchanger.

The solution presented in Figure 10.22(b) utilizes all the advantages of System 1, 2 and 3, because it is also equipped with the rotary heat exchanger. When outdoor conditions allow to provide comfort without dehumidifying the ambient air, the primary airflow is delivered to bypass of the desiccant wheel and then to the HMX. In this case the rotary heat exchanger is used to pre-cool the working airflow before it enters the exchanger and also to pre-heat the regeneration airflow. The pre-cooling of working air without changing its humidity ratio leads to the two earlier-established benefits: the colder air results in lower supply air temperatures and lower water consumption. The benefits from pre-cooling of the working airflow in System 3 are visible in Figure 10.23(a) and (b). This simulation was performed for the same conditions as in previous analysis. It can be seen that Modified System 3 achieves lower supply air temperatures and higher cooling capacity than other analyzed Systems. The differences vary from 0.5-1.2°C (System 2) to 4°C (System 1). This shows that presented solution has the highest potential of wide application. It is able to keep the highest temperature effectiveness and minimize the exploitation costs with the bypass system. However, it is important to mention that in many cases limiting factor is the price of the considered system. In this case System 1 is definitely the cheapest solution. However, Modified System 3 has some benefits over the System 3: it uses two fans, instead of three. The bypass and dampers system is much cheaper than the additional fan. The cost of Modified System 3 with the rotary exchanger would also be similar to the System 2. This show that sometimes the most effective solution does not have to be the most expensive one.
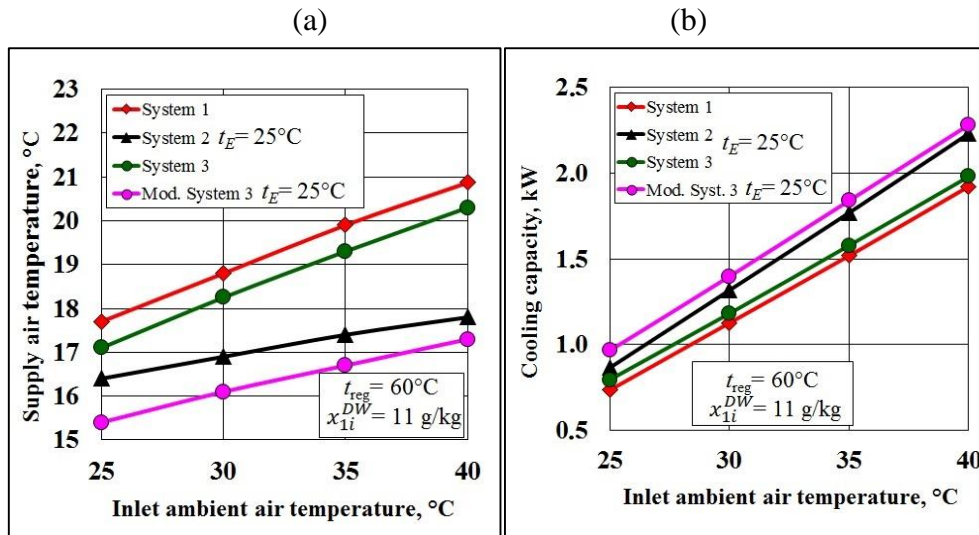
(a)                    (b)



Fig. 10.23. Comparison of Modified System 3 with rotary exchanger with other solutions. (a) Supply air temperature. (b) Cooling capacity.

## 10.3. Conclusions from the section

In this Section the potential of application of the cross-flow M-Cycle air cooler in selected air conditioning systems was investigated. Two types of systems were analyzed: typical air conditioning system equipped with R410a cooling coil in Polish climate conditions and the SDEC system, which is based on combination of evaporative cooling and a desiccant wheel. The typical air conditioning system was realizing mixing and displacement ventilation in the office building with room exposed on the different world directions. In SDEC system, the system equipped with the M-Cycle HMX was compared with typical desiccant system based on the rotary exchanger and evaporative coolers. After that, the different arrangements of the SDEC systems equipped with the cross-flow M-Cycle HMX were analyzed.

It was established that:

- The M-Cycle air cooler has a high potential to be applied in air conditioning systems in Polish climate conditions.
  - The operation costs of the systems equipped with the cross-flow M-Cycle air cooler are significantly lower than of the typical mechanical compression systems.
  - HMX has the highest application potential for displacement ventilation, where it can operate as the only cooling source, while the size of the cooling coil can be minimized and used only as a backup.
  - In case of the mixing ventilation, the M-Cycle air cooler needs to operate with the cooling coil during peak hours, however, it still significantly decreases its power, to the level where operational costs are minimal.
  - In both cases the cross-flow M-Cycle HMX saves energy not only by sensibly cooling the outdoor air, but also by preventing from too high dehumidification on the cooling coil.

- The cross-flow M-Cycle air cooler also has a high potential of application in the SDEC systems.
  - The M-Cycle system allows for higher temperature effectiveness than the traditional desiccant system even when the desiccant wheel is regenerated with lower temperature. The additional advantage of the M-Cycle exchanger is that it does not add moisture to the airflow, which allows providing more comfort to the conditioned spaces.
- Desiccant systems equipped with the cross-flow is sensitive on the variety of factors.
  - Under very hot and humid inlet conditions the system may require additional heat for the regeneration of the desiccant wheel in order to provide satisfying indoor conditions. The results also showed that the system is sensitive on the ambient and regeneration airflow rate and rotational speed of the desiccant wheel and it is less sensitive on the humidity ratio change between supply and exhaust airflow.
- Depending on the different arrangements, the SDEC systems equipped with the M-Cycle unit may show different effectiveness and sensitivity on the above-mentioned factors.
  - First system (only desiccant wheel with HMX and heat source) was the simplest solution and it showed the lowest temperature effectiveness, but its construction allowed for keeping the thermal comfort in conditioned space regardless of the inlet parameters. The second system (System 1 equipped with rotary exchanger) showed highest temperature effectiveness, but it was sensitive on the exhaust air parameters. The third system (System 1 when dehumidified air is delivered only to the initial channels) showed higher temperature effectiveness than System 1 and lower than System 2, when all systems supplied the same amount of air to the conditioned space. It also allowed obtaining significantly higher cooling capacity than first and second arrangement, when all systems dehumidified the same airflow. The main disadvantage of System 3 was its complicated structure and sensitivity on outdoor humidity. In too humid outdoor conditions, this solution could not provide thermal comfort.
  - Using the established data the modifications of the System 3 were presented. This solution combines the advantages of all compared systems and it eliminates their disadvantages. It allows operating with high efficiency, minimal energy and water consumption and provide thermal comfort regardless on the outdoor conditions. Therefore, this solution has the highest potential of implementation.

## 11. Summary and final conclusions

This thesis investigated the Maisotsenko cycle heat and mass exchanger used in air conditioning systems: the cross-flow M-Cycle air cooler. The heat and mass transfer process were analyzed with ε-NTU-models, 14 mathematical models of the M-Cycle HMXs were developed in total for the purpose of this thesis ("ideal" M-Cycle with dense perforation, 9 different models of

HMX with different arrangement of the initial part, modified cross-flow M-Cycle unit with different primary and working air entrance location, regenerative air cooler, perforated regenerative air cooler and the modified counter-flow air cooler). Additionally, mathematical models of the parallel-flow, counter-flow and cross-flow evaporative air coolers and the model of the desiccant wheel were developed to fully analyze the heat and mass transfer process in the considered exchanger and its application potential. The initial studies with the basic evaporative cooling cycles allowed preparing initial assumptions for the mathematical model of the M-Cycle air cooler and to establish the most characteristic features of the combined heat and mass transfer in indirect evaporative air coolers (such as occurrence of two active heat and mass transfer zones and violation of the Lewis relation).

The modified Runge-Kutta method and original algorithms, allowing to take into account uneven fin temperature distribution under combined heat and mass transfer conditions and effect of airflows mixing in wet channels under different arrangements of the initial part of the HMX were applied to numerically solve the sets of differential equations under variable initial conditions. The computation model results were validated against experimental data obtained both from tests performed by author and from experimental data available in the existing literature. The positive results of this validation indicated that the sufficient accuracy in simulation could be obtained. The model is therefore suitable for use in analyzing the heat and mass transfer processes occurring inside considered HMX and predicting its operational performance. The performance of the HMX was investigated and parametrically evaluated by transitional simulation under various ambient and working and operational conditions under different geometrical arrangements.

The heat and mass transfer analysis allowed establishing that:

- o The processes of heat and mass transfer are characterized by a complex and diverse temperature and moisture distributions, which are significantly different from the dependences found in typical evaporative heat exchangers,
- o Heat and mass transfer process in the wet channel are strongly deformed and characterized by temperature and humidity oscillation due to continuous mixing the wet airflow 4 with dry airflow 3,
- o The active zones of heat and mass transfer may occur several times in one HMX.
- o The shape of the channel has significant impact on heat and mass transfer distribution on plate and fin surface,
- o Due to the occurrence of different active heat and mass transfer zones in the exchanger with different boundary conditions characterizing the coupled heat and mass transfer process in each of these determined zones, the Lewis relation unity in the M-Cycle HMX is violated as in case of the counter and cross-flow evaporative air coolers.

From the sensitivity analysis under variable operational conditions it was established that:

- o M-Cycle heat and mass exchanger is most effective in hot and dry climates,
- o The heat and mass transfer performance strongly depends on inlet air temperature and humidity, geometrical size of the channels, type of plate-fin

surface, uniformity of water distribution, primary air velocity and working to primary air heat capacity ratio,

o Dew point effectiveness and wet bulb effectiveness are not adequate indicators for cross-flow M-Cycle air cooler performance, when they are considered as only efficiency factors.

From the comparative analysis between the different M-Cycle coolers it was established that:

o The cross-flow M-Cycle HMX has the highest application potential from other forms of M-Cycle. The counter-flow M-Cycle exchangers, which are closer to the ideological basis of the process, achieve a little higher temperature effectiveness, however, due to the unfavorable structure, their cooling capacity is much lower,

o The high effectiveness of the cross-flow M-Cycle air cooler lies in its initial part, which allows to form a unique temperature distribution which is similar to the temperature distribution in the counter-flow evaporative air coolers. This allows the cross-flow unit to achieve temperature effectiveness close to the effectiveness of the counter-flow units.

From the performance analysis of the different variants of the cross-flow M-Cycle exchangers it was established that:

o The existing cross-flow M-Cycle air cooler can be improved by keeping the uniform airflow distribution inside the channels and modifying the initial part arrangement:

▪ The best proportions between initial and product side are 1:7 and 2:8,

▪ When there is enough space in the air handling unit, the initial part of the exchanger can be expand while product part remains unchanged.

o The modified version of the cross-flow HMX with primary and working air entering from the opposite sides of the exchanger can be a better solution in some air conditioning systems, because it can operate in supply-exhaust airflow regime. The boundary values for the exhaust air parameters, which allow overcoming the efficiency of the original unit were established and presented.

After above-mentioned analysis, the cross-flow M-Cycle heat exchanger was statistically analyzed and its structure was optimized. The statistical analysis allowed establishing the regression equations for "black box" models of the characteristic efficiency factors, including outlet air temperature, specific cooling capacity respected to the volume of HMX structure, dew point effectiveness and coefficient of performance ($COP_{1+2}$). The optimization was based on five independent variables (inlet air temperature and relative humidity, primary air mass flow rate, working to primary air heat capacity ratio and relative length of the initial part) and their influence on $\hat{Q}$, $\varepsilon_{DP}$ and $COP_{1+2}$. The optimization allowed establishing the optimal geometrical and operational parameters of the exchanger and the climate conditions for its rational operation. The analysis of the values of Harrington function in climate parameters from selected cities worldwide showed that investigated HMX can be applied in most of them and it is suitable for the Polish climate conditions. Therefore, the assumed tesis for this dissertation if fulfilled.

The optimized HMX was analyzed in terms of its application potential in two air conditioning systems: typical air handling unit with cooling coil supplied by R410a mechanical compression system and the desiccant system with rotary dehumidifier regenerated with air with relatively low temperature which can be obtained by the solar panels in moderate climate conditions. Both analysis showed that cross-flow M-Cycle air cooler has high application potential.

In case of the typical air conditioning system, HMX allowed for significant reduction of operational costs (up to 4.6 times in mixing ventilation and up to 23 times in the displacement ventilation). In the displacement system the considered air cooler is able to operate as the only cooling source, while in the mixing system it requires additional cooling coil during peak hours. In case of the desiccant systems, considered unit allowed achieving higher effectiveness than typical system equipped with direct evaporative coolers and rotary exchanger and it allowed keeping the comfort conditions inside the conditioned spaces at lower regeneration air temperature. The analysis of the different arrangements of the SDEC systems equipped with the cross-flow M-Cycle air cooler allowed finding the most effective solution in terms of cooling performance.

The obtained results show the attractiveness of the M-Cycle heat exchanger and allow extending the potential of useful utilization of evaporative cooling for the purpose of air conditioning. The carried analyses are hoped to be beneficial for researchers around the world and to be useful in designing the indirect evaporative air cooling units.

## References

[1]    L. Pérez-Lombard, J. Ortiz and C. Pout, "A review on buildings energy consumption information," *Energy and Buildings,* pp. 394-398, Vol. 40, 2008.

[2]    Z. Duan, Z. Changhong, X. Zhang, M. Mustafa, B. Alimohammadisagvand, A. Hasan and X. Zhao, "Indirect evaporative cooling: Past, present and future potentials," *Renewable and Sustainable Energy Reviews,* p. 6823–6850, Vol. 16, 2012.

[3]    I. E. Agency, "Transition to Sustainable Buildings: Clean Energy Solutions Center Book Launch," 2013.

[4]    B. Polska, "Raport: Stan energetyczny budynków w Polsce (in Polish), http://www.elektroonline.pl/," 2012.

[5]    "HVAC Costs," 1 2016. [Online]. Available: http://hvaccosts.rheemecosense.com/.

[6]    U. E. I. Administration, " Residential Energy Consumption Survey," 2009.

[7]    Z. Duan, "Investigation of a Novel Dew Point Indirect Evaporative Air Conditioning System for Buildings," *A Thesis submitted to the The University of Nottingham for the degrees of Doctor,* 2011.

[8]    L. Bellemo, B. Elmegaard, L. O. Reinholdt, M. R. Kærn, A. Jakobsen and W. B. Markussen, "Modelling and analysis of a desiccant cooling system using the regenerative indirect evaporative cooling process," *ECOS 2013, Proceedings of the 26th International Conference on Efficiency, Cost, Optimization, Simulation and Environmental Impact of Energy Systems, Guilin (China),* p. 109–122, 16–19 July, 2013.

[9]    B. Riangvilaikul and S. Kumar, "An experimental study of a novel dew point evaporative cooling system," *Energy Buildings,* p. 637–644, Vol. 42, 2010.

[10] B. Riangvilaikul and S. Kumar, "Numerical study of a novel dew point evaporative cooling system," *Energy and Buildings,* p. 2241–2250, Vol. 42, 2010.

[11] A. Hasan, "Indirect evaporative cooling of air to a sub-wet bulb temperature," *Applied Thermal Engineering,* pp. 2460-2468, Vol. 30, 2010.

[12] S. Anisimov and D. Pandelidis, "Numerical study of the Maisotsenko cycle heat and mass exchanger," *International Journal of Heat and Mass Transfer,* pp. 75-96, Vol. 75, 2014.

[13] "Wikipedia," 1 2016. [Online]. Available: https://en.wikipedia.org/wiki/Evaporative_cooler.

[14] M. Bahadori, "Passive Cooling Systems in Iranian Architecture," *Scientific American,* pp. 144-154, 02 1978.

[15] L. Gillan, "Maisotsenko cycle for cooling process," *Clean Air,* pp. 1-18, Vol. 9, 2008.

[16] S. Anisimov and D. Pandelidis, "Modelowanie matematyczne wymienników do pośredniego ochładzania powietrza za pomocą parowania cieczy o krzyżowym układzie przepływu czynników (in Polish)," *Ciepłownictwo Ogrzewnictwo Wentylacja (Distric Heating, Heating, Ventilation),* pp. 335-341, Vol. 8, 2012.

[17] Y. Xuan, F. Xiao, X. Niu and X. W. S. Huang, "Research and application of evaporative cooling in China: A review (I)- Research," *Renewable and Sustainable Energy Reviews,* pp. 3535-3546, Vol. 16, 2012.

[18] "JDR Group," 1 2016. [Online]. Available: http://www.jdr-websites.co.uk/.

[19] S. Anisimov and D. Pandelidis, "Porównanie pracy pośrednich wymienników wyparnych o różnych schematach przepływu powietrza: wyniki symulacji numerycznej (in Polish)," *Ciepłownictwo Ogrzewnictwo Wentylacja (District Heating, Heating, Ventilation),* pp. 126-129, Vol. 3, 2013.

[20] "Euroclima," 1 2016. [Online]. Available: www.euroclima.com.

[21] S. Anisimov and D. Pandelidis, "Heat and mass transfer processes in counter-flow indirect evaporative air cooler," in *Proceedings of the Environmental Engineering International Conference*, Sankt Petersburg, Russia, 2012.

[22] A. Hasan, "Going below the wet bulb temperature by indirect evaporative cooling: Analysis using a modified ε-NTU method," *Applied Energy,* p. 237–245, Vol. 89, 2012.

[23] X. Zhao, S. Liu and S. B. Riffat, "Comparative study of heat and mass exchanging materials for indirect evaporative cooling systems," *Building and Environment,* p. 1902–1911, Vol. 43, 2008.

[24] C. Higgins and H. Reichmuth, "Desert CoolAire package unit technical assessment: Field performance of a prototype hybrid indirect evaporative airconditioner," New Buildings Institute, 2007.

[25] Y. Jiang and X. Xie, "Theoretical and testing performance of an innovative indirect evaporative chiller," *Solar Energy,* p. 2041–55, Vol. 84, 2010.

[26] V. Maisotsenko, L. Gillan and A. G. R. Gillan, "Fabrication materials and techniques for plate heat and mass exchangers for indirect evaporative coolers". USA Patent US 20100018234 A1, 2008.

[27] V. Gómez, F. Rey Martínez, D. Varel, M. Molina Leyva and R. Herrero Martin, "Description and experimental results of a semi-indirect ceramic evaporative cooler," *International Journal of Refrigeration,* pp. 654-662, Vol. 28, 2005.

[28] D. R. Crum, J. W. Mitchell and B. W. A., "Indirect evaporative cooler performance," *ASHRAE Trans,* p. 1261–75, Vol. 93, 1987.

[29]   D. Pandelidis, S. Anisimov and W. Worek, "Performance study of the Maisotsenko Cycle heat exchangers in different air-conditioning applications," *International Journal of Heat and Mass Transfer,* p. 207–221, Vol. 81, 2015.

[30]   D. Pandelidis, S. Anisimov and W. Worek, "Performance study of counter-flow indirect evaporative air coolers," *Energy and Buildings,* pp. 53-64, Vol. 109, 2015.

[31]   D. Pandelidis and S. Anisimov, "Oszczędności energetyczne i ekonomiczne wynikające z zastosowania wymiennika wyparnego w klimatyzacji cz. 1 (in Polish)," *Chłodnictwo & Klimatyzacja (Refrigeration & Air Conditioning),* pp. 58-61, Vol. 1-2, 2014.

[32]   D. Pandelidis and S. Anisimov, "Oszczędności energetyczne i ekonomiczne wynikające z zastosowania wymiennika wyparnego w klimatyzacji. Cz. 2," *Chłodnictwo & Klimatyzacja (Refrigeration & Air Conditioning),* pp. 38-41, Vol. 3, 2014.

[33]   P. Kowalski, *Wymiana ciepła i masy w obrotowym osuszaczu solarnego systemu klimatyzacyjnego (in Polish),* Wrocław, Poland: A Thesis submitted to Wrocław University of Technology for the degree of Doctor of Philosophy, 2013.

[34]   D. Pandelidis, "Gruntowy wymiennik ciepła współpracujący z solarnym układem klimatyzacji. Cz. 1 (in Polish)," *Chłodnictwo (Refrigeration),* pp. 32-36, Vol. 6, 2014.

[35]   D. Pandelidis, "Gruntowy wymiennik ciepła współpracujący z solarnym układem klimatyzacji. Cz. 2 (in Polish)," *Chłodnictwo (Refrigeration),* pp. 24-27, Vol. 49, 2014.

[36]   D. Pandelidis, "Gruntowy wymiennik ciepła współpracujący z solarnym układem klimatyzacji. Cz. 3 (in Polish)," *Chłodnictwo (Refrigeration),* pp. 28-33, Vol. 8 2014.

[37]   G. Heidarinejad, M. Bozorgmehra, S. Delfanib and J. Esmaeelianb, "Experimental investigation of two-stage indirect/ direct evaporative cooling system in various climatic conditions," *Building and Environment,* p. 2073–9, Vol. 44, 2009.

[38]   G. Heidarinejad, M. F. Farahani and S. Delfani, "Investigation of a hybrid system of nocturnal radiative cooling and direct evaporative cooling," *Building and Environment,* p. 1521–1528, Vol. 45, 2010.

[39]   V. Khalajzadeh, M. F. Farahani and G. Heidarinejad, "A novel integrated system of ground heat exchanger and indirect evaporative cooler," *Energy and Buildings,* p. 604–610, Vol. 49, 2012.

[40]   L. Elberling, "Laboratory Evaluation of the Coolerado Cooler-Indirect Evaporative Cooling Unit," *Pacific Gas and Electric Company (Report),* 2006.

[41]   E. D. Rogdakis, I. P. Koronaki and D. N. Tertipis, "Experimental and computational evaluation of a Maisotsenko evaporative cooler at Greek climate," *Energy and Buildings,* p. 497–506, Vol. 70, 2014.

[42]   V. Maisotsenko, A. Cimerzan and M. P. N. Zexer, "Device for indirect evaporative air cooling (in Russian)". Soviet Union Patent 979796, 08 1976.

[43]   C. Zhan, X. Zhao, S. Smith and S. B. Riffat, "Numerical study of a M-Cycle cross-flow heat exchanger for indirect evaporative cooling," *Building and Environment,* p. 657–668, Vol. 46, 2011.

[44]   S. Anisimov and D. Pandelidis, "Porównanie pracy pośrednich wymienników wyparnych o różnych schematach przepływu powietrza: model matematyczny (in Polish)," *Ciepłownictwo Ogrzewnictwo Wentylacja (District Heating, Heating, Ventilation) ,* pp. 75-78, Vol. 2, 2013.

[45]   S. Anisimov, D. Pandelidis and J. Danielewicz, "Numerical analysis of selected evaporative exchangers with the Maisotsenko cycle," *Energy Conversion and Management,* pp. 452-464, Vol. 88, 2014.

[46] D. Zube and L. Gillan, "Evaluating Coolerado Corportion's heat-mass exchanger performance through experimental analysis," *International Journal of Energy for a Clean Environment ("Special Issue on M-Cycle Fundamentals and Applications"),* pp. 101-116, Vol. 12, 2-4 2011.

[47] S. Anisimov, D. Pandelidis, A. Jedlikowski and V. Polushkin, "Performance Investigation of a M-cycle cross-flow heat exchanger used for indirect evaporative cooling," *Energy,* pp. 593-606, Vol. 76, 2014.

[48] S. Anisimov, D. Pandelidis and J. Danielewicz, "Numerical study and optimization of the combined indirect evaporative air cooler for air-conditioning systems," *Energy,* pp. 452-464, Vol. 80, 2015.

[49] D. Pandelidis and S. Anisimov, "Numerical analysis of the selected operational and geometrical aspects of the M-Cycle heat and mass exchanger," *Energy and Buildings,* pp. 413-424, Vol. 87, 2015.

[50] X. Zhao, J. Li and S. B. Riffat, "Numerical study of a novel counter-flow heat and mass exchanger for dew point evaporative cooling," *Applied Thermal Engineering,* pp. 1942-1951, Vol. 28, 2008.

[51] C. Zhan, Z. Duan, X. Zhao, S. Smith, H. Jin and S. Riffat, "Comparative study of the performance of the M-cycle counter-flow and cross-flow heat exchangers for indirect evaporative cooling - Paving the path toward sustainable cooling of buildings," *Energy,* p. 6790–805, Vol. 36, 2011.

[52] W. T. Ray, "Conditioning liquids and air and other gases". USA Patent No. US 19865929, 1935.

[53] D. Pescod, "A heat exchanger for energy saving in an air-conditioning plant," *Trans ASHRAE,* 238–51 Vol. 85, 1979.

[54] I. L. Maclaine-Cross and P. J. Banks, "A general theory of wet surface heat exchangers and its application to regenerative evaporative cooling," *Journal of Heat Transfer,* p. 579–585, Vol. 103, 1981.

[55] S. T. Hsu, Z. Lavan and W. Worek, "Optimization of wet-surface heat exchangers," *Energy,* p. 757–770, Vol. 14, 1989.

[56] P. J. Erens and A. A. Dreyer, "Modelling of indirect evaporative air coolers," *International Journal of Heat and Mass Transfer,* pp. 17-26, Vol. 36, 1993.

[57] R. Navon and H. Arkin, "Feasibility of direct-indirect evaporative cooling for residences, based on studies with a desert cooler," *Building and Environment,* p. 393–399, Vol. 29-3, 1994.

[58] H. El-Dessouky, A. Al-Haddad and F. Al-Juwayhel, "A modified analysis of counter flow wet cooling towers," *Journal of Heat Transfer Trans ASME,* p. 617–26, Vol. 119, 1997.

[59] T. Tulsidasani, R. L. Sawhney, S. P. Singh and M. S. Sodha, "Recent research on an indirect evaproative cooler (IEC) part 1: optimization of the COP," *International Journal of Energy Research,* p. 238–51, Vol. 21, 1997.

[60] N. J. Stoitchkov and G. I. Dimitrov, "Effectiveness of crossflow plate heat exchanger for indirect evaporative cooling," *International Journal of Refrigeration,* p. 463–471, Vol. 21, 1998.

[61] J. F. San Jose Alonso, F. J. Rey Martinez, V. Gomez and M. A. Alvarez-Guerra Plasencia, "Simulation model of an indirect evaporative cooler," *Energy and Buildings,* p. 23–27, Vol. 29, 1998.

[62] X. C. Guo and T. S. Zhao, "A parametric study of an indirect evaporative air cooler," *International Communications in Heat and Mass Transfer,* p. 217–226, Vol. 25, 1998.

[63] K. A. Joudi and S. M. Mehdi, "Application of indirect evaporative cooling to variable domestic cooling load," *Energy Conversion and Management,* p. 1931–1951, Vol. 41, 2000.

[64] V. Maisotsenko, L. Gillan and A. H. T. Gillan, "Method and plate apparatus for dew point evaporative cooler". USA Patent US 7197887 B2, 2000.

[65] C. Song, D. Lee and S. Ro, "Cooling enhancement in an air-cooled finned heat exchanger by thin water film evaporation," *International Journal of Heat and Mass Transfer,* p. 1241–1249, Vol. 46 2003.

[66] H. El-Dessouky, H. Ettouney and S. Al-Zeefari, "Performance analysis of two-stage evaporative coolers," *Chemical Engineering Journal,* p. 255–266, Vol. 102, 2004.

[67] J. Lebrun, C. A. Silva, F. Trebilcock and E. Winandy, "Simplified models for direct and indirect contact cooling towers and evaporative condensers," *Building Services Engineering Research& Technology,* p. 25–31, Vol. 25, 2004.

[68] F. J. Rey Martinez, E. V. Gómez, R. H. Martin, J. M. Gutiérrez and F. V. Diez, "Comparative study of two different evaporative systems: an indirect evaporative cooler and a semi-indirect ceramic evaporative cooler," *Energy and Buildings,* p. 696–708, Vol. 36, 2004.

[69] J. C. Kloppers and D. G. Kröger, "The Lewis factor and its influence on the performance prediction of wet-cooling towers," *International Journal of Thermal Sciences,* p. 879–884, Vol. 44, 2005.

[70] M. N. Golubovic, H. D. Hettiarachchi, W. Belding and W. M. Worek, "A new method for the experimental determination of Lewis' relation," *International Communications in Heat and Mass Transfer,* p. 929–935, Vol. 33, 2006.

[71] R. Chengqin and Y. Hongxing, "An analytical model for the heat and mass transfer processes in indirect evaporative cooling with parallel/counter flow configurations," *International Journal of Heat and Mass Transfer,* p. 617–27, Vol. 49, 2006.

[72] H. D. M. Hettiarachchi, D. Golubovic, F. Mihajlo and W. M. Worek, "The effect of longitudinal heat conduction in cross flow indirect evaporative air coolers," *Applied Thermal Engineering,* p. 1841–1848, Vol. 27, 2007.

[73] G. Qiu, "A Novel Evaporative/Desiccant Cooling System," *A Thesis submitted to the The University of Nottingham for the degrees of Doctor of Philosophy,* 2007.

[74] S. Alizadeh, "Performance of a solar liquid desiccant air conditioner – an experimental and theoretical approach," *Solar Energy,* p. 563–572, Vol. 82, 2008.

[75] X. Zhao, S. Yang, Z. Duan and S. B. Riffat, "Feasibility study of a novel dew point air conditioning system for China building application," *Building and Environment,* p. 1990–1999, Vol. 44, 2009.

[76] E. Kozubal and S. Slayzak, "Coolerado 5 Ton RTU performance: western cooling challenge results," *National Renewable Energy Laboratory,* 2009.

[77] M. F. Farahani, G. Heidarinejad and S. Delfani, "A two-stage system of nocturnal radiative and indirect evaporative cooling for conditions in Tehran," *Energy and Buildings,* p. 2131–2138, Vol. 42, 2010.

[78] S. Anisimov and V. M. D. Vasiljev, "Heat and Mass Transfer in Plastic Indirect Evaporative Air Cooler under Combined Flow Conditions," in *Proceedings of Healthy Buildings Conference*, Espoo, Finland, 2000.

[79] T. Miyazaki, A. Akisawa and I. Nikai, "The cooling performance of a building integrated evaporative cooling system driven by solar energy," *Energy and Buildings,* p. 2211–2218, Vol. 43, 2011.

[80] S. Jaber and S. Ajib, "Evaporative cooling as an efficient system in Mediterranean region," *Applied Thermal Engineering,* p. 2590–2596, Vol. 31, 2011.

[81] W. Chen, "Thermal analysis on the cooling performance of a wet porous evaporative plate for building," *Energy Conversion and Management,* p. 2217–2226, Vol. 52, 2011.

[82] R. K. Kulkarni and S. P. S. Rajput, "Performance evaluation of two stage indirect/ direct evaporative cooler with alternative shapes and cooling media in direct stage," *International Journal of Applied Engineering Research,* p. 1–13, Vol. 1, 2011.

[83] F. Bruno, "On-site experimental testing of a novel dew point evaporative cooler," *Energy and Buildings,* p. 3475–3483, Vol. 43, 2011.

[84] E. Tavakoli and R. Hosseini, "Numerical analysis of 3D cross flow between corrugated parallel plates in evaporative coolers," *Energy Conversion and Management,* p. 884–892, Vol. 52, 2011.

[85] M. Farmahini-Farahani and H. Heidarinejad, "Increasing effectiveness of evaporative cooling by pre-cooling using nocturnally stored water," *Applied Thermal Engineering,* p. 117–123, Vol. 38, 2012.

[86] H. Caliskan, I. Dincer and A. Hepbasli, "A comparative study on energetic, exergetic and environmental performance assessments of novel M-Cycle based air coolers for buildings," *Energy Conversion and Management,* p. 69–79, Vol. 56, 2012.

[87] H. Caliskan, I. Dincer and A. Hepbasli, "Thermodynamic analyses and assessments of various thermal energy storage systems for buildings," *Energy Conversion and Management,* p. 109–122, Vol. 62, 2012.

[88] W. M. Worek, M. Khinkis, D. Kalensky and V. Maisotsenko, "Integrated Desiccant-Indirect Evaporative Cooling System Utilizing the Maisotsenko Cycle," *Proc. of the ASME 2012 Summer Heat Transfer Conf., HT2012-58039,* 2012.

[89] P. Finocchiaro, M. Beccali and B. Nocke, "Advanced solar assisted desiccant and evaporative cooling system equipped with wet heat exchangers," *Solar Energy,* p. 608–18, Vol. 86, 2012.

[90] R. Boukhanouf, A. Alharbi, H. G. Ibrahim and M. Kanzari, "Investigation of a sub-wet bulb temperature evaporative cooler for buildings," *Proceedings of Sustainable Building Conference,* pp. 70-79, 2013.

[91] M. Kanzari, R. Boukhanouf and H. G. Ibrahim, "Mathematical modeling of a sub-wet bulb temperature evaporative cooling using porous ceramic materials," *International Journal of Chemical, Materials Science and Engineering,* p. 147–153, Vol. 7, 2013.

[92] J. Woods and E. Kozubal, "A desiccant-enhanced evaporative air conditioner: Numerical model and experiments," *Energy Conversion and Management,* p. 208–220, Vol. 65, 2013.

[93] I. Uçkan, T. Yılmaz, E. Hürdogan and O. Büyükalaca, "Experimental investigation of a novel configuration of desiccant based evaporative air conditioning system," *Energy Conversion and Management,* p. 606–615, Vol. 65, 2013.

[94] J. Lee, B. Choi and D. Lee, "Comparison of configurations for a compact regenerative evaporative cooler," *International Journal of Heat and Mass Transfer,* p. 192–198, Vol. 65, 2013.

[95] X. Cui, K. J. Chua, M. R. Islam and W. Yang, "Fundamental formulation of a modified LMTD method to study indirect evaporative heat exchangers," *Energy Conversion and Management,* p. 372–381, Vol. 88, 2014.

[96] M. Jradi and S. B. Riffat, "Experimental and numerical investigation of a dew point cooling system for thermal comfort in buildings," *Applied Energy,* p. 524–535, Vol. 132, 2014.

[97] S. A. El-Agouz and A. E. Kabeel, "Performance of desiccant air conditioning system with geothermal energy under different climatic conditions," *Energy Conversion and Management,* p. 464–475, Vol. 88, 2014.

[98] L. C. Sosa and G. Gómez-Azpeitia, "Cooling average potential of evaporative cooling system in dry warm climate," *Energy Procedia,* p. 2554–2563, Vol. 57, 2014.

[99] W. Z. Gao, Y. P. Cheng, A. G. Jiang, T. Liu and K. Anderson, "Experimental investigation on integrated liquid desiccant - Indirect evaporative air cooling system utilizing the Maisotesenko-Cycle," *Applied Thermal Engineering,* p. 288–296, Vol. 88, 2015.

[100] H. Montazeri, B. Blocken and J. L. M. Hensen, "CFD analysis of the impact of physical parameters on evaporative cooling by a mist spray system," *Applied Thermal Engineering,* p. 608–622, Vol. 75, 2015.

[101] D. Q. Zenga, H. Li, Y. J. Dai and A. X. Xie, "Numerical analysis and optimization of a solar hybrid one-rotor two-stage desiccant cooling and heating system," *Applied Thermal Engineering,* p. 474–483, Vol. 73, 2015.

[102] E. G. Cruz and E. Krüger, "Evaluating the potential of an indirect evaporative passive cooling system for Brazilian dwellings," *Building and Environment,* p. 265–273, Vol. 87, 2015.

[103] G. Heidarinejad and S. Moshari, "Novel modeling of an indirect evaporative cooling system with cross-flow configuration," *Energy and Buildings,* pp. 351-362, Vol. 92, 2015.

[104] X. Cui, K. J. Chua, M. R. Islam and K. C. Ng, "Performance evaluation of an indirect pre-cooling evaporative heat exchanger operating in hot and humid climate," *Energy Conversion and Management,* p. 140–150, Vol. 120, 2015.

[105] H. H. Balyani, A. Sohani, H. Sayyaadi and R. Karami, "Acquiring the Best Cooling Strategy Based on Thermal Comfort and 3E Analyses for Small Scale Residential Buildings at Diverse Climatic Conditions," *International Journal of Refrigeration,* p. 112–137, Vol. 57, 2015.

[106] C. Wani, S. Ghodke and C. Shrivastava, "A Review on Potential of Maisotsenko Cycle in Energy Saving Applications Using Evaporative Cooling," *International Journal of Advance Research in Science, Engineering and Technology ,* pp. 15-20, Vol. 01, 2012.

[107] D. La, Y. Dai, Y. li, R. Wang and T. Ge, "Technical development of rotary desiccant dehumidification and air conditioning: A review," *Renewable and Sustainable Energy Reviews,* pp. 130-147, Vol. 14, 2010.

[108] K. Chua, S. Chou, W. Yang and J. Yan, "Achieving better energy-efficient air conditioning – A review of technologies and strategies," *Applied Energy,* pp. 87-104, Vol. 104, 2013.

[109] L. Zaheed and R. Jachuck, "Review of polymer compact heat exchangers, with special emphasis on a polymer film unit," *Applied Thermal Engineering ,* p. 2323–2358, Vol. 24, 2004.

[110] T. Urbas, "Onet," 1 2016. [Online]. Available: http://urbas.blog.onet.pl/.

[111] D. Tertipis, Modelling and experimental evaluation of evaporative cooling systems, Athens, Greece: Thesis submitted to the University of Athens for the degrees of Doctor of Philosophy, 2014.

[112] B. Weerts, NSIDC green data center project: Coolerado and modeling an application of the Maisotsenko cycle, Boulder, CO, USA: Thesis submitted to the Faculty of the Graduate School of the University of Colorado for the degrees of Master of Science Civil Engineering, 2012.

[113] S. Anisimov and D. Pandelidis, "Theoretical study of the basic cycles for indirect evaporative air cooling," *International Journal of Heat and Mass Transfer,* pp. 974-989, Vol. 84, 2015.

[114] V. Bogoslovski and M. Poz, Fundamentals of physics of heating, ventilation and air conditioning units design (in Russian), Moscow, Russia: Strojizdat, 1983.

[115] S. Patankar, Numerical heat and mass transfer and fluid flow, Washington DC: Hemisphere Publishing Corp. , 1980.

[116] R. Shah and D. Sekulic, Fundamentals of heat exchanger design, Hoboken, NJ, USA: John Wiley & Sons Inc, 2003.

[117] W. Kays and A. London, Compact Heat Exchangers, McGraw Hill, NY, USA, 1984.

[118] S. Anisimov and A. Ermoshkin, *Analysis of counter-flow indirect evaporative air coolers,* Sankt Petersburg, Russia, 1991.

[119] R. Holmberg, "Sensible and latent heat transfer in cross-counter-flow gas-to-gas heat exchanger," *ASME Journal of Heat Transfer,* p. 173–7, Vol. 111, 1989.

[120] A. Žukauskas and J. Žiugžda, Heat transfer in laminar flow of fluid (in Russian), Vilnius, Lithuania: Mintis, 1969.

[121] W. Lewis, "The evaporation of liquid into a gas – a correction," *Mechanical Engineer,* p. 567–573, Vol. 55, 1933.

[122] W. Lewis, "The evaporation of liquid into a gas," *Transactions of ASME,* pp. 325-340, Vol. 44, 1922.

[123] L. Berman, Evaporative cooling of circulating water (in Russian), Gosenergoizdat, Russia, 1957.

[124] L. Berman, "On the validity of the analogy between heat and mass transfer and the Lewis relation in air conditioning units and cooling towers (in Russian)," *Refrigerating Technics,* pp. 34-37, Vol. 2, 1974.

[125] V. Bogoslovski and S. Bulkin, "Heat transfer calculation between air and water (in Russian)," in *Thermal Conditions in Building Structures, Ventilation, Air Conditioning and Heat Supply Systems*, Snakt Petersburg, Russia , 1980, pp. 20-23.

[126] A. Guhman, Application of the theory of similarity to the study of heat and mass transfer processes (in Russian), Moscow, Russia: High School, 1974.

[127] O. Kokorin, Evaporative cooling for the purposes of air-conditioning (in Russian), Moscow, Russia: Stoizdat, 1965.

[128] V. Maisotsenko, "Mathematical modeling of heat and mass transfer in regenerative indirect evaporative air coolers (in Russian)," *Refrigerating Technics,* pp. 40-43, Vol. 1, 1987.

[129] D. Pandelidis, S. Anisimov and W. Worek, "Comparison study of the counter-flow regenerative evaporative heat exchangers with numerical methods," *Applied Thermal Engineering,* pp. 211-224, Vol. 84, 2015.

[130] S. Anisimov and D. Pandelidis, "Heat and mass transfer processes in indirect evaporative air conditioners through the Maisotsenko cycle," *International Journal of Energy for Clean Environment,* p. 273–286 , Vol. 12, 2011.

[131] S. Anisimov, A. Jedlikowski and D. Pandelidis, "Frost formation in the cross-flow plate heat exchanger for energy recovery," *International Journal of Heat and Mass Transfer,* pp. 201-217, Vol. 90, 2015.

[132] S. Anisimov, D. Pandelidis and A. Jedlikowski, "Performance study of the indirect evaporative air cooler and heat recovery exchanger in air conditioning system during the summer and winter operation," *Energy,* pp. 205-225, Vol. 89, 2015.

[133] A. S. 133-2001, *Method of Testing Direct Evaporative Air Coolers,* 2001.

[134] D. Pandelidis and S. Anisimov, "Numerical analysis of the heat and mass transfer processes in selected M-Cycle heat exchangers for the dew point evaporative cooling," *Energy Conversion and Management,* pp. 62-83, Vol. 90, 2015.

[135] C. Coolerado, *M50 air conditioner brochure,* 2014.

[136] D. Pandelidis and S. Anisimov, "Numerical study of perforated indirect evaporative air cooler," *International Journal of Energy for a Clean Environment ("Special Issue on M-Cycle Fundamentals and Applications"),* pp. 239-250, Vol. 2-4, 2011.

[137] S. Anisimov and J. Żuchowicki, "Renewable energy utilization in indirect evaporative air coolers of air conditioning system," in *Proceedings of the Minian International Conference "Towards a Safe and Clean Environment" TSCE`05*, Minia-Hurghada, Egipt, 2005.

[138] S. Anisimov, D. Pandelidis and M. V., "Numerical analysis of heat and mass transfer processes through the Maisotsenko cycle," in *Proceedings of the 10th International Conference on Heat Transfer, Fluid Mechanics and Thermodynamics, HEFAT2014*, Orlando, Florida, USA, 2014.

[139] D. Pandelidis and S. Anisimov, "Application of a statistical design for analyzing basic performance characteristics of the cross-flow Maisotsenko cycle heat exchanger," *International Journal of Heat and Mass Transfer,* pp. 45-61, Vol. 95, 2016.

[140] S. Ahnazarova and V. Kafarov, Methods of optimization experiments in chemical technology, Moscow, Russia: MA, Graduate School, 1985.

[141] E. Betiku, O. Omilakin, S. Ajala, A. Okeleye, A. Taiwo and B. Solomon, "Mathematical modeling and process parameters optimization studies by artificial neural network and response surface methodology: A case of non-edible neem (Azadirachta indica) seed oil biodiesel synthesis," *Energy,* pp. 266-273, Vol. 72, 2014.

[142] D. Bas and I. Boyaci, "Modeling and optimization I: Usability of response surface methodology," *Journal of Food Engineering,* pp. 836-845, Vol. 78 2007.

[143] J. Harrington, "The desirability function," *Industrial Quality Control,* pp. 494-498, Vol. 21, 1965.

[144] H. Trautmann and C. Weihs, "On the distribution of the desirability function index using Harrington's desirability function," *Metrika,* p. 207–213, Vol. 62/2, 2006.

[145] S. Anisimov, " Optimization of heat and mass transfer in heat exchanger, used as indirect evaporative coolers in air conditioning system," in *Proceedings of the 6-th All-Russian HVAC Engineers Fellowship Congress*, Sankt-Petersburg, Russia, 1998.

[146] S. Anisimov, V. Vasiljev, S. Klimov and S. Bolotin, "Optimization of heat recovery in the heat exchangers used in air-conditioning units," in *Proceedings of the 23rd Multivariate Optimization and Computer Aided Design*, Mielno, Poland, 2005.

[147] J. Hendiger, P. Ziętek and M. Chludzińska, Wentylacja i klimatyzacja (in Polish), Warsaw, Poland: Venture Industries, 2009.

[148] T. I. R. f. U. D. o. E. DOE/GO-102007-2325, "Coolerado Cooler Helps to Save Cooling Energy and Dollars," www.eere.energy.gov/femp/, 2007.

[149] T. Kotruchow, "Budujemydom.pl," 1 2016. [Online]. Available: http://www.budujemydom.pl/wentylacja-i-klimatyzacja/11935-w-jakim-stopniu-klimatyzacja-obciaza-domowy-budzet.

[150] W. Gao, W. Worek, V. Konduru and K. Adensin, "Numerical study on performance of a desiccant cooling system with indirect evaporative cooler," *Energy and Buildings ,* p. 16–24, Vol. 86, 2015.

[151] C. Coolerado, *Energy Recovery Ventilator (ERV) brochure,* 2015.

[152] K. Rajski, Wymiana ciepła i masy w zraszanym wymienniku płytowym o prostokątnych kanałach powietrznych (in Polish), Wroclaw, Poland: A Thesis submitted to Wrocław University of Technology for the degree of Doctor of Philosophy, 2015.

## List of figure captions

Fig. 1.1. Energy consumption in XXIst century. (a) Energy consumption in EU, 2012 [3]. (b) Energy consumption in Poland, 2012 [4]. (c) Energy consumption in households worldwide, 2012 [5]. (d) Increase in air conditioning in American Households [6].

Fig. 1.2. The scheme of an ancient windcatcher [13].

Fig. 1.3. Evaporative cooling today. (a) A misting fan in Athens, Greece (author's photograph). (b) A traditional air cooler in Mirzapur, Uttar Pradesh, India [13].

Fig. 1.4. Direct evaporative air coolers. (a) Operation scheme. (b) Scheme of a typical DEC unit [18].

Fig. 1.5. Heat and mass transfer in DEC process

Fig. 1.6. Indirect evaporative cooling. (a) Heat and mass transfer on psychrometric chart. (b) ETA PAC air handling unit by corporation Euroclima equipped with double cross-flow indirect evaporative cooler [20]. (c) Parallel-flow IEC. (d) Counter-flow IEC. (e) Cross-flow IEC.

Fig. 1.7. Materials used for evaporative air coolers. (a) PVC package. (b) Aluminum package. (c) Metal wool porous structure. (d) Cellulose-blended fibre sheets. (e) Ceramic porous structure. (f) Rigid porous paper structure used for DEC packages.

Fig. 1.8. A combined system of indirect and direct evaporative air coolers.

Fig. 1.9. A combined system of indirect evaporative air cooler and typical cooling coil.

Fig. 1.10. Scheme of the typical SDEC system.

Fig. 1.11. SDEC system with IEC and air ground heat exchanger [34].

Fig. 1.12. System with nocturnal cooling or a water ground heat exchanger.

Fig. 1.13. The psychrometric interpretation of the Maisotsenko cycle in a regenerative HMX.

Fig. 1.14. Maisotsenko cycle development process. (a) Standard indirect evaporative air cooler. (b) Adiabatic counter-flow evaporative air cooler. (c) Regenerative M-Cycle evaporative air cooler. (d) Modified counter-flow evaporative air cooler with the M-Cycle.

Fig. 1.15. Cross-flow Maisotsenko cycle HMX. (a) Scheme of the unit. (b) Actual air cooler manufactured by Coolerado Corp. (author's photograph).

Fig. 1.16. The combined evaporative air cooler patented by Ray [52] in 1935.

Fig. 1.17. The regenerative M-Cycle air cooler patented by Maisotsenko [42] in 1976.

Fig. 1.18. One of the first versions of the cross-flow M-Cycle air cooler patented by Maisotsenko in 2002.

Fig. 1.19. Different versions of the cross-flow M-Cycle HMXs which were tested over the years (author's photograph).

Fig. 1.20. The Coolerado's hybrid H80 unit based on the M-Cycle HMX and a mechanical compression system [76]. (a) Operation scheme. (b) The actual unit.

Fig. 1.21. Testing bench used by Riangvilaikul and Kumar [9].

Fig. 1.22. ISAW TAC-150 cross-flow M-Cycle HMX investigated by Zhao et al. [43]. (a) Unit's scheme. (b) Temperature distribution: primary and the working air strams.

Fig. 1.23. The SDEC system with the M-Cycle HMX.

Fig. 1.24. Scheme of the M-Cycle HMX analyzed in this study.

Fig. 1.25. Structure of the M-Cycle HMX analyzed in this study (author's photographs). (a) The general look of the structure. (b) Dry and wet channels. (c) Connection of two HMXs in one unit with the water tank. (d) Dry channels structure (single HMX). (e) Wet channels structure (single HMX).

Fig. 1.26. Dry and wet channels of the M-Cycle HMX analyzed in this study. (a) Dry channels. (b) Wet channels.

Fig. 1.27. Different arrangements of the initial part in the cross-flow M-Cycle air cooler. (a) Ideal arrangement (dense perforation). (b) Currently produced arrangement obtained with the numerical results. (c) Different

arrangements tested at the Coolerado Corp. part 1. (d) Different arrangements tested at the Coolerado Corp. part 2.

Fig. 2.1. Basic cycles for indirect evaporative air cooling analyzed in the section. (a) parallel-flow (P). (b) counter-flow (C). (c) cross-flow (CR). (d) regenerative flow (R).

Fig. 2.2. Schematic of heat and mass transfer in differential control volumes in the product part of the investigated HMXs. (a) parallel-flow exchanger. (b) counter-flow and regenerative exchangers. (c) cross-flow exchanger.

Fig. 2.3. Initial conditions at the entrance to appropriate air channels. (a) Parallel-flow HMX. (b) Counter-flow HMX. (c) Regenerative HMX. (d) Cross-flow HMX.

Fig. 2.4. Combined heat and mass transfer analysis for the basic evaporative cycles. (a) Psychrometric chart. (b) Temperature distribution in parallel-flow IEC. (c) Temperature distribution in counter-flow IEC. (d) Temperature distribution in regenerative IEC. (e) Temperature distribution in cross-flow IEC. (f) Humidity ratio distribution in parallel-flow IEC. (g) Humidity ratio distribution in counter-flow IEC. (h) Humidity ratio distribution in regenerative IEC. (i) Humidity ratio distribution in cross-flow IEC.

Fig. 2.5. Water film temperature distribution. (a) Parallel-flow IEC. (b) Counter-flow IEC. (c) Regenerative IEC. (d) Cross-flow IEC.

Fig. 2.6. Characteristic effectiveness indexes as a function of dimensionless operating parameters. (a) Dew point effectiveness as a function of $W_2/W_1$ ratio. (b) Dew point effectiveness as a function of $NTU_1$ number. (c) Specific cooling capacity as a function of $W_2/W_1$ ratio. (d) Specific cooling capacity as a function of $NTU_1$ number.

Fig. 3.1. M-Cycle heat and mass exchanger structure. 1: primary airflow. 2: working airflow (wet channels in product part). 3: working airflow (dry channels in initial part). 4: working airflow (wet channels in initial part).

Fig. 3.2. Maisotsenko cycle HMX structure characteristics (all photographs are made by author). (a) Structure of wet and dry channels with nomenclature. (b) General view of the device. (c) Channels structure. (d) Dry channel with coating material. (d) ) Wet channel with wicking material.

Fig. 3.3. Maisotsenko Cycle mathematical model assumptions for the air streams. (a) Dry channels. (b) Wet channels.

Fig. 3.4. Schematic of heat and mass transfer in differential control volumes in the product part of the investigated HMX. (a) At the entrance part of the wet channel (detail view on the wet channel). (b) At the entrance part of the wet channel (detail view on the dry channel). (c) At the exit part of the wet channel (detail view on the wet channel). (d) At the exit part of the wet channel (detail view on the dry channel). (e) For the dry channel fin. (f) For the wet channel fin at the entrance part of the wet channel. (g) For the wet channel fin at the exit part of the wet channel.

Fig. 3.5. A schematic of the fin geometry and details of thermal boundary conditions for the fins in dry and wet channels.

Fig. 3.6. A schematic of the "ideal" perforation in the initial part of the cross-flow Maisotsenko cycle air cooler.

Fig. 3.7. Maisotsenko Cycle mathematical model calculation algorithm illustrations. (a) Processes in the product part. (b) Processes in the wet channels of the initial part (working air stream 4). (c) Processes in the dry channels of the initial part (working air stream 3).

Fig. 4.1. Testing bench at Coolerado Corporation facilities in Denver, CO, USA (all photographs are made by author). (a) General scheme of the measurement station. (b) Photo of the bench inside the test chamber. (c) Three-dimensional visualization of the testing bench inside test chamber with all equipment. (d) Three-dimensional visualization of the pre-condition unit. (e) Thermometers used in the experiment. (f) Photo of the testing chamber. (g) Manometer used in the experiment. (h) Calibration of the Omega K-type thermocouple used for measuring the wet bulb temperature inside the channels of the exchanger (comparison of probe with the primer paint and probe cover with wetted material).

Fig. 4.2. (a) Photo of the dry plate (all photographs are made by author). (b) Photograph of the wet plate. (c) Infra-red photograph of the product part of the exchanger. (d) Infra-red photograph of the exhaust part of the exchanger. (e) Measuring points inside the dry part of the exchanger: scheme. (f) Measuring points inside the wet part of the exchanger: scheme. (g) Measuring points inside the dry part of the exchanger: channel plate with the signed points. (h) Measuring points inside the wet part of the exchanger: channel plate with the signed points.

Fig. 4.3. Comparison between model and experiment under variable inlet air temperature at different levels of humidity ratio. (a) Average outlet product airflow temperature $\bar{t}_{1o}$. (b) Specific cooling capacity $\hat{Q}_G$ (respected to 1 kg/s of product airflow). (c) Wet bulb effectiveness $\varepsilon_{WB}$. (d) Dew point effectiveness $\varepsilon_{DP}$.

Fig. 4.4. Comparison between model and experiment under variable airflow rate. (a) Average outlet product airflow temperature $\bar{t}_{1o}$ .(b) Specific cooling capacity $\hat{Q}_G$ . (c) Wet bulb effectiveness $\varepsilon_{WB}$ . (d) Dew point effectiveness $\varepsilon_{DP}$ .

Fig. 4.5. Correlation between the model and the experiment. (a) Average outlet temperature of the primary flow $t1o$. (b) Average outlet temperature of the working flow $t2o$. (c) Average outlet humidity ratio of the working flow $x2o$. (d) Wet bulb effectiveness.

Fig. 4.6. Comparison of temperature distribution across the channels of the exchanger. (a) Profiles of primary and working air temperature in the dry channel. (b) Profiles of working air temperature in the wet channel. (c) Profiles of primary and working air temperature in the dry channel. (d) Profiles of working air temperature in the wet channel.

Fig. 4.7. Comparison of temperature distribution across the channels of the exchanger. (a) Profiles of primary air temperature in the dry channel: experiment. (b) Profiles of primary air temperature in the dry channel: model. (c) Profiles of working air temperature in the wet channel: experiment. (d) Profiles of working air temperature in the wet channel: model.

Fig. 4.8. Psychrometric paths of the working air stream inside the heat exchanger. (a) For the dry channel 1 and wet channels $A–F$: experiment. (b) For the dry channel 1 and wet channels $A–F$: model. (c) For the dry channel 1 and 2 and wet channels $G–L$: experiment. (d) For the dry channel 1 and 2 and wet channels $G–L$: model.

Fig. 5.1. Simulation results for the initial part of the HMX. (a) Heat and mass transfer processes on the psychrometric chart. (b) Air stream 3 temperature distribution (dry channel). (c) Temperature and humidity ratio profiles (average values) in the wet channel along $Y$ axis (exchanger with 10 holes). (d) Temperature and humidity ratio profiles (average values) in the wet channel along $Y$ axis (exchanger with 20 holes). (e) Air stream 4 temperature distribution: surface plot. (f) Air stream 4 humidity ratio distribution: surface plot.

Fig. 5.2. Simulation results for the product part. (a) Heat and mass transfer processes on the psychrometric chart. (b) Average heat flux distribution along the $Y$ axis. (c) Local sensible and latent heat flux distribution along the $Y$ axis (section $X=0.5$) - bar chart. (d) Local sensible and latent heat flux distribution along the $Y$ axis (section $X=1.0$)- bar chart. (e) Air stream 2 temperature distribution: surface plot. (f) Air stream 1 temperature distribution: surface plot.

Fig. 5.3. Dry channels characteristics (nomenclature $1^{st},2^{nd}$…: number of dry initial part channels; $1_{st}$; $2_{nd}$…: number of product part channels). (a) Original HMX (V0). (b) Variant 1 (V1). (c) Variant 2 (V2). (d) Variant 3 (V3). (e) Variant 4 (V4). (f) Variant 5 (V5). (g) Variant 6 (V6). (h) Variant 7 (V7).

Fig. 5.4. Wet channels characteristics (nomenclature $1^{st},2^{nd}$…: number of wet working air channels). (a) Original HMX (V0). (b) Variant 1 (V1). (c) Variant 2 (V2). (d) Variant 3 (V3). (e) Variant 4 (V4). (f) Variant 5 (V5). (g) Variant 6 (V6). (h) Variant 7 (V7).

Fig. 5.9. Simulation results for heat transfer surface. (a) Average latent and sensible heat flux on the plate and fins surface- exchanger with the flat channels (bar chart along the $X$ axis). (b) Average latent and sensible heat flux on the plate and fins surface- exchanger with flat channels (bar chart along the $Y$ axis). (c) Local latent and sensible heat flux on the plate and fins surface- exchanger with the square channels (bar chart along the $X$ axis: section $Y$-0.5). (d) Local latent and sensible heat flux on the plate and fins surface- exchanger with the square channels (bar chart along the $X$ axis: section $Y$-1.0). (e) Local latent and sensible heat flux on the plate and fins surface- exchanger with the triangle channels (bar chart along the $X$ axis: section $Y$-0.5). (f) Local latent and sensible heat flux on the plate and fins surface- exchanger with the triangle channels (bar chart along the $X$ axis: section $Y$-1.0). (g) Outlet temperature and specific cooling capacity $QG$ for the different $\lambda$ coefficient values (■- HMX with square channels; ▲ - HMX with triangle channels; ▬- HMX with flat channels). (h) Outlet temperature and specific cooling capacity $QG$ for different $\sigma$ coefficient values (HMX with flat channels).

Fig. 6.1. Impact of air inlet parameters on cooling effectiveness. (a) Dew point effectiveness and outlet product air temperature as a function of inlet air temperature (constant inlet relative humidity). (b) Specific cooling capacity and outlet product air temperature as a function of inlet air temperature (constant inlet relative humidity). (c) Dew point effectiveness and outlet product air temperature as a function of inlet air relative humidity (constant inlet temperature). (d) Specific cooling capacity and outlet product air temperature as a function of inlet air relative humidity (constant inlet temperature). (e) Impact of the inlet relative humidity on the

dew point effectiveness. (f) Dew point effectiveness and outlet product air temperature as a function of inlet air temperature (constant inlet humidity ratio). (g) Specific cooling capacity and outlet product air temperature as a function of inlet air temperature (with constant inlet humidity ratio).

Fig. 6.2. Impact of exchanger geometry on cooling efficiency. (a) Dew point effectiveness and outlet product air temperature as a function of channel height (HMX with flat channels). (b) Specific cooling capacity and outlet product air temperature as a function of channel height (HMX with flat channels). (c) Dew point effectiveness and outlet product air temperature as a function of $L_X$ ( ■- HMX with square channels; ▲- HMX with triangle channels; ▬- exchanger with flat channels). (d) Specific cooling capacity and outlet product air temperature as a function of $L_X$. (e) Dew point effectiveness and outlet product air temperature as a function of $L_Y$ (HMX with flat channels). (f) Specific cooling capacity and outlet product air temperature: function of $L_Y$ (HMX with flat channels).

Fig. 6.3. Impact of operational parameters on cooling effectiveness. (a) Dew point effectiveness and outlet air temperature as a function of airflow velocity. (b) Specific cooling capacity and outlet air temperature as a function of airflow velocity. (c) Dew point effectiveness and outlet air temperature as a function of $W_2/W_1$ ratio. (d) Specific cooling capacity and outlet air temperature as a function of $W_2/W_1$ ratio.

Figure 7.1. Different versions of the airflow arrangement in the M-Cycle heat and mass exchangers. (a) Modified counter- flow HMX. (b) Regenerative HMX. (c) Regenerative HMX with perforation. (d) Cross-flow HMX. (e) Modified cross-flow HMX.

Figure 7.2. Airflow distribution in the dry and wet channels. (a) Modified counter-flow HMX (V1). (b) Regenerative HMX with perforation (V3). (c) Modified cross-flow HMX (V5).

Fig. 7.3. Numerical simulation results. (a) Average outlet product air temperature $t1o$ and specific cooling capacity $Q$ vs. inlet air temperature (at constant inlet air relative humidity). (b) $t1o$ and $Q$ vs. inlet air relative humidity (at constant inlet air temperature). (c) $t1o$ and $Q$ vs primary airflow velocity (at constant inlet air parameters). (d) $t1o$ and $Q$ vs NTU (at constant inlet air parameters). (e) Wet bulb effectiveness vs NTU (at constant inlet air parameters). (f) $t1o$ and $Q$ vs. S/P ratio (at constant inlet air parameters).

Figure 7.4. Temperature and heat flux distribution in the channels of the considered HMXs. (a) Temperature distribution for V1 HMX. (b) Temperature distribution for V2 HMX. (c) Temperature distribution for V3 HMX. (d) Temperature distribution for V4 HMX. (e) Temperature distribution for V5 HMX. (f) Heat flux distribution for units V1−V5.

Fig. 8.1. Analyzed HMXs. (a) Original cross-flow HMX (HMX1). (b) Modified cross-flow HMX (HMX2).

Fig. 8.2. Analyzed heat exchangers in different applications for air conditioning systems. (a) HMX1 in air conditioning system with fan coils. (b) HMX2 in air conditioning system with fan coils. (c) HMX2 in air conditioning system with heat pump. (d) HMX1 in air conditioning system with desiccant wheel.

Fig. 8.3. Simulation results for HMXs operating in different air conditioning systems. (a) Outlet temperatures HMX1: t1i=30°C; RH1i=25 to 50%; HMX2: t1i=30°C; t3i=21 to 26°C; RH3i=40 to 60%. (b) Heat flux distribution inside the primary air channels. (c) Outlet temperatures: HMX1: t1i=32.5°C; RH1i=20 to 50%; HMX2: t1i=30°C; t3i=21 to 26°C;  RH3i=40 to 60%. (d) Outlet temperatures: HMX1: t1i=35°C; RH1i=20 to 50%; HMX2: t1i=30°C; t3i=21 to 26°C; RH3i=40 to 60%.

Fig. 8.4. Heat recovery units before the HMX1. (a) System with cross-flow recuperator; (b) System with recirculation. (c) Simulation results for the HMX1 operating with heat recovery unit, recirculation and desiccant wheel.

Fig. 8.5. Basic unit for the analysis (dry and wet channels with numeration respectively).

Fig. 8.6. Assumed airflow distributions inside the wet channels. (a) Even airflow distribution. (b) Uneven airflow distribution: 40% of the working air stream is transferred through the first five channels. (c) Uneven airflow distribution: 45% of the working air stream is transferred through the first five channels. (d) Uneven airflow distribution: 60% of the working air stream is transferred through the first five channels.

Fig. 8.7. Impact of uneven airflow distribution on the cooling performance. (a) Outlet air temperature- function of inlet air temperature. (b) Outlet air temperature- function of the primary airflow rate. (c) Cooling capacity- function of inlet air temperature. (d) Cooling capacity- function of the primary airflow rate. (e) $COP_1$- function of inlet air temperature. (f) $COP_1$- function of the primary airflow rate. (g) $COP_{1+2}$- function of inlet air temperature. (h) $COP_{1+2}$- function of the primary airflow rate.

Fig. 8.8. Different methods of achieving even airflow distribution. (a) Increasing hydraulic resistance of the channels at the entry region. (b) Using a Tichelmann airflow scheme. (c) Suggested location of the exhaust diffuser in Coolerado units to create the Tichelmann airflow scheme.

Fig. 8.9. Assumed heat exchangers. (a) Basic unit- 1. (b) Basic unit with additional dry working air channel- 2. (c) Basic unit with two additional dry working air channels- 3.

Fig. 8.10. Influence of the size of the initial part on the cooling performance. (a) Outlet air temperature- function of inlet air temperature. (b) Outlet air temperature- function of primary airflow rate. (c) Cooling capacity- function of inlet air temperature. (d) Cooling capacity- function of primary airflow rate. (e) $COP_1$- function of inlet air temperature. (f) $COP_1$- function of primary airflow rate. (g) $COP_{1+2}$- function of inlet air temperature. (h) $COP_{1+2}$- function of primary airflow rate.

Fig. 8.11. Assumed heat exchangers. (a) Basic unit- 1. (b) Unit with six primary air channels and two dry working air channels- 2. (c) Unit with five primary air channels and three dry working air channels- 3.

Fig. 8.12. Impact of increasing the initial part at cost of product part on cooling performance. (a) Outlet air temperature- function of inlet air temperature. (b) Outlet air temperature- function of the primary airflow rate. (c) Cooling capacity- function of inlet air temperature. (d) Cooling capacity- function of the primary airflow rate. (e) $COP_1$- function of inlet air temperature. (f) $COP_1$- function of the primary airflow rate. (g) $COP_{1+2}$- function of inlet air temperature. (h) $COP_{1+2}$- function of the primary airflow rate.

Fig. 8.14. Simulation results for constant inlet relative humidity and variable temperature. (a) Outlet temperatures. (b) Wet bulb effectiveness.

Fig. 8.16. Impact of inlet air humidity on cooling effectiveness. (a) Outlet air temperatures (constant inlet air temperature, variable inlet relative humidity). (b) Wet bulb effectiveness (constant inlet air temperature, variable inlet relative humidity). (c) Outlet air temperatures (constant inlet humidity ratio). (d) Wet bulb effectiveness (constant inlet humidity ratio). (e) Cooling capacity (constant inlet humidity ratio).

Fig. 8.16. Simulation results for different airflow rates. (a) Outlet air temperatures for variable primary and working airflow (working to primary airflow ratio equal 1). (b) Cooling capacity for variable primary and working airflow (working to primary airflow ratio equal 1). (c) Impact of variable working and primary airflow on outlet air temperatures for V0,V4 and V7 units. (d) Impact of different working to primary airflow ratios on cooling performance of selected units.

Fig. 9.1. Independent variables chosen for the modeling purpose

Fig. 9.2. The coefficients of determination $R^2$ for regression equations of the analyzed factors. (a) Outlet product airflow temperature. (b) Specific cooling capacity. (c) Dew point effectiveness. (d) COP.

Fig. 9.3. Single-parameter optimization results. (a) Influence of $G_1$ on $\varepsilon_{DP}$. (b) Influence of $G_1$ on $\hat{Q}$. (c) Influence of $G_1$ on COP. (d) Influence of $\overline{l}_Y^{work}$ on $\varepsilon_{DP}$. (e) Influence of $\overline{l}_Y^{work}$ on $\hat{Q}$. (f) Influence of $\overline{l}_Y^{work}$ on COP. (g) Influence of $W_2/W_1$ on $\varepsilon_{DP}$. (h) Influence of $W_2/W_1$ on $\hat{Q}$. (i) Influence of $W_2/W_1$ on COP.

Fig. 9.4. The unitless scales of desirability for individual efficiency indexes.

Fig. 9.5. Ternary plots obtained from the simplex-lattice design for inlet airflow conditions $t_{1i}$ = 32.5°C and $RH_{1i}$ = 50%. (a) Impact of weights values on the Harrington function. (b) Impact of weights values on the $G_1^{opt}$. (c) Impact of weights values on the $(W_2/W_1)^{opt}$. (d) Impact of weights values on the $(\overline{l}_Y^{work})^{opt}$. (e) Impact of weights values on the $(\varepsilon_{DP})^{opt}$. (f) Impact of weights values on $d_1(\varepsilon_{DP})^{opt}$. (g) Impact of weights values on the $(\hat{Q})^{opt}$. (h) Impact of weights values on the $d_2(\hat{Q})^{opt}$. (i) Impact of weights values on the $(COP)^{opt}$. (j) Impact of weights values on the $d_3(COP)^{opt}$.

Fig. 9.6. Character of the Desirability Index $D$ under conditions $t_{1i}$ = 32.5°C and $RH_{1i}$ = 50%. (a) At the fixed level of the $W_2/W_1$: contour plot. (b) At the fixed level of the $W_2/W_1$: three-dimensional plot. (c) At the fixed level of the $\overline{l}_Y^{work}$: contour plot. (d) At the fixed level of the $\overline{l}_Y^{work}$: three-dimensional plot. (e) At the fixed level of the $G_1$: contour plot. (f) At the fixed level of the $G_1$: three-dimensional plot.

Fig. 9.7. Character of the Desirability Index. (a) At the fixed level of the $W_2/W_1$, $t_{1i}$ = 25.0°C and $RH_{1i}$ = 30%. (b) At the fixed level of the $W_2/W_1$, $t_{1i}$ = 40.0°C and $RH_{1i}$ = 70%. (c) at the fixed level of the , $t_{1i}$ = 25.0°C and $RH_{1i}$ = 30%. (d) At the fixed level of the $\overline{l}_Y^{work}$, $t_{1i}$ = 40.0°C and $RH_{1i}$ = 70%. (e) at the fixed level of the $G_1$, $t_{1i}$ =

25.0°C and $RH_{1i}$ = 30%. (f) At the fixed level of the $G_1$, $t_{1i}$ = 40.0°C and $RH_{1i}$ = 70%.(g) At the fixed level of the $G_1$=0.1, $W_2/W_1$=0.6, $\overline{l_y^{work}}$ =0.125. (h) At the fixed level of the $G_1$=0.26, $W_2/W_1$=1.4, $\overline{l_y^{work}}$ =0.625.

Fig. 9.8. Optimal individual values of influence factors at different climate conditions. (a) Primary air mass flow rate. (b) Working to primary air ratio. (c) Relative length of the initial part of exchanger.

Fig. 9.9. Climatic zones of preferable application of the HMX. (a) Contour plot. (b) Three-dimensional plot.

Fig. 10.1. Analyzed systems. (a) AHU with the M-Cycle unit. (b) AHU with the rotary heat exchanger. (c) Coolerado AHU with 240 M-Cycle HMXs blocked in one device (with cooling capacity equal 315 kW). (d) Scheme of the system with mixing ventilation. (e) Scheme of the system with displacement ventilation.

Fig. 10.2. Outlet air temperatures obtained by the HMX in Wroclaw climate.

Fig. 10.3. Comparison between AC system with the M-Cycle HMX and traditional AC system. (a) Coverage of the required cooling capacities for "south room": M-Cycle system. (b) Coverage of the required cooling capacities for "south room": traditional system. (c) Coverage of the required cooling capacities for "west room": M-Cycle system. (d) Coverage of the required cooling capacities for "west room": traditional system. (e) Coverage of the required cooling capacities for "east room": M-Cycle system. (f) Coverage of the required cooling capacities for "east room": traditional system.

Fig. 10.4. Comparison between AC system with the M-Cycle HMX and traditional AC system on psychrometric chart. (a) "South room": M-Cycle system. (b) "South room": traditional system.

Fig. 10.5. Comparison between AC system with the M-Cycle HMX and traditional AC system. (a) Coverage of the required cooling capacities for "south room": M-Cycle system. (b) Coverage of the required cooling capacities for "south room": traditional system. (c) Coverage of the required cooling capacities for "west room": M-Cycle system. (d) Coverage of the required cooling capacities for "west room": traditional system. (e) Coverage of the required cooling capacities for "east room": M-Cycle system. (f) Coverage of the required cooling capacities for "east room": traditional system.

Fig. 10.6. Comparison between AC system with the M-Cycle HMX and traditional AC system on psychrometric chart. (a) "South room": M-Cycle system. (b) "South room": traditional system.

Fig. 10.7. Comparison between AC system with the M-Cycle HMX and traditional AC system: daily operation costs. (a) Mixing ventilation. (b) Displacement ventilation.

Fig.10.8. Scheme of the typical SDEC system.

Fig. 10.9. Analyzed M-Cycle desiccant system. (a) The scheme of the system. (b) The scheme of the desiccant wheel.

Fig. 10.10. General scheme of the system with initial conditions.

Fig. 10.11. Comparison between traditional and novel desiccant air conditioning systems. (a) Traditional system. (b) System with the M-Cycle HMX. (c) System with the M-Cycle HMX and rotary heat exchanger.

Fig. 10.12. Impact of inlet ambient air temperature on the system performance.

Fig. 10.13. Impact of inlet ambient air humidity ratio on the system performance.

Fig. 10.14. Impact of regeneration air temperature on the system performance.

Fig. 10.15. Impact of airflow rates on the system performance. (a) Ambient airflow rate ($V_{reg}$=150 m³/h). (b) Regeneration airflow rate ($V_1$=600 m³/h).

Fig. 10.16. Impact of airflow rates on the system performance.

Fig. 10.17. Impact of humidity ratio change between supply and exhaust airflow on the system performance.

Fig. 10.18. Analyzed systems. (a) System 1. (b) System 2. (c) System 3.

Fig. 10.19. Assumptions for mathematical model. (a) Inlet conditions: System 1. (b) Inlet conditions: System 2. (c) Inlet conditions: System 3.

Fig. 10.20. Comparison under the same supply airflow rate. (a) Comparison under variable inlet temperature: supply air temperatures. (b) Comparison under variable inlet temperature: cooling capacities. (c) Comparison under variable inlet humidity ratio: supply air temperatures. (d) Comparison under variable inlet humidity ratio:

cooling capacities. (e) Comparison under variable regeneration air temperature: supply air temperatures. (f) Comparison under variable regeneration air temperature: cooling capacities.

Fig. 10.21. Comparison under the same dehumidified airflow rate. (a) Comparison under variable inlet temperature: supply air temperatures. (b) Comparison under variable inlet temperature: cooling capacities. (c) Comparison under variable inlet humidity ratio: supply air temperatures. (d) Comparison under variable inlet humidity ratio: cooling capacities. (e) Comparison under variable regeneration air temperature: supply air temperatures. (f) Comparison under variable regeneration air temperature: cooling capacities.

Fig. 10.22. Proposed modifications of System 3. (a) Modified System 3 with bypass. (b) Modified System 3 with bypass and rotary exchanger.

Fig. 10.23. Comparison of Modified System 3 with rotary exchanger with other solutions. (a) Supply air temperature. (b) Cooling capacity.

## List of table captions

Table 1.1. Prosperities of selected materials used of evaporative air coolers

150-250

Table 1.2. Parametric data chosen for analysis of the selected IEC units.

Table 2.1. Lewis factor values for selected $W_2/W_1$ ratios at $t_{1i}$=35°C, RH$_{1i}$=30%, NTU$_1$=2.3

Table 4.1. Assumed exchanger construction parameters

Table 5.1. Assumptions for numerical simulation channels type.

Table 7.1. Differences between inlet and outlet air temperatures ($t_{1i}$–$t_{1o}$) for two inlet conditions.

Table 7.2. Outlet air temperature $t_{1o}$ and specific cooling capacity $Q$ for inlet air temperature equal 30°C.

Table 7.3. Outlet air temperature $t_{1o}$ and specific cooling capacity $Q$ for inlet RH equal 45%.

Table 7.4. Outlet air temperature $t_{1o}$ and specific cooling capacity $Q$ for different air stream velocities.

Table 7.5. Outlet air temperature $t_{1o}$ and specific cooling capacity $Q$ for two levels of NTU.

Table 7.6. Outlet air temperature $t_{1o}$ and specific cooling capacity $Q$ for different levels of $W_2/W_1$.

Table 7.7. Optimal $W_2/W_1$ ratios for V2 HMX available in literature.

Table 7.8. Influence of selected operational parameters on efficiency of V1-V5 HMXs.

Table 8.1. The reference operating conditions for the analyzed exchangers

Table 8.2. Outlet temperature, specific cooling capacity and wet bulb effectiveness of HMX1 and HMX2

Table 8.3. Selected boundary temperature and relative humidity values for the exhaust air entering the working air channels in HMX2 allowing overcoming the performance of HMX1

Tab. 8.4. Lowest temperature of the pre-cooled working airflow in the dry channels

Tab. 8.5. Lowest temperature of the pre-cooled working airflow in the dry channels

Table 9.1. Independent variables and their coded and actual levels for CCD

Table 9.2. CCD setting in the original and coded form* of the independent parameters ($X_1…X_k$) and experimental results for the response variable $\hat{Y}_{1i}$ (outlet product airflow temperature $\bar{t}_{1o}$ )

Table 9.3. Repeatability and regression coefficients deviation

## Appendix A. Calculation algorithm of the model describing the cross-flow evaporative cooler

The following section presents the algorithm of calculations for the differential equations describing the cross-flow heat and mass exchanger. Algorithms for other exchangers is omitted, due to the fact that they were presented in existing studies [145]. Moreover, the algorithm for the cross-flow cooler is more complicated than of the other three coolers because it describes the calculation of the partial differential equations. It is important to study this algorithm as a basis for the analyzed M-Cycle unit, because it operates under the cross-flow scheme as well [134]. To discretize and numerically solve the developed set of differential-algebraic equations (i.e. (2.3), (2.9), (2.15), (2.18) and (2.20) from **Section 2** of presented thesis) the numerical method on the base of modified Runge-Kutta scheme is used to approximate derivatives over the uniform grid along the independent variables of $\bar{X}$ and $\bar{Y}$ (Figs. A1 and A2). The calculations were carried out by "*layer by layer*" in the working airflow direction ($\bar{Y}$-axis) starting from the initial section ($i=0$) ($\bar{X}=0$) (Fig. A2). The changes of the working airflow parameters within $(k, l)$-th elementary calculation cell from the node ($l-1$) to another ($l$) in the section ($i=k$) were determined on the base of the relevant *ordinary* differential equations applicable to the calculated elementary cell by fourth-order Runge-Kutta method (Fig A1(a) and A2(c))

$$\begin{cases} dt_2^{(k,l)}/d\bar{Y} = \mathrm{NTU}_2'' \left[ \left( \left(t_{p2}^{(k,l-1)}\right)' - t_2^{(k,l-1)} \right) += \right. \\ \left. + \left(\frac{\sigma_p}{\mathrm{Le}}\right)_2 \left(\frac{c_g}{c_p}\right)_2 \left( \left(t_{p2}^{(k,l-1)}\right)' - t_2^{(k,l-1)} \right) \left( \left(x_{p2}^{(k,l-1)}\right)' - x_2^{(k,l-1)} \right) \right] = \\ = \Omega \left( t_2^{(k,l-1)}, \left(t_{p2}^{(k,l-1)}\right)', x_2^{(k,l-1)}, \left(x_2^{(k,l-1)}\right)' \right) \\ dx_2^{(k,l)}/d\bar{Y} = \mathrm{NTU}_2'' \left(\frac{1}{\mathrm{Le}_2}\right) \sigma_{p2} \left( \left(x_{p2}^{(k,l-1)}\right)' - x_2^{(k,l-1)} \right) = \\ = \psi \left( x_2^{(k,l-1)}, \left(x_{p2}^{(k,l-1)}\right)' \right) \end{cases} \quad (A1)$$

under additional conditions, connected with the energy balance equations developed for the airflow/plate surface interface in the dry and wet passages

$$\begin{cases} \left[\left(\dfrac{W_1}{W_2}\right)\mathrm{NTU}_1\left(t_{p1}^{(k,l-1)}-t_1^{(k,l-1)}\right)+\mathrm{NTU}_2\left(\left(t_{p2}^{(k,l-1)}\right)'-t_2^{(k,l-1)}\right)+ \\[2mm] \qquad +\mathrm{NTU}_2\left(\dfrac{\sigma_p r_o}{c_p \mathrm{Le}}\right)_2\left(\left(x_{p2}^{(k,l-1)}\right)'-x_2^{(k,l-1)}\right)=0 \\[2mm] \left(\dfrac{\lambda_{plt}}{\delta_{plt}}\right)\left(t_{p1}^{(k,l-1)}-\left(t_{p2}^{(k,l-1)}\right)'\right)\approx\alpha_1\left(t_1^{(k,l-1)}-t_{p1}^{(k,l-1)}\right) \end{cases} \tag{A1*}$$

The changes of the main airflow temperature within $(k, l)$-th elementary cell from the node $(k-1)$ to another $(k)$ were determined similarly (Fig. A1(b))

$$dt_1^{(k,l)}/d\overline{X}=\mathrm{NTU}_1\left(\frac{t_{p1}^{(k-1,l)}+t_{p1}^{(k,l)}}{2}-t_1^{(k-1,l)}\right)=\theta\left(t_1^{(k-1,l)},t_{p1}^{(k-1,l)},t_{p1}^{(k,l)}\right) \tag{A2}$$

under additional conditions, connected with the energy balance equations developed for the airflow/plate surface interface in the dry and wet passages

$$\begin{cases} \left[\left(\dfrac{W_1}{W_2}\right)\mathrm{NTU}_1\left(\dfrac{t_{p1}^{(k-1,l)}+t_{p1}^{(k,l)}}{2}-t_1^{(k-1,l)}\right)+\mathrm{NTU}_2\left(\dfrac{\left(t_{p2}^{(k-1,l)}\right)'+\left(t_{p2}^{(k,l)}\right)'}{2}-\dfrac{t_2^{(k-1,l)}+t_2^{(k,l)}}{2}\right)+\right. \\[3mm] \qquad +\mathrm{NTU}_2\left(\dfrac{\sigma_p r_o}{c_p \mathrm{Le}}\right)_2\left(\dfrac{\left(x_{p2}^{(k-1,l)}\right)'+\left(x_{p2}^{(k,l)}\right)'}{2}-\dfrac{x_2^{(k-1,l)}+x_2^{(k,l)}}{2}\right)=0 \\[3mm] \left(\dfrac{\lambda_{plt}}{\delta_{plt}}\right)\left(\dfrac{t_{p1}^{(k-1,l)}+t_{p1}^{(k,l)}}{2}-\dfrac{\left(t_{p2}^{(k-1,l)}\right)'+\left(t_{p2}^{(k,l)}\right)'}{2}\right)\approx\alpha_1\left(t_1^{(k-1,l)}-\dfrac{t_{p1}^{(k-1,l)}+t_{p1}^{(k,l)}}{2}\right) \end{cases} \tag{A2*}$$

The calculated values of the primary and working airflow parameters $t_1^{k,l}$, $t_2^{k,l}$, $x_2^{k,l}$ are the initial values for the next cell $(k, l+1)$ in the layer $(k)$. In this manner one can calculate "*layer by layer*" from the section $\overline{Y}=0$ to the section $\overline{Y}=1.0$ for a given value of $(i=k)$. A similar sequence of calculations is taken for the next layer $(i=k+1)$.

There is a certain specificity for the zero section calculations $(i=0)$ ( $\overline{X}=0$ ) (Fig. A2(a)). In this case the changes of the working airflow parameters were determined taking into account that the temperature of the primary airflow in this layer is constant and equaled to the inlet temperature $t_{1i}$ .

$$\begin{cases} dt_2^{(0,l)}/d\overline{Y} = \mathrm{NTU}_2'' \left[ \left( \left( t_{p2}^{(0,l-1)} \right)' - t_2^{(0,l-1)} \right) + \right. \\ \left. + \left( \frac{\sigma_p}{\mathrm{Le}} \right)_2 \left( \frac{c_g}{c_p} \right)_2 \left( \left( t_{p2}^{(0,l-1)} \right)' - t_2^{(0,l-1)} \right) \left( \left( x_{p2}^{(0,l-1)} \right)' - x_2^{(0,l-1)} \right) \right] = \\ \qquad = \Omega \left[ t_2^{(0,l-1)}, \left( t_{p2}^{(0,l-1)} \right)', x_2^{(0,l-1)}, \left( x_{p2}^{(0,l-1)} \right)' \right] \\ dx_2^{(0,l)}/d\overline{Y} = \mathrm{NTU}_2'' \left( \frac{1}{\mathrm{Le}_2} \right) \sigma_{p2} \left[ \left( x_{p2}^{(0,l-1)} \right)' - x_2^{(0,l-1)} \right] = \\ \qquad = \psi \left[ x_2^{(0,l-1)}, \left( x_{p2}^{(0,l-1)} \right)' \right] \end{cases} \qquad \text{(A2**)}$$

under additional conditions, connected with the energy balance equations developed for the airflow/plate surface interface in the dry and wet passages

$$\begin{cases} \left[ \left( \frac{W_1}{W_2} \right) \mathrm{NTU}_1 \left( t_{p1}^{(0,l-1)} - t_{1i} \right) + \mathrm{NTU}_2 \left( \left( t_{p2}^{(0,l-1)} \right)' - t_2^{(0,l-1)} \right) + \\ \qquad + \mathrm{NTU}_2 \left( \frac{\sigma_p r_o}{c_p \mathrm{Le}} \right)_2 \left( \left( x_{p2}^{(0,l-1)} \right)' - x_2^{(0,l-1)} \right) = 0 \\ \left( \frac{\lambda_{plt}}{\delta_{plt}} \right) \left( t_{p1}^{(0,l-1)} - \left( t_{p2}^{(0,l-1)} \right)' \right) \approx \alpha_1 \left( t_{1i} - t_{p1}^{(0,l-1)} \right) \end{cases} \qquad \text{(A2***)}$$

Similarly, when calculating the primary airflow temperature in the layer ($j$=0) ($\overline{Y}=0$) it should be taken into account that the working airflow parameters are constant and equaled to the inlet values $t_{2i}$ and $x_{2i}$ (see Fig A2(b)).

$$dt_1^{(k,0)}/d\overline{X} = \mathrm{NTU}_1 \left( \frac{t_{p1}^{(k-1,0)} + t_{p1}^{(k,0)}}{2} - t_1^{(k-1,0)} \right) = \theta \left( t_1^{(k-1,0)}, t_{p1}^{(k-1,0)}, t_{p1}^{(k,0)} \right) \qquad \text{(A3**)}$$

under additional conditions, connected with the energy balance equations developed for the airflow/plate surface interface in the dry and wet passages

$$\left[ \begin{array}{l} \left| \left(\dfrac{W_1}{W_2}\right) \mathrm{NTU}_1 \left( \dfrac{t_{p1}^{(k-1,0)} + t_{p1}^{(k,0)}}{2} - t_1^{(k-1,0)} \right) + \mathrm{NTU}_2 \left( \dfrac{\left(t_{p2}^{(k-1,0)}\right)' + \left(t_{p2}^{(k,0)}\right)'}{2} - t_{2i} \right) + \right. \\[4mm] \left. + \mathrm{NTU}_2 \left( \dfrac{\sigma_p r_o}{c_p \mathrm{Le}} \right)_2 \left| \dfrac{\left(x_{p2}^{(k-1,0)}\right)' + \left(x_{p2}^{(k,0)}\right)'}{2} - x_{2i} \right| = 0 \right. \\[4mm] \left| \left(\dfrac{\lambda_{plt}}{\delta_{plt}}\right) \right| \dfrac{t_{p1}^{(k-1,0)} + t_{p1}^{(k,0)}}{2} - \dfrac{\left(t_{p2}^{(k-1,0)}\right)' + \left(t_{p2}^{(k,0)}\right)'}{2} \right| \approx \alpha_1 \left| t_1^{(k-1,0)} - \dfrac{t_{p1}^{(k-1,0)} + t_{p1}^{(k,0)}}{2} \right| \end{array} \right] \qquad (A3^{***})$$

It should be noted that Eqs. (2.3), (2.9), (2.15), (2.18) and (2.20) (from **Section 2** of presented thesis) were used to define the air-plate interface temperatures on each step of numerical integration by iteration method. Optimum values of the external parameters of this equation were defined to accelerate the convergence of the selected Wegstein iteration method. The accuracy of numerical method was checked by computing the identical variants on various space domain grids. Convergence test showed that the optimum number of grid nodes and, consequently, the minimum time of computation within the given tolerance of accuracy (0.5% thermal and mass balance error) was reached at the step size of 0.01 in the $\bar{X}$ and $\bar{Y}$ directions. The implementation scheme of the proposed algorithm and the flow sheet of programming used in this calculation are presented in Figs. A1-A3.
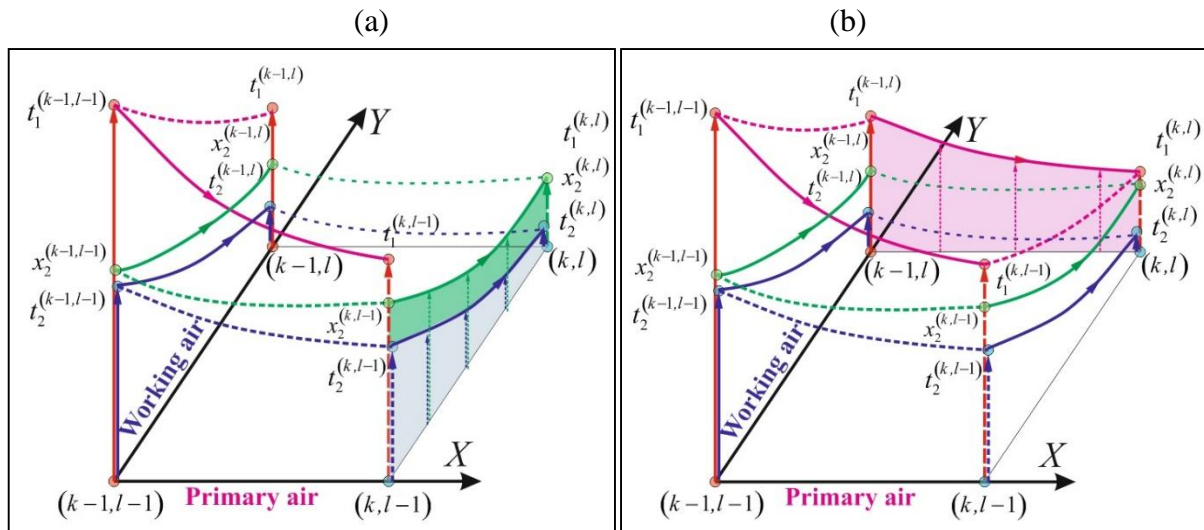


Fig. A1. Calculating algorithm for the elementary cell $(k, l)$.
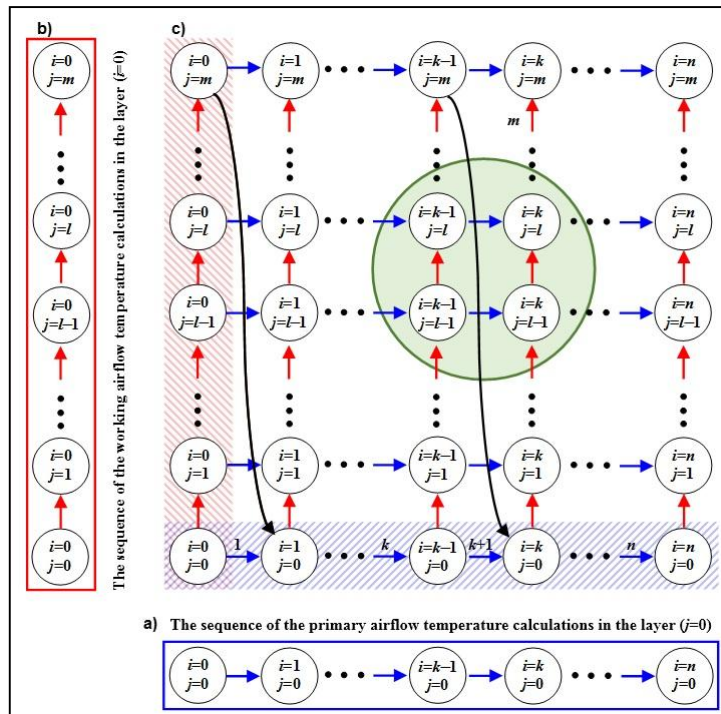
Fig. A2. The Sequence of calculations.
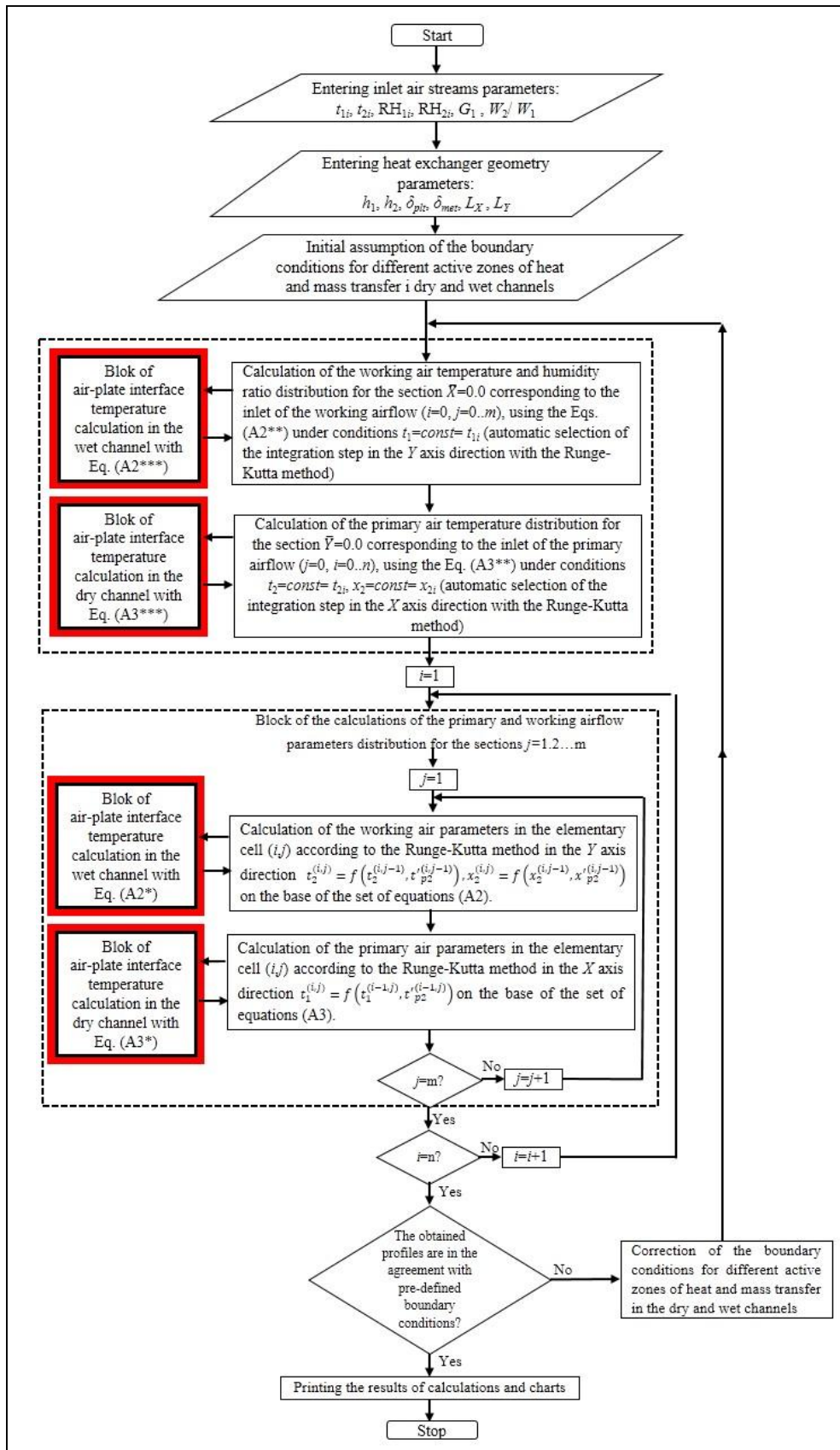
Fig. A3. Flow sheet of programming.

## Appendix B. Validation of the mathematical models of cross-flow and regenerative evaporative air cooler against existing experimental data

This Appendix present the validation of the models describing the cross-flow and regenerative air coolers against existing experimental data. The accuracy of the mathematical model prediction is considered to be similar for parallel and counter-flow HMXs. The similar construction of those units and the nearly identical differential equations describing the heat and mass transfer processes occurring in considered exchangers allows assuming that the accuracy of the mathematical models describing them is also similar.

Equation (B1) was used to calculate the discrepancies (this method was used in other studies connected with indirect evaporative air cooling, e.g. [60]).

$$((\bar{t}_{1o})^{\text{experiment}} - (\bar{t}_{1o})^{\text{model}} / (\bar{t}_{1o})^{\text{experiment}}) \cdot 100\% \qquad (B1)$$

### B1. Cross-flow IEC

The mathematical model of the cross-flow heat and mass exchanger was validated against existing experimental data presented by Martinez et. al [68]. The exchanger in Martinez' paper (Fig. B1) was made of 25 flat plates with the following geometric dimensions:
- thickness: $3 \cdot 10^{-3}$ m,
- length: 0.3 m,
- area: 2.25 m$^2$,
- geometry: flat plates,
- material: aluminum.



Fig. B1. Photograph of the exchanger used by Martinez et al. [68].

The scheme of the measurement station is presented in Figure B2.(a). It consists of fan delivering the airflow to the recuperator, a room with the heat pump to heat the secondary airflow and a water supply system. The measured parameters were the temperature (in points T

in Figure B2.(a)), relative humidity (RH in Fig. B2.(a)) and pressure drop along the cooler ($\Delta$P in Fig. B2.(a)) to calculate the airflow rate. The details of the experiment can be found in [68].

The model was set to the same operating conditions as for the experimental cases, including the exchanger geometry and inlet airflow conditions. The comparison between the data obtained from the model and experiment is visible in Figure B2.(b).The model was compared for three type of conditions presented in the Martinez study: dry conditions ($RH_i < 30\%$), moderate conditions ($30\% < RH_i < 60\%$) and humid conditions ($RH_i < 60\%$) under variable inlet air temperature. The highest discrepancies between outlet temperature obtained by simulation and experiment were 0.55°C for inlet air temperature equal 24.5°C for dry conditions, the maximal discrepancy obtained from Eq. (B1) is equal to 3.2%. The coefficient of correlation $R^2$ between experimental and numerical results was calculated and established as equal 0.985. Presented analysis allows assuming that the results obtained by model and the experiment are similar, therefore it can be assumed that the model can be used to analyze the cross-flow heat and mass exchanger.

(a)                                                        (b)
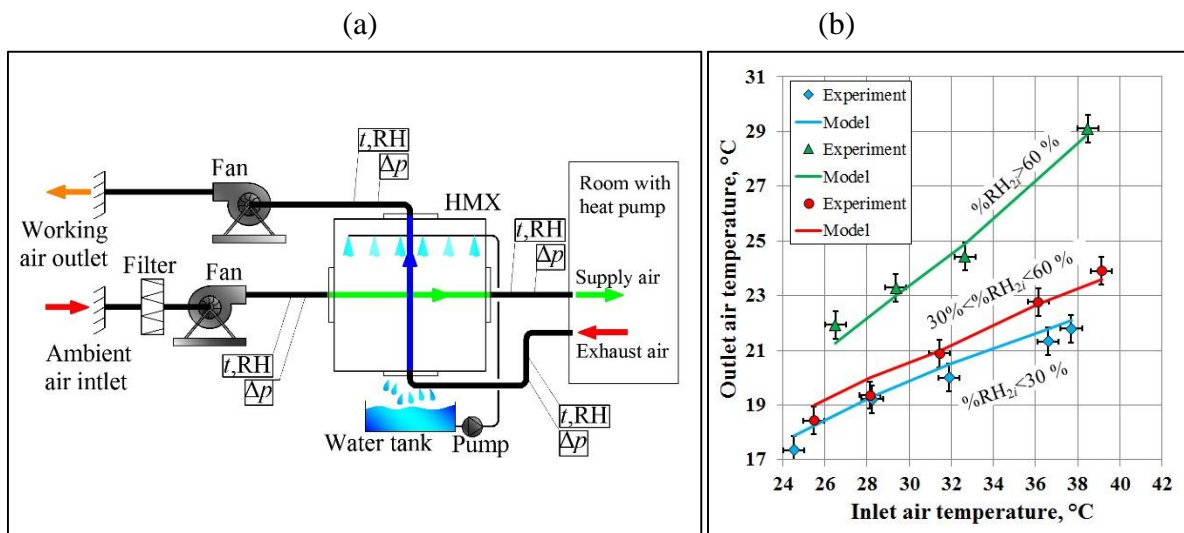


Fig. B2. Validation of the mathematical model describing cross-flow exchanger. (a) Scheme of the testing bench in study by Martinez et al. [68]. (b) Comparison between the mathematical model and experimental results.

## B2. Regenerative IEC

The model describing the regenerative HMX was validated against existing experimental data published by Riangvilaikul and Kumar [9]. The tests were conducted at the Asian Institute of Technology, Thailand. The experimental facility for dew point evaporative cooling system in Riangvilaikul and Kumar's study consisted of the air-preconditioning unit, the regenerative HMX and the measurement devices (Fig. B3). The preconditioning unit was equipped with 1.5 kW pre-heater, 1.5 kW re-heater (Fig. B3(a)) and a 5 kW water boiler system for humidification purposes. The air temperature and humidity ratio was controlled by a cooling coil. The intake air fan was able to regulate the desirable amount of air flow precisely with the variable speed drive controller. The exchanger body was insulated to reduce heat losses, the conditions inside the testing chamber were close to ideal [9]. The analyzed HMX was 1.2 m

long, the wall separating the channels was 0.5 mm thick, the channel width was equal 80 mm, while the height of the channel was equal 5 mm. The parameters measured was the airflow rate ($G$), dry and wet bulb temperatures (DB and WB in Fig. B3(a)).

Riangvilaikul and Kumar's studies contain two type of experiments: steady state operation and dynamic studies. The model describing the regenerative HMX is compared to the steady state operation studies, due to its basic assumptions (see **Section 2.1** of presented thesis). The model was set to the same operating conditions as for experimental cases- the same geometry of the HMX, the same inlet airflow parameters and the same airflow velocity. This analysis established the accuracy of the model in predicting the performance of the real regenerative indirect evaporative air cooler.

(a)                                                        (b)
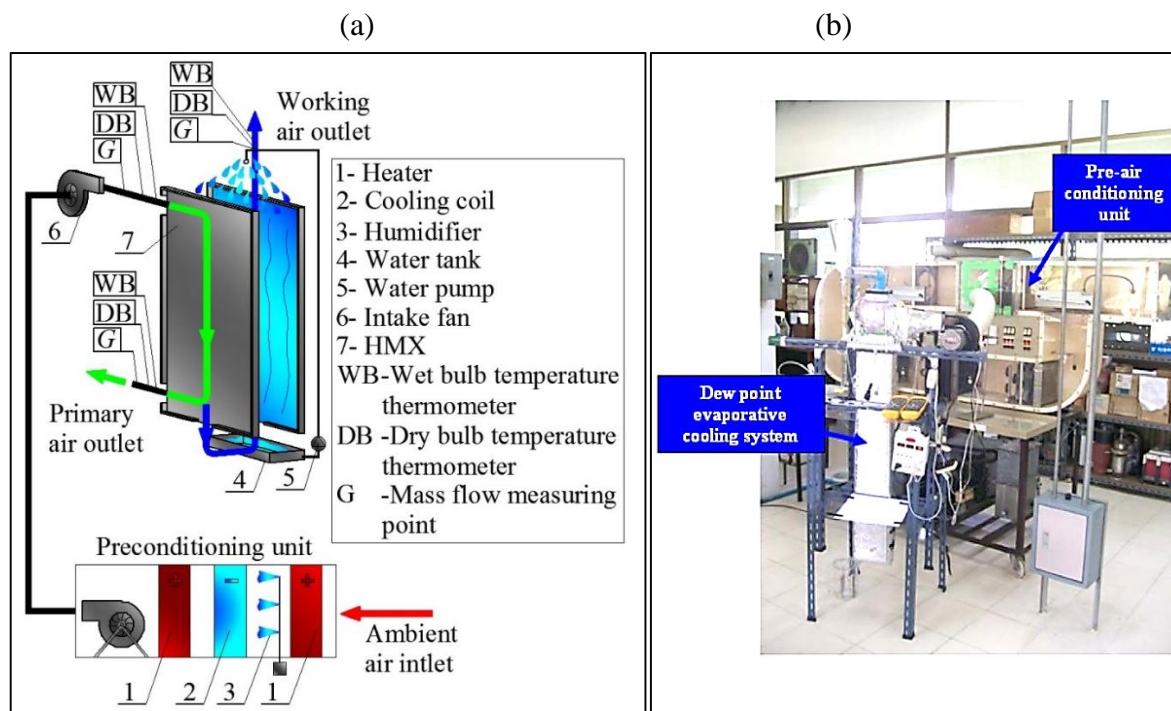


Fig. B3. Validation of the mathematical model describing regenerative exchanger. (a) Scheme of the testing bench in study by Riangvilaikul and Kumar [9]. (b) Photograph of the testing bench [9].

The model was set to the same operating conditions as for the experimental cases, including the exchanger geometry and inlet airflow conditions. The validation of the mathematical model is presented in Fig. B3(a) and (b) (constant inlet temperature and humidity ratio, variable airflow velocity) and in Fig. B3(c)-(f) (constant airflow velocity, variable inlet temperature and humidity ratio). In the first case comparison was presented for two hypothetical conditions: dry ($x_{1i}$=11.2 g/kg: Fig. B3(a)) and humid ($x_{1i}$=20.0 g/kg: Fig. B3(b)), while for the second case four hypothetical conditions were considered: very dry ($x_{1i}$=6.9 g/kg: Fig. B3(c)), dry ($x_{1i}$=11.2 g/kg: Fig. B3(d)), humid ($x_{1i}$=20.0 g/kg: Fig. B3(e)) and very humid ($x_{1i}$=26.4 g/kg: Fig. B3(f)).

For the first case (Fig. B3(a) and (b)), the differences in obtained supply air temperature, calculated from the equation were at most 4%, the coefficient of determination $R^2$ between experiment and model was established as equal 0.998. For the second case (Fig. B3(c)-(f)), discrepancies between the model and experiment are at most 2% (i.e. the highest differences in

outlet air temperatures are 0.2°C) and the $R^2$ correlation is equal 0.999. It can be seen that the experimental and simulation results show satisfactory agreement, thus the model can be successfully used to predict performance of the regenerative HMX. It should be mentioned that similar agreement with the same experimental results was obtained by models presented by Riangvilaikul and Kumar and by Zhao et al. [10] and [50]. The results of the author's model were also compared with other existing mathematical models with good agreement (the comparison can be found in [129]).

(a) (b)

(c) (d)
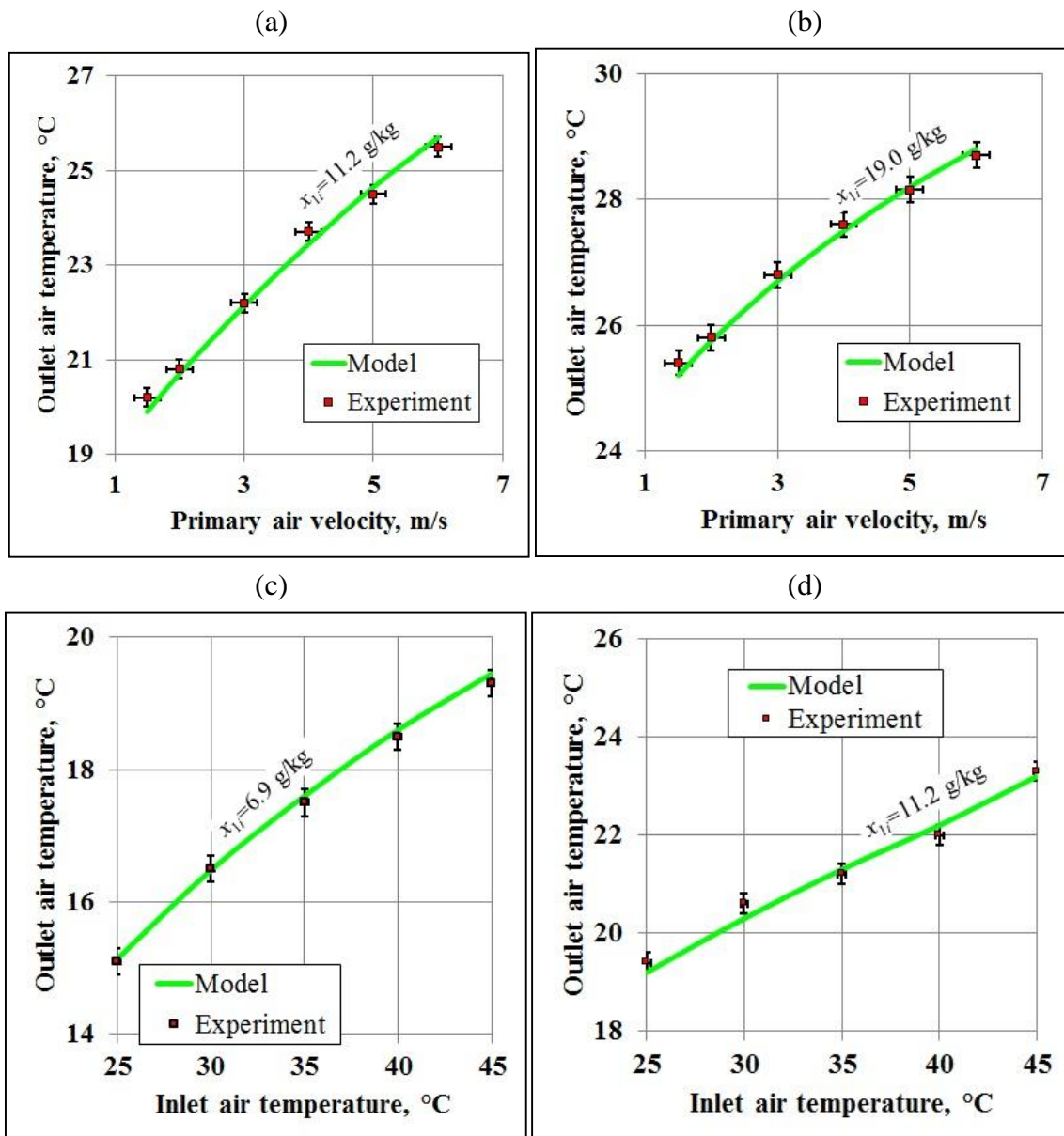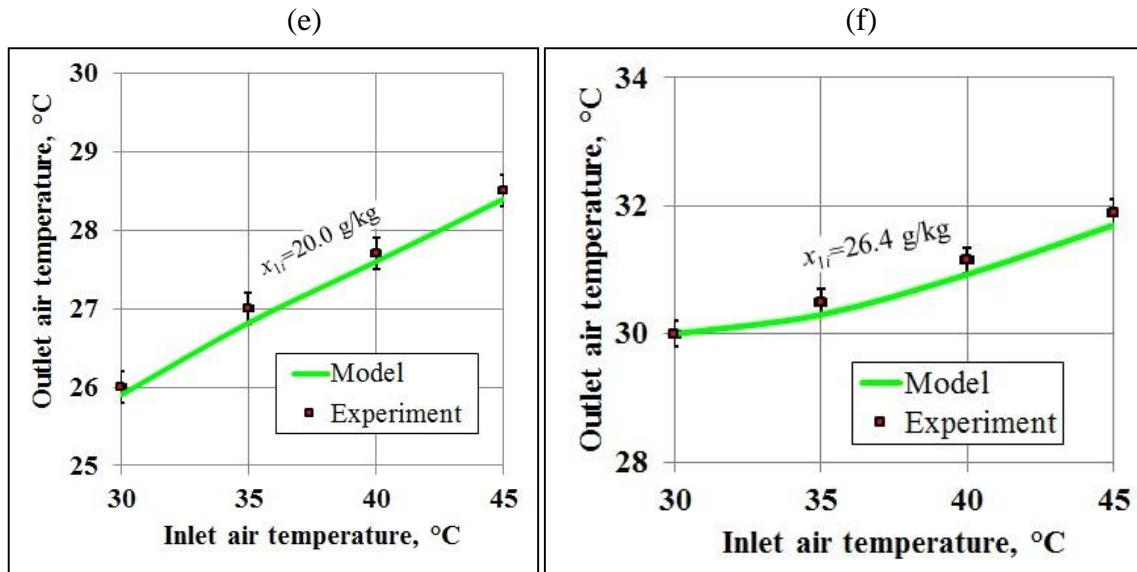
Fig. B3. Validation of the ε-NTU method results against experimental measurements data from [9]. (a) Outlet product air temperature at variable velocity $v_1$ and constant inlet air parameters ($x_{1i}$=11.2 g/kg). (b) Outlet product air temperature at variable velocity $v_1$ and constant inlet air parameters ($x_{1i}$ =19.0 g/kg). (c) Outlet product air temperature at variable inlet air temperature $t_{1i}$ and constant velocity $v_1$ ($x_{1i}$ =6.9 g/kg). (d) Outlet product air temperature at variable inlet air temperature $t_{1i}$ and constant velocity $v_1$ ($x_{1i}$ =11.2 g/kg). (e) Outlet product air temperature at variable inlet air temperature $t_{1i}$ and constant velocity $v_1$ ($x_{1i}$ =20.0 g/kg). (f) Outlet product air temperature at variable inlet air temperature $t_{1i}$ and constant velocity $v_1$ ($x_{1i}$ =26.4 g/kg).

# Appendix C. Calculation algorithm for the model of the realistic M-Cycle air cooler (universal section method)

The main disadvantage of the algorithm for the "ideal" M-Cycle presented in **Section 3.3.1** of the presented thesis is the fact that it cannot be used to analyze the impact of different perforation arrangements on the cooling performance of the M-Cycle air cooler, because it has to include a perforation with density equal to the integration step. The second disadvantage is that it has to include the rectangular shape of the initial part of the air cooler. In case of currently produced M-Cycle unit the first channel of the initial part is shorter than other two (see Fig. 1.27(d) and (e) and Fig. 1.28(b) in **Section 1** of the presented thesis). For the above-mentioned reasons the new algorithm has to be implemented in order to overcome the disadvantages of the algorithm for the "ideal" M-Cycle. The new method presented in this Appendix is universal and it can be used to calculate any type of the cross-flow M-Cycle air cooler. Due to its mechanism it is named The Section Method.

From the standpoint of the thermodynamic processes, the Maisotsenko Cycle heat exchangers can be divided into identical square sections, which can be considered as a small cross-flow indirect evaporative coolers with different distribution of inlet airflow parameters depending on the previous sections outlet airflow parameters. The original, currently- produced, M-Cycle air cooler is used as an example (Fig. C1). If the dry channels (Fig. C1(a)) and the wet channels (Fig. C1(b)) are presented on the same sheet (Fig. C1(c)) it can be seen that they are creating small square sections of the elementary cross-flow air coolers. Figure C1(c) shows such exchanger divided into the numbered sections.

(a)             (b)

(c)



(d)                                    (e)
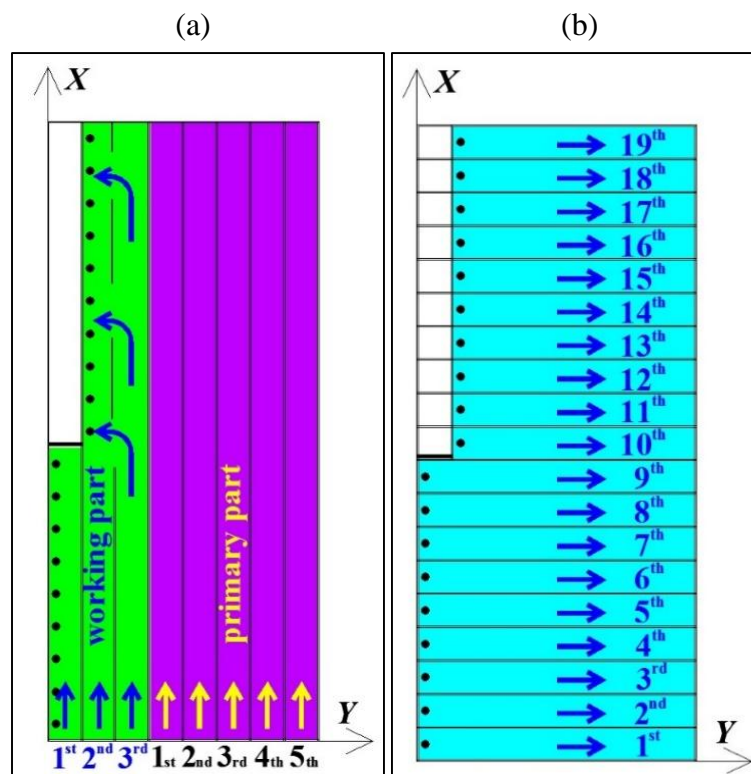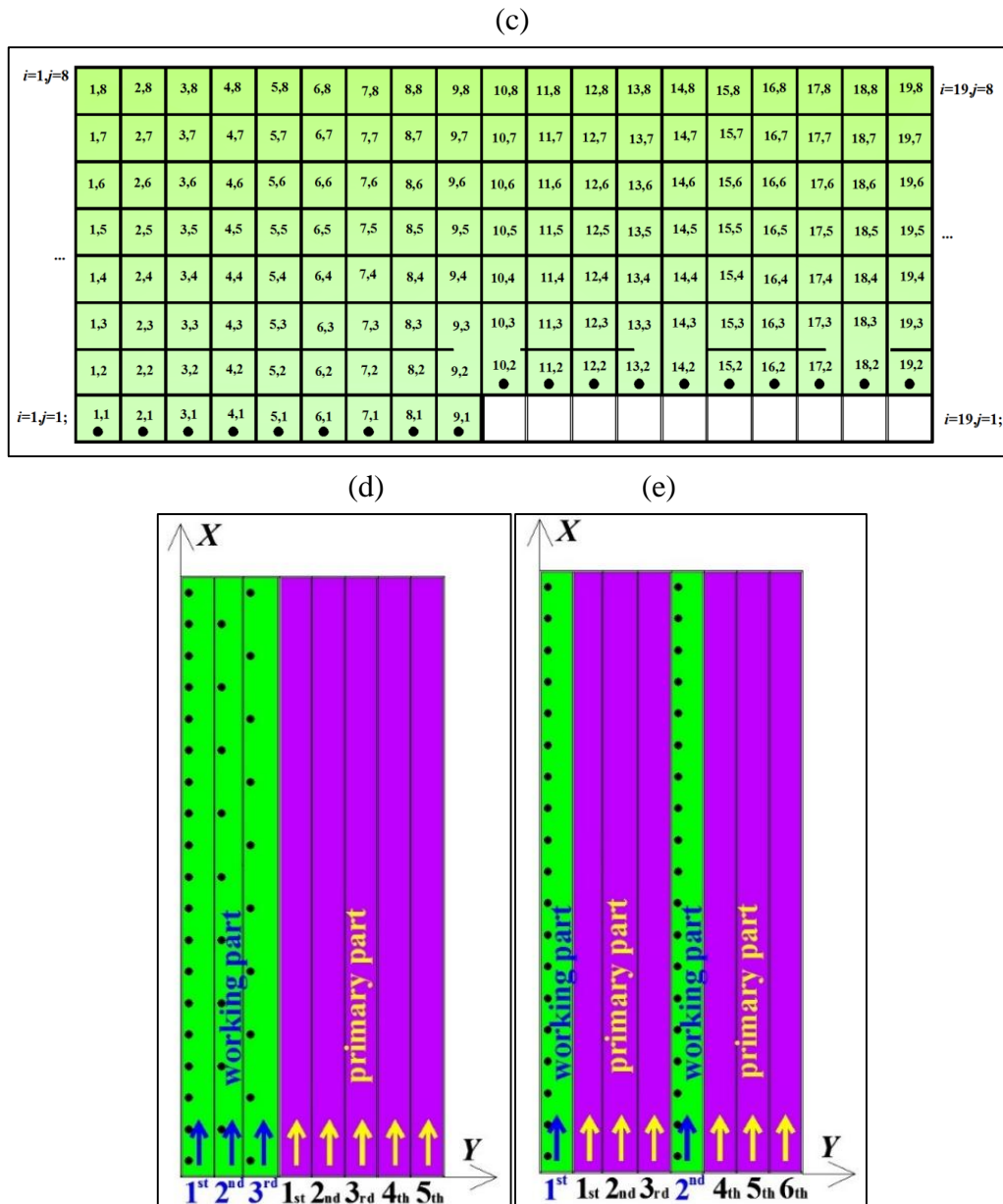


Fig. C1. Explanation of the section method. (a) Currently produced M-Cycle air cooler: dry channels. (b) Currently produced M-Cycle air cooler: wet channels. (c) Currently produced M-Cycle air cooler divided into the numbered the sections (dry and wet channel on the same sheet). (d) Different arrangement of the M-Cycle air cooler: Example No. 1. (e) Different arrangement of the M-Cycle air cooler: Example No. 2.

There are two types of assumed sections: *ordinary* cross-flow section without perforated holes (no mixing of the air streams occurs) and section *with airflow mixing* with perforated holes (the premixing process occurs at the entrance of the considered "*elementary*" cross-flow section). The number of sections inside each type of the M-Cycle heat exchanger is determined on the basis of the holes distribution and the length of dry and the wet channels. It can be seen that any type of the cross-flow M-Cycle air cooler can be divided into the sections, therefore this method allows analyzing and comparing different arrangements of the initial part in the M-Cycle HMXs. The examples of different versions of such air coolers are visible in Figure C1(d)

and (e). The section numeration is shown schematically in Fig. C1(c). The sections numeration is characterized by the two numbers $(i,j)$, where the number $i$ corresponds to the number of sections along the $X$ axis, while the number $j$ corresponds to the number of sections along the $Y$ axis (Fig. C1(c)). The number $i$ changes from 1 to 19, the number $j$ changes from 1 to 8 in case of the presented air cooler. Each section is treated as an independent cross-flow HMX and it is calculated separately.

Each section has the internal calculation web, with nodes changing from (0) to ($n$) along $X_{i,j}$ axis and from (0) to ($m$) along $Y_{i,j}$ axis (Fig. C2(a)). Inside the section, differential equations of heat and mass transfer are solved with modified Runge-Kutta method, similar to the method presented for the typical cross-flow evaporative cooler (see **Appendix A**), but with different plate calculation mechanism, due to the fact that it must include the existence of fins. The process of the sample calculations for nodes $(0,0 \div m)$ in the longitudinal section ($i=0$) along the $Y_{i,j}$ axis is shown in Figure C2(a).

The elementary working air stream $(\dot{G}_2)_{i,j} = (G_2)_{i,j} \dfrac{dX_{i,j}}{l_{sec}}$ enters the node (0,0) with known parameters $(t_2^{0,0})_{i,j}$ and $(x_2^{0,0})_{i,j}$. After passing the elementary segment $d\bar{Y}_{i,j}$ between nodes (0,0) and (0,1) its temperature changes by the value $\dfrac{\partial (t_2^{0,0})_{i,j}}{\partial \bar{Y}_{i,j}} d\bar{Y}_{i,j}$, while its humidity ratio changes by the value $\dfrac{\partial (x_2^{0,0})_{i,j}}{\partial \bar{Y}_{i,j}} d\bar{Y}_{i,j}$, therefore the parameters in the node (0,1) are equal

$(t_2^{0,1})_{i,j} = (t_2^{0,0})_{i,j} + \dfrac{\partial (t_2^{0,0})_{i,j}}{\partial \bar{Y}_{i,j}} d\bar{Y}_{i,j}$ and $(x_2^{0,1})_{i,j} = (x_2^{0,0})_{i,j} + \dfrac{\partial (x_2^{0,0})_{i,j}}{\partial \bar{Y}_{i,j}} d\bar{Y}_{i,j}$. The process is repeated along the $Y_{i,j}$ axis for all the calculating nodes in the longitudinal section ($i=0$).

The airflow parameters in the last node $(0,m)$ are equal $(t_2^{0,m})_{i,j} = (t_2^{0,0})_{i,j} + (\Delta t_2^{0,0 \div m})_{i,j}$ and $(x_2^{0,m})_{i,j} = (x_2^{0,0})_{i,j} + (\Delta x_2^{0,0 \div m})_{i,j}$, where $(\Delta t_2^{0,0 \div m})_{i,j} = \int_0^1 \dfrac{\partial (t_2^{0,0 \div m})_{i,j}}{\partial \bar{Y}_{i,j}} d\bar{Y}_{i,j}$ and $(\Delta x_2^{0,0 \div m})_{i,j} = \int_0^1 \dfrac{\partial (x_2^{0,0 \div m})_{i,j}}{\partial \bar{Y}_{i,j}} \partial \bar{Y}_{i,j}$. The algorithm of determination of the airflow parameters distribution in the dry channel is similar as in the case of the wet channel, the only difference is the uniform field of the humidity ratio on the channel surface (no mass transfer).

The notation process for the airflow parameters in the dry and the wet channels on the boundary between two ordinary sections is shown schematically in Fig. C2(b) and (c). Airflow 1 in the dry passage is passing by and exchanging heat with the working airflow 2 in the wet channel. At the end of the example section $(i,j)$ the exit airflow parameters are established in each calculation node $(n,0 \div m)$ (see Fig. C2(b)). For example, in the node $(n,m)$ the outlet air airflow temperature in the dry passage is equal $(t_1^{n,m})_{i,j}$ and the humidity ratio is equal $(x_1^{n,m})_{i,j} = x_{1i} = const$. The outlet airflow parameters from the section $(i,j)$ become the inlet airflow parameters for the adjacent section $(i+1,j)$, therefore they are rewritten node by node. For example, $(t_1^{n,m})_{i,j}$ becomes $(t_1^{0,m})_{i+1,j}$, humidity ratio is constant, therefore $(x_1^{n,m})_{i,j}$ becomes $(x_1^{0,m})_{i+1,j} = x_{1i} = const$ and so on. Air mass flow rate doesn't change $(G_1)_{i,j} =$

$(G_1)_{i,j+1}$, therefore the NTU$_1$ values are the same in the sections $(i,j)$ and $(i+1,j)$. The process of assigning the working airflow parameters node by node on the boundary of two adjacent sections $(i,j)$ and $(i,j+1)$ for the wet channel is identical as in the case of the dry channel, but with consideration that the working airflow humidity ratio is not constant, therefore it is rewritten in the same way as the temperature (see Fig. C2(c)).

As mentioned before, there are two type of sections: the ordinary cross-flow sections and the sections with of mixing air streams. Processes occurring in the wet channels of the sections with the airflows mixing are shown in Figure C2(d). It can be seen that the mixing process occurs on the boundary between the two adjacent sections $(i+1,j)$ and $(i+1,j+1)$, therefore it is carried out before the integration of the differential equations (mixing occurs outside the calculation algorithm). This simplifies the solution process and allows each section to be treated as a typical cross-flow evaporative cooler. In the mixing sections, after the working air stream passes the section $(i+1,j)$, its average temperature $(\bar{t}_{2o})_{i+1,j}$ and humidity ratio $(\bar{x}_{2o})_{i+1,j}$ are established, by averaging temperatures and humidity ratios in all the nodes $(0 \div n,m)$ at the exit of the section $(i+1,j)$:

$$(\bar{t}_{2o})_{i+1,j} = \frac{\sum_{k=0}^{k=n}\left(t_2^{k,m}\right)_{i+1,j}}{n+1} \tag{3.40}$$

$$(\bar{x}_{2o})_{i+1,j} = \frac{\sum_{k=0}^{k=n}\left(x_2^{k,m}\right)_{i+1,j}}{n+1} \tag{3.41}$$

A certain part of the airflow 1 from the dry channel $(\Delta G_1)_{i+1,j+1}$ with known parameters $(\bar{t}_{1i})_{i+1,j+1}$ and $(\bar{x}_{1i})_{i+1,j+1} = x_{1i}$ is mixed with the working airflow $(G_2)_{i+1,j}$ at the entrance to the section $(i+1,j+1)$. It should be mentioned that due to the fact that mixing algorithm occurs outside the calculation process, the value of the air streams 1 and 2 is not elementary and it can be previously established. This allows analyzing the impact of uneven airflow distribution through the channels on the performance of the M-Cycle air coolers. The inlet working airflow parameters in the section $(i+1,j+1)$ can be calculated from the equations:

$$(\bar{t}_{2i})_{i+1,j+1} = \frac{(\bar{t}_{2o})_{i+1,j}(G_2)_{i+1,j}+(\bar{t}_{1i})_{i+1,j+1}(\Delta G_1)_{i+1,j+1}}{(G_2)_{i+1,j}+(\Delta G_1)_{i+1,j+1}} \tag{3.42}$$

$$(\bar{x}_{2i})_{i+1,j+1} = \frac{(\bar{x}_{2o})_{i+1,j}(G_2)_{i+1,j}+(\bar{x}_{1i})_{i+1,j+1}(\Delta G_1)_{i+1,j+1}}{(G_2)_{i+1,j}+(\Delta G_1)_{i+1,j+1}} \tag{3.43}$$

After establishing $(\bar{t}_{2i})_{i+1,j+1}$ and $(\bar{x}_{2i})_{i+1,j+1}$, the values are assigned to the working airflow parameters in all the beginning calculation nodes at for the section $(i+1,j+1)$: $\left(t_2^{0 \div n,0}\right)_{i+1,j+1} = (\bar{t}_{2i})_{i+1,j+1}$, $\left(x_2^{0 \div n,0}\right)_{i+1,j+1} = (\bar{x}_{2i})_{i+1,j+1}$. This shows the main difference in the calculation algorithms developed for the *ordinary* sections and the sections with airflows mixing: at the entrance to the *ordinary* section there's always non-uniform temperature and humidity distribution, whereas at the entrance to the mixing sections the

airflows parameters distribution is considered to be uniform (no temperature and moisture distribution in the point of mixing is assumed). The inlet air mass flow rate for the section $(i{+}1,j{+}1)$ is equal $(G_2)_{i+1,j+1} = (G_2)_{i+1,j} + (\Delta G_1)_{i+1,j+1}$. Based on the corrected air mass flow rate $(G_2)_{i+1,j+1}$, new value of the $(\text{NTU}_2)_{i+1,j+1}$ is calculated for the section $(i{+}1,j{+}1)$.

(a)



(b)

(c)



(d)



(e)

(f)
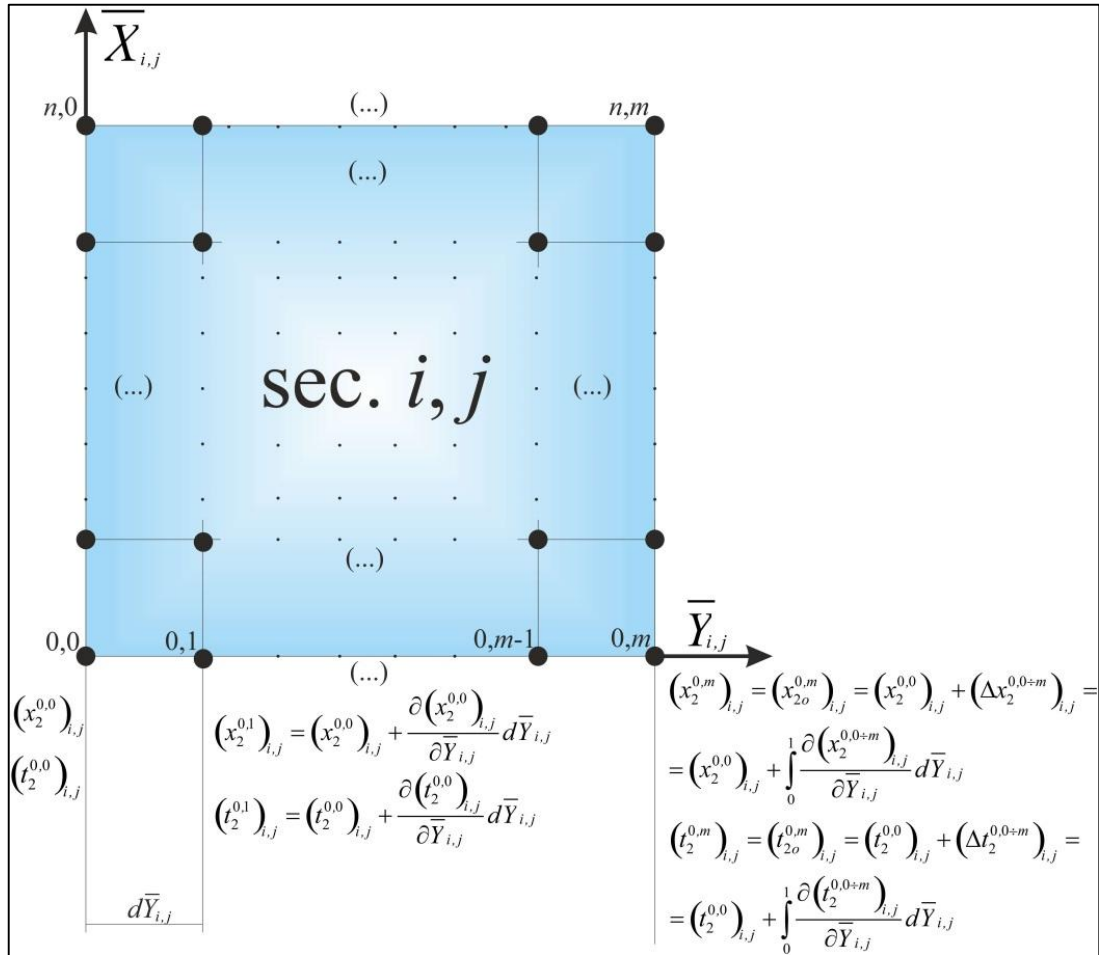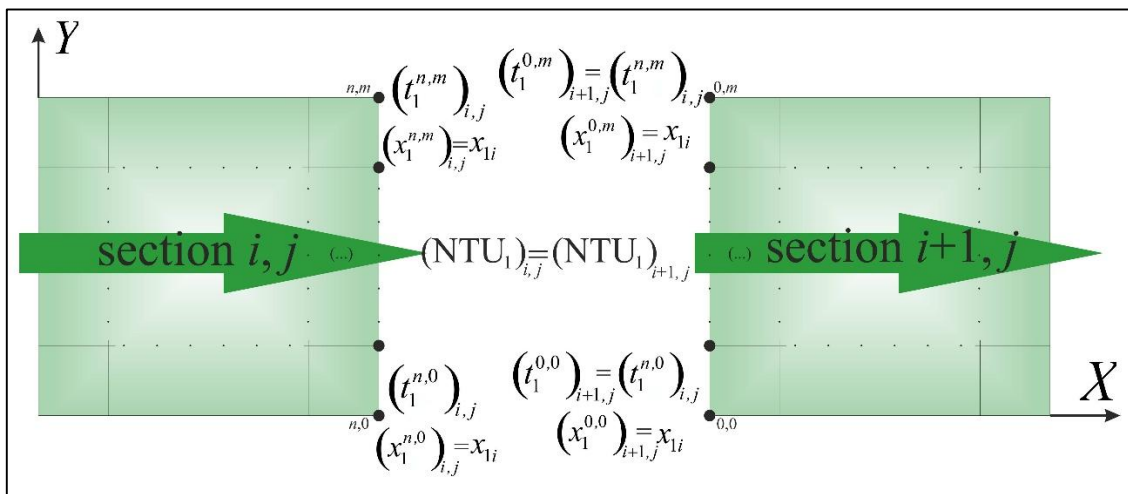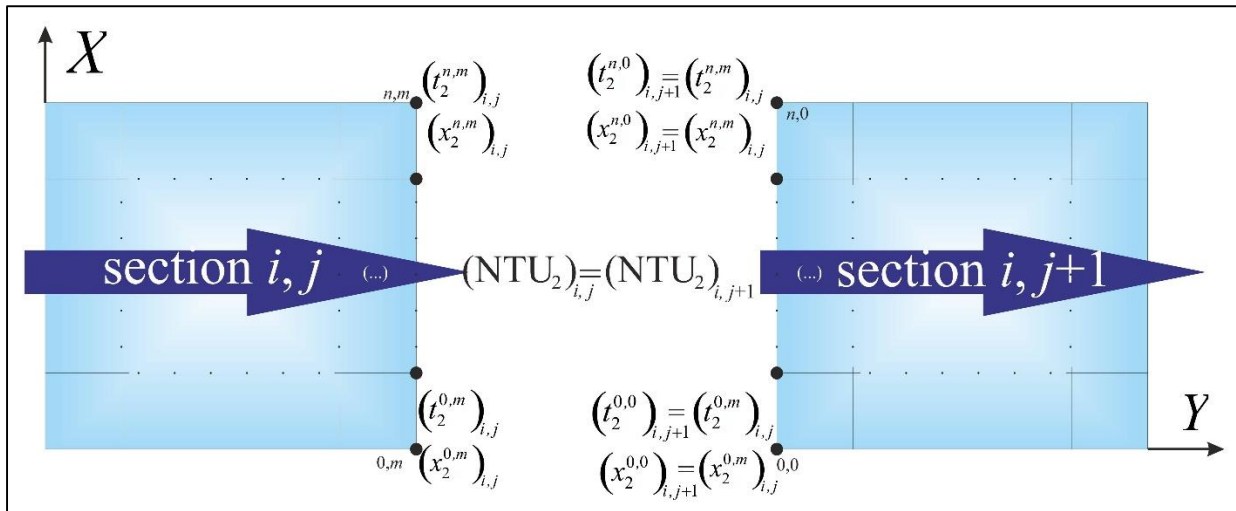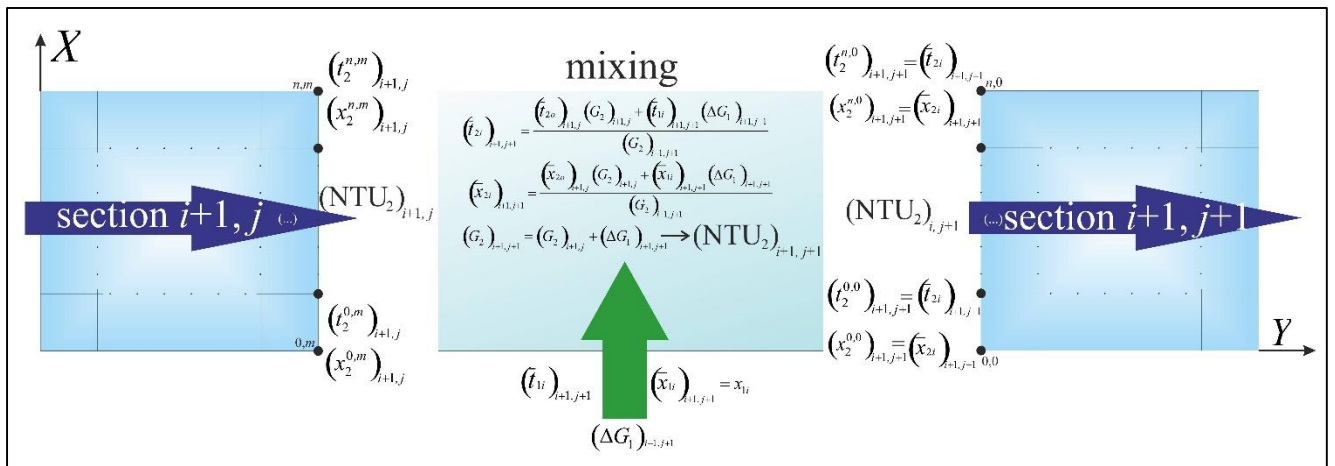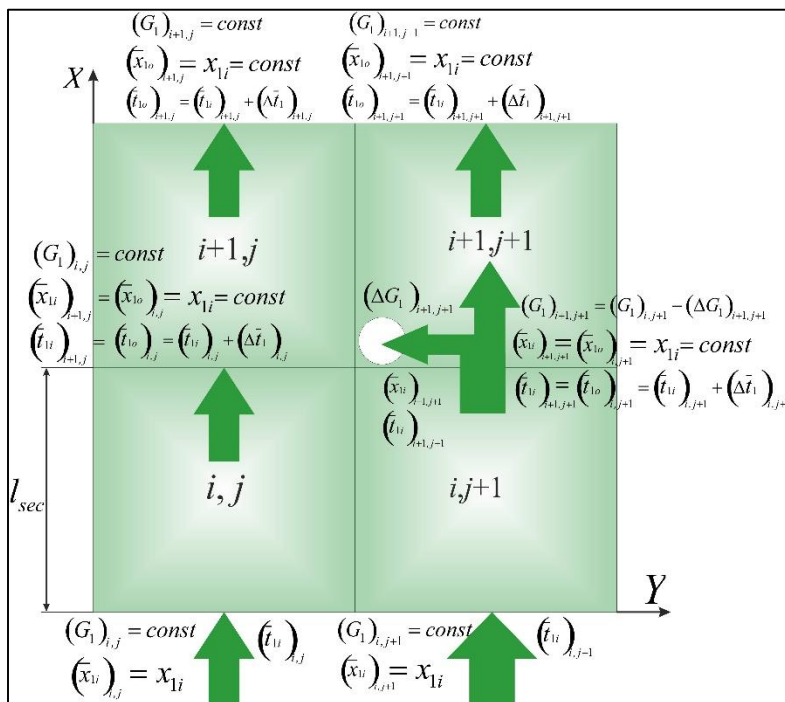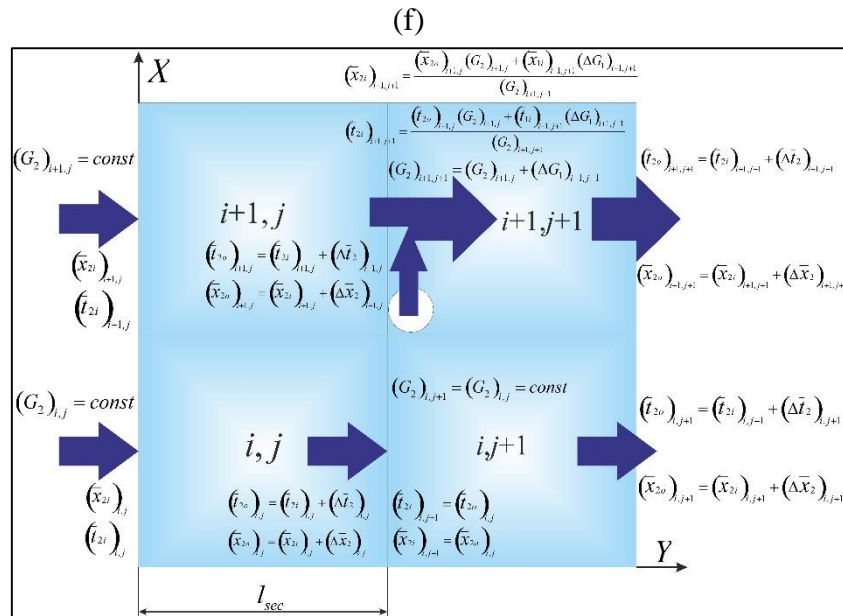


Fig. C2. Maisotsenko Cycle mathematical model calculation algorithm illustrations. (a) Calculation nodes inside the example section. (b) Notation scheme for the *ordinary* section in the dry channel. (c) Notation scheme for the *ordinary* section in the wet channel. (d) Notation scheme for the mixing section in the wet channel. (e) Four example sections for the dry channel. (f) Four example sections for the wet channel.

Establishing inlet airflow parameters in the mixing sections in the dry channels is more simple (Fig. C2(e)): the airflow temperature and humidity ratio are assigned node by node, like in case of an *ordinary* section, the only algorithmic difference is the change of the NTU value (in the example case case $(NTU_1)_{i+1,j+1}$) on the boundary between the sections $(i,j+1)$ and $(i+1,j+1)$, due to the reduction of the air mass flow rate by the value of $(\Delta G_1)_{i+1,j+1}$. After establishing initial distributions of the airflows parameters at the entrance to the dry and wet channels the calculation process starts. Figures C2(e) and (f) present the example fragment of dry and wet channel with *ordinary* and *mixing* sections. It can be seen how the algorithm process is realized in any type of the M-Cycle heat exchanger: for every section the inlet parameters are established before calculation process (they are rewritten or the they calculated from the mixing equations) and the integration process inside each section is realized as in the typical cross-flow air cooler. It is visible that different arrangements of the M-Cycle units can be created with the appropriate combination of mixing and ordinary sections.

The above-described algorithm is realized in the original multi-module computer simulation program, which integrates the set of differential equations with different initial conditions, depending on the considered section type. The section scheme depends on the assumed type of the investigated heat exchanger.

## Appendix D. Flow sheets of programming for the computer programs describing cross-flow M-Cycle air cooler.

The main difference in program schemes between the previously-presented cross-flow IEC (**Appendix A**) and the cross-flow M-Cycle air coolers, except the mixing algorithms, lies in the calculaiton of the energy balance on the strucutre with fins. Therefore new flow sheets of the programming must be implemented. Both programs (Ideal M-Cycle and Section Method) are using the same plate and fin temperature calculation algorithm (Fig. D1), however in case of the ideal M-Cyle the mixing of the air streams is implemented in every calculation step in the initial part, whereas in the section method the mixing process occurs before the integration prcoess and every section is calculated under previously established conditions. Due to this fact, the temperature distribution inside the channels of the cooler in case of the algorithm of the "ideal" M-Cycle is caluculated by dynamic transfer of the parameters to the Air-Plate Interface Calculation Block, while in case of the Section Method the established initial conditions are transferred to the Section Caluclation Block, where the temperature distributions are caluclated with the Air-Plate Interface Calculation Block.

All the above-described algorithms are realized in the original multi-module computer simulation programs. Their accuracy has been preliminary validated by solving examples with familiar analytical solutions and by solving the same examples with different integration steps. The smallest number of numerical web nodes was achieved for $\bar{X}$ and $\bar{Y}$ axis step equal to 0.01. The flow sheet of programing for the model of the Ideal M-Cycle is presented in Figure D2, while the flow sheet of programing for the model of the Section Method is presented in Figure D3.
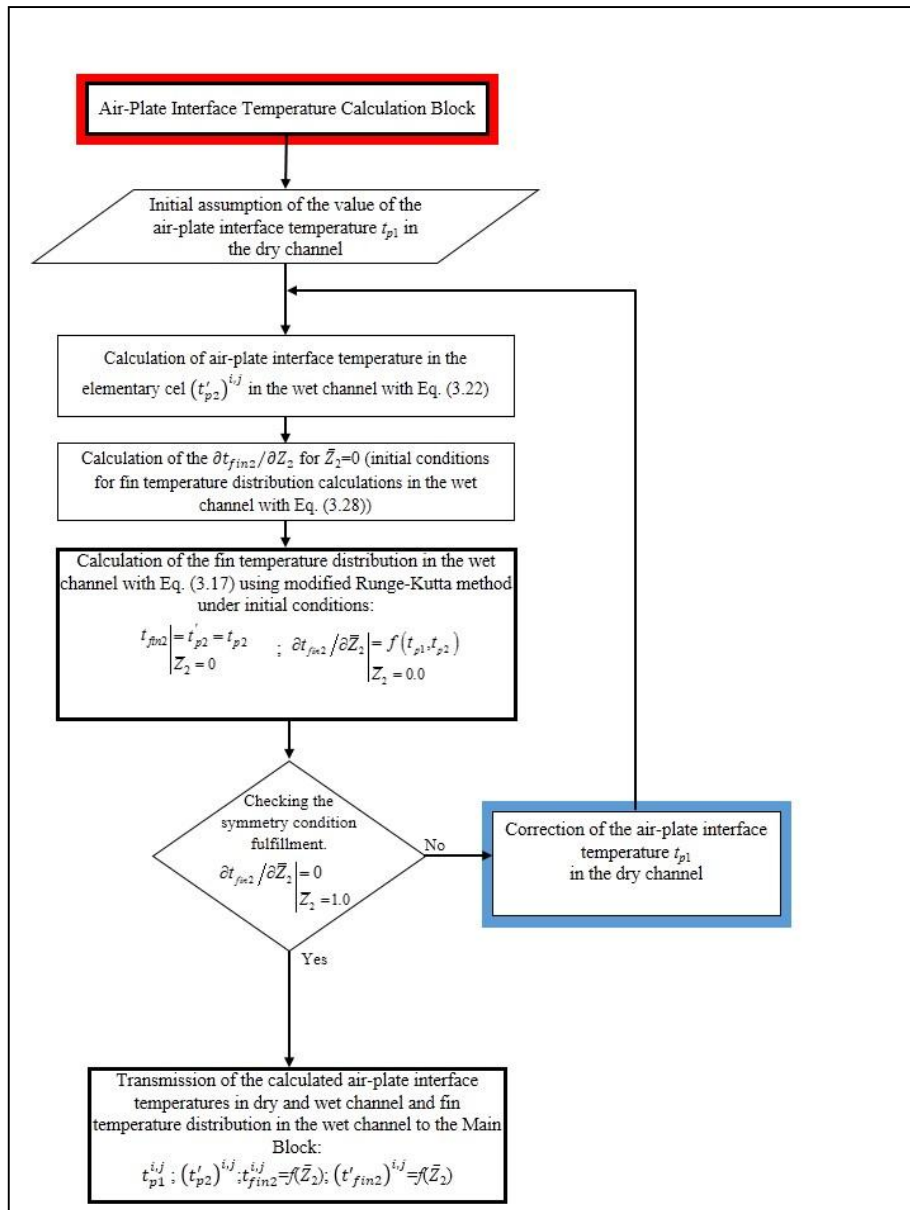
Fig. D1. Air plate temperature calculation block used in both programs.
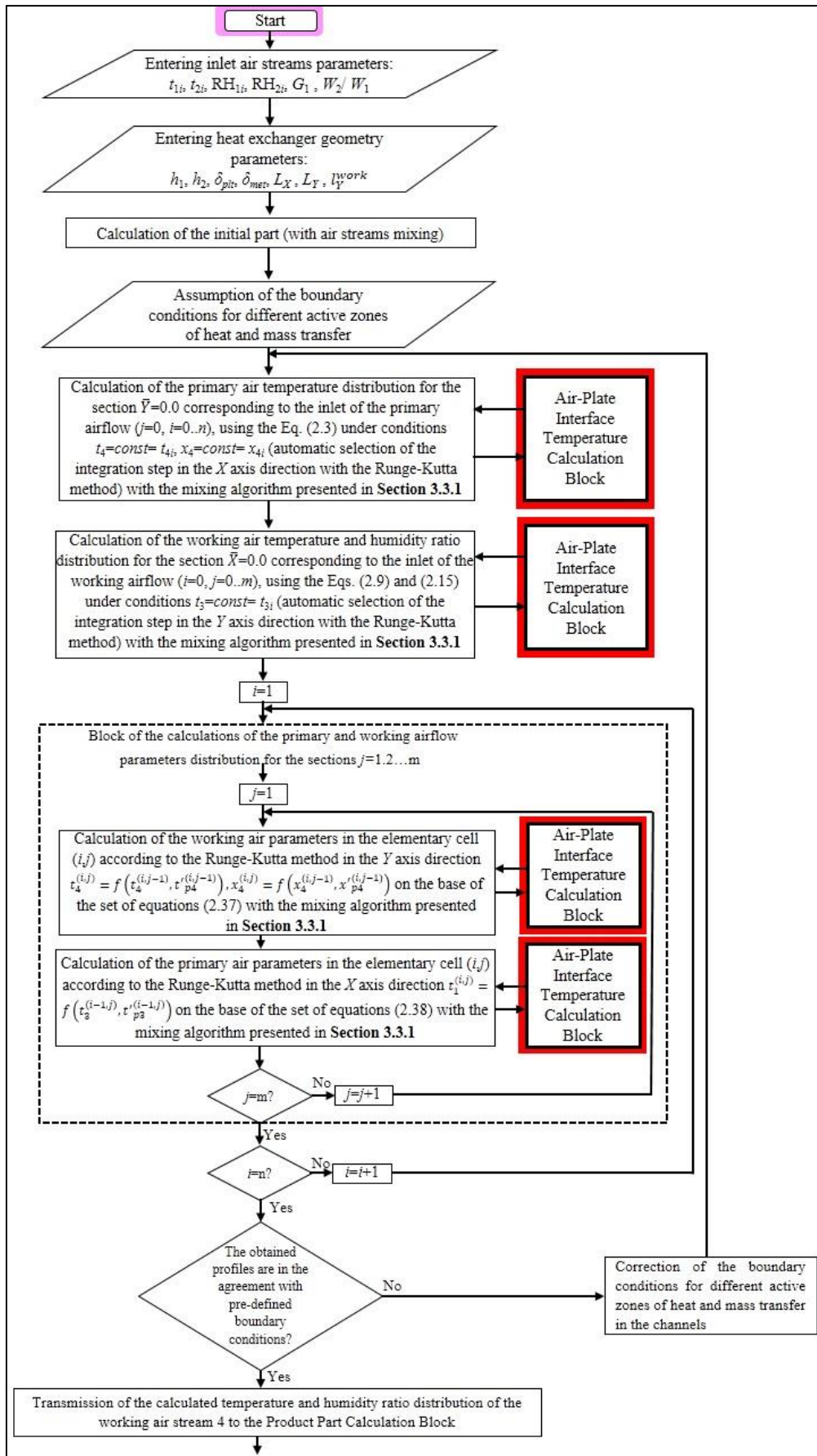
Fig. D2. Flow sheet of programing: model of the "ideal" M-Cycle.
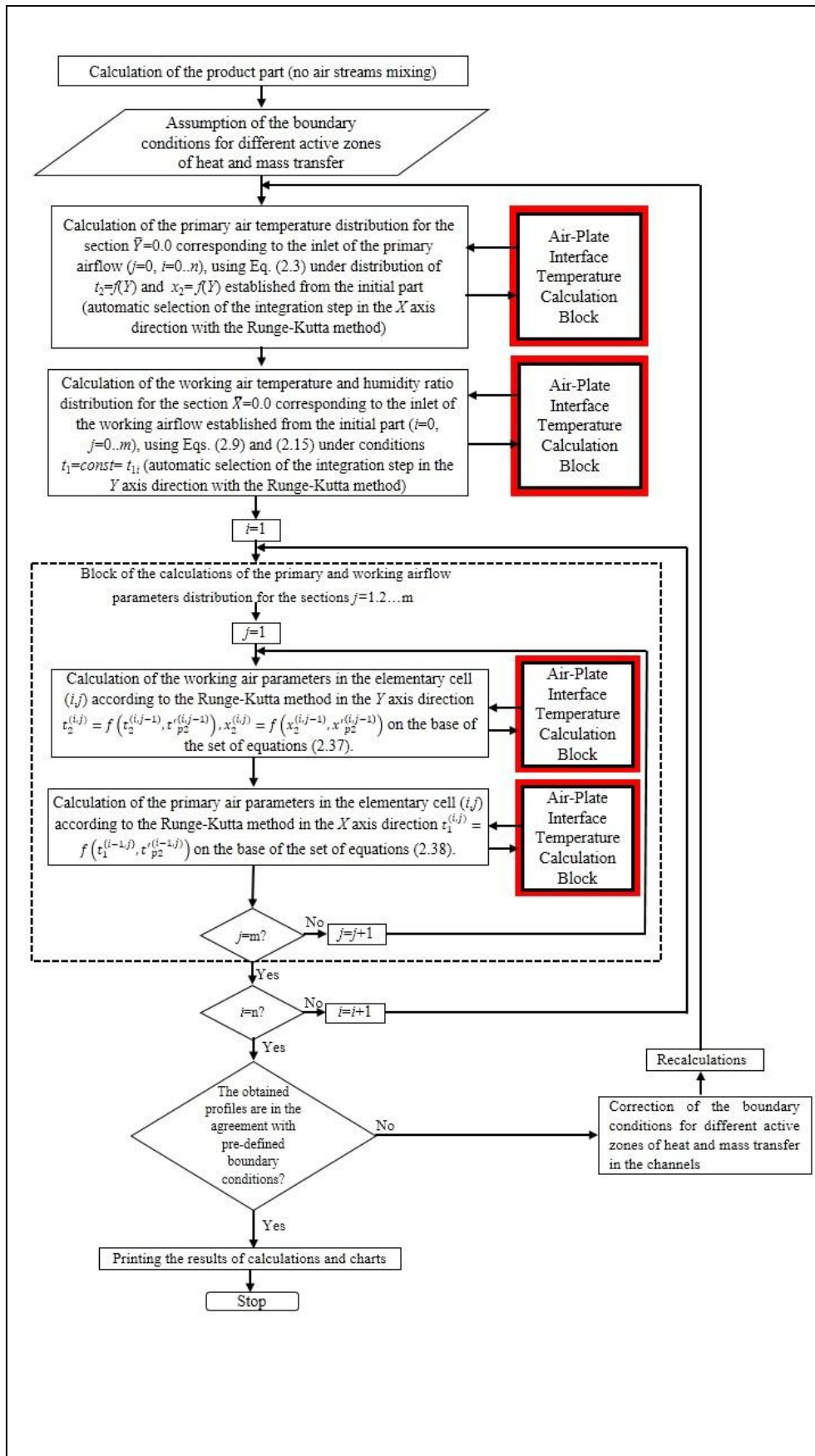
Fig. D2. Continued
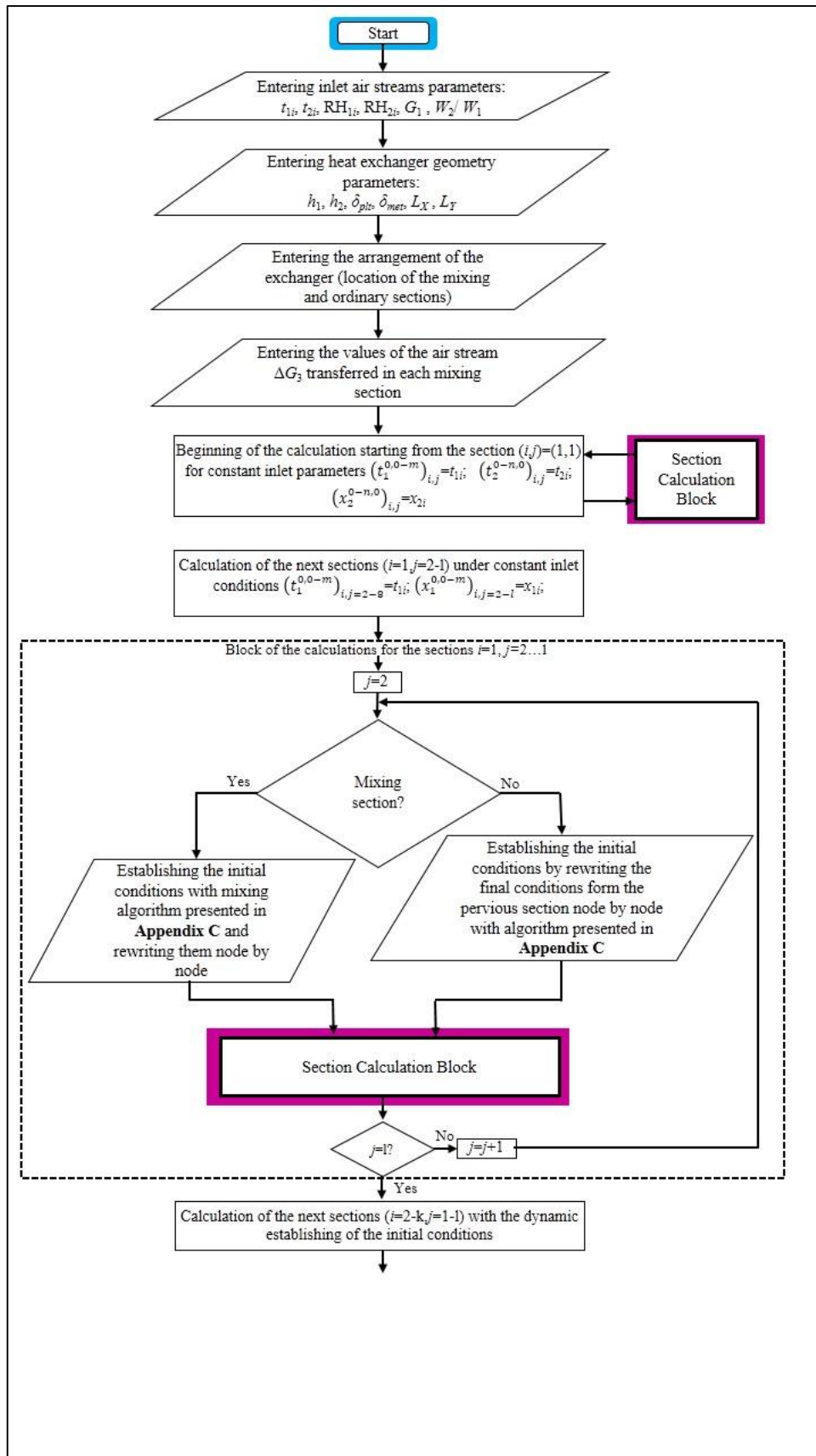
Fig. D3. Flow sheet of programing: universal Section Method.
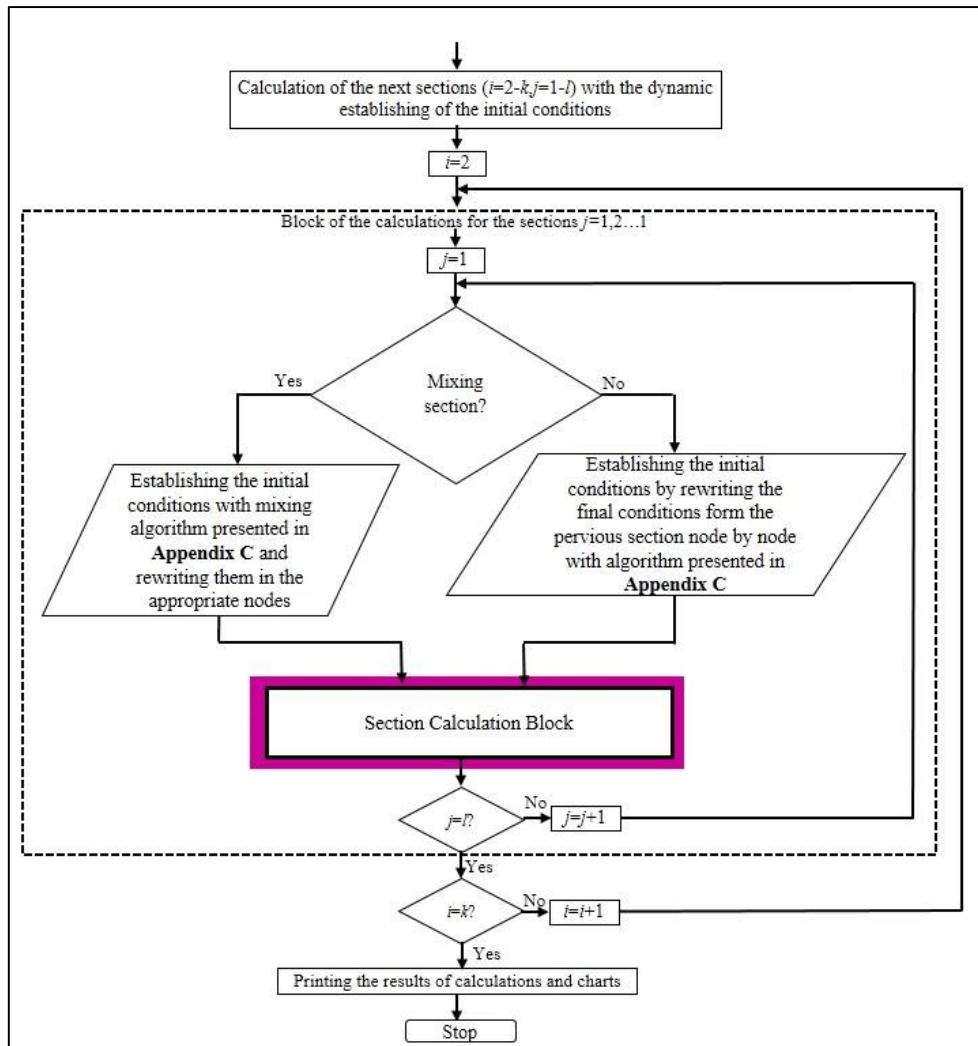
Fig. D3. Continued
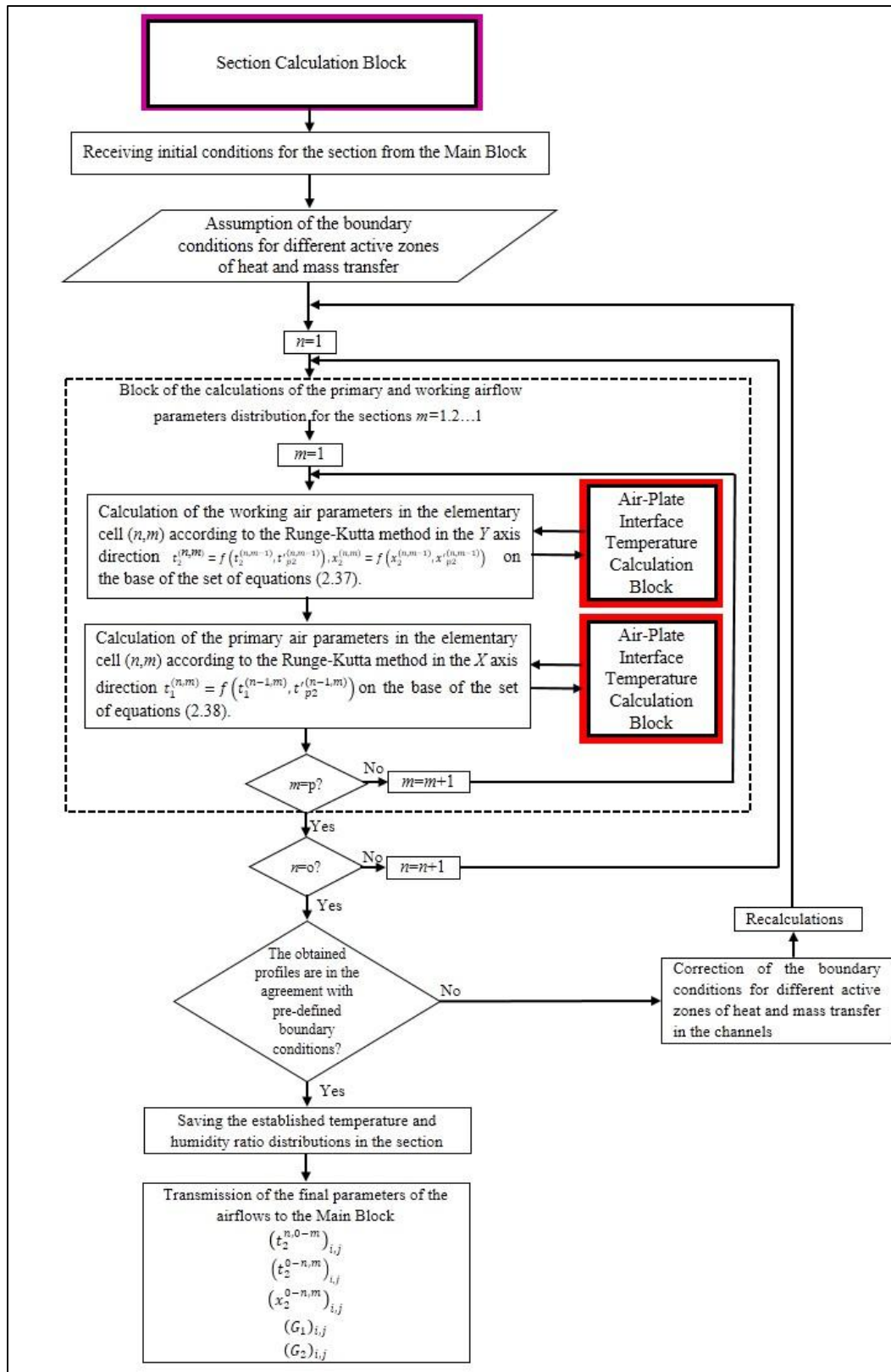
Fig. D4. Flow sheet of programing: Section Calculation Block for universal Section Method.

## Appendix E. Analysis of the accuracy of the experiment performed by author

### E.1. Analysis of the experiment accuracy

As it was mentioned earlier, the parameters measured directly on the experiments were dry and wet bulb temperatures and pressure drop on the at the orifice plates. The ranges of operating parameters for numerical and experimental study are listed in Table E1.

Table E1. Range of operating parameters for numerical and experimental study

| Specification | Unit | Range |
|---|---|---|
| Primary flow rate, $V_1$ | m³/h | (95–400) |
| Secondary flow rate, $V_2$ ($V_{3i}$) | m³/h | (70–350) |
| Inlet air temperature, $t_{1i}$, ($t_{3i}$) | °C | (20–44) |
| Inlet air humidity ratio, $x_{1i}$, ($x_{3i}$) | g/kg | (9–26) |

In order to calculate the accuracy of the direct measurements the method of maximal uncertainty $\Delta x$ was used. This method is based on the assumption that the range of the measured unit where the real value occurs can be calculated. The standard uncertainty can be calculated from the equation:

$$u(x) = \frac{\Delta x}{\sqrt{3}} \tag{E1}$$

Accuracies of the parameters measured directly along with the standard uncertainties are established in Table E2.

Table E2. Standard uncertainties of the parameters measured directly

| Measured unit | Measuring device | $\Delta x$ | $u(x)$ |
|---|---|---|---|
| Dry bulb temperature (inlet and outlet of the HMX) | VWR Traceable thermometer | 0.2°C | $\pm 0.115$ °C |
| Wet bulb temperature (inlet and outlet of the HMX) | VWR Traceable thermometer | 0.2°C | $\pm 0.115$ °C |
| Dry bulb temperature (primary and working channels of the HMX) | Omega K-type thermocouple | 0.2°C | $\pm 0.115$ °C |
| Wet bulb temperature (working channels of the HMX) | Omega K-type thermocouple | 0.2°C | $\pm 0.115$ °C |
| Pressure drop on the orifice plates | Manometer | 0.254 mm | $\pm 0.147$ mm |

In case of the parameters measured indirectly the measured value $y$ is calculated from the functional dependence (E2):

$$y = f\left(x_1, x_2, x_3, ..., x_k, ..., x_K\right) \tag{E2}$$

where: $x_1, x_2, x_3, \ldots x_k, \ldots x_K$ are the parameters measured directly.

This method is realized with the assumption that those parameters and their standard uncertainties are known. The composed standard uncertainty of direct non-correlated measurements is calculated from Eq. (E3).

$$u_c(y) = \sqrt{\sum_{k=1}^{K}\left(\frac{\partial f}{\partial x_k}\right)^2 u^2(x_k)} \tag{E3}$$

The composed standard uncertainty allows establishing value of the measured parameter, however, in order to analyse the compatibility of the measured values with other results or for the commercial purposes the expanded uncertainty $U$ for direct measurements and $U_c$ for the indirect measurements have to be applied.

$$U_c(y) = k \cdot u_c(y) \tag{E4}$$

where: $k$ is the expansion coefficient adequate to the distrust level, usually $k=2$ most of the experimental cases the value of $k$ equal 2 is recommended [152], therefore in the presented study the $k$ is equal to 2).

The standard and expanded uncertainty has the same unit as measured value. In order to calculate the relative uncertainty (standard and expanded) in the percent scale, Eq. (E5) is needed.

$$U_r(y) = \frac{U_c(y)}{y} \cdot 100\% \tag{E5}$$

The indirect parameters calculated to validate the model from the parameters measured directly are listed as follows:
- Air mass flow rate

$$0.03398 \cdot \alpha \cdot \frac{\pi \cdot d^2}{4} \cdot \sqrt{\frac{2\Delta p}{\rho}} \tag{E.6}$$

where: α- dimensionless flow coefficient from the characteristics of the orifice plate: α=0.7
0.03398- correction coefficient established by Coolerado Corporation during the pre-calibration

- Humidity ratio of the airflow is obtained with the psychrometric method [152].
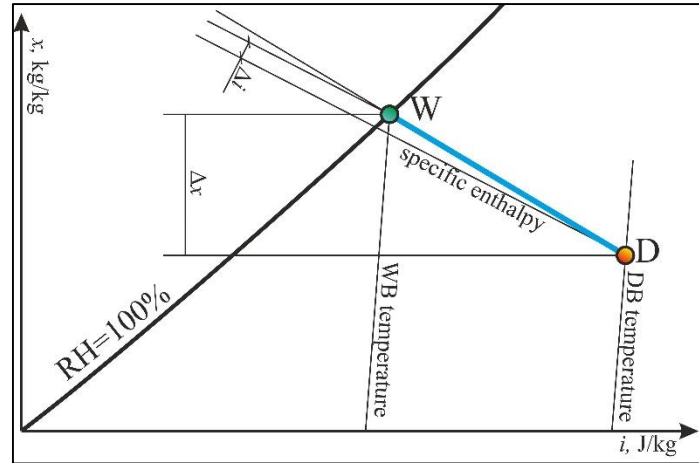
Fig. E1. Characteristic points (dry bulb temperature $t_{DB}$ and wet bulb temperature $t_{WB}$) for psychrometric method of measuring air humidity ratio [152].

Humidity ratio in the point D in Figure E1 was calculated with the following equation:

$$x_D = x_W - \Delta x \ , \ \text{kg/kg} \tag{E7}$$

Where humidity ratio in point W- $x_W$ was calculated using Eq. E8.

$$x_W = 0.622 \frac{p_w}{P_b - p_w} \ , \ \text{kg/kg} \tag{E8}$$

The slope of the characteristic line of the dry air state is calculated from the following equation:

$$\frac{i_W - i_D}{\Delta x} = c_W \cdot t_W \tag{E9}$$

where:

-$i_W$- specific enthalpy of air in the point W

$$i_W = c_p \cdot t_W + x_W \left( q^o + c_g \cdot t_W \right) \ , \ \text{kJ/kg}$$

-$i_D$- specific enthalpy of air in the point D

$$i_D = c_p \cdot t_D + \left( x_W - \Delta x \right) \left( q^o + c_g \cdot t_s \right) \ , \ \text{kJ/kg}$$

-$c_W$- specific heat of water

$$c_w = 4.206328 - 1.131471 \cdot 10^{-3} \cdot t_W + 1.224984 \cdot 10^{-5} \cdot t_W^2 \ , \ \text{kJ/(kg \cdot K)}$$

Using the above-mentioned equations the enthalpy of the air in point D can be established:

$$i_D = \frac{a + x_W \cdot d - \dfrac{d \cdot b}{c_w \cdot x_W} - \dfrac{d \cdot x_W \cdot c}{c_W \cdot t_W}}{1 - \dfrac{d}{c_W \cdot x_W}} \ , \ \text{kJ/kg} \tag{E10}$$

where $a = c_p \cdot t_D$; $b = c_p \cdot t_W$; $c = c_g \cdot t_W + q^o$; $d = c_g \cdot t_D + q^o$

- Wet bulb thermal effectiveness

$$\varepsilon_{WB} = \frac{t_{1i} - \overline{t}_{1o}}{t_{1i} - t_{1i}^{WB}} \tag{E11}$$

- Dew point thermal effectiveness

$$\varepsilon_{DP} = \frac{t_{1i} - \overline{t}_{1o}}{t_{1i} - t_{1i}^{DP}} \tag{E12}$$

- Cooling capacity

$$Q_1 = G_1 c_{p1} \left( t_{1i} - \overline{t}_{1o} \right) \tag{E13}$$

The expanded composed uncertainties for the measured parameters are presented in Table E3.

Table E3. Expanded composed and standard uncertainties for the parameters measured

| Parameters | | | Expanded composed and standard uncertainties | | |
|---|---|---|---|---|---|
| Parameter measured | Equation | Unit | Min | average | max |
| Air mass flow rate | (4.6) | kg/s | 1.12 | 2.16 | 4.95 |
| Air humidity ratio | (2.29) | g/kg | 3.90 | 5.05 | 6.53 |
| Wet bulb effectiveness | (4.9) | - | 2.12 | 3.37 | 4.65 |
| Dew point effectiveness | (4.10) | - | 2.19 | 3.21 | 4.48 |
| Cooling capacity | (4.11) | kW | 3.92 | 5.44 | 8.13 |
| Specific enthalpy of the airflow | (4.15) | kJ/kg | 2.08 | 2.40 | 2.86 |
| Air mass flow rate | (4.6) | kg/s | 1.12 | 2.16 | 4.95 |

## E.2. Analysis of the energy balance during experiment

To additionally check the accuracy of the experiment, an energy balance analysis based on the measured temperatures (dry bulb and wet bulb) and airflow rates was carried out and carefully examined.

The energy balance equation for the primary air stream is given as

$$Q_1 = G_1 c_{p1} \left( t_{1i} - \overline{t}_{1o} \right) \tag{E14}$$

The energy balance equation for the secondary air stream is given as

$$Q_2 = G_2\left(\bar{h}_{2o} - h_{3i}\right) \tag{E15}$$

where

$$\bar{i}_{2o} = c_{p2}\bar{t}_{2o} + \left(r_o + c_{g2}\bar{t}_{2o}\right)\bar{x}_{2o} \tag{E16}$$

$$\bar{i}_{3i} = \bar{i}_{1i} = c_{p1}t_{1i} + \left(r_o + c_{g1}t_{1i}\right)x_{1i} \tag{E17}$$

The energy balance equation for the water film can be calculated using the following relation

$$Q_W = G_W c_W \left(t_{Wo} - t_{Wi}\right) \tag{E18}$$

The overall heat energy conservation equation for the HMX is with Eq. (E19)

$$Q_1 = Q_2 + Q_W \tag{E19}$$

This equation indicates that amount of energy lost by the primary air stream in the dry channels should be equal to the energy absorbed by the working air stream and water film in the wet channels. It should be noted that in the case of the examined HMX, when consumed water rate corresponds to sufficient evaporation and keeping up the material of plates in hygroscopic saturated condition, the working airflow heat capacity $W_2 = G_2 c_{p2}$ is much larger than of the water $W_w = G_w c_w$ Taking this into account the impact of the energy absorbed by the water film $Q_w$ in energy conservation equation (E19) is negligible ($Q_w \approx 0$), energy balance equation is given as:

$$Q_1 \approx Q_2 \tag{E20}$$
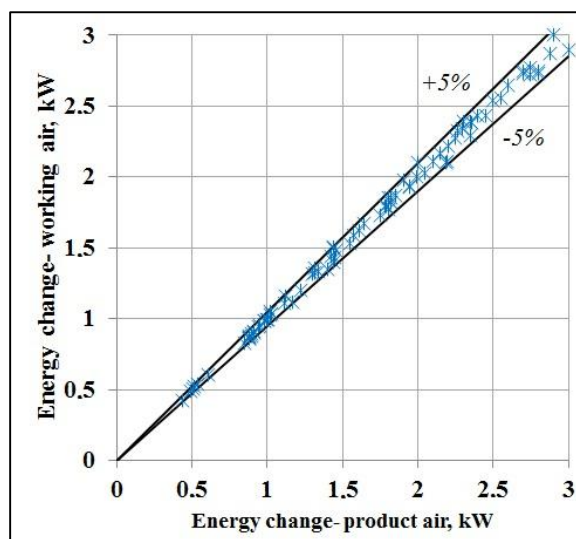


Fig. E2. The energy balance between the primary and the working airflow in the performed experiment.

The verification of the correctness of the experiment was based on energy balance equation (E20). If this check in terms of energy change in the primary airflow $Q_1$ (Eq. E14) and corresponding results of energy change for the working airflow $Q_2$ (Eq. E15) is satisfied the obtained experimental data can be considered as accurate. The results of analysis of the energy balance are presented in Figure E2. It can be seen that the obtained experimental data shows that energy balance is satisfied within a reasonable accuracy of ±5%. Therefore it can be stated that the experiment can be treated as accurate.

## Appendix F. Validation against existing experimental data

This Appendix compares the data obtained from the model and the experiment with other experimental studies concerning the cross-flow Maisotsenko cycle air cooler in order to see if the data obtained differs in the significant matter from data obtained by other authors. Not all of the studies allowed for the direct comparison of the data, due to the fact that their cases all of the necessary physical and operational parameters were not provided. The studies which allowed for the direct comparison are performed by Weerts [112] and by Zube [46]. In case of other studies only the general values of the obtained wet bulb effectiveness will be compared.

### F.1. Data obtained by Weerts

Weerts [112] performed his study at The National Snow and Ice Data Center, is located at the University of Colorado's East Campus in Boulder, Colorado, USA. The measurement station was set to test the M-Cycle air coolers which were for air-conditioning of the data center in the  room 376 on the third (top) floor in building RL-2. The cooling system design includes a unique cooling system that uses both airside economization and a Maisotsenko Cycle air conditioners. The major pieces of equipment in this system include a rooftop air handling unit powered by a 7.5 kilowatt fan motor via a variable frequency drive, eight Coolerado M50 air conditioners and hot aisle containment (Fig. F1). Weerts' studies [112] were performed for inlet airflow values varying between 1095 $m^3$/h to 4050 $m^3$/h (at supply to working airflow ratio equal 1:1), air inlet temperature varying from 17.3°C (63.1 °F) to 32.3°C (90.1 °F) and air inlet relative humidity varying from 7.4% to 62.9%. Weerts measured inlet and outlet parameters of primary and working air streams. He used HMP45C sensors (manufacturer: Campbell Scientific) with accuracy of 0.05°C and 2.0% for relative humidity to measure the outlet temperature and relative humidity of the airflow. For inlet air temperature and humidity he used ZW-007 sensors (manufacturer: HOBO), with 0.21°C and 2.5% measure accuracy. A hot wire anemometer 407123 (manufacturer: Extech Instruments) with 3.0% accuracy was used to determine the velocity profile for airflow. All these measurement sensors were linked to a CR10X data logger (manufacturer: Campbell Scientific) and a computer for data recording and analyses. The signals were scanned and reported at 3 minute intervals. The data was saved with the same intervals.

The model was set to the same operating conditions as for the experimental cases: the same inlet airflow temperature and relative humidity and the same airflow rates. Modeling results compared with experimental data collected by Weerts, including the outlet primary and working air temperature, primary air outlet relative humidity and working air outlet humidity ratio are shown respectively in Figure F2(a)−(d).

(a)



(b)
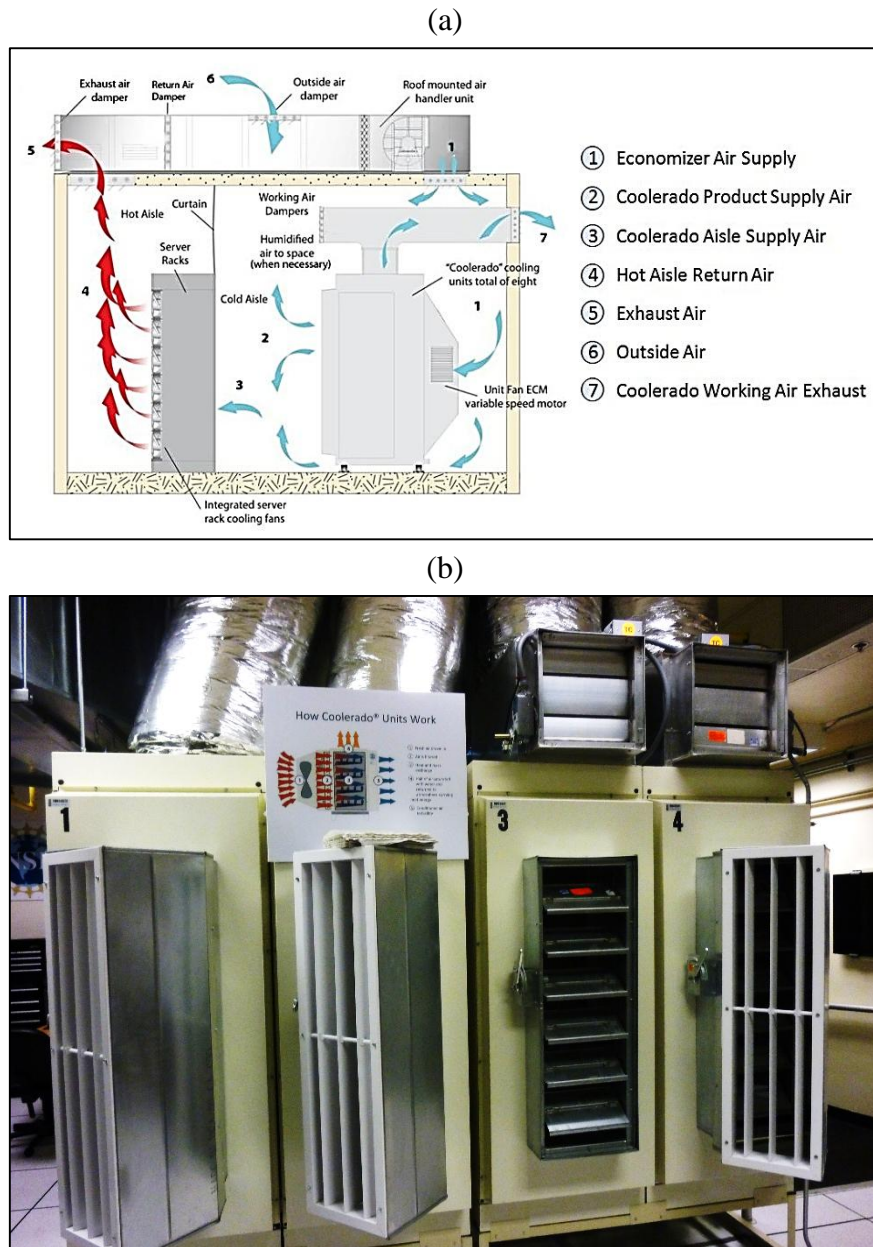


Fig. F1. Measurement station used by Weerts [112]. (a) Scheme of the experimental setup. (b) Photograph of the tested Coolerado units with the cross-flow M-Cycle air coolers.

Due to the fact that the Weerts experiment wasn't performed to obtain the direct trends in the outlet parameters, the correlation method was used to compare the model and the experiment. Discrepancies in the primary stream outlet temperature are up to 5%, the correlation between the experiment and the simulation data is equal 0.998 (Fig. F2(a)). The highest discrepancies for the outlet relative humidity of the primary airflow and the measured values are equal 7%, the correlation is equal to 0.979 (Fig. F2(b)). In case of the working airflow, the correlation between the outlet temperature is equal 0.981 (Fig. F2(c)), the discrepancies are at most 7%. For the ream outlet humidity ratio the correlation is equal 0.971, the maximal differences are equal 0.6 g/kg (Fig. F2(d)).
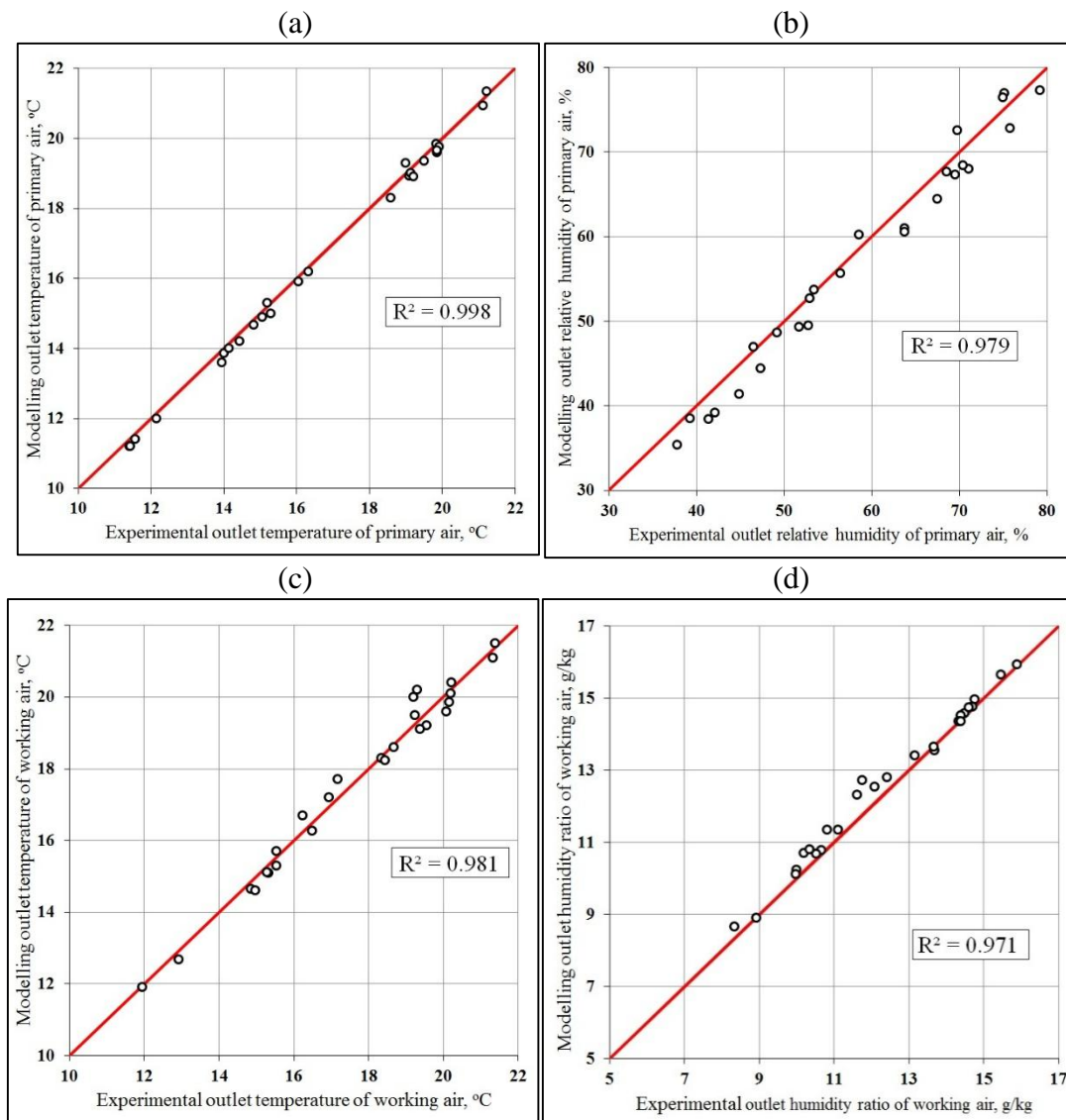
Fig. F2. M-Cycle mathematical model results compared to the Weerts data [112]. (a) Outlet temperature of the primary air stream. (b) Outlet temperature- working air stream. (c) Outlet relative humidity of the primary stream; (d) Outlet humidity ratio of the working air stream.

## F.2. Data obtained by Zube

Another comparison was prepared for the experimental data obtained by Zube [46]. Zube used the same testing bench in Coolerado Corporation as it was used by author, with different M-Cycle air cooler (the same type, but different unit). Zube analyzed the average temperatures inside the heat exchanger with analogous method to author (using similar grid with measurement points (Fig. F3). For measuring temperature he used pre-calibrated Fieldpiece HS26 Stick Meter with Thermocouple ATH4 Accessory Head (manufacturer Fieldpiece) with 0.2°C accuracy. Primary and working air inlet temperature was equal 40.0°C (104°F), inlet humidity ratio was equal 12 g/kg. Airflow rate was measured with Fieldpiece HS26 Stick Meter with Manometer ADMN2 Accessory Head (manufacturer Fieldpiece), the primary airflow rate was equal 461 m³/h, the working airflow rate was equal 342 m³/h. Air

temperature was measured in 11 points along primary air stream flow direction (points A-K in Fig. F3) and in 4 points in the secondary air stream flow direction (points 1-4 in Fig. F3).
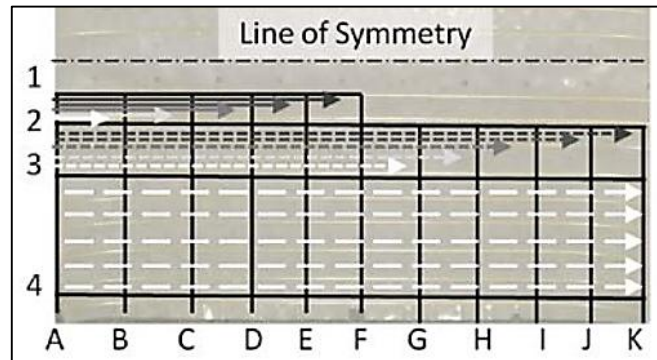


Fig. F3. Scheme of the grid used by Zube.

Modeling results compared with experimental data collected by Zube, including the average primary 1 and working airstream 3 temperature profiles are shown in Fig. F4(a) and (b) respectively. The main purpose of this comparison, as in case presented in section 4.1.7, is to find out if trends of temperature drop profiles between model and experiment are similar. Deviation of primary stream temperature profiles are at most 1.1°C (Fig. F4(a)), which can be considered as satisfying value. Despite the inaccuracy of measuring devices, the measurements inside the channels are very sensitive to the location of the probe. Therefore there is always a high uncertainty level if the measured temperature is representative for the point. It can be seen that the general trend is similar and the outlet air temperature is very close to the simulation results (0.3°C temperature difference). The same trend is visible in case of the average working air stream parameters (Fig. F4(b)). The maximal differences between the temperature obtained by model and the experiment are equal 1.1°C. Final temperature of the working air stream is close to experimental results: difference is equal 0.3°C. Average temperature differences for primary air stream are equal 0.6°C and 0.5°C for working air stream.
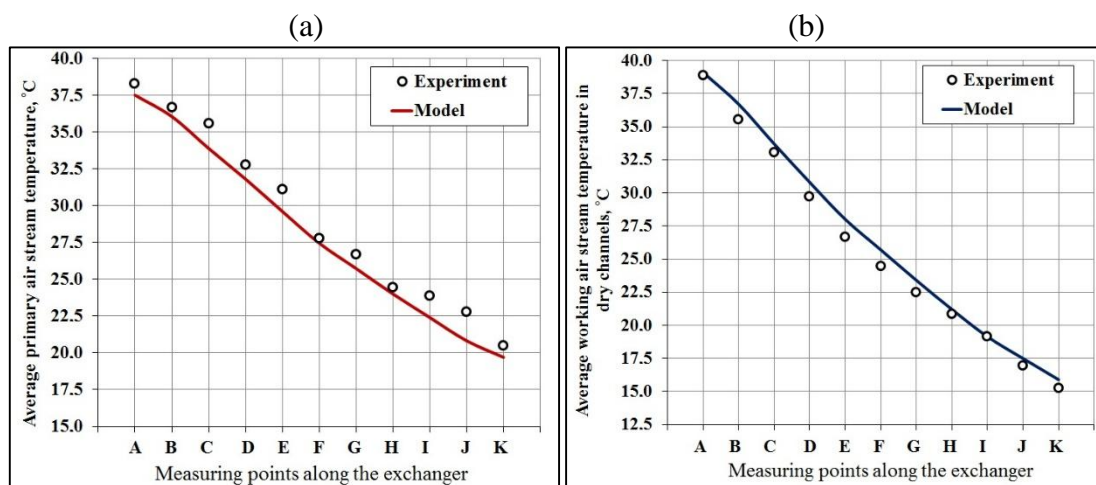


Fig. F4. Comparison between the mathematical model and the data obtained by Zube [46]. (a) Distribution of the average primary air temperature along the dry channels. (b) Distribution of the average working air temperature along the dry channels.

### F.3. Other studies

Additionally, the general outlet results can be compared with other studies. In Gillan's study [15] the present experimental research results provide similar values of outlet performance indices. The obtained outlet product air temperature for various inlet air conditions differs from the inlet airflow wet bulb temperature in the range of $\pm(0.5–3.3)°C$, while in the Gillan's study, the outlet temperature differed from the inlet airflow wet bulb temperature in the range of $\pm(0.55°C–2.7)°C$. The insufficient differences can be explained by measurement inaccuracy and changing ambient conditions.

Another experimental study of the M-Cycle heat exchanger was performed by Caliskan et. all [86] for energetic and energetic analysis purpose. The achieved wet bulb effectiveness obtained by Caliskan varies from 0.74 to 1.04, while the wet bulb effectiveness obtained in this study varies from 0.85 to 1.15. The difference can be explained by the fact that Caliskan's study was performed in real state conditions, where inlet parameters were changing dynamically, while presented experiments were performed under static inlet air conditions.

Eberling analyzed the performance and operational cost of the Coolerado Cooler based on the cross-flow M-Cycle heat and mass exchanger [40]. In case of the Eberling's tests, the obtained wet bulb effectiveness varied from 0.81 to 0.96. The differences can be explained by the fact that Eberling used older variant of the cross-flow M-Cycle air cooler, which was later replaced by the unit analyzed in this thesis. Also, this study was performed under real state conditions, as in the Caliskan case, which also may had influence on the results.

It can be seen that the general results of the experimental and modeling results obtained by author are similar to the results obtained by other authors. It is noteworthy that the character of obtained dependency of the investigated HMX cooling performance in relation to inlet air conditions corresponds to the results noted in previous works, devoted to the study of the analogical heat exchanger – the regenerative evaporative coolers [10], [50], [51].

## Appendix G. Mathematical model of the modified counter-flow evaporative air cooler (basic M-Cycle)

The modified counter-flow evaporative air cooler is transformed into a repeatable structure in order to perform numerical analysis (Fig. G1). In case of this unit the working air is delivered to the middle channel and it is separated to two wet channels which contact with the primary air from the opposite side. For the purpose of mathematical modeling, the primary air stream is marked as 1, the working airflow in the wet channels which contacts with the primary air is marked as 2, the working airflow in the dry channels is marked as 3.

The scheme of the heat and mass transfer in the in differential control volume in the V1 HMX is presented in Figure G2. The model is developed on the heat and mass balance considerations in the form of differential equations made up for the separated air streams and the energy balance equations developed for the plate surfaces in the dry and wet passages.
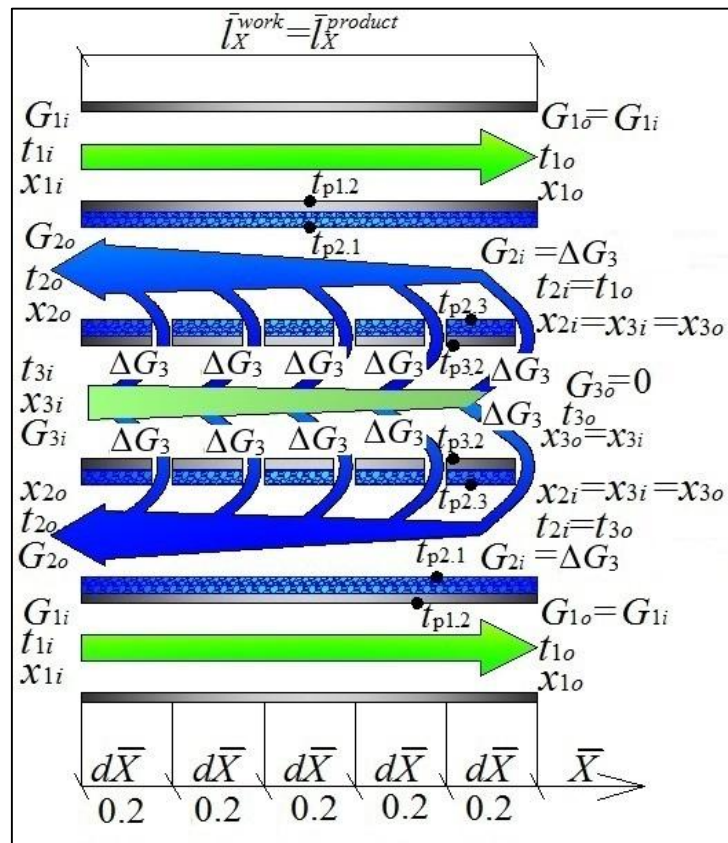


Figure G1. Airflow distribution in the dry and wet channels of the considered unit.
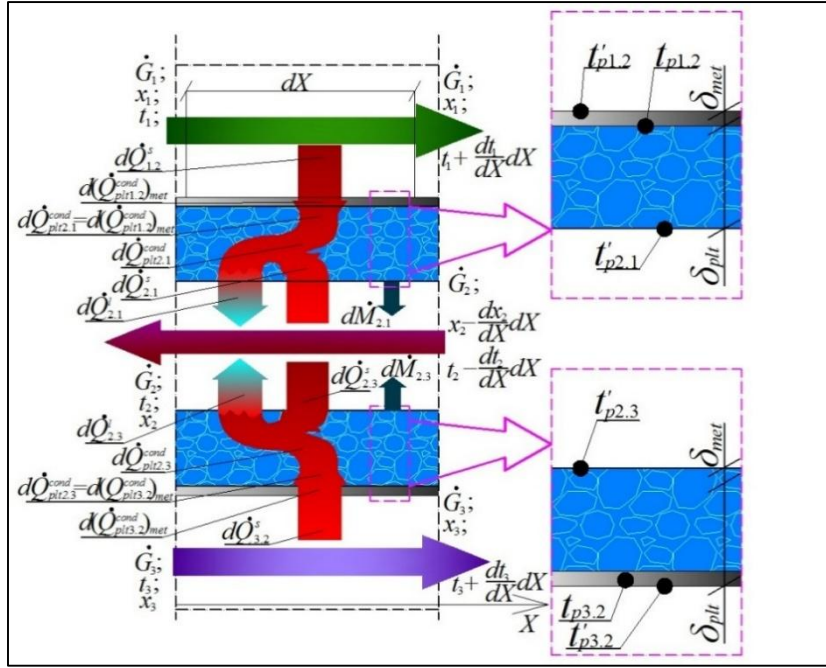
Figure G2. Schematic of heat and mass transfer in differential control volume in the V1 HMX.

According to the above-mentioned assumptions the following heat and mass balance equations can be written for the air streams passing through control volume of the channels in the V1 HMX [45]. Due to the fact that conversion of the basic energy balance equations is analogous to the method used of other evaporative coolers in the presented thesis (see **Section 2 and 3**), the conversion process is omitted in this Appendix and only the final forms of the equations are presented.

- For the primary air stream 1 in the dry channel:
- ➢ The energy conservation balance considering only sensible heat transfer on the plate surface (Fig. G2).

$$\frac{dt_1}{d\bar{\bar{X}}} = \mathrm{NTU}_{1.2}\left(t_{p1.2} - t_1\right)$$
(G1)

- For the working air stream 3 in the dry channel
- ➢ The energy conservation balance considering only sensible heat transfer on the plate surface (Fig. G2).

$$\frac{dt_3}{d\bar{\bar{X}}} = \mathrm{NTU}_{3.2}\left(t_{p3.2} - t_3\right)$$
(G2)

- For the working air stream 2 in the wet channel:
- ➢ The energy conservation balance (taking into account the specific heat capacity of the evaporated moisture).

$$\frac{dt_2}{d\bar{\bar{X}}} = -\mathrm{NTU}_{2.1}\left(t'_{p2.1} - t_2\right)\left[1 + \left(\frac{\sigma_p}{\mathrm{Le}}\right)_{2.1}\left(\frac{c_g}{c_p}\right)_2\left(x'_{p2.1} - x_2\right)\right] -$$

$$-\mathrm{NTU}_{2.3}\left(t'_{p2.3}-t_2\right)\left[1+\left(\frac{\sigma_p}{\mathrm{Le}}\right)_{2.3}\left(\frac{c_g}{c_p}\right)_2\left(x'_{p2.3}-x_2\right)\right] \tag{G3}$$

➢ The mass conservation balance for the water vapor inside the wet channel 2.

$$\frac{dx_2}{d\bar{\bar{X}}}=-\mathrm{NTU}_{2.1}\left(\frac{\sigma_p}{\mathrm{Le}}\right)_{2.1}\left(x'_{p2.1}-x_2\right)-\mathrm{NTU}_{2.3}\left(\frac{\sigma_p}{\mathrm{Le}}\right)_{2.3}\left(x'_{p2.3}-x_2\right) \tag{G4}$$

Additionally the mathematical model is supplemented by energy balance equations developed
   ➢ For the airflow/plate surface interface 1.2 in the dry primary air stream passage 1 (Fig. G2).

$$\left(\frac{\lambda_{plt}}{\delta_{plt}}\right)_{1.2}\left(t_{p1.2}-t'_{p2.1}\right)=\alpha_{1.2}\left(t_1-t_{p1.2}\right) \tag{G5}$$

   ➢ For the airflow/plate surface interface 2.1 in the wet working air stream passage 2 (Fig. G2).

$$\left(\frac{\lambda_{plt}}{\delta_{plt}}\right)_{1.2}\left(t_{p1.2}-t'_{p2.1}\right)+\alpha_{2.1}\left(t_2-t'_{p2.1}\right)=\frac{1}{c_{p2}}\left(\frac{\sigma_p\alpha q^{\circ}}{\mathrm{Le}}\right)_{2.1}\left(x'_{p2.1}-x_2\right) \tag{G6}$$

Simultaneous rearranging Eqs. (G5) and (G6) gives the following balance relationship:

$$\mathrm{NTU}_{1.2}\left(t_{p1.2}-t_1\right)+\left(\frac{W_2}{W_1}\right)\mathrm{NTU}_{2.1}\left[\left(t'_{p2.1}-t_2\right)+\frac{1}{c_{p2}}\left(\frac{\sigma_p q^{\circ}}{\mathrm{Le}}\right)_{2.1}\left(x'_{p2.1}-x_2\right)\right]=0 \tag{G7}$$

   ➢ For the airflow/plate surface interface 3.2 in the dry working air stream passage 3 (Fig. G2).

$$\left(\frac{\lambda_{plt}}{\delta_{plt}}\right)_{3.2}\left(t_{p3.2}-t'_{p2.3}\right)=\alpha_{3.2}\left(t_3-t_{p3.2}\right) \tag{G8}$$

   ➢ For the airflow/plate surface interface 2.3 in the wet working air stream passage 2 (Fig. G2).

$$\left(\frac{\lambda_{plt}}{\delta_{plt}}\right)_{3.2}\left(t_{p3.2}-t'_{p2.3}\right)+\alpha_{2.3}\left(t_2-t'_{p2.3}\right)=\frac{1}{c_{p2}}\left(\frac{\sigma_p\alpha q^{\circ}}{\mathrm{Le}}\right)_{2.3}\left(x'_{p2.3}-x_2\right) \tag{G9}$$

Simultaneous rearranging Eqs. (G8) and (G9) gives the following balance relationship:

$$\left(\frac{W_3}{W_1}\right)\mathrm{NTU}_{3.2}\left(t_{p3.2}-t_3\right)+\left(\frac{W_2}{W_1}\right)\mathrm{NTU}_{2.3}\left[\left(t'_{p2.3}-t_2\right)+\frac{1}{c_{p2}}\left(\frac{\sigma_p q^o}{\mathrm{Le}}\right)_{2.3}\left(x'_{p2.3}-x_2\right)\right]=0$$

(G10)

To complete, the set of simultaneous differential equations the boundary conditions, establishing initial thermodynamic parameters values of exchanged air streams at the entrance to the appropriate channels of the product part of the heat exchangers (Fig. G2) are needed. For the airflow parameters at the inlet to the dry channels.

$$t_1\bigg|\begin{array}{l}=t_{1i}=t_{3i}\\\overline{X}=0.0\\\overline{Y}=\left(0.0\div1.0\right)\end{array}\quad;\qquad x_1\bigg|\begin{array}{l}=x_{1i}=x_{3i}=const\\\overline{X}=\left(0.0\div1.0\right)\\\overline{Y}=\left(0.0\div1.0\right)\end{array}$$

(G11)

- For the working airflow parameters at the inlet to the wet channels.
- 

$$t_2\bigg|\begin{array}{l}=t_{2i}=t_{3o}\\\overline{Y}=\left(0.0\div1.0\right)\\\overline{X}=1.0\end{array}\quad;\qquad x_2\bigg|\begin{array}{l}=x_{2i}=x_{3o}=x_{3i}\\\overline{Y}=\left(0.0\div1.0\right)\\\overline{X}=1.0\end{array}$$

(G12)

The proposed set of the governing equations describing the heat and mass transfer process in the working part of the V1 HMX is also additionally supplemented by the algebraic equations, describing the process of air streams mixing in the wet channels [45]. Computer simulation was executed using modified Runge-Kutta method in the Wolfram Mathematica environment. It should be mentioned that validation of the model describing V1 HMX is omitted due to the fact that differential equations describing heat and mass transfer in those units is analogous to the ones describing the validated models of exchanger V2, therefore its accuracy is considered to be similar.

## Appendix H. Additional information for Section 9.1.

CCDs for $\hat{Q}$, $\varepsilon_{DP}$ and COP are presented in Tables H.1,H.3 and H.5 respectively, their tests of significance for the regression coefficients are presented in Table H.2,H.4 and H.6 respectively.

Table H.1.CCD setting in the original and coded form* of the independent parameters (X1…Xk) and experimental results for the response variable $\hat{Y}_{2i}$ (specific cooling capacity $\hat{Q}$ )

| Types of | Run | $X_1$, | $X_2$, | $X_3$, | $X_4$, | $X_5$, | Observed | Predicted | Deviations |
|---|---|---|---|---|---|---|---|---|---|
| The full factorial portion of the CCD ($n^*=2^k=32$) | 1 | 36.25(+1) | 60(+1) | 0.22(+1) | 1.2(+1) | 0.5(+1) | 7.5 | 7.6 | -0.1 |
| | 2 | 36.25(+1) | 60(+1) | 0.22(+1) | 1.2(+1) | 0.25(−1) | 8.7 | 8.8 | -0.1 |
| | 3 | 36.25(+1) | 60(+1) | 0.22(+1) | 0.8(−1) | 0.5(+1) | 7.4 | 7.4 | 0.0 |
| | 4 | 36.25(+1) | 60(+1) | 0.22(+1) | 0.8(−1) | 0.25(−1) | 8.6 | 8.6 | 0.0 |
| | 5 | 36.25(+1) | 60(+1) | 0.14(−1) | 1.2(+1) | 0.5(+1) | 5.9 | 5.9 | 0.0 |
| | 6 | 36.25(+1) | 60(+1) | 0.14(−1) | 1.2(+1) | 0.25(−1) | 6.4 | 6.4 | 0.0 |
| | 7 | 36.25(+1) | 60(+1) | 0.14(−1) | 0.8(−1) | 0.5(+1) | 5.7 | 5.7 | 0.0 |
| | 8 | 36.25(+1) | 60(+1) | 0.14(−1) | 0.8(−1) | 0.25(−1) | 6.3 | 6.2 | 0.2 |
| | 9 | 36.25(+1) | 40(−1) | 0.22(+1) | 1.2(+1) | 0.5(+1) | 12.0 | 12.1 | -0.1 |
| | 10 | 36.25(+1) | 40(−1) | 0.22(+1) | 1.2(+1) | 0.25(−1) | 14.0 | 13.8 | 0.2 |
| | 11 | 36.25(+1) | 40(−1) | 0.22(+1) | 0.8(−1) | 0.5(+1) | 11.8 | 11.9 | -0.1 |
| | 12 | 36.25(+1) | 40(−1) | 0.22(+1) | 0.8(−1) | 0.25(−1) | 13.7 | 13.6 | 0.1 |
| | 13 | 36.25(+1) | 40(−1) | 0.14(−1) | 1.2(+1) | 0.5(+1) | 9.4 | 9.4 | 0.0 |
| | 14 | 36.25(+1) | 40(−1) | 0.14(−1) | 1.2(+1) | 0.25(−1) | 10.3 | 10.4 | -0.1 |
| | 15 | 36.25(+1) | 40(−1) | 0.14(−1) | 0.8(−1) | 0.5(+1) | 9.2 | 9.2 | 0.0 |
| | 16 | 36.25(+1) | 40(−1) | 0.14(−1) | 0.8(−1) | 0.25(−1) | 10.2 | 10.2 | 0.0 |
| | 17 | 28.75(−1) | 60(+1) | 0.22(+1) | 1.2(+1) | 0.5(+1) | 6.2 | 6.1 | 0.1 |
| | 18 | 28.75(−1) | 60(+1) | 0.22(+1) | 1.2(+1) | 0.25(−1) | 7.3 | 7.3 | -0.1 |
| | 19 | 28.75(−1) | 60(+1) | 0.22(+1) | 0.8(−1) | 0.5(+1) | 6.1 | 5.9 | 0.1 |
| | 20 | 28.75(−1) | 60(+1) | 0.22(+1) | 0.8(−1) | 0.25(−1) | 7.1 | 7.1 | 0.0 |
| | 21 | 28.75(−1) | 60(+1) | 0.14(−1) | 1.2(+1) | 0.5(+1) | 4.9 | 5.0 | -0.1 |
| | 22 | 28.75(−1) | 60(+1) | 0.14(−1) | 1.2(+1) | 0.25(−1) | 5.4 | 5.4 | 0.0 |
| | 23 | 28.75(−1) | 60(+1) | 0.14(−1) | 0.8(−1) | 0.5(+1) | 4.8 | 4.8 | 0.0 |
| | 24 | 28.75(−1) | 60(+1) | 0.14(−1) | 0.8(−1) | 0.25(−1) | 5.3 | 5.2 | 0.1 |
| | 25 | 28.75(−1) | 40(−1) | 0.22(+1) | 1.2(+1) | 0.5(+1) | 9.8 | 9.8 | 0.0 |
| | 26 | 28.75(−1) | 40(−1) | 0.22(+1) | 1.2(+1) | 0.25(−1) | 11.4 | 11.5 | 0.0 |
| | 27 | 28.75(−1) | 40(−1) | 0.22(+1) | 0.8(−1) | 0.5(+1) | 9.5 | 9.6 | 0.0 |
| | 28 | 28.75(−1) | 40(−1) | 0.22(+1) | 0.8(−1) | 0.25(−1) | 11.1 | 11.3 | -0.2 |
| | 29 | 28.75(−1) | 40(−1) | 0.14(−1) | 1.2(+1) | 0.5(+1) | 7.8 | 7.6 | 0.1 |
| | 30 | 28.75(−1) | 40(−1) | 0.14(−1) | 1.2(+1) | 0.25(−1) | 8.6 | 8.6 | 0.0 |
| | 31 | 28.75(−1) | 40(−1) | 0.14(−1) | 0.8(−1) | 0.5(+1) | 7.5 | 7.4 | 0.1 |
| | 32 | 28.75(−1) | 40(−1) | 0.14(−1) | 0.8(−1) | 0.25(−1) | 8.3 | 8.4 | -0.1 |
| The axial (star) portion of the CCD ($n_\alpha=2k=10$) | 33 | 40.0(+α) | 50(0) | 0.18(0) | 1.0(0) | 0.375(0) | 10.2 | 10.3 | 0.0 |
| | 34 | 25.0(−α) | 50(0) | 0.18(0) | 1.0(0) | 0.375(0) | 6.9 | 7.0 | -0.1 |
| | 35 | 32.5(0) | 70(+α) | 0.18(0) | 1.0(0) | 0.375(0) | 4.9 | 5.02 | -0.1 |
| | 36 | 32.5(0) | 30(−α) | 0.18(0) | 1.0(0) | 0.375(0) | 12.8 | 12.7 | 0.1 |
| | 37 | 32.5(0) | 50(0) | 0.26(+α) | 1.0(0) | 0.375(0) | 10.5 | 10.4 | 0.1 |
| | 38 | 32.5(0) | 50(0) | 0.1(−α) | 1.0(0) | 0.375(0) | 5.8 | 5.9 | -0.1 |
| | 39 | 32.5(0) | 50(0) | 0.18(0) | 1.4(+α) | 0.375(0) | 8.7 | 8.7 | 0.0 |
| | 40 | 32.5(0) | 50(0) | 0.18(0) | 0.6(−α) | 0.375(0) | 8.2 | 8.3 | -0.1 |
| | 41 | 32.5(0) | 50(0) | 0.18(0) | 1.0(0) | 0.625(+α) | 7.0 | 7.0 | 0.0 |
| | 42 | 32.5(0) | 50(0) | 0.18(0) | 1.0(0) | 0.125(−α) | 9.2 | 9.1 | 0.0 |
| Set of the center points of the CCD ($n_R=8$) | 43 | 32.5(0) | 50(0) | 0.18(0) | 1.0(0) | 0.375(0) | 8.6 | 8.6 | 0.0 |
| | 44 | 32.5(0) | 50(0) | 0.18(0) | 1.0(0) | 0.375(0) | 8.8 | 8.6 | 0.1 |
| | 45 | 32.5(0) | 50(0) | 0.18(0) | 1.0(0) | 0.375(0) | 8.4 | 8.6 | -0.2 |
| | 46 | 32.5(0) | 50(0) | 0.18(0) | 1.0(0) | 0.375(0) | 8.6 | 8.6 | 0.0 |
| | 47 | 32.5(0) | 50(0) | 0.18(0) | 1.0(0) | 0.375(0) | 8.8 | 8.6 | 0.1 |
| | 48 | 32.5(0) | 50(0) | 0.18(0) | 1.0(0) | 0.375(0) | 8.4 | 8.6 | -0.2 |
| | 49 | 32.5(0) | 50(0) | 0.18(0) | 1.2(0) | 0.5(0) | 8.6 | 8.6 | 0.0 |
| | 50 | 32.5(0) | 50(0) | 0.18(0) | 1.2(0) | 0.25(0) | 8.8 | 8.6 | 0.1 |

* Values in parenthesis are the coded forms of variables.

Table H.2.Test of significance for regression coefficients of predicted model equation for $\hat{Y}_2$ (specific cooling capacity $\hat{Q}$ )

| Term | Coefficient estimated | $t_j$ | $t_p$ | Statistically significant |
|---|---|---|---|---|
| $b_0$ | 8.63 | 414 | | *Yes* |
| $b_1$ | 0.82 | 27.2 | | *Yes* |
| $b_2$ | -1.92 | 64 | | *Yes* |
| $b_3$ | 1.14 | 37.9 | | *Yes* |
| $b_4$ | 0.106 | 3.53 | | *Yes* |
| $b_5$ | -0.539 | 17.9 | | *Yes* |
| $b_{12}$ | -0.219 | 5.93 | | **Yes** |
| $b_{13}$ | 0.136 | 3.69 | | **Yes** |
| $b_{14}$ | -0.009 | 0.23 | | No |
| $b_{15}$ | -0.039 | 1.05 | | No |
| $b_{23}$ | -0.246 | 6.66 | 2.37 | **Yes** |
| $b_{24}$ | -0.031 | 0.85 | | No |
| $b_{25}$ | 0.124 | 3.38 | | **Yes** |
| $b_{34}$ | 0.0114 | 0.31 | | No |
| $b_{35}$ | -0.183 | 4.97 | | **Yes** |
| $b_{45}$ | -0.003 | 0.07 | | No |
| $b_{11}$ | -0.0075 | 1.01 | | No |
| $b_{22}$ | 0.058 | 8.49 | | **Yes** |
| $b_{33}$ | -0.119 | 17.5 | | **Yes** |
| $b_{44}$ | -0.039 | 5.67 | | **Yes** |
| $b_{55}$ | -0.143 | 21.0 | | **Yes** |

Table H.3. CCD setting in the original and coded form* of the independent parameters ($X_1 \ldots X_k$) and experimental results for the response variable $\hat{Y}_{3i}$ (dew point effectiveness $\varepsilon_{DP}$)

| Types of | Run | $X_1$, | $X_2$, | $X_3$, | $X_4$, | $X_5$, | Observed | Predicted | Deviations |
|---|---|---|---|---|---|---|---|---|---|
| | 1 | 36.25(+1) | 60(+1) | 0.22(+1) | 1.2(+1) | 0.5(+1) | 0.58 | 0.59 | -0.01 |
| | 2 | 36.25(+1) | 60(+1) | 0.22(+1) | 1.2(+1) | 0.25(−1) | 0.68 | 0.68 | 0.00 |
| | 3 | 36.25(+1) | 60(+1) | 0.22(+1) | 0.8(−1) | 0.5(+1) | 0.57 | 0.58 | -0.01 |
| | 4 | 36.25(+1) | 60(+1) | 0.22(+1) | 0.8(−1) | 0.25(−1) | 0.67 | 0.66 | 0.00 |
| | 5 | 36.25(+1) | 60(+1) | 0.14(−1) | 1.2(+1) | 0.5(+1) | 0.71 | 0.71 | 0.00 |
| | 6 | 36.25(+1) | 60(+1) | 0.14(−1) | 1.2(+1) | 0.25(−1) | 0.78 | 0.78 | 0.00 |
| | 7 | 36.25(+1) | 60(+1) | 0.14(−1) | 0.8(−1) | 0.5(+1) | 0.70 | 0.70 | 0.00 |
| | 8 | 36.25(+1) | 60(+1) | 0.14(−1) | 0.8(−1) | 0.25(−1) | 0.77 | 0.76 | 0.01 |
| The full factorial portion of the CCD ($n^*=2^k=32$) | 9 | 36.25(+1) | 40(−1) | 0.22(+1) | 1.2(+1) | 0.5(+1) | 0.53 | 0.53 | 0.00 |
| | 10 | 36.25(+1) | 40(−1) | 0.22(+1) | 1.2(+1) | 0.25(−1) | 0.62 | 0.62 | 0.00 |
| | 11 | 36.25(+1) | 40(−1) | 0.22(+1) | 0.8(−1) | 0.5(+1) | 0.52 | 0.52 | 0.00 |
| | 12 | 36.25(+1) | 40(−1) | 0.22(+1) | 0.8(−1) | 0.25(−1) | 0.61 | 0.60 | 0.00 |
| | 13 | 36.25(+1) | 40(−1) | 0.14(−1) | 1.2(+1) | 0.5(+1) | 0.66 | 0.65 | 0.00 |
| | 14 | 36.25(+1) | 40(−1) | 0.14(−1) | 1.2(+1) | 0.25(−1) | 0.72 | 0.72 | 0.00 |
| | 15 | 36.25(+1) | 40(−1) | 0.14(−1) | 0.8(−1) | 0.5(+1) | 0.64 | 0.64 | 0.00 |
| | 16 | 36.25(+1) | 40(−1) | 0.14(−1) | 0.8(−1) | 0.25(−1) | 0.71 | 0.70 | 0.00 |
| | 17 | 28.75(−1) | 60(+1) | 0.22(+1) | 1.2(+1) | 0.5(+1) | 0.51 | 0.51 | 0.00 |
| | 18 | 28.75(−1) | 60(+1) | 0.22(+1) | 1.2(+1) | 0.25(−1) | 0.60 | 0.59 | 0.00 |
| | 19 | 28.75(−1) | 60(+1) | 0.22(+1) | 0.8(−1) | 0.5(+1) | 0.50 | 0.49 | 0.00 |
| | 20 | 28.75(−1) | 60(+1) | 0.22(+1) | 0.8(−1) | 0.25(−1) | 0.58 | 0.58 | 0.00 |
| | 21 | 28.75(−1) | 60(+1) | 0.14(−1) | 1.2(+1) | 0.5(+1) | 0.63 | 0.63 | 0.00 |
| | 22 | 28.75(−1) | 60(+1) | 0.14(−1) | 1.2(+1) | 0.25(−1) | 0.70 | 0.69 | 0.00 |
| | 23 | 28.75(−1) | 60(+1) | 0.14(−1) | 0.8(−1) | 0.5(+1) | 0.61 | 0.61 | 0.00 |
| | 24 | 28.75(−1) | 60(+1) | 0.14(−1) | 0.8(−1) | 0.25(−1) | 0.68 | 0.68 | 0.00 |
| | 25 | 28.75(−1) | 40(−1) | 0.22(+1) | 1.2(+1) | 0.5(+1) | 0.46 | 0.45 | 0.01 |
| | 26 | 28.75(−1) | 40(−1) | 0.22(+1) | 1.2(+1) | 0.25(−1) | 0.54 | 0.54 | 0.00 |
| | 27 | 28.75(−1) | 40(−1) | 0.22(+1) | 0.8(−1) | 0.5(+1) | 0.45 | 0.43 | 0.01 |
| | 28 | 28.75(−1) | 40(−1) | 0.22(+1) | 0.8(−1) | 0.25(−1) | 0.52 | 0.52 | 0.00 |
| | 29 | 28.75(−1) | 40(−1) | 0.14(−1) | 1.2(+1) | 0.5(+1) | 0.57 | 0.57 | 0.00 |
| | 30 | 28.75(−1) | 40(−1) | 0.14(−1) | 1.2(+1) | 0.25(−1) | 0.63 | 0.64 | -0.01 |
| | 31 | 28.75(−1) | 40(−1) | 0.14(−1) | 0.8(−1) | 0.5(+1) | 0.55 | 0.55 | 0.00 |
| | 32 | 28.75(−1) | 40(−1) | 0.14(−1) | 0.8(−1) | 0.25(−1) | 0.61 | 0.62 | -0.01 |
| The axial (star) portion of the CCD ($n_\alpha=2k=10$) | 33 | 40.0(+α) | 50(0) | 0.18(0) | 1.0(0) | 0.375(0) | 0.70 | 0.70 | 0.00 |
| | 34 | 25.0(−α) | 50(0) | 0.18(0) | 1.0(0) | 0.375(0) | 0.53 | 0.53 | 0.00 |
| | 35 | 32.5(0) | 70(+α) | 0.18(0) | 1.0(0) | 0.375(0) | 0.67 | 0.67 | 0.00 |
| | 36 | 32.5(0) | 30(−α) | 0.18(0) | 1.0(0) | 0.375(0) | 0.55 | 0.55 | 0.00 |
| | 37 | 32.5(0) | 50(0) | 0.26(+α) | 1.0(0) | 0.375(0) | 0.53 | 0.53 | -0.01 |
| | 38 | 32.5(0) | 50(0) | 0.1(−α) | 1.0(0) | 0.375(0) | 0.76 | 0.75 | 0.00 |
| | 39 | 32.5(0) | 50(0) | 0.18(0) | 1.4(+α) | 0.375(0) | 0.63 | 0.63 | 0.00 |
| | 40 | 32.5(0) | 50(0) | 0.18(0) | 0.6(−α) | 0.375(0) | 0.60 | 0.60 | 0.00 |
| | 41 | 32.5(0) | 50(0) | 0.18(0) | 1.0(0) | 0.625(+α) | 0.51 | 0.51 | 0.00 |
| | 42 | 32.5(0) | 50(0) | 0.18(0) | 1.0(0) | 0.125(−α) | 0.66 | 0.66 | 0.01 |
| Set of the center points of the CCD ($n_K=8$) | 43 | 32.5(0) | 50(0) | 0.18(0) | 1.0(0) | 0.375(0) | 0.62 | 0.62 | 0.00 |
| | 44 | 32.5(0) | 50(0) | 0.18(0) | 1.0(0) | 0.375(0) | 0.63 | 0.62 | 0.01 |
| | 45 | 32.5(0) | 50(0) | 0.18(0) | 1.0(0) | 0.375(0) | 0.61 | 0.62 | -0.01 |
| | 46 | 32.5(0) | 50(0) | 0.18(0) | 1.0(0) | 0.375(0) | 0.62 | 0.62 | 0.00 |
| | 47 | 32.5(0) | 50(0) | 0.18(0) | 1.0(0) | 0.375(0) | 0.63 | 0.62 | 0.01 |
| | 48 | 32.5(0) | 50(0) | 0.18(0) | 1.0(0) | 0.375(0) | 0.61 | 0.62 | -0.01 |
| | 49 | 32.5(0) | 50(0) | 0.18(0) | 1.2(0) | 0.5(0) | 0.63 | 0.62 | 0.01 |
| | 50 | 32.5(0) | 50(0) | 0.18(0) | 1.2(0) | 0.25(0) | 0.61 | 0.62 | -0.01 |

\* Values in parenthesis are the coded forms of variables.

Table H.4.Test of significance for regression coefficients of predicted model equation for $\acute{Y}_3$ (dew point effectiveness $\varepsilon_{DP}$)

| Term | Coefficient estimated | $t_j$ | $t_p$ | Statistically significant |
|------|------|------|------|------|
| $b_0$ | 0.623 | 476 | | *Yes* |
| $b_1$ | 0.0419 | 20.2 | | *Yes* |
| $b_2$ | 0.0291 | 15.4 | | *Yes* |
| $b_3$ | -0.055 | 29.3 | | *Yes* |
| $b_4$ | 0.0076 | 4.03 | | *Yes* |
| $b_5$ | -0.038 | 20.1 | | *Yes* |
| $b_{12}$ | -0.0097 | 0.42 | | No |
| $b_{13}$ | -0.002 | 0.85 | | No |
| $b_{14}$ | -0.001 | 0.45 | | No |
| $b_{15}$ | -0.0018 | 0.77 | | No |
| $b_{23}$ | -0.0017 | 0.77 | 2.37 | No |
| $b_{24}$ | -0.0005 | 0.20 | | No |
| $b_{25}$ | -0.002 | 0.85 | | No |
| $b_{34}$ | -0.0007 | 0.31 | | No |
| $b_{35}$ | -0.005 | 2.45 | | *Yes* |
| $b_{45}$ | -0.0002 | 0.07 | | No |
| $b_{11}$ | -0.0016 | 3.75 | | *Yes* |
| $b_{22}$ | -0.0031 | 7.16 | | *Yes* |
| $b_{33}$ | 0.0052 | 12.1 | | *Yes* |
| $b_{44}$ | -0.0024 | 5.61 | | *Yes* |
| $b_{55}$ | -0.01 | 23.64 | | *Yes* |

Table H.5.CCD setting in the original and coded form* of the independent parameters ($X_1 \ldots X_k$) and experimental results for the response variable $\hat{Y}_{4i}$ (COP)

| Types of | Run | $X_1$, | $X_2$, | $X_3$, | $X_4$, | $X_5$, | Observed | Predicted | Deviations |
|---|---|---|---|---|---|---|---|---|---|
| The full factorial portion of the CCD ($n^* = 2^k = 32$) | 1 | 36.25(+1) | 60(+1) | 0.22(+1) | 1.2(+1) | 0.5(+1) | 40.7 | 39.3 | 1.4 |
| | 2 | 36.25(+1) | 60(+1) | 0.22(+1) | 1.2(+1) | 0.25(−1) | 25.8 | 28.9 | -3.2 |
| | 3 | 36.25(+1) | 60(+1) | 0.22(+1) | 0.8(−1) | 0.5(+1) | 84.6 | 85.7 | -1.1 |
| | 4 | 36.25(+1) | 60(+1) | 0.22(+1) | 0.8(−1) | 0.25(−1) | 55.0 | 53.2 | 1.9 |
| | 5 | 36.25(+1) | 60(+1) | 0.14(−1) | 1.2(+1) | 0.5(+1) | 78.2 | 78.8 | -0.6 |
| | 6 | 36.25(+1) | 60(+1) | 0.14(−1) | 1.2(+1) | 0.25(−1) | 46.7 | 43.5 | 3.2 |
| | 7 | 36.25(+1) | 60(+1) | 0.14(−1) | 0.8(−1) | 0.5(+1) | 161.9 | 167.2 | -5.3 |
| | 8 | 36.25(+1) | 60(+1) | 0.14(−1) | 0.8(−1) | 0.25(−1) | 100.0 | 105.7 | -5.7 |
| | 9 | 36.25(+1) | 40(−1) | 0.22(+1) | 1.2(+1) | 0.5(+1) | 65.1 | 61.6 | 3.5 |
| | 10 | 36.25(+1) | 40(−1) | 0.22(+1) | 1.2(+1) | 0.25(−1) | 41.3 | 36.9 | 4.3 |
| | 11 | 36.25(+1) | 40(−1) | 0.22(+1) | 0.8(−1) | 0.5(+1) | 134.6 | 139.8 | -5.3 |
| | 12 | 36.25(+1) | 40(−1) | 0.22(+1) | 0.8(−1) | 0.25(−1) | 87.8 | 89.0 | -1.2 |
| | 13 | 36.25(+1) | 40(−1) | 0.14(−1) | 1.2(+1) | 0.5(+1) | 125.9 | 130.4 | -4.5 |
| | 14 | 36.25(+1) | 40(−1) | 0.14(−1) | 1.2(+1) | 0.25(−1) | 75.3 | 76.7 | -1.4 |
| | 15 | 36.25(+1) | 40(−1) | 0.14(−1) | 0.8(−1) | 0.5(+1) | 259.4 | 246.6 | 12.8 |
| | 16 | 36.25(+1) | 40(−1) | 0.14(−1) | 0.8(−1) | 0.25(−1) | 160.7 | 166.8 | -6.1 |
| | 17 | 28.75(−1) | 60(+1) | 0.22(+1) | 1.2(+1) | 0.5(+1) | 33.6 | 30.2 | 3.4 |
| | 18 | 28.75(−1) | 60(+1) | 0.22(+1) | 1.2(+1) | 0.25(−1) | 21.4 | 25.1 | -3.7 |
| | 19 | 28.75(−1) | 60(+1) | 0.22(+1) | 0.8(−1) | 0.5(+1) | 69.2 | 67.8 | 1.4 |
| | 20 | 28.75(−1) | 60(+1) | 0.22(+1) | 0.8(−1) | 0.25(−1) | 45.4 | 43.8 | 1.6 |
| | 21 | 28.75(−1) | 60(+1) | 0.14(−1) | 1.2(+1) | 0.5(+1) | 65.5 | 64.1 | 1.4 |
| | 22 | 28.75(−1) | 60(+1) | 0.14(−1) | 1.2(+1) | 0.25(−1) | 39.4 | 37.2 | 2.3 |
| | 23 | 28.75(−1) | 60(+1) | 0.14(−1) | 0.8(−1) | 0.5(+1) | 134.2 | 139.7 | -5.5 |
| | 24 | 28.75(−1) | 60(+1) | 0.14(−1) | 0.8(−1) | 0.25(−1) | 83.6 | 86.6 | -3.1 |
| | 25 | 28.75(−1) | 40(−1) | 0.22(+1) | 1.2(+1) | 0.5(+1) | 52.9 | 47.3 | 5.6 |
| | 26 | 28.75(−1) | 40(−1) | 0.22(+1) | 1.2(+1) | 0.25(−1) | 33.8 | 31.1 | 2.6 |
| | 27 | 28.75(−1) | 40(−1) | 0.22(+1) | 0.8(−1) | 0.5(+1) | 108.8 | 112.8 | -4.0 |
| | 28 | 28.75(−1) | 40(−1) | 0.22(+1) | 0.8(−1) | 0.25(−1) | 71.2 | 70.4 | 0.7 |
| | 29 | 28.75(−1) | 40(−1) | 0.14(−1) | 1.2(+1) | 0.5(+1) | 103.6 | 106.4 | -2.8 |
| | 30 | 28.75(−1) | 40(−1) | 0.14(−1) | 1.2(+1) | 0.25(−1) | 62.5 | 61.2 | 1.3 |
| | 31 | 28.75(−1) | 40(−1) | 0.14(−1) | 0.8(−1) | 0.5(+1) | 211.5 | 209.9 | 1.5 |
| | 32 | 28.75(−1) | 40(−1) | 0.14(−1) | 0.8(−1) | 0.25(−1) | 131.9 | 138.5 | -6.6 |
| The axial (star) portion of the CCD ($n_\alpha = 2k = 10$) | 33 | 40.0(+α) | 50(0) | 0.18(0) | 1.0(0) | 0.375(0) | 91.7 | 91.6 | 0.1 |
| | 34 | 25.0(−α) | 50(0) | 0.18(0) | 1.0(0) | 0.375(0) | 62.2 | 58.2 | 3.9 |
| | 35 | 32.5(0) | 70(+α) | 0.18(0) | 1.0(0) | 0.375(0) | 43.8 | 38.1 | 5.7 |
| | 36 | 32.5(0) | 30(−α) | 0.18(0) | 1.0(0) | 0.375(0) | 114.5 | 116.3 | -1.8 |
| | 37 | 32.5(0) | 50(0) | 0.26(+α) | 1.0(0) | 0.375(0) | 45.1 | 51.0 | -5.9 |
| | 38 | 32.5(0) | 50(0) | 0.1(−α) | 1.0(0) | 0.375(0) | 168.8 | 162.7 | 6.1 |
| | 39 | 32.5(0) | 50(0) | 0.18(0) | 1.4(+α) | 0.375(0) | 41.0 | 44.0 | -3.0 |
| | 40 | 32.5(0) | 50(0) | 0.18(0) | 0.6(−α) | 0.375(0) | 185.5 | 177.4 | 8.1 |
| | 41 | 32.5(0) | 50(0) | 0.18(0) | 1.0(0) | 0.625(+α) | 93.9 | 97.5 | -3.6 |
| | 42 | 32.5(0) | 50(0) | 0.18(0) | 1.0(0) | 0.125(−α) | 29.3 | 25.3 | 4.0 |
| Set of the center points of the CCD ($n_R = 8$) | 43 | 32.5(0) | 50(0) | 0.18(0) | 1.0(0) | 0.375(0) | 77.1 | 77.9 | -0.8 |
| | 44 | 32.5(0) | 50(0) | 0.18(0) | 1.0(0) | 0.375(0) | 83.8 | 77.9 | 5.8 |
| | 45 | 32.5(0) | 50(0) | 0.18(0) | 1.0(0) | 0.375(0) | 71.6 | 77.9 | -6.4 |
| | 46 | 32.5(0) | 50(0) | 0.18(0) | 1.0(0) | 0.375(0) | 80.5 | 77.9 | 2.6 |
| | 47 | 32.5(0) | 50(0) | 0.18(0) | 1.0(0) | 0.375(0) | 83.8 | 77.9 | 5.8 |
| | 48 | 32.5(0) | 50(0) | 0.18(0) | 1.0(0) | 0.375(0) | 71.6 | 77.9 | -6.4 |
| | 49 | 32.5(0) | 50(0) | 0.18(0) | 1.2(0) | 0.5(0) | 82.0 | 77.9 | 4.0 |
| | 50 | 32.5(0) | 50(0) | 0.18(0) | 1.2(0) | 0.25(0) | 74.5 | 77.9 | -3.4 |

* Values in parenthesis are the coded forms of variables.

Table H.6. Test of significance for regression coefficients of predicted model equation for $\hat{Y}_{4i}$ (COP)

| Term | Coefficient estimated | $t_j$ | $t_p$ | Statistically significant |
|------|------|------|------|------|
| $b_0$ | 78 | 108 | | *Yes* |
| $b_1$ | 8.34 | 7.98 | | *Yes* |
| $b_2$ | -19.55 | 18.7 | | *Yes* |
| $b_3$ | -27.91 | 26.7 | | *Yes* |
| $b_4$ | -31.92 | 30.5 | | *Yes* |
| $b_5$ | 19.43 | 18.6 | | *Yes* |
| $b_{12}$ | -2.29 | 1.79 | | No |
| $b_{13}$ | -2.425 | 1.89 | | No |
| $b_{14}$ | -3.191 | 2.5 | | *Yes* |
| $b_{15}$ | 2.11 | 1.65 | | *Yes* |
| $b_{23}$ | 6.307 | 4.93 | 2.37 | *Yes* |
| $b_{24}$ | 6.958 | 5.44 | | *Yes* |
| $b_{25}$ | -4.587 | 3.58 | | *Yes* |
| $b_{34}$ | 9.503 | 7.42 | | *Yes* |
| $b_{35}$ | -7.256 | 5.67 | | *Yes* |
| $b_{45}$ | -6.539 | 5.11 | | *Yes* |
| $b_{11}$ | -0.75 | 0.83 | | No |
| $b_{22}$ | -0.168 | 0.18 | | No |
| $b_{33}$ | 7.237 | 7.92 | | *Yes* |
| $b_{44}$ | 8.915 | 9.75 | | *Yes* |
| $b_{55}$ | -4.832 | 5.30 | | *Yes* |

## Appendix I. Sensitivity analysis on the influence factors on the basis of regression models

The impact of independent factors on the performance characteristics were analyzed through the RSM approach on the surface plots in Figures I1–I5. Three-dimensional plots are presented for different combination of pairs of independent parameters varied from minimal to maximal assumed value ($-\alpha...+\alpha$ in **Section 9** of presented thesis), while other missing independent variables remain unchanged on the same level (at the center points of the CCD in **Section 9** of presented thesis).

It can be observed that effect of different independent input variables on the exchanger's performance may be more or less significant. As it is seen from the plot (Fig. I1(a)) the inlet air temperature has a little higher impact on the outlet primary airflow temperature than inlet air relative humidity. The impact of these two independent variables on the specific cooling capacity, dew point effectiveness and COP is similar (Fig. I1(b)-(d)). Both the input variables (inlet air temperature and relative humidity) are characterized by high statistical significance in terms of the selected performance characteristics, because heat and mass transfer process runs more effectively under dry and hot inlet airflow conditions, as it was established in the previous sections. Another pair of input variables compared in terms of their impact on the performance factors was inlet air relative humidity and primary air mass flow rate. It can be observed that inlet airflow relative humidity has more significant impact on the outlet primary airflow temperature (Fig. I1(e)), while impact of both variables on the specific cooling capacity and dew point effectiveness is similar. It is also clear visible that the primary air mass flow rate has higher impact on the COP (Fig. I1(h)). Two main reasons may cause this effect. The first one is that the air mass flow rate determines the value of the main heat transfer parameter NTU: a higher supply air mass flow rate reduces the NTU value, which results in the higher outlet primary airflow temperature. The second one is that the value of air mass flow rate also impacts on the pressure drops along the channels, which results in the changes in the electrical energy consumed by the fan. It should be noted that the value of the inlet air relative humidity changes only one component of the COP (cooling capacity), therefore its impact is lower than influence of the supply air mass flow rate.

(a)



(b)



(c)



(d)



(e)



(f)
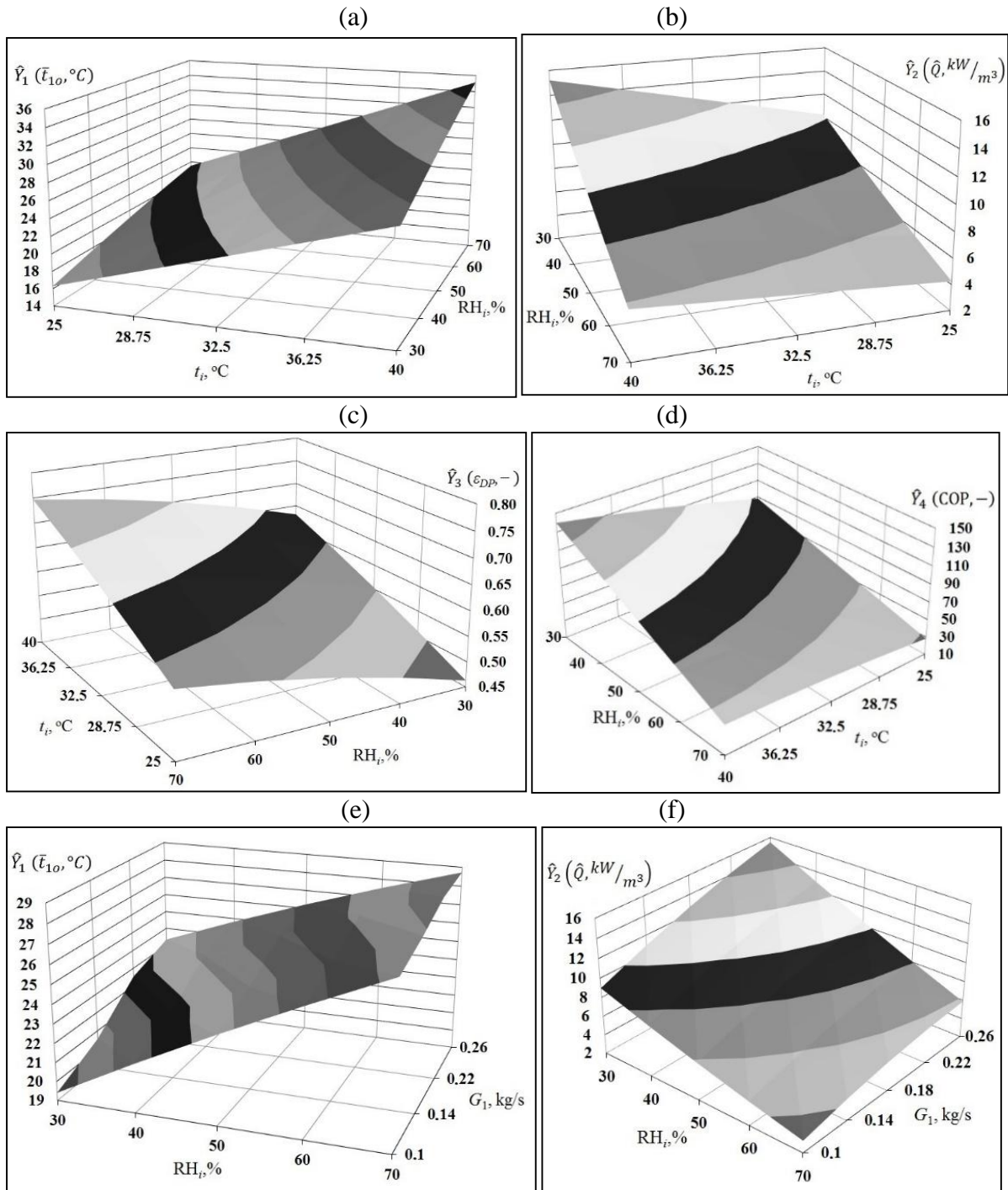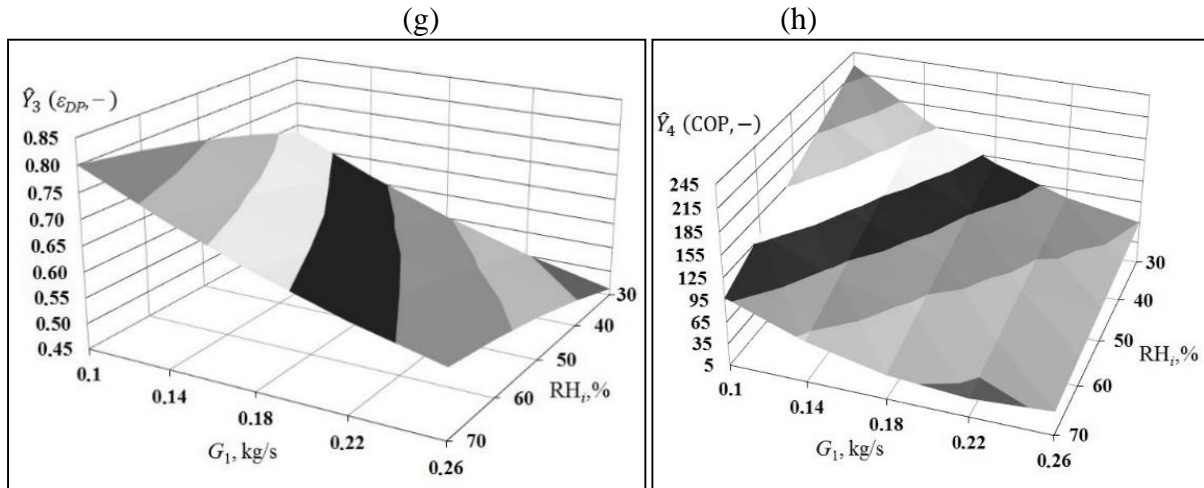
Fig. I1. Impact of independent variables on performance factors. (a) $t_i$ and $RH_i$ on $\hat{Y}_1(\bar{t}_{lo})$. (b) $t_i$ and $RH_i$ on $\hat{Y}_2(\hat{Q})$. (c) $t_i$ and $RH_i$ on $\hat{Y}_3(\varepsilon_{DP})$. (d) $t_i$ and $RH_i$ on $\hat{Y}_4(COP)$. (e) $G_1$ and $RH_i$ on $\hat{Y}_1(\bar{t}_{lo})$. (f) $G_1$ and $RH_i$ on $\hat{Y}_2(\hat{Q})$. (g) $G_1$ and $RH_i$ on $\hat{Y}_3(\varepsilon_{DP})$. (h) $G_1$ and $RH_i$ on $\hat{Y}_4(COP)$.

The impact of another pair of independent variables (primary air mass flow rate and working to primary air heat capacity ratio) on the performance factors is presented in Fig. I2(a)−(d). It can be seen that the primary air mass flow rate has more significant impact on all of the examined performance factors than the working to primary air heat capacity ratio. It was connected that the values of independent variable $W_2/W_1$ were selected in the range where it allows keeping a relatively high efficiency of the exchanger. $W_2/W_1$ ratio has a significant influence on the COP (Fig. I2(d)), because it effects on two components of this performance factor, like in the case of the primary air mass flow rate (cooling capacity and theoretical energy consumption). It may be seen from Fig. I2(e)−(h) that working to primary air heat capacity ratio has lower influence on the outlet primary airflow temperature, specific cooling capacity and dew point effectiveness than relative width of the dry initial part ($\bar{l}_Y^{work}$), but it has a higher impact on the COP. It was also noted that statistical significance of these two variables is relatively low in compare to the other independent variables (primary air mass flow rate, inlet air temperature and relative humidity). For example, the changes of the $\bar{l}_Y^{work}$ and $W_2/W_1$ from −$\alpha$ to +$\alpha$ results in only 1.8 and 0.8°C changes in outlet primary airflow temperature. Variations of inlet air temperature from −$\alpha$ to +$\alpha$ causes a 12.2°C difference, changes of inlet air relative humidity RH results in 6.7°C difference, while variation of primary air mass flow rate causes 3.0°C difference in outlet primary airflow temperatures. This shows that these two independent variables can be assumed as less significant for the M-Cycle HMX performance.

(a)

(b)



(c)

(d)



(e)

(f)

(g)               (h)
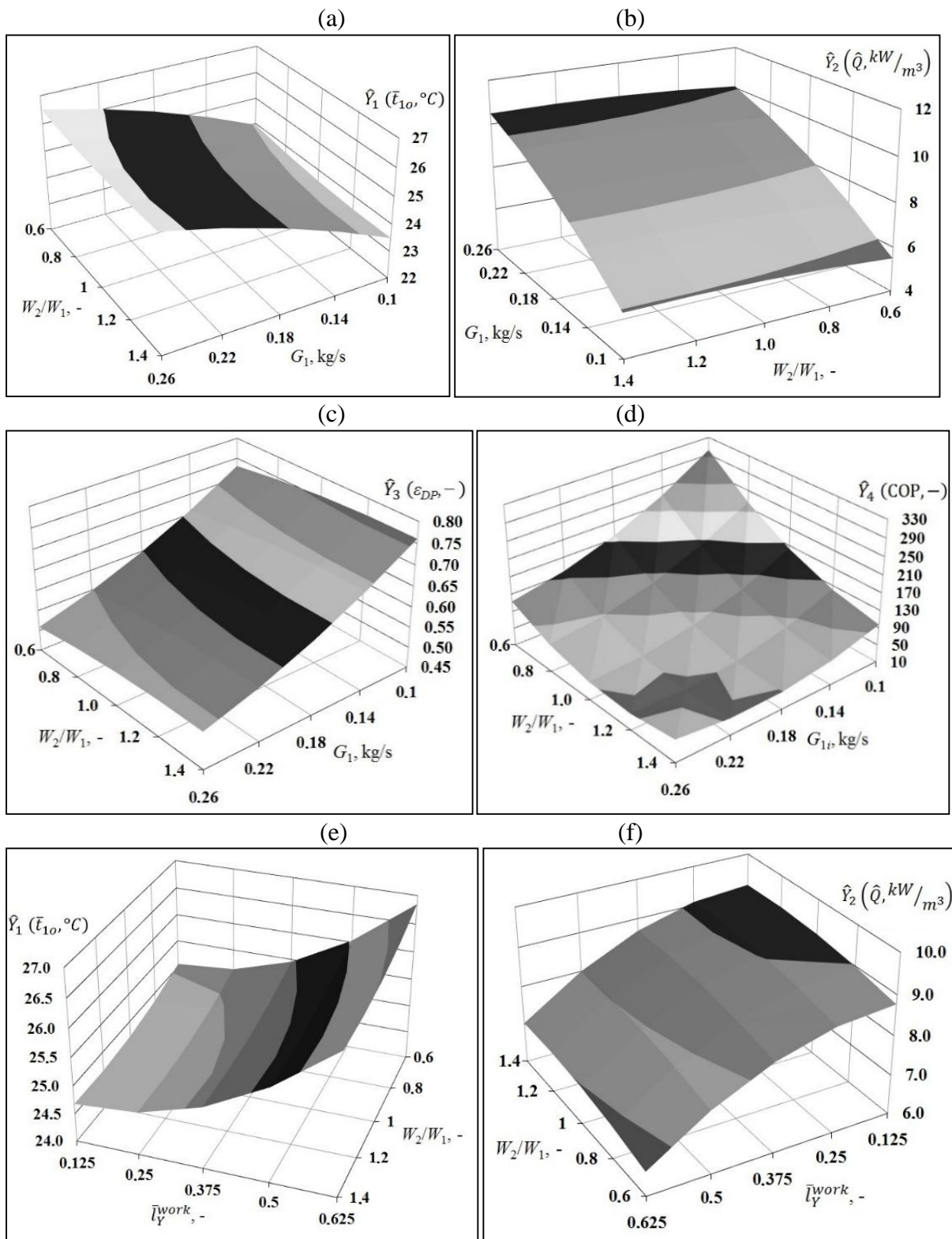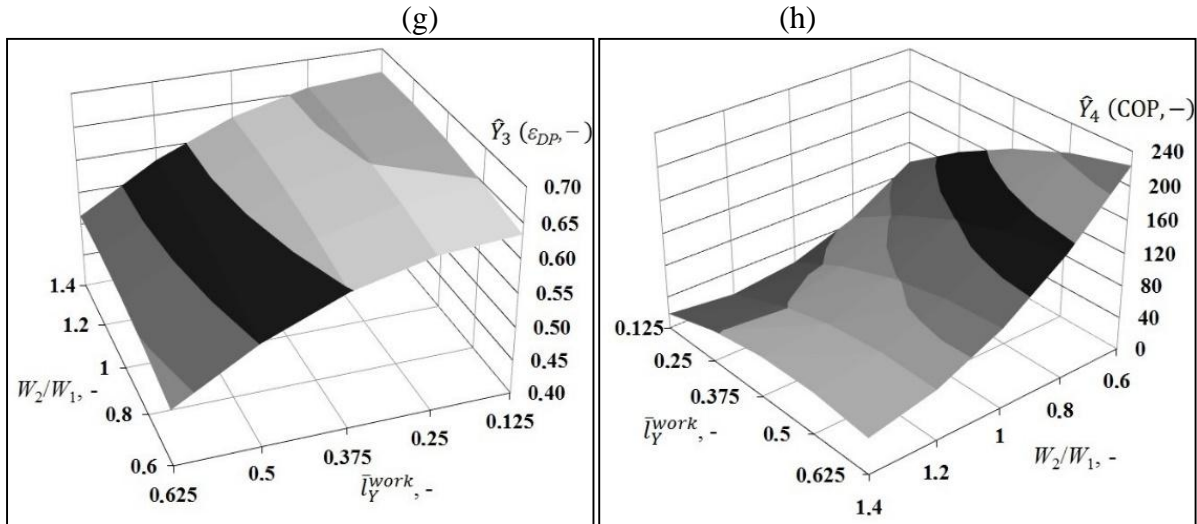


Fig. I2. Impact of independent variables on performance factors. (a) $G_1$ and $W_2/W_1$ on $\hat{Y}_1(\bar{t}_{1o})$. (b) $G_1$ and $W_2/W_1$ on $\hat{Y}_2(\hat{Q})$. (c) $G_1$ and $W_2/W_1$ on $\hat{Y}_3(\varepsilon_{DP})$. (d) $G_1$ and $W_2/W_1$ on $\hat{Y}_4(COP)$. (e) $W_2/W_1$ and $\bar{l}_Y^{work}$ on $\hat{Y}_1(\bar{t}_{1o})$. (f) $W_2/W_1$ and $\bar{l}_Y^{work}$ on $\hat{Y}_2(\hat{Q})$. (g) $W_2/W_1$ and $\bar{l}_Y^{work}$ on $\hat{Y}_3(\varepsilon_{DP})$. (h) $W_2/W_1$ and $\bar{l}_Y^{work}$ on $\hat{Y}_4(COP)$.

The comparison of impact of other pairs of input variables on the examined performance factors is presented in Figures I3–I5. The influence of primary air mass flow rate and working to primary airflow heat capacity ratio on the performance factors under different values of inlet air temperature is given in Fig. I3. It is clearly seen that inlet air temperature affects the outlet primary airflow temperature more significantly than primary air mass flow rate and working to primary air heat capacity ratio (Fig. I3(a) and (e)). Impact of inlet air temperature and primary air mass flow rate is similar on the specific cooling capacity and dew point effectiveness (Fig. I3(b) and (c)). Working to primary air heat capacity ratio has lower significance than inlet air temperature in terms of those two performance factors (Fig. I3(f) and (g)). It can be also seen that impact of the inlet air temperature on the COP is lower than $G_1$ and $W_2/W_1$ ratio (Fig. I3(d) and (h)).

(a)               (b)
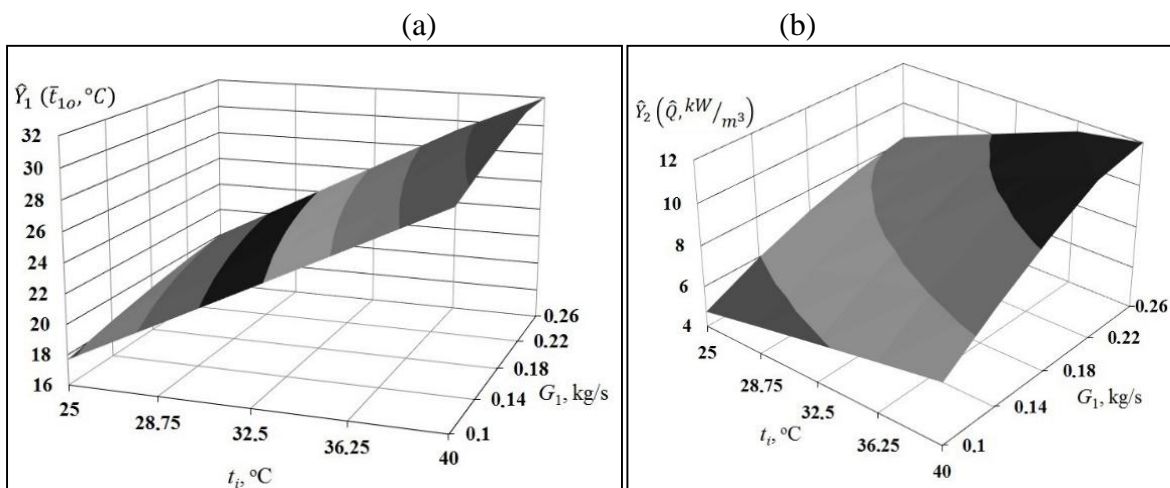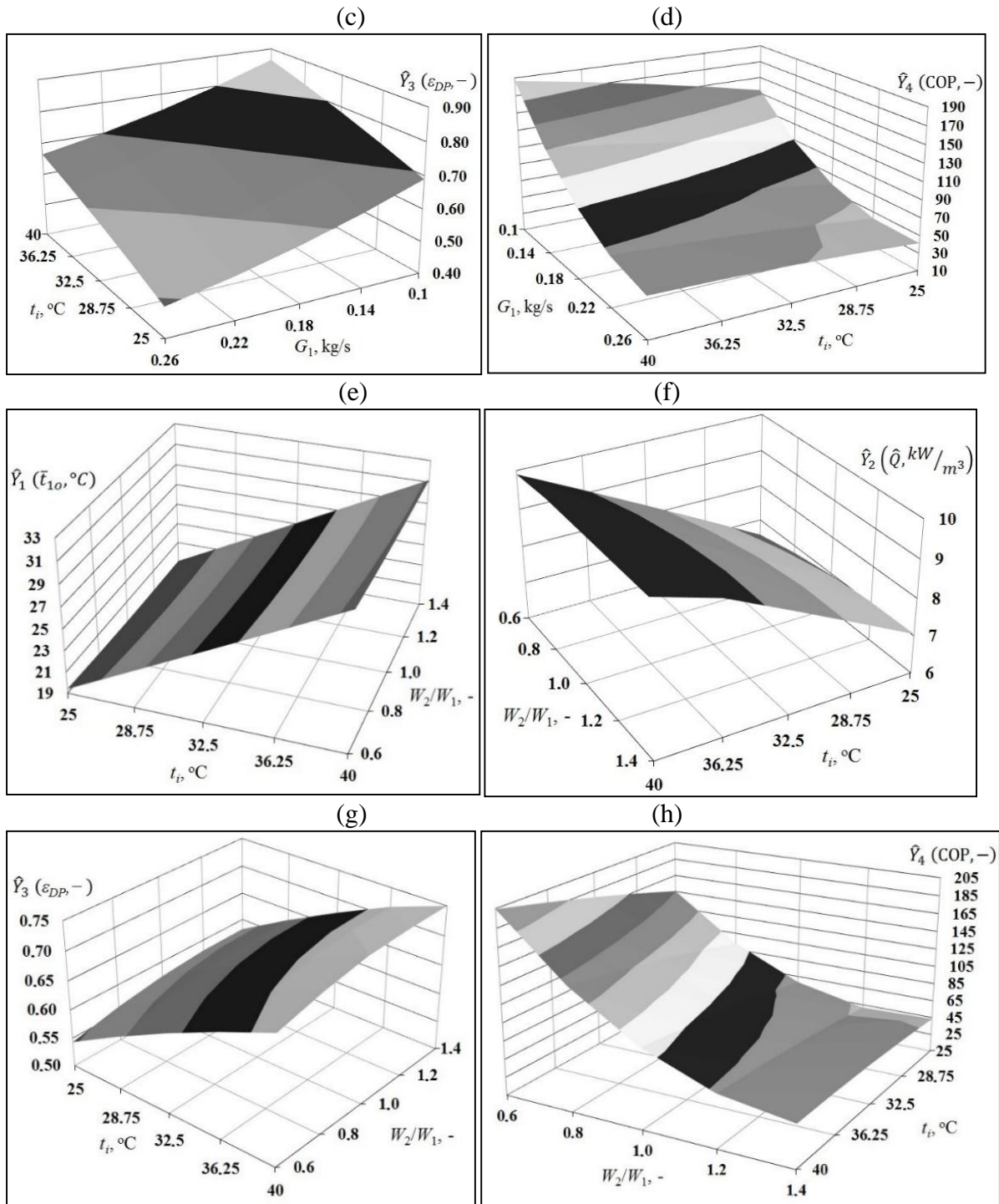
Fig. I3. Impact of independent variables on performance factors. (a) $t_i$ and $G_1$ on $\hat{Y}_1(\bar{t}_{1o})$. (b) $t_i$ and $G_1$ on $\hat{Y}_1(\bar{t}_{1o})$. (c) $t_i$ and $G_1$ on $\hat{Y}_3(\varepsilon_{DP})$. (d) $t_i$ and $G_1$ on COP. (e) $t_i$ and $W_2/W_1$ on $\hat{Y}_1(\bar{t}_{1o})$. (f) $t_i$ and $W_2/W_1$ on $\hat{Y}_2(\hat{Q})$. (g) $t_i$ and $W_2/W_1$ on $\hat{Y}_3(\varepsilon_{DP})$. (h) $t_i$ and $W_2/W_1$ on $\hat{Y}_4(\text{COP})$.

The impact of inlet air temperature and relative width of the dry initial part on the performance factors is presented in Fig. I4(a)–(d). It can be observed that inlet air temperature has higher influence on outlet primary airflow temperature, cooling capacity and dew point effectiveness

than relative width of the dry initial part (Fig. I4(a)–(c)), but it has lower impact on the COP factor (Fig. I4(d)). Figure I4 (e)–(h) shows the impact of inlet air relative humidity and working to primary air heat capacity ratio. Inlet air relative humidity is more significant than working to primary air heat capacity ratio in terms of outlet primary airflow temperature, specific cooling capacity and dew point effectiveness (Fig. I4(e)–(g)) and is less significant in terms of the COP in compare with $W_2/W_1$ ratio (Fig. I4(h)).



(a)  (b)  (c)  (d)  (e)  (f)

(g)  (h)
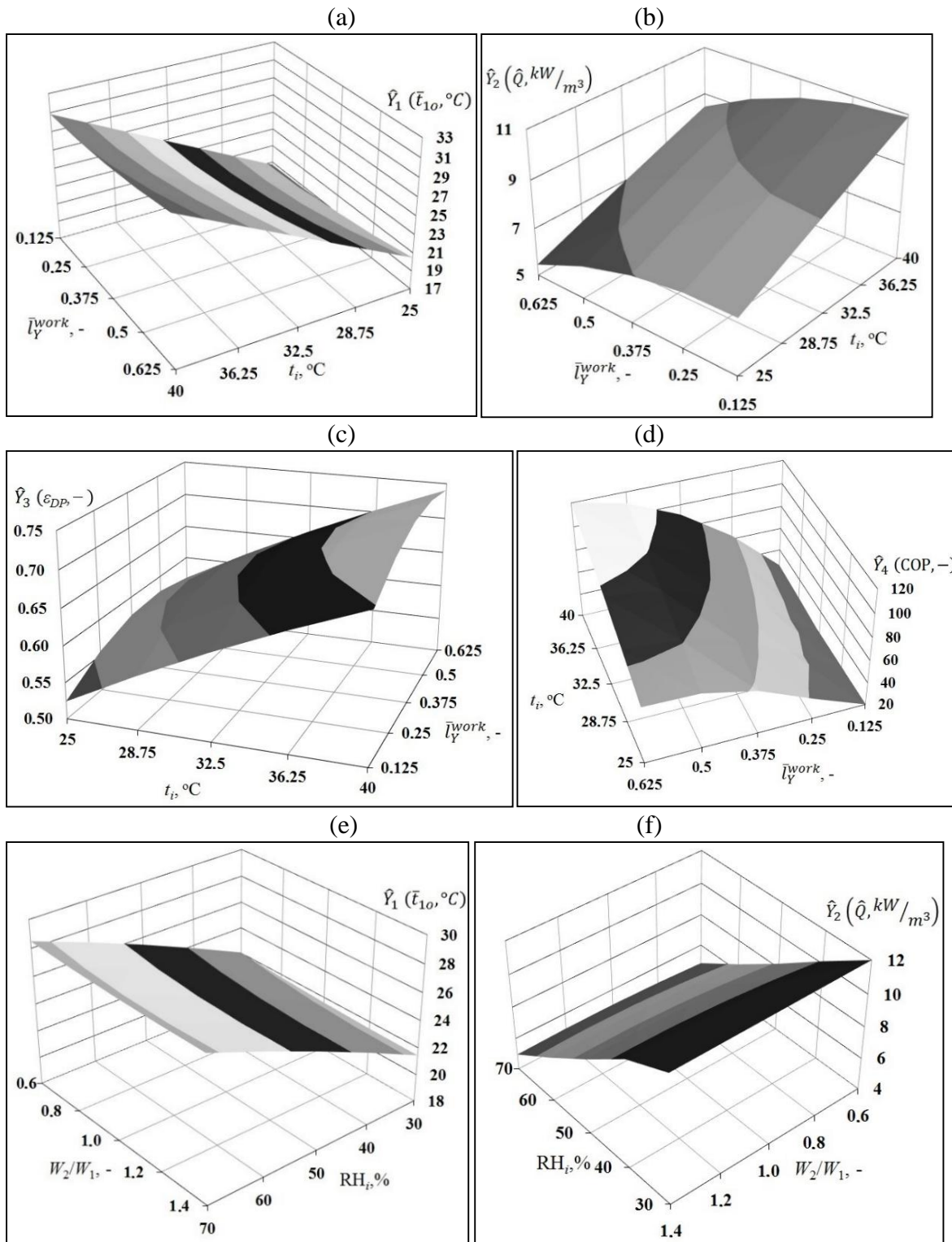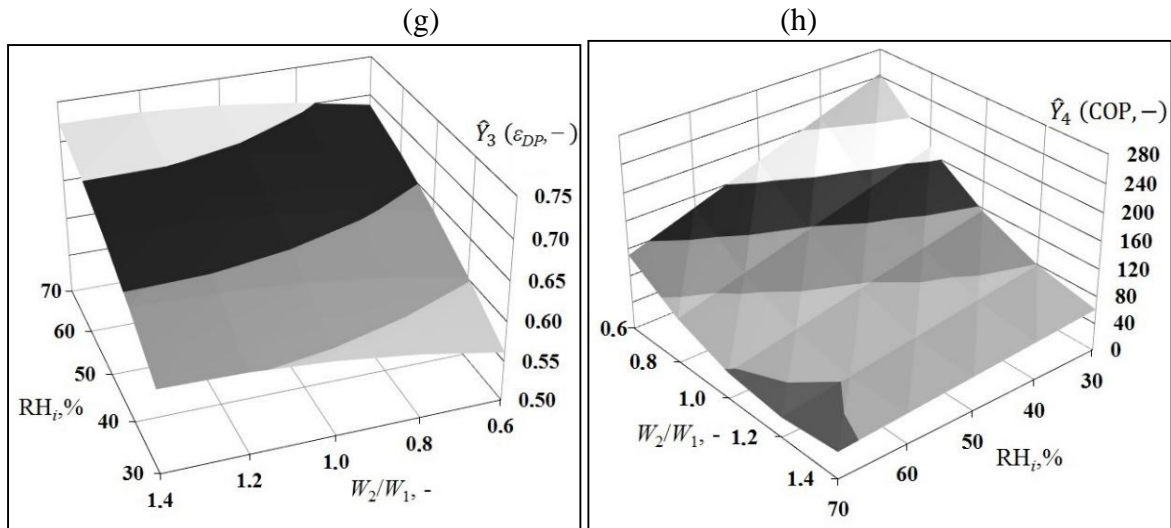
Fig. I4. Impact of independent variables on performance factors. (a) ti and $\overline{l}_Y^{work}$ on $\hat{Y}_1(\overline{t}_{1o})$. (b) ti and $\overline{l}_Y^{work}$ on $\hat{Y}_2(\hat{Q})$. (c) ti and $\overline{l}_Y^{work}$ on $\hat{Y}_3(\varepsilon_{DP})$. (d) ti and $\overline{l}_Y^{work}$ on $\hat{Y}_4(COP)$. (e) RHi and W2/W1 on $\hat{Y}_1(\overline{t}_{1o})$. (f) RHi and W2/W1 on $\hat{Y}_2(\hat{Q})$. (g) RHi and W2/W1 on $\hat{Y}_3(\varepsilon_{DP})$. (h) RHi and W2/W1 on $\hat{Y}_4(COP)$.

Figure I5 shows the comparison between the last pairs of factors: inlet air relative humidity with relative width of the dry initial part and primary air mass flow rate with relative width of the dry initial part. It is visible that inlet air relative humidity has more impact on the outlet primary airflow temperature, cooling capacity and dew point effectiveness than relative width of the dry initial part (Fig. I5(a)−(c)) and it is less significant in terms of the COP (Fig. I5(d)). Primary air mass flow rate is more significant than relative width of the dry initial part in terms of all examined performance factors (Fig. I5(e) − (h)).

(a)  (b)

(c)

(d)



(e)

(f)



(g)

(h)
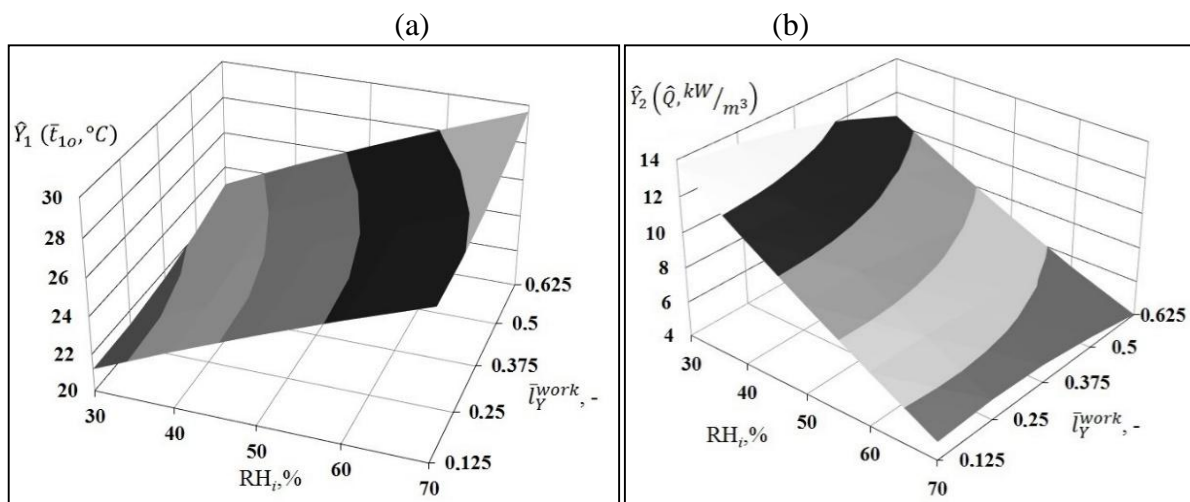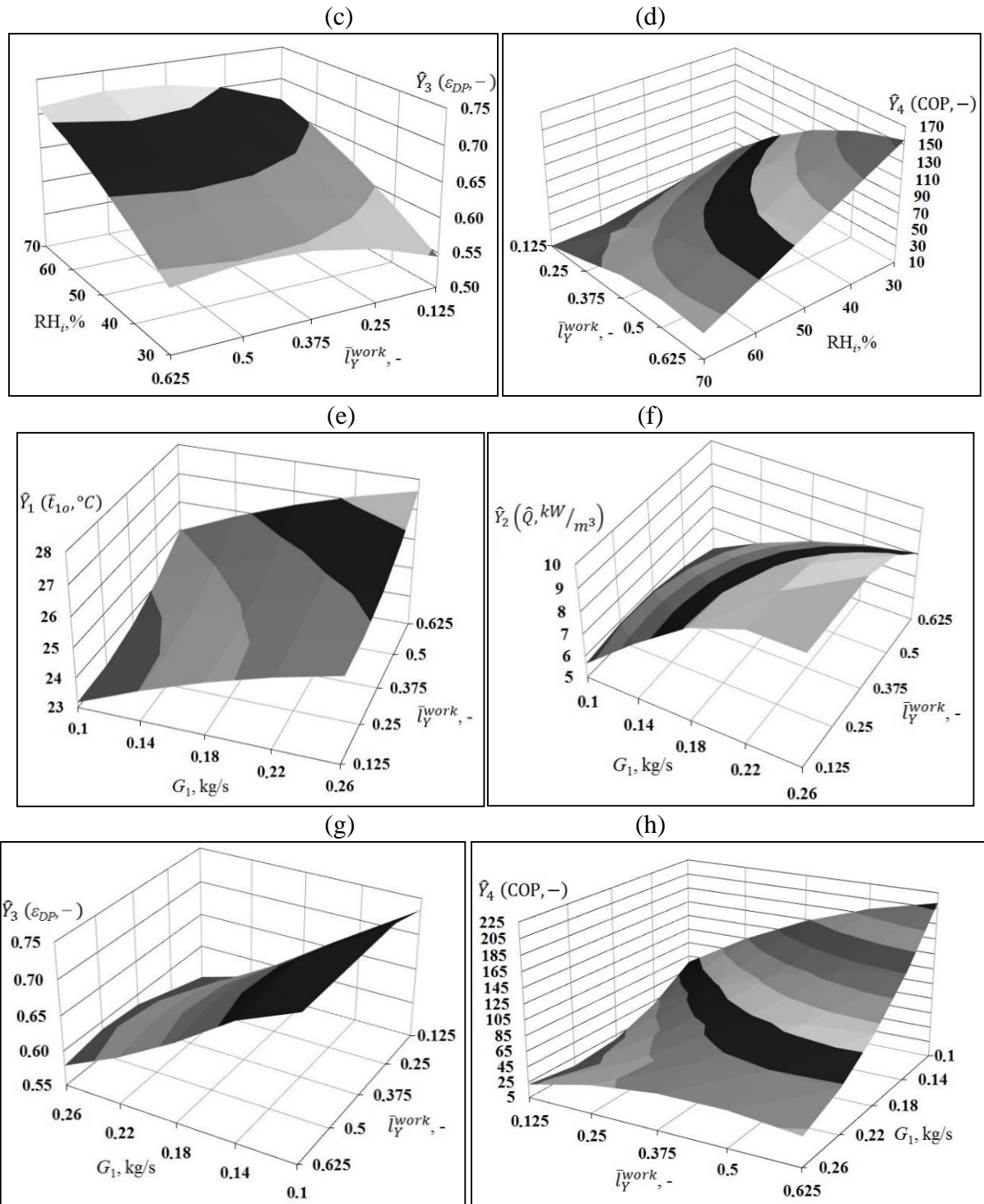


Fig. I5. Impact of independent variables on performance factors. (a) $RH_i$ and $\overline{l}_Y^{work}$ on $\hat{Y}_1(\overline{t}_{1o})$. (b) $RH_i$ and $\overline{l}_Y^{work}$ on $\hat{Y}_2(\hat{Q})$. (c) $RH_i$ and $\overline{l}_Y^{work}$ on $\hat{Y}_3(\varepsilon_{DP})$. (d) $RH_i$ and $\overline{l}_Y^{work}$ on $\hat{Y}_4(COP)$. (e) $G_1$ and $\overline{l}_Y^{work}$ on $\hat{Y}_1(\overline{t}_{1o})$. (f) $G_1$ and $\overline{l}_Y^{work}$ on $\hat{Y}_2(\hat{Q})$. (g) $G_1$ and $\overline{l}_Y^{work}$ on $\hat{Y}_3(\varepsilon_{DP})$. (h) $G_1$ and $\overline{l}_Y^{work}$ on $\hat{Y}_4(COP)$.

## Appendix J. Mathematical model of the desiccant wheel

This Appendix requires additional nomenclature to describe the desiccant wheel. It is established in Table J.1.The initial conditions for the mathematical model and the operational scheme of desiccant wheel is presented in Figure J1. The mathematical model used in this thesis is very typical [33], [150], therefore to process of conversion of the heat and mass transfer equations is omitted and only the final energy balance equations are presented. The full conversion of the same type of equation can be seen in many scientific papers, e.g. in PhD thesis presented by Kowalski [33].

Table J.1. Nomenclature used for mathematical model of the desiccant wheel

| | | |
|---|---|---|
| $L_Z$ | [m] | Streamwise length of the desiccant wheel |
| $M_M$ | [kg] | Mass |
| $q^{sorp}$ | [kJ/kg] | Heat of sorption |
| $W$ | [kg/kg] | Moisture content of desiccant material |
| $Z_1$ | [m] | Coordinate along the process airflow direction: desiccant wheel |
| $Z_2$ | [m] | Coordinate along the regeneration airflow direction: desiccant wheel |
| **Special characters:** | | |
| $\Delta\tau_1$ | [s] | Absorption stage duration |
| $\Delta\tau_2$ | [s] | Desorption stage duration |
| $\Delta\bar{\tau}_1 = \Delta\tau_1/\tau_o$ | [s] | Non-dimensional absorption stage duration |
| $\Delta\bar{\tau}_2 = \Delta\tau_2/\tau_o$ | [s] | Non-dimensional desorption stage duration |
| | [s] | Time |
| $\tau$ | [s] | Time of one revolution of the wheel |
| $\tau_o = (\Delta\tau_1 + \Delta\tau_2)$ | [s] | Non-dimensional time of one revolution of the wheel |
| $\bar{\tau}_o = (\Delta\bar{\tau}_1 + \Delta\bar{\tau}_2) = 1.0$ | | |
| **Non dimensional coordinates:** | | |
| $i$ | [-] | Wheel revolution counter ($i=(1\ldots n)$) |
| $j$ | [-] | Stage counter ($j=1$ – absorption stage, $j=2$ – desorption stage) |
| NTU* | [-] | Number of transfer units: desiccant material |
| $\bar{Z}$ | [-] | $\bar{Z}=Z/L_Z$ – relative $Z$ coordinate |
| **Subscripts** | | |
| 1 | | Process airflow in desiccant wheel |
| 2 | | Regeneration airflow in desiccant wheel |
| $d$ | | Desiccant material |
| $DW$ | | Desiccant wheel |
| $reg$ | | Regeneration airflow (desiccant wheel) |
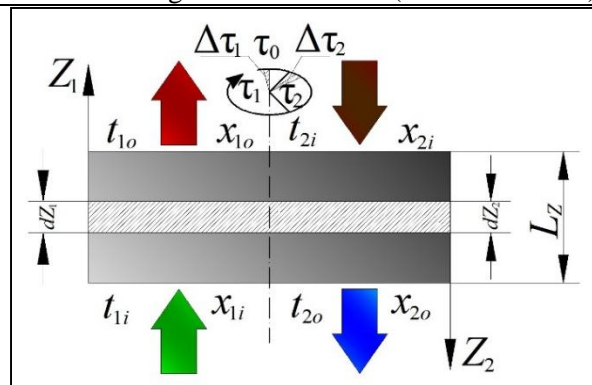


Fig. J1. Assumptions for mathematical model.

The governing equations for the mathematical model of the rotary dehumidifier are presented below. The energy conservation balance for the process airflow:

$$\frac{\partial t_1}{\partial \bar{\bar{Z}}_1} = \text{NTU}_1 \left( t_{d1} - t_1 \right) \tag{J1}$$

where $\text{NTU}_1 = \alpha_1 F_1 / (G_1 c_{p1})$.

The mass conservation balance for the process airflow:

$$\frac{\partial x_1}{\partial \bar{\bar{Z}}_1} = \text{NTU}_1 \frac{1}{\text{Le}_1} \left( x_{d1} - x_1 \right) \tag{J2}$$

The mass conservation balance for desiccant matrix in the process sector:

$$\frac{\partial W_{d1}}{\partial \bar{\tau}} = \text{NTU}_1^* \left( \frac{c_d}{c_p \text{Le}} \right)_1 \left( x_1 - x_{d1} \right) \tag{J3}$$

where $\text{NTU}_1^* = \alpha_1 F_1 \tau_o / (M_{d1} c_{d1})$.

The energy conservation balance for desiccant matrix in the process sector:

$$\frac{\partial t_{d1}}{\partial \bar{\tau}} = \text{NTU}_1^* \left( t_1 - t_{d1} \right) + \left( \frac{\partial W_{d1}}{\partial \bar{\tau}} \right) \frac{1}{c_{d1}} \left[ q_1^{sorp} + c_{g1} \left( t_1 - t_{d1} \right) \right] \tag{J4}$$

or

$$\frac{\partial t_{d1}}{\partial \bar{\tau}} = \text{NTU}_1^* \left( t_1 - t_{d1} \right) + \text{NTU}_1^* \frac{1}{c_{p1} \text{Le}_1} \left( x_1 - x_{d1} \right) \left[ q_1^{sorp} + c_{g1} \left( t_1 - t_{d1} \right) \right] \tag{J5}$$

Regeneration part
The energy conservation balance for the regeneration airflow:

$$\frac{\partial t_2}{\partial \bar{\bar{Z}}_2} = \text{NTU}_2 \left( t_{d2} - t_2 \right) + \frac{\partial x_2}{\partial \bar{\bar{Z}}_2} \left( \frac{c_{g2}}{c_{p2}} \right) \left( t_{d2} - t_2 \right) \tag{J5}$$

or

$$\frac{\partial t_2}{\partial \bar{\bar{Z}}_2} = \text{NTU}_2 \left( t_{d2} - t_2 \right) \left[ 1 + \left( \frac{c_g}{c_p \text{Le}} \right)_2 \left( x_{d2} - x_2 \right) \right] \tag{J6}$$

where $\text{NTU}_2 = \alpha_2 F_2 / (G_2 c_{p2})$.

The mass conservation balance for the regeneration airflow:

$$\frac{\partial x_2}{\partial \overline{Z}_2} = \mathrm{NTU}_2 \frac{1}{\mathrm{Le}_2}\left(x_{d2} - x_2\right) \tag{J7}$$

The mass conservation balance for desiccant matrix in the regeneration sector:

$$\frac{\partial W_{d2}}{\partial \overline{\tau}} = \mathrm{NTU}_2^*\left(\frac{c_d}{c_p \mathrm{Le}}\right)_2 \left(x_2 - x_{d2}\right) \tag{J8}$$

where $\mathrm{NTU}_2^* = \alpha_2 F_2 \tau_o / (M_{d2} c_{d2})$.

The energy conservation balance for desiccant matrix in the regeneration sector:

$$\frac{\partial t_{d2}}{\partial \overline{\tau}} = \mathrm{NTU}_2^*\left(t_2 - t_{d2}\right) + \frac{\partial W_{d2}}{\partial \overline{\tau}}\left(\frac{q^{sorp}}{c_d}\right)_2 \tag{J9}$$

or

$$\frac{\partial t_{d2}}{\partial \overline{\tau}} = \mathrm{NTU}_2^*\left[\left(t_2 - t_{d2}\right) + \left(\frac{q^{sorp}}{c_p \mathrm{Le}}\right)_2 \left(x_2 - x_{d2}\right)\right] \tag{J10}$$

The mathematical model is supplemented with initial, switching and boundary conditions. Initial conditions:

$$t_{d1}\left(\overline{\tau}, \overline{Z}_1\right)\Big|_{\substack{\overline{Z}_1 = (0.0\ldots 1.0) \\ \overline{\tau} = 0}} = t_{do}\left(\overline{Z}_1\right) \quad ; \qquad W_{d1}\left(\overline{\tau}, \overline{Z}_1\right)\Big|_{\substack{\overline{Z}_1 = (0.0\ldots 1.0) \\ \overline{\tau} = 0}} = W_{do}\left(\overline{Z}_1\right) \tag{J11}$$

Boundary conditions:
    Absorption side:

$$t_1\left(\overline{\tau}, \overline{Z}_1\right)\Big|_{\substack{\overline{Z}_1 = 0.0 \\ \overline{\tau} = ((i-1)\ldots(\Delta\overline{\tau}_1 + (i-1)))}} = t_{1i}^{DW} = const \quad ; \qquad x_1\left(\overline{\tau}, \overline{Z}_1\right)\Big|_{\substack{\overline{Z}_1 = 0.0 \\ \overline{\tau} = ((i-1)\ldots(\Delta\overline{\tau}_1 + (i-1)))}} = x_{1i}^{DW} = const \tag{J12}$$

    Desorption side:

$$t_2\left(\overline{\tau}, \overline{Z}_2\right)\Big|_{\substack{\overline{Z}_2 = 0.0 \\ \overline{\tau} = ((\Delta\overline{\tau}_1 + (i-1))\ldots i)}} = t_{2i}^{DW} = const \quad ; \qquad x_2\left(\overline{\tau}, \overline{Z}_2\right)\Big|_{\substack{\overline{Z}_2 = 0.0 \\ \overline{\tau} = ((\Delta\overline{\tau}_1 + (i-1))\ldots i)}} = x_{2i}^{DW} = const \tag{J13}$$

Switching conditions:

$$t_{d2}\left(\overline{\tau},\overline{Z}_2\right)\Big| = t_{d1}\left(\overline{\tau},\overline{Z}_1\right) \qquad\qquad W_{d2}\left(\overline{\tau},\overline{Z}_2\right)\Big| = W_{d1}\left(\overline{\tau},\overline{Z}_1\right)$$

$$\begin{aligned}
&\Big|\overline{Z}_1 = \left(0.0\ldots 1.0\right) && \Big|\overline{Z}_1 = \left(0.0\ldots 1.0\right) \\
&\Big|\overline{Z}_2 = \left(0.0\ldots 1.0\right); && \Big|\overline{Z}_2 = \left(0.0\ldots 1.0\right); \\
&\Big|\overline{Z}_2 = 1-\overline{Z}_1 && \Big|\overline{Z}_2 = 1-\overline{Z}_1 \\
&\Big|\overline{\tau} = \varDelta\overline{\tau}_1 + \left(i-1\right) && \Big|\overline{\tau} = \varDelta\overline{\tau}_1 + \left(i-1\right)
\end{aligned} \qquad (J14)$$

$$t_{d1}\left(\overline{\tau},\overline{Z}_1\right)\Big| = t_{d2}\left(\overline{\tau},\overline{Z}_2\right) \qquad\qquad W_{d1}\left(\overline{\tau},\overline{Z}_1\right)\Big| = W_{d2}\left(\overline{\tau},\overline{Z}_2\right)$$

$$\begin{aligned}
&\Big|\overline{Z}_1 = \left(0.0\ldots 1.0\right) && \Big|\overline{Z}_1 = \left(0.0\ldots 1.0\right) \\
&\Big|\overline{Z}_2 = \left(0.0\ldots 1.0\right); && \Big|\overline{Z}_2 = \left(0.0\ldots 1.0\right)\cdot \\
&\Big|\overline{Z}_1 = 1-\overline{Z}_2 && \Big|\overline{Z}_1 = 1-\overline{Z}_2 \\
&\Big|\overline{\tau} = i && \Big|\overline{\tau} = i
\end{aligned} \qquad (J15)$$

Conditions of the quasi-steady mode realization (Cyclical steady state conditions, which are independent of the stating conditions)

$$t_{d1}\left(\overline{\tau},\overline{Z}_1\right)\Big| = t_{d1}\left(\overline{\tau}*,\overline{Z}_1\right) \qquad\qquad W_{d1}\left(\overline{\tau},\overline{Z}_1\right)\Big| = W_{d1}\left(\overline{\tau}*,\overline{Z}_1\right)$$

$$\begin{aligned}
&\Big|\overline{Z}_1 = \left(0.0\ldots 1.0\right) && \Big|\overline{Z}_1 = \left(0.0\ldots 1.0\right) \\
&\Big|\overline{\tau} = i; && \Big|\overline{\tau} = i \cdot \\
&\Big|\overline{\tau}* = i+1 && \Big|\overline{\tau}* = i+1
\end{aligned} \qquad (J16)$$

The humidity ratio of air in equilibrium with the desiccant matrix is defined as a function of matrix temperature and moisture content of desiccant matrix [33]

$$x_d = x_d\left(t_d, W_d\right) \qquad (J17)$$

Simulation of multi-cycle heat and mass transfer process in a rotary desiccant wheel consisted of a dehumidification process followed by a regeneration process in a cyclic manner. This is much more complicated task in comparison with a single simulation cycle [20]. In the case of traditional way of simulation, it is necessary to calculate the first phase (dehumidification), then the second one (regeneration), and then repeat such sequence of calculations for the next cycle. Computations should be repeated for a large number of intermediate cycles in order to approach quasi steady-state conditions. Such method of simulation requires a significant time of computing, which is an obstacle in the research process. Consequently, first and foremost, it is necessary to minimize the time of approaching a cyclic steady-state mode. One of the ways to solve this problem is to find a rational approximation of the initial conditions. The effectiveness of this approach is based on the fact that a cyclic steady-state mode does not depend on the

initial conditions and is a result of an asymptotic process. Preliminary series of numerical simulations allowed to establish an optimal distribution of the initial parameters, based on an asymptotic assumptions of the investigated heat and mass transfer processes realized in the rotor of desiccant wheel at a matrix rotation frequency higher than critical value (turns per minute, $n_o > 7$ min$^{-1}$) [33]. In this case, the temperature and moisture content of desiccant material within each cross-section remains practically substantially constant during the whole cycle (the psychrometric representation of processes occurring under critical operational conditions in the desiccant wheel are visible in Figure J2). This fact allows the heat and mass transfer in the matrix of desiccant wheel to be described by the set of ordinary differential equations of heat and mass conservation balances. The governing equations for the mathematical model of desiccant rotary wheel at rotation frequency higher than critical value are presented below.

(a)



(b)
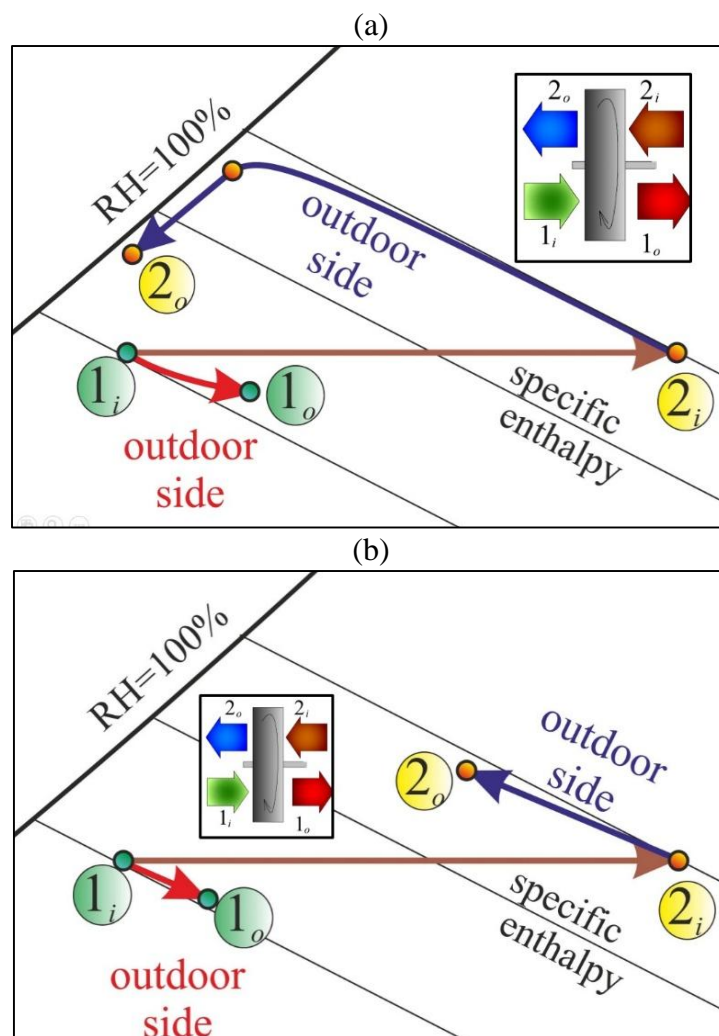


Fig. J2. Psychrometric representation of process occurring in desiccant wheel under: (a) very fast rotational speed (b) very slow rotational speed.

The energy conservation balance for the process airflow:

$$\frac{dt_1}{d\bar{Z}} = \text{NTU}_1 (t_d - t_1) \tag{J18}$$

where $\mathrm{NTU}_1 = \alpha_1 F_1 / (G_1 c_{p1})$.

The mass conservation balance for the process airflow:

$$\frac{dx_1}{d\bar{Z}} = \mathrm{NTU}_1 \frac{1}{\mathrm{Le}_1} (x_d - x_1) \tag{J19}$$

The energy conservation balance for the regeneration airflow:

$$\frac{dt_2}{d\bar{Z}} = -\mathrm{NTU}_2 (t_d - t_2) + \frac{dx_2}{d\bar{Z}} \left( \frac{c_{g2}}{c_{p2}} \right) (t_d - t_2) \tag{J20}$$

or

$$\frac{dt_2}{d\bar{Z}} = -\mathrm{NTU}_2 (t_d - t_2) \left[ 1 + \left( \frac{c_g}{c_p \mathrm{Le}} \right)_2 (x_d - x_2) \right] \tag{J21}$$

where $\mathrm{NTU}_2 = \alpha_2 F_2 / (G_2 c_{p2})$.

The mass conservation balance for the regeneration airflow:

$$\frac{dx_2}{d\bar{Z}} = -\mathrm{NTU}_2 \frac{1}{\mathrm{Le}_2} (x_d - x_2) \tag{J22}$$

The energy conservation balance for desiccant matrix

$$\mathrm{NTU}_1 (t_d - t_1) + \mathrm{NTU}_1 (t_d - t_1) \left( \frac{c_g}{c_p \mathrm{Le}} \right)_1 (x_1 - x_d) + \mathrm{NTU}_1 \left( \frac{q^{sorp}}{c_p \mathrm{Le}} \right)_1 (x_d - x_1) +$$
$$+ \left( \frac{W_2}{W_1} \right) \mathrm{NTU}_2 (t_d - t_2) + \left( \frac{W_2}{W_1} \right) \mathrm{NTU}_2 \left( \frac{q^{sorp}}{c_p \mathrm{Le}} \right)_2 (x_d - x_2) = 0 \tag{J23}$$

or

$$\frac{dt_1}{d\bar{Z}} - \left( \frac{W_2}{W_1} \right) \frac{dt_2}{d\bar{Z}} - \frac{dx_1}{d\bar{Z}} \left[ \left( \frac{q^{sorp}}{c_p} \right)_1 + \left( \frac{c_g}{c_p} \right)_1 (t_d - t_1) \right] + \left( \frac{W_2}{W_1} \right) \frac{dx_2}{d\bar{Z}} \left[ \left( \frac{q^{sorp}}{c_p} \right)_2 + \left( \frac{c_g}{c_p} \right)_2 (t_d - t_2) \right] = 0 \tag{J24}$$

The mass conservation balance for desiccant matrix:

$$\mathrm{NTU}_1 \frac{1}{\mathrm{Le}_1} (x_d - x_1) + \left( \frac{W_2}{W_1} \right) \mathrm{NTU}_2 \frac{1}{\mathrm{Le}_2} (x_d - x_2) = 0 \tag{J25}$$

Or

$$\frac{dx_1}{d\bar{\bar{Z}}} - \left(\frac{W_2}{W_1}\right)\frac{dx_2}{d\bar{\bar{Z}}} = 0 \qquad\qquad (J26)$$

Simplified energy conservation balance for desiccant matrix

$$\frac{dt_1}{d\bar{\bar{Z}}} - \left(\frac{W_2}{W_1}\right)\frac{dt_2}{d\bar{Z}} + \frac{dx_1}{d\bar{Z}}\left(\frac{c_g}{c_p}\right)(t_1 - t_2) \approx 0 \qquad\qquad (J24*)$$

The moisture content of desiccant matrix in equilibrium with the moist air is defined as a function temperature and humidity ratio of air [33]

$$W_d = W_d\left(t_d, x_d\right) \qquad\qquad (J27)$$

The mathematical model given by Eqs. (J18)–(J27) is supplemented by boundary conditions Eqs. (J12) and (J13) for absorption and desorption process. It should be emphasized that in this case the developed model, Eqs. (J18)–(J27), is considered to estimate a rational initial approximation of cyclic steady-state mode. Taking into account that obtained profiles of the temperature and moisture content of desiccant matrix characterize the distribution of average values of these parameters in a quasi-steady mode, it is expedient to move initial conditions (K11) into another time layer corresponding to the mid-stage of the dehumidification phase.

$$t_{d1}\left(\bar{\tau}, \bar{Z}_1\right)\Big|_{\substack{\bar{Z}_1 = (0.0\ldots 1.0) \\ \bar{\tau} = \Delta\bar{\tau}_1/2}} = t_{do}\left(\bar{Z}_1\right) \qquad ; \qquad W_{d1}\left(\bar{\tau}, \bar{Z}_1\right)\Big|_{\substack{\bar{Z}_1 = (0.0\ldots 1.0) \\ \bar{\tau} = \Delta\bar{\tau}_1/2}} = W_{do}\left(\bar{Z}_1\right) \qquad (J28)$$

Both models are implemented in a multi-module computer simulation program. A four-dimensional computational numerical code using a modified Runge-Kutta method was implemented using the Wolfram Mathematica environment.

## J.1. Validation of the mathematical model describing desiccant wheel against existing experimental data

The mathematical model describing the desiccant wheel was validated against existing experimental data collected by Kowalski [33] at testing bench at Wroclaw University of Technology, Wroclaw, Poland. The measurement station used by Kowalski was equipped with basic air treatment devices: air filters, heaters and humidifiers for both the outdoor and regeneration airflow (Fig. J3). The parameters of the desiccant wheel used in the tests are established in Table J2.

Table J.2. Parameters of the desiccant wheel used by Kowalski [33]

| Desiccant wheel parameters | |
|---|---|
| Specific heat capacity (silica gel), J/(kg K) | 750 |
| Channel type | Sinusoidal |
| Channel height, mm | 1.24 |
| Channel width, mm | 2.21 |
| Wall thickness, mm | 0.2 |
| Channel length, m | 0.1 |
| Wheel diameter, m | 0.45 |
| Percent of wheel used for regeneration airflow, % | 25 |
| Rotary speed, turns per hour | 8 |

The inlet ambient air temperature in Kowalski's test varied from 18.2 to 34.2°C, the regeneration air temperature varied from 30.5 to 101.0°C, the ambient air humidity ratio changed from 4.1-12.2 g/kg, the regeneration air humidity ratio varied from 4.4 to 15.9 g/kg, the outdoor airflow rate varied from 358 to 650 m³/h, the regeneration airflow rate varied from 80 to 215 m³/h. The parameters measured included the air temperature, relative humidity, mass flow rate and the pressure drop on the exchanger.

(a)



(b)                                                          (c)
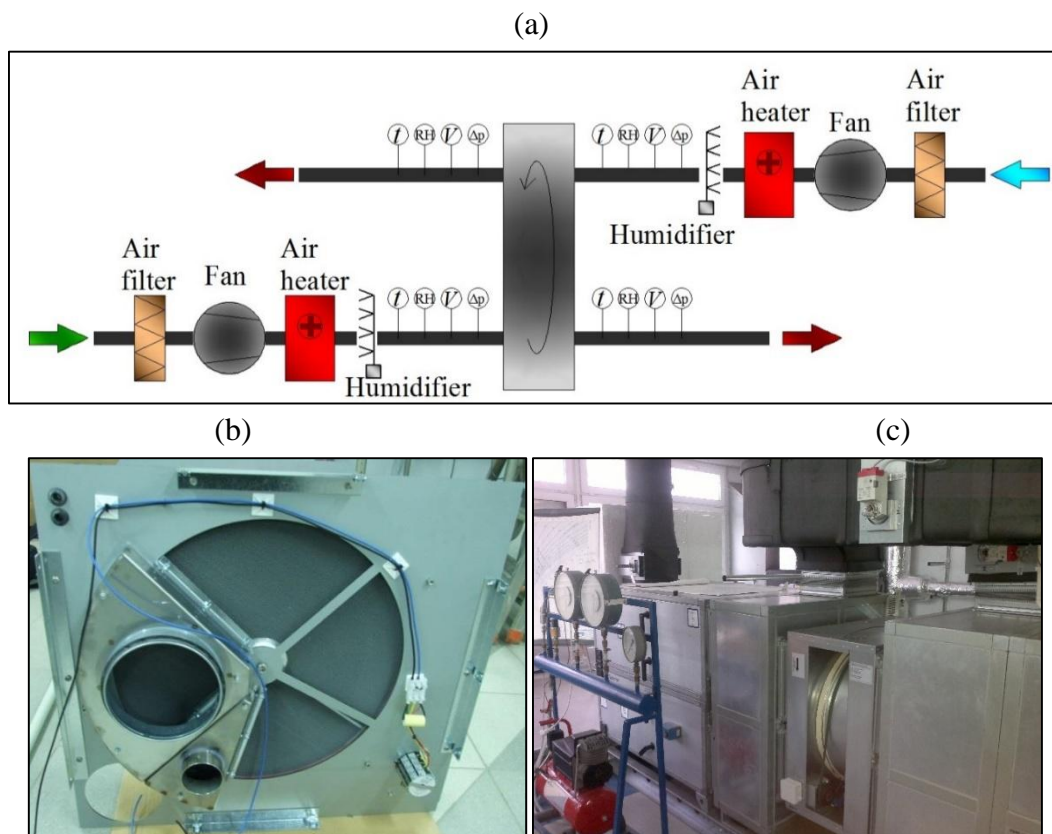


Fig. J3. Measurement station used by Kowalski at Wroclaw University of Technology [33]. (a) Scheme of the testing bench. (b) Photograph of the tested desiccant wheel. (c) Photograph of the testing bench.

The comparison between mathematical model and the experimental results is presented in Figure J4. The comparison include the drop in humidity ratio of the outdoor airflow for one variable parameter and the other remaining unchanged. The analyzed parameters include: variable outdoor and regeneration air temperature (Fig. J4(a) and (b)), variable ambient and regeneration air humidity ratio (Fig. J4(c) and (d)) and variable ambient and regeneration airflow rate (Fig. J4(e) and (f)). The discrepancies between the experimental and simulation results are at most 0.4 g/kg, the correlation coefficient $R^2$ is equal 0.971. It can be seen that the model and the experimental results show satisfactory agreement and trend, therefore the model can be used for numerical analysis of the desiccant wheel.

(a)

(b)



(c)

(d)

(e)                       (f)
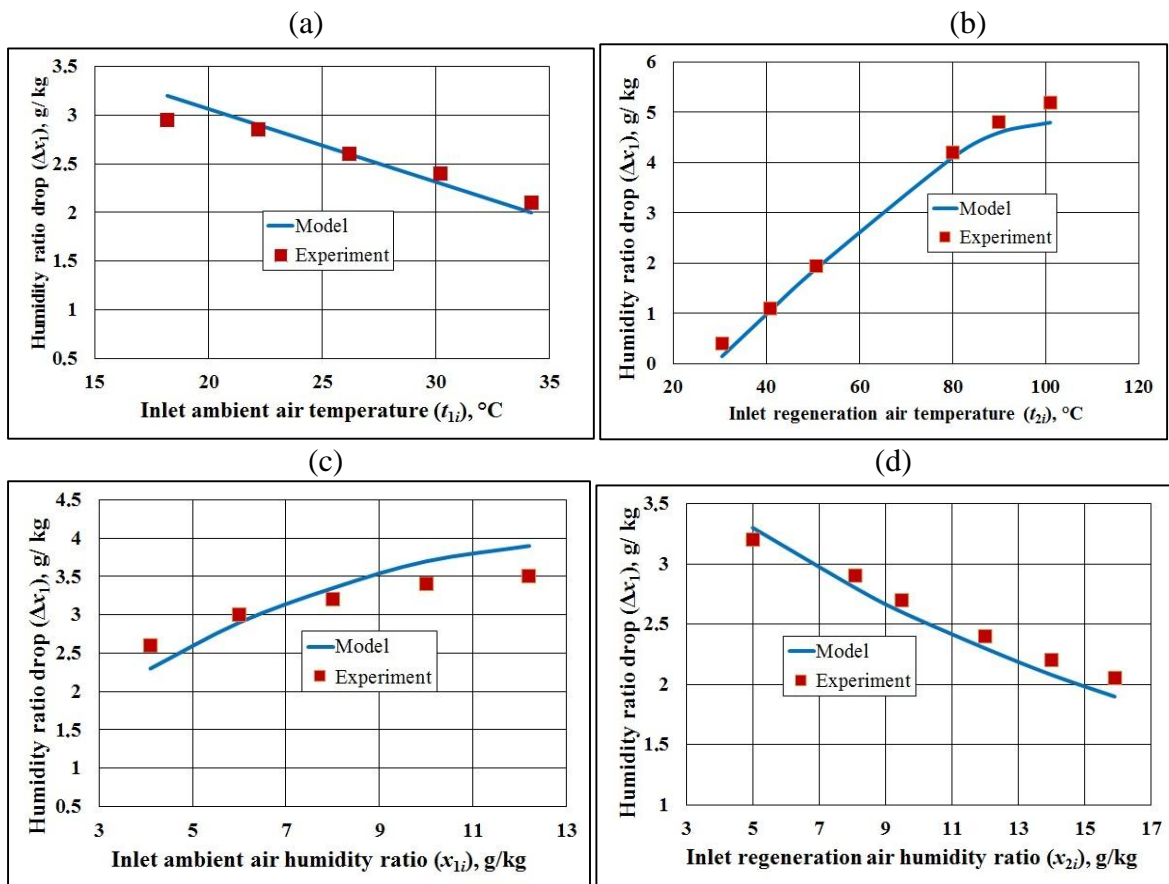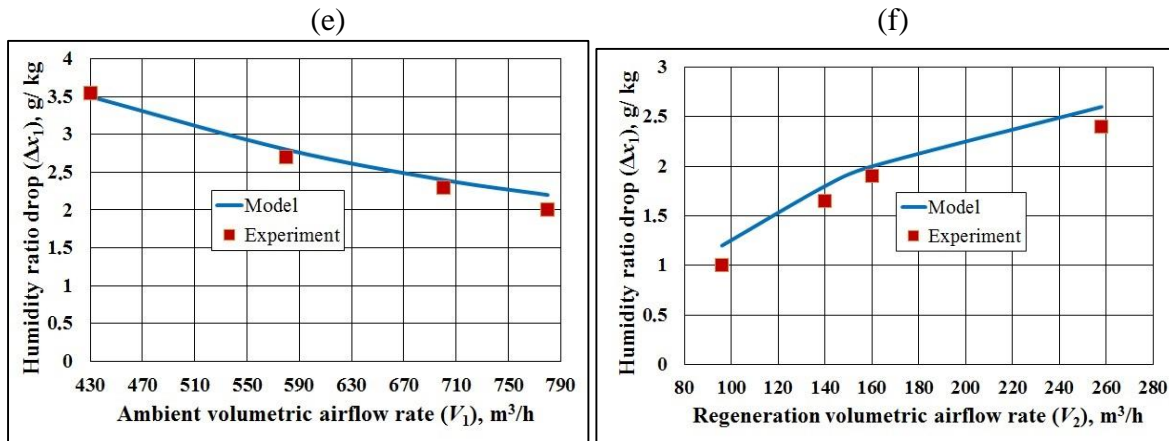


Fig. J4. Validation of mathematical model describing the desiccant wheel against data collected by Kowalski [33]. (a) Ambient air humidity ratio drop at variable inlet ambient air temperature. (b) Ambient air humidity ratio drop at variable inlet regeneration air temperature. (c) Ambient air humidity ratio drop at variable inlet ambient air humidity ratio. (d) Ambient air humidity ratio drop at variable inlet regeneration air humidity ratio. (e) Ambient air humidity ratio drop at variable inlet ambient airflow rate. (f) Ambient air humidity ratio drop at variable inlet regeneration airflow rate.

## Appendix K. Root code of the program describing ideal cross-flow M-Cycle air cooler

The root code for the computer program describing ideal cross-flow M-Cycle air cooler in the Pascal environment is presented below. Due to the fact that the other computer codes take too much space, they are omitted in this Appendix and they are presented in the CD room attached to the paper version of the thesis.

```
Procedure  Fct_Z_var_ad;
        VAR   i, j : INTEGER;
    begin
      Y[1]:=t1_z_0; Y[2]:=Y[1]; Y[3]:=P[d2N]; TNEW[1,1]:=t1_z_0;
      for j:=1 to Ndim do  YY[j]:= Y[j];
      X_tw:=X_Start+Step_X*0.0; Z_tw:=0;
      Praw_ZoX_var_Ad(X_tw,YY,Dery);
      for j:=1 to Ndim do
        begin
          AN[j]:=TOLD[1,j]; AK[j]:=YY[j]; TNEW[1,j]:=YY[j]
        end; {for j}
      t2_do_Miszania:= YY[2]; d2_do_Mieszania:=YY[3];
      AN[Ndim+1]:=TOLD[1,Ndim+1]; AK[Ndim+1]:=tw1;
      AN[Ndim+2]:=TOLD[1,Ndim+2]; AK[Ndim+2]:=tw2;
      TNEW[1,Ndim+1]:=tw; TNEW[1,Ndim+2]:=tw2; TNEW[1,Ndim+3]:=dw2;
     TNEW[1,Ndim+4]:=t2_do_Mieszania; TNEW[1,Ndim+5]:=d2_do_Mieszania;
      z:=0.0;
      for i:=2 to N_z do
        begin
          X:=X_Start;
          Z:=Z_Array[i]; Z_Start:=Z_Array[i-1]; Step_Z:=Z-Z_Start;
          for j:=1 to Ndim do  Y[j]:=TOLD[i,j];
          tw1:=TOLD[I,Ndim+1]; tw:=TOLD[i,Ndim+2];
          Rk3_Ad(X, Y, Yp { Praw_Zo_X_var_Ad });
          Praw_Zo_X_var_Ad(X_Start,Y,Dery);
          Z_tw:=Z_Start+Step_Z*0.9999;
          t2_do_Mieszania:=Y[2]; d2_do_Mieszania:=Y[3];
            Y[2]:=(Y[2]*Z_Start+Y[1]*Step_Z)/(Z_Start+Step_Z);
            Y[3]:=(Y[3]*Z_Start+P[d2N]*Step_Z)/(Z_Start+Step_Z);
          { Praw_Zo_Xvar_Ad(X_Start,Y,Dery);}

          for j:=1 to Ndim do
            begin
              AN[j]:=TOLD[i,j]; AK[j]:=Y[j]; TNEW[i,j]:=Y[j]
            end;  {for j}
      AN[Ndim+1]:=TOLD[i,Ndim+1]; AK[Ndim+1]:=tw1;
      AN[Ndim+2]:=TOLD[i,Ndim+2]; AK[Ndim+2]:=tw2;
       TNEW[i,Ndim+]:=tw1; TNEW[i,Ndim+2]:=tw2; TNEW[i,Ndim+3]:=dw2;
      TNEW[i,Ndim+4]:=t2_do_Mieszania; TNEW[i,Ndim+5]:=d2_do_Mieszania;
        end; {for i}
    end; {Procedure  Fct_Z_var_ad}
   Procedure  Fct_Z_var_Proces;

FUNCTION F_tw2 (tw2_Local: Single ) : Single;
        VAR   dw2_Local, F : Single ;
        BEGIN  { FUNCTION F_tw2}
        D_of_Air( 1.0, tw2_Local, dw2_Local);
        F:=(Lambda_Sc/Delta_plate*
          (tw1-tw2_Local)*(1-Delta_Zeb_1/s_Zeb_1)+
          P[Alfa_2]*(Ytw[2]-tw2_Local)*(1-Delta_Zeb_2/s_Zeb_2)+
          P[Alfa_2]*2500.0/P[Lewis]*(Ytw[3]-dw2_Local)*
        (1-Delta_Zeb_2/s_Zeb_2))*Waga_tw2
```

```
        + tw2_Local;
       F:=(P[Alfa_1]*(Ytw[1]-tw1)*(1-Delta_Zeb_1/s_Zeb_1)+
         P[Alfa_2]*(Ytw[2]-tw2_Local)*(1-Delta_Zeb_2/s_Zeb_2)+
         P[Alfa_2]*2500.0/P[Lewis]*(Ytw[3]-dw2_Local)*
         (1-Delta_Zeb_2/s_Zeb_2))*Waga_tw2
        + tw2_Local;
       F_tw2:=F;
      END;  {FUNCTION F_tw2}
    FUNCTION F_t_Wall(tw : Single ) : Single;
      VAR   dw, tw2_Initial_Local, tw2_Local, dw2_Local, F : Single ;
          {tw1, tw2 dw2 ? Ł«®˘ «ĕ-ëĄ ŻĄfĄ¬Ą--ëĄ!!!!}
       BEGIN  { FUNCTION F_t Wall }
       D_of_Air( 1.0, tw, dw );
       tw1:=tw; dw1:=dw;
       tw2_Initial_Local:= Pt1Wet_bulb] {tw2_Local tw};
       Rtmi_tw2 (tw2_Local, Nevjazka_tw2, Ytw[1], Ytw[2], Eps_tw2, Iter_tw2, Jerror_tw2);
 Rtwi_tw2 (tw2_Local, Nevjazka_tw2, F_tw2, tw2_Initial_Local, Eps_tw2, Iter_tw2, Jerror_tw2);
(1-Delta_Zeb_1/s_Zeb_1)*(1/(P[Alfa_1]*(1-Delta_Zeb_1/s_Zeb_1))+
(Delta_plate/Lambda_Sc)*
1/(1-Delta_Zeb_2/s_Zeb_2));
       D_of_Air(1.0, tw2Local, dw2_Local);
       tw2:=tw2_Local; dw2:=dw2_Local;
       D_of_Air( 1.0, tw, dw );
       tw1:=tw; dw1:=dw;          Calka_Delta_tw_Zeb2:=(tw2_Local- Ytw[2]);
       Calka_Delta_dw_Zeb2:=(dw2_Local- Ytw[3]);
       F:=(P[Alfa_1]*(Ytw[1]-tw1)*P[Psi1]+
         P[Alfa_2]{+C_vap_C_p*Dery[3]}*
         ((1-Delta_Zeb_2/s_Zeb_2)*
         (Ytw[2]-tw2_Local)+
         (2*h_Zeb_2/s_Zeb_2)*(-Calka_Delta_tw_Zeb2)) +
         2500*P[Alfa_2]/P[Lewis]*
         ((1-Delta_Zeb_2/s_Zeb_2)*
         (Ytw[3]-dw2_Local)+
         (2*h_Zeb_2/s_Zeb_2)*(-Calka_Delta_dw_Zeb2)))*Waga_tw2
         + tw;
       F_t_Wall := F;
      END;  { FUNCTION F_t Wall}
    FUNCTION F_t_Wall_Pro(tw : Single ) : Single;
      VAR   dw, tw2_Initial_Local, tw2_Local, dw2_Local, F : Single ;
          {tw1, tw2 dw2 ? Ł«®˘ «ĕ-ëĄ ŻĄfĄ¬Ą--ëĄ!!!!}
       BEGIN  { FUNCTION F_t_Wall_Pro}
       D_of_Air( 1.0, tw, dw );
       tw1:=tw; dw1:=dw;
       tw2_Initial_Local:= P[t1Wet_bulb] {tw2_Local tw};
       Rtmi_tw2 (tw2_Local, Nevjazka_tw2, Ytw[1], Ytw[2], Eps_tw2, Iter_tw2, Jerror_tw2);
 Rtwi_tw2 (tw2_Local, Nevjazka_tw2, F_tw2, tw2_Initial_Local, Eps_tw2, Iter_tw2, Jerror_tw2);
       tw2_Local:=Ytw[1]-P[Alfa_1]*(Ytw[1]-tw1)*
(1-Delta_Zeb_1/s_Zeb_1)*(1/(P[Alfa_1]*(1-Delta_Zeb_1/s_Zeb_1))+
(Delta_plate/Lambda_Sc)*
1/(1-Delta_Zeb_2/s_Zeb_2));
       D_of_Air(1.0, tw2_Local, dw2_Local);
       tw2:=tw2_Local; dw2:=dw2_Local;
       D_of_Air( 1.0, tw, dw );
       tw1:=tw; dw1:=dw;
       Calka_Delta_tw_Zeb2:=(tw2_Local- Ytw[2]);
       Calka_Delta_dw_Zeb2:=(dw2_Local- Ytw[3]);
       F:=(P[Alfa_1]*(Ytw[1]-tw1)*P[Psi1]+
         P[Alfa_2]{+C_vap_C_p*Dery[3]}*
         ((1-Delta_Zeb_2/s_Zeb_2)*
         (Ytw[2]-tw2_Local)+
         (2*h_Zeb_2/s_Zeb_2)*(-Calka_Delta_tw_Zeb2)) +
         2500*P[Alfa_2]/P[Lewis_2]*
         ((1-Delta_Zeb_2/s_Zeb_2)*
         (Ytw[3]-dw2_Local)+
         (2*h_Zeb_2/s_Zeb_2)*(-Calka_Delta_dw_Zeb2)))*Waga_tw2
         + tw;
       F_t_Wall_Pro := F;
```

```
      END; { FUNCTION F_t_Wall_Pro}
     FUNCTION F_t_Wall_Ad(tw : Single ) : Single;
       VAR  dw, tw2_Initial_Local, tw2_Local, dw2_Local, F : Single ;
        BEGIN  { FUNCTION F_t_Wall_Ad}
         D_of_Air( 1.0, tw, dw );
         tw1:=tw; dw1:=dw;
         tw2_Initial_Local:= P[t1Wet_bulb] {tw2_Local tw};
         tw2_Local:=Ytw[1]-P[Alfa_3]*(Ytw[1]-tw1)*
   (1-Delta_Zeb_1/s_Zeb_1)*(1/(P[Alfa_3]*(1-Delta_Zeb_1/s_Zeb_1))+
   (Delta_plate/Lambda_Sc)*
   1/(1-Delta_Zeb_2/s_Zeb_2));
         tw2:=tw2_Local; dw2:=dw2_Local;
         D_of_Air( 1.0, tw, dw );
         tw1:=tw; dw1:=dw;
         Calka_Delta_tw_Zeb2:=(tw2_Local- Ytw[2]);
         Calk_Delta_dw_Zeb2:=(dw2_Local- Ytw[3]);
         F:=(P[Alfa_3]*(Ytw[1]-tw1)*P[Psi3]+
           P[Alfa_4]{+C_vap_C_p*Dery[3]}*
           ((1-Delta_Zeb_2/s_Zeb_2)*
           (Ytw[2]-tw2_Local)+
           (2*h_Zeb_2/s_Zeb_2)*(-Calka_Delta_tw_Zeb2)) +
           2500*P[Alfa_4]/P[Lewis_4]*
           ((1-Delta_Zeb_2/s_Zeb_2)*
           (Ytw[3]-dw2_Local)+
           (2*h_Zeb_2/s_Zeb_2)*(-Calka_Delta_dw_Zeb2)))*Waga_tw2
           + tw;
         F_t_Wall_Ad:= F;
       END;  { FUNCTION F_t_Wall_Ad}



Procedure Rk3_Ad(VAR X : Single; VAR Y, Yp : NdimType
            {PROCEDURE Praw_Zo_X_var_Ad( X : Single; Y, : NdimType);} );
     Var k1,q1, X_RK : Single;
     Begin
Prmt[1]:=Z_Start; Prmt[2]:=Z_Start+Step_Z; Prmt[3]:=Step_Z;
       Z_tw:=Z_Start+0.0*Step_Z; X_tw:=X_Start+Step_X*0.0; X_RK:=X_tw;
       Praw_Zo_X_var_Ad(X_RK, Y, Yp);
       k1:=Step_X*Yp[1]; Y[1]:=Y[1]+0.5*k1; q1:=k1;
 X:=X_Start+Step_X*0.5; {X$:=X} an1:=(AN[1]+AK[1])*0.5; ak1:=Y[1];
       for j:=1 to Ndim do YY[J]:=(AN[J]+AK[J])*0.5;
       Dery[1]:=1.e-3; Dery[2]:=1.e-3; Dery[3]:=1.0-(Dery[1]+Dery[2]);
       Z_tw:=Z_Start+0.0*Step_Z; X_tw:=X_Start+Step_X*0.0;
       RKGS_Xo_Z_var_Ad(Prmt, YY, Dery, {Ndim,} Jhlf,{ Praw_Xo_Z_var_Ad, Outp_Xo_Z_var,}Aux);
       Y[2]:=YY[2];  Y[3]:=YY[3];
Z_tw:=Z_Start+0.0*Step_Z; X_tw:=X_Start+Step_X*0.0; X_RK:=X_tw;
       Praw_Zo_X_var_Ad(X_RK, Y, Yp);
       k1:=Step_X*Yp[1];  Y[1]:=Y[1]+SQM*(k1-q1);
       q1:=q1+sqm*(3.*(k1-q1)-k1);
{ X:=X_Start+Step_X*0.5; AN1:=AN1;}  AK1:=Y[1];
       for j:=1 to Ndim do  YY[J]:=(AN[J]+AK[J])*0.5;
       Dery[1]:=1.e-3; Dery[2]:=1.e-3; Dery[3]:=1.0-(Dery[1]+Dery[2]);
       Z_tw:=Z_Start+0.0*Step_Z; X_tw:=X_Start+Step_X*0.0;
       RKGS_Xo_Z_var_Ad(Prmt, YY, Dery, {Ndim,} Jhlf,{ Praw_Xo_Z_var_Ad, Outp_Xo_Z_var,}Aux);

       Y[2]:=YY[2]; Y[3]:=YY[3]; { X:=X_Start+Step_X*0.5; AN1:=AN1;}  AK1:=Y[1];
       for j:=1 to Ndim do  YY[J]:=(AN[J]+AK[J])*0.5;
       Dery[1]:=1.e-3; Dery[2]:=1.e-3; Dery[3]:=1.0-(Dery[1]+Dery[2]);
       Z_tw:=Z_Start+0.0*Step_Z; X_tw:=X_Start+Step_X*0.0;
       RKGS_Xo_Z_var_Ad(Prmt, YY, Dery, {Ndim,} Jhlf,{ Praw_Xo_Z_var_Ad, Outp_Xo_Z_var,}Aux);
       Y[2]:=YY[2];  Y[3]:=YY[3];
Z_tw:=Z_Start+0.0*Step_Z; X_tw:=X_Start+Step_X*0.0; X_RK:=X_tw;
       Praw_Zo_X_var_Ad(X_RK, Y, Yp);
       k1:=Step_X*Yp[1]; Y[1]:=Y[1]+sqp*(k1-q1);
       q1:=q1+sqp*(3.*(k1-q1)-k1);
X:=X_Start+Step_X; { X$:=X}  AN1:=AK[1]; AK1:=Y[1];
       for j:=1 to Ndim do  YY[J]:=AK[J];
```

```
        Dery[1]:=1.e-3; ery[2]:=1.e-3; Dery[3]:=1.0-(Dery[1]+Dery[2]);
        Z_tw:=Z_Start+0.0*Step_Z; X_tw:=X_Start+Step_X*0.0;
        RKGS_Xo_Z_var_Ad(Prmt, YY, Dery, {Ndim,} Jhlf,{ Praw_Xo_Z_var_Ad, Outp_Xo_Z_var,}Aux);
        Y[2]:=YY[2];  Y[3]:=YY[3];
  X:=X_Start+Step_X
 do  YY[J]:=AK[J];
        Dery[1]:=1.e-3; Dery[2]:=1.e-3; Dery[3]:=1.0-(Dery[1]+Dery[2]);
        Z_tw:=Z_Start+0.0*Step_Z; X_tw:=X_Start+Step_X*0.0;
        RKGS_Xo_Z_var_Ad(Prmt, YY, Dery, {Ndim,} Jhlf,{ Praw_Xo_Z_var_Ad, Outp_Xo_Z_var,}Aux);
        Y[2]:=YY[2];  Y[3]:=YY[3];
Z_tw:=Z_Start+0.0*Step_Z; X_tw:=X_Start+Step_X*0.0; X_RK:=X_tw;
        Praw_Zo_X_var_
1]; Y[1]:=Y[1]+s1_6*(k1-2.0*q1);
X:=X_Start+Step_X; {X$:=XC; AN1:=AK[1];}  AK1:=Y[1];
        for j:=1 to Ndim do  YY[J]:=AK[J];
        Dery[1]:=1.e-3; Dery[2]:=1.e-3; Dery[3]:=1.0-(Dery[1]+Dery[2]);
        Z_tw:=Z_Start+0.0*Step_Z; X_tw:=X_Start+Step_X*0.0;
        RKGS_Xo_Zvar_Ad(Prmt, YY, Dery, {Ndim,} Jhlf,{ Praw_Xo_Z_var_Ad, Outp_Xo_Z_var,}Aux);
        Y[2]:=YY[2];  Y[3]:=YY[3];
     end;
Procedure Rk3_Pro(VAR X : Single; VAR Y, Yp : NdimType
           {PROCEDURE Praw_Zo_X_var_Pro( X : Single; Y, : NdimType);} );
     Var k1,q1, X_RK : Single;
     Begin
Z_tw:=Z_Start+0.0*Step_Z; X_tw:=X_Start+Step_X*0.0; X_RK:=X_tw;
        Praw_Zo_X_var_Pro(X_RK, Y, Yp);
        k1:=Step_X*Yp[1]; Y[1]:=Y[1]+0.5*k1; q1:=k1;
X:=X_Start+Step_X*0.5; {X$:=X} an1:=(AN[1]+AK[1])*0.5;  ak1:=Y[1];
        for j:=1 to Ndim do YY[J]:=(AN[J]+AK[J])*0.5;
        Dery[1]:=1.e-3; Dery[2]:=1.e-3; Dery[3]:=1.0-(Dery[1]+Dery[2]);
        Z_tw:=Z_Start+0.0*Step_Z; X_tw:=X_Start+Step_X*0.0;
        RKGSXo_Z_var_Pro(Prmt, YY, Dery, {Ndim,} Jhlf,{ Praw_Xo_Z_var_Pro, Outp_Xo_Z_var,}Aux);
        Y[2]:=YY[2];  Y[3]:=YY[3];
Z_tw:=Z_Start+0.0*Step_Z; X_tw:=X_Start+Step_X*0.0; X_RK:=X_tw;
        Praw_Zo_X_var_Pro(X_RK, Y, Yp);
        k1:=Step_X*Yp[1];   Y[1]:=Y[1]+SQM*(k1-q1);
        q1:=q1+sqm*(3.*(k1-q1)-k1);
{ X:=X_Start+Step_X*0.5; AN1:=AN1;}  AK1:=Y[1];
        for j:=1 to Ndim do  YY[J]:=(AN[J]+AK[J])*0.5;
        Dery[1]:=1.e-3; Dery[2]:=1.e-3; Dery[3]:=1.0-(Dery[1]+Dery[2]);
        Z_tw:=Z_Start+0.0*Step_Z; X_tw:=X_Start+Step_X*0.0;
        RKGS_Xo_Z_var_Pro(Prmt, YY, Dery, {Ndim,} Jhlf,{ Praw_Xo_Z_var_Pro, Outp_Xo_Z_var,}Aux);
        Y[2]:=YY[2];  Y[3]:=YY[3];
Z_tw:=Z_Start+0.0*Step_Z; X_tw:=X_Start+Step_X*0.0; X_RK:=X_tw;
        Praw_Zo_X_var_Pro(X_RK, Y, Yp);
        k1:=Step_X*Yp[1]; Y[1]:=Y[1]+sqp*(k1-q1);
        q1:=q1+sqp*(3.*(k1-q1)-k1);
X:=X_StartStep_X; { X$:=X}  AN1:=AK[1]; AK1:=Y[1];
        for j:=1 to Ndim do  YY[J]:=AK[J];
        Dery[1]:=1.e-3; Dery[2]:=1.e-3; Dery[3]:=1.0-(Dery[1]+Dery[2]);
        Z_tw:=Z_Start+0.0*Step_Z; X_tw:=X_Start+Step_X*0.0;
        RKGS_Xo_Z_var_Pro(Prmt, YY, Dery, {Ndim,} Jhlf,{ Praw_Xo_Z_var_Pro, Outp_Xo_Z_var,}Aux);
        Y[2]:=YY[2];  Y[3]:=YY[3];
Z_tw:=Z_Start+0.0*Step_Z; X_tw:=X_Start+Step_X*0.0; X_RK:=X_tw;
        Praw_Zo_X_var_Pro(X_RK, Y, Yp);
        k1:=Step_X*Yp[1]; Y[1]:=Y[1]+s1_6*(k1-2.0*q1);
X:=X_Start+Step_X; {X$:=XC; AN1:=AK[1];}  AK1:=Y[1];
        for j:=1 to Ndim do  YY[J]:=AK[J];
        Dery[1]:=1.e-3; Dery[2]:=1.e-3; Dery[3]:=1.0-(Dery[1]+Dery[2]);
        Z_tw:=Z_Start+0.0*Step_Z; X_tw:=X_Start+Step_X*0.0;
vr_Pro(Prmt, YY, Dery, {Ndim,} Jhlf,{ Praw_Xo_Z_var_Pro, Outp_Xo_Z_var,}Aux);
        Y[2]:=YY[2];  Y[3]:=YY[3];
     end;  {Procedure Rk3_Pro}
Procedure Rk3_Ad_All(VAR X : Single; VAR Y, Yp : NdimType
           {PROCEDURE Praw_Zo_X_var_Ad( X : Single; Y, : NdimType);} );
     Var k1,q1, X_RK : Single;
Prmt[1]:=Z_Start; Prmt[2]:=Z_Start+Step_Z; Prmt[3]:=Step_Z;
```

```
        Z_t:=ZStart+0.0*Step_Z; X_tw:=X_Start+Step_X*0.0; X_RK:=X_tw;
        Praw_Zo_X_var_Ad(X_RK, Y, Yp);
        k1:=Step_X*Yp[1]; Y[1]:=Y[1]+0.5*k1; q1:=k1;       begin
        X:=X_Start+Step_X*0.5; {X$:=X} an1:=(AN[1]+AK[1])*0.5; ak1:=Y[1];
        for j:=1 to Ndim do YY[J]:=(AN[J]+AK[J])*0.5;
        Dery[1]:=1.e-3; Dery[2]:=1.e-3; Dery[3]:=1.0-(Dery[1]+Dery[2]);
        Z_tw:=Z_Start+0.0*Step_Z; X_tw:=X_Start+Step_X*0.0;
        RKGS_Xo_Z_var_Ad_All(Prmt, YY, Dery, {Ndim,} Jhlf,
        { Praw_Xo_Z_var_Ad_All, Outp_Xo_Z_var,}Aux);
        Y[2]:=YY[2]; Y[3]:=YY[3]; Z_tw:=Z_Start+0.0*Step_Z; X_tw:=X_Start+Step_X*0.0; X_RK:=X_tw;
        Praw_Zo_X_var_Ad(X_RK, Y, Yp);
        k1:=Step_X*Yp[1]; Y[1]:=Y[1]+SQM*(k1-q1);
        q1:=q1+sqm*(3.*(k1-q1)-k1);
{ X:=X_Start+Step_X*0.5; AN1:=AN1;}   AK1:=Y[1];
        for j:=1 to Ndim do  YY[J]:=(AN[J]+AK[J])*0.5;
        Dery[1]:=1.e-3; Dery[2]:=1.e-3; Dery[3]:=1.0-(Dery[1]+Dery[2]);
        Z_tw:=Z_Start+0.0*Step_Z; X_tw:=X_Start+Step_X*0.0;
        RKGSXo_Z_var_Ad_All(Prmt, YY, Dery, {Ndim,} Jhlf,
        { Praw_Xo_Z_var_Ad_All, Outp_Xo_Z_var,}Aux);
        Y[2]:=YY[2]; Y[3]:=YY[3];
Z_tw:=Z_Start+0.0*Step_Z; X_tw:=X_Start+Step_X*0.0; X_RK:=X_tw;
        Praw_Zo_Xvar_Ad(X_RK, Y, Yp);
        k1:=Step_X*Yp[1]; Y[1]:=Y[1]+sqp*(k1-q1);
        q1:=q1+sqp*(3.*(k1-q1)-k1);
X:=X_Start+Step_X; { X$:=X} AN1:=AK[1]; AK1:=Y[1];
        for j:=1 to Ndim do  YY[J]:=AK[J];
        Dery[1]:=1.e-3; Dery[2]:=1.e-3; Dery[3]:=1.0-(Dery[1]+Dery[2]);
        Z_tw:=Z_Start+0.0*Step_Z; X_tw:=X_Start+Step_X*0.0;
        RKGS_Xo_Z_var_Ad_All(Prmt, YY, Dery, {Ndim,} Jhlf,
        { Praw_Xo_Z_var_Ad_All, Outp_Xo_Z_var,}Aux);
        Y[2]:=YY[2]; Y[3]:=YY[3];
        Z_tw:=Z_Start+0.0*Step_Z; X_tw:=X_Start+Step_X*0.0; X_RK:=X_tw;
        Praw_Zo_X_var_Ad(X_RK, Y, Yp);
        k1:=Step_X*Yp[1]; Y[1]:=Y[1]+s1_6*(k1-2.0*q1);
X:=X_Start+Step_X; {X$:=XC; AN1:=AK[1];}  AK1:=Y[1];
        for j:=1 to Ndim do  YY[J]:=AK[J];
        Dery[1]:=1.e-3; Dery[2]:=1.e-3; Dery[3]:=1.0-(Dery[1]+Dery[2]);
        Z_tw:=Z_Start+0.0*Step_Z; X_tw:=X_Start+Step_X*0.0;
        RKGS_Xo_Z_var_Ad_All(Prmt, YY, Dery, {Ndim,} Jhlf,
        { Praw_Xo_Z_var_Ad_All, Outp_Xo_Z_var,}Aux);
        Y[2]:=YY[2]; Y[3]:=YY[3];
      end; Procedure Rk3_Pro_All(VAR X : Single; VAR Y, Yp : NdimType
            {PROCEDURE Praw_Zo_X_var_Pro( X : Single; Y, : NdimType);} );
      Var k1,q1, X_RK : Single;
     begin rmt[1]:=Z_Start; Prmt[2]:=Z_Start+Step_Z; Prmt[3]:=Step_Z;
        Z_tw:=Z_Start+0.0*Step_Z; X_tw:=X_Start+Step_X*0.0; X_RK:=X_tw;
        Praw_Zo_X_var_Pro(X_RK, Y, Yp);
        k1:=Step_X*Yp[1]; Y[1]:=Y[1]+0.5*k1; q1:=k1;
X:=X_Start+Step_X*0.5; {X$:=X} an1:=(AN[1]+AK[1])*0.5; ak1:=Y[1];
        for j:=1 to Ndim do  YY[J]:=(AN[J]+AK[J])*0.5;
        Dery[1]:=1.e-3; Dery[2]:=1.e-3; Dery[3]:=1.0-(Dery[1]+Dery[2]);
        Z_tw:=Z_Start+0.0*Step_Z; X_tw:=X_Start+Step_X*0.0;
        RKGS_Xo_Z_var_Pro_All(Prmt, YY, Dery, {Ndim,} Jhlf,
        { Praw_Xo_Z_var_Pro_All, Outp_Xo_Z_var,}Aux);
        Y[2]:=YY[2]; Y[3]:=YY[3]; { X:=X_Start+Step_X*0.5; AN1:=AN1;}  AK1:=Y[1];
        for j:=1 to Ndim do  YY[J]:=(AN[J]+AK[J])*0.5;
        Dery[1]:=1.e-3; Dery[2]:=1.e-3; Dery[3]:=1.0-(Dery[1]+Dery[2]);
        Z_tw:=Z_Start+0.0*Step_Z; X_tw:=X_Start+Step_X*0.0;
        RKGS_Xo_Z_var_Pro_All(Prmt, YY, Dery, {Ndim,} Jhlf,
        { Praw_Xo_Z_var_Pro_All, Outp_Xo_Z_var,}Aux);
        Y[2]:=YY[2]; Y[3]:=YY[3];
Z_tw:=Z_Start+0.0*Step_Z; X_tw:=X_Start+Step_X*0.0; X_RK:=X_tw;
        Praw_Zo_X_var_Pro(X_RK, Y, Yp);
        k1:=Step_X*Yp[1]; Y[1]:=Y[1]+sqp*(k1-q1);
        q1:=q1+sqp*(3.*(k1-q1)-k1);
X:=X_Start+Step_X; { X$:=X} AN1:=AK[1]; AK1:=Y[1];
        for j:=1 to Ndim do  YY[J]:=AK[J];
```

```
        Dery[1]:=1.e-3; Dery[2]:=1.e-3; Dery[3]:=1.0-(Dery[1]+Dery[2]);
        Z_tw:=Z_Start+0.0*Step_Z; X_tw:=X_Start+Step_X*0.0;
        RKGS_Xo_Z_var_Pro_All(Prmt, YY, Dery, {Ndim,} Jhlf,
        { Praw_Xo_Z_var_Pro_All, Outp_Xo_Z_var,}Aux);
        Y[2]:=YY[2];  Y[3]:=YY[3];
  Z_tw:=Z_Start+0.0*Step_Z; X_tw:=X_Start+Step_X*0.0; X_RK:=X_tw;
        Praw_Zo_X_var_Pro(X_RK, Y, Yp);
        k1:=Step_X*Yp[1]; Y[1]:=Y[1]+s1_6*(k1-2.0*q1); X:=X_Start+Step_X; {X$:=XC; AN1:=AK[1];} AK1:=Y[1];
        for j:=1 to Ndim do  YY[J]:=AK[J];
        Dery[1]:=1.e-3; Dery[2]:=1.e-3; Dery[3]:=1.0-(Dery[1]+Dery[2]);
        Z_w:=Z_Start+0.0*Step_Z; X_tw:=X_Start+Step_X*0.0;
        RKGS_Xo_Z_var_Pro_All(Prmt, YY, Dery, {Ndim,} Jhlf,
        { Praw_Xo_Z_var_Pro_All, Outp_Xo_Z_var,}Aux);
        Y[2]:=YY[2];  Y[3]:=YY[3];
      end;

  begin
     if irow > 0 then
       begin
       n:=Ndim;
       if n > irow then  n:=irow;
       for i:=1 to irow do
         begin
           delta:=abs(arg[i]-Z);
           if  delta > b  then  b:=delta;
           Work[i]:=delta
         end; {for i}
       b:=b+1.0;
       for j:=1 to n do
         begin
           delta:=b;
           for  i:=1 to irow  do
             begin
               if Work[i] < delta  then
                 begin
                   ii:=i; delta:=Work[i]
                 end  {if Work[i] < delta}
             end;  {for i}
           arg_sort[j]:=arg[ii];
(*         if icol <> 1 then
             begin
               f_sort[2*j-1]:=val[ii]; iii:=ii+irow;  f_sort[2*j]:=val[iii];
             end  {if icol <> 1}
           else {if icol = 1}        *)  f_sort[j]:=val[ii];
           Work[ii]:=b
         end  {for j}
     end {if irow > 0}
   end;  {Procedure Atsg}
egin
     ier:=2; delt2:=0.0;
     if Ndim > 1  then
       begin
        for j:=2 to Ndim do
          begin
            delt1:=delt2; iend:=j-1;
            for i:=1 to iend do
              begin
                h:=arg_sort[i]-arg_sort[j];
                if h <> 0.0   then
                  f_sort[j]:=(f_sort[i]*(Z-arg_sort[j])-f_sort[j]*(Z-arg_sort[i]))/h
                else  {if h = 0.0}
                  begin
                    ier:=3; j:=iend; goto 8
                  end; {else ==> if h = 0.0}
              end; {for i}
            delt2:=abs(f_sort[j]-f_sort[iend]);
            if j > 2 then
```

```
        begin
          if delt2 <= eps then
            begin
              ier:=0; goto 8
            end; {if delt2 <= eps}
          if j >=5 then
            if delt2 >= delt1 then
              begin
              ier:=1; j:=iend; goto 8
              end; {if delt2 >= delt1}
        end;  {if j > 2}
      end;  {for j:}
    end {if Ndim > 1}
    else  {if Ndim <= 1}
    if Ndim < 1  then  goto 9;
    j:= Ndim;
8:    y:= f_sort[j];

9:  end;   {Procedure Ali}
   Procedure OTPT( Z:Single; Var YGR : y_Gr_Type);
     Var  P_partial2, t2Dew_Point : Single;
         I, j : integer;
  Begin
    for j:=1 to (Ndim+5) do
     begin
       for i:=1 to N_z do  t_Aux[i]:=Tnew[i,j];
       Atsg(Z, Z_Array, t_Aux, Work, N_z, 1, arg_sort, f_sort,N_Z);
       Ali(Z, arg_sort, f_sort, Ygr[j], N_Z, eps_t, i_error);
     End;
         if (Z <= L_ad) then
           Ygr[9]:=1.005*YGR[1]+(2500.+1.807*YGR[1])*P[d2N]
         Else
           Ygr[9]:=1.005*YGR[1]+(2500.+1.807*YGR[1])*P[d1N];
         Ygr[10]:=1.005*YGR[2]+(2500.+1.807*YGR[2])*YGR[3];
   end;
PROCEDURE D_of_Air( Fi, t : Single; VAR d : Single) ;
       LABEL  10 ;
       VAR t_ps, Ps  : Single;
        BEGIN   { PROCEDURE D_of_Air }
         t_ps:=t; Ps:=P[press] - 1.0;
         IF  t >= t_press  THEN  GOTO 10;
         IF  t < -60.0  THEN t_ps:= -60.0;
         Ps:= 1.3332 * EXP( Ln10*(156.0+8.12*t_ps)/(236.0+t_ps) );
  10:       d:= 0.622 * Fi / ( P[press] / Ps - Fi );
         END;     PROCEDURE Fi_of_Air( t, d : Single; VAR Fi : Single) ;
       Label  10;
       VAR  t_ps, Ps : Single;
        BEGIN   { PROCEDURE Fi_of_Air }
         t_ps:=t; Ps:=P[press] - 1.0;
         IF  t >= t_press  THEN  GOTO 10;
         IF  t < -60.0  THEN t_ps:= -60.0;
         Ps:= 1.3332 * EXP( Ln10*(156.0+8.12*t_ps)/(236.0+t_ps) );
  10:       Fi:= D * P[press] / ( Ps * ( d + 0.622 ));
         END;
 PROCEDURE Fi_of_Air( t, d : Single; VAR Fi : Single) ;
       Label  10;
       VAR  t_ps, Ps : Single;
        BEGIN   { PROCEDURE Fi_of_Air }
         t_ps:=t; Ps:=P[press] - 1.0;
         IF  t >= t_press  THEN  GOTO 10;
         IF  t < -60.0  THEN t_ps:= -60.0;
         Ps:= 1.3332 * EXP( Ln10*(156.0+8.12*t_ps)/(236.0+t_ps) );
  10:       Fi:= D * P[press] / ( Ps * ( d + 0.622 ));
         END;   { PROCEDURE Fi_of_Air }
         D_of_Air(P[Fi2N],P[t2N],P[d2N]);
         F_Wall1:=2.0*Lx*Ly; F_Wall2:=2.0*Lx*Ly; D_Ekv:=2.0*Delta;
         F_Wall1_Pro:=2.0*Lx*(Ly*L_user); F_Wall2_Pro:= F_Wall1_Pro;
```

```
      F_Wall3_Ad:=2.0*Lx*(Ly*L_Ad); F_Wall4_Ad:= F_Wall3_Ad;
      P_partial:=P[press]*P[d1N]/(0.622+P[d1N]);
      PLn:=  LN(P_partial/1.3332) / LN10 ;
      P[t1Dew_Point]:= (PLn*236.0-156.0) / (8.12-PLn);
      E1N:=1.005*P[t1N] + (2500. + 1.807*P[t1N]) * P[d1N];
      EN:=E1N;
      Rtmi ( P[t1Wet_bulb],Nevjazka, {FctWet_bulb,} P[t1Dew_Point],
          P[t1N], Eps_tWet_bulb, Iter_tWet_bulb, Jerror );


      P_partial:=P[press]*P[d2N]/(0.622+P[d2N]);
      PLn:=  LN(P_partial/1.3332) / LN10 ;
      P[t2Dew_Point]:= (PLn*236.0-156.0) / (8.12-PLn);
      E2N:=1.005*P[t2N] + (2500. + 1.807*P[t2N]) * P[d2N];
      EN:=E2N;
      Rtmi ( P[t2Wet_bulb],Nevjazka, {FctWet_bulb,} P[t2Dew_Point],
          P[t2N], Eps_tWet_bulb, Iter_tWet_bulb, Jerror );
      RoFlow1:=353./(273.+P[t1N]);
      RoFlow2:=353./(273.+P[t2N]);
      RoFlow3:=353./(273.+P[t2N]);
      RoFlow4:=353./(273.+P[t2N]);
      W1_Pro:=P[w1];
      G1_Pro:=W1_Pro*Delta*Ly*L_user*RoFlow1; G2_Pro:=G1_Pro*G2_G1;
      G4_Ad:=G2_Pro; G3_Ad:=G2_Pro;
      P[w2]:= G2_Pro/((Delta*Lx)*RoFlow2);
      W2_Pro:=G2_Pro/((Delta*Lx)*RoFlow2);
      W4_Ad:=G4_Ad/((Delta*Lx)*RoFlow4);
      W3_Ad:=G3_Ad/((Delta*Ly*L_ad)*RoFlow3);
      Re1_Delta_Pro:=W1_Pro*Delta/Nju;
      Re1_D_Ekv_Pro:=Re1_Delta_Pro*D_Ekv/Delta;
      Pe1_Delta_Pro:=RE1_Delta_Pro*Pr;
      Gz1_Delta_Pro:=Pe1_Delta_Pro*(Delta/Lx);
 {    Nu1_D_Ekv_q_const_Pro:=0.071*EXP(LN(Re1_D_Ekv_Pro)*0.64);
      Nu1_Delta_q_const_Pro:=Nu1_D_Ekv_q_const_Pro*(Delta/D_Ekv);}
      Nu1_Delta_q_const_Pro:=1.755*EXP(LN(Gz1_Delta_Pro)/3.0);
               IF Nu1_Delta_q_const_Pro < Nu_Critial_q_Const  THEN
          Nu1_Delta_q_const_Pro:=Nu_Critial_q_Const;
      Alfa1_q_const_Pro:=Nu1_Delta_q_const_Pro*Lambda/Delta;
      Fo1_q_const_Pro:=Alfa1_q_const_Pro*F_Wall1_Pro/(G1_Pro*C_p1);
      M1_q_const_Pro:=
         sqrt(2.0*Alfa1_q_const_Pro/(Lambda_Zeb_1*Delta_Zeb_1));
 {    Nu1_Delta_tw_const_Pro:=1.64*EXP(LN(Gz1_Delta_Pro)*0.64);   }
      Nu1_Delta_tw_const_Pro:=1.533*EXP(LN(Gz1_Delta_Pro)/3.0);
      IF  Nu1_Delta_tw_const_Pro < Nu_Critial_tw_Const  THEN
          Nu1_Delta_tw_const_Pro:=Nu_Critial_tw_Const;
      Alfa1_tw_const_Pro:= Nu1_Delta_tw_const_Pro*Lambda/Delta;
      Fo1_tw_const_Pro:=Alfa1_tw_const_Pro*F_Wall1_Pro/(G1_Pro*C_p1);
      M1_tw_const_Pro:=
        sqrt(2.0*Alfa1_tw_const_Pro/(Lambda_Zeb_1*Delta_Zeb_1));
      Re2_Delta_Pro:=W2_Pro*Delta/Nju;
      Re2_D_Ekv_Pro:=Re2_Delta_Pro*D_Ekv/Delta;
      Pe2_Delta_Pro:=RE2_Delta_Pro*Pr;
      Gz2_Delta_Pro:=Pe2_Delta_Pro*(Delta/(Ly*L_user));
 {    Nu2_D_Ekv_q_const_Pro:=0.071*EXP(LN(Re2_D_Ekv_Pro)*0.64);
      Nu2_Delta_q_const_Pro:=Nu1_D_Ekv_q_const_Pro*(Delta/D_Ekv);}
      Nu2_Delta_q_const_Pro:=1.755*EXP(LN(Gz2_Delta_Pro)/3.0);
      IF  Nu2_Delta_q_const_Pro < Nu_Critial_q_Const  THEN
          Nu2_Delta_q_const_Pro:=Nu_Critial_q_Const;
      Alfa2_q_const_Pro:=Nu2_Delta_q_const_Pro*Lambda/Delta;
      Fo2_q_const_Pro:=Alfa2_q_const_Pro*F_Wall2_Pro/(G2_Pro*C_p2);
      M2_q_const_Pro:=
         sqrt(2.0*Alfa2_q_const_Pro/(Lambda_Zeb_2*Delta_Zeb_2));
 {    Nu2_Delta_tw_const_Pro:=1.64*EXP(LN(Gz2_Delta_Pro)*0.64);   }
      Nu2_Delta_tw_const_Pro:=1.533*EXP(LN(Gz2_Delta_Pro)/3.0);
      IF  Nu2_Delta_tw_const_Pro < Nu_Critial_tw_Const  THEN
          Nu2_Delta_tw_const_Pro:=Nu_Critial_tw_Const;
      Alfa2_tw_const_Pro:= Nu2_Delta_tw_const_Pro*Lambda/Delta;
      Fo2_tw_const_Pro:=Alfa2_tw_const_Pro*F_Wall2_Pro/(G2_Pro*C_p2);
```

```
   M2_tw_const_Pro:=
   Re3_D_Ekv_Ad:=Re3_Delta_Ad*D_Ekv/Delta;
   Pe3_Delta_Ad:=RE3_Delta_Ad*Pr;
   Gz3_Delta_Ad:=Pe3_Delta_Ad*(Delta/Lx);
   Nu3_Delta_q_const_Ad:=1.755*EXP(LN(Gz3_Delta_Ad)/3.0);
   IF Nu3_Delta_q_const_Ad < Nu_Critial_q_Const THEN
      Nu3_Delta_q_const_Ad:=Nu_Critial_q_Const;
   Alfa3_q_const_Ad:=Nu3_Delta_q_const_Ad*Lambda/Delta;
   Fo3_q_const_Ad:=Alfa3_q_const_Ad*F_Wall3_Ad/(G3_Ad*C_p2);
   M3_q_const_Ad:=
      sqrt(2.0*Alfa3_q_const_Ad/(Lambda_Zeb_1*Delta_Zeb_1));
   Nu3_Delta_tw_const_Ad:=1.533*EXP(LN(Gz3_Delta_Ad)/3.0);
   IF Nu3_Delta_tw_const_Ad < Nu_Critial_tw_Const THEN
      Nu3_Delta_tw_const_Ad:=Nu_Critial_tw_Const;
   Alfa3_tw_const_Ad:= Nu3_Delta_tw_const_Ad*Lambda/Delta;
   Fo3_tw_const_Ad:=Alfa3_tw_const_Ad*F_Wall3_Ad/(G3_Ad*C_p2);
   M3_tw_const_Ad:=
      sqrt(2.0*Alfa3_tw_const_Ad/(Lambda_Zeb_1*Delta_Zeb_1));
   Re4_Delta_Ad:=(W4_Ad/2)*Delta/Nju;
   Re4_D_Ekv_Ad:=Re4_Delta_Ad*D_Ekv/Delta;
   Pe4_Delta_Ad:=RE4_Delta_Ad*Pr;
   Gz4_Delta_Ad:=Pe4_Delta_Ad*(Delta/(Ly*L_Ad));
{   Nu4_D_Ekv_q_const_Ad:=0.071*EXP(LN(Re4_D_Ekv_Ad)*0.64);
   Nu4_Delta_q_const_Ad:=Nu4_D_Ekv_q_const_Ad*(Delta/D_Ekv);}
   Nu4_Delta_q_const_Ad:=1.755*EXP(LN(Gz4_Delta_Ad)/3.0);
   IF Nu4_Delta_q_const_Ad < Nu_Critial_q_Const THEN
      Nu4_Delta_q_const_Ad:=Nu_Critial_q_Const;
   Alfa4_q_const_Ad:=Nu4_Delta_q_const_Ad*Lambda/Delta;
   Fo4_q_const_Ad:=Alfa4_q_const_Ad*F_Wall4_Ad/(G4_Ad*C_p2);
   M4_q_const_Ad:=
      sqrt(2.0*Alfa4_q_const_Ad/(Lambda_Zeb_2*Delta_Zeb_2));
{   Nu4_Delta_tw_const_Ad:=1.64*EXP(LN(Gz4_Delta_Ad)*0.64);   }
   Nu4_Delta_tw_const_Ad:=1.533*EXP(LN(Gz4_Delta_Ad)/3.0);
   IF Nu4_Delta_tw_const_Ad < Nu_Critial_tw_Const THEN
      Nu4_Delta_tw_const_Ad:=Nu_Critial_tw_Const;
   Alfa4_tw_const_Ad:=Nu4_Delta_tw_const_Ad*Lambda/Delta;
   Fo4_tw_const_Ad:=Alfa4_tw_const_Ad*F_Wall4_Ad/(G4_Ad*C_p2);
   M4_tw_const_Ad:=
      sqrt(2.0*Alfa4_tw_const_Ad/(Lambda_Zeb_2*Delta_Zeb_2));
   WRITELN(KIO_M_Cycle);
   WRITELN(KIO_M_Cycle,' Delta =',Delta:8,' Lx =',Lx:5:2,
   ' Ly =',Ly:5:2, ' L_ad/Ly =', L_ad:6:3);
   WRITELN(KIO_M_Cycle,' t1_Pro(p) =',P[t1N]:7:2, ' t3_Ad(p) =',P[t2N]:7:2,
   ' Fi1_Pro(p) =',P[Fi1N]*100.0:7:2,
   ' Fi3_Ad(p) =',P[Fi2N]*100.0:7:2);
   WRITELN(KIO_M_Cycle,' W1_Pro =', W1_Pro:7:3,
       ' W2_Pro = ', W2_Pro:7:3,
       ' W3_Ad = ', W3_Ad:7:3,
       ' W4_Ad = ', W4_Ad:7:3,
       ' W1_Pro/W3_Ad =',P[W1_W2]:7:3); WRITELN(KIO_M_Cycle);
   WRITELN(KIO_M_Cycle,' x1_Pro(p) =',P[d1N]*1000.:7:2,
   ' x3_Ad(p) =',P[d2N]*1000.:7:2,' P(bar.) =',P[press]:7:1,
   ' tw(p) = ???');
   WRITELN(KIO_M_Cycle,' t1p_Pro(m.) =', P[t1Wet_bulb]:7:2,
   ' t3p_Ad(m.) =', P[t2Wet_bulb]:7:2,
   ' t1p_Pro(r) =',P[t1Dew_Point]:7:2,
   ' t3p_Ad(r) =',P[t2Dew_Point]:7:2); WRITELN(KIO_M_Cycle);
   WRITEN(KIO_M_Cycle,' G1_Pro(50kan.) =',G1_Pro*50.0*3600.0:7:1,
   ' G2_Pro(50kan.) =', G2_Pro*50.0*3600.0:7:1,
   ' G3_Ad(50kan.) =', G3_Ad*50.0*3600.0:7:1,
   ' G4_Ad(50kan.) =', G4_Ad*50.0*3600.0:7:1);
   WRITELN(KIO_M_Cycle,' Re1_Delta_Pro =', Re1_Delta_Pro:7:2,
   ' Re2_Delta_Pro =', Re2_Delta_Pro:7:2,
   ' Re3_Delta_Ad =', Re3_Delta_Ad:7:2,
   ' Re4_Delta_Ad =', Re4_Delta_Ad:7:2);
   WRITELN(KIO_M_Cycle,' Pe1_Delta_Pro =', Pe1_Delta_Pro:7:2,
   ' Pe2_Delta_Pro =', Pe2_Delta_Pro:7:2,
```

```
                ' Pe3_Delta_Ad =', Pe3_Delta_Ad:7:2,
                ' Pe4_Delta_Ad =', Pe4_Delta_Ad:7:2);
         END;        { PROCEDURE Def_Initial }
 PROCEDURE  Graf_I_d_diagramma(VAR t,d : graf_I_d_type;
    NPoint, Nt, Nd, Ngrafn, Ngrafk : INTEGER; Delta_t : Single);

    LABEL  80, 65, 50, 2600, 2700, 2800, 200 ;
    CONST  A :  ARRAY[1..26]
         d1 : ARRAY[1..71] of CHAR =
    TYPE  jStringType = ARRAY[1..71] of INTEGER   ;
    VAR   j, i, kFi, LL, k, js, Lh1, jj, ii, Ld, Li, kd,
         kd1  : INTEGER ;
                   tmin, tmax, dmin, dmax, dmin_i, Fimin, ht, hd,
         hdx, Enmin, Enmax, hEn, ty, dd, di, dg     : Single;
         dx, En : ARRAY [1..6] of Single;
         Fi  : ARRAY [1..6] of Single;
         B, ddd : ARRAY[1..71] of CHAR;
         jString  : jStringType;
      BEGIN    { PROCEDURE  Graf }
       tmin:= t[1,Ngrafn]; tmax:=t[1,Ngrafn];
       dmin:= d[1,Ngrafn]; dmax:=d[1,Ngrafn];
       FOR i:=1 TO  Npoint  DO
        FOR j:=Ngrafn  TO  Ngrafk  DO
          BEGIN
           IF  tmin > t[i,j]  THEN  tmin:=t[i,j];
           IF  tmax < t[i,j]  THEN  tmax:=t[i,j];
           IF  dmin > d[i,j]  THEN  dmin:=d[i,j];
           IF  dmax < d[i,j]  THEN  dmax:=d[i,j]
          END;  { FOR i } { FOR j }
       tmax:=Round(tmax)+1; tmin:=Round(tmin)-Delta_t;
       dmax:=Round(dmax)+1; dmin:=Round(dmin)-1;
       IF  dmin < 0.0  THEN  dmin:=0.0;
       dmin_i:=dmin*0.001; Fi_of_Air(tmax,dmin_i,Fimin);
       i:=Trunc(Fimin*10.0);  Fimin:=(i DIV 2 + 1)*2*0.1;
       hd:=(dmax-dmin)/(Nd-1); ht:=(tmax-tmin)/(Nt-1);
       hdx:=(dmax-dmin)/5.0;
       For  j:=1 To 6 Do  dx[j]:=dmin+hdx*(j-1);
       Writeln;   Write(' ',dx[1]:4:1,' ');
       For j:=2 To 6 Do Write('        ', dx[j]:5:2);
       Writeln;
       Writeln(KIO_M_Cycle);  Write(KIO_M_Cycle,' ',dx[1]:4:1,' ');
       For j:=2 To 6 Do Write(KIO_M_Cycle,'        ', dx[j]:5:2);
       Writeln(KIO_M_Cycle);
       i:=Trunc(Fimin*10.0) ;  kFi:=i DIV 2 +1;
       For j:=kFi To 6 Do  Fi[j]:=Fimin+0.2*(j-kFi);
       Enmin:=Round(1.005*tmin+(2500.+1.807*tmin)*dmin_i)+1;
       Enmax:=Int(1.005*tmax+(2500.+1.807*tmax)*dmax*0.001)-1;
       hEn:=(Enmax-Enmin)/5.0;
       For  j:=1 To  6 Do  En[j]:=Enmax-hEn*(j-1);
       LL:=1;
       For  k:=1  To  Nt   Do
        Begin
          ty:=tmax-ht*(k-1);
         For  js:=1  TO  Nd  DO
           Begin
            jString[js]:=0;  B[js]:=' '
           End;  { For  js }
         For  i:=1  TO  Npoint  DO
           FOR  j:=Ngrafn  TO  Ngrafk  DO
             Begin
               jj:=j+11;
               Lh1:=Round((tmax-t[i,j])/ht) + 1;
               If  Lh1 <> k  THEN  Goto 80;
               ii:=Round((d[i,j]-dmin)/hd) + 1;
               If  jString[ii] <> 0  THEN  B[ii]:= '#'
                ELSE
                 BEGIN
```

```
                   jString[ii]:=ii; B[ii]:=A[jj]
                  END;   { If jString[ii] = 0 }
 80:           END;   { FOR j }   { FOR i }
          For j:=kFi To  6  Do
            Begin
             D_of_Air(Fi[j], ty, dd);
             Ld:=Round((dd*1000.-dmin)/hd)+1;
             If Ld < 1 Then  Goto 50;
             If Ld > Nd Then  Goto 65;
             If jString[Ld] <> 0  THEN  Goto 50;
             jString[Ld]:=Ld; B[Ld]:=A[2*j-1];
 50:         End; { For j }
 65:      For j:=1  To  6  Do
            Begin
             di:=(En[j]-1.005*ty)/(2500.+1.807*ty)*1000.0;
             Li:=Round((di-dmin)/hd)+1;
             If  (Li >= 1) AND (Li <= Nd) AND (jString[Li]= 0) Then
               Begin
               jString[Li]:= Li; B[Li]:= '+'
               End  {(Li >= 1) AND (Li <= Nd) AND (jString[Li]= 0)}
            End;  { For j }
          D_of_Air(1.0, ty, dg); kd:=Round((dg*1000.-dmin)/hd) + 1;
          If  (k = Nt) OR (kd >= Nd) Then  Goto 2600;
          If LL <> k  Then  Goto 2700;
          kd1:=kd+1;
          For j:=1 To  6  Do
            Begin
             js:=(j-1)*14+1;
             If  (js > kd) AND (jString[js]=0)  Then
               Begin
                jString[js]:=js; B[js]:='!'
               End   { Jf (js > kd)  OR  (jString[js]=js) }
            End;  { For j }
          For js:=kd1 To  Nd  Do
            Begin
              If  jString[js] = 0  THEN
                Begin
                  jString[js]:= js; B[js]:=' '
                End   { If jString[js] = 0 }
            End;  { For js }
 2600:     If LL <> k  Then  Goto 2700;
          For js:=1  To  Nd  Do
            Begin
              ddd[js]:=d1[js];
              If jString[js] <> 0  THEN  ddd[js]:=B[js];
            End;    { For js }
          Writeln(KIO_M_Cycle,ty:5:1,ddd:71);
          Writeln(ty:5:1,ddd:71); LL:=LL+6; Goto 200;
 2700:     For js:=1  TO  Nd  DO
            Begin
             ddd[js]:=d2[js];
             If jString[js] <> 0  THEN  ddd[js]:=B[js];
            End;  { For js }
          Writeln(KIO_M_Cycle,'    ',ddd:71);
          Writeln('    ',ddd:71);
 200:     End;   { For k }
        Writeln(KIO_M_Cycle);  Write(KIO_M_Cycle,' ',dx[1]:4:1,' ');
        For j:=2 To 6 Do Write(KIO_M_Cycle,'        ', dx[j]:5:2);
        Writeln(KIO_M_Cycle);
        Writeln;  Write(' ',dx[1]:4:1,' ');
        For j:=2 To 6 Do Write('        ', dx[j]:5:2);
        Writeln
       END;
PROGRAM M_KIO(KIO_M_Cycle,INPUT,OUTPUT);
    CONST K1_Alfa1=1.0; Nju=15.7E-6; RoFlow=1.2;
        C_p1=1.005E+3; C_p2=1.005E+3; C_vap=1.807E+3;
        Lambda=2.52E-2; Pr=0.708; FiWall=1.0;
```

```
        Nu_Critial_tw_Const=3.77; Nu_Critial_q_Const=4.12;
        Ln10=2.302585; C_vap_C_p=1.798010 ;
        Lambda_Sc=0.6;Lambda_Zeb_1=0.6; Lambda_Zeb_2=0.6;
        Lambda_Folia=100; {Lambda_Warstwa_Wody_2=0.6;}
        eps_t=0.0001; eps_d=1.e-5;
        sqm=0.2928932; sqp=1.707107; s1_6=0.1666667;
     Ndim = 3; Ndim_Zeb2 = 2; Ndim_X_max=4001;
     Ndim_Z_max=4001; Ndim_Z_max_Zeb2=4001;
     N_Graf=6; N_Z_Grag=N_Graf; N_X_Grag=N_Graf;
     N_Graf_56=56; N_Z_Grag_56=N_Graf_56;  N_X_Grag_56=N_Graf_56;


      LABEL   100;
   TYPE Data = (t1N, t2N, d1N, d2N, Fi1N, Fi2N, t1Wet_bulb,
            t2Wet_Bulb, t1Dew_Point, t2Dew_Point, press,
            tWall, K1Alfa1, Fo1, Fo2, Fo3, Fo4,
            w1, w2, W1_W2, Lewis, Lewis_2, Lewis_4, m1, m2, m3, m4,
            Psi1, Psi2, Psi3, Psi4, Alfa_1, Alfa_2, Alfa_3, Alfa_4);
        StartingData = ARRAY [ Data ] of Single;
        NdimArray = 1..Ndim;
        NdimArray_Zeb2= 1..Ndim_Zeb2
        PrmtType = ARRAY [1..5] of Single;
        NdimType = ARRAY [ NdimArray ] of Single;
        AuxType = ARRAY [ 1..8,NdimArray ] of Single;
        PrmtType_Zeb2= ARRAY [1..5] of Single;
        NdimType_Zeb2= ARRAY [ NdimArray_Zeb2] of Single;
        AuxType_Zeb2= ARRAY [ 1..8,NdimArray_Zeb2] of Single;
        graf_I_d_type = ARRAY [1..12,1..10] of Single ;
        Ndim_Array_X = 1..Ndim_X_max;
        Ndim_Array_X_Type = ARRAY [ Ndim_Array_X ] of Single;
        Ndim_Array_Z = 1..Ndim_Z_max;
        Ndim_Array_Z_Type = ARRAY [ Ndim_Array_Z ] of Single;
        Ndim_Array_Z_Zeb2= 1..Ndim_Z_max_Zeb2;
        Ndim_Array_Z_Type_Zeb2= ARRAY [Ndim_Array_Z_Zeb2] of Single;
        Ndim_Array_Told_Tnew_Type =
              ARRAY [Ndim_Array_Z, 1..Ndim+5] of Single;
        Ndim_Array_T_X_var_Type =
              ARRAY [Ndim_Array_X, 1..Ndim+5] of Single;
        Ndim_Array_X_graf_Type = ARRAY [1..Ndim_X_max,1..N_X_Grag+1,1..Ndim+5] of Single ;
        Ndim_Array_Z_graf_Type = ARRAY [1..Ndim_Z_max,1..N_Z_Grag+1,1..Ndim+5] of Single ;
        grafType = ARRAY [1..N_Graf_56,1..2*(N_Graf+1)] of Single ;
   FUNC_F_t_Wall = FUNCTION (X_Root : Single) : Single;
     VAR P : StartingData;
             Prmt : PrmtType;
        Prmt_Zeb2 : PrmtType_Zeb2;
        Y, Dery, YY, Yp, Ytw : NdimType;
        Y_Zeb2, Dery_Zeb2, YY_Zeb2, Yp_Zeb2 : NdimType_Zeb2;
        Aux : AuxType;
        Aux_Zeb2 : AuxType_Zeb2;
        tGraf_I_d, DGraf_I_d  : graf_I_d_type;
        tGraf_I_d_Ad, DGraf_I_d_Ad, tGraf_I_d_Pro, DGraf_I_d_Pro
            : Array [1..12] of Single;
        Array_X_graf : Ndim_Array_X_graf_Type;
        Array_Z_graf : Ndim_Array_Z_graf_Type;
        Graf_aux : grafType;
        X_Array : Ndim_Array_X_Type;
        Z_Array, arg_sort, f_sort, Work, t_aux : Ndim_Array_Z_Type;
        Told, Tnew, t_d_mean_Z : Ndim_Array_Told_Tnew_Type;
        T_X_var_Z_L_ad, T_X_var_Z_0 : Ndim_Array_T_X_var_Type;
        T_Zeb2_Os_Z : Ndim_Array_T_Zeb2_Os_Z_Type;
        AN, AK : Array[1..Ndim+2] of single ;
        YGR : y_Gr_Type;
        Y_Zeb2_Print : Y_Zeb2_Print_Type;
        tw1, dw1, tw2, dw2, tw_Zeb2, dw_Zeb2, d_Zeb2, CN_Zeb2,
        Nevjazka, Nevjazka_tw2, t2_do_Mieszania, d2_do_Mieszania,
        tw1_Initial, t_Dew_Point_Initial, tw2_Initial,
        Eps_tw1, Eps_tw2, Eps_tw_Zeb2,
        t_press, PLn, E1N, E2N, EN, DN,
```

Delta, Delta_plate, Lx, Ly, P_partial, F_Wall1, F_Wall2,
V_packing,
Delta_Zeb_1, h_Zeb_1, s_Zeb_1,
Delta_Zeb_2, h_Zeb_2, s_Zeb_2,
Delta_Warstwa_Wody_W2, Delta_Warstwa_Wody_Zeb_2,
Delta_Warstwa_Wody_W2_Calka,
Eps_tWet_bulb, Eps_tWall, G1, G2, D_Ekv,
Re1_D_Ekv, Re1_Delta, Gz1_Delta, Pe1_Delta, RoFlow1,
Re2_D_Ekv, Re2_Delta, Gz2_Delta, Pe2_Delta, RoFlow2,
Nu1_Delta_q_const, Nu1_D_Ekv_q_const, Nu1_Delta_tw_const,
Nu2_Delta_q_const, Nu2_D_Ekv_q_const, Nu2_Delta_tw_const,
Nu1_1_zone, Nu1_2_zone, Nu1_3_zone,
Nu2_1_zone, Nu2_2_zone, Nu2_3_zone,
Nu2_2_zone_mass, Nu2_3_zone_mass, Nu1, Nu2, Nu2_mass,
Fo1_tw_const, Fo1_q_const, Fo2_tw_const,  Fo2_q_const,
Fo1_1_zone, Fo1_2_zone, Fo1_3_zone,
Fo2_1_zone, Fo2_2_zone, Fo2_3_zone,
Fo2_2_zone_mass, Fo2_3_zone_mass,
M1_1_zone, M1_2_zone, M1_3_zone,
M2_1_zone, M2_2_zone, M2_3_zone,
th1_1_zone, th1_2_zone, th1_3_zone,
th2_1_zone, th2_2_zone, ch2_1_zone, ch2_2_zone,
Psi1_1_zone, Psi1_2_zone, Psi1_3_zone,
Psi2_1_zone, Psi2_2_zone,
th_1, th_2, th_3, th_4,
F_Wall1_Pro, F_Wall2_Pro, F_Wall3_Ad, F_Wall4_Ad,
RoFlow3, RoFlow4,
W1_Pro, W2_Pro, W3_Ad, W4_Ad,
G1_Pro, G2_Pro, G3_Ad, G4_Ad,
Re1_Delta_Pro, Re1_D_Ekv_Pro, Pe1_Delta_Pro, Gz1_Delta_Pro,
Re2_Delta_Pro, Re2_D_Ekv_Pro, Pe2_Delta_Pro, Gz2_Delta_Pro,
Re3_Delta_Ad, Re3_D_Ekv_Ad, Pe3_Delta_Ad, Gz3_Delta_Ad,
Re4_Delta_Ad, Re4_D_Ekv_Ad, Pe4_Delta_Ad, Gz4_Delta_Ad,
Nu1_D_Ekv_q_const_Pro, Nu2_D_Ekv_q_const_Pro,
Nu3_D_Ekv_q_const_Ad, Nu4_D_Ekv_q_const_Ad,
Nu1_Delta_q_const_Pro, Nu2_Delta_q_const_Pro,
Nu3_Delta_q_const_Ad, Nu4_Delta_q_const_Ad,
Nu1_Delta_tw_const_Pro, Nu2_Delta_tw_const_Pro,
Nu3_Delta_tw_const_Ad, Nu4_Delta_tw_const_Ad,
Alfa1_q_const_Pro, Alfa2_q_const_Pro,
Alfa3_q_const_Ad, Alfa4_q_const_Ad,
Alfa1_tw_const_Pro, Alfa2_tw_const_Pro,
Alfa3_tw_const_Ad, Alfa4_tw_const_Ad,
Alfa2_1_zone_mass, Nu2_1_zone_mass, Lewis2_1_zone, Lewis2_2_zone,
Alfa3_1_zone, Alfa3_2_zone, Alfa4_1_zone, Alfa4_2_zone,
Alfa_2_zone_mass, Alfa4_1_zone_mass,
Nu3_1_zone, Nu3_2_zone, Nu4_1_zone, Nu4_2_zone,
Nu4_1_zone_mass, Nu4_2_zone_mass, Lewis4_1_zone, Lewis4_2_zone,
M3_1_zone, M3_2_zone, M4_1_zone, M4_2_zone,
th3_1_zone, th3_2_zone, th4_1_zone, th4_2_zone,
Psi3_1_zone, Psi3_2_zone, Psi4_1_zone, Psi4_2_zone,
ch4_1_zone, ch4_2_zone,
Fo1_q_const_Pro, Fo2_q_const_Pro, Fo3_q_const_Ad, Fo4_q_const_Ad,
Fo1_tw_const_Pro, Fo2_tw_const_Pro,
Fo3_tw_const_Ad, Fo4_tw_const_Ad,
Fo3_1_zone, Fo3_2_zone, Fo4_1_zone, Fo4_2_zone,
M1_q_const_Pro, M2_q_const_Pro, M3_q_const_Ad, M4_q_const_Ad,
M1_tw_const_Pro, M2_tw_const_Pro,
M3_tw_const_Ad, M4_tw_const_Ad,
Fa_3, Fa_4, delta_P3, delta_P4, W3_average, W4_average,
t3_average, t4_average, N_3, N_4, N_3_4,
Calka_t_Zeb2, Calka_d_Zeb2, Calka_tw_Zeb2, Calka_dw_Zeb2,
Calka_Delta_Warstwa_Wody_Zeb_2, Calka_Delta_tw_Zeb2,
Calka_Delta_dw_Zeb2, Delta_Folia,
t_Zeb2_Nacz, d_Zeb2_Nacz, tw_Zeb2_Nacz, dw_Zeb2_Nacz,
Delta_Warstwa_Wody_Zeb_2_Nacz, Delta_Warstwa_Wody_Zeb_2_Kon,
t_Zeb2_Kon, d_Zeb2_Kon, tw_Zeb2_Kon, dw_Zeb2_Kon, C_Zeb2_Kon,

Calka_t1_Kon, Calka_t2_Kon, Calka_d2_Kon,
Calka_t1_Kon_Adiabat, Calka_t1_Kon_User,
AddTw2_3_zone, Waga_C_Zeb2, Waga_t_Zeb2, Waga_tw2,
Waga_C_Zeb2_Waga_t_Zeb2,
Alfa1_tw_const, K1_tw_const, Alfa1_q_const, K1_q_const,
Alfa2_tw_const,  Alfa2_q_const,
M1_tw_const, M1_q_const, M2_tw_const, M2_q_const,
Alfa1_1_zone, K1_1_zone, Alfa1_2_zone, K1_2_zone, Alfa1_3_zone,
K1_3_zone, Alfa2_Zeb2,
Alfa2_1_zone, Alfa2_2_zone, Alfa2_3_zone,
Alfa2_2_zone_mass, Alfa2_3_zone_mass,
Alfa1, K1, Alfa2,
XPrintStart, StepPrint, Step,
t1k, t2k, d1k, d2k, Delta_t1, Effect,
t1n_Adiabat, t1k_Adiabat, d1n_Adiabat, d1k_Adiabat,
t2n_Adiabat, t2k_Adiabat, d2n_Adiabat, d2k_Adiabat,
E1n_Adiabat, E1k_Adiabat, E2n_Adiabat, E2k_Adiabat,
Fi1n_Adiabat, Fi1k_Adiabat, Fi2n_Adiabat, Fi2k_Adiabat,
t1n_User, t1k_User, d1n_User, d1k_User,
t2n_User, t2k_User, d2n_User, d2k_User,
E1n_User, E1k_User, E2n_User, E2k_User,
Fi1n_User, Fi1k_User, Fi2n_User, Fi2k_User,
E2_do_mieszania, Fi2_do_mieszania,
Delta_t1_diabat, Delta_t2_Adiabat, Delta_d2_Adiabat,
Delta_E2_Adiabat,
Q2_Total_Adiabat, Q2_Latent_Adiabat, Q2_Sensible_Adiabat,
DeltaQ_Adiabat, Q1_Adiabat, Q_average_Adiabat,
Q_N_Adiabat, Q_N_plus_bypass_Adiabat,
Delta_t1_User, Delta_t2_User, Delta_d2_User, Delta_E2_User,
Q2_Total_User, Q2_Latent_User, Q2_Sensible_User,
DeltaQ_User, Q1_User, Q_average_User,
Q_N_User, Q_N_plus_bypass_User,
Q1, Q2, DeltaQ, E1, E2, E1k, Fi1, Fi2,
Delta_t2, Delta_d2, Q2_Sensible,
Q2_Latent, Q2_Total, Q_average,
t1k_Initial,  Eps_t1k, Delta_t1k,
X_tw, Z_tw, L_user, L_ad, Poprawka_G1, Poprawka_G2,
Delta_G1, G2_var,
Step_X, Step_Z, Step_Z_Zeb2, Step_Print_X, Step_Print_Z,
Step_Graf_X, Step_Graf_Z, Z_Start, X_Start, Z_Start_Print,
Z, Z_Zeb2, X, XXX, X_Print, Step_Z_0_X_Var_N_x,
h_Graf_X_56, h_Graf_Z_56, X_Graf, t1_z_0, an1, ak1, asr1,
t2_z_L_ad_X_Old, d2_z_L_ad_X_Old,
t2_z_L_ad_X_New, d2_z_L_ad_X_New,
t1_z_L_ad_X_Old, t1_z_L_ad_X_New,
Fi1k, Fi2k, E2k, t1_average, t2_average,w1_average,
w2_average, Fa_1, Fa_2, delta_P1, delta_P2,
N_1, N_2, N_1_2, Q_N,
N_1_plus_bypass, N_1_2_plus_bypass, Q_N_plus_bypass,
tDew_Point, Z_Dry, Z_wet, Z_frost,
Lewis_2_zone, Lewis_3_zone, Lewis_Zeb2, F_sum,
E1_Dew_Point, d2N_sat, E2k_theoretic, Effect_enthalpy,
teta_rosy, teta_Wet_Bulb, G2_G1, G2_G1_critical,
W1_cp, W2_cp, W_cp_min,
Q1_Jawne, Q2_Jawne, Q2_Utajone, Q2_Calkowite,
Q1_Jawne_Wzgledne, Q2_Jawne_Wzgledne, Q2_Utajone_Wzgledne,
Q1_Jawne_Scianka, Q1_Jawne_Zebro, Q2_Jawne_Scianka, Q2_Jawne_Zebro,
Q2_Utajone_Scianka, Q2_Utajone_Zebro, Q2_Calkowite_Zebro,
Q1_Jawne_Scianka_Wzgledne, Q1_Jawne_Zebro_Wzgledne,
Q2_Jawne_Scianka_Wzgledne, Q2_Jawne_Zebro_Wzgledne,
Q2_Utajone_Scianka_Wzgledne, Q2_Utajone_Zebro_Wzgledne,
Q2_Calkowite_Zebro_Wzgledne,
Q3_Jawne, Q4_Jawne, Q4_Utajone, Q4_Calkowite,
Q3_Jawne_Wzgledne, Q4_Jawne_Wzgledne, Q4_Utajone_Wzgledne,
Q3_Jawne_Scianka, Q3_Jawne_Zebro, Q4_Jawne_Scianka, Q4_Jawne_Zebro,
Q4_Utajone_Scianka, Q4_Utajone_Zebro, Q4_Calkowite_Zebro,
Q3_Jawne_Scianka_Wzgledne, Q3_Jawne_Zebro_Wzgledne,

```
        Q4_Jawne_Scianka_Wzgledne, Q4_Jawne_Zebro_Wzgledne,
        Q4_Utajone_Scianka_Wzgledne, Q4_Utajone_Zebro_Wzgledne,
        Q4_Calkowite_Zebro_Wzgledne
                : Single;
        Jhlf, Jhlf_Zeb2, Iter_tw1, Iter_tw2, Iter_tw_Zeb2,
        Jerror, Jerror_tw2, Jerror_tw_Zeb2_Ice,
        JPrint, Iter_tWet_bulb,
        Iter_tWall, J, J_Print_file, i, i5,
        J_graf_X,
        N_x, N_z, N_Z_Zeb2, Index_graf_Z, k, i_X, i_Z, j_Z, J_Print_X, L,
        J_Print_X_Flag, J_Graf_X_Flag, j_X, i_error, N_Z_Print,
        N_X_Print, i_Flag_wet_Zeb2_q, N_Z_Zeb2_Warstwa_Wody, N_z_User, L_NX
                : Integer;
        Buf : ARRAY [1..2048] of CHAR;
        KIO_M_Cycle : TEXT ;
  {$I D_Fi.pas} {$I CrosOtpt.pas} {$I F_tDew.pas} {$I Root.pas}
{$I Cros_Ftw.pas} {$I PrawOutp.pas} {$I Rkgs.pas} {$I Def_Init.pas}
{$I PRINT_Al.pas} {$I PRINT_Ad.pas} {$I PRINT_Pr.pas}
{$I cros_Rk.pas}  {$I cros_Fct.pas} {$I Graf.pas}
{$I I_d.pas} {$I Graf_Ad.pas} {$I Graf_Pro.pas} {$I Graf_All.pas}
{$I Print_Fo.pas} {$I SHAPKA.pas}
        BEGIN  { Program }
         ASSIGN(KIO_M_Cycle,'KIO_M_Cycle_Output.pas'); Rewrite(KIO_M_Cycle);
         {  FLUSH(KIO_M_Cycle); }
         SetTextBuf(KIO_M_Cycle, Buf);
        Eps_tWet_bulb:=1.0E-4; Iter_tWet_bulb:=200;
        Eps_tWall:=5.0E-7; Iter_tWall:=200;
        Eps_tw2:=Eps_tWall; Iter_tw2:=Iter_tWall;
        Eps_tw_Zeb2:=Eps_tWall; Iter_tw_Zeb2:=Iter_tWall;
        Prmt[4]:=3.E-7;
             P[t1N]:=+20.4;     P[t2N]:=+20.4;
             P[Fi1N]:=0.60;     P[Fi2N]:=0.60;
             P[w1]:=3.2;        G2_G1:=1.0;
             L_ad:=0.25;        L_user:=1-L_ad;
        P[press]:=1000.; P[K1Alfa1]:=K1_Alfa1;   {P[Lewis]:=1.0;}
           P_partial:=P[press]*P[d1N]/(0.622+P[d1N]);
        Delta:=3.0E-3; Lx:=0.5; Ly:=0.25; Delta_plate:=1.0e-3;
        Delta_Zeb_1:=1.0e-3; h_Zeb_1:=0.5*Delta; s_Zeb_1:=8*Delta;
        Delta_Zeb_2:=1.0e-3; h_Zeb_2:=0.5*Delta; s_Zeb_2:=8*Delta;
        Delta_Folia:=0.002e-3;
        Delta_Warstwa_Wody_W2:=0.50E-3;
        Delta_Warstwa_Wody_Zeb_2:= Delta_Warstwa_Wody_W2;
        Delta_Warstwa_Wody_W2_Calka:=Delta_Warstwa_Wody_W2/h_Zeb_2;
              Def_Initial;
        P[Fo1]:=Fo1_2_zone; P[Fo2]:=Fo2_2_zone;
        P[Fo3]:=Fo3_2_zone; P[Fo4]:=Fo4_2_zone;
        P[Alfa_1]:=Alfa1_2_zone; P[Alfa_2]:= Alfa2_2_zone;
        P[Alfa_3]:=Alfa3_2_zone; P[Alfa_4]:= Alfa4_2_zone;
        P[m1]:= M1_2_zone; P[m2]:= M2_2_zone;
        P[m3]:= M3_2_zone; P[m4]:= M4_2_zone;
        P[Psi1]:=Psi1_2_zone; P[Pi2]:=Psi2_2_zone;
        P[Psi3]:=Psi3_2_zone; P[Psi4]:=Psi4_2_zone;
        P[Lewis_2]:=Lewis2_2_zone; P[Lewis_4]:=Lewis4_2_zone;
        th_1:=th1_2_zone; th_2:= th2_2_zone;
        th_3:=th3_2_zone; th_4:= th2_2_zone;
           Waga_C_Zeb2:=1/(1+h_Zeb_2*M2_1_zone/th2_1_zone);
           Waga_t_Zeb2:=1-Waga_C_Zeb2;
           WRITELN(KIO_M_Cycle,' Waga_t_Zeb2 =', Waga_t_Zeb2:7:4,
           ' Waga_C_Zeb2 =', Waga_C_Zeb2:7:4); WRITELN(KIO_M_Cycle);
           Waga_C_Zeb2_Waga_t_Zeb2:=0.2*Waga_C_Zeb2/Waga_t_Zeb2;
              Waga_tw2:= 1.0/P[Alfa_2];
              J_Print_file:=1;
        WRITELN(KIO_M_Cycle);
        WRITELN(KIO_M_Cycle,' Afa1=', P[Alfa_1]:6:2,
        ' Alfa2=', P[Alfa_2]:6:2);
        WRITELN(KIO_M_Cycle,' Fo1 =', P[Fo1]:7:2,
        ' Fo2 =', P[Fo2]:7:2);
```

```
        WRITELN(KIO_M_Cycle,' M1 =', P[m1] :7:2,
' M2 =', P[m2] :7:2);
        WRITELN(KIO_M_Cycle,' Psi1 =', P[Psi1]:7:2);
        WRITELN(KIO_M_Cycle, ' Lewis_2=', P[Lewis_2]:5:3 );
        WRITELN (KIO_M_Cycle);
        WRITELN(KIO_M_Cycle,' Alfa3=', P[Alfa_3]:6:2,
' Alfa4=', P[Alfa_4]:6:2);
        WRITELN(KIO_M_Cycle,' Fo3 =', P[Fo3]:7:2,
 ' Fo4 =', P[Fo4]:7:2);
        WRITELN(KIO_M_Cycle,' M3 =', P[m3] :7:2,
' M4 =', P[m4] :7:2);
        WRITELN(KIO_M_Cycle,' Psi3 =', P[Psi3]:7:2);
        WRITELN(KIO_M_Cycle, ' Lewis_4=', P[Lewis_4]:5:3 );
        WRITELN (KIO_M_Cycle);
      D_of_Air(P[Fi2N],P[t2N],P[d2N]);
      E2N:=1.005*P[t2N] + (2500. + 1.807*P[t2N]) * P[d2N];
      t1n_Adiabat:=P[t2N]; Fi1n_Adiabat:=P[Fi2N];
      D_of_Air(Fi1n_Adiabat, t1n_Adiabat, d1n_Adiabat);
      E1n_Adiabat:=1.005*t1n_Adiabat+
      (2500. + 1.807*t1n_Adiabat)*d1n_Adiabat;
        WRITELN(KIO_M_Cycle);
        WRITELN(KIO_M_Cycle,
        WRITELN(KIO_M_Cycle,'
        WRITELN(KIO_M_Cycle);
        WRITELN(KIO_M_Cycle,'
        WRITELN (KIO_M_Cycle);
         N_x:=201; N_z:=201;
         Step_X:=1.0/(N_x-1);  Step_Z:=1.0/(N_z-1);
         {Step_Z_Zeb2:= Step_Z;}
         Step_Print_X:=0.5; Step_Print_Z:=1.0/5; Z_Start_Print:=0;
         Step_Z_0_X_Var_N_x:=Step_X;
         Step_Graf_X:=1.0/(N_X_Grag-1);
         Step_Graf_Z:=1.0/(N_Z_Grag-1);
         h_Graf_X_56:=1.0/(N_X_Grag_56-1);
         h_Graf_Z_56:=1.0/(N_Z_Grag_56-1);;
              N_Z_Print:=Round(1.0/Step_Print_Z)+1;
              N_X_Print:=Round(1.0/Step_Print_X)+1;
       WRITELN(KIO_M_Cycle,' Step_X =', Step_X:7:3,
 ' Step_Z =', Step_Z:7:3{, ' Step_Z_Zeb2 =', Step_Z_Zeb2:7:3});
      {N_x:=Round(1.0/Step_X)+1; N_z:=Round(L_ad/Step_Z)+1;}
      {(N_Z_Zeb2:=Round(1.0/Step_Z_Zeb2)+1;}
      {N_Z_Zeb2_Warstwa_Wody:=
        Round(Delta_Warstwa_Wody_W2_Calka/Step_Z_Zeb2)+1;}
      for j:=1 to N_x do  X_Array[j]:=Step_X*(j-1);
      for j:=1 to N_z do  Z_Array[j]:=0+Step_Z*(j-1);
      for j:=1 to N_z do
       Begin
        if (Z_Array[j] <= L_ad) then N_z_User:=j;
       End;
      Calka_t1_Kon:=0; Calka_t2_Kon:=0; Calka_d2_Kon:=0;
      Calka_t1_Kon_Adiabat:=0; Calka_t1_Kon_User:=0;
              Index_graf_Z:=1;
      for k:=1 to Ndim+5 do
       for j:=1 to N_X_Grag+1 do
        for i:=1 to N_X do
          Array_X_graf[i,j,k]:=0.0;
      for k:=1 to Ndim+5 do
       for j:=1 to N_Z_Grag+1 do
        for i:=1 to N_Z do
          Array_Z_graf[i,j,k]:=0.0;
      i_X:=0; Z_Start:=0.0; X_Start:=0.0; J_Print_X:=0;
      XPrintStart:=0.0-1.E-5;
      Y[1]:=P[t2N]; Y[2]:=Y[1]; Y[3]:=P[d2N];
      tw1:=P[t1Wet_bulb];X_tw:=0; Z_tw:=0;
      Praw_Zo_X_var_Ad(0.0,Y,Dery);  {¤«ď ®ŻfĄ¤Ą«Ą-¨ď tw}
      t2_do_Mieszania:=Y[2]; d2_do_Mieszania:=Y[3];
      for j:=1 to Ndim do
```

```
      begin
        for i:=1 to N_x do T_X_var_Z_0[i,j]:=Y[J];
      end; {for j}
    for i:=1 to N_x do
      begin
        T_X_var_Z_0[i,Ndim+1]:=tw1;
        T_X_var_Z_0[i,Ndim+2]:=tw2;
        T_X_var_Z_0[i,Ndim+3]:=dw2;
        T_X_var_Z_0[i,Ndim+4]:=t2_do_Mieszania;
        T_X_var_Z_0[i,Ndim+5]:=d2_do_Mieszania;
      end; {for i}
    X_Start:=0.0; i_Z:=0; j_Z:=0;
    for j:=1 to Ndim do  Y[J]:=T_X_var_Z_0[1,j];
    tw1:=P[t1Wet_bulb];X_tw:=0; Z_tw:=0; Z_Start:=0.0;
    for j:=1 to Ndim do
      begin
        YY[j]:=Y[j]; TOLD[1,j]:=Y[J]
      end; {for j}
    Z_Start:=0.0;
    an1:=T_X_var_Z_0[1,1]; ak1:=T_X_var_Z_0[1,1];
    Praw_Xo_Z_var_Ad(0.0,Y,Dery);
    t2_do_Mieszania:= Y[2]; d2_do_Mieszania:=Y[3];
    TOLD[1,Ndim+1]:=tw1; TOLD[1,Ndim+2]:=tw2; TOLD[1,Ndim+3]:=dw2;
    TOLD[1,Ndim+4]:=t2_do_Mieszania; TOLD[1,Ndim+5]:=d2_do_Mieszania;
    z:=0.0; X_Start:=0.0;
    for i:=2 to N_Z do
      begin
        z:=Z_Array[i]; Z_Start:=Z_Array[i-1]; Step_Z:=Z-Z_Start;
        Dery[1]:=1.E-3; Dery[2]:=1.E-3;
        Dery[3]:=1.0-(Dery[1]+Dery[2]);
        Prmt[1]:=Z_Start; Prmt[2]:=Z_Start+Step_Z; Prmt[3]:=Step_Z;
        Prmt[4]:=3.E-7;
        Y[1]:=P[t2N];
        an1:=P[t2N]; ak1:=P[t2N];
        RKGS_Xo_Z_var_Ad(Prmt, Y, Dery, {Ndim,}
        Jhlf,{Praw_Xo_Z_var_Ad, Outp_Xo_Z_var,} Aux );
        Z_tw:=Z_Start+Step_Z*0.9999;
        t2_do_Mieszania:=Y[2]; d2_do_Mieszania:=Y[3];
        Y[2]:=(Y[2]*Z_Start+Y[1]*Step_Z)/(Z_Start+Step_Z);
        Y[3]:=(Y[3]*Z_Start+P[d2N]*Step_Z)/(Z_Start+Step_Z);
        for j:=1 to Ndim do  TOLD[i,j]:=Y[J];
        TOLD[i,Ndim+1]:=tw1; TOLD[i,Ndim+2]:=tw2;
        TOLD[i,Ndim+3]:=dw2;
        TOLD[i,Ndim+4]:=t2_do_Mieszania;
        TOLD[i,Ndim+5]:=d2_do_Mieszania;
      end {for i};
    for j:=1 to Ndim+5 do
      for i:=1 to N_Z do
        begin
          TNEW[i,j]:=TOLD[i,j]; t_d_mean_Z[i,j]:=0.0;
        end;
    for i:=2 to N_Z do
      begin
        for k:=1 to Ndim+5 do
          Array_X_graf[1,N_X_Grag+1,k]:=
            Array_X_graf[1,N_X_Grag+1,k]+
            (TNEW[i-1,k]+TNEW[i,k])*0.5*Step_Z;
      end; {for i}
    for k:=1 to Ndim+5 do
        Array_X_graf[1,N_X_Grag+1,k]:=
          Array_X_graf[1,N_X_Grag+1,k]/1.0;
    for j:=1 to N_Z_Grag do
      begin
        Z:=0+Step_Graf_Z*(j-1);  Otpt(Z,Ygr);
        for k:=1 to Ndim+5 do  Array_X_graf[1,j,k]:=Ygr[k];
      end; {for j}
    for i:=1 to N_Z_Grag_56 do
```

```
        begin
          Z:=0+h_Graf_Z_56*(i-1); Otpt(Z,YGR);
          for k:=1 to Ndim+5 do
            Array_Z_graf[i,Index_graf_Z,k]:=Ygr[k];
        end; {for i}
  Index_graf_Z:=Index_graf_Z+1;
  {Goto 100;}
  i_Z:=0; z:=0.0; J_Print_X:=1; J_graf_X:=1;
  {for L:=2 to 3 do}
  for L:=2 to N_x do
    begin
      X:=X_Array[L]; X_Start:=X_Array[L-1]; Step_X:=X-X_Start;
      XXX:=X; X_Print:=-1.E-5+Step_Print_X*J_Print_X;
      if XXX >= X_Print
        then
          begin
            J_Print_X_Flag:=1; J_Print_X:=J_Print_X+1
          end { if XXX >= X_Print }
        else J_Print_X_Flag:=0;
      X_Graf:=-1.e-5+Step_Graf_X*J_graf_X;
      if XXX >= X_Graf
        then
          begin
            J_Graf_X_Flag:=1; J_Graf_X:=J_Graf_X+1
          end { if XXX >= X_Graf }
        else J_Graf_X_Flag:=0;
      for j:=1 to Ndim do  Y[J]:=T_X_var_Z_0[L,j];
      t1_z_0:=T_X_var_Z_0[L,1];
      if J_Print_X_Flag=1  then
        begin
          Prt_Ad(X_Array[L],+1)
        end; {if J_Print_X_Flag=1}
  for j:=1 to Ndim+5 do
    T_X_var_Z_L_ad[L,j]:=TNEW[N_Z,j];
  for i:=2 to N_Z do
    begin
      for k:=1 to Ndim+5 do
        Array_X_graf[L,N_X_Grag+1,k]:=
          Array_X_graf[L,N_X_Grag+1,k]+
          (TNEW[i-1,k]+TNEW[i,k])*0.5*Step_Z;
    end; {for i}
  for k:=1 to Ndim+5 do
      Array_X_graf[L,N_X_Grag+1,k]:=
        Array_X_graf[L,N_X_Grag+1,k]/1.0;
    for j:=1 to N_Z_Grag do
      begin
        Z:=0+Step_Graf_Z*(j-1); Otpt(Z,Ygr);
        for k:=1 to Ndim+5 do Array_X_graf[L,j,k]:=Ygr[k];
      end; {for j}
    for j:=1 to Ndim+5 do
      for i:=1 to N_Z do
        t_d_mean_Z[i,j]:=t_d_mean_Z[i,j]+
        (TOLD[i,j]+TNEW[i,j])*0.5*(X_Array[L]-X_Array[L-1]);
    if J_Graf_X_Flag = 1 then
      begin
        for i:=1 to N_Z_Grag_56 do
          begin
            Z:=0+h_Graf_Z_56*(i-1); Otpt(Z,YGR);
            for K:=1 to Ndim+5 do
              Array_Z_graf[i,Index_graf_Z,k]:=YGR[k];
          end; {for i}
        Index_graf_Z:=Index_graf_Z+1;
      end;  {if J_Graf_X_Flag = 1}
    for j:=1 to Ndim+5 do
      for i:=1 to N_z do TOLD[i,j]:=TNEW[i,j];
    end;{for L}
  t2n_Adiabat:=t_d_mean_Z[1,2]; d2n_Adiabat:=P[d2N];
```

```
      Fi_of_Air(t2n_Adiabat, d2n_Adiabat, Fi2n_Adiabat);
      E2n_Adiabat:=1.005*t2n_Adiabat+
      (2500. + 1.807*t2n_Adiabat)*d2n_Adiabat;
      t2k_Adiabat:=t_d_mean_Z[N_z,2]; d2k_Adiabat:=t_d_mean_Z[N_z,3];
      Fi_of_Air(t2k_Adiabat, d2k_Adiabat, Fi2k_Adiabat);
      E2k_Adiabat:=1.005*t2k_Adiabat+
      (2500. + 1.807*t2k_Adiabat)*d2k_Adiabat;
      for i:=1 to N_z do
        Calka_t1_Kon_Adiabat:=Calka_t1_Kon_Adiabat+TNEW[i,1];
      t1k_Adiabat:=Calka_t1_Kon_Adiabat/N_z;
      d1k_Adiabat:=d1n_Adiabat;
      Fi_of_Air(t1k_Adiabat, d1k_Adiabat, Fi1k_Adiabat);
      E1k_Adiabat:=1.005*t1k_Adiabat+
      (2500. + 1.807*t1k_Adiabat)*d1k_Adiabat;
      for j:=1 to Ndim+5 do
        for i:=1 to N_Z do  TNEW[i,j]:=t_d_mean_Z[i,j];
      for i:=1 to N_Z_Grag_56 do
        begin
          Z:=0+h_Graf_Z_56*(i-1); Otpt(Z,YGR);
          for k:=1 to Ndim+5 do  Array_Z_graf[i,N_Z_Grag+1,k]:=Ygr[k];
        end; {for i}
      for i:=1 to N_x do Z_Array[i]:=X_Array[i];
              N_Z:=N_x;
      for j:=1 to N_X_Grag+1 do
        begin
          for k:=1 to Ndim+5 do
            for i:=1 to N_x do  TNEW[i,k]:=Array_X_graf[i,j,k];
          for i:=1 to N_X_Grag_56 do
            begin
              X:=h_Graf_X_56*(i-1);  Otpt(X,YGR);
              for k:=1 to Ndim+5 do Array_X_graf[i,j,k]:=YGR[k];
            end; {for i}
        end; {for j}
      PrintEnd_Ad;
       Graf_Ad;
      WRITELN(KIO_M_Cycle);
      WRITELN(KIO_M_Cycle,'
      WRITELN(KIO_M_Cycle);
      WRITELN(KIO_M_Cycle,'
      WRITELN(KIO_M_Cycle,
      WRITELN(KIO_M_Cycle,'
      WRITELN (KIO_M_Cycle);
      WRITELN(KIO_M_Cycle);
      WRITELN(KIO_M_Cycle,' Alfa1=', P[Alfa_1]:6:2,
      ' Alfa2=', P[Alfa_2]:6:2);
      WRITELN(KIO_M_Cycle,' Fo1 =', P[Fo1]:7:2,
       ' Fo2 =', P[Fo2]:7:2);
      WRITELN(KIO_M_Cycle,' M1 =', P[m1] :7:2,
      ' M2 =', P[m2] :7:2);
      WRITELN(KIO_M_Cycle,' Psi1 =', P[Psi1]:7:2);
      WRITELN(KIO_M_Cycle, ' Lewis =', P[Lewis]:5:3 );
      WRITELN (KIO_M_Cycle);
      D_of_Air(P[Fi2N],P[t2N],P[d2N]);
      E2N:=1.005*P[t2N] + (2500. + 1.807*P[t2N]) * P[d2N];
      t1n_Adiabat:=P[t2N]; Fi1n_Adiabat:=P[Fi2N];
      D_of_Air(Fi1n_Adiabat, t1n_Adiabat, d1n_Adiabat);
      E1n_Adiabat:=1.005*t1n_Adiabat+
      (2500. + 1.807*t1n_Adiabat)*d1n_Adiabat;
      D_of_Air(P[Fi1N],P[t1N],P[d1N]);
      E1N:=1.005*P[t1N] + (2500. + 1.807*P[t1N]) * P[d1N];
      t1n_User:=P[t1N]; Fi1n_User:=P[Fi1N];
      D_of_Air(Fi1n_User, t1n_User, d1n_User);
      E1n_User:=1.005*t1n_User+
      (2500. + 1.807*t1n_User)*d1n_User;
      t2n_User:=t2k_Adiabat; d2n_User:=d2k_Adiabat;;
      Fi_of_Air(t2n_User, d2n_User, Fi2n_User);
      E2n_User:=1.005*t2n_User+
```

```
(2500. + 1.807*t2n_User)*d2n_User;
  Step_X:=1.0/(N_x-1); Step_Z:=1.0/(N_z-1);
  {Step_Z_Zeb2:= Step_Z;}
  {Step_Print_X:=0.1;} Step_Print_Z:=1.0/10;
  Z_Start_Print:=0;
  Step_Graf_X:=1.0/(N_X_Grag-1);
  Step_Graf_Z:=1.0/(N_Z_Grag-1);
  h_Graf_X_56:=1.0/(N_X_Grag_56-1);
  h_Graf_Z_56:=1.0/(N_Z_Grag_56-1);;
  N_Z_Print:=Round(1.0/Step_Print_Z)+1;
      N_X_Print:=Round(1.0/Step_Print_X)+1;
 WRITELN(KIO_M_Cycle,' Step_X =', Step_X:7:3,
  ' Step_Z =', Step_Z:7:3, ' Step_Z_Zeb2 =', Step_Z_Zeb2:7:3);
{(N_Z_Zeb2:=Round(1.0/Step_Z_Zeb2)+1;}
{N_Z_Zeb2_Warstwa_Wody:=
    Round(Delta_Warstwa_Wody_W2_Calka/Step_Z_Zeb2)+1;}
for j:=1 to N_x do  X_Array[j]:=Step_X*(j-1);
for j:=1 to N_z do  Z_Array[j]:=0+Step_Z*(j-1);
N_z_User:=N_z;
Calka_t1_Kon:=0; Calka_t2_Kon:=0; Calka_d2_Kon:=0;
Calka_t1_Kon_Adiabat:=0; Calka_t1_Kon_User:=0;
            Index_graf_Z:=1;
for k:=1 to Ndim+5 do
  for j:=1 to N_X_Grag+1 do
    for i:=1 to N_X do
      Array_X_graf[i,j,k]:=0.0;
for k:=1 to Ndim+5 do
  for j:=1 to N_Z_Grag+1 do
    for i:=1 to N_Z do
      Array_Z_graf[i,j,k]:=0.0;
          Shapka_Pro;
X_Start:=0; i_Z:=0; j_Z:=0;
Y[1]:=P[t1N];
Y[2]:=T_X_var_Z_L_ad[1,2]; Y[3]:=T_X_var_Z_L_ad[1,3];
tw1:=T_X_var_Z_L_ad[1,Ndim+1]; X_tw:=0;
Z_tw:=0; Z_Start:=0;
for j:=1 to Ndim do
  begin
    YY[j]:=Y[j]; TOLD[1,j]:=Y[J]
  end; {for j}
an1:=P[t1N]; ak1:=P[t1N];
Praw_Xo_Z_var_Pro(0,Y,Dery);
t2_do_Mieszania:=Y[2]; d2_do_Mieszania:=Y[3];
TOLD[1,Ndim+1]:=tw1; TOLD[1,Ndim+2]:=tw2; TOLD[1,Ndim+3]:=dw2;
TOLD[1,Ndim+4]:=t2_do_Mieszania; TOLD[1,Ndim+5]:=d2_do_Mieszania;
z:=0; X_Start:=0;
Y[1]:=P[t1N];
Y[2]:=T_X_var_Z_L_ad[1,2]; Y[3]:=T_X_var_Z_L_ad[1,3];
for i:=2 to N_Z do
  begin
    z:=Z_Array[i]; Z_Start:=Z_Array[i-1]; Step_Z:=Z-Z_Start;
    Dery[1]:=1.E-3; Dery[2]:=1.E-3;
    Dery[3]:=1.0-(Dery[1]+Dery[2]);
    Prmt[1]:=Z_Start; Prmt[2]:=Z_Start+Step_Z; Prmt[3]:=Step_Z;
    Prmt[4]:=3.E-7;
    Y[1]:=P[t1N];
    an1:=P[t1N]; ak1:=P[t1N];
    RKGS_Xo_Z_var_Pro(Prmt, Y, Dery, {Ndim,} Jhlf,
    { Praw_Xo_Z_var_Pro, Outp_Xo_Z_var,} Aux );
    t2_do_Mieszania:=Y[2]; d2_do_Mieszania:=Y[3];
    Praw_Zo_X_var_Pro(X_Start,Y,Dery);
    for j:=1 to Ndim do TOLD[i,j]:=Y[J];
    TOLD[i,Ndim+1]:=tw1; TOLD[i,Ndim+2]:=tw2;
    TOLD[i,Ndim+3]:=dw2;
    TOLD[i,Ndim+4]:=t2_do_Mieszania;
    TOLD[i,Ndim+5]:=d2_do_Mieszania;
  end {for i};
```

```
     for j:=1 to Ndim+5 do
       for i:=1 to N_Z do
         begin
           TNEW[i,j]:=TOLD[i,j]; t_d_mean_Z[i,j]:=0.0;
         end;
     for i:=2 to N_Z do
       begin
         for k:=1 to Ndim+5 do
           Array_X_graf[1,N_X_Grag+1,k]:=Array_X_graf[1,N_X_Grag+1,k]+(TNEW[i-
1,k]+TNEW[i,k])*0.5*Step_Z;
       end; {for i}
     for k:=1 to Ndim+5 do
         Array_X_graf[1,N_X_Grag+1,k]:=
           Array_X_graf[1,N_X_Grag+1,k]/1.0;
     for j:=1 to N_Z_Grag do
       begin
         Z:=0+Step_Graf_Z*(j-1); Otpt(Z,Ygr);
         for k:=1 to Ndim+5 do  Array_X_graf[1,j,k]:=Ygr[k];
       end; {for j}
     Prt_Pro(0.0,Jhlf);
     for i:=1 to N_Z_Grag_56 do
       begin
         Z:=0+h_Graf_Z_56*(i-1); Otpt(Z,YGR);
         for k:=1 to Ndim+5 do
           Array_Z_graf[i,Index_graf_Z,k]:=Ygr[k];
       end; {for i}
     Index_graf_Z:=Index_graf_Z+1;
     {Goto 100;}
     i_Z:=0; z:=L_ad; J_Print_X:=1; J_graf_X:=1;
     {for L:=2 to 3 do}
     for L:=2 to N_x do
       begin
         X:=X_Array[L]; X_Start:=X_Array[L-1]; Step_X:=X-X_Start;
         XXX:=X; X_Print:=-1.E-5+Step_Print_X*J_Print_X;
         if XXX >= X_Print
           then
             begin
               J_Print_X_Flag:=1; J_Print_X:=J_Print_X+1
             end { if XXX >= X_Print }
           else J_Print_X_Flag:=0;
         X_Graf:=-1.e-5+Step_Graf_X*J_graf_X;
         if XXX >= X_Graf
           then
             begin
               J_Graf_X_Flag:=1; J_Graf_X:=J_Graf_X+1
             end { if XXX >= X_Graf }
           else J_Graf_X_Flag:=0;
     t1_z_L_ad_X_Old:=TOLD[1,1];
     t2_z_L_ad_X_Old:=T_X_var_Z_L_ad[(L-1),2];
     d2_z_L_ad_X_Old:=T_X_var_Z_L_ad[(L-1),3];
     t2_z_L_ad_X_New:=T_X_var_Z_L_ad[L,2];
     d2_z_L_ad_X_New:=T_X_var_Z_L_ad[L,3];
     TOLD[1,2]:=t2_z_L_ad_X_Old;
     TOLD[1,3]:=d2_z_L_ad_X_Old;
         Fct_Z_var_Proces;
         if J_Print_X_Flag=1  then
           begin
             Prt_Pro(X_Array[L],+1)
           end; {if J_Print_X_Flag=1}
         for i:=2 to N_Z do
           begin
             for k:=1 to Ndim+5 do
               Array_X_graf[L,N_X_Grag+1,k]:=Array_X_graf[L,N_X_Grag+1,k]+(TNEW[i-
1,k]+TNEW[i,k])*0.5*Step_Z;
           end; {for i}
       for k:=1 to Ndim+5 do
           Array_X_graf[L,N_X_Grag+1,k]:=
```

```
                  Array_X_graf[L,N_X_Grag+1,k]/1.0;
            for j:=1 to N_Z_Grag do
              begin
                Z:=0+Step_Graf_Z*(j-1); Otpt(Z,Ygr);
                for k:=1 to Ndim+5 do Array_X_graf[L,j,k]:=Ygr[k];
              end; {for j}
            for j:=1 to Ndim+5 do
              for i:=1 to N_Z do
                t_d_mean_Z[i,j]:=t_d_mean_Z[i,j]+
                (TOLD[i,j]+TNEW[i,j])*0.5*(X_Array[L]-X_Array[L-1]);
            if J_Graf_X_Flag = 1 then
              begin
                for i:=1 to N_Z_Grag_56 do
                  begin
                    Z:=0+h_Graf_Z_56*(i-1); Otpt(Z,YGR);
                    for K:=1 to Ndim+5 do
                      Array_Z_graf[i,Index_graf_Z,k]:=YGR[k];
                  end; {for i}
                Index_graf_Z:=Index_graf_Z+1;
              end;  {if J_Graf_X_Flag = 1}
            for j:=1 to Ndim+5 do
              for i:=1 to N_z do TOLD[i,j]:=TNEW[i,j];
          end;{for L}
    t2k_User:=t_d_mean_Z[N_z,2]; d2k_User:=t_d_mean_Z[N_z,3];
    Fi_of_Air(t2k_User, d2k_User, Fi2k_User);
    E2k_User:=1.005*t2k_User +
    (2500. + 1.807*t2k_User)*d2k_User;
    for i:=1 to N_z do
      Calka_t1_Kon_User:=Calka_t1_Kon_User+TNEW[i,1];
    t1k_User:=Calka_t1_Kon_User/N_z;
    d1k_User:=d1n_User;
    Fi_of_Air(t1k_User, d1k_User, Fi1k_User);
    E1k_User:=1.005*t1k_User+
    (2500. + 1.807*t1k_User)*d1k_User;
    for j:=1  to Ndim+5 do
      for i:=1 to N_Z do  TNEW[i,j]:=t_d_mean_Z[i,j];
    for i:=1 to N_Z_Grag_56 do
      begin
        Z:=0+h_Graf_Z_56*(i-1); Otpt(Z,YGR);
        for k:=1 to Ndim+5 do
          Array_Z_graf[i,N_Z_Grag+1,k]:=Ygr[k];
      end; {for i}
    for i:=1 to N_x do Z_Array[i]:=X_Array[i];
           N_Z:=N_x;
    for j:=1 to N_X_Grag+1 do
      begin
        for k:=1 to Ndim+5 do
          for i:=1 to N_x do  TNEW[i,k]:=Array_X_graf[i,j,k];
        for i:=1 to N_X_Grag_56 do
          begin
            X:=h_Graf_X_56*(i-1); Otpt(X,YGR);
            for k:=1 to Ndim+5 do Array_X_graf[i,j,k]:=YGR[k];
          end; {for i}
      end; {for j}
    WRITELN(KIO_M_Cycle);
    WRITELN(KIO_M_Cycle,'
    WRITELN (KIO_M_Cycle);
    WRITELN(KIO_M_Cycle);
    WRITELN(KIO_M_Cycle,' ,
    WRITELN (KIO_M_Cycle);
    WRITELN(KIO_M_Cycle);
    WRITELN(KIO_M_Cycle,' Alfa1=', P[Alfa_1]:6:2,
    ' Alfa2=', P[Alfa_2]:6:2);
    WRITELN(KIO_M_Cycle,' Fo1 =', P[Fo1]:7:2,
    ' Fo2 =', P[Fo2]:7:2);
    WRITELN(KIO_M_Cycle,' M1 =', P[m1] :7:2,
    ' M2 =', P[m2] :7:2);
```

```
WRITELN(KIO_M_Cycle,' Psi1 =', P[Psi1]:7:2);
WRITELN(KIO_M_Cycle, ' Lewis_2=', P[Lewis_2]:5:3 );
WRITELN (KIO_M_Cycle);
WRITELN(KIO_M_Cycle,' Alfa3=', P[Alfa_3]:6:2,
' Alfa4=', P[Alfa_4]:6:2);
WRITELN(KIO_M_Cycle,' Fo3 =', P[Fo3]:7:2,
' Fo4 =', P[Fo4]:7:2);
WRITELN(KIO_M_Cycle,' M3 =', P[m3] :7:2,
' M4 =', P[m4] :7:2);
WRITELN(KIO_M_Cycle,' Psi3 =', P[Psi3]:7:2);
WRITELN(KIO_M_Cycle, ' Lewis_4=', P[Lewis_4]:5:3 );
WRITELN (KIO_M_Cycle);
D_of_Air(P[Fi2N],P[t2N],P[d2N]);
E2N:=1.005*P[t2N] + (2500. + 1.807*P[t2N]) * P[d2N];
t1n_Adiabat:=P[t2N]; Fi1n_Adiabat:=P[Fi2N];
D_of_Air(Fi1n_Adiabat, t1n_Adiabat, d1n_Adiabat);
E1n_Adiabat:=1.005*t1n_Adiabat+
D_of_Air(P[Fi1N],P[t1N],P[d1N]);
E1N:=1.005*P[t1N] + (2500. + 1.807*P[t1N]) * P[d1N];
t1n_User:=P[t1N]; Fi1n_User:=P[Fi1N];
D_of_Air(Fi1n_User, t1n_User, d1n_User);
E1n_User:=1.005*t1n_User+
(2500. + 1.807*t1n_User)*d1n_User;
t2n_User:=t2k_Adiabat; d2n_User:=d2k_Adiabat;;
Fi_of_Air(t2n_User, d2n_User, Fi2n_User);
E2n_User:=1.005*t2n_User+
(2500. + 1.807*t2n_User)*d2n_User;
  Step_X:=1.0/(N_x-1);  Step_Z:=1.0/(N_z-1);
  {Step_Z_Zeb2:= Step_Z;}
  Step_Print_X:=0.1; Step_Print_Z:=1.0/10; Z_Start_Print:=0;
  Step_Z_0_X_Var_N_x:=Step_X;

  Step_Graf_X:=1.0/(N_X_Grag-1);
  Step_Graf_Z:=1.0/(N_Z_Grag-1);
  h_Graf_X_56:=1.0/(N_X_Grag_56-1);
  h_Graf_Z_56:=1.0/(N_Z_Grag_56-1);;
        N_Z_Print:=Round(1.0/Step_Print_Z)+1;
        N_X_Print:=Round(1.0/Step_Print_X)+1;
 WRITELN(KIO_M_Cycle,' Step_X =', Step_X:7:3,
 ' Step_Z =', Step_Z:7:3{, ' Step_Z_Zeb2 =', Step_Z_Zeb2:7:3});
{(N_Z_Zeb2:=Round(1.0/Step_Z_Zeb2)+1;}
{N_Z_Zeb2_Warstwa_Wody:=
   Round(DeltaWarstwa_Wody_W2_Calka/Step_Z_Zeb2)+1;}
for j:=1 to N_x do  X_Array[j]:=Step_X*(j-1);
for j:=1 to N_z do  Z_Array[j]:=0+Step_Z*(j-1);
for j:=1 to N_z do
 Begin
  if (Z_Array[j] <= L_ad) then N_z_User:=j;
 End;
Calka_t1_Kon:=0; Calka_t2_Kon:=0; Calka_d2_Kon:=0;
Calka_t1_Kon_Adiabat:=0; Calka_t1_Kon_User:=0;
          Index_graf_Z:=1;
for k:=1 to Ndim+5 do
 for j:=1 to N_X_Grag+1 do
  for i:=1 to N_X do
    Array_X_graf[i,j,k]:=0.0;
for k:=1 to Ndim+5 do
 for j:=1 to N_Z_Grag+1 do
  for i:=1 to N_Z do
    Array_Z_graf[i,j,k]:=0.0;
i_X:=0; Z_Start:=0.0; X_Start:=0.0; J_Print_X:=0;
XPrintStart:=0.0-1.E-5;
Y[1]:=P[t2N]; Y[2]:=Y[1]; Y[3]:=P[d2N];
tw1:=P[t1Wet_bulb];X_tw:=0; Z_tw:=0;
Praw_Zo_X_var_Ad(0.0,Y,Dery); {¤«ď ®ŽfĄ¤Ą«Ą-¨ď tw}
t2_do_Mieszania:=Y[2]; d2_do_Mieszania:=Y[3];
for j:=1 to Ndim do
```

```
      begin
        for i:=1 to N_x do T_X_var_Z_0[i,j]:=Y[J];
      end; {for j}
    for i:=1 to N_x do
      begin
        T_X_var_Z_0[i,Ndim+1]:=tw1;
        T_X_var_Z_0[i,Ndim+2]:=tw2;
        T_X_var_Z_0[i,Ndim+3]:=dw2;
        T_X_var_Z_0[i,Ndim+4]:=t2_do_Mieszania;
        T_X_var_Z_0[i,Ndim+5]:=d2_do_Mieszania;
      end; {for i}
    X_Start:=0.0; i_Z:=0; j_Z:=0;
    for j:=1 to Ndim do  Y[J]:=T_X_var_Z_0[1,j];
    tw1:=P[t1Wet_bulb];X_tw:=0; Z_tw:=0; Z_Start:=0.0;
    for j:=1 to Ndim do
      begin
        YY[j]:=Y[j]; TOLD[1,j]:=Y[J]
      end; {for j}
    Z_Start:=0.0;
    an1:=T_X_var_Z0[1,1]; ak1:=T_X_var_Z_0[1,1];
    Praw_Xo_Z_var_Ad(0.0,Y,Dery); {do obliczenia tw1}
    t2_do_Mieszania:=Y[2]; d2_do_Mieszania:=Y[3];
    TOLD[1,Ndim+1]:=tw1; TOLD[1,Ndim+2]:=tw2; TOLD[1,Ndim+3]:=dw2;
    TOLD[1,Ndim+4]:=t2_do_Mieszania; TOLD[1,Ndim+5]:=d2_do_Mieszania;
    for i:=2 to N_Z do
      begin
        z:=Z_Array[i]; Z_Start:=Z_Array[i-1]; Step_Z:=Z-Z_Start;
        Dery[1]:=1.E-3; Dery[2]:=1.E-3;
        Dery[3]:=1.0-(Dery[1]+Dery[2]);
        Prmt[1]:=Z_Start; Prmt[2]:=Z_Start+Step_Z; Prmt[3]:=Step_Z;
        Prmt[4]:=3.E-7;
        Z_tw:=Z_Start+Step_Z*0.9999;
        if (Z_tw < L_ad) then
          begin
            Y[1]:=P[t2N];
            an1:=P[t2N]; ak1:=P[t2N];
            RKGS_Xo_Z_var_Ad_All(Prmt, Y, Dery, {Ndim,}
            Jhlf,{Praw_Xo_Z_var_Ad_All, Outp_Xo_Z_var,} Aux );
            Praw_Xo_Z_var_Ad_All(X_Start,Y,Dery);
            Z_tw:=Z_Start+Step_Z*0.9999;
            t2_do_Mieszania:=Y[2]; d2_do_Mieszania:=Y[3];
            Y[2]:=(Y[2]*Z_Start+Y[1]*Step_Z)/(Z_Start+Step_Z);
            Y[3]:=(Y[3]*Z_Start+P[d2N]*Step_Z)/(Z_Start+Step_Z);
          End;{ if (Z_tw < L_ad)}
        if (Z_tw >= L_ad) then
          begin
            Y[1]:=P[t1N];
            an1:=P[t1N]; ak1:=P[t1N];
RKGS_Xo_Z_var_Pro_All(Prmt, Y, Dery, {Ndim,}
          Jhlf,{ Praw_Xo_Z_var_Pro_All, Outp_Xo_Z_var,} Aux );
          Praw_Xo_Z_var_Pro_All(X_Start,Y,Dery);
        for j:=1 to Ndim do  TOLD[i,j]:=Y[J];
        TOLD[i,Ndim+1]:=tw1; TOLD[i,Ndim+2]:=tw2;
        TOLD[i,Ndim+3]:=dw2;
        TOLD[i,Ndim+4]:=t2_do_Mieszania;
      for j:=1 to Ndim+5 do
        for i:=1 to N_Z do
          begin
            TNEW[i,j]:=TOLD[i,j]; t_d_mean_Z[i,j]:=0.0;
          end;
      for i:=2 to N_Z do
        begin
          for k:=1 to Ndim+5 do
            Array_X_graf[1,N_X_Grag+1,k]:=
              Array_X_graf[1,N_X_Grag+1,k]+
              (TNEW[i-1,k]+TNEW[i,k])*0.5*Step_Z;
        end; {for i}
```

```
for k:=1 to Ndim+5 do
     Array_X_graf[1,N_X_Grag+1,k]:=
      Array_X_graf[1,N_X_Grag+1,k]/1.0;
for j:=1 to N_Z_Grag do
  begin
    Z:=0+Step_Graf_Z*(j-1);  Otpt(Z,Ygr);
    for k:=1 to Ndim+5 do  Array_X_graf[1,j,k]:=Ygr[k];
  end; {for j}
for i:=1 to N_Z_Grag_56 do
  begin
    Z:=0+h_Graf_Z_56*(i-1); Otpt(Z,YGR);
    for k:=1 to Ndim+5 do
     Array_Z_graf[i,Index_graf_Z,k]:=Ygr[k];
  end; {for i}
Index_graf_Z:=Index_graf_Z+1;
{Goto 100;}
i_Z:=0; z:=0.0; J_Print_X:=1; J_graf_X:=1;
{for L:=2 to 3 do}
for L:=2 to N_x do
  begin
   X:=X_Array[L]; X_Start:=X_Array[L-1]; Step_X:=X-X_Start;
   if XXX >= X_Print
    then
     begin
      J_Print_X_Flag:=1; J_Print_X:=J_Print_X+1
     end { if XXX >= X_Print }
    else J_Print_X_Flag:=0;
   X_Graf:=-1.e-5+Step_Graf_X*J_graf_X;
   if XXX >= X_Graf
    then
     begin
      J_Graf_X_Flag:=1; J_Graf_X:=J_Graf_X+1
     end { if XXX >= X_Graf }
    else J_Graf_X_Flag:=0;
   for j:=1 to Ndim do  Y[J]:=T_X_var_Z_0[L,j];
   t1_z_0:=T_X_var_Z_0[L,1];
   if J_Print_X_Flag=1  then
     begin
       Prt_All(X_Array[L],+1)
     end; {if J_Print_X_Flag=1}
for i:=2 to N_Z do
  begin
    for k:=1 to Ndim+5 do
     Array_X_graf[L,N_X_Grag+1,k]:=
      Array_X_graf[L,N_X_Grag+1,k]+
      (TNEW[i-1,k]+TNEW[i,k])*0.5*Step_Z;
for k:=1 to Ndim+5 do
     Array_X_graf[L,N_X_Grag+1,k]:=
      Array_X_graf[L,N_X_Grag+1,k]/1.0;
   for j:=1 to N_Z_Grag do
     begin
       Z:=0+Step_Graf_Z*(j-1); Otpt(Z,Ygr);
       for k:=1 to Ndim+5 do Array_X_graf[L,j,k]:=Ygr[k];
     end; {for j}
   for j:=1 to Ndim+5 do
     for i:=1 to N_Z do
      t_d_mean_Z[i,j]:=t_d_mean_Z[i,j]+
      (TOLD[i,j]+TNEW[i,j])*0.5*(X_Array[L]-X_Array[L-
   if J_Graf_X_Flag = 1 then
     begin
       for i:=1 to N_Z_Grag_56 do
         begin
           Z:=0+h_Graf_Z_56*(i-1); Otpt(Z,YGR);
           for K:=1 to Ndim+5 do
             Array_Z_graf[i,Index_graf_Z,k]:=YGR[k];
         end; {for i}
       Index_graf_Z:=Index_graf_Z+1;
```

```
        end;  {if J_Graf_X_Flag = 1}
      for j:=1 to Ndim+5 do
        for i:=1 to N_z do TOLD[i,j]:=TNEW[i,j];
      end;{for L}
   t2n_Adiabat:=t_d_mean_Z[1,2]; d2n_Adiabat:=P[d2N];
  Fi_of_Air(t2n_, Fi2n_Adiabat);
  E2n_Adiabat:=1.005*t2n_Adiabat+
  (2500. + 1.807*t2n_Adiabat)*d2n_Adiabat;
  t2k_Adiabat:=t_d_mean_Z[N_z_User,2];
  d2k_Adiabat:=t_d_mean_Z[N_z_User,3];
  Fi_of_Air(t2k_Adiabat, d2k_Adiabat, Fi2k_Adiabat);
  E2k_Adiabat:=1.005*t2k_Adiabat+
  (2500. + 1.807*t2k_Adiabat)*d2k_Adiabat;
  for i:=1 to N_z_User do
    Calka_t1_Kon_Adiabat:=Calka_t1_Kon_Adiabat+TNEW[i,1];
  t1k_Adiabat:=Calka_t1_Kon_Adiabat/N_z_User;
  d1k_Adiabat:=d1n_Adiabat;
  Fi_of_Air(t1k_Adiabat, d1k_Adiabat, Fi1k_Adiabat);
  E1k_Adiabat:=1.005*t1k_Adiabat+
  (2500. + 1.807*t1k_Adiabat)*d1k_Adiabat;
  t2k_User:=t_d_mean_Z[N_z,2]; d2k_User:=t_d_mean_Z[N_z,3];
  Fi_of_Air(t2k_User, d2k_User, Fi2k_User);
  E2k_User:=1.005*t2k_User+
  (2500. + 1.
  for i:= N_z_User to N_z do
    Calka_t1_Kon_User:=Calka_t1_Kon_User+TNEW[i,1];
  t1k_User:=Calka_t1_Kon_User/(N_z-N_z_User+1);
  d1k_User:=d1n_User;
  Fi_of_Air(t1k_User, d1k_User, Fi1k_User);
  E1k_User:=1.005*t1k_User+
  (2500. + 1.807*t1k_User)*d1k_User;
  for j:=1  to Ndim+5 do
    for i:=1 to N_Z do  TNEW[i,j]:=t_d_mean_Z[i,j];
  for i:=1 to N_Z_Grag_56 do
    begin
      Z:=0+h_Graf_Z_56*(i-1); Otpt(Z,YGR);
      for k:=1 to Ndim+5 do  Array_Z_graf[i,N_Z_Grag+1,k]:=Ygr[k];
    end; {for i}
  for i:=1 to N_x do Z_Array[i]:=X_Array[i];
          N_Z:=N_x;
  for j:=1 to N_X_Grag+1 do
    begin
      for k:=1 to Ndim+5 do
        for i:=1 to N_x do  TNEW[i,k]:=Array_X_graf[i,j,k];
      for i:=1 to N_X_Grag_56 do
        begin
          X:=h_Graf_X_56*(i-1);  Otpt(X,YGR);
          for k:=1 to Ndim+5 do Array_X_graf[i,j,k]:=YGR[k];
        end; {for i}
    end; {for j}
   PrintEnd_All;
   Graf_All;
       PrintEnd_All;
100:          Close(KIO_M_Cycle);
  END.  { Program }
  PROCEDURE Praw_Zo_X_var_Ad( X : Single; Y : NdimType ; VAR Dery : NdimType);
   VAR  tw_Initial_Local, tw, dw : Single;
     { tw1, dw1, P, C_var_C_p, Dery   - Global }
    BEGIN    { PROCEDURE Praw_Zo_X_var_Ad }
    Ytw[1]:=Y[1]; Ytw[2]:=Y[2]; Ytw[3]:=Y[3];
    tw_Initial_Local:= tw1; {P[t1Wet_bulb]}
    Rtwi( tw, Nevjazka, F_t_Wall_Ad, tw_Initial_Local,
        Eps_tWall, Iter_tWall, Jerror);
    D_of_Air( 1.0, tw, dw );
    tw1:=tw; dw1:=dw;
    {tw2:=tw1; dw2:= dw1;}
    Dery[2]:=0.0; Dery[3] := 0.0;
```

```
    Dery[1] :=P[Fo3]/Poprawka_G1*(tw1-Y[1])*P[Psi3];
  END;  { PROCEDURE Praw_Zo_X_var_Ad}
 PROCEDURE Praw_Zo_X_var_z_Mieszaniem_Ad( X : Single; Y : NdimType ; VAR Dery : NdimType);
   VAR  tw_Initial_Local, tw, dw : Single;
    { tw1, dw1, P, C_var_C_p, Dery   - Global }

  BEGIN    { PROCEDURE Praw_Zo_X_var_z_Mieszaniem_Ad}
   Ytw[1]:=Y[1]; Y[2]:=Y[1]; Ytw[2]:=Y[2]; Ytw[3]:=Y[3];
   tw_Initial_Local:= tw1; {P[t1Wet_bulb]}
   Rtwi( tw, Nevjazka, F_t_Wall_Ad, tw_Initial_Local,
      Eps_tWall, Iter_tWall, Jerror);
   D_of_Air( 1.0, tw, dw );
   tw1:=tw; dw1:=dw;
   {tw2:=tw1; dw2:= dw1;}
   Dery[2]:=0.0; Dery[3] := 0.0;
   Dery[1] :=P[Fo3]/Poprawka_G1*(tw1-Y[1])*P[Psi3];
  END; { PROCEDURE Praw_Zo_X_var_z_Mieszaniem_Ad}
 PROCEDURE Praw_Zo_X_var_Pro( X : Single; Y : NdimType ; VAR Dery : NdimType);
  VAR  tw_Initial_Local, tw, dw : Single;
    { tw1, dw1, P, C_var_C_p, Dery   - Global }
   Ytw[1]:=Y[1]; Ytw[2]:=Y[2]; Ytw[3]:=Y[3];
   tw_Initial_Local:= tw1; {P[t1Wet_bulb]}
   Rtwi( tw, Nevjazka, F_t_Wall_Pro, tw_Initial_Local,
      Eps_tWall, Iter_tWall, Jerror);
   D_of_Air( 1.0, tw, dw );
   tw1:=tw; dw1:=dw;
   {tw2:=tw1; dw2:= dw1;}
   Dery[2]:=0.0; Dery[3] := 0.0;
   Dery[1] :=P[Fo1]/Poprawka_G1*(tw1-Y[1])*P[Psi1];
  END; { PROCEDURE Praw_Zo_X_var_Pro}
 PROCEDURE Outp_Zo_X_var_z_Mieszaniem_Print_Ad(X : Single; Y, Dery : NdimType;
          Jhlf {, Ndim}  : INTEGER; Prmt : PrmtType);
   LABEL  10;
   VAR  XPrint, Ew2, Fiw2, tw, dw, tw_Initial_Local : Single;
    BEGIN    { PROCEDURE Outp_Zo_X_var_z_Mieszaniem_Print_Ad}
    IF J_Print_X = 0  THEN  Praw_Zo_X_var_z_Mieszaniem_Ad(X, Y ,Dery);
    { ELSE }
     XPrint:= XPrintStart + Step_Print_X*J_Print_X;
     IF  (X > XPrint)  AND  (XPrint <= Prmt[2])  THEN
     Begin  {Print}
      J_Print_X:=J_Print_X+1;
    Ytw[1]:=Y[1]; Y[2]:=Y[1]; Ytw[2]:=Y[2]; Ytw[3]:=Y[3];
    tw_Initial_Local:= tw1; {P[t1Wet_bulb]}
    Rtwi( tw, Nevjazka, F_t_Wall_Ad, tw_Initial_Local,
       Eps_tWall, Iter_tWall, Jerror);
    D_of_Air( 1.0, tw, dw );
    tw1:=tw; dw1:=dw;
    {tw2:=tw1; dw2:= dw1;}
    Calka_Delta_tw_Zeb2:=(tw2-Y[2]);
    Calka_Delta_dw_Zeb2:=(dw2-Y[3]);
    Q3_Jawne:=P[Alfa_3]*(tw1-Y[1])*P[Psi3];
    Q4_Jawne:=P[Alfa_4] {+C_vap_C_p*Dery[3]}*
      ((1-Delta_Zeb_2/s_Zeb_2)*(tw2-Y[2])+
      (2*h_Zeb_2/s_Zeb_2)*Calka_Delta_tw_Zeb2);
    Q4_Utajone:=2500*P[Alfa_4]/P[Lewis_4]*
      ((1-Delta_Zeb_2/s_Zeb_2)*(dw2-Y[3])+
      (2*h_Zeb_2/s_Zeb_2)*Calka_Delta_dw_Zeb2);
    Q4_Calkowite:=(Q4_Jawne+Q4_Utajone);
    Q3_Jawne_Wzgledne:=Q3_Jawne/Q4_Utajone*100.0;
    Q4_Jawne_Wzgledne:=Q4_Jawne/Q4_Utajone*100.0;
    Q4_Utajone_Wzgledne:=(Q3_Jawne_Wzgledne+Q4_Jawne_Wzgledne);
    Q3_Jawne_Scianka:=P[Alfa_3]*(tw1-Y[1])*
           (1-Delta_Zeb_1/s_Zeb_1);
    Q3_Jawne_Zebro:=P[Alfa_3]*(tw1-Y[1])*
          (2*th_3/(P[m3]*s_Zeb_1));
    Q4_Jawne_Scianka:=P[Alfa_4] {+C_vap_C_p*Dery[3]}*
      ((1-Delta_Zeb_2/s_Zeb_2)*(tw2-Y[2]));
```

```
        Q4_Jawne_Zebro:=P[Alfa_4] {+C_vap_C_p*Dery[3]}*
          ((2*h_Zeb_2/s_Zeb_2)*Calka_Delta_tw_Zeb2);
        Q4_Utajone_Scianka:=2500*P[Alfa_4]/P[Lewis_4]*
          ((1-Delta_Zeb_2/s_Zeb_2)*(dw2-Y[3]));
        Q4_Utajone_Zebro:=2500*P[Alfa_4]/P[Lewis_4]*
          ((2*h_Zeb_2/s_Zeb_2)*Calka_Delta_dw_Zeb2);
        Q4_Calkowite_Zebro:=(Q4_Jawne_Zebro+Q4_Utajone_Zebro);
        Q3_Jawne_Scianka_Wzgledne:=Q3_Jawne_Scianka/Q4_Utajone*100.0;
        Q3_Jawne_Zebro_Wzgledne:=Q3_Jawne_Zebro/Q4_Utajone*100.0;
        Q4_Jawne_Scianka_Wzgledne:=Q4_Jawne_Scianka/Q4_Utajone*100.0;
        Q4_Jawne_Zebro_Wzgledne:=Q4_Jawne_Zebro/Q4_Utajone*100.0;
        Q4_Utajone_Scianka_Wzgledne:=Q4_Utajone_Scianka/Q4_Utajone*100.0;
        Q4_Utajone_Zebro_Wzgledne:=Q4_Utajone_Zebro/Q4_Utajone*100.0;
        Q4_Calkowite_Zebro_Wzgledne:=Q4_Calkowite_Zebro/Q4_Utajone*100.0;
        E1:=1.005*Y[1] + (2500. + 1.807*Y[1])*P[d2N];
        E2:=1.005*Y[2] + (2500. + 1.807*Y[2])*Y[3];
   E2:=1.005*(Y[2]*Z_Start+Y[1]*Step_Z)/(Z_Start+Step_Z)
  +(2500+1.807*(Y[2]*Z_Start+Y[1]*Step_Z)/(Z_Start+Step_Z))*
   (Y[3]*Z_Start+P[d2N]*Step_Z)/(Z_Start+Step_Z);
        Ew2:=1.005*tw2 + (2500. + 1.807*tw2)*dw2;
        Fi_of_Air( Y[1], P[d2N], Fi1);
        Fi_of_Air( Y[2], Y[3], Fi2);
   Fi_of_Air((Y[2]*Z_Start+Y[1]*Step_Z)/(Z_Start+Step_Z),
     (Y[3]*Z_Start+P[d2N]*Step_Z)/(Z_Start+Step_Z), Fi2);
        if X <= 1.e-5 then
          WRITELN('*',X:5:2,' *',Z:5:2,' *',Y[1]:7:2,' *',Y[2]:7:2,
          ' *', tw1:8:4,' *',P[d2N]*1000.:7:2,
          ' *',Y[3]*1000.:7:2,' *',dw1*1000.:7:2,
          ' *  ',Jhlf:3,'  *')
         else    {if not Z_print <= 1.e-5}
          WRITELN('*',X:5:2,' *','    *',Y[1]:7:2,' *',Y[2]:7:2,
          ' *', tw1:8:4,' *',P[d2N]*1000.:7:2,
          ' *',Y[3]*1000.:7:2,' *',dw1*1000.:7:2,
          ' *  ',Jhlf:3,'  *');
        WRITELN('*     ','*     ',
        '*',E1:7:2,' *',E2:7:2,
        ' *',Ew2:7:2,' *',Fi1*100.:7:2,
        ' *',Fi2*100.:7:2,' *',Fiw2*100.:7:2,
        ' *        *');
        WRITELN('*     ','*     ',
        '*','     ','  *','       ',
        ' *', tw2:8:4,' *','       ',
        ' *','     ',' *', dw2*1000.:8:4,
        ' *        *');
        if X <= 1.e-5 then
          WRITELN(KIO_M_Cycle,'*',X:5:2,' *',Z:5:2,' *',Y[1]:7:2,' *',Y[2]:7:2,
          ' *', tw1:8:4,' *', P[d2N]*1000.:7:2,
          ' *',Y[3]*1000.:7:2,' *',dw1*1000.:7:2,
          ' *  ',Jhlf:3,'  *')
         else    {if not Z_print <= 1.e-5}
          WRITELN(KIO_M_Cycle,'*',X:5:2,' *','    *',Y[1]:7:2,' *',Y[2]:7:2,
          ' *', tw1:8:4,' *', P[d2N]*1000.:7:2,
          ' *',Y[3]*1000.:7:2,' *',dw1*1000.:7:2,
          ' *  ',Jhlf:3,'  *');
        WRITELN(KIO_M_Cycle, '*     ','*     ',
        '*',E1:7:2,' *',E2:7:2,
        ' *',Ew2:7:2,' *',Fi1*100.:7:2,
        ' *',Fi2*100.:7:2,' *',Fiw2*100.:7:2,
        ' *        *');
        WRITELN(KIO_M_Cycle, '*     ','*     ',
        '*','     ','  *','       ',
        ' *', tw2:8:4,' *','       ',
        ' *','     ',' *', dw2*1000.:8:4,
        ' *        *');
        WRITELN(KIO_M_Cycle, '*     ','*     ',
        '*', Q3_Jawne:7:1,' *', Q4_Jawne:7:1,
        ' *', Q4_Utajone:7:1,' * ', Q3_Jawne_Wzgledne:6:1,
```

```
                   ' *', Q4_Jawne_Wzgledne:6:1,' *', Q4_Utajone_Wzgledne:6:1,
                   ' *      *');
                WRITELN(KIO_M_Cycle, '*    ','*    ',
                 '*', Q3_Jawne_Scianka_Wzgledne:7:2,' *',
                  Q3_Jawne_Zebro_Wzgledne:7:2,
                 ' *', Q4_Jawne_Scianka_Wzgledne:7:2,' *',
                 Q4_Jawne_Zebro_Wzgledne:7:2,
                 ' *', Q4_Utajone_Scianka_Wzgledne:7:2,' *',
                 Q4_Utajone_Zebro_Wzgledne:7:2, ' *',
                 Q4_Calkowite_Zebro_Wzgledne:7:2, ' *');
                For i:=1 TO 85 Do  WRITE(KIO_M_Cycle,'*'); WRITELN(KIO_M_Cycle);
             End; {IF (X > XPrint) AND (XPrint <= Prmt[2])} { ELSE }
          End;   { PROCEDURE Outp_Zo_X_var_z_Mieszaniem_Print_Ad}
      PROCEDURE Outp_Zo_X_var_z_Mieszaniem_N_x_Ad(X : Single; Y, Dery : NdimType;
                  Jhlf {, Ndim}  : INTEGER; Prmt : PrmtType);
       LABEL  10;
       VAR  XPrint, Ew2, Fiw2, tw, dw, tw_Initial_Local : Single;
         BEGIN    { PROCEDURE Outp_Zo_X_var_z_Mieszaniem_N_x_Ad}
           IF  J_Print_X = 0  THEN  Praw_Zo_X_var_z_Mieszaniem_Ad( X, Y ,Dery); { ELSE }
           XPrint:= XPrintStart +Step_Z_0_X_Var_N_x*J_Print_X;
           IF  (X > XPrint)  AND  (XPrint <= Prmt[2])  THEN
             Begin  {Print}
              J_Print_X:=J_Print_X+1;
              Ytw[1]:=Y[1]; Y[2]:=Y[1]; Ytw[2]:=Y[2]; Ytw[3]:=Y[3];
              tw_Initial_Local:= tw1; {P[t1Wet_bulb]}
              Rtwi( tw, Nevjazka, F_t_Wall_Ad, tw_Initial_Local,
               Eps_tWall, Iter_tWall, Jerror);
              D_of_Air( 1.0, tw, dw );
              tw1:=tw; dw1:=dw;
              {tw2:=tw1; dw2:= dw1;}
              for j:=1 to Ndim do  T_X_var_Z_0[L_NX,j]:=Y[J];
              T_X_var_Z_0[L_NX,Ndim+1]:=tw1;
              T_X_var_Z_0[L_NX,Ndim+2]:=tw2;
              T_X_var_Z_0[L_NX,Ndim+3]:=dw2;
              T_X_var_Z_0[L_NX,Ndim+4]:=t2_do_Mieszania;
              T_X_var_Z_0[L_NX,Ndim+5]:=d2_do_Mieszania;
              L_NX:=L_NX+1;
             End; {IF (X > XPrint) AND (XPrint <= Prmt[2])} { ELSE }
          End;    { PROCEDURE Outp_Zo_X_var_z_Mieszaniem_N_x_Ad}
      PROCEDURE Praw_Xo_Z_var_Ad( Z : Single; Y : NdimType ; VAR  Dery : NdimType);
        VAR  tw_Initial_Local, tw, dw : Single;
         { tw1, dw1, P, C_var_C_p, Dery   - Global }
         BEGIN    { PROCEDURE Praw_Xo_Z_var_Ad}
         asr1:=an1+(ak1-an1)*(Z-Z_Start)/Step_Z;
         YY[1]:=asr1; YY[2]:=Y[2];  YY[3]:=Y[3];
            Poprawka_G2:=Z_Start;
         if Z_Start < 0.0001 then  Poprawka_G2:=1.0;
         Ytw[1]:=YY[1]; Ytw[2]:=YY[2]; Ytw[3]:=YY[3];
         tw_Initial_Local:=P[t1Wet_bulb];
            Rtwi( tw, Nevjazka, F_t_Wall_Ad, tw_Initial_Local,
              Eps_tWall, Iter_tWall, Jerror);
          D_of_Air( 1.0, tw, dw );
          tw1:=tw; dw1:=dw;
         Calka_Delta_tw_Zeb2:=(tw2 - YY[2]);
         Calka_Delta_dw_Zeb2:=(dw2 - YY[3]);
          Dery[3] :=P[Fo4]/Poprawka_G2/P[Lewis_4]*((1-Delta_Zeb_2/s_Zeb_2)*
             (dw2 - YY[3])+(2*h_Zeb_2/s_Zeb_2)*Calka_Delta_dw_Zeb2);
          Dery[2] :=P[Fo4]/Poprawka_G2*((1-Delta_Zeb_2/s_Zeb_2)*(tw2 -YY[2])+
             (2*h_Zeb_2/s_Zeb_2)*Calka_Delta_tw_Zeb2);
      PROCEDURE Praw_Xo_Z_var_Pro( Z : Single; Y : NdimType ; VAR  Dery : NdimType);
        VAR  tw_Initial_Local, tw, dw : Single;
         { tw1, dw1, P, C_var_C_p, Dery   - Global }
         BEGIN    { PROCEDURE Praw_Xo_Z_var_Pro}
         asr1:=an1+(ak1-an1)*(Z-Z_Start)/Step_Z;
         YY[1]:=asr1; YY[2]:=Y[2];  YY[3]:=Y[3];
         Ytw[1]:=YY[1]; Ytw[2]:=YY[2]; Ytw[3]:=YY[3];
         tw_Initial_Local:=P[t1Wet_bulb];
```

```
          Rtwi( tw, Nevjazka, F_t_Wall_Pro, tw_Initial_Local,
            Eps_tWall, Iter_tWall, Jerror);
        D_of_Air( 1.0, tw, dw );
         tw1:=tw; dw1:=dw;
      Calka_Delta_tw_Zeb2:=(tw2 - YY[2]);
      Calka_Delta_dw_Zeb2:=(dw2 - YY[3]);
        Dery[3] :=P[Fo2]/Poprawka_G2/P[Lewis_2]*((1-Delta_Zeb_2/s_Zeb_2)*
            (dw2 - YY[3])+(2*h_Zeb_2/s_Zeb_2)*Calka_Delta_dw_Zeb2);
        Dery[2] :=P[Fo2]/Poprawka_G2*((1-Delta_Zeb_2/s_Zeb_2)*(tw2 -YY[2])+
            (2*h_Zeb_2/s_Zeb_2)*Calka_Delta_tw_Zeb2);
     PROCEDURE Praw_Xo_Z_var_Ad_All( Z : Single; Y : NdimType ; VAR  Dery : NdimType);
      VAR  tw, dw, tw_Initial_Local : Single;
        { tw1, dw1, P, C_var_C_p, Dery   - Global }
       BEGIN   { PROCEDURE Praw_Xo_Z_var_Ad_All}
        asr1:=an1+(ak1-an1)*(Z-Z_Start)/Step_Z;
        YY[1]:=asr1; YY[2]:=Y[2];  YY[3]:=Y[3];
         Poprawka_G2:=Z_Start/L_ad;
        if Z_Start < 0.0001 then  Poprawka_G2:=1.0;
        Ytw[1]:=YY[1]; Ytw[2]:=YY[2]; Ytw[3]:=YY[3];
        tw_Initial_Local:=P[t1Wet_bulb];
          Rtwi( tw, Nevjazka, F_t_Wall_Ad, tw_Initial_Local,
            Eps_tWall, Iter_tWall, Jerror);
        D_of_Air( 1.0, tw, dw );
         tw1:=tw; dw1:=dw;
      Calka_Delta_tw_Zeb2:=(tw2 - YY[2]);
      Calka_Delta_dw_Zeb2:=(dw2 - YY[3]);
        Dery[3] :=P[Fo4]*(1/L_ad)/Poprawka_G2/P[Lewis_4]*
            ((1-Delta_Zeb_2/s_Zeb_2)*
            (dw2 - YY[3])+(2*h_Zeb_2/s_Zeb_2)*Calka_Delta_dw_Zeb2);
        Dery[2] :=P[Fo4]*(1/L_ad)/Poprawka_G2*((1-Delta_Zeb_2/s_Zeb_2)*
            (tw2 -YY[2])+
        Dery[1] :=0.0;
       END; { PROCEDURE Praw_Xo_Z_var_Ad_All}
     PROCEDURE Praw_Xo_Z_var_Pro_All( Z : Single; Y : NdimType ; VAR  Dery : NdimType);
       VAR  tw_Initial_Local, tw, dw : Single;
          { tw1, dw1, P, C_var_C_p, Dery   - Global }
        BEGIN    { PROCEDURE Praw_Xo_Z_var_Pro_All }
         asr1:=an1+(ak1-an1)*(Z-Z_Start)/Step_Z;
         YY[1]:=asr1; YY[2]:=Y[2];  YY[3]:=Y[3];
         Ytw[1]:=YY[1]; Ytw[2]:=YY[2]; Ytw[3]:=YY[3];
         tw_Initial_Local:=P[t1Wet_bulb];
           Rtwi( tw, Nevjazka, F_t_Wall_Pro, tw_Initial_Local,
             Eps_tWall, Iter_tWall, Jerror);
         D_of_Air( 1.0, tw, dw );
          tw1:=tw; dw1:=dw;
{Warto?ci tw2 ¨ dw2 policzono ˇ p/p F_t_Wall przez Rtwi ¨ przekazane s? jako zmienne globalne}
         Calka_Delta_tw_Zeb2:=(tw2 - YY[2]);
         Calka_Delta_dw_Zeb2:=(dw2 - YY[3]);
          Dery[3] :=P[Fo2]*(1/(1-L_ad))/Poprawka_G2/P[Lewis_2]*
              ((1-Delta_Zeb_2/s_Zeb_2)*
              (dw2 - YY[3])+(2*h_Zeb_2/s_Zeb_2)*Calka_Delta_dw_Zeb2);
          Dery[2] :=P[Fo2]*(1/(1-L_ad))/Poprawka_G2*
              ((1-Delta_Zeb_2/s_Zeb_2)*(tw2 -YY[2])+
              (2*h_Zeb_2/s_Zeb_2)*Calka_Delta_tw_Zeb2);
          Dery[1] :=0.0;
        END; { PROCEDURE Praw_Xo_Z_var_Pro_All}
      PROCEDURE Outp_Xo_Z_var( X : Single; Y, Dery : NdimType;
              Jhlf {, Ndim}  : INTEGER; Prmt : PrmtType);
        BEGIN    { PROCEDURE Outp_Xo_Z_var}
        End;    { PROCEDURE Outp_Xo_Z_var}
       PROCEDURE Outp( X : Single; Y, Dery : NdimType;
              Jhlf {, Ndim}  : INTEGER; Prmt : PrmtType);
        BEGIN    { PROCEDURE Outp }
        End;     { PROCEDURE Outp}
      PROCEDURE Prt_Ad( X : Single; jhlf:integer );
      Var Z_print, Z_print_Ad, Fiw2, Ew2, d1_Print : Single;
         dry_wet_Flag  : ARRAY [1..3] of CHAR;
```

```
     Frost_Flag  : ARRAY [1..5] of CHAR;
    j, i : integer;
  Begin {PROCEDURE Prt_Ad }
   for j:=1 to N_Z_Print do
     begin
      Z_print:=Z_Start_Print+Step_Print_Z *(j-1);
      OTPT(Z_print,YGR);
      Z_print_Ad:=Z_print*L_ad;
      D_of_Air( 1.0, Ygr[4], dw1);
      Ew2:=1.005*Ygr[5]+(2500.+1.807*Ygr[5])* Ygr[6];
      E2_do_mieszania:=1.005*Ygr[7]+(2500.+1.807*Ygr[7])*Ygr[8];
     Fi_of_Air( Ygr[1], d1_Print, Fi1);
     Fi_of_Air( Ygr[2], Ygr[3], Fi2);
     Fi_of_Air( Ygr[5], Ygr[6], Fiw2);
     Fi_of_Air( Ygr[7], Ygr[8], Fi2_do_mieszania);
    Calka_Delta_tw_Zeb2:=(Ygr[5]-Ygr[2]);
    Calka_Delta_dw_Zeb2:=(Ygr[6]-Ygr[3]);
     Q3_Jawne:=P[Alfa_3]*(Ygr[4]-Ygr[1])*P[Psi3];
     Q4_Jawne:=P[Alfa_4] {+C_vap_C_p*Dery[3]}*
       ((1-Delta_Zeb_2/s_Zeb_2)*
       (Ygr[5]-Ygr[2])+
       (2*h_Zeb_2/s_Zeb_2)*Calka_Delta_tw_Zeb2);
     Q4_Utajone:=2500*P[Alfa_4]/P[Lewis_4]*
       ((1-Delta_Zeb_2/s_Zeb_2)*
       (Ygr[6]-Ygr[3])+
       (2*h_Zeb_2/s_Zeb_2)*Calka_Delta_dw_Zeb2);
     Q4_Calkowite:=(Q4_Jawne+Q4_Utajone);
     Q3_Jawne_Wzgledne:=Q3_Jawne/Q4_Utajone*100.0;
     Q4_Jawne_Wzgledne:=Q4_Jawne/Q4_Utajone*100.0;
     Q4_Utajone_Wzgledne:=(Q3_Jawne_Wzgledne+Q4_Jawne_Wzgledne);
     Q3_Jawne_Scianka:=P[Alfa_3]*(Ygr[4]-Ygr[1])*
              (1-Delta_Zeb_1/s_Zeb_1);
     Q3_Jawne_Zebro:=P[Alfa_3]*(Ygr[4]-Ygr[1])*
            (2*th_3/(P[m3]*s_Zeb_1));
     Q4_Jawne_Scianka:=P[Alfa_4] {+C_vap_C_p*Dery[3]}*
       ((1-Delta_Zeb_2/s_Zeb_2)*
       (Ygr[5]-Ygr[2]));
     Q4_Jawne_Zebro:=P[Alfa_4] {+C_vap_C_p*Dery[3]}*
       ((2*h_Zeb_2/s_Zeb_2)*Calka_Delta_tw_Zeb2);
     Q4_Utajone_Scianka:=2500*P[Alfa_4]/P[Lewis_4]*
       ((1-Delta_Zeb_2/s_Zeb_2)*
       (Ygr[6]-Ygr[3]));
     Q4_Utajone_Zebro:=2500*P[Alfa_4]/P[Lewis_4]*
       ((2*h_Zeb_2/s_Zeb_2)*Calka_Delta_dw_Zeb2);
     Q4_Calkowite_Zebro:=(Q4_Jawne_Zebro+Q4_Utajone_Zebro);
     Q3_Jawne_Scianka_Wzgledne:=Q3_Jawne_Scianka/Q4_Utajone*100.0;
     Q3_Jawne_Zebro_Wzgledne:=Q3_Jawne_Zebro/Q4_Utajone*100.0;
     Q4_Jawne_Scianka_Wzgledne:=Q4_Jawne_Scianka/Q4_Utajone*100.0;
     Q4_Jawne_Zebro_Wzgledne:=Q4_Jawne_Zebro/Q4_Utajone*100.0;
     Q4_Utajone_Scianka_Wzgledne:=Q4_Utajone_Scianka/Q4_Utajone*100.0;
     Q4_Utajone_Zebro_Wzgledne:=Q4_Utajone_Zebro/Q4_Utajone*100.0;
     Q4_Calkowite_Zebro_Wzgledne:=Q4_Calkowite_Zebro/Q4_Utajone*100.0;
     if Z_print <= (Z_Start_Print+1.e-5) then
        WRITELN('*',X:5:2,' *',Z_print_Ad:5:2,' *',Ygr[1]:7:2,
        ' *',Ygr[2]:7:2,
        ' *',Ygr[4]:7:2,' *', d1_Print*1000.:7:2,
        ' *',Ygr[3]*1000.:7:2,' *',dw1*1000.:7:2,
        ' *         *')
      else    {if not Z_print <= (Z_Start_Print+1.e-5)}
        WRITELN('*       *',Z_print_Ad:5:2,
        ' *',Ygr[1]:7:2,' *',Ygr[2]:7:2,
        ' *',Ygr[4]:7:2,' *',d1_Print*1000.:7:2,
        ' *',Ygr[3]*1000.:7:2,' *',dw1*1000.:7:2,
        ' *         *');
      WRITELN('*       ','*       ','*',Ygr[9]:7:2,' *', Ygr[10]:7:2,
        ' *',Ew2:7:2,' *',Fi1*100.:7:2,
        ' *',Fi2*100.:7:2,' *',Fiw2*100.:7:2,
```

```
         ' *         *');
        WRITELN('*     ','*     ',
        '*','  ',' ','*','  ',' ',
        ' *', Ygr[5]:7:2,' *',' ',' ',
        ' *',' ',' *', Ygr[6]*1000.:7:2,
        ' *         *');
       For i:=1 TO 85 Do WRITE('*'); WRITELN;
       if Z_print <=(Z_Start_Print+1.e-5) then
          WRITELN(KIO_M_Cycle,'*',X:5:2,
          ' *', Z_print_Ad:5:2,' *',Ygr[1]:7:2,
          ' *',Ygr[2]:7:2,
          ' *',Ygr[4]:7:2,' *', d1_Print*1000.:7:2,
          ' *',Ygr[3]*1000.:7:2,' *',dw1*1000.:7:2,
          ' *         *')
       else    {if not Z_print <=(Z_Start_Print+1.e-5)}
          WRITELN(KIO_M_Cycle,'*     *',Z_print_Ad:5:2,
          ' *',Ygr[1]:7:2,' *',Ygr[2]:7:2,
          ' *',Ygr[4]:7:2,' *', d1_Print*1000.:7:2,
          ' *',Ygr[3]*1000.:7:2,' *',dw1*1000.:7:2,
          ' *         *');
        WRITELN(KIO_M_Cycle,'*     ','*     ',
        '*        *',Ygr[7]:7:2,
        ' *', Ygr[5]:7:2,' *     ',
        ' *', Ygr[8]*1000.:7:2,' *', Ygr[6]*1000.:7:2,
        ' *         *');
       WRITELN(KIO_M_Cycle,'*     ','*     ',
          '*',Ygr[9]:7:2,' *', Ygr[10]:7:2,
          ' *',Ew2:7:2,' *',Fi1*100.:7:2,
          ' *',Fi2*100.:7:2,' *',Fiw2*100.:7:2,
          ' *         *');
       WRITELN(KIO_M_Cycle,'*     ','*     ',
          '*        *', E2_do_mieszania:7:2,
          ' *       *',Fi2_do_mieszania*100.:7:2,
          ' *       *');
        WRITELN(KIO_M_Cycle,'*     ','*     ',
        '*', Q3_Jawne:7:1,' *', Q4_Jawne:7:1,
        ' *', Q4_Utajone:7:1,' *', Q3_Jawne_Wzgledne:6:1,
        ' *', Q4_Jawne_Wzgledne:6:1,' *', Q4_Utajone_Wzgledne:6:1,
        ' *         *');
        WRITELN(KIO_M_Cycle,'*     ','*     ',
        '*', Q3_Jawne_Scianka_Wzgledne:7:2,' *',
        Q3_Jawne_Zebro_Wzgledne:7:2,
        ' *', Q4_Jawne_Scianka_Wzgledne:7:2,' *',
        Q4_Jawne_Zebro_Wzgledne:7:2,
        ' *', Q4_Utajone_Scianka_Wzgledne:7:2,' *',
        Q4_Utajone_Zebro_Wzgledne:7:2,
        ' *', Q4_Calkowite_Zebro_Wzgledne:7:2, ' *');
       For i:=1 TO 85 Do WRITE(KIO_M_Cycle,'*'); WRITELN(KIO_M_Cycle);
      end; {for j}
    end; {PROCEDURE Prt_Ad}
   PROCEDURE Prt_Pro( X : Single; jhlf:integer );
   Var Z_print, Z_print_Pro, Fiw2, Ew2, d1_Print : Single;
     dry_wet_Flag  : ARRAY [1..3] of CHAR;
     Frost_Flag  : ARRAY [1..5] of CHAR;
     j, i : integer;
   Begin {PROCEDURE Prt_Pro }
     for j:=1 to N_Z_Print do
      begin
        Z_print:=Z_Start_Print+Step_Print_Z *(j-1);
        OTPT(Z_print,YGR);
        Z_print_Pro:=L_ad+Z_print*1-L_ad);
        D_of_Air( 1.0, Ygr[4], dw1);
        Ew2:=1.005*Ygr[5]+(2500.+1.807*Ygr[5])* Ygr[6];
        E2_domieszania:=1.005*Ygr[7]+(2500.+1.807*Ygr[7])*Ygr[8];
       Fi_of_Air( Ygr[1], d1_Print, Fi1);
       Fi_of_Air( Ygr[2], Ygr[3], Fi2);
       Fi_of_Air( Ygr[5], Ygr[6], Fiw2);
```

```
  Fi_of_Air( Ygr[7], Ygr[8], Fi2_do_mieszania);
Calka_Delta_tw_Zeb2:=(Ygr[5]-Ygr[2]);
Calka_Delta_dw_Zeb2:=(Ygr[6]-Ygr[3]);
Q1_Jawne:=P[Alfa_1]*(Ygr[4]-Ygr[1])*P[Psi1];
 Q2_Jawne:=P[Alfa_2] {+C_vap_C_p*Dery[3]}*
  ((1-Delta_Zeb_2/s_Zeb_2)*
  (Ygr[5]-Ygr[2])+
  (2*h_Zeb_2/s_Zeb_2)*Calka_Delta_tw_Zeb2);
 Q2_Utajone:=2500*P[Alfa_2]/P[Lewis_2]*
  ((1-Delta_Zeb_2/s_Zeb_2)*
  (Ygr[6]-Ygr[3])+
  (2*h_Zeb_2/s_Zeb_2)*Calka_Delta_dw_Zeb2);
 Q2_Calkowite:=(Q2_Jawne+Q2_Utajone);
 Q1_Jawne_Wzgledne:=Q1_Jawne/Q2_Utajone*100.0;
 Q2_Jawne_Wzgledne:=Q2_Jawne/Q2_Utajone*100.0;
 Q2_Utajone_Wzgledne:=(Q1_Jawne_Wzgledne+ Q2_Jawne_Wzgledne);
 Q1_Jawne_Scianka:=P[Alfa_1]*(Ygr[4]-Ygr[1])*
          (1-Delta_Zeb_1/s_Zeb_1);
 Q1_Jawne_Zebro:=P[Alfa_1]*(Ygr[4]-Ygr[1])*
        (2*th_1/(P[m1]*s_Zeb_1));
 Q2_Jawne_Scianka:=P[Alfa_2] {+C_vap_C_p*Dery[3]}*
  ((1-Delta_Zeb_2/s_Zeb_2)*
  (Ygr[5]-Ygr[2]));
 Q2_Jawne_Zebro:=P[Alfa_2] {+C_vap_C_p*Dery[3]}*
  ((2*h_Zeb_2/s_Zeb_2)*Calka_Delta_tw_Zeb2);
 Q2_Utajone_Scianka:=2500*P[Alfa_2]/P[Lewis_2]*
  ((1-Delta_Zeb_2/s_Zeb_2)*
  (Ygr[6]-Ygr[3]));
 Q2_Utajone_Zebro:=2500*P[Alfa_2]/P[Lewis_2]*
  ((2*h_Zeb_2/s_Zeb_2)*Calka_Delta_dw_Zeb2);
 Q2_Calkowite_Zebro:=(Q2_Jawne_Zebro+Q2_Utajone_Zebro);
 Q1_Jawne_Scianka_Wzgledne:=Q1_Jawne_Scianka/Q2_Utajone*100.0;
 Q1_Jawne_Zebro_Wzgledne:=Q1_Jawne_Zebro/Q2_Utajone*100.0;
 Q2_Jawne_Scianka_Wzgledne:=Q2_Jawne_Scianka/Q2_Utajone*100.0;
 Q2_Jawne_Zebro_Wzgledne:=Q2_Jawne_Zebro/Q2_Utajone*100.0;
 Q2_Utajone_Scianka_Wzgledne:=Q2_Utajone_Scianka/Q2_Utajone*100.0;
 Q2_Utajone_Zebro_Wzgledne:=Q2_Utajone_Zebro/Q2_Utajone*100.0;
 Q2_Calkowite_Zebro_Wzgledne:=Q2_Calkowite_Zebro/Q2_Utajone*100.0;
 if Z_print <= (Z_Start_Print+1.e-5) then
     WRITELN('*',X:5:2,' *',Z_print_Pro:5:2,' *',Ygr[1]:7:2,
     ' *',Ygr[2]:7:2,
     ' *',Ygr[4]:7:2,' *', d1_Print*1000.:7:2,
     ' *',Ygr[3]*1000.:7:2,' *',dw1*1000.:7:2,
     ' *        *')
 else    {if not Z_print <= (Z_Start_Print+1.e-5)}
     WRITELN('*      *',Z_print_Pro:5:2,
     ' *',Ygr[1]:7:2,' *',Ygr[2]:7:2,
     ' *',Ygr[4]:7:2,' *',d1_Print*1000.:7:2,
     ' *',Ygr[3]*1000.:7:2,' *',dw1*1000.:7:2,
     ' *        *');
  WRITELN('*       ','*        ','*',Ygr[9]:7:2,' *', Ygr[10]:7:2,
     ' *',Ew2:7:2,' *',Fi1*100.:7:2,
     ' *',Fi2*100.:7:2,' *',Fiw2*100.:7:2,
     ' *        *');
   WRITELN('*    ','*     ',
   '*','     ','* ','     ',
   ' *', Ygr[5]:7:2,' *','      ',
   ' *','     ','* ', Ygr[6]*1000.:7:2,
   ' *        *');
  For i:=1 TO  85  Do  WRITE('*'); WRITELN;
  if Z_print <=(Z_Start_Print+1.e-5) then
     WRITELN(KIO_M_Cycle,'*',X:5:2,
     ' *',Z_print_Pro:5:2,' *',Ygr[1]:7:2,
     ' *',Ygr[2]:7:2,
     ' *',Ygr[4]:7:2,' *', d1_Print*1000.:7:2,
     ' *',Ygr[3]*1000.:7:2,' *',dw1*1000.:7:2,
     ' *        *')
```

```
    else    {if not Z_print <=(Z_Start_Print+1.e-5)}
        WRITELN(KIO_M_Cycle,'*      *',Z_print_Pro:5:2,
      ' *',Ygr[1]:7:2,' *',Ygr[2]:7:2,
      ' *',Ygr[4]:7:2,' *', d1_Print*1000.:7:2,
      ' *',Ygr[3]*1000.:7:2,' *',dw1*1000.:7:2,
      ' *        *');

      WRITELN(KIO_M_Cycle,'*     ','*     ',
      '*        *',Ygr[7]:7:2,
      ' *', Ygr[5]:7:2,' *       ',
      ' *', Ygr[8]*1000.:7:2,' *', Ygr[6]*1000.:7:2,
      ' *        *');            WRITELN(KIO_M_Cycle,'*     ','*     ',
      '*',Ygr[9]:7:2,' *', Ygr[10]:7:2,
      ' *',Ew2:7:2,' *',Fi1*100.:7:2,
      ' *',Fi2*100.:7:2,' *',Fiw2*100.:7:2,
      ' *        *');
    WRITELN(KIO_M_Cycle,'*     ','*     ',
       '*        *', E2_do_mieszania:7:2,
      ' *      *        *',Fi2_do_mieszania*100.:7:2,
      ' *      *        *');
    WRITELN(KIO_M_Cycle,'*     ','*     ',
    '*', Q1_Jawne:7:1,' *', Q2_Jawne:7:1,
    ' *', Q2_Utajone:7:1,' * ', Q1_Jawne_Wzgledne:6:1,
    ' * ', Q2_Jawne_Wzgledne:6:1,' * ', Q2_Utajone_Wzgledne:6:1,
    ' *        *');
    WRITELN(KIO_M_Cycle,'*     ','*     ',
    '*', Q1_Jawne_Scianka_Wzgledne:7:2,' *',
    Q1_Jawne_Zebro_Wzgledne:7:2,
    ' *', Q2_Jawne_Scianka_Wzgledne:7:2,' *',
    Q2_Jawne_Zebro_Wzgledne:7:2,
    ' *', Q2_Utajone_Scianka_Wzgledne:7:2,' *',
    Q2_Utajone_Zebro_Wzgledne:7:2,
    ' *', Q2_Calkowite_Zebro_Wzgledne:7:2, ' *');
    For i:=1 TO 85 Do  WRITE(KIO_M_Cycle,'*'); WRITELN(KIO_M_Cycle);
    end; {for j}
end; {PROCEDURE Prt_Pro}
PROCEDURE Prt_All( X : Single; jhlf:integer );
Var Z_print, Fiw2, Ew2, d1_Print : Single;
  dry_wet_Flag : ARRAY [1..3] of CHAR;
  Frost_Flag : ARRAY [1..5] of CHAR;
  j, i : integer;
Begin {PROCEDURE Prt}
  for j:=1 to N_Z_Print do
    begin
      Z_print:=Z_Start_Print+Step_Print_Z *(j-1);
      OTPT(Z_print,YGR);
      D_of_Air( 1.0, Ygr[4], dw1);
      Ew2:=1.005*Ygr[5]+(2500.+1.807*Ygr[5])* Ygr[6];
      E2_do_mieszania:=1.005*Ygr[7]+(2500.+1.807*Ygr[7])*Ygr[8];
    if (Z_print <= L_ad) then
      d1_Print:=P[d2N]
    Else
      d1_Print:=P[d1N];
    Fi_of_Air( Ygr[1], d1_Print, Fi1);
    Fi_of_Air( Ygr[2], Ygr[3], Fi2);
    Fi_of_Air( Ygr[5], Ygr[6], Fiw2);
    Fi_of_Air( Ygr[7], Ygr[8], Fi2_do_mieszania);
   Calka_Delta_tw_Zeb2:=(Ygr[5]-Ygr[2]);
   Calka_Delta_dw_Zeb2:=(Ygr[6]-Ygr[3]);
  if (Z_print <= L_ad) then
    Begin
   Q3_Jawne:=P[Alfa_3]*(Ygr[4]-Ygr[1])*P[Psi3];
   Q4_Jawne:=P[Alfa_4] {+C_vap_C_p*Dery[3]}*
     ((1-Delta_Zeb_2/s_Zeb_2)*
     (Ygr[5]-Ygr[2])+
     (2*h_Zeb_2/s_Zeb_2)*Calka_Delta_tw_Zeb2);
   Q4_Utajone:=2500*P[Alfa_4]/P[Lewis_4]*
```

```
        ((1-Delta_Zeb_2/s_Zeb_2)*
        (Ygr[6]-Ygr[3])+
        (2*h_Zeb_2/s_Zeb_2)*Calka_Delta_dw_Zeb2);
    Q4_Calkowite:=(Q4_Jawne+Q4_Utajone);
    Q3_Jawne_Wzgledne:=Q3_Jawne/Q4_Utajone*100.0;
    Q4_Jawne_Wzgledne:=Q4_Jawne/Q4_Utajone*100.0;
    Q4_Utajone_Wzgledne:=(Q3_Jawne_Wzgledne+Q4_Jawne_Wzgledne);
    Q3_Jawne_Scianka:=P[Alfa_3]*(Ygr[4]-Ygr[1])*
            (1-Delta_Zeb_1/s_Zeb_1);
    Q3_Jawne_Zebro:=P[Alfa_3]*(Ygr[4]-Ygr[1])*
          (2*th_3/(P[m3]*s_Zeb_1));
    Q4_Jawne_Scianka:=P[Alfa_4] {+C_vap_C_p*Dery[3]}*
      ((1-Delta_Zeb_2/s_Zeb_2)*
      (Ygr[5]-Ygr[2]));
    Q4_Jawne_Zebro:=P[Alfa_4] {+C_vap_C_p*Dery[3]}*
      ((2*h_Zeb_2/s_Zeb_2)*Calka_Delta_tw_Zeb2);
    Q4_Utajone_Scianka:=2500*P[Alfa_4]/P[Lewis_4]*
      ((1-Delta_Zeb_2/s_Zeb_2)*
      (Ygr[6]-Ygr[3]));
    Q4_Utajone_Zebro:=2500*P[Alfa_4]/P[Lewis_4]*
      ((2*h_Zeb_2/s_Zeb_2)*Calka_Delta_dw_Zeb2);
    Q4_Calkowite_Zebro:=(Q4_Jawne_Zebro+Q4_Utajone_Zebro);
    Q3_Jawne_Scianka_Wzgledne:=Q3_Jawne_Scianka/Q4_Utajone*100.0;
    Q3_Jawne_Zebro_Wzgledne:=Q3_Jawne_Zebro/Q4_Utajone*100.0;
    Q4_Jawne_Scianka_Wzgledne:=Q4_Jawne_Scianka/Q4_Utajone*100.0;
    Q4_Jawne_Zebro_Wzgledne:=Q4_Jawne_Zebro/Q4_Utajone*100.0;
    Q4_Utajone_Scianka_Wzgledne:=Q4_Utajone_Scianka/Q4_Utajone*100.0;
    Q4_Utajone_Zebro_Wzgledne:=Q4_Utajone_Zebro/Q4_Utajone*100.0;
    Q4_Calkowite_Zebro_Wzgledne:=Q4_Calkowite_Zebro/Q4_Utajone*100.0;
    if Z_print <= (Z_Start_Print+1.e-5) then
        WRITELN('*',X:5:2,' *',Z_print:5:2,' *',Ygr[1]:7:2,
        ' *',Ygr[2]:7:2,
        ' *',Ygr[4]:7:2,' *', d1_Print*1000.:7:2,
        ' *',Ygr[3]*1000.:7:2,' *',dw1*1000.:7:2,
        ' *        *')
    else    {if not Z_print <= (Z_Start_Print+1.e-5)}
        WRITELN('*      *',Z_print:5:2,' *',Ygr[1]:7:2,' *',Ygr[2]:7:2,
        ' *',Ygr[4]:7:2,' *',d1_Print*1000.:7:2,
        ' *',Ygr[3]*1000.:7:2,' *',dw1*1000.:7:2,
        ' *        *');
    WRITELN('*      ','*      ','*',Ygr[9]:7:2,' *', Ygr[10]:7:2,
        ' *',Ew2:7:2,' *',Fi1*100.:7:2,
        ' *',Fi2*100.:7:2,' *',Fiw2*100.:7:2,
        ' *        *');
    WRITELN('*     ','*      ',
      '*','      ',' *','     ',
      ' *', Ygr[5]:7:2,' *','     ',
      ' *','      ',' *', Ygr[6]*1000.:7:2,
      ' *        *');
    For i:=1 TO  85  Do  WRITE('*'); WRITELN;
    if Z_print <=(Z_Start_Print+1.e-5) then
        WRITELN(KIO_M_Cycle,'*',X:5:2,' *',Z_print:5:2,' *',Ygr[1]:7:2,
        ' *',Ygr[2]:7:2,
        ' *',Ygr[4]:7:2,' *', d1_Print*1000.:7:2,
        ' *',Ygr[3]*1000.:7:2,' *',dw1*1000.:7:2,
        ' *        *')
    else    {if not Z_print <=(Z_Start_Print+1.e-5)}
        WRITELN(KIO_M_Cycle,'*      *',Z_print:5:2,
        ' *',Ygr[1]:7:2,' *',Ygr[2]:7:2,
        ' *',Ygr[4]:7:2,' *', d1_Print*1000.:7:2,
        ' *',Ygr[3]*1000.:7:2,' *',dw1*1000.:7:2,
      WRITELN(KIO_M_Cycle,'*     ','*      ',
      '*      *',Ygr[7]:7:2,
      ' *', Ygr[5]:7:2,' *       ',
      ' *', Ygr[8]*1000.:7:2,' *', Ygr[6]*1000.:7:2,
      ' *        *');
    WRITELN(KIO_M_Cycle,'*     ','*      ',
```

```
         '*',Ygr[9]:7:2,' *', Ygr[10]:7:2,
         ' *',Ew2:7:2,' *',Fi1*100.:7:2,
         ' *',Fi2*100.:7:2,' *',Fiw2*100.:7:2,
         ' *       *');
    WRITELN(KIO_M_Cycle,'*    ','*     ',
       '*       *', E2_do_mieszania:7:2,
       ' *      *       *',Fi2_do_mieszania*100.:7:2,
       ' *      *        *');
    WRITELN(KIO_M_Cycle,'*    ','*     ',
      '*', Q3_Jawne:7:1,' *', Q4_Jawne:7:1,
      ' *', Q4_Utajone:7:1,' * ', Q3_Jawne_Wzgledne:6:1,
      ' * ', Q4_Jawne_Wzgledne:6:1,' * ', Q4_Utajone_Wzgledne:6:1,
      ' *       *');
    WRITELN(KIO_M_Cycle,'*    ','*     ',
      '*', Q3_Jawne_Scianka_Wzgledne:7:2,' *',
      Q3_Jawne_Zebro_Wzgledne:7:2,
      ' *', Q4_Jawne_Scianka_Wzgledne:7:2,' *',
      Q4_Jawne_Zebro_Wzgledne:7:2,
      ' *', Q4_Utajone_Scianka_Wzgledne:7:2,' *',
      Q4_Utajone_Zebro_Wzgledne:7:2,
      ' *', Q4_Calkowite_Zebro_Wzgledne:7:2, ' *');
   End { if (Z_print <= L_ad)}
  Else { if (Z_print > L_ad)}
   Begin
  Q1_Jawne:=P[Alfa_1]*(Ygr[4]-Ygr[1])*P[Psi1];
  Q2_Jawne:=P[Alfa_2] {+C_vap_C_p*Dery[3]}*
    ((1-Delta_Zeb_2/s_Zeb_2)*
    (Ygr[5]-Ygr[2])+
    (2*h_Zeb_2/s_Zeb_2)*Calka_Delta_tw_Zeb2);
  Q2_Utajone:=2500*P[Alfa_2]/P[Lewis_2]*
    ((1-Delta_Zeb_2/s_Zeb_2)*
    (Ygr[6]-Ygr[3])+
    (2*h_Zeb_2/s_Zeb_2)*Calka_Delta_dw_Zeb2);
  Q2_Calkowite:=(Q2_Jawne+Q2_Utajone);
  Q1_Jawne_Wzgledne:=Q1_Jawne/Q2_Utajone*100.0;
  Q2_Jawne_Wzgledne:=Q2_Jawne/Q2_Utajone*100.0;
  Q2_Utajone_Wzgledne:=(Q1_Jawne_Wzgledne+ Q2_Jawne_Wzgledne);
  Q1_Jawne_Scianka:=P[Alfa_1]*(Ygr[4]-Ygr[1])*
          (1-Delta_Zeb_1/s_Zeb_1);
  Q1_Jawne_Zebro:=P[Alfa_1]*(Ygr[4]-Ygr[1])*
         (2*th_1/(P[m1]*s_Zeb_1));
  Q2_Jawne_Scianka:=P[Alfa_2] {+C_vap_C_p*Dery[3]}*
    ((1-Delta_Zeb_2/s_Zeb_2)*
    (Ygr[5]-Ygr[2]));
  Q2_Jawne_Zebro:=P[Alfa_2] {+C_vap_C_p*Dery[3]}*
    ((2*h_Zeb_2/s_Zeb_2)*Calka_Delta_tw_Zeb2);
  Q2_Utajone_Scianka:=2500*P[Alfa_2]/P[Lewis_2]*
    ((1-Delta_Zeb_2/s_Zeb_2)*
    (Ygr[6]-Ygr[3]));
  Q2_Utajone_Zebro:=2500*P[Alfa_2]/P[Lewis_2]*
    ((2*h_Zeb_2/s_Zeb_2)*Calka_Delta_dw_Zeb2);
  Q2_Calkowite_Zebro:=(Q2_Jawne_Zebro+Q2_Utajone_Zebro);
  Q1_Jawne_Scianka_Wzgledne:=Q1_Jawne_Scianka/Q2_Utajone*100.0;
  Q1_Jawne_Zebro_Wzgledne:=Q1_Jawne_Zebro/Q2_Utajone*100.0;
  Q2_Jawne_Scianka_Wzgledne:=Q2_Jawne_Scianka/Q2_Utajone*100.0;
  Q2_Jawne_Zebro_Wzgledne:=Q2_Jawne_Zebro/Q2_Utajone*100.0;
  Q2_Utajone_Scianka_Wzgledne:=Q2_Utajone_Scianka/Q2_Utajone*100.0;
  Q2_Utajone_Zebro_Wzgledne:=Q2_Utajone_Zebro/Q2_Utajone*100.0;
  Q2_Calkowite_Zebro_Wzgledne:=Q2_Calkowite_Zebro/Q2_Utajone*100.0;
   if Z_print <= (Z_Start_Print+1.e-5) then
       WRITELN('*',X:5:2,' *',Z_print:5:2,' *',Ygr[1]:7:2,
       ' *',Ygr[2]:7:2,
       ' *',Ygr[4]:7:2,' *', d1_Print*1000.:7:2,
       ' *',Ygr[3]*1000.:7:2,' *',dw1*1000.:7:2,
       ' *       *')
   else    {if not Z_print <= (Z_Start_Print+1.e-5)}
       WRITELN('*      *',Z_print:5:2,' *',Ygr[1]:7:2,' *',Ygr[2]:7:2,
```

```
                ' *',Ygr[4]:7:2,' *',d1_Print*1000.:7:2,
                ' *',Ygr[3]*1000.:7:2,' *',dw1*1000.:7:2,
                ' *        *');
      WRITELN('*      ','*      ','*',Ygr[9]:7:2,' *', Ygr[10]:7:2,
                ' *',Ew2:7:2,' *',Fi1*100.:7:2,
                ' *',Fi2*100.:7:2,' *',Fiw2*100.:7:2,
                ' *        *');
      WRITELN('*     ','*      ',
                '*',' ',',' *',' ',
                ' *', Ygr[5]:7:2,' *,' ',
                ' *,' ',',' *', Ygr[6]*1000.:7:2,
                ' *         *');
      For i:=1 TO  85  Do  WRITE('*'); WRITELN;
      if Z_print <=(Z_Start_Print+1.e-5) then
          WRITELN(KIO_M_Cycle,'*',X:5:2,' *',Z_print:5:2,' *',Ygr[1]:7:2,
                ' *',Ygr[2]:7:2,
                ' *',Ygr[4]:7:2,' *', d1_Print*1000.:7:2,
                ' *',Ygr[3]*1000.:7:2,' *',dw1*1000.:7:2,
                ' *         *')
      else     {if not Z_print <=(Z_Start_Print+1.e-5)}
          WRITELN(KIO_M_Cycle,'*       *',Z_print:5:2,
                ' *',Ygr[1]:7:2,' *',Ygr[2]:7:2,
                ' *',Ygr[4]:7:2,' *', d1_Print*1000.:7:2,
                ' *',Ygr[3]*1000.:7:2,' *',dw1*1000.:7:2,
          WRITELN(KIO_M_Cycle,'*     ','*      ',
                '*        *',Ygr[7]:7:2,
                ' *', Ygr[5]:7:2,' *       ',
                ' *', Ygr[8]*1000.:7:2,' *', Ygr[6]*1000.:7:2,
                ' *          *');
      WRITELN(KIO_M_Cycle,'*      ','*      ',
                '*',Ygr[9]:7:2,' *', Ygr[10]:7:2,
                ' *',Ew2:7:2,' *',Fi1*100.:7:2,
                ' *',Fi2*100.:7:2,' *',Fiw2*100.:7:2,
                ' *        *');
      WRITELN(KIO_M_Cycle,'*      ','*      ',
                '*        *', E2_do_mieszania:7:2,
                ' *       *         *',Fi2_do_mieszania*100.:7:2,
                ' *       *          *');
      WRITELN(KIO_M_Cycle,'*      ','*      ',
                '*', Q1_Jawne:7:1,' *', Q2_Jawne:7:1,
                ' *', Q2_Utajone:7:1,' *', Q1_Jawne_Wzgledne:6:1,
                ' *', Q2_Jawne_Wzgledne:6:1,' *', Q2_Utajone_Wzgledne:6:1,
                ' *        *');
      WRITELN(KIO_M_Ccle,'*      ','*      ',
                '*', Q1_Jawne_Scianka_Wzgledne:7:2,' *',
                Q1_Jawne_Zebro_Wzgledne:7:2,
                ' *', Q2_Jawne_Scianka_Wzgledne:7:2,' *',
                Q2_Jawne_Zebro_Wzgledne:7:2,
                ' *', Q2_Utajone_Scianka_Wzgledne:7:2,' *',
                Q2_Utajone_Zebro_Wzgledne:7:2,
                ' *', Q2_Calkowite_Zebro_Wzgledne:7:2, ' *');
      End; { if (Z_print > L_ad)}
      For i:=1 TO  85  Do  WRITE(KIO_M_Cycle,'*'); WRITELN(KIO_M_Cycle);
    end; {for j}
  end; {PROCEDURE Prt_All}
    PROCEDURE Rtmi  ( VAR X,F_value : Single; {$F+}
            {FUNCTION FctWet_bulb (X_Root : Single) : Single;}
             X_Left, X_Right, Eps : Single;
             Iter_X : INTEGER; VAR Jerror : INTEGER);
    LABEL   4, 14, 16, 17  ;
    VAR  X_L, X_R, Tol, F_L, F_R, Tolf, A, D_X,
       X_M, F_M  : Single;
       J, K  :  INTEGER;
     BEGIN
       Jerror:=0; X_L:=X_Left; X_R:=X_Right; X:=X_L;
```

```
          Tol:=X; F_value:=FctWet_bulb(Tol);
          IF  F_value = 0.0  THEN  GOTO  16;     { ELSE }
          F_L:=F_value; X:=X_R; Tol:=X;
          F_value:=FctWet_bulb(Tol);
          IF  F_value = 0.0  THEN  GOTO  16;     { ELSE }
          F_R:=F_value;
          IF  ( F_L * F_R ) > 0.0  THEN
           BEGIN   { IF  ( F_L * F_R ) > 0.0 }
            Jerror:=2; GOTO 16;
           END;   { IF  ( F_L * F_R ) > 0.0 }   { ELSE }
  4:       J:=J + 1;
          FOR  K:=1  TO  Iter_X  DO
           BEGIN   { FOR  K }
            X:=0.5*(X_L+X_R); Tol:=X; F_value:=FctWet_bulb(Tol);
            IF  F_value = 0.0  THEN  GOTO  16; { ELSE }
            IF  ( F_L * F_R ) < 0.0   THEN
             BEGIN   { IF  ( F_L * F_R ) < 0.0 }
              Tol:=X_L; X_L:=X_R; X_R:=Tol;
              Tol:=F_L; F_L:=F_R; F_R:=Tol;
             END;   { IF  ( F_L * F_R ) < 0.0 } { ELSE }
            Tol:=F_value - F_L; A:=F_value * Tol; A:=A+A;
            IF  A < (F_R * (F_R - F_L))  THEN
             IF  J <= Iter_X  THEN  GOTO  17; { ELSE } { ELSE }
            X_R:=X; F_R:=F_value;
            Tol:=Eps; A:=ABS( X_R );
            IF  A > 1.0  THEN  Tol:=Tol * A;  { ELSE }
            IF  ABS(X_R - X_L) <= Tol  THEN
             IF ABS(F_R - F_L) <= Tolf  THEN  GOTO  14; { ELSE }
           END;    { FOR  K }
  14:      IF  ABS(F_R) > ABS(F_L)  THEN
          BEGIN   { IF  ABS(F_R) > ABS(F_L) }
           X:=X_L; F_value:=F_L;
          END;   { IF  ABS(F_R) > ABS(F_L) }
          GOTO 16;    { To end of Procedure }
  17:      A:=F_R - F_value;
          D_X:=(X-X_L)*F_L*(1.0+F_value*(A-Tol)/(A*(F_R-F_L)))/Tol;
          X_M:=X; F_M:=F_value; X:=X_L-D_X;
          Tol:=X; F_value:=FctWet_bulb(Tol);
          IF  F_value = 0.0  THEN  GOTO  16; { To end of Procedure }
          Tol:=Eps; A:=ABS(X);
          IF  A > 1.0  THEN  Tol:=Tol * A; { ELSE }
           IF  ABS(D_X) <= Tol  THEN
            IF  ABS(F_value) <= Tolf  THEN  GOTO  16; { ELSE }
          IF  (F_value * F_L) < 0.0  THEN
           BEGIN   { IF  (F_value * F_L) < 0.0 }
            X_R:=X; F_R:=F_value; GOTO  4;
           END;    { IF  (F_value * F_L) < 0.0 } { ELSE }
          X_L:=X; F_L:=F_value; X_R:=X_M; F_R:=F_M; GOTO  4;
  16:      END {$F-} ;  { PROCEDURE Rtmi }
        PROCEDURE Rtmi_tw2 ( VAR X,F_value : Single; {$F+}
               {FUNCTION F_tw2 (X_Root : Single) : Single;}
                 X_Left, X_Right, Eps : Single;
                 Iter_X : INTEGER; VAR Jerror : INTEGER);
        LABEL  4, 14, 16, 17  ;
        VAR  X_L, X_R, Tol, F_L, F_R, Tolf, A, D_X,
          X_M, F_M, tw2, dw2, F  : Single;
          J, K  :  INTEGER;
         BEGIN
          Jerror:=0; X_L:=X_Left; X_R:=X_Right; X:=X_L;
          Tol:=X;
```

```
          tw2:=Tol;
          D_of_Air( 1.0, tw2, dw2);
          F:=(Lambda_Sc/Delta_plate*(tw2-tw1)*(1-Delta_Zeb_1/s_Zeb_1)+
          P[Alfa_2]*(tw2-Ytw[2])*
          (1-Delta_Zeb_2/s_Zeb_2)+
          P[Alfa_2]*2500.0/P[Lewis]*(dw2-Ytw[3])*
          (1-Delta_Zeb_2/s_Zeb_2))*Waga_tw2
          {+ tw2};
          F_value:=F;
          IF  F_value = 0.0  THEN  GOTO 16;     { ELSE }
          F_L:=F_value; X:=X_R; Tol:=X;
          tw2:=Tol;
          D_of_Air( 1.0, tw2, dw2);
          F:=(Lambda_Sc/Delta_plate*(tw2-tw1)*(1-Delta_Zeb_1/s_Zeb_1)+
          P[Alfa_2]*(tw2-Ytw[2])*
          (1-Delta_Zeb_2/s_Zeb_2)+
          P[Alfa_2]*2500.0/P[Lewis]*(dw2-Ytw[3])*
          (1-Delta_Zeb_2/s_Zeb_2))*Waga_tw2
          {+ tw2};
          F_value:=F;
          IF  F_value = 0.0  THEN  GOTO 16;     { ELSE }
          F_R:=F_value;
          IF ( F_L * F_R ) > 0.0   THEN
           BEGIN  { IF ( F_L * F_R ) > 0.0 }
            Jerror:=2;  GOTO 16;
           END;   { IF ( F_L * F_R ) > 0.0 }  { ELSE }
 4:       J:=J + 1;
          FOR  K:=1  TO  Iter_X  DO
           BEGIN   { FOR  K }
            X:=0.5*(X_L+X_R); Tol:=X;
          tw2:=Tol;
          D_of_Air( 1.0, tw2, dw2);
          F:=(Lambda_Sc/Delta_plate*(tw2-tw1)*(1-Delta_Zeb_1/s_Zeb_1)+
          P[Alfa_2]*(tw2-Ytw[2])*
          (1-Delta_Zeb_2/s_Zeb_2)+
          P[Alfa_2]*2500.0/P[Lewis]*(dw2-Ytw[3])*
          (1-Delta_Zeb_2/s_Zeb_2))*Waga_tw2
          {+ tw2};
          F_value:=F;
             IF  F_value = 0.0  THEN  GOTO 16; { ELSE }
             IF ( F_L * F_R ) < 0.0   THEN
              BEGIN   { IF ( F_L * F_R ) < 0.0 }
               Tol:=X_L; X_L:=X_R; X_R:=Tol;
               Tol:=F_L; F_L:=F_R; F_R:=Tol;
              END;   { IF ( F_L * F_R ) < 0.0 } { ELSE }
             Tol:=F_value - F_L; A:=F_value * Tol; A:=A+A;
             IF  A < (F_R * (F_R - F_L))  THEN
              IF  J <= Iter_X  THEN GOTO 17; { ELSE } { ELSE }
             X_R:=X; F_R:=F_value;
             Tol:=Eps; A:=ABS( X_R );
             IF  A > 1.0  THEN  Tol:=Tol * A;  { ELSE }
             IF  ABS(X_R - X_L) <= Tol  THEN
              IF ABS(F_R - F_L) <= Tolf  THEN  GOTO 14; { ELSE }
           END;    { FOR  K }
 14:      IF  ABS(F_R) > ABS(F_L)  THEN
          BEGIN   { IF  ABS(F_R) > ABS(F_L) }
           X:=X_L; F_value:=F_L;
          END;   { IF  ABS(F_R) > ABS(F_L) }
          GOTO 16;   { To end of Procedure }
 17:      A:=F_R - F_vale;
```

```
            D_X:=(X-X_L)*F_L*(1.0+F_value*(A-Tol)/(A*(F_R-F_L)))/Tol;
            X_M:=X; F_M:=F_value; X:=X_L-D_X;
            Tol:X;
           tw2:=Tol;
           D_of_Air( 1.0, tw2, dw2);
           F:=(Lambda_Sc/Delta_plate*(tw2-tw1)*(1-Delta_Zeb_1/s_Zeb_1)+
           P[Alfa_2]*(tw2-Ytw[2])*
           (1-Delta_Zeb_2/s_Zeb_2)+
           P[Alfa_2]*2500.0/P[Lewis]*(dw2-Ytw[3])*
           (1-Delta_Zeb_2/s_Zeb_2))*Waga_tw2
           {+ tw2};
           F_value:=F;
            IF  F_value = 0.0  THEN  GOTO 16; { To end of Procedure }
            Tol:=Eps; A:=ABS(X);
            IF  A > 1.0  THEN  Tol:=Tol * A; { ELSE }
             IF  ABS(D_X) <= Tol  THEN
               IF  ABS(F_value) <= Tolf  THEN  GOTO 16; { ELSE }
            IF  (F_value * F_L) < 0.0  THEN
             BEGIN   { IF  (F_value * F_L) <  0.0 }
              X_R:=X; F_R:=F_value; GOTO  4;
             END;    { IF  (F_value * F_L) <  0.0 }  { ELSE }
            X_L:=X; F_L:=F_value; X_R:=X_M; F_R:=F_M; GOTO  4;
  16:      END {$F-} ;  { PROCEDURE Rtmi_tw2}
       PROCEDURE Rtwi ( VAR X,F_value : Single;
                  F_t_Wall : FUNC_F_t_Wall;
                  X_Initial, Eps : Single;
                  Iter_X : INTEGER; VAR Jerror : INTEGER);
        LABEL  8  ;
        VAR  A, B, Tol, D  : Single;
          J  : INTEGER;
         BEGIN   { PROCEDURE Rtwi }
          Jerror:=0; Tol:=X_Initial; X:=F_t_Wall(Tol); A:=X-X_Initial;
          B:=-A; Tol:=X; F_value:=X-F_t_Wall(Tol);
          FOR J:=1 TO  Iter_X  DO
           BEGIN  { FOR J }
            IF  F_value = 0.0  THEN  GOTO 8;   { ELSE }
            B:=B/F_value - 1.0;
            IF  B = 0.0  THEN
              BEGIN  { IF  B = 0.0 }
          Jerror:=1;
  8:      END;    { PROCEDURE Rtwi }
                F_tw2 : FUNC_F_t_Wall;
                 X_Initial, Eps : Single;
                 Iter_X : INTEGER; VAR Jerror : INTEGER);
        LABEL  8  ;
        VAR  A, B, Tol, D   : Single;
          J  : INTEGER;
         BEGIN   { PROCEDURE Rtwi_tw2 }
          Jerror:=0; Tol:=X_Initial; X:=F_tw2(Tol); A:=X-X_Initial;
          B:=-A; Tol:=X; F_value:=X-F_tw2(Tol);
          FOR J:=1 TO  Iter_X  DO
           BEGIN  { FOR J }
            IF  F_value = 0.0  THEN  GOTO 8;   { ELSE }
            B:=B/F_value - 1.0;
            IF  B = 0.0  THEN
              BEGIN  { IF  B = 0.0 }
               Jerror:=2;WRITELN(Jerror);  GOTO 8;
              END;  { IF  B = 0.0 }
             A:=A/B; X:=X+A; B:=F_value; Tol:=X;
             F_value:=X-F_tw2(Tol);
```

```
                 Tol:=Eps; D:=ABS(X);
                  IF  D > 1.0  THEN  Tol:=Tol*D;     { ELSE }
                  IF  ABS(A) <= Tol  THEN
                    IF ABS(F_value) <= (10.0*Tol) THEN GOTO 8; { ELSE }
                END;   { FOR J }
              Jerror:=1;
    8:        END;  { PROCEDURE Rtwi_tw2 }
          PROCEDURE  RKGS_Xo_Z_var_Ad( VAR Prmt : PrmtType; VAR Y, Dery : NdimType;
                    { Ndim : INTEGER; } VAR Jhlf : INTEGER;
                    { PROCEDURE Praw_Xo_Z_var_Ad( Z : Single; Y, Dery : NdimType);
                     PROCEDURE Outp_Xo_Z_var(Z : Single; Y, Dery : NdimType;
                          Jhlf  : INTEGER;
                          Prmt : PrmtType);}
                 VAR Aux : AuxType );
          LABEL    4, 9, 10, 18, 36, 39, 40        ;
          VAR A, B, C : ARRAY [1..4] Of Single;
            Z, Zend, H, TestZend, Test_Z_H_Zend, Aj, Bj, Cj,
            R1, R2, Delt, Z_H    :Single;
            J, Jrec, Jtest, Jstep, Jend, Jj, Jmod :  INTEGER;
          BEGIN      {
            FOR J:=1 TO  Ndim  DO  Aux[8, J]:= 0.6666667 * Dery[ J ];
            Z:=Prmt[1]; Zend:=Prmt[2]; H:=Prmt[3]; Prmt[5]:=0.0;
                      Praw_Xo_Z_var_Ad( Z, Y , Dery  );
            TestZend := H*(Zend-Z);
           IF TestZend > 0.0  THEN
            BEGIN
             A[1]:=0.5; A[2]:=0.2928932; A[3]:=1.707107; A[4]:=0.1666667;
             B[1]:=2.0; B[2]:=1.0; B[3]:=1.0; B[4]:=2.0;
             C[1]:=0.5; C[2]:=0.2928932; C[3]:=1.707107; C[4]:=0.5;
             FOR  J := 1  TO  Ndim  DO
              BEGIN
                Aux[1,J]:=Y[J]; Aux[2,J]:=Dery[J];
                Aux[3,J]:=0.0; Aux[6,J]:=0.0
              END;   { FOR J }
            Jrec:=0; H:=H+H; Jhlf:=-1; Jstep:=0; Jend:=0;
    4:       Test_Z_H_Zend:= (Z+H-Zend)*H;
           IF  Test_Z_H_Zend >= 0.0  THEN  Jend:= 1; { ELSE }
           IF   Test_Z_H_Zend >  0.0  THEN  H:= Zend - Z; { ELSE }
           Outp_Xo_Z_var( Z, Y, Dery, Jrec, { Ndim,} Prmt );
           IF Prmt[5] <> 0.0  THEN  GOTO 40;  { ELSE }
           Jtest:=0;
    9:      Jstep:=Jstep+1; {IF Jtest <= 0} {IF (Jtep-Jmod-Jmod) <> 0}
           Jj:=1;
    10:     Aj:=A[Jj]; Bj:=B[Jj]; Cj:=C[Jj];  {IF Jj < 4}
           FOR J:=1  TO  Ndim  DO
            BEGIN
             R1:=H*Dery[J]; R2:=Aj*(R1-BJ*Aux[6,J]); Y[J]:=Y[J]+R2;
             R2:=R2+R2+R2; Aux[6,J]:=Aux[6,J]+R2-Cj*R1
            END;   { FOR J }
           IF  Jj < 4  THEN
            BEGIN
             Jj:=Jj+1;
             IF  Jj <> 3  THEN  Z:=Z+0.5*H;  { ELSE }
             Praw_Xo_Z_var_Ad( Z, Y  , Dery  );
             GOTO 10
            END;     { IF Jj < 4  THEN }    { ELSE }
            BEGIN
             FOR J:=1  TO  Ndim  DO  Aux[4,J]:=Y[J];
             Jtest:=1; Jstep:=Jstep+Jstep-2;
    18:        Jhlf:=Jhlf+1; Z:=Z-H; H:=0.5*H;
```

```
       FOR J:=1 TO Ndim DO
         BEGIN
           Y[J]:=Aux[1,J]; Dery[J]:=Aux[2,J];
           Aux[6,J]:=Aux[3,J]
         END;    { FOR J }
        GOTO 9
       END
      Jmod:=Jstep DIV 2;
      IF (Jstep-Jmod-Jmod) <> 0 THEN
       BEGIN
         Praw_Xo_Z_var_Ad( Z, Y , Dery );
          FOR J:=1 TO Ndim DO
           BEGIN
             Aux[5,J]:=Y[J]; Aux[7,J]:=Dery[J]
           END;    { FOR J }
          GOTO 9
       END
      Delt:=0.0;
      FOR J:=1 TO Ndim DO
      Delt:=Delt+Aux[8,J]*ABS(Aux[4,J]-Y[J]);
      IF Delt > Prmt[4] THEN
        BEGIN
          IF Jhlf >= 10 THEN GOTO 36; { ELSE }
          FOR J:=1 TO Ndim DO Aux[4,J]:=Aux[5,J];
          Jstep:=Jstep+Jstep-4; Z:=Z-H; Jend:=0; GOTO 18
        END; { IF Delt > Prmt[4] THEN } { ELSE }
      Praw_Xo_Z_var_Ad( Z, Y , Dery );
      FOR J:=1 TO Ndim DO
          BEGIN
            Aux[1,J]:=Y[J]; Aux[2,J]:=Dery[J]; Y[J]:=Aux[5,J];
            Aux[3,J]:=Aux[6,J]; Dery[J]:=Aux[7,J]
          END;    { FOR J }
      Z_H:=Z-H;
      Outp_Xo_Z_var( Z_H,Y, Dery, Jhlf, { Ndim,} Prmt );
      IF Prmt[5] <> 0.0 THEN GOTO 40; { ELSE }
      FOR J:=1 TO Ndim DO
          BEGIN
            Y[J]:=Aux[1,J]; Dery[J]:=Aux[2,J]
          END;    { FOR J }
      Jrec:=Jhlf;
      IF Jend > 0 THEN GOTO 39; { ELSE }
      Jhlf:=Jhlf-1; Jstep:=Jstep DIV 2; H:=H+H;
      IF Jhlf < 0 THEN GOTO 4; { ELSE }
      Jmod:=Jstep DIV 2;
      IF (Jstep-Jmod-Jmod) <> 0 THEN GOTO 4; { ELSE }
      IF (Delt-0.02*Prmt[4]) > 0 THEN GOTO 4; { ELSE }
      Jhlf:=Jhlf-1; Jstep:=Jstep DIV 2; H:=H+H; GOTO 4;
36:     Jhlf:=11; Praw_Xo_Z_var_Ad(Z, Y , Dery );
      END; { IF TestZend > 0.0 THEN } { ELSE }
      IF TestZend = 0.0 THEN Jhlf:=12;
      IF TestZend < 0.0 THEN Jhlf:=13;
39:   Outp_Xo_Z_var(Z,Y,Dery,Jhlf, {Ndim,} Prmt); { IF Jend >= 0 THEN }
40:   END; { IF Prmt[5] <> 0.0 }  { PROCEDURE RKGS_Xo_Z_var_Ad}
    PROCEDURE RKGS_Xo_Z_var_Pro( VAR Prmt : PrmtType; VAR Y, Dery : NdimType;
            { Ndim : INTEGER; } VAR Jhlf : INTEGER;
            { PROCEDURE Praw_Xo_Z_var_Pro( Z : Single; Y, Dery : NdimType);
             PROCEDURE Outp_Xo_Z_var(Z : Single; Y, Dery : NdimType;
                     Jhlf : INTEGER;
                     Prmt : PrmtType);}
            VAR Aux : AuxType );
```

```
        LABEL   4, 9, 10, 18, 36, 39, 40      ;
        VAR A, B, C : ARRAY [1..4] Of Single;
          Z, Zend, H, TestZend, Test_Z_H_Zend, Aj, Bj, Cj,
          R1, R2, Delt, Z_H   :Single;
          J, Jrec, Jtest, Jstep, Jend, Jj, Jmod :  INTEGER;
        BEGIN      { PROCEDURE  RKGS_Xo_Z_var_Pro}
          FOR  J:=1 TO Ndim DO  Aux[8, J]:= 0.6666667 * Dery[ J ];
          Z:=Prmt[1]; Zend:=Prmt[2]; H:=Prmt[3]; Prmt[5]:=0.0;
                  Praw_Xo_Z_var_Pro( Z, Y , Dery  );
          TestZend := H*(Zend-Z);
         IF TestZend > 0.0  THEN
          BEGIN
          A[1]:=0.5; A[2]:=0.2928932; A[3]:=1.707107; A[4]:=0.1666667;
          B[1]:=2.0; B[2]:=1.0; B[3]:=1.0; B[4]:=2.0;
          C[1]:=0.5; C[2]:=0.2928932; C[3]:=1.707107; C[4]:=0.5;
          FOR  J := 1 TO  Ndim  DO
           BEGIN
             Aux[1,J]:=Y[J]; Aux[2,J]:=Dery[J];
             Aux[3,J]:=0.0; Aux[6,J]:=0.0
           END;   { FOR J }
          Jrec:=0; H:=H+H; Jhlf:=-1; Jstep:=0; Jend:=0;
 {Start of A Runge-Kutta step }
           {IF Jhlf < 0 THEN  }  {IF (Jstep-Jmod-Jmod) <> 0 THEN }
              {IF (Delt-0.02*Prmt[4]) > 0  THEN }
   4:        Test_Z_H_Zend:= (Z+H-Zend)*H;
           IF  Test_Z_H_Zend >= 0.0  THEN  Jend:= 1; { ELSE }
           IF   Test_Z_H_Zend >  0.0  THEN  H:= Zend - Z; { ELSE }
           Outp_Xo_Z_var( Z, Y, Dery, Jrec, { Ndim,} Prmt );
           IF Prmt[5] <> 0.0  THEN  GOTO 40; { ELSE }
           Jtest:=0;
   9:        Jstep:=Jstep+1; {IF Jtest <= 0} {IF (Jtep-Jmod-Jmod) <> 0}
           Jj:=1;
  10:        Aj:=A[Jj]; Bj:=B[Jj]; Cj:=C[Jj];  {IF Jj < 4}
           FOR  J:=1 TO  Ndim  DO
            BEGIN
             R1:=H*Dery[J]; R2:=Aj*(R1-BJ*Aux[6,J]); Y[J]:=Y[J]+R2;
             R2:=R2+R2+R2; Aux[6,J]:=Aux[6,J]+R2-Cj*R1
            END;   { FOR J }
           IF  Jj < 4  THEN
            BEGIN
             Jj:=Jj+1;
             IF  Jj <> 3  THEN  Z:=Z+0.5*H;  { ELSE }
             Praw_Xo_Z_var_Pro( Z, Y  , Dery  );
             GOTO 10
            END;
           IF  Jtest <= 0  THEN
            BEGIN
             FOR  J:=1 TO  Ndim  DO  Aux[4,J]:=Y[J];
             Jtest:=1; Jstep:=Jstep+Jstep-2;
  18:         Jhlf:=Jhlf+1; Z:=Z-H; H:=0.5*H;
             FOR  J:=1 TO  Ndim  DO
              BEGIN
                Y[J]:=Aux[1,J]; Dery[J]:=Aux[2,J];
                Aux[6,J]:=Aux[3,J]
              END;   { FOR J }
             GOTO 9
            END;
           Jmod:=Jstep DIV 2;
           IF  (Jstep-Jmod-Jmod) <> 0 THEN
            BEGIN
```

```
           Praw_Xo_Z_var_Pro( Z, Y , Dery );
           FOR  J:=1  TO  Ndim  DO
            BEGIN
              Aux[5,J]:=Y[J]; Aux[7,J]:=Dery[J]
            END;   { FOR J }
           GOTO 9
          END;
        Delt:=0.0;
        FOR  J:=1  TO  Ndim  DO
        Delt:=Delt+Aux[8,J]*ABS(Aux[4,J]-Y[J]);
        IF  Delt > Prmt[4]  THEN
          BEGIN
            IF  Jhlf >= 10  THEN  GOTO  36; { ELSE }
            FOR  J:=1  TO  Ndim  DO  Aux[4,J]:=Aux[5,J];
            Jstep:=Jstep+Jstep-4; Z:=Z-H; Jend:=0; GOTO 18
          END; { IF Delt > Prmt[4] THEN } { ELSE }
        Praw_Xo_Z_var_Pro( Z, Y , Dery );
        FOR  J:=1  TO  Ndim  DO
            BEGIN
              Aux[1,J]:=Y[J]; Aux[2,J]:=Dery[J]; Y[J]:=Aux[5,J];
              Aux[3,J]:=Aux[6,J]; Dery[J]:=Aux[7,J]
            END;   { FOR J }
        Z_H:=Z-H;
        Outp_Xo_Z_var( Z_H,Y, Dery, Jhlf, { Ndim,} Prmt );
        IF Prmt[5] <> 0.0  THEN  GOTO 40;  { ELSE }
        FOR  J:=1  TO  Ndim  DO
            BEGIN
              Y[J]:=Aux[1,J]; Dery[J]:=Aux[2,J]
            END;   { FOR J }
        Jrec:=Jhlf;
        IF  Jend > 0  THEN  GOTO  39; { ELSE }
        Jhlf:=Jhlf-1; Jstep:=Jstep DIV 2; H:=H+H;
        IF  Jhlf < 0  THEN  GOTO  4; { ELSE }
        Jmod:=Jstep DIV 2;
        IF (Jstep-Jmod-Jmod) <> 0 THEN  GOTO 4;  { ELSE }
        IF (Delt-0.02*Prmt[4]) > 0  THEN  GOTO  4;  { ELSE }
        Jhlf:=Jhlf-1; Jstep:=Jstep DIV 2; H:=H+H; GOTO 4;
36:      Jhlf:=11; Praw_Xo_Z_var_Pro(Z, Y , Dery );
        END;  { IF TestZend > 0.0  THEN } { ELSE }
        IF TestZend = 0.0  THEN  Jhlf:=12;
        IF TestZend < 0.0  THEN  Jhlf:=13;
39:    Outp_Xo_Z_var(Z,Y,Dery,Jhlf, {Ndim,} Prmt); {IF  Jend >= 0  THEN }
40:    END; { IF Prmt[5] <> 0.0 }  { PROCEDURE  RKGS_Xo_Z_var_Pro}
    PROCEDURE  RKGS_Xo_Z_var_Ad_All( VAR Prmt : PrmtType; VAR Y, Dery : NdimType;
            { Ndim : INTEGER; } VAR Jhlf : INTEGER;
            { PROCEDURE Praw_Xo_Z_var_Ad_All( Z : Single; Y, Dery : NdimType);
             PROCEDURE Outp_Xo_Z_var(Z : Single; Y, Dery : NdimType;
                      Jhlf : INTEGER;
                      Prmt : PrmtType);}
             VAR Aux : AuxType );
    LABEL   4, 9, 10, 18, 36, 39, 40       ;
    VAR A, B, C : ARRAY [1..4] Of Single;
       Z, Zend, H, TestZend, Test_Z_H_Zend, Aj, Bj, Cj,
       R1, R2, Delt, Z_H    :Single;
       J, Jrec, Jtest, Jstep, Jend, Jj, Jmod :  INTEGER;
    BEGIN
      FOR  J:=1  TO  Ndim  DO  Aux[8, J]:= 0.6666667 * Dery[ J ];
      Z:=Prmt[1]; Zend:=Prmt[2]; H:=Prmt[3]; Prmt[5]:=0.0;
            Praw_Xo_Z_var_Ad_Al( Z, Y , Dery);
      TestZend := H*(Zend-Z);
```

```
         IF TestZend > 0.0  THEN
          BEGIN
           A[1]:=0.5; A[2]:=0.2928932; A[3]:=1.707107; A[4]:=0.1666667;
           B[1]:=2.0; B[2]:=1.0; B[3]:=1.0; B[4]:=2.0;
           C[1]:=0.5; C[2]:=0.2928932; C[3]:=1.707107; C[4]:=0.5;
           FOR  J := 1  TO  Ndim  DO
            BEGIN
              Aux[1,J]:=Y[J]; Aux[2,J]:=Dery[J];
              Aux[3,J]:=0.0; Aux[6,J]:=0.0
            END;  { FOR J }
           Jrec:=0; H:=H+H; Jhlf:=-1; Jstep:=0; Jend:=0;
              {IF Jhlf < 0 THEN  } {IF (Jstep-Jmod-Jmod) <> 0 THEN }
                {IF (Delt-0.02*Prmt[4]) > 0  THEN }
  4:        Test_Z_H_Zend:= (Z+H-Zend)*H;
           IF Test_Z_H_Zend >= 0.0 THEN Jend:= 1; { ELSE }
           IF  Test_Z_H_Zend >  0.0 THEN H:= Zend - Z; { ELSE }
           Outp_Xo_Z_var( Z, Y, Dery, Jrec, { Ndim,} Prmt );
           IF Prmt[5] <> 0.0  THEN  GOTO 40; { ELSE }
           Jtest:=0;
  9:        Jstep:=Jstep+1; {IF Jtest <= 0} {IF (Jtep-Jmod-Jmod) <> 0}
           Jj:=1;
 10:         Aj:=A[Jj]; Bj:=B[Jj]; Cj:=C[Jj];  {IF Jj < 4}
           FOR  J:=1  TO  Ndim  DO
            BEGIN
             R1:=H*Dery[J]; R2:=Aj*(R1-BJ*Aux[6,J]); Y[J]:=Y[J]+R2;
             R2:=R2+R2+R2; Aux[6,J]:=Aux[6,J]+R2-Cj*R1
            END;   { FOR J }
           IF  Jj < 4  THEN
            BEGIN
              Jj:=Jj+1;
              IF  Jj <> 3  THEN  Z:=Z+0.5*H;  { ELSE }
              Praw_Xo_Z_var_Ad_All( Z, Y, Dery);
              GOTO 10
            END
           IF  Jtest <= 0  THEN
            BEGIN
             FOR  J:=1 TO  Ndim  DO  Aux[4,J]:=Y[J];
             Jtest:=1; Jstep:=Jstep+Jstep-2;
 18:          Jhlf:=Jhlf+1; Z:=Z-H; H:=0.5*H;
             FOR  J:=1  TO  Ndim  DO
              BEGIN
                Y[J]:=Aux[1,J]; Dery[J]:=Aux[2,J];
                Aux[6,J]:=Aux[3,J]
              END;   { FOR J }
             GOTO 9
            END;
           Jmod:=Jstep DIV 2;
           IF  (Jstep-Jmod-Jmod) <> 0 THEN
            BEGIN
             Praw_Xo_Z_var_Ad_All( Z, Y, Dery );
             FOR  J:=1  TO  Ndim  DO
              BEGIN
                Aux[5,J]:=Y[J]; Aux[7,J]:=Dery[J]
              END;   { FOR J }
             GOTO 9
            END;  { IF (Jtep-Jmod-Jmod) <> 0 THEN } { ELSE }
           Delt:=0.0;
           FOR  J:=1  TO  Ndim  DO
           Delt:=Delt+Aux[8,J]*ABS(Aux[4,J]-Y[J]);
           IF  Delt > Prmt[4]  THEN
```

```
              BEGIN
                IF  Jhlf >= 10  THEN  GOTO  36; { ELSE }
                FOR  J:=1  TO  Ndim  DO  Aux[4,J]:=Aux[5,J];
                Jstep:=Jstep+Jstep-4; Z:=Z-H; Jend:=0; GOTO 18
              END; { IF Delt > Prmt[4] THEN } { ELSE }
            Praw_Xo_Z_var_Ad_All(Z, Y, Dery);
            FOR  J:=1  TO  Ndim  DO
                BEGIN
                  Aux[1,J]:=Y[J]; Aux[2,J]:=Dery[J]; Y[J]:=Aux[5,J];
                  Aux[3,J]:=Aux[6,J]; Dery[J]:=Aux[7,J]
                END;    { FOR J }
            Z_H:=Z-H;
            Outp_Xo_Z_var( Z_H,Y, Dery, Jhlf, { Ndim,} Prmt );
            IF Prmt[5] <> 0.0  THEN  GOTO 40; { ELSE }
            FOR  J:=1  TO  Ndim  DO
                BEGIN
                  Y[J]:=Aux[1,J]; Dery[J]:=Aux[2,J]
                END;    { FOR J }
            Jrec:=Jhlf;
            IF  Jend > 0  THEN  GOTO  39; { ELSE }
            Jhlf:=Jhlf-1; Jstep:=Jstep DIV 2; H:=H+H;
            IF  Jhlf < 0  THEN  GOTO  4; { ELSE }
            Jmod:=Jstep DIV 2;
            IF (Jstep-Jmod-Jmod) <> 0  THEN  GOTO  4; { ELSE }
            IF (Delt-0.02*Prmt[4]) > 0  THEN  GOTO  4; { ELSE }
            Jhlf:=Jhlf-1; Jstep:=Jstep DIV 2; H:=H+H; GOTO 4;
36:         Jhlf:=11; Praw_Xo_Z_var_Ad_All(Z, Y , Dery );
            END; { IF TestZend > 0.0 THEN } { ELSE }
            IF TestZend = 0.0  THEN  Jhlf:=12;
            IF TestZend < 0.0  THEN  Jhlf:=13;
39:         Outp_Xo_Z_var(Z,Y,Dery,Jhlf, {Ndim,} Prmt); { IF Jend >= 0  THEN }
40:      END; { IF Prmt[5] <> 0.0 }  { PROCEDURE RKGS_Xo_Z_var_Ad_All}
      PROCEDURE  RKGS_Xo_Z_var_Pro_All( VAR Prmt : PrmtType; VAR Y, Dery : NdimType;
              { Ndim : INTEGER; } VAR Jhlf : INTEGER;
              { PROCEDURE Praw_Xo_Z_var_Pro_All( Z : Single; Y, Dery : NdimType);
               PROCEDURE Outp_Xo_Z_var(Z : Single; Y, Dery : NdimType;
                         Jhlf  : INTEGER;
                         Prmt : PrmtType);}
              VAR Aux : AuxType );
      LABEL   4, 9, 10, 18, 36, 39, 40        ;
      VAR A, B, C : ARRAY [1..4] Of Single;
         Z, Zend, H, TestZend, Test_Z_H_Zend, Aj, Bj, Cj,
         R1, R2, Delt, Z_H   :Single;
         J, Jrec, Jtest, Jstep, Jend, Jj, Jmod : INTEGER;
      BEGIN
        FOR  J:=1  TO  Ndim  DO  Aux[8, J]:= 0.6666667 * Dery[ J ];
        Z:=Prmt[1]; Zend:=Prmt[2]; H:=Prmt[3]; Prmt[5]:=0.0;
               Praw_Xo_Z_var_Pro_All( Z, Y , Dery);
        TestZend := H*(Zend-Z);
        IF TestZend > 0.0  THEN
        BEGIN
        A[1]:=0.5; A[2]:=0.2928932; A[3]:=1.707107; A[4]:=0.1666667;
        B[1]:=2.0; B[2]:=1.0; B[3]:=1.0; B[4]:=2.0;
        C[1]:=0.5; C[2]:=0.2928932; C[3]:=1.707107; C[4]:=0.5;
        FOR  J := 1  TO  Ndim  DO
          BEGIN
            Aux[1,J]:=Y[J]; Aux[2,J]:=Dery[J];
            Aux[3,J]:=0.0; Aux[6,J]:=0.0
          END; { FOR J }
        Jrec:=0; H:=H+H; Jhlf:=-1; Jstep:=0; Jend:=0;
```

```
          {IF Jhlf < 0 THEN  } {IF (Jstep-Jmod-Jmod) <> 0 THEN }
              {IF (Delt-0.02*Prmt[4]) > 0  THEN }
  4:       Test_Z_H_Zend:= (Z+H-Zend)*H;
          IF  Test_Z_H_Zend >= 0.0  THEN Jend:= 1; { ELSE }
          IF   Test_Z_H_Zend >  0.0  THEN H:= Zend - Z; { ELSE }
          Outp_Xo_Z_var( Z, Y, Dery, Jrec, { Ndim,} Prmt );
          IF Prmt[5] <> 0.0  THEN  GOTO 40;  { ELSE }
          Jtest:=0;
  9:       Jstep:=Jstep+1; {IF Jtest <= 0} {IF (Jtep-Jmod-Jmod) <> 0}
          Jj:=1;
  10:       Aj:=A[Jj]; Bj:=B[Jj]; Cj:=C[Jj];  {IF Jj < 4}
          FOR J:=1  TO  Ndim  DO
           BEGIN
           R1:=H*Dery[J]; R2:=Aj*(R1-BJ*Aux[6,J]); Y[J]:=Y[J]+R2;
           R2:=R2+R2+R2; Aux[6,J]:=Aux[6,J]+R2-Cj*R1
           END;    { FOR J }
          IF  Jj < 4  THEN
           BEGIN
            Jj:=Jj+1;
            IF  Jj <> 3  THEN  Z:=Z+0.5*H;  { ELSE }
            Praw_Xo_Z_var_Pro_All(Z, Y, Dery);
            GOTO 10
           END;
          IF  Jtest <= 0  THEN
           BEGIN
            FOR  J:=1  TO  Ndim  DO  Aux[4,J]:=Y[J];
            Jtest:=1; Jstep:=Jstep+Jstep-2;
  18:          Jhlf:=Jhlf+1; Z:=Z-H; H:=0.5*H;
            FOR  J:=1  TO  Ndim  DO
             BEGIN
              Y[J]:=Aux[1,J]; Dery[J]:=Aux[2,J];
              Aux[6,J]:=Aux[3,J]
             END;    { FOR J }
            GOTO 9
           END;  { IF Jtest <= 0  THEN } { ELSE }
          Jmod:=Jstep DIV 2;
          IF  (Jstep-Jmod-Jmod) <> 0  THEN
           BEGIN
            Praw_Xo_Z_var_Pro_All(Z, Y, Dery );
            FOR  J:=1  TO  Ndim  DO
             BEGIN
              Aux[5,J]:=Y[J]; Aux[7,J]:=Dery[J]
             END;    { FOR J }
            GOTO 9
           END;
          Delt:=0.0;
          FOR J:=1  TO  Ndim  DO
          Delt:=Delt+Aux[8,J]*ABS(Aux[4,J]-Y[J]);
          IF  Delt > Prmt[4]  THEN
           BEGIN
            IF  Jhlf >= 10  THEN  GOTO 36; { ELSE }
            FOR  J:=1  TO  Ndim  DO  Aux[4,J]:=Aux[5,J];
            Jstep:=Jstep+Jstep-4; Z:=Z-H; Jend:=0; GOTO 18
           END;  { IF  Delt > Prmt[4]  THEN } { ELSE }
          Praw_Xo_Z_var_Pro_All(Z, Y, Dery);
          FOR J:=1  TO  Ndim  DO
             BEGIN
              Aux[1,J]:=Y[J]; Aux[2,J]:=Dery[J]; Y[J]:=Aux[5,J];
              Aux[3,J]:=Aux[6,J]; Dery[J]:=Aux[7,J]
             END;   { FOR J }
```

```
        Z_H:=Z-H;
        Outp_Xo_Z_var( Z_H,Y, Dery, Jhlf, { Ndim,} Prmt );
        IF Prmt[5] <> 0.0  THEN  GOTO 40;  { ELSE }
        FOR  J:=1  TO  Ndim  DO
           BEGIN
             Y[J]:=Aux[1,J]; Dery[J]:=Aux[2,J]
           END;   { FOR J }
        Jrec:=Jhlf;
        IF  Jend > 0  THEN  GOTO  39;
        Jhlf:=Jhlf-1; Jstep:=Jstep DIV 2; H:=H+H;
        IF  Jhlf < 0  THEN  GOTO  4;  { ELSE }
        Jmod:=Jstep DIV 2;
        IF (Jstep-Jmod-Jmod) <> 0  THEN  GOTO  4;  { ELSE }
        IF (Delt-0.02*Prmt[4]) > 0  THEN  GOTO  4;  { ELSE }
        Jhlf:=Jhlf-1; Jstep:=Jstep DIV 2; H:=H+H; GOTO 4;
36:       Jhlf:=11; Praw_Xo_Z_var_Pro_All(Z, Y , Dery );
        END; { IF TestZend > 0.0  THEN }  { ELSE }
        IF TestZend = 0.0  THEN  Jhlf:=12;
        IF TestZend < 0.0  THEN  Jhlf:=13;
39:     Outp_Xo_Z_var(Z,Y,Dery,Jhlf, {Ndim,} Prmt);  { IF  Jend >= 0  THEN }
40:    END;  { IF Prmt[5] <> 0.0 }   { PROCEDURE  RKGS_Xo_Z_var_Pro_All}
      PROCEDURE  RKGS_Zo_X_var_Aux_Pro( VAR Prmt : PrmtType; VAR Y, Dery : NdimType;
               { Ndim : INTEGER; } VAR Jhlf : INTEGER;
               { PROCEDURE Praw_Zo_X_var_Pro( X : Single; Y, Dery : NdimType);
                PROCEDURE Outp(X : Single; Y, Dery : NdimType;
                       Jhlf  : INTEGER;
                       Prmt : PrmtType);}
              VAR Aux : AuxType );
      LABEL   4, 9, 10, 18, 36, 39, 40       ;
      VAR A, B, C : ARRAY [1..4] Of Single;
        X, Xend, H, TestXend, Test_X_H_Xend, Aj, Bj, Cj,
        R1, R2, Delt, X_H   :Single;
        J, Jrec, Jtest, Jstep, Jend, Jj, Jmod :  INTEGER;
      BEGIN
        FOR  J:=1  TO  Ndim  DO  Aux[8, J]:= 0.6666667 * Dery[ J ];
        X:=Prmt[1]; Xend:=Prmt[2]; H:=Prmt[3]; Prmt[5]:=0.0;
                Praw_Zo_X_var_Pro( X, Y , Dery );
        TestXend := H*(Xend-X);
        IF TestXend > 0.0  THEN
        BEGIN
        A[1]:=0.5; A[2]:=0.2928932; A[3]:=1.707107; A[4]:=0.1666667;
        B[1]:=2.0; B[2]:=1.0; B[3]:=1.0; B[4]:=2.0;
        C[1]:=0.5; C[2]:=0.2928932; C[3]:=1.707107; C[4]:=0.5;
        FOR  J := 1  TO  Ndim  DO
          BEGIN
            Aux[1,J]:=Y[J]; Aux[2,J]:=Dery[J];
            Aux[3,J]:=0.0; Aux[6,J]:=0.0
          END;  { FOR J }
        Jrec:=0; H:=H+H; Jhlf:=-1; Jstep:=0; Jend:=0;
         {IF Jhlf < 0  THEN  } {IF (Jstep-Jmod-Jmod) <> 0  THEN }
            {IF (Delt-0.02*Prmt[4]) > 0  THEN }
 4:      Test_X_H_Xend:= (X+H-Xend)*H;
        IF  Test_X_H_Xend >= 0.0  THEN  Jend:= 1;  { ELSE }
        IF   Test_X_H_Xend > 0.0  THEN  H:= Xend - X;  { ELSE }
        Outp ( X, Y, Dery, Jrec, { Ndim,} Prmt );
        IF Prmt[5] <> 0.0  THEN  GOTO 40;  { ELSE }
        Jtest:=0;
 9:      Jstep:=Jstep+1; {IF Jtest <= 0} {IF (Jtep-Jmod-Jmod) <> 0}
        Jj:=1;
10:      Aj:=A[Jj]; Bj:=B[Jj]; Cj:=C[Jj];  {IF Jj < 4}
```

```
            FOR  J:=1  TO  Ndim  DO
             BEGIN
              R1:=H*Dery[J]; R2:=Aj*(R1-BJ*Aux[6,J]); Y[J]:=Y[J]+R2;
              R2:=R2+R2+R2; Aux[6,J]:=Aux[6,J]+R2-Cj*R1
             END;    { FOR J }
            IF  Jj < 4  THEN
             BEGIN
              Jj:=Jj+1;
              IF  Jj <> 3  THEN  X:=X+0.5*H;  { ELSE }
              Praw_Zo_X_var_Pro( X, Y , Dery );
              GOTO 10
             END;
             BEGIN
              FOR J:=1  TO  Ndim  DO  Aux[4,J]:=Y[J];
              Jtest:=1; Jstep:=Jstep+Jstep-2;
18:           Jhlf:=Jhlf+1; X:=X-H; H:=0.5*H;
              FOR J:=1  TO  Ndim  DO
               BEGIN
                Y[J]:=Aux[1,J]; Dery[J]:=Aux[2,J];
                Aux[6,J]:=Aux[3,J]
               END;
              GOTO 9
             END;
            Jmod:=Jstep DIV 2;
            IF  (Jstep-Jmod-Jmod) <> 0 THEN
             BEGIN
               Praw_Zo_X_var_Pro( X, Y , Dery );
               FOR J:=1  TO  Ndim  DO
                BEGIN
                 Aux[5,J]:=Y[J]; Aux[7,J]:=Dery[J]
                END;    { FOR J }
               GOTO 9
             END;
            Delt:=0.0;
            FOR J:=1  TO  Ndim  DO
            Delt:=Delt+Aux[8,J]*ABS(Aux[4,J]-Y[J]);
            IF  Delt > Prmt[4]  THEN
             BEGIN
               IF  Jhlf >= 10  THEN  GOTO  36; { ELSE }
               FOR J:=1  TO  Ndim  DO  Aux[4,J]:=Aux[5,J];
               Jstep:=Jstep+Jstep-4; X:=X-H; Jend:=0; GOTO 18
             END; { IF  Delt > Prmt[4]  THEN } { ELSE }
            Praw_Zo_X_var_Pro( X, Y , Dery );
            FOR J:=1  TO  Ndim  DO
               BEGIN
                Aux[1,J]:=Y[J]; Aux[2,J]:=Dery[J]; Y[J]:=Aux[5,J];
                Aux[3,J]:=Aux[6,J]; Dery[J]:=Aux[7,J]
               END;    { FOR J }
            X_H:=X-H;
            Outp( X_H,Y, Dery, Jhlf, { Ndim,} Prmt );
            IF Prmt[5] <> 0.0  THEN  GOTO 40; { ELSE }
            FOR J:=1  TO  Ndim  DO
               BEGIN
                Y[J]:=Aux[1,J]; Dery[J]:=Aux[2,J]
               END;    { FOR J }
            Jrec:=Jhlf;
            IF  Jend > 0  THEN  GOTO 39; { ELSE }
            Jhlf:=Jhlf-1; Jstep:=Jstep DIV 2; H:=H+H;
            IF  Jhlf < 0  THEN  GOTO 4; { ELSE }
            Jmod:=Jstep DIV 2;
```

```
        IF (Jstep-Jmod-Jmod) <> 0  THEN  GOTO  4;  { ELSE }
        IF (Delt-0.02*Prmt[4]) > 0  THEN  GOTO  4;  { ELSE }
        Jhlf:=Jhlf-1; Jstep:=Jstep DIV 2; H:=H+H; GOTO 4;
36:       Jhlf:=11; Praw_Zo_X_var_Pro(X, Y , Dery );
        END;  { IF TestXend > 0.0  THEN }  { ELSE }
        IF TestXend = 0.0  THEN  Jhlf:=12;
        IF TestXend < 0.0  THEN  Jhlf:=13;
39:     Outp(X,Y,Dery,Jhlf, {Ndim,} Prmt);  { IF  Jend >= 0  THEN }
40:     END;  { IF Prmt[5] <> 0.0 }   { PROCEDURE  RKGS_Zo_X_var_Aux_Pro}
```